

DISS. ETH NO. 24586

THE ROLE OF BIOTRANSFORMATION ON THE TOXICOKINETICS OF
FUNGICIDES IN AQUATIC INVERTEBRATES

A thesis submitted to attain the degree of
DOCTOR OF SCIENCES of ETH ZURICH
(Dr. sc. ETH Zurich)

presented by

ANDREA RÖSCH

MSc Marine Environmental Sciences, University of Oldenburg

born on 07.03.1986

citizen of Germany

accepted on the recommendation of
Prof. Dr. Juliane Hollender (examiner)
Dr. Roman Ashauer (co-examiner)
Prof. Dr. Nina Cedergreen (co-examiner)
Prof. Dr. Kristopher McNeill (co-examiner)

2017

Table of Contents

Summary	vii
Zusammenfassung.....	xi
Chapter 1. Introduction	1
1.1 Pesticides in the Aquatic Environment	3
1.2 Pesticide Mixtures, Regulation and Risk Assessment	4
1.3 Aquatic Invertebrates as Test Species: <i>Gammarus pulex</i> and <i>Hyalella azteca</i>	5
1.4 Toxicokinetic Processes in Aquatic Organisms	6
1.5 Knowledge Gaps, Objectives, and Content of the Thesis	11
References	13
Chapter 2. How Biotransformation influences Toxicokinetics of Azole Fungicides in the Aquatic Invertebrate <i>Gammarus pulex</i>.....	19
Abstract	21
2.1 Introduction	22
2.2 Material and Methods.....	23
2.3 Result and Discussion.....	28
Acknowledgment	42
References	43
Chapter S2. Supporting Information: How Biotransformation influences Toxicokinetics of Azole Fungicides in the Aquatic Invertebrate <i>Gammarus pulex</i>.....	49
SI.A Chemicals and Solutions.....	51
SI.B Analytical Method.....	52
SI.C Quality Control	55
SI.D SIEVE Settings.....	58
SI.E Exposure Medium Concentrations.....	59
SI.F Sampling during the Kinetic Experiment	60
SI.G Sulfate Deconjugation Experiment	60
SI.H Toxicokinetics and Bayesian Statistics	61
SI.I Identified Biotransformation Products	65
SI.J Effects of Biotransformation on the Polarity of Biotransformation Products	106
References	107

Chapter 3. The Synergistic Potential of Azole Fungicides in the Aquatic Invertebrate *Gammarus pulex*..... 109

Abstract	111
3.1 Introduction	112
3.2 Material and Methods.....	114
3.3 Results and Discussion	119
Acknowledgment	130
References	131

Chapter S3. Supporting Information: The Synergistic Potential of Azole Fungicides in the Aquatic Invertebrate *Gammarus pulex*..... 137

SI.A Chemicals and Solutions.....	139
SI.B Test Organisms.....	140
SI.C Analytical Method.....	141
SI.D Quality Control	143
SI.E Biotransformation Product Identification with SIEVE Software.....	145
SI.F Sampling During the Kinetic Experiment	146
SI.G Sulfate and Glucose Deconjugation Experiment.....	146
SI.H Modeling Bioaccumulation and Biotransformation Kinetics.....	147
SI.I Exposure Medium Concentrations, Internal Concentrations and Bioaccumulation Factors (BAFs).....	158
SI.J Internal Concentration Measurements of Binary Mixtures	178
SI.K Toxicity Prediction based on Concentration Addition (CA).....	184
SI.L Dose-Response Fitting.....	185
SI.M Half Maximal Inhibitory Concentrations based on <i>in vivo</i> ECOD Activity ($IC_{50, ECODS}$)	186
SI.N Inhibitory Concentrations based on Internal Concentration Measurements ($IC_{50/10, PRZ, AZS}$).....	187
SI.O Lethal Concentrations of Azoxystrobin (LC_{50S}) in the Presence and Absence of Prochloraz.....	188
SI.P Data Evaluation of the Video-Tracking of Gammarids	189
SI.Q Identified Biotransformation Products for Azoxystrobin.....	192
References	208

Chapter 4. Comparing Biotransformation of two Fungicides and the Potential of Cytochrome P450 Inhibition in two Aquatic Invertebrates 211

Abstract	213
4.1 Introduction	214
4.2 Material and Methods	216
4.3 Results and Discussion	220
Acknowledgment	237
References	238

Chapter S4. Supporting Information: Comparing Biotransformation of two Fungicides and the Potential of Cytochrome P450 Inhibition in two Aquatic Invertebrates 245

SI.A Chemicals and Solutions	247
SI.B Quality Control	248
SI.C Biotransformation Product Identification in <i>H. azteca</i> by Suspect and Nontarget Screening using Compound Discoverer	249
SI.D Sampling during the <i>H. azteca</i> Kinetic Experiment	250
SI.E Modeling Bioaccumulation and Biotransformation Kinetics	251
SI.F Exposure Medium Concentrations, Internal Concentrations and Bioaccumulation Factors (BAFs) for <i>H. azteca</i>	254
SI.G Determination of $IC_{50, PRZ, AZS}$ in <i>H. azteca</i>	261
SI.H Dose-Response Fitting of $IC_{50, PRZ, AZS}$ in <i>H. azteca</i>	262
SI.I Comparison of different <i>H. azteca</i> Sample Wet Weights for Detection and Quantification of Biotransformation Products	263
SI.J Identified Biotransformation Products for Azoxystrobin and Prochloraz in <i>H. azteca</i>	265
References	313

Chapter 5. Conclusion, Outlook and Open Questions 315

5.1 Prediction and Identification of Biotransformation Products	317
5.2 (Semi)-Quantification of Biotransformation Products	318
5.3 Prediction of Toxicokinetic Processes	318
5.4 Relevance of Synergism in Pesticide Mixtures	321
5.5 Toxicokinetic-(Toxicodynamic) Modeling to assess the Importance of Biotransformation and Synergistic Interactions	321
5.6 Chemical Testing using Aquatic Invertebrates	322
References	323

Curriculum Vitae	327
Acknowledgments	329

Summary

In areas with mainly agricultural land use, pesticides are frequently detected in the ng L^{-1} to $\mu\text{g L}^{-1}$ range in surface water bodies and may pose a risk to aquatic ecosystems. Different pesticides including herbicides, insecticides and fungicides are co-occurring, leading to complex mixtures and combined effects cannot be excluded. Once released into surface waters, pesticides can be taken up by aquatic organisms and may bioaccumulate. Biotransformation describes the enzyme-catalyzed transformation of chemicals inside organisms and is a key toxicokinetic process that can greatly influence the bioaccumulation potential of chemicals by reducing the internal concentration in an organism and modifying toxicity.

Within this thesis, it was the goal to improve the understanding of the role of fungicide biotransformation on bioaccumulation and resulting toxicity in the two aquatic invertebrate species *Gammarus pulex* and *Hyalella azteca*. Based on previous effect measurements, azole fungicides are known to cause synergistic effects in mixtures. However, a mechanistic process understanding is lacking that provides proof that the observed synergism is actually caused by altered enzyme activity thereby affecting biotransformation. Using high-resolution tandem mass spectrometry (HRMS/MS), biotransformation products (BTPs) for selected frequently applied azole and strobilurin fungicides were identified. Through toxicokinetic modeling of uptake, biotransformation and elimination processes, the importance of biotransformation in reducing parent compound bioaccumulation was evaluated and compared in the two selected test species. Additionally, the influence of azoles on internal concentrations of a substrate and associated BTPs and on toxicity was investigated in detail to gain a mechanistic understanding of synergistic effects caused by azole fungicides.

First, biotransformation of seven frequently used azole fungicides (triazoles: cyproconazole, epoxiconazole, fluconazole, propiconazole, tebuconazole and imidazoles: ketoconazole, prochloraz) was investigated in *G. pulex* in 24 h screening experiments. Additionally, kinetic experiments were performed to model toxicokinetic processes of prochloraz and epoxiconazole. The active moiety of azole fungicides is either a triazole or imidazole ring, both of which are known to interact with cytochrome P450 monooxygenases (CYPs) that are critical in enzymatic detoxification reactions of chemicals. Therefore, special attention was given to the active moiety and its preservation during biotransformation. By the use of HRMS/MS, between one (ketoconazole) and six (epoxiconazole) BTPs were tentatively identified per parent compound, except for fluconazole and prochloraz. Bioaccumulation factors (BAFs) ranged from approximately $0.4 - 50 \text{ L kg}_{\text{ww}}^{-1}$ and were in general low compared to the threshold of 2000 L kg^{-1} given in the European REACH regulation. For fluconazole, no BTPs were detected, which is in accordance with its low bioaccumulation ($\text{BAF} \approx 0.4 \text{ L kg}_{\text{ww}}^{-1}$) and much higher polarity ($\log D_{\text{ow}} \approx 0.7$) compared to the other selected azoles. In contrast, prochloraz showed extensive biotransformation reactions with 18 identified BTPs that were mainly characterized by imidazole ring loss or cleavage. Overall,

most BTPs were formed by oxidation and conjugation reactions. Different conjugation reactions were identified, including those with sulfate, with glutathione resulting in cysteine products, with glucose-sulfate, with phosphate and with acetate. Ring loss or cleavage was only observed for imidazoles, which is in line with the general mechanism of oxidative ring openings of imidazoles, likely influencing their bioactivity. Biotransformation only played a minor role with regard to the reduction of parent compound bioaccumulation, with the exception of prochloraz.

Second, the synergistic potential of six selected azole fungicides (triazoles: cyproconazole, epoxiconazole, propiconazole, tebuconazole and imidazoles: ketoconazole, prochloraz) was studied mechanistically and the azole CYP inhibition strength was investigated in *G. pulex*. The strobilurin fungicide azoxystrobin was chosen as a co-occurring substrate. Eighteen BTPs were identified for azoxystrobin by HRMS/MS screening approaches, revealing a complex biotransformation pathway. BTPs were mainly characterized by oxidation and conjugation reactions with sulfate, glucose, glucose-sulfate, and glutathione resulting in cysteine products. Binary fungicide mixtures, composed of 40 and 80 $\mu\text{g L}^{-1}$ azoxystrobin and similar molar concentrations of one of the selected azole fungicides, were tested, and only prochloraz showed a strong inhibitory potential, measured both in terms of internal concentrations of azoxystrobin and associated BTPs and in terms of acute toxicity. Bioaccumulation of azoxystrobin ($\text{BAF} \approx 5 \text{ L kg}_{\text{ww}}^{-1}$) was doubled in the presence of prochloraz. By determining the half-maximal inhibitory concentration of prochloraz ($\text{IC}_{50, \text{PRZ}, \text{AZ}}$) via internal concentration measurements, it was shown that the threshold where CYP inhibition starts (10% CYP inhibition expressed as $\text{IC}_{10, \text{PRZ}, \text{AZ}}: 4 \pm 2 \mu\text{g L}^{-1}$) is close to azole concentrations measured in Swiss surface waters. However, synergism by prochloraz was not only caused by the inhibition of CYP-catalyzed biotransformation reactions of azoxystrobin. Toxicokinetic modeling and derived increased uptake rate constants, an increase in total internal concentrations of azoxystrobin and associated BTPs, and *in vivo* assays for measuring CYP activities suggested that the presence of prochloraz additionally lead to increased azoxystrobin uptake. Video-tracking of *G. pulex* confirmed that increased uptake was due to prochloraz-induced hyperactivity, leading to increased movement and consequently increased ventilation rates.

Finally, fungicide biotransformation was investigated in *H. azteca* and compared with those in *G. pulex*. Similar BTPs were identified for azoxystrobin and prochloraz in *H. azteca* and *G. pulex* indicating a conservation of enzymes across the two aquatic invertebrate species. BTPs were mainly formed by oxidation and conjugation reactions. However, in addition to conjugation reactions with glucose, sulfate, glucose-sulfate, and glutathione resulting in cysteine products identified in both species, new conjugation reactions with taurine and glucose-malonyl were identified in *H. azteca*. Toxicokinetic modeling of azoxystrobin and associated BTPs indicated that biotransformation is more relevant for the reduction of parent compound bioaccumulation in *H. azteca* compared to *G. pulex*. However, bioaccumulation was low for azoxystrobin ($\text{BAF} \approx 5 \text{ L kg}_{\text{ww}}^{-1}$) and prochloraz ($\text{BAF} \approx 50 - 160 \text{ L kg}_{\text{ww}}^{-1}$) in both species compared to REACH criteria. Furthermore, estimated kinetic rate constants confirmed the importance of secondary BTPs such as conjugation reactions in aquatic

organisms. Determined half-maximal inhibitory concentrations ($IC_{50, PRZ, AZS}$) of prochloraz suggested that *H. azteca* was by a factor of five less sensitive to prochloraz-induced CYP inhibition compared to *G. pulex*. However, these species sensitivity differences seem to be of minor importance with regard to risk assessment, since assessment factors are applied to account for interspecies variability.

Overall, the results of this thesis show the importance of identifying BTPs and including biotransformation as a separate process into toxicokinetic modeling, as it enables differentiation between elimination routes and reveals the relevance of biotransformation. The synergistic effects of azole fungicides caused by enzyme inhibition as well as by altered uptake behavior indicate that understanding of mechanistic processes is important for predictive risk assessment and can be supported by toxicokinetic modeling. Although synergism is often linked to high threshold concentrations, synergism can also occur close to environmental realistic concentrations – as observed for prochloraz – highlighting the importance of identifying and including potent synergists into risk assessment.

Zusammenfassung

In Gebieten mit vorwiegend landwirtschaftlicher Landnutzung werden häufig Pestizide mit Konzentrationen im ng L^{-1} bis $\mu\text{g L}^{-1}$ Bereich in Oberflächengewässern nachgewiesen, die eine Gefahr für aquatische Ökosysteme darstellen. Verschiedene Pestizide, darunter Herbizide, Insektizide und Fungizide, können gemeinsam auftreten, was zu komplexen Mischungen führt. Hierbei können Kombinationswirkungen nicht ausgeschlossen werden. Pestizide können sobald sie in Oberflächengewässer eingetragen sind von aquatischen Organismen aufgenommen werden und dort bioakkumulieren. Die enzymkatalysierte Umwandlung von Chemikalien in Organismen bezeichnet man als Biotransformation. Sie stellt einen Schlüsselprozess dar, der einen grossen Einfluss auf das Bioakkumulationspotential von Chemikalien haben kann, indem er die interne Chemikalienkonzentration reduziert und dadurch die Toxizität beeinflusst.

Das Ziel dieser Arbeit war es, das Verständnis der Fungizidbiotransformation in zwei Süsswasserinvertebraten, den Flohkrebsarten *Gammarus pulex* und *Hyalella azteca* zu verbessern und die Rolle von Biotransformation bezüglich Bioakkumulation und der daraus resultierenden Toxizität zu untersuchen. Mit Hilfe von hochauflösender Tandem-Massenspektrometrie (HRMS/MS) wurden Biotransformationsprodukte (BTPs) für sieben häufig verwendete Azol- und Strobilurinfungizide detektiert und identifiziert. Durch die Modellierung von toxikokinetischen Prozessen (Aufnahme, Biotransformation, Elimination) konnte die Bedeutung der Biotransformation bezüglich ihrer Funktion die Bioakkumulation der Ausgangssubstanz zu reduzieren bewertet und in den ausgewählten Testorganismen verglichen werden. Es ist bekannt, dass Azolfungizide synergistische Effekte in Mischungen erzeugen können. Allerdings basiert dieses Wissen auf Effektstudien und es mangelt bisher an einem mechanistischen Prozessverständnis, das den vermuteten Mechanismus einer veränderten Biotransformation durch Enzyminhibition, die durch Azolfungizide hervorgerufen wird, bestätigt. Deshalb wurde in dieser Studie der Einfluss von Azolfungiziden auf die internen Konzentrationen eines Substrats und seiner gebildeten BTPs sowie auf die Toxizität detailliert untersucht, um ein mechanistisches Verständnis des Synergismus, der durch Azolfungizide hervorgerufen wird, zu gewinnen.

Im ersten Teil wurde die Biotransformation von sieben häufig angewendeten Azolfungiziden (Triazole: Cyproconazol, Epoxiconazol, Fluconazol, Propiconazol, Tebuconazol und Imidazole: Ketoconazol, Prochloraz) in *G. pulex* in 24 h-Screeningexperimenten untersucht. Zusätzlich wurden kinetische Experimente durchgeführt, um toxikokinetische Prozesse von Prochloraz und Epoxiconazol zu modellieren. Die aktive Gruppe von Azolen ist der Triazol- bzw. Imidazolring, von dem man weiss, dass er mit Cytochrome P450 Monooxygenasen (CYPs) wechselwirkt, die hochgradig in enzymatische Detoxifizierungsreaktionen von Chemikalien involviert sind. Deshalb wurde ein besonderes Augenmerk auf den aktiven Triazol- bzw. Imidazolring und auf seine Erhaltung während Biotransformationsprozessen gelegt. Mittels HRMS/MS wurden pro Ausgangssubstanz zwischen einem (Ketoconazol) und

sechs (Epoconazol) BTPs vorläufig identifiziert. Ausnahmen bildeten Fluconazol und Prochloraz. Bioakkumulationsfaktoren (BAFs) bewegten sich zwischen 0.4 und $50 \text{ L kg}_{\text{ww}}^{-1}$ und waren somit niedrig im Vergleich zur Europäischen REACH Verordnung, die Substanzen mit $\text{BAFs} > 2000 \text{ L kg}^{-1}$ als bioakkumulativ einstuft. Für Fluconazol wurden keine BTPs nachgewiesen, was mit seiner geringen Bioakkumulation ($\text{BAF} \approx 0.4 \text{ L kg}_{\text{ww}}^{-1}$) und viel höheren Polarität ($\log D_{\text{ow}} \approx 0.7$) im Vergleich zu den anderen ausgewählten Azolfungiziden übereinstimmt. Im Gegensatz dazu wurde Prochloraz umfassend biotransformiert. 18 BTPs, die vorwiegend durch Ringspaltungen und Ringverluste gekennzeichnet waren, wurden identifiziert. Im Allgemeinen wurden BTPs vorwiegend durch Oxidations- und Konjugationsreaktionen gebildet. Es wurden verschiedene Konjugationsreaktionen mit Sulfat, mit Glutathion woraus Cysteinprodukte resultierten, mit Glucose-Sulfat, mit Phosphat und mit Acetat identifiziert. Ringspaltungen und Ringverluste wurden nur für Imidazole beobachtet, was mit dem generellen Mechanismus der oxidativen Ringöffnung von Imidazolen übereinstimmt und wahrscheinlich die Bioaktivität dieser BTPs beeinflusst. Biotransformation spielte nur eine untergeordnete Rolle bezüglich der Reduzierung der Bioakkumulation der Ausgangsverbindungen, wobei wiederum Prochloraz eine Ausnahme bildete.

Im zweiten Teil wurde das synergistische Potential von sechs ausgewählten Azolfungiziden (Triazole: Cyproconazol, Epoconazol, Propiconazol, Tebuconazol und Imidazole: Ketoconazol, Prochloraz) mechanistisch in *G. pulex* untersucht und die CYP-Inhibitionsstärke der Azole erforscht. Als gleichzeitig auftretendes Substrat wurde das Strobilurinfungizid Azoxystrobin ausgewählt. Für Azoxystrobin wurden 18 BTPs mittels HRMS/MS identifiziert, wobei ein komplexer Biotransformationsweg aufgedeckt wurde. BTPs wurden vorwiegend durch Oxidationsreaktionen und Konjugationsreaktionen mit Sulfat, mit Glucose, mit Glucose-Sulfat und mit Glutathion woraus Cysteinprodukte resultierten, gebildet. Von den getesteten binären Fungizidmischungen, zusammengesetzt aus 40 und $80 \mu\text{g L}^{-1}$ Azoxystrobin sowie gleichen molaren Konzentrationen eines der ausgewählten Azolfungizide, zeigte nur Prochloraz eine starke inhibierende Wirkung, welche in Form der internen Konzentrationen von Azoxystrobin und seinen BTPs sowie durch akute Toxizität gemessen wurde. Die Bioakkumulation von Azoxystrobin ($\text{BAF} \approx 5 \text{ L kg}_{\text{ww}}^{-1}$) verdoppelte sich in Gegenwart von Prochloraz. Durch die Bestimmung der halbmaximalen Inhibitionskonzentration von Prochloraz ($\text{IC}_{50, \text{PRZ, AZ}}$) via interne Konzentrationsmessungen wurde gezeigt, dass die Grenze, ab der CYP-Inhibition beginnt (10% CYP-Inhibition ausgedrückt durch $\text{IC}_{10, \text{PRZ, AZ}}: 4 \pm 2 \mu\text{g L}^{-1}$), sich in der Nähe von Azolkonzentrationen befindet, die in Schweizer Oberflächengewässern gemessen werden. Der durch Prochloraz hervorgerufene Synergismus wurde jedoch nicht nur durch CYP-Inhibition verursacht. Toxikokinetische Modellierung und dadurch erhaltene erhöhte Aufnahmeraten, eine Zunahme der totalen internen Konzentration von Azoxystrobin und seinen BTPs sowie *in vivo*-Assays zur Messung der CYP-Aktivität deuteten darauf hin, dass die Gegenwart von Prochloraz zusätzlich zu einer erhöhten Azoxystrobinaufnahme führte. Videotracking von *G. pulex* bestätigte, dass die erhöhte Aufnahme durch Prochloraz-induzierte Hyperaktivität hervorgerufen wurde, welche zu verstärkter Bewegung und somit zu erhöhten Ventilationsraten führte.

Im dritten Teil wurde die Fungizidbiotransformation in *H. azteca* untersucht und mit der in *G. pulex* verglichen. Es wurden überwiegend ähnliche BTPs für Azoxystrobin und Prochloraz in *H. azteca* und *G. pulex* identifiziert, was auf eine Konservierung von Enzymen in den beiden Flohkrebsarten hindeutet. BTPs wurden überwiegend durch Oxidations- und Konjugationsreaktionen gebildet. Zusätzlich zu Konjugationsreaktionen mit Glucose, Sulfat, Glucose-Sulfat, und Glutathion, woraus Cysteinprodukte resultierten, die in beiden Arten identifiziert wurden, wurden in *H. azteca* neue Konjugationsreaktionen mit Taurin und Glucose-Malonyl identifiziert. Die toxikokinetische Modellierung von Azoxystrobin und seinen BTPs wies darauf hin, dass Biotransformation in *H. azteca* relevanter für die Reduzierung der Bioakkumulation der Ausgangsverbindung ist als in *G. pulex*. Verglichen mit der Europäischen REACH Verordnung war jedoch die Bioakkumulation von Azoxystrobin ($BAF \approx 5 \text{ L kg}_{\text{ww}}^{-1}$) und Prochloraz ($BAF \approx 50 - 160 \text{ L kg}_{\text{ww}}^{-1}$) in beiden Arten gering. Des Weiteren wurde durch die ermittelten kinetischen Raten die Bedeutung von sekundären BTPs, wie zum Beispiel von Konjugationsprodukten, in aquatischen Organismen bestätigt. Die bestimmten halbmaximalen Inhibitionskonzentrationen von Prochloraz ($IC_{50, \text{PRZ}, \text{AZ}}$) deuteten darauf hin, dass *H. azteca* im Vergleich zu *G. pulex* um einen Faktor von etwa fünf weniger sensitiv bezüglich Prochloraz-induzierter CYP-Inhibition war. Dieser Sensitivitätsunterschied der beiden Arten scheint jedoch vernachlässigbar in Bezug auf die öko-toxikologische Risikobewertung zu sein, da dort Sicherheitsfaktoren angewendet werden, um zwischenartige Unterschiede zu berücksichtigen.

Insgesamt zeigt diese Arbeit, wie wichtig es ist, BTPs zu identifizieren und Biotransformation als separaten Prozess in die toxikokinetische Modellierung miteinzubeziehen, da dadurch die Unterscheidung zwischen verschiedenen Eliminationswegen ermöglicht wird. Dies zeigt die Bedeutung von Biotransformation auf. Der durch Azole erzeugte Synergismus, hervorgerufen durch Enzyminhibition sowie durch veränderte Aufnahmeraten, deutet darauf hin, dass ein mechanistisches Prozessverständnis entscheidend für eine voraussagende öko-toxikologische Risikoabschätzung ist, die durch toxikokinetische Modellierung unterstützt werden kann. Obwohl Synergismus häufig an hohe Grenzkonzentrationen gebunden ist, können synergistische Effekte auch in der Nähe von realistischen Umweltkonzentrationen auftreten, wie in dieser Arbeit für Prochloraz. Somit ist es entscheidend, die wirksamsten Synergisten zu identifizieren und in der Risikoabschätzung zu berücksichtigen.

Chapter 1. Introduction

1.1 Pesticides in the Aquatic Environment

Thousands of known and unknown anthropogenic compounds from sources such as industry, household or agriculture are released into surface water bodies all over the world, thereby adversely affecting aquatic ecosystems.¹ These organic micropollutants are detected ubiquitously in surface waters with concentrations in the ng L^{-1} to $\mu\text{g L}^{-1}$ range,²⁻³ the consequences of which are losses in biodiversity and ecosystem services, such as supply of clean drinking water. In areas of predominant agricultural land use, pesticides pose one of the major threats to aquatic organisms. Pesticides are designed to act on target organisms; however, as soon as pesticides enter the environment, nontarget organisms are exposed as well and may suffer from acute or chronic effects.^{1, 4} Major pesticide substance classes are herbicides, fungicides and insecticides. In Switzerland, around 2200 tonnes of pesticides are sold every year, in which fungicides (used to control fungal pathogens), and herbicides (used to control undesired plants) each make up ~40%, and insecticides (used to control undesired insects) make up ~20%.⁵

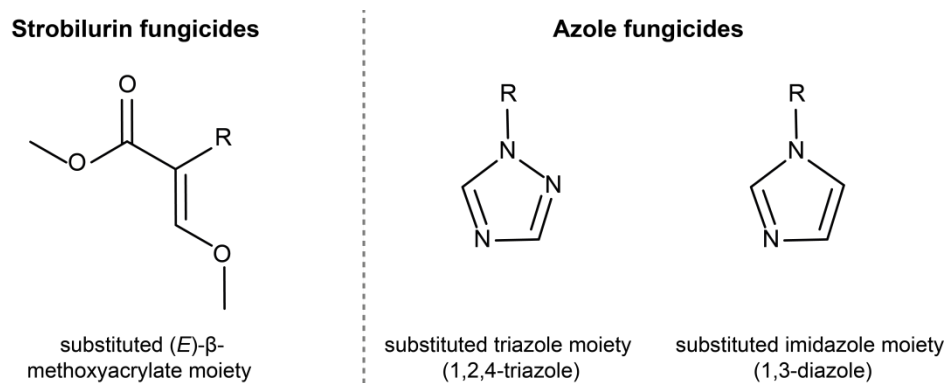


Figure 1-1: Active moieties of strobilurin and azole fungicides. Azoxystrobin carries the (E)-β-methoxyacrylate moiety, while there are other strobilurin fungicides that contain modified toxicophores such as an (E)-methyl methoxyiminoacetate group.

Among agricultural systemic fungicides, **strobilurins** and **azoles** (Figure 1-1) are two of the most frequently applied fungicide classes worldwide against diverse fungal diseases⁶⁻⁷ and have been measured at concentrations in the low ng L^{-1} to low $\mu\text{g L}^{-1}$ range in aquatic ecosystems.⁸⁻¹⁴ Their main fields of application are grains, orchards, vineyards and potatoes.^{6, 15} Six strobilurin and 15 azole fungicides are authorized in Switzerland in the year 2017 and co-formulated mixtures of strobilurins and azoles are commercially available.¹⁶

Azoxystrobin was the first patent among the strobilurin fungicides – first sold in 1996, its invention was based on a group of fungicidal naturally occurring compounds containing the β-methoxyacrylate active moiety. The strobilurin fungicides received remarkable commercial success since they can act against all major groups of pathogenic plant fungi. Prior to that, comparable plant protection was only achieved through different fungicide mixtures. The fungicidal activity of strobilurins results from their ability to inhibit mitochondrial respiration in fungi by interfering with the cytochrome bc_1 complex, located in fungal and eukaryotic inner mitochondrial cell membranes. The toxicity of strobilurins towards birds, mammals and bees

is considered to be low, whereas strobilurins pose a higher risk towards aquatic organisms.¹⁷⁻²⁰ Median-lethal concentrations (LC₅₀s) of azoxystrobin representing only acute toxicity towards aquatic invertebrates range between 150 and 350 µg L⁻¹.²¹⁻²³

Azole fungicides, including the triazoles and the imidazoles, belong to the class of ergosterol-biosynthesis-inhibitors (EBIs), also known as C14 α-demethylase inhibitors. Ergosterol is an essential constituent of fungal cell membranes important for its structure and function. EBIs are able to interrupt the ergosterol biosynthesis by inhibiting the specific cytochrome P450 monooxygenase (CYP) isoform – the lanosterol-14 α-demethylase – that catalyzes the reaction from lanosterol to ergosterol.²⁴⁻²⁵ Azole fungicides are moderately toxic towards aquatic invertebrates with LC₅₀s in the low mg L⁻¹ range.^{21, 26-29}

1.2 Pesticide Mixtures, Regulation and Risk Assessment

To date, ecotoxicological risk assessment is usually based on standardized single substance testing in the laboratory using model organisms from major trophic levels (primary producer, primary consumer, secondary consumer). More comprehensive approaches include the use of species sensitivity distributions or mesocosm studies. Nontarget aquatic fungi are normally not included as test organisms, although they might be the most sensitive species towards fungicides. Consequently, the risk of fungicides might be underestimated. **Environmental quality standards (EQSs)** can be derived by dividing the effect concentration of the most sensitive trophic level by an assessment factors, to account for differences in species sensitivities, to extrapolate from laboratory to field data, and from short term to long term exposure. Assessment factors can vary between 2 and 1000 depending on the amount and/or quality of underlying ecotoxicological data.³⁰ A distinction is made between acute EQSs (MAC-EQS: maximum allowable concentration) and chronic EQSs (AA-EQS: annual average concentration). If environmental concentrations exceed the EQSs, there is potential risk for aquatic organisms. EQSs are included in the European water framework directive (WFD) to assess the water quality with respect to ecotoxicological effects.³¹ In Switzerland, the water protection ordinance prescribes a maximum concentration of 0.1 µg L⁻¹ per single substance in surface waters.³² However, EQSs are expected to be included into the water protection ordinance in 2018 and the Swiss Centre for Applied Ecotoxicology proposes acute and chronic EQSs on behalf of the Swiss Federal Office for the Environment.³³ EQSs are available for azoxystrobin and selected azole fungicides (cyproconazole, epoxiconazole and tebuconazole) and are located in the very low µg L⁻¹ range (0.2 - 1.4 µg L⁻¹) for acute and chronic EQSs. No EQSs for azoxystrobin and azole fungicides are given in the WFD since EQSs are only listed for a limited number of priority substances.

With the knowledge that aquatic organisms are exposed to complex chemical mixtures that vary over time, in concentration and composition, a better understanding of potential mixture effects is required. Toxicity testing of every combination of chemical mixture in the environment is not feasible due to the large number of potential mixtures. Nevertheless, the inclusion of **mixture effects** of chemicals into the Water Framework Directive and into the

REACH regulation are under discussion.³⁴⁻³⁵ Models have been developed to predict mixture effects. Concentration Addition (CA) and Independent Action (IA) are the two major concepts to predict mixture toxicity. CA, first formulated by Loewe and Muischnek (1926)³⁶, is mainly used for substances with similar modes of action, whereas IA, established by Bliss (1939)³⁷, is mainly applied for substances with different modes of action. Both models assume that chemicals do not interact. CA has been shown to be a conservative first tier approach, which can also be used for dissimilar acting chemicals.^{34, 38-40} In addition, IA is dependent on binary response data and predictions on data such as sublethal endpoints (e.g. growth) do not fit the underlying theory. If chemicals in a mixture jointly cause a higher effect than predicted by either of the models, the phenomenon is called **synergism**. Underlying mechanisms responsible for synergistic interactions are diverse and interactions between chemicals can affect different processes such as bioavailability, uptake, internal transport, biotransformation, binding at the target site, and excretion.³⁹ However, two reviews reported that only in a small fraction (approximately 5%) of investigated pesticide mixtures, effects were greater than two compared to the model of CA.³⁹⁻⁴⁰

In addition to the complex mixtures composed of single substances present in the environment, every substance can undergo abiotic and biotic biotransformation processes, which further complicates risk assessment. As an example, the EU's Pesticide Directive requires the assessment of major and relevant transformation products of plant protection products before approval.⁴¹ However, further investigations on how to prioritize transformation products with regard to their environmental risk are needed.⁴²

1.3 Aquatic Invertebrates as Test Species: *Gammarus pulex* and *Hyalella azteca*

Among the order *Amphipoda*, the family *Gammaridae* has a widespread distribution across Europe and Asia and lives in freshwater, brackish and marine habitats. The genus *Gammarus* contains more than 200 described species of which 100 species are only found in freshwater habitats in the Northern Hemisphere.⁴³⁻⁴⁴ One of the most diverse amphipod genus found in Switzerland is *Gammarus*, containing six native and two non-native species. Especially the two native *Gammarus* species, the *Gammarus fossarum* species complex and *Gammarus pulex* are widely distributed in Switzerland.⁴⁵ *Gammarus spp.* are key organisms in many freshwater ecosystems and as shredders they highly contribute to the detritus processing in streams. *Gammarus spp.* often represent the dominant species in terms of number and/or biomass and are prey for fish.⁴⁶ Due to their high sensitivity towards a wide range of stressors, they are often used as bioindicators and for ecotoxicological testing.^{44, 47-48} Additionally, their slow growth and relatively large size makes them suitable test species for bioaccumulation studies.⁴⁹⁻⁵² However, *Gammarus spp.* is not easily cultured in the lab and organisms need to be collected from the field for testing.

The American relative to *Gammarus spp.* is the amphipod *Hyalella azteca* out of the family *Hyalellidae*. They inhabit preferably warm lakes and streams and are found in North and South America. In favored habitats they can reach high densities of >20 000 organisms/m².

They are used as standardized test species for sediment and water quality assessment mainly in North America.⁵³⁻⁵⁶ In contrast to *Gammarus spp.*, *H. azteca* can be easily cultured in the lab. Thus, a homogenous test population is available over the entire year, leading to less variability in organisms size and enzyme composition compared to the collection of field organisms, such as *Gammarus spp.*

1.4 Toxicokinetic Processes in Aquatic Organisms

1.4.1 Biotransformation Processes in Aquatic Invertebrates

Biotransformation describes the enzyme-catalyzed transformation of chemicals inside an organism into biotransformation products (BTPs) with different physicochemical properties compared to the parent compound. In order for biotransformation to occur, chemicals need to reach the enzyme to undergo enzymatic transformation. In aquatic invertebrates such as in *Amphipoda*, the hepatopancreas represents the main detoxification tissue. Biotransformation of bioactive compounds often leads to detoxification by altering the active site. However, in some cases biotransformation leads to bioactivation by enzymatically introducing an active group or by modifying an inactive to an active molecule.⁵⁷

BTPs are usually more hydrophilic than their precursors, facilitating the excretion from the organism. However, different studies reported that more polar BTPs compared to their precursors were retained longer in the organism and were not excreted faster.^{49-50, 52, 58} Since many BTPs are hydrophilic and ionized they cannot easily cross cell membranes composed of lipid bilayers. Nevertheless, their intracellular mobility is increased and their tissue distribution is different compared to those of the parent compound.^{57, 59}

Major biotransformation reactions include oxidation, reduction, hydrolysis and conjugation reactions. Monooxygenation by **cytochrome P450 enzymes** (CYPs) is one of the most frequent enzymatic reaction. The CYP superfamily of heme-containing metalloenzymes catalyzes a wide variety of endogenous and exogenous compounds and is known to be present in all kingdoms of life.⁶⁰⁻⁶³ CYPs play an important role in the detoxification of chemicals mainly by oxidizing a large variety of substrates. Most common reactions catalyzed by CYPs include hydroxylation of aliphatic or aromatic carbons, N-, S- and O-oxidations, as well as oxidative dehalogenations. The majority of reactions catalyzed by CYPs are oxidations. However, CYPs are also known to catalyze reactions such as reductions (e.g. reductive dehalogenations or hydrogenations) and ester cleavages. In addition to CYP monooxygenases, **flavin-containing monooxygenases** are mainly known to catalyze the formation of N- and S-oxides^{62, 64} and **hydrolysis** reactions of amides and carboxylic esters are catalyzed by esterases.⁶⁵ The coupling of an endogenous molecule to a newly introduced functional group or to a functional group already present at the parent compound is called **conjugation reaction**. Major conjugation reactions include methylation, sulfonation, glucuronidation, glucosidation and acetylation of nucleophiles, amino acid conjugation of carboxylic acids, as well as nucleophilic addition of glutathione to electrophiles. The endogenous molecule is usually carried by a cofactor (with exceptions

such as glutathione and amino acid conjugation) and transferases catalyze these reactions.⁶⁶ Since many chemicals already exhibit diverse functional groups and do not necessarily require previous reactions to make the molecule accessible for conjugation, the terminology of “Phase I” (redox and hydrolysis reactions) and “Phase II” (conjugation reactions) – still used a lot in the field of drug metabolism – is not fully appropriate and should be avoided.⁶⁷

Activities of almost all enzymes aforementioned have been detected in aquatic organisms.⁶¹ Especially conjugation reactions – either by directly conjugating functional groups of the parent compound or by conjugating previously enzymatically introduced functional groups – have been shown to be main routes of biotransformation in aquatic invertebrates.^{49-50, 52, 68-71} Toxicity of chemicals is generally regarded to decrease through biotransformation. Therefore, biotransformation is a key process that can greatly influence the toxicity and bioaccumulation of chemicals.

To characterize different biotransformation processes, BTPs need to be identified. Mass spectrometry has become an emerging analytical tool in environmental sciences during the last two decades. Gas chromatography-mass spectrometry (GC-MS) has been the preferred analytical method to quantify and identify organic pollutants for a long time and is still widely used, particularly for non-polar analytes.⁷² With the invention of electrospray ionization⁷³, liquid chromatography-(tandem) mass spectrometry (LC-(MS)/MS) allowed for the analysis of more polar non-volatile compounds without the need of prior derivatization. Since many contaminants in aquatic environments and thereof formed BTPs are polar, LC-(MS)/MS methods have often become the analytical technique of choice.⁷⁴⁻⁷⁵ Especially the use of **high-resolution mass spectrometry** (HRMS) in environmental analysis offers high resolving power and mass determination to part-per-million accuracy, which thereby enables the screening of predicted BTP exact masses (suspect screening) or the screening of unknown BTPs (nontarget screening) (e.g. by comparing extracted ion chromatograms of treatment and control samples).⁷⁶⁻⁷⁷ Finally, structure elucidation is done by the interpretation of HRMS/MS spectra. However, in many cases reference standards of BTPs are not available for final confirmation and the level of identification confidence is communicated based on a classification scheme.⁷⁸

1.4.2 Bioaccumulation and Bioconcentration

Bioaccumulation and bioconcentration describe the processes that lead to higher chemical concentrations inside an organism compared to the surrounding medium. Both processes differ in their uptake routes. Bioconcentration considers the accumulation of waterborne chemicals through non-dietary uptake routes, such as respiratory and dermal surfaces, whereas bioaccumulation also includes uptake via food. For many aquatic organisms, the main uptake route of neutral polar organic micropollutants is from water and bioconcentration is therefore a net result of uptake, distribution, elimination and biotransformation processes.^{57, 79}

Bioaccumulation factors (BAFs) can be expressed as the ratio of the internal concentration of a chemical in an organism and the concentration in the surrounding medium at steady state:

$$\text{BAF} = \frac{C_{\text{organism}}}{C_{\text{water}}} \quad [\text{L kg}^{-1}] \quad (1)$$

A correlation between bioconcentration factors (BCFs) and physicochemical properties of neutral organic chemicals (*n*-octanol-water partition coefficient K_{ow}) is known for many aquatic organism (see review of Katagi (2010)⁶¹). These correlations are based on fugacity driven bioconcentration models and can approximately predict BCFs for neutral organic chemicals.⁸⁰ The underlying principle is that the hydrophobicity of chemicals is the driving force that determines the partitioning between water and the lipid constituents of the organism. Uptake via passive diffusion is the major uptake route and uptake is driven by the fugacity difference between water and the organism. This correlation is linear for neutral compounds with log K_{ow} s between approximately 1 and 6; above this no simple relationship exists between lipophilicity and BCF (see review by MacKay and Fraser (2000)⁸¹). However, in addition to physicochemical factors, bioconcentration is influenced by physiological factors of the organism (lipid content and organism size), physicochemical factors of the chemical (e.g. steric factors), and strongly by biochemical factors of the organism as enzymatic biotransformation can significantly increase the elimination of a chemical.⁷⁹ Therefore, even predicting BCFs of neutral organic chemicals only based on physicochemical properties has its limitations.

Kinetic models can be applied to understand the underlying **toxicokinetic processes** (“what the organism does to the chemical”) of bioaccumulation, such as uptake, internal distribution, biotransformation and elimination of a chemical (Figure 1-2).⁸² If the organism is regarded as a single well-mixed compartment and first-order kinetics are assumed for chemical uptake and elimination rates, the time course of the internal concentration of a chemical can be described by a one-compartment first-order kinetic model⁸³⁻⁸⁴ with the following ordinary differential equation:

$$\frac{dC_{in}(t)}{dt} = C_{water}(t) \cdot k_u - C_{in}(t) \cdot k_{e, total} \quad (2)$$

where $C_{in}(t)$ [nmol kg^{-1}] is the time course of the internal concentration of the chemical and $C_{water}(t)$ [nmol L^{-1}] describes the time course of the chemical in the water. Uptake of the chemical via food, dermal and respiratory surfaces is described by the uptake rate constant k_u [$\text{L kg}^{-1} \text{d}^{-1}$], whereas $k_{e, total}$ [d^{-1}] is the total elimination of the chemical. Total elimination mainly consists of elimination via dermal and respiratory surfaces, elimination via faeces and elimination due to biotransformation. Thereby kinetic BAFs (BAF_k s) can be calculated, which represent the balance of k_u and the total elimination rate $k_{e, total}$ (equation 3). Rate constants are assumed to be constant and do not change over time, therefore no steady state is required.

$$\text{BAF}_k = \frac{k_u}{k_{e, total}} \quad [\text{L kg}^{-1}] \quad (3)$$

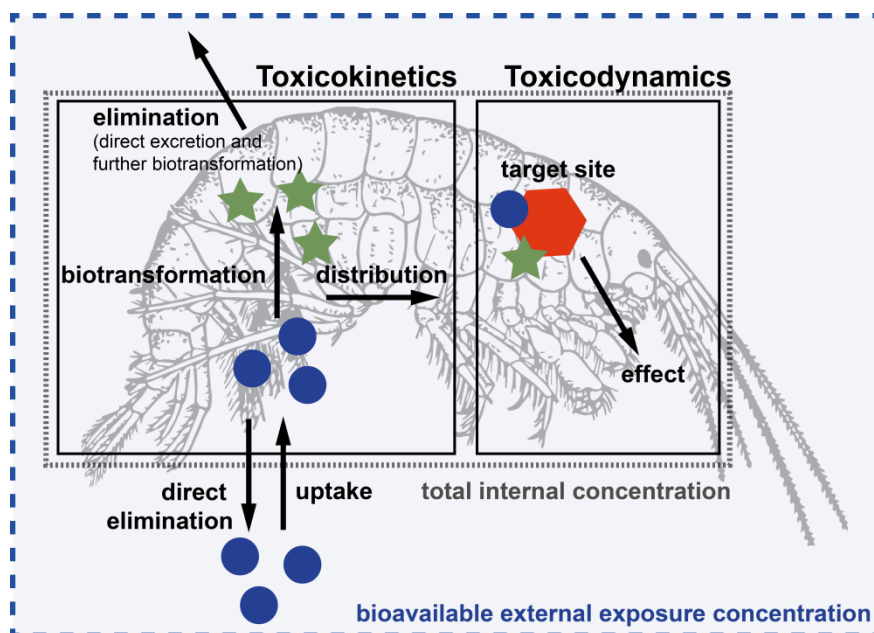


Figure 1-2: Relationship between external exposure concentration, toxicokinetic and toxicodynamic processes that lead to an effect at the target site.

If suitable analytical techniques such as HRMS/(MS) are available that allow for the detection and identification of BTPs, BTPs can be included into the kinetic model. Thereby, the time courses of internal concentrations of the parent compound and of associated BTPs can be modeled. However, a detailed understanding of the underlying biotransformation pathway is necessary to assign primary BTPs (formed directly from the parent compound) and secondary BTPs (where a direct precursor BTP was identified). Consequently, a detailed model that includes the time courses of primary and secondary BTPs can separate the lumped rate constant $k_{e, total}$ [d^{-1}] into the different underlying processes, *i.e.*, into direct elimination of the parent compound via dermal and respiratory surfaces and elimination via faeces (k_e [d^{-1}]), and into elimination due to primary biotransformation ($k_{Mx, 1st}$ [d^{-1}]) (equation 4). Thereby the importance of biotransformation can be estimated since primary biotransformation rate constants $k_{Mx, 1st}$ indicate how much biotransformation adds to the total reduction of parent compound bioaccumulation.

$$k_{e, total} = k_e + \sum k_{Mx, 1st} \quad [d^{-1}] \quad (4)$$

1.4.3 Linking Toxicokinetic Processes to an Effect

To exert a detrimental effect, the chemical has to reach the target site via toxicokinetic processes (Figure 1-2). **Toxicodynamics** (“what the chemical does to the organism”) describes the interaction of a chemical at the target site that leads to an effect.^{82, 85} To address differences in species sensitivities towards chemicals, toxicokinetic and toxicodynamic processes need to be considered. Moving from nominal external exposure concentrations to bioavailable external exposure concentrations and finally to internal concentrations has greatly improved the interpretation of toxicological effects.⁸⁶

Main target sites include membranes, proteins/peptides and genetic material. Partitioning into membranes causes non-specific damage of membrane structure and functioning. This reversible effect caused by any chemical is called baseline toxicity (minimum toxicity).⁸⁷ For neutral baseline toxicants (log K_{ow} range of 1 to 5), internal concentrations are a good approximate for target site concentrations. Therefore, whole body internal lethal concentrations (ILC_{50s}, concept of lethal body burden) are fairly constant for baseline toxicants. This implies that the potency of neutral baseline toxicants is solely dependent on their bioconcentration potential.⁸⁷⁻⁹⁰ Besides baseline toxicity, many chemicals exhibit additionally specific and/or multiple modes of action such as interactions with receptors (e.g., acetylcholine or estrogen receptors) or enzymes (e.g., acetylcholinesterase or CYP).⁸⁷ For specific acting chemicals, simple partitioning models are usually not sufficient to estimate the concentration at the target site. However, to understand toxicological effects, whole-body internal concentrations are much more suitable surrogates of the effective dose than external exposure concentrations, although measuring or modeling the target site concentration would be the ultimate goal.⁸⁶⁻⁸⁷

An example of specifically acting compounds are azole fungicides. **Azole fungicides are well-known inhibitors of CYP.** Besides the use of azoles as agricultural fungicides, azole fungicides such as ketoconazole and fluconazole are used as pharmaceuticals to treat fungal infections. Therefore, most knowledge of the inhibition potential of azole fungicides stems from pharmacokinetic interaction studies within human risk assessment and pharmaceutical registration.⁹¹⁻⁹³ The imidazole and triazole rings represent the active moiety by interacting with the CYP. Thus, biotransformation reactions occurring at the active site of the azole can alter the CYP inhibition potential. The nucleophilic free electron pair of the nitrogen in the heterocycle coordinates to the heme-iron, thereby preventing the binding of molecular oxygen and interrupting the CYP catalytic cycle. Additionally, hydrophobic interactions of the ring substituents in the binding cavity of the CYP are required as the complex formation is dependent on electronic and steric interactions of the lipophilic substituent in the enzyme binding cavity.⁹⁴⁻⁹⁵

Several studies have shown that azole fungicides can enhance the effect of other pesticides, such as pyrethroids, towards aquatic species.⁹⁶⁻¹⁰⁰ The observed synergism based on effect measurements with endpoints such as mortality or immobilization is proposed to be caused by inhibited CYP-catalyzed biotransformation reactions, which lead to an accumulation of the parent compound and thereby to increased toxicity.

1.5 Knowledge Gaps, Objectives, and Content of the Thesis

As described in the preceding sections, biotransformation is a key toxicokinetic process that can greatly add to the reduction of parent compound bioaccumulation, thereby reducing the internal concentration in an organism and modifying its toxicity. The overall goal of this theses was to provide a **better understanding of the general role of biotransformation in aquatic invertebrates** such as in *G. pulex* and *H. azteca*.

To date, most studies that investigate bioconcentration processes in aquatic organisms rely on modeled uptake and elimination kinetics based only on internal concentration measurements of the parent compound, which impedes assessing the importance of biotransformation. Therefore, we aimed to use HRMS/MS suspect and nontarget screening approaches to identify BTPs of different fungicides and include them in toxicokinetic modeling. Estimated toxicokinetic rate constants could be used to evaluate and compare the role of biotransformation in the selected aquatic invertebrate species *G. pulex* and *H. azteca*.

Until now, the known synergism in mixtures containing an azole has mostly been studied by effect measurements which did not allow for a mechanistic process understanding. Therefore, a further goal of this work was to investigate the supposed principle of synergism – the inhibition of CYP-catalyzed biotransformation reactions – mechanistically by determining internal parent compound and BTP concentrations.

More specifically, we aimed to answer the following research questions:

- (1) How much does biotransformation add to the reduction of parent compound bioaccumulation of selected azole and strobilurin fungicides?** (Chapter 2, 3 and 4)
- (2) Does biotransformation alter the active moiety of azole fungicides, leading to a loss of their specific mode of action?** (Chapter 2 and 4)
- (3) Is the known synergism in mixtures containing an azole caused by CYP inhibition?** (Chapter 3)
- (4) How do biotransformation pathways, toxicokinetics and susceptibility to CYP inhibition differ in *G. pulex* and *H. azteca*?** (Chapter 4)

To address research questions 1 and 2, in **Chapter 2**, the biotransformation of seven frequently used azole fungicides was investigated in *G. pulex*. Therefore, five triazole fungicides (cyproconazole, epoxiconazole, fluconazole, propiconazole, and tebuconazole) and two imidazole fungicides (ketoconazole and prochloraz) were selected that exhibit different physicochemical properties ($\log D_{ow}$ from 0.6 to 4.3) to study the biotransformation of structurally related compounds. Due to the specific mode of action of azole fungicides as CYP inhibitors, it was of interest if the active moiety (the triazole or imidazole ring) was conserved during biotransformation, such that the resulting BTPs could still act as CYP inhibitors and maintain their antifungal activity. The structures of BTPs were elucidated with HRMS/MS using suspect and nontarget screening. To understand the role of biotransformation in reducing bioaccumulation of the respective azole parent compound,

toxicokinetic rates of uptake, elimination and biotransformation were determined using toxicokinetic modeling.

To address research question 3 on the known synergism in mixtures containing an azole, in **Chapter 3** the synergistic potential of azole fungicides was studied mechanistically in *G. pulex*. Internal concentrations of the strobilurin fungicide azoxystrobin and associated BTPs were measured in the presence and absence of an azole fungicide potentially acting as CYP inhibitor and thereby inhibiting CYP-catalyzed biotransformation reactions of azoxystrobin. Six azole fungicides – four triazoles (cyproconazole, epoxiconazole, propiconazole, and tebuconazole) and two imidazoles (ketoconazole and prochloraz) – were selected to test their inhibition potential with regard to CYP-catalyzed biotransformation reactions. In addition, we aimed to determine the CYP inhibition strengths of the selected azoles in terms of half-maximal inhibitory concentrations (IC_{50} s). Thus, CYP inhibition potencies of the selected azoles could be compared and IC_{50} s could be evaluated in the context of environmentally realistic concentrations.

Chapter 4 focused on biotransformation routes in two aquatic invertebrate species (*G. pulex* and *H. azteca*) to address research question 4 concerning species sensitivity differences. Therefore, two fungicides (the strobilurin fungicide azoxystrobin and the azole fungicide prochloraz), whose biotransformation pathways and toxicokinetics were investigated in *G. pulex* in Chapter 2 and 3, were selected as test compounds. Biotransformation pathways, toxicokinetic rate constants, and susceptibility to CYP inhibition were used to assess potential differences in species' sensitivity towards the same chemicals.

Chapter 5 summarizes the main findings, draws general conclusions and further questions raised by this work are highlighted.

References

- [1] Schwarzenbach, R. P.; Escher, B. I.; Fenner, K.; Hofstetter, T. B.; Johnson, C. A.; Von Gunten, U.; Wehrli, B., The challenge of micropollutants in aquatic systems. *Science* **2006**, *313* (5790), 1072-1077.
- [2] Loos, R.; Carvalho, R.; Antonio, D. C.; Cornero, S.; Locoro, G.; Tavazzi, S.; Paracchini, B.; Ghiani, M.; Lettieri, T.; Blaha, L.; Jarosova, B.; Voorspoels, S.; Servaes, K.; Haglund, P.; Fick, J.; Lindberg, R. H.; Schwesig, D.; Gawlik, B. M., EU-wide monitoring survey on emerging polar organic contaminants in wastewater treatment plant effluents. *Water Res.* **2013**, *47* (17), 6475-6487.
- [3] Schaefer, R. B.; von der Ohe, P. C.; Kuehne, R.; Schueuermann, G.; Liess, M., Occurrence and Toxicity of 331 Organic Pollutants in Large Rivers of North Germany over a Decade (1994 to 2004). *Environmental Science & Technology* **2011**, *45* (14), 6167-6174.
- [4] Malaj, E.; von der Ohe, P. C.; Grote, M.; Kuehne, R.; Mondy, C. P.; Usseglio-Polatera, P.; Brack, W.; Schaefer, R. B., Organic chemicals jeopardize the health of freshwater ecosystems on the continental scale. *Proceedings of the National Academy of Sciences of the United States of America* **2014**, *111* (26), 9549-9554.
- [5] BLW, Agrarbericht, Swiss Federal Office for the Agriculture. **2016**.
- [6] IUPAC International Union of Pure and Applied Chemistry. Pesticide Properties Database. <http://sitem.herts.ac.uk/aeru/iupac/>.
- [7] Global Fungicides Market (Type, Crop Type and Geography - Size, Share, Global Trends, Company Profiles, Analysis, Segmentation and Forecast, 2013 - 2020. http://www.researchandmarkets.com/research/7dtjwc/global_fungicides.
- [8] Rasmussen, J. J.; Baattrup-Pedersen, A.; Wiberg-Larsen, P.; McKnight, U. S.; Kronvang, B., Buffer strip width and agricultural pesticide contamination in Danish lowland streams: Implications for stream and riparian management. *Ecol. Eng.* **2011**, *37* (12), 1990-1997.
- [9] Kahle, M.; Buerge, I. J.; Hauser, A.; Müller, M. D.; Poiger, T., Azole Fungicides: Occurrence and Fate in Wastewater and Surface Waters. *Environmental Science & Technology* **2008**, *42* (19), 7193-7200.
- [10] Battaglin, W.; Sandstrom, M.; Kuivila, K.; Kolpin, D.; Meyer, M., Occurrence of Azoxystrobin, Propiconazole, and Selected Other Fungicides in US Streams, 2005–2006. *Water Air Soil Pollut* **2011**, *218* (1-4), 307-322.
- [11] Kuzmanović, M.; Ginebreda, A.; Petrović, M.; Barceló, D., Risk assessment based prioritization of 200 organic micropollutants in 4 Iberian rivers. *Sci. Total Environ.* **2015**, *503-504*, 289-299.
- [12] Moschet, C.; Wittmer, I.; Simovic, J.; Junghans, M.; Piazzoli, A.; Singer, H.; Stamm, C.; Leu, C.; Hollender, J., How a complete pesticide screening changes the assessment of surface water quality. *Environ. Sci. Technol.* **2014**, *48* (10), 5423-5432.
- [13] Berenzen, N.; Hümmer, S.; Liess, M.; Schulz, R., Pesticide Peak Discharge from Wastewater Treatment Plants into Streams During the Main Period of Insecticide Application: Ecotoxicological Evaluation in Comparison to Runoff. *Bull. Environ. Contam. Toxicol.* **2003**, *70* (5), 0891-0897.
- [14] Doppler, T.; Mangold, S.; Wittmer, I.; Spycher, S.; Comte, R.; Stamm, C.; Singer, H., Hohe PSM-Belastung in schweizer Bächen. *Aqua und Gas* **2017**, *4*, 46-56.
- [15] Moschet, C.; Wittmer, I.; Stamm, C.; Singer, H.; Hollender, J., Insektizide und Fungizide in Fließgewässern. Wichtig zur Beurteilung der Gewässerqualität. *Aqua & Gas* **2015**, *95* (4), 54-65.
- [16] BLW, Pflanzenschutzmittelverzeichnis. Federal Office for the Agriculture. <http://www.psm.admin.ch/psm/produkte/index.html?lang=de>, 2017.
- [17] Rodrigues, E. T.; Lopes, I.; Pardal, M. A., Occurrence, fate and effects of azoxystrobin in aquatic ecosystems: a review. *Environment international* **2013**, *53*, 18-28.
- [18] Bartlett, D. W.; Clough, J. M.; Godwin, J. R.; Hall, A. A.; Hamer, M.; Parr-Dobrzanski, B., The strobilurin fungicides. *Pest Management Science* **2002**, *58* (7), 649-662.

- [19] Bartlett, D. W.; Clough, J. M.; Godfrey, C. R. A.; Godwin, J. R.; Hall, A. A.; Heaney, S. P.; Maund, S. J., Understanding the strobilurin fungicides. *Pestic. Outlook* **2001**, *12* (4), 143-148.
- [20] EFSA, Conclusion on the peer review of the pesticide risk assessment of the active substance azoxystrobin. *EFSA Journal* **2010**, *8* (4).
- [21] Beketov, M. A.; Liess, M., Potential of 11 pesticides to initiate downstream drift of stream macroinvertebrates. *Arch. Environ. Contam. Toxicol.* **2008**, *55* (2), 247-53.
- [22] Zubrod, J. P.; Baudy, P.; Schulz, R.; Bundschuh, M., Effects of current-use fungicides and their mixtures on the feeding and survival of the key shredder *Gammarus fossarum*. *Aquat. Toxicol.* **2014**, *150*, 133-143.
- [23] Warming, T. P.; Mulderu, G.; Christoffersen, K. S., Clonal variation in physiological responses of *Daphnia magna* to the strobilurin fungicide azoxystrobin. *Environ. Toxicol. Chem.* **2009**, *28* (2), 374-380.
- [24] Henry, M. J.; Sisler, H. D., Effects of sterol biosynthesis-inhibiting (SBI) fungicides on cytochrome P-450 oxygenations in fungi. *Pestic. Biochem. Physiol.* **1984**, *22* (3), 262-275.
- [25] Copping, L. G.; Hewitt, H. G., Chemistry and Mode of Action of Crop Protection agents. *Royal Society of Chemistry Cambridge, UK* **1998**.
- [26] Nyman, A. M.; Schirmer, K.; Ashauer, R., Toxicokinetic-toxicodynamic modelling of survival of *Gammarus pulex* in multiple pulse exposures to propiconazole: Model assumptions, calibration data requirements and predictive power. *Ecotoxicology* **2012**, *21* (7), 1828-1840.
- [27] Adam, O.; Badot, P. M.; Degiorgi, F.; Crini, G., Mixture toxicity assessment of wood preservative pesticides in the freshwater amphipod *Gammarus pulex* (L.). *Ecotoxicology and Environmental Safety* **2009**, *72* (2), 441-449.
- [28] Estimation Programs Interface Suite™ for Microsoft® Windows, v 4.11. United States Environmental Protection Agency, Washington, DC, USA. 2013.
- [29] Haeba, M. H.; Hilscherova, K.; Mazurova, E.; Blaha, L., Selected endocrine disrupting compounds (vinclozolin, flutamide, ketoconazole and dicofol): Effects on survival, occurrence of males, growth, molting and reproduction of *Daphnia magna*. *Environ Sci Pollut Res* **2008**, *15* (3), 222-227.
- [30] Common Implementation Strategy for the Water Framework Directive (2000/60/EC). Guidance Document No. 27. Technical Guidance For Deriving Environmental Quality Standards 2011.
- [31] European Commission, Common Implementation Strategy for the Water Framework Directive (2000/60/EC). 2011.
- [32] Gewässerschutzverordnung (GSchV) vom 28. Oktober 1998 (Stand am 1. Mai 2017) SR 814.201.
- [33] Oekotoxzentrum, Vorschläge für akute und chronische Qualitätskriterien für ausgewählte schweizrelevante Substanzen. **2017**.
- [34] Backhaus, T.; Faust, M., Predictive Environmental Risk Assessment of Chemical Mixtures: A Conceptual Framework. *Environmental Science & Technology* **2012**, *46* (5), 2564-2573.
- [35] European Commission, COM(2012) 252 final - Communication from The Commission to The Council, The combination effects of chemicals - Chemical mixtures. 2012.
- [36] Loewe, S.; Muischnek, H., Über Kombinationswirkungen - Mitteilung: Hilfsmittel der Fragestellung. *Archiv für Experimentelle Pathologie und Pharmakologie* **1926**, *114* (5-6), 313-326.
- [37] Bliss, C. I., The toxicity of poisons applied jointly. *Annals of Applied Biology* **1939**, *26* (3), 585-615.
- [38] Rodney, S. I.; Teed, R. S.; Moore, D. R. J., Estimating the Toxicity of Pesticide Mixtures to Aquatic Organisms: A Review. *Human and Ecological Risk Assessment* **2013**, *19* (6), 1557-1575.
- [39] Cedergreen, N., Quantifying synergy: A systematic review of mixture toxicity studies within environmental toxicology. *PLoS ONE* **2014**, *9* (5), e96580.

- [40] Belden, J. B.; Gilliom, R. J.; Lydy, M. J., How well can we predict the toxicity of pesticide mixtures to aquatic life? *Integrated environmental assessment and management* **2007**, 3 (3), 364-372.
- [41] EU Regulation (EC) No 1107/2009 of the European Parliament and of the Council of 21 October 2009 concerning the placing of plant protection products on the market and repealing Council Directives 79/117/EEC and 91/414/EEC.
- [42] Escher, B. I.; Fenner, K., Recent advances in environmental risk assessment of transformation products. *Environ. Sci. Technol.* **2011**, 45 (9), 3835-3847.
- [43] Karaman, G. S.; Pinkster, S., Freshwater Gammarus species from Europe, North Africa and adjacent regions of Asia (Crustacea-Amphipoda) part 1. Gammarus pulex – group and related species. **1977**.
- [44] Kunz, P. Y.; Kienle, C.; Gerhardt, A., Gammarus spp. in aquatic ecotoxicology and water quality assessment: toward integrated multilevel tests. *Rev. Environ. Contam. Toxicol.* **2010**, 205, 1-76.
- [45] Altermatt, F.; Alther, R.; Fišer, C.; Jokela, J.; Konec, M.; Küry, D.; Mächler, E.; Stucki, P.; Westram, A. M., Diversity and Distribution of Freshwater Amphipod Species in Switzerland (Crustacea: Amphipoda). *PLOS ONE* **2014**, 9 (10), e110328.
- [46] Macneil, C.; Dick, J. T. A.; Elwood, R. W., The trophic ecology of freshwater Gammarus spp. (Crustacea: Amphipoda): Problems and perspectives concerning the functional feeding group concept. *Biological Reviews of the Cambridge Philosophical Society* **1997**, 72 (3), 349-364.
- [47] Maltby, L.; Clayton, S. A.; Wood, R. M.; McLoughlin, N., Evaluation of the Gammarus pulex in situ feeding assay as a biomonitor of water quality: Robustness, responsiveness, and relevance. *Environ. Toxicol. Chem.* **2002**, 21 (2), 361-368.
- [48] Fässler, S.; Stöckli, A., Das Fehlen von Bachflohkrebsen. *Aqua und Gas* **2013**, 4, 62-72.
- [49] Rösch, A.; Anliker, S.; Hollender, J., How Biotransformation Influences Toxicokinetics of Azole Fungicides in the Aquatic Invertebrate Gammarus pulex. *Environmental Science & Technology* **2016**, 50 (13), 7175-7188.
- [50] Ashauer, R.; Hintermeister, A.; O'Connor, I.; Elumelu, M.; Hollender, J.; Escher, B. I., Significance of xenobiotic metabolism for bioaccumulation kinetics of organic chemicals in gammarus pulex. *Environ. Sci. Technol.* **2012**, 46 (6), 3498-3508.
- [51] Ashauer, R.; Caravatti, I.; Hintermeister, A.; Escher, B. I., Bioaccumulation kinetics of organic xenobiotic pollutants in the freshwater invertebrate Gammarus pulex modeled with prediction intervals. *Environ. Toxicol. Chem.* **2010**, 29 (7), 1625-36.
- [52] Rösch, A.; Gottardi, M.; Vignet, C.; Cedergreen, N.; Hollender, J., Mechanistic Understanding of the Synergistic Potential of Azole Fungicides in the Aquatic Invertebrate Gammarus pulex. *Environmental Science & Technology* **2017**, 51 (21), 12784-12795.
- [53] EPA, Methods for measuring the toxicity and bioaccumulation of sediment-associated contaminants with freshwater invertebrates. **2000**.
- [54] Borgmann, U.; Ralph, K. M.; Norwood, W. P., Toxicity test procedures for Hyalella azteca, and chronic toxicity of cadmium and pentachlorophenol to H. azteca, Gammarus fasciatus, and Daphnia magna. *Archives of Environmental Contamination and Toxicology* **1989**, 18 (5), 756-764.
- [55] Ingersoll, C. G.; Brunson, E. L.; Dwyer, F. J.; Ankley, G. T.; Benoit, D. A.; Norberg-King, T. J.; Burton, G. A.; Hoke, R. A.; Landrum, P. F.; Winger, P. V., Toxicity and bioaccumulation of sediment-associated contaminants using freshwater invertebrates: A review of methods and applications. *Environ. Toxicol. Chem.* **1995**, 14 (11), 1885-1894.
- [56] Bartlett, A. J.; Struger, J.; Grapentine, L. C.; Palace, V. P., Examining impacts of current-use pesticides in Southern Ontario using in situ exposures of the amphipod Hyalella azteca. *Environ. Toxicol. Chem.* **2016**, 35 (5), 1224-1238.
- [57] Sijm, D. T. H. M.; Rikken, M. G. J.; Rorije, E.; Traas, T. P.; Mclachlan, M. S.; Peijnenburg, W. J. G. M., Transport, Accumulation and Transformation Processes. In *Risk Assessment of Chemicals: An Introduction*, Leeuwen, C. J. v.; Vermeire, T. G., Eds. Springer Netherlands: Dordrecht, 2007; pp 73-158.

- [58] Jeon, J.; Kurth, D.; Ashauer, R.; Hollender, J., Comparative toxicokinetics of organic micropollutants in freshwater crustaceans. *Environ. Sci. Technol.* **2013**, *47* (15), 8809-17.
- [59] Gobas, F. A. P. C.; Opperhuizen, A.; Hutzinger, O., Bioconcentration of hydrophobic chemicals in fish: Relationship with membrane permeation. *Environ. Toxicol. Chem.* **1986**, *5* (7), 637-646.
- [60] Snyder, M. J., Cytochrome P450 enzymes in aquatic invertebrates: Recent advances and future directions. *Aquat. Toxicol.* **2000**, *48* (4), 529-547.
- [61] Katagi, T., Bioconcentration, Bioaccumulation, and Metabolism of Pesticides in Aquatic Organisms. In *Reviews of Environmental Contamination and Toxicology, Vol 204*, Whitacre, D. M., Ed. 2010; Vol. 204, pp 1-132.
- [62] Guengerich, F. P., Common and uncommon cytochrome P450 reactions related to metabolism and chemical toxicity. *Chem. Res. Toxicol.* **2001**, *14* (6), 611-650.
- [63] Sole, M.; Livingstone, D. R., Components of the cytochrome P450-dependent monooxygenase system and 'NADPH-independent benzo a pyrene hydroxylase' activity in a wide range of marine invertebrate species. *Comparative Biochemistry and Physiology C-Toxicology & Pharmacology* **2005**, *141* (1), 20-31.
- [64] Testa, B.; Kramer, S. D., The biochemistry of drug metabolism - An introduction - Part 2. Redox reactions and their enzymes. *Chemistry & Biodiversity* **2007**, *4* (3), 257-405.
- [65] Testa, B.; Kraemer, S. D., The biochemistry of drug metabolism - An introduction Part 3. Reactions of hydrolysis and their enzymes. *Chemistry & Biodiversity* **2007**, *4* (9), 2031-2122.
- [66] Testa, B.; Kraemer, S. D., The Biochemistry of Drug Metabolism - An Introduction Part 4. Reactions of Conjugation and Their Enzymes. *Chemistry & Biodiversity* **2008**, *5* (11), 2171-2336.
- [67] Josephy, P. D.; Guengerich, F. P.; Miners, J. O., "Phase I" and "Phase II" drug metabolism: Terminology that we should phase out? *Drug Metabolism Reviews* **2005**, *37* (4), 575-580.
- [68] Kukkonen, J.; Oikari, A., Sulphate conjugation is the main route of pentachlorophenol metabolism in *Daphnia magna*. *Comparative Biochemistry and Physiology - C Pharmacology Toxicology and Endocrinology* **1988**, *91* (2), 465-468.
- [69] Jeon, J.; Kurth, D.; Hollender, J., Biotransformation pathways of biocides and pharmaceuticals in freshwater crustaceans based on structure elucidation of metabolites using high resolution mass spectrometry. *Chem. Res. Toxicol.* **2013**, *26* (3), 313-24.
- [70] Ikenaka, Y.; Ishizaka, M.; Eun, H.; Miyabara, Y., Glucose-sulfate conjugates as a new phase II metabolite formed by aquatic crustaceans. *Biochem. Biophys. Res. Commun.* **2007**, *360* (2), 490-495.
- [71] Ikenaka, Y.; Eun, H.; Ishizaka, M.; Miyabara, Y., Metabolism of pyrene by aquatic crustacean, *Daphnia magna*. *Aquat. Toxicol.* **2006**, *80* (2), 158-165.
- [72] Barcelo, D.; Petrovic, M., Challenges and achievements of LC-MS in environmental analysis: 25 years on. *Trac-Trends in Analytical Chemistry* **2007**, *26* (1), 2-11.
- [73] Whitehouse, C. M.; Dreyer, R. N.; Yamashita, M.; Fenn, J. B., Electrospray Interface for Liquid Chromatographs and Mass Spectrometers. *Anal. Chem.* **1985**, *57* (3), 675-679.
- [74] Giger, W., Hydrophilic and amphiphilic water pollutants: using advanced analytical methods for classic and emerging contaminants. *Analytical and Bioanalytical Chemistry* **2009**, *393* (1), 37-44.
- [75] Alder, L.; Greulich, K.; Kempe, G.; Vieth, B., Residue analysis of 500 high priority pesticides: Better by GC-MS or LC-MS/MS? *Mass Spectrom. Rev.* **2006**, *25* (6), 838-865.
- [76] Kind, T.; Fiehn, O., Advances in structure elucidation of small molecules using mass spectrometry. *Bioanalytical reviews* **2010**, *2* (1-4), 23-60.
- [77] Krauss, M.; Singer, H.; Hollender, J., LC-high resolution MS in environmental analysis: From target screening to the identification of unknowns. *Analytical and Bioanalytical Chemistry* **2010**, *397* (3), 943-951.
- [78] Schymanski, E. L.; Jeon, J.; Gulde, R.; Fenner, K.; Ruff, M.; Singer, H. P.; Hollender, J., Identifying Small Molecules via High Resolution Mass Spectrometry: Communicating Confidence. *Environmental Science & Technology* **2014**, *48* (4), 2097-2098.

- [79] Barron, M. G., Bioconcentration. Will water-borne organic chemicals accumulate in aquatic organisms? *Environmental Science & Technology* **1990**, *24* (11), 1612-1618.
- [80] Mackay, D., Correlation of Bioconcentration Factors. *Environmental Science & Technology* **1982**, *16* (5), 274-278.
- [81] Mackay, D.; Fraser, A., Bioaccumulation of persistent organic chemicals: Mechanisms and models. *Environ. Pollut.* **2000**, *110* (3), 375-391.
- [82] Rozman, K. K.; Doull, J., Dose and time as variables of toxicity. *Toxicology* **2000**, *144* (1-3), 169-178.
- [83] Spacie, A.; Hamelink, J. L., Alternative Models for Describing the Bioconcentration of Organics in Fish. *Environ. Toxicol. Chem.* **1982**, *1* (4), 309-320.
- [84] Landrum, P. F.; Lee li, H.; Lydy, M. J., Toxicokinetics in aquatic systems: Model comparisons and use in hazard assessment. *Environ. Toxicol. Chem.* **1992**, *11* (12), 1709-1725.
- [85] McCarty, L. S.; Mackay, D., Enhancing ecotoxicological modeling and assessment. *Environ. Sci. Technol.* **1993**, *27* (9), 1719-1728.
- [86] Escher, B. I.; Hermens, J. L. M., Internal exposure: Linking bioavailability to effects. *Environ. Sci. Technol.* **2004**, *38* (23), 455A-462A.
- [87] Escher, B. I.; Hermens, J. L. M., Modes of action in ecotoxicology: Their role in body burdens, species sensitivity, QSARs, and mixture effects. *Environmental Science & Technology* **2002**, *36* (20), 4201-4217.
- [88] Veith, G. D.; Call, D. J.; Brooke, L. T., Structure Toxicity Relationships for the Fathead Minnow, Pimephales Promelas: Narcotic Industrial Chemicals. *Canadian Journal of Fisheries and Aquatic Sciences* **1983**, *40* (6), 743-748.
- [89] Konemann, H., Quantitative Structure-Activity Relationships in Fish Toxicity Studies. Part 1. Relationship for 50 Industrial Pollutants. *Toxicology* **1981**, *19* (3), 209-221.
- [90] McCarty, L. S.; Mackay, D.; Smith, A. D.; Ozburn, G. W.; Dixon, D. G., Residue-based Interpretation of Toxicity and Bioconcentration QSARs from Aquatic Bioassays - Neutral Narcotic Organics. *Environ. Toxicol. Chem.* **1992**, *11* (7), 917-930.
- [91] Venkatakrisnan, K.; von Moltke, L. L.; Greenblatt, D. J., Effects of the antifungal agents on oxidative drug metabolism - Clinical relevance. *Clin. Pharmacokinet.* **2000**, *38* (2), 111-180.
- [92] Lynch, T.; Price, A., The effect of cytochrome P450 metabolism on drug response, interactions, and adverse effects. *American Family Physician* **2007**, *76* (3), 391-396.
- [93] Gubbins, P. O., Triazole antifungal agents drugdrug interactions involving hepatic cytochrome P450. *Expert Opinion on Drug Metabolism and Toxicology* **2011**, *7* (11), 1411-1429.
- [94] Kraemer, S. D.; Testa, B., The Biochemistry of Drug Metabolism - An Introduction Part 7. Intra-Individual Factors Affecting Drug Metabolism. *Chemistry & Biodiversity* **2009**, *6* (10), 1477-1660.
- [95] Ortiz De Montellano, P. R.; Almira Correia, M., *Inhibition of cytochrome P450 enzymes*. 1995; p 305-364.
- [96] Nørgaard, K. B.; Cedergreen, N., Pesticide cocktails can interact synergistically on aquatic crustaceans. *Environ Sci Pollut Res* **2010**, *17* (4), 957-967.
- [97] Bjergager, M. B.; Hanson, M. L.; Solomon, K. R.; Cedergreen, N., Synergy between prochloraz and esfenvalerate in *Daphnia magna* from acute and subchronic exposures in the laboratory and microcosms. *Aquat. Toxicol.* **2012**, *110-111*, 17-24.
- [98] Bjergager, M.-B. A.; Hanson, M. L.; Lissemore, L.; Henriquez, N.; Solomon, K. R.; Cedergreen, N., Synergy in microcosms with environmentally realistic concentrations of prochloraz and esfenvalerate. *Aquat. Toxicol.* **2011**, *101* (2), 412-422.
- [99] Cedergreen, N.; Kamper, A.; Streibig, J. C., Is prochloraz a potent synergist across aquatic species? A study on bacteria, daphnia, algae and higher plants. *Aquat. Toxicol.* **2006**, *78* (3), 243-252.
- [100] Kretschmann, A.; Gottardi, M.; Dalhoff, K.; Cedergreen, N., The synergistic potential of the azole fungicides prochloraz and propiconazole toward a short α -cypermethrin pulse increases over time in *Daphnia magna*. *Aquat. Toxicol.* **2015**, *162*, 94-101.

Chapter 2. How Biotransformation influences Toxicokinetics of Azole Fungicides in the Aquatic Invertebrate *Gammarus pulex*

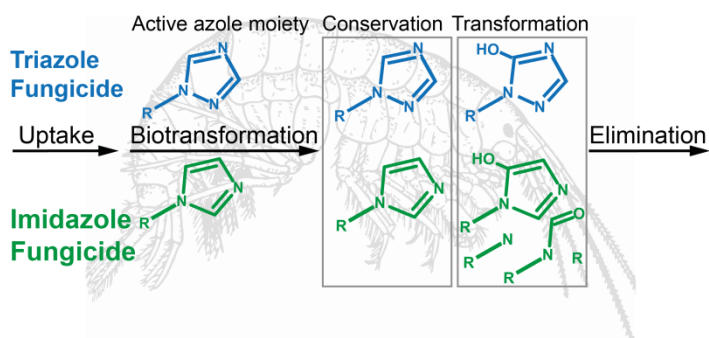
Andrea Rösch^{1,2}, Sabine Anliker^{1,2}, Juliane Hollender^{1,2*}

¹ Eawag, Swiss Federal Institute of Aquatic Science and Technology, 8600 Dübendorf, Switzerland

² Institute of Biogeochemistry and Pollutant Dynamics, ETH Zürich, 8092 Zürich, Switzerland

* Corresponding Author: Phone: +41 58 765 5493. e-mail: juliane.hollender@eawag.ch

Published in *Environmental Science and Technology*, DOI: 10.1021/acs.est.6b01301



Abstract

Biotransformation is a key process that can greatly influence the bioaccumulation potential and toxicity of organic compounds. In this study biotransformation of seven frequently usedazole fungicides (triazoles: cyproconazole, epoxiconazole, fluconazole, propiconazole, tebuconazole and imidazoles: ketoconazole, prochloraz) was investigated in the aquatic invertebrate *Gammarus pulex* in a 24 h exposure experiment. Additionally, temporal trends of the whole body internal concentrations of epoxiconazole, prochloraz, and their respective biotransformation products (BTPs) were studied to gain insight into toxicokinetic processes such as uptake, elimination and biotransformation. By the use of high resolution tandem mass spectrometry in total 37 BTPs were identified. Between one (ketoconazole) and six (epoxiconazole) BTPs were identified per parent compound except for prochloraz, which showed extensive biotransformation reactions with 18 BTPs detected that were mainly formed through ring cleavage or ring loss. In general, most BTPs were formed by oxidation and conjugation reactions. Ring loss or ring cleavage was only observed for the imidazoles as expected from the general mechanism of oxidative ring openings of imidazoles, likely affecting the bioactivity of these BTPs. Overall, internal concentrations of BTPs were up to three orders of magnitude lower than that of the corresponding parent compound. Thus, biotransformation did not dominate toxicokinetics and only played a minor role in elimination of the respective parent compound, with the exception of prochloraz.

2.1 Introduction

Aquatic organisms are exposed to a mixture of numerous pollutants originating from industrial, agricultural, and domestic activities. One of the most widely used classes of antifungal agents are azole fungicides, which include among others triazoles and imidazoles (see Figure 2-1). These fungicides are applied in agriculture as well as in pharmacology against various fungal infections.¹ Azoles enter the aquatic environment via runoff from agricultural areas and effluents from wastewater treatment plants. Hence, azoles are frequently detected in surface waters with concentrations ranging from low ng L⁻¹ to low µg L⁻¹.²⁻⁴ In a recent pesticide screening in Swiss surface waters several azoles have been detected up to a concentration of 100 ng L⁻¹.⁵ Azole fungicides are moderately toxic toward aquatic invertebrates with LC₅₀ values in the low mg L⁻¹ range.⁶⁻¹⁰

The anti-fungal activity of azoles results from their ability to inhibit the cytochrome P450 (CYP) catalyzed ergosterol biosynthesis in fungi. Binding between the azole and the enzyme occurs via the nucleophilic nitrogen in the specific azole moiety and the iron of the enzyme which is responsible for converting lanosterol to ergosterol. This leads to a depletion of ergosterol, which is essential for the structure and functioning of fungal cell membranes.¹¹⁻¹² Thus, biotransformation reactions taking place at the active azole moiety of the fungicide can affect its antifungal activity. The huge enzyme class of CYP monooxygenases catalyzes a wide variety of oxidative reactions in metabolism and in nontarget organisms CYPs are an important enzyme class active in the detoxification of xenobiotics. In aquatic species, such as in daphnids it has been observed that azole fungicides can enhance the effect of other pesticides such as of pyrethroids.¹³⁻¹⁷ This synergistic effect is supposed to be caused by the inhibition of CYP, and hence by less biotransformation of the toxic pesticide.

Gammarids are small crustaceans belonging to the order of amphipoda and are an important keystone species in lotic aquatic ecosystems. They represent one of the most sensitive aquatic invertebrate species and therefore they are often used as model organism for ecotoxicological studies and for biomonitoring.¹⁸⁻²¹ Chemical exposure concentrations are closely related to internal concentrations inside organisms and can determine the effect of a chemical. Key factors regulating the internal chemical concentration are uptake and elimination processes including biotransformation – also termed toxicokinetics – which describe the time course of the toxicant concentration inside the organism.²²⁻²³

Biotransformation within an organism determines the bioaccumulation potential of a specific azole fungicide as well as the bioaccumulation of co-occurring substances. To date, very little information is available about the biotransformation of azoles in aquatic invertebrates. Therefore, the goals of this study were first to investigate biotransformation of seven selected azole fungicides in *Gammarus pulex* and second to get insight into toxicokinetic processes, *i.e.*, the time course of chemical uptake, biotransformation, and elimination. Five frequently used triazole fungicides (cyproconazole: CP, epoxiconazole: EP, fluconazole: FLU, propiconazole: PRP, and tebuconazole: TEB) and two imidazole fungicides (ketoconazole: KET and prochloraz: PRZ) with different physicochemical properties (log D_{ow} from 0.6 to 4.3, see Table 2-1) were chosen to explore the role of structural similarity in relation to

biotransformation. Since the azole ring represents the active moiety of these fungicides, it was of interest if this part of the molecule remains intact during biotransformation and can therefore still act as CYP inhibitor and maintain its antifungal activity. By determining the kinetic rate constants of uptake, biotransformation, and elimination we aimed to investigate the role of biotransformation in relation to the reduction of bioaccumulation of the respective parent compounds.

2.2 Material and Methods

2.2.1 Chemicals, Solutions and Test Organisms

Detailed information about all chemicals and solutions used during experiments and instrumental analysis are provided in the Supporting Information (SI) A.

Adult *G. pulex* were collected from a small creek near Zürich, Switzerland (E 702150, N 2360850) between October and December 2014. The sampling area is characterized by relatively little agricultural use and is located in a small nature reserve. Male and female *G. pulex* were not differentiated since a reliable assignment of sex is only possible with an examination under a microscope using inactive and therefore dead organisms.²⁴ Prior to the experiments, organisms were acclimatized for 3-5 days to the test conditions (11 °C, 12 h light / 12 h dark cycle) in an aquarium with aerated artificial pond water (APW)²⁵ composed of 0.12 g L⁻¹ MgSO₄ · 7 H₂O, 0.065 g L⁻¹ NaHCO₃, 0.0058 g L⁻¹ KCl, and 0.29 g L⁻¹ CaCl₂ · 2 H₂O. *G. pulex* were fed with horse chestnut (*Aesculus hippocastanum*) leaves inoculated with *Cladosporium herbarum* to facilitate the decomposition of the leaves, thereby making them more edible.²⁵

2.2.2 Experimental Design

Biotransformation Product Screening Experiment

Biotransformation product (BTP) screening experiments were carried out separately for each selected azole fungicide. Exposure solutions were prepared in APW at nominal concentrations of 200 µg L⁻¹. 600 mL-glass beakers were filled in duplicate with 500 mL exposure solution and four organisms were added to each beaker. To provide food and shelter and to avoid cannibalism, four horse chestnut leaf discs (diameter: 2 cm) were added to each beaker. After incubation for 24 h at test conditions, the organisms were sieved, rinsed with nanopure water, blotted dry on tissue, transferred into 2 mL-microcentrifuge tubes, and weighed. After addition of 100 µL isotopically labeled internal standard mix solution (100 µg L⁻¹), 500 µL MeOH, and 300 mg of 1 mm zirconia/silica beads (BioSpec Products, Inc., USA), the extraction and homogenization was carried out with a FastPrep bead beater (MP Biomedicals, Switzerland) in two cycles of 15 s at 6 m s⁻¹ (cooling on ice in between). Afterwards, samples were centrifuged (6 min, 10 000 rpm, 20 °C) and filtered through 0.45 µm regenerated cellulose filters (BGB Analytic AG, Switzerland). Filters were washed with 400 µL MeOH and the filtrate pooled with the extract. Additionally, different controls were performed, *i.e.*, without target chemicals (“chemical negative, food and

organism positive”), without organisms (“organism negative, chemical and food positive”) and one with only chemicals (“organism and food negative, chemical positive”). To quantify the aqueous concentrations the exposure medium was sampled at the beginning and the end of the experiments. All samples were stored at -20 °C until chemical analysis.

Toxicokinetic Experiment

G. pulex were exposed separately to epoxiconazole and prochloraz at concentrations of 100 µg L⁻¹ for 24 h, and were afterwards transferred to clean media for a 120 h depuration phase. During both the exposure and depuration phase *G. pulex* (four organisms per beaker) were sampled in duplicate at different time points (see SI F). Immediately after sampling 200 µL of isotopically labeled internal standard mix solution (100 µg L⁻¹) and 400 µL of MeOH were added.

Unless stated otherwise, the sample preparation was similar to the one described above.

2.2.3 Chemical Analysis

All samples were analyzed by online solid phase extraction coupled to liquid chromatography high resolution tandem mass spectrometry (online-SPE-LC-HRMS/MS).²⁶ Automated online-SPE served for sample clean-up and enrichment. By using a mixed bed multilayer cartridge a broad range of compounds with different polarities, molecular sizes, and charges was retained and enriched. Detection of analytes was performed by using a quadrupole-orbitrap mass spectrometer (Q Exactive, Thermo Fisher Scientific Inc.) with electrospray ionization (ESI). Full scan acquisition for a mass range of 100 – 1000 m/z with a resolution of 70 000 (at m/z 200) was performed in polarity-switching mode followed by five (positive mode) and two (negative mode) data-dependent MS/MS scans with a resolution of 17 500 (at m/z 200) and an isolation window of 1 m/z. For triggering data-dependent MS/MS acquisition a mass list with suspected BTPs (between 450 and 1300 masses per parent compound) was set up based on *in silico* pathway prediction and scientific literature (see SI B).

Quantification was based on internal standard calibration (Trace Finder software 3.1 (Thermo Scientific)). Amounts of BTPs were estimated based on the calibration curve of their parent compound since no reference standards could be obtained. For more details about the analytical procedure, quantification, and quality control refer to SI B and SI C.

2.2.4 Biotransformation Product Identification by Suspect and Nontarget Screening

SIEVE software version 2.1 and 2.2 (Thermo Scientific) for differential expression analysis was used to compare treatment and control samples (see SI D).

As a first step a suspect screening was carried out. Therefore, the mass list with the suspected BTPs was uploaded to SIEVE and used for peak identification. Peaks only detected in the treatment samples with a peak intensity >10⁶ in at least one replicate sample and with a minimum of three scans in the extracted ion chromatogram were regarded as possible BTPs. For prochloraz and epoxiconazole, where kinetic data were available, the

concentrations of the suspected BTPs should increase in the uptake phase and decrease in the depuration phase.

As a second step a nontarget screening was conducted to discover additional not predicted BTPs. Therefore, in addition to the above mentioned criteria two extra criteria were used – a new integrated intensity threshold of 0.1% of the integrated intensity of the parent compound and an integrated intensity ratio between treatment and control samples of more than 10.

2.2.5 Structure Elucidation

Structure elucidation was based on the interpretation of (1) the exact mass and the isotopic pattern to assign molecular formulas and of (2) MS/MS spectra to identify diagnostic fragments or losses characteristic for one specific structure (D) or for several positional isomers (d).

Structure elucidation was assisted by the fragmentation prediction tool Mass Frontier (version 7.0, HighChem, Slovakia) and by molecular structure generation including MS and MS/MS information with Molgen-MSMS.²⁷

For some tentatively identified BTPs additional evidence was given by enzyme deconjugation experiments (e), by biotransformation pathway information (p), or by the same structure and/or MS/MS spectra already reported in scientific literature (l, m). Enzymatic sulfate deconjugation was carried out experimentally analogous to Kukkonen and Oikari (1988)²⁸ (see SI G). The letters in parentheses (D, d, e, p, l, m) indicate the identification confidence of the BTPs shown in Table 2-1. For triazoles the presence of the ionized triazole moiety ($m/z = 70.0400$) in the MS/MS spectra provided further evidence that identified BTPs were actually formed from a triazole parent compound (see SI I). Furthermore confidence levels proposed by Schymanski et al. (2014)²⁹ were assigned to communicate identification confidence.

2.2.6 Modeling Bioaccumulation and Biotransformation Kinetics

Model Structure

To estimate the rate constants for the toxicokinetic processes a one-compartment first-order model was applied. Build Your Own Model (BYOM) version 1.5, a set of multiple scripts and functions, programmed by Tjalling Jager (<http://debtox.nl/about.html>) was used for modeling bioaccumulation and biotransformation kinetics in Matlab R2012b/R2015b. Although the term BTP is preferred, M for metabolite is used within the equations for simplicity.

The time courses of the parent compounds are described by the following ordinary differential equation:

$$\frac{dC_{in,p}(t)}{dt} = C_{water}(t) \cdot k_u - C_{in,p}(t) \cdot k_e - C_{in,p}(t) \cdot (k_{M1,1st} + \dots + k_{Mx,1st}) \quad (1)$$

where $C_{in,p}(t)$ [$\text{nmol kg}_{\text{wet weight (ww)}}^{-1}$] is the time course of the whole body internal concentration of the parent compound in *G. pulex* and $C_{\text{water}}(t)$ is the time course of the parent compound concentration in the medium [nmol L^{-1}]. Uptake of the parent compound via food, dermal and respiratory surfaces is described by the uptake rate constant k_u [$\text{L kg}_{\text{ww}}^{-1} \text{d}^{-1}$], whereas direct elimination of the parent compound via excretion through dermal and respiratory surfaces is described by the elimination rate constant k_e [d^{-1}]. $k_{Mx,1st}$ and $k_{Mx,2nd}$ [d^{-1}] are the rate constants for biotransformation for the primary and secondary BTPs, respectively.

We differentiate between primary BTPs, that are formed directly from the parent compound in separate independent pathways, and secondary BTPs, where a direct precursor BTP was identified. The time courses of the BTPs are described as follows:

For the primary BTPs:

$$\begin{aligned} \frac{dC_{in,M1,1st}(t)}{dt} = & C_{in,p}(t) \cdot k_{M1,1st} - C_{in,M1,1st}(t) \cdot k_{eM1,1st} \\ & - C_{in,M1,1st}(t) \cdot (k_{M1,2nd} + \dots + k_{Mx,2nd}) \end{aligned} \quad (2)$$

For the secondary BTPs:

$$\begin{aligned} \frac{dC_{in,M1,2nd}(t)}{dt} = & C_{in,M1,1st}(t) \cdot k_{M1,2nd} - C_{in,M1,2nd}(t) \cdot k_{eM1,2nd} \\ & - C_{in,M1,2nd}(t) \cdot (k_{M1,further} + \dots + k_{Mx,further}) \end{aligned} \quad (3)$$

where $C_{in,Mx,1st}(t)$ and $C_{in,Mx,2nd}(t)$ [$\text{nmol kg}_{\text{ww}}^{-1}$] are the time courses of the whole body internal concentration of the primary and secondary BTPs, respectively, and $k_{eMx,1st}$ and $k_{eMx,2nd}$ are the elimination rate constants of the primary and secondary BTPs, respectively. For BTPs where no successors were identified, the elimination rate $k_{eMx,1st \text{ or } 2nd}$ includes direct excretion and elimination due to further biotransformation. Otherwise, an additional elimination term was added depending on the number of successors (see equations 2 and 3).

Model Calibration and Parameter Estimation

For model calibration the equations were solved numerically (Runge-Kutta method) and fitted to the measured internal concentrations of the parent compounds and their BTPs. All parameters were fitted simultaneously by minimizing the sum of squares (Nelder-Mead Simplex method) between measured and simulated internal concentration. All parameters were restricted to positive values and no weighting of particular data sets was applied. As exposure concentration the average measured medium concentration during the uptake phase was used. During the depuration phase the medium concentration was set to zero, which was confirmed by the analysis of the exposure medium. For simulating the time courses of the internal concentrations of the parent compounds and their BTPs the best fit parameters were used. 95% confidence intervals were calculated for all parameters using profile likelihoods.

Bioaccumulation Factor and Elimination Half-Lives

Bioaccumulation factors (BAFs) [L kg^{-1}] can either be calculated at steady state at a specific time point based on the ratio of the internal concentration of a parent compound and the water concentration:

$$\text{BAF} = \frac{C_{\text{in,p}}(t)}{C_{\text{water}}(t)} \quad (4)$$

or based on the kinetic rate constants:

$$\text{kinetic BAF (BAF}_k) = \frac{k_u}{k_e + k_{\text{M1,1st}} + \dots + k_{\text{Mx,1st}}} \quad (5)$$

Ashauer et al. (2012)³⁰ showed that the dietary uptake of 15 organic chemicals ($\log K_{\text{ow}}$ from 0.33 to 5.18) in *G. pulex* contributed to less than 1% of the total uptake. Thus, the measured BAFs are close to the bioconcentration factors (BCFs).

Elimination half-lives ($t_{1/2}$) [h] were calculated based on the total elimination for parent compounds and BTPs. For parent compounds these calculations are valid under the assumption of constant water concentrations (C_{water}). For BTPs, even though BTP formation is considered during both the uptake and depuration phase (see equations 2 and 3), for the calculation of half-lives we have to assume that no further BTP formation occurs during the depuration phase (reasonable assumption in the case of a fast elimination of the parent compounds).

For parent compounds:

$$t_{1/2,p} = \frac{\ln 2}{k_e + k_{\text{M1,1st}} + \dots + k_{\text{Mx,1st}}} \quad (6)$$

For BTPs where one or more direct successor is known:

$$t_{1/2,\text{M1,1stor2nd}} = \frac{\ln 2}{k_{\text{eM1,1stor2nd}} + k_{\text{M1,2ndor further}} + \dots + k_{\text{Mx,2ndor further}}} \quad (7)$$

For BTPs where no direct successor is known:

$$t_{1/2,\text{M1,1stor2nd}} = \frac{\ln 2}{k_{\text{eM1,1stor2nd}}} \quad (8)$$

2.3 Result and Discussion

2.3.1 Identified Biotransformation Products and Biotransformation Reactions

Exposure medium concentrations were measured at the beginning and at the end of the experiments. Medium concentrations were in general less than 20% lower than nominal concentrations and were comparable to “chemical positive” control samples. Medium concentrations declined during the 24 h exposure phase on average by 3% in the BTP screening experiment and by 14% in the kinetic experiment (see SI E). Mortality was only observed during the exposure to PRP in the BTP screening experiment. Exposure times of 24 h were regarded as sufficient to gain an understanding about predominant biotransformation processes, as toxicokinetic studies in gammarids³⁰⁻³¹ have shown that steady state was reached after 24 h exposure for chemicals with comparable log D_{ow} values.

In total 37 BTPs were tentatively identified in *G. pulex* for six out of the seven selected azole fungicides. The identification confidence for each BTP as described in the section *Structure Elucidation* is stated in Table 2-1. Even though no reference standards could be obtained for the detected BTPs, we are often able to report only one structure based on diagnostic fragments for one structure (D) or based on diagnostic fragments for positional isomers in combination with pathway information (metabolic logic) (d, p). According to the identification confidence levels proposed by Schymanski et al. (2014)²⁹ 17 BTPs match level 2b (*probable structure: diagnostic evidence for one structure*) and 20 BTPs match level 3 (*tentative candidates: e.g., positional isomers*). Annotated MS/MS spectra for each BTP are reported in the SI I and are available electronically in the MassBank database.³² Mass errors between theoretical and measured mass were generally < 3 ppm.

The naming of BTPs is as follows: e.g., CP_M308a at which the first letters (CP) represent the abbreviation of the parent compound, M stands for metabolite, the following number represents m/z, and the final letter differentiates between isobaric BTPs.

Fluconazole was the only parent compound where no BTPs were detected. This is in accordance with its low bioaccumulation caused by its much higher polarity (log D_{ow} = 0.7, Table 2-1) compared to the other selected azoles and with previous studies in humans and wastewater treatment.³³⁻³⁵ Brammer et al. (1991)³⁵ found 80% of fluconazole unchanged in human urine and identified only two minor BTPs, a glucuronide conjugate and an N-oxide.

For the six remaining azoles between one (KET) and 18 (PRZ) BTPs were identified per parent compound. Out of the 37 detected BTPs, 29 were predicted with *in silico* prediction and by literature research (see SI B). The remaining eight BTPs were found with the nontarget screening approach.

Biotransformation of azoles took place via different reactions. The most common biotransformation reactions observed were oxidations and conjugations as well as the combination of the two. An overview of all biotransformation reactions identified for each azole, with differentiation between reactions occurring at the active moiety or at the remaining molecule, is depicted in Figure 2-1. Hydroxylation was the most prevalent reaction

observed for all azoles and occurred at the aliphatic part of the molecule, the chlorophenyl moiety, and at the azole ring. In some cases hydroxylation products were further oxidized to ketones.

Different conjugation reactions were identified including those with sulfate (for EP and PRZ), with glutathione resulting in cysteine products (for EP and PRZ), with glucose-sulfate (for PRZ), with phosphate (for TEB), and with acetate (for PRZ). Sulfate and glucose-sulfate conjugation products were further confirmed by enzymatic deconjugation experiments. Several studies report sulfate, glucose and glucose-sulfate conjugates being major BTPs for different organic contaminants in aquatic invertebrates.^{28, 30, 36-37} The glutathione conjugates and resulting cysteine products confirmed the recent results of Jeon et al. (2013)²⁶, where glutathione conjugates and cysteine products have been detected for the first time in freshwater crustaceans. Nucleophilic addition of glutathione to electrophiles (e.g., epoxides) is in agreement with common observations of glutathione conjugation during biotransformation.³⁸ To date phosphate conjugation has been only described for insects and has been rarely observed in vertebrate species.³⁹⁻⁴⁰ Acetylations are known for the mammalian metabolism of xenobiotics⁴¹ and have been observed in algae, macrophytes and bivalves⁴² as well as during microbial biotransformation⁴³. However, phosphate conjugation and acetylation have not been detected in aquatic crustaceans previously.

For the two compounds epoxiconazole and prochloraz showing the highest BAFs (see Table 2-1) most diverse biotransformation reactions including conjugations were detected. Conjugation products might have also been formed for the other studied azoles but at concentrations below LOQ. Nevertheless, due to the enrichment capability of the online-SPE method, the sensitivity and broad scan range (100-1000 m/z) of the LC-HRMS/MS method, the low limits of quantification (LOQ) for all azoles and BTPs ($\text{LOQ}^1 < 0.5 \text{ nmol kg}_{\text{ww}}^{-1}$, see SI C), and the combined suspect and nontarget screening approaches, we assume not to have missed any relevant BTP.

¹ LOQs for gammarid extracts were recalculated, such that the molar amount of the parent compounds in the lowest calibration standard was adjusted to the average sample wet weight per injection, instead of the average sample wet weight per sample, as was previously done. Recalculation resulted in LOQs which were 10x higher than reported. This recalculation did not change the quantification and interpretation of the results however, since all reported values were still above the recalculated LOQs.

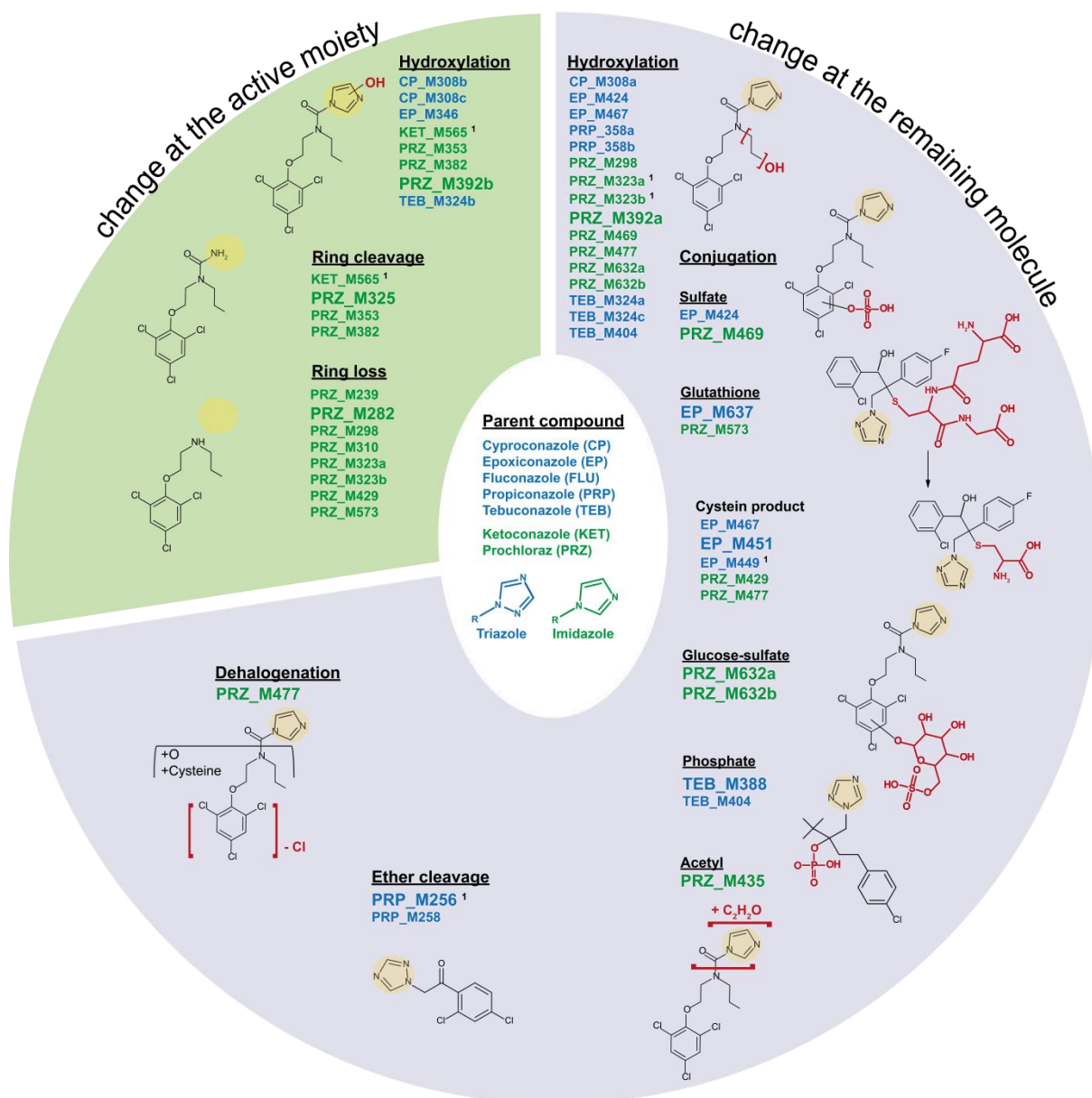


Figure 2-1: Overview of identified biotransformation products (BTPs) in *G. pulex* after 24 h exposure to 200 µg L⁻¹ of the respective azole fungicide. Structural changes between the BTPs and its parent compound are highlighted in red. In case the exact position of structural change is not known the effected moiety is marked with red brackets and the change is labeled. Below each reaction the BTPs are listed, where this reaction happened as well (imidazoles: marked in green, triazoles: marked in blue). The active moiety (imidazole or triazole ring) is highlighted in yellow. The larger font size indicates the name of the depicted structure. ¹ marks BTPs that undergo further oxidation (formation of ketones).

Comparison of Triazole and Imidazole Biotransformation

Large differences in biotransformation reactions were present between triazoles and imidazoles. Ring cleavages or ring losses were only observed for imidazoles. For prochloraz most biotransformation reactions (13 out of 18) (see Figure 2-2) took place at the azole functional moiety. For ketoconazole only one imidazole ring oxidation product was observed (KET_M565). These results also fit within expectations since the imidazole ring cleavage is known to be initiated by formation of an epoxide⁴⁴⁻⁴⁵, which is not possible for triazoles due to a lack of two adjacent carbon atoms in the triazole ring (see Figure 2-1). In the case of triazoles, ring hydroxylation (for CP, EP, and TEB) represented the only change occurring at the active moiety.

Conservation of the Ring Functional Moiety

As mentioned above, for prochloraz most biotransformation reactions resulted in a cleavage or loss of the imidazole ring. In contrast, for the remaining azoles biotransformation reactions rarely occurred at the active azole moiety, whereby their antifungal activity and their CYP inhibitory potential may be conserved. But even changes at the active moiety can be regarded as negligible, since the internal concentrations of the respective parent compounds were much higher than those of the BTPs, with the exception of prochloraz (see section *Influence of Azole Biotransformation on Bioaccumulation*).

Crucial for azole-CYP complex formation are steric and electronic effects of the substituents, the position of substitution at the ring, and hydrophobic interactions between the azole and the CYP.⁴⁶ Therefore, it remains unclear whether ring hydroxylation hinders one of the nitrogen atoms to coordinate with the heme active site.

Since azoles are known to act as CYP inhibitors one could hypothesize that they might be able to inhibit their own biotransformation. However, prochloraz which is known to be a strong CYP inhibitor in other aquatic species^{14, 16-17, 47}, showed the highest biotransformation potential. Prochloraz can be an inhibitor and a substrate at the same time⁴⁶ and the internal concentration of prochloraz determines the proportion of inhibited CYP. Therefore, knowledge of the inhibition potency would provide information about the strength of inhibition and thus the amount of available active CYP.⁴⁸

Comparison with Literature Data for other Species

To the best of our knowledge, no study exists about the biotransformation of azole fungicides in aquatic crustaceans. Furthermore, there is also no research which compares biotransformation of imidazoles and triazoles.

For the imidazole fungicides prochloraz and ketoconazole various studies support our findings about the frequent ring opening. In *G. pulex* oxidation of the imidazole ring was observed resulting in the aldehyde product PRZ_M353 and the thereof formed BTP PRZ_M325. These BTPs were also observed in rat (PRZ_353/325)⁴⁹⁻⁵⁰, rainbow trout (PRZ_M353)⁵¹, and plants (PRZ_M353/325).⁵²

Conjugation reactions showed some differences between aquatic invertebrates and the other organisms. Glucuronic acid (rainbow trout, rat) and sulfate (rat) conjugations were identified in the afore mentioned studies. This is consistent with the findings of James (1987)⁵³ that glucuronidations are more common in fish, whereas glucosidations may represent a more important pathway in invertebrates.

The microsomal metabolism of ketoconazole has been studied extensively due to its importance as antifungal drug and its ability to act as specific inhibitor of CYP3A4.⁵⁴⁻⁵⁷ Biotransformation of ketoconazole in human and rat microsomes led to the oxidation of the imidazole and/or piperazine moiety. KET_M565 identified in this study was also the most abundant BTP in rat and human microsomes.⁵⁷

According to literature, biotransformation of triazoles is not that conserved over different organisms as it seems for imidazoles. In contrast to our findings, microbial biotransformation of tebuconazole led to ring cleavages.⁵⁸⁻⁵⁹ In rats, extensive biotransformation of cyproconazole was observed with the major BTP being formed by oxidative removal of the triazole ring.⁵² In human urine, hydroxyl and carboxyl products of tebuconazole were identified as major BTPs, both free and as glucuronide conjugates.⁶⁰ For propiconazole, the large majority of BTPs identified in mammals contained the unchanged triazole ring which is in line with our results.⁵² Little data is available for epoxiconazole. Contrary to our results, in *in vitro* experiments with rat and trout hepatic microsomes, and with human CYP3A4 no BTPs were identified for epoxiconazole.⁶¹⁻⁶² Despite the diversity of reactions, BTPs resulting from the cleavage of the triazole ring were rarely observed, which is in agreement with expectations since no epoxide can be formed on the ring to initiate cleavage (see above).

In conclusion, we detected several BTPs in *G. pulex* that have been previously identified in other organisms such as mammals or rats. However, cross-species extrapolation of biotransformation reactions is precarious without a thorough understanding of the underlying mechanisms and enzymes.

Table 2-1: Overview of parent compounds and respective biotransformation products formed in *G. pulex*. Biotransformation products are listed according to their relative peak intensity. Mean values for the retention time (RT) and the bioaccumulation factor (BAF) are provided for the replicate samples. Below each biotransformation product the abbreviation (S) stands for “identified by suspect screening”, whereas (N) stands for “identified by nontarget screening”. The asterisk marks biotransformation products where the active azole moiety was altered.

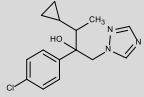
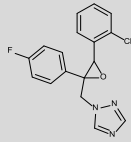
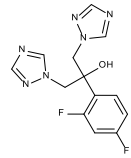
Compound	Formula [M] Exact mass of [M+H] ⁺ / [M-H] ⁻ ⁱⁱⁱ⁾	RT [min]	Elemental change ^{iv)}	Description	Log D _{ow} ^{v)}	Identification confidence ^{vi)} /level according to Schymanski et al. (2014) ^{29/} ^{vii)}
Cyproconazole (CP) 	C ₁₅ H ₁₈ ClN ₃ O 292.1211	15.7		parent compound	2.9	/1/
BAF (t₂₄) ⁱ⁾: 12 L kg _{ww} ⁻¹						
CP_M308a (S)	C ₁₅ H ₁₈ ClN ₃ O ₂ 308.1160	13.5	+ O	aliphatic hydroxylation	1.5-1.9	I ⁵² , /3/
CP_M308b * (S)	C ₁₅ H ₁₈ ClN ₃ O ₂ 308.1160	14.1	+ O	triazole ring hydroxylation	3.1	d, /3/
CP_M308c * (S)	C ₁₅ H ₁₈ ClN ₃ O ₂ 308.1160	14.7	+ O	triazole ring hydroxylation	3.2	d, /3/
Epoxiconazole (EP) 	C ₁₇ H ₁₃ ClFN ₃ O 330.0804	16.0		parent compound	3.7	/1/
BAF (t₂₄) ⁱ⁾: 49 L kg _{ww} ⁻¹ BAF_k ⁱⁱ⁾: 33 L kg _{ww} ⁻¹						
EP_M346 * (S)	C ₁₇ H ₁₃ ClFN ₃ O ₂ 346.0753	15.0	+ O	triazole ring hydroxylation	4.0-4.1	d, /3/
EP_M449 (S)	C ₂₀ H ₁₈ ClFN ₄ O ₃ S 449.0845	13.9	+ C ₃ H ₇ NO ₂ S - H ₂	cysteine product, further oxidation	0.8	/3/
EP_M451 (S)	C ₂₀ H ₂₀ ClFN ₄ O ₃ S 451.1001	12.6	+ C ₃ H ₇ NO ₂ S	cysteine product	0.4	D, /2b/
EP_M467 (S)	C ₂₀ H ₂₀ ClFN ₄ O ₄ S 467.0951	11.5	+ O + C ₃ H ₇ NO ₂ S	hydroxylation, cysteine product	0.1	d, /3/
EP_M424 (S)	C ₁₇ H ₁₃ ClFN ₃ O ₅ S 424.0176	12.2	+ O + SO ₃	aliphatic hydroxylation, sulfate conjugation	0.8	e, /3/
EP_M637 (S)	C ₂₇ H ₃₀ ClFN ₆ O ₇ S 637.1642	12.4	+ C ₁₀ H ₁₇ N ₃ O ₆ S	glutathione conjugation	-5.1	D, /2b/
Fluconazole FLU) 	C ₁₃ H ₁₂ F ₂ N ₆ O 307.1113	7.5		parent compound	0.6	/1/
BAF (t₂₄) ⁱ⁾: 0.4 L kg _{ww} ⁻¹						

Table 2-1 continued.

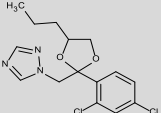
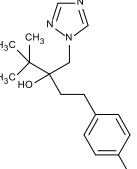
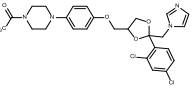
Compound	Formula [M] Exact mass of [M+H] ⁺ / [M-H] ⁻ ⁱⁱⁱ⁾	RT [min]	Elemental change ^{iv)}	Description	Log D _{ow} ^{v)}	Identification confidence ^{vi)} /level according to Schymanski et al. (2014) ^{29/ vii)}
Propiconazole (PRP) 	C ₁₅ H ₁₇ Cl ₂ N ₃ O ₂ 342.0771	17.0		parent compound	4.3	/1/
BAF (t₂₄) ⁱ⁾: 27 L kg_{ww}⁻¹						
PRP_M358a (S)	C ₁₅ H ₁₇ Cl ₂ N ₃ O ₃ 358.0720	13.9	+ O	aliphatic hydroxylation	2.8-4.0	d, l ⁶¹ , m ⁶¹ , /3/
PRP_M358b (S)	C ₁₅ H ₁₇ Cl ₂ N ₃ O ₃ 358.0720	14.5	+ O	aliphatic hydroxylation	2.8-4.0	d, l ⁶¹ , m ⁶¹ , /3/
PRP_M258 (N)	C ₁₀ H ₉ Cl ₂ N ₃ O 258.0195	12.3	- C ₅ H ₈ O	partial loss of dioxolane containing the propyl moiety (ether cleavage)	2.0	D, l ⁵² , /2b/
PRP_M256 (S)	C ₁₀ H ₇ Cl ₂ N ₃ O 256.0039	11.6	- C ₅ H ₁₀ O	partial loss of dioxolane containing the propyl moiety (ether cleavage), further oxidation	2.2	D, l ⁵² , /2b/
Tebuconazole (TEB) 	C ₁₆ H ₂₂ ClN ₃ O 308.1524	16.8		parent compound	3.7	/1/
BAF (t₂₄) ⁱ⁾: 31 L kg_{ww}⁻¹						
TEB_M324a (S)	C ₁₆ H ₂₂ ClN ₃ O ₂ 324.1473	15.1	+ O	aliphatic hydroxylation	2.4	d, l ⁶² , /2b/
TEB_M388 (N)	C ₁₆ H ₂₃ ClN ₃ O ₄ P 388.1187	15.8	+ HPO ₃	phosphate conjugation	-0.2	D, /2b/
TEB_M404 (N)	C ₁₆ H ₂₃ ClN ₃ O ₅ P 404.1137	12.6	+ O + HPO ₃	aliphatic hydroxylation, phosphate conjugation	-1.5	D, /2b/
TEB_M324b * (S)	C ₁₆ H ₂₂ ClN ₃ O ₂ 324.1473	15.9	+ O	triazole ring hydroxylation	4.0-4.1	d /3/
TEB_M324c (S)	C ₁₆ H ₂₂ ClN ₃ O ₂ 324.1473	16.3	+ O	hydroxylation	2.4	d, l ⁶² , /3/
Ketoconazole (KET) 	C ₂₆ H ₂₈ Cl ₂ N ₄ O ₄ 531.1560	13.6		parent compound	4.2	/1/
BAF (t₂₄) ⁱ⁾: 9.2 L kg_{ww}^{-1 viii)}						
KET_M565 * (S)	C ₂₆ H ₃₀ Cl ₂ N ₄ O ₆ 565.1615	14.6	+ H ₂ O ₂	imidazole ring oxidation	2.2	d, l ^{55, 57} , m ⁵⁷ , /3/

Table 2-1 continued.

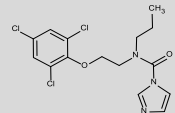
Compound	Formula [M] Exact mass of [M+H] ⁺ / [M-H] ⁱⁱⁱ⁾	RT [min]	Elemental change ^{iv)}	Description	Log D _{ow} ^{v)}	Identification confidence ^{vi)} /level according to Schymanski et al. (2014) ^{29/ vii)}
Prochloraz (PRZ) 	C ₁₅ H ₁₆ Cl ₃ N ₃ O ₂ 376.0381	16.2		parent compound	3.6	/1/
BAF (t₂₄)ⁱ⁾: 57 L kg _{ww} ⁻¹ BAF_kⁱⁱ⁾: 50 L kg _{ww} ⁻¹						
PRZ_M282 * (N)	C ₁₁ H ₁₄ Cl ₃ ON 282.0214	13.2	- C ₄ H ₂ N ₂ O	loss of imidazole ring and CO	2.4	D, p, /2b/
PRZ_M353 * (S)	C ₁₃ H ₁₅ Cl ₃ O ₃ N ₂ 353.0221	16.9	- C ₂ HN + O	partial loss of hydroxylated imidazole ring, aldehyde formation	3.4	D, p, l ^{49, 51-52} , m ⁵¹ , /2b/
PRZ_M323b * (S)	C ₁₂ H ₁₂ Cl ₃ O ₃ N 323.9956	16.0	- C ₃ H ₄ N ₂ + O	imidazole ring loss, aliphatic hydroxylation and further oxidation to a ketone	2.6-3.2	d, /3/
PRZ_M323a * (S)	C ₁₂ H ₁₂ Cl ₃ O ₃ N 323.9956	15.7	- C ₃ H ₄ N ₂ + O	imidazole ring loss, aliphatic hydroxylation and further oxidation to a ketone	2.3-2.6	d, /3/
PRZ_M392b * (S)	C ₁₅ H ₁₆ Cl ₃ N ₃ O ₃ 392.0330	15.3	+ O	imidazole ring hydroxylation	2.3	d, p, /3/
PRZ_M392a (S)	C ₁₅ H ₁₆ Cl ₃ N ₃ O ₃ 392.0330	13.9	+ O	aliphatic hydroxylation	2.1-2.5	d, /3/
PRZ_M325 * (S)	C ₁₂ H ₁₅ Cl ₃ O ₂ N ₂ 325.0272	17.1	- C ₃ HN	partial loss of imidazole ring	3.4	D, p, l ^{49-50, 52} , /2b/
PRZ_M298 * (N)	C ₁₁ H ₁₄ O ₂ NCl ₃ 298.0163	12.9	- C ₄ H ₂ N ₂ O + O	loss of imidazole ring and CO, hydroxylation	1.4-2.9	/3/
PRZ_M429 * (S)	C ₁₅ H ₁₉ Cl ₃ O ₄ N ₂ S 429.0204	16.6	- C ₃ H ₂ N ₂ + C ₃ H ₅ NO ₂ S	loss of imidazole ring, cysteine product	1.4	D, /2b/
PRZ_M239 * (N)	C ₈ H ₈ ONCl ₃ 239.9744	12.6	- C ₇ H ₈ N ₂ O	remaining chlorophenyl moiety and C ₂ H ₅ NO	1.4	D, /2b/
PRZ_M435 * (S)	C ₁₇ H ₂₁ Cl ₃ N ₄ O ₃ 435.0752	14.9	+ C ₂ H ₂ O	acetylation at CO- imidazole ring moiety; NH ₄ ⁺ adduct	-	d, /3/
PRZ_M382 * (S)	C ₁₄ H ₁₈ Cl ₃ N ₃ O ₃ 382.0487	16.6	- CH ₂ + °O	partial loss of hydroxylated imidazole ring	2.2-3.2	d, p, /2b/
PRZ_M632a (N)	C ₂₁ H ₂₆ Cl ₃ N ₃ O ₁₁ S 632.0281	10.4	+ O + C ₆ H ₁₀ O ₈ S	aromatic hydroxylation, glucose and sulfate conjugation	-1.3	D, e, /2b/
PRZ_M469 (S)	C ₁₅ H ₁₆ Cl ₃ N ₃ O ₆ S 469.9753	11.1	+ O + SO ₃	aromatic hydroxylation, sulfate conjugation	0.5	D, e, /2b/
PRZ_M310 * (S)	C ₁₂ H ₁₄ O ₂ NCl ₃ 310.0163	16.8/ 17.5	- C ₃ H ₂ N ₂	loss of imidazole ring	3.7	D, /2b/
PRZ_M632b (N)	C ₂₁ H ₂₆ Cl ₃ N ₃ O ₁₁ S 632.0281	11.1	+ O + C ₆ H ₁₀ O ₈ S	aromatic hydroxylation, glucose and sulfate conjugation	-1.3	D, e, /2b/

Table 2-1 continued.

Compound	Formula [M] Exact mass of [M+H] ⁺ / [M-H] ⁻ ⁱⁱⁱ⁾	RT [min]	Elemental change ^{iv)}	Description	Log D _{ow} ^{v)}	Identification confidence ^{vi)} /level according to Schymanski et al. (2014) ^{29/ vii)}
PRZ_M477 (S)	C ₁₈ H ₂₂ Cl ₂ N ₄ O ₅ S 477.0761	11.2	+ C ₃ H ₆ NO ₂ S + O - Cl	cysteine product, hydroxylation, dehalogenation	-	d, /3/
PRZ_M573 * (S)	C ₁₉ H ₂₃ Cl ₃ O ₈ N ₄ S 573.0375	13.8	- C ₃ H ₂ N ₂ - C ₃ H ₆ + C ₁₀ H ₁₅ N ₃ O ₆ S	loss of imidazole ring, loss of propyl side chain, glutathione conjugation	-1.9	/3/

ⁱ⁾ See Equation 4 in section *Modeling Bioaccumulation and Biotransformation Kinetics* for the calculation of BAFs at steady state.

ⁱⁱ⁾ See Equation 5 in section *Modeling Bioaccumulation and Biotransformation Kinetics* for the calculation of kinetic BAFs (BAF_ks).

ⁱⁱⁱ⁾ [M-H]⁻ only for the sulfate-containing BTPs because they are more sensitive in negative ionization mode. However, they were quantified in positive ionization mode because the respective parent compounds were also detected in positive ionization mode.

^{iv)} The elemental change refers to the change in the molecular formula of the BTP in comparison with the parent compound.

^{v)} Log D_{ow} values were predicted by MarvinSketch version 14.10.20.0 at pH 7.9 and 25 °C. Log D_{ow} values correspond to corrected log K_{ow} values to account for pH-dependent dissociation. At pH 7.9 all selected target compounds are neutral thus log D_{ow} is equal to log K_{ow}.

If different positional isomers are possible for one BTP, a range of log D_{ow} values is given.

^{vi)} D: diagnostic fragment for one structure; d: diagnostic fragment for positional isomers; e: enzyme deconjugation; l: structure reported in literature; m: MS/MS data from literature; p: biotransformation pathway information; d, p: diagnostic fragment for positional isomers (d) in combination with pathway information (p) give evidence for one possible structure.

^{vii)} Levels are defined as follows: 5 (exact mass), 4 (unequivocal molecular formula), 3 (tentative candidates: e.g., positional isomers), 2 (probable structure: library spectrum match (a) or diagnostic evidence for one structure (b)) and 1 (confirmed structure).

^{viii)} No mean value is reported due to inconsistent medium concentrations in the replicate sample. For details refer to SI I.

2.3.2 Influence of Azole Biotransformation on Bioaccumulation

Toxicokinetic Modeling of Epoxiconazole and Prochloraz: Assumptions, Difficulties, Parameter Estimation, and Parameter Correlation

Epoxiconazole and prochloraz were selected to investigate toxicokinetic processes since they exhibited highest bioaccumulation and most diverse biotransformation reactions in the screening experiment. To avoid potential toxic effects caused by bioaccumulation lower exposure concentrations ($100 \mu\text{g L}^{-1}$) were chosen compared to those used in the screening experiment ($200 \mu\text{g L}^{-1}$). Therefore, three BTPs each for epoxiconazole and prochloraz were not detected during the kinetic experiment, as they already showed low peak intensities in the screening experiment ($1 \cdot 10^6 - 2 \cdot 10^6$).

All three BTPs detected for epoxiconazole were modeled as primary BTPs because no direct precursor was observed. Obviously, some BTPs have formed in several consecutive steps, yet we did not observe the intermediate products.

The estimation of kinetic rate constant was challenging for prochloraz due to the high number of identified BTPs (15). The number of BTPs defines the number of parameters ($k_{M1, 1st / 2nd}$ - $k_{Mx, 1st / 2nd}$ and $k_{eM1, 1st / 2nd} - k_{eMx, 1st / 2nd}$) built-into the model equations necessary to describe the time series of the internal concentration of each BTP. If too many parameters have to be fitted based on the number of underlying data, then the model becomes less reliable. In order to decrease the number of parameters, the use of reaction types rather than single BTPs was considered. But this adjustment did not help to decrease the number of parameters because BTPs were predominantly formed by more than one reaction (e.g., PRZ_M353: partial loss of the hydroxylated imidazole ring and further oxidation to an aldehyde).

As a first step we tried to elucidate the biotransformation pathway, to identify primary and secondary BTPs and thereby define the model equations. BTPs were formed without delay, i.e., no chronology of formation was observed, which would have assisted in pathway elucidation. We propose the biotransformation pathway of prochloraz depicted in Figure 2-2 based on common drug biotransformation reactions, metabolic logic and known reactions occurring at the imidazole ring.⁴⁴⁻⁴⁵ The cascade of reactions taking place at the imidazole ring is described to start via an epoxide formation at the double bond between C4-C5. The proposed pathway was reviewed by model calibration and by profiling likelihoods to calculate robust confidence intervals for each parameter. In general, the proposed pathway is supported by the model results and the modeled outcome is depicted in Figure 2-3 (see also SI H). However, the elimination rate constants of two secondary BTPs ($k_{eM, PRZ_M325, 2nd}$, $k_{eM, PRZ_M310, 2nd}$) resulted in confidence intervals that hit the limits of the parameter values. Moreover, the elimination rate constants of four BTPs ($k_{eM, PRZ_M298, 2nd}$, $k_{eM, PRZ_M382, 2nd}$, $k_{eM, PRZ_M392a, 1st}$, $k_{eM, PRZ_M392b, 1st}$) exhibited large confidence intervals, where the limits of the parameter values ranged up to four orders of magnitude (see SI H). Reasons for unidentified parameters or large confidence intervals might be the not fully elucidated model structure with its high number of parameters, or possible correlation of some parameters to one or more others. A Bayesian correlation analysis was conducted that confirmed the latter

assumption (see SI H). Experimentally determined rate constants of BTPs would have helped to decrease the model uncertainty but this was not possible since the BTPs were not commercially available as reference standards.

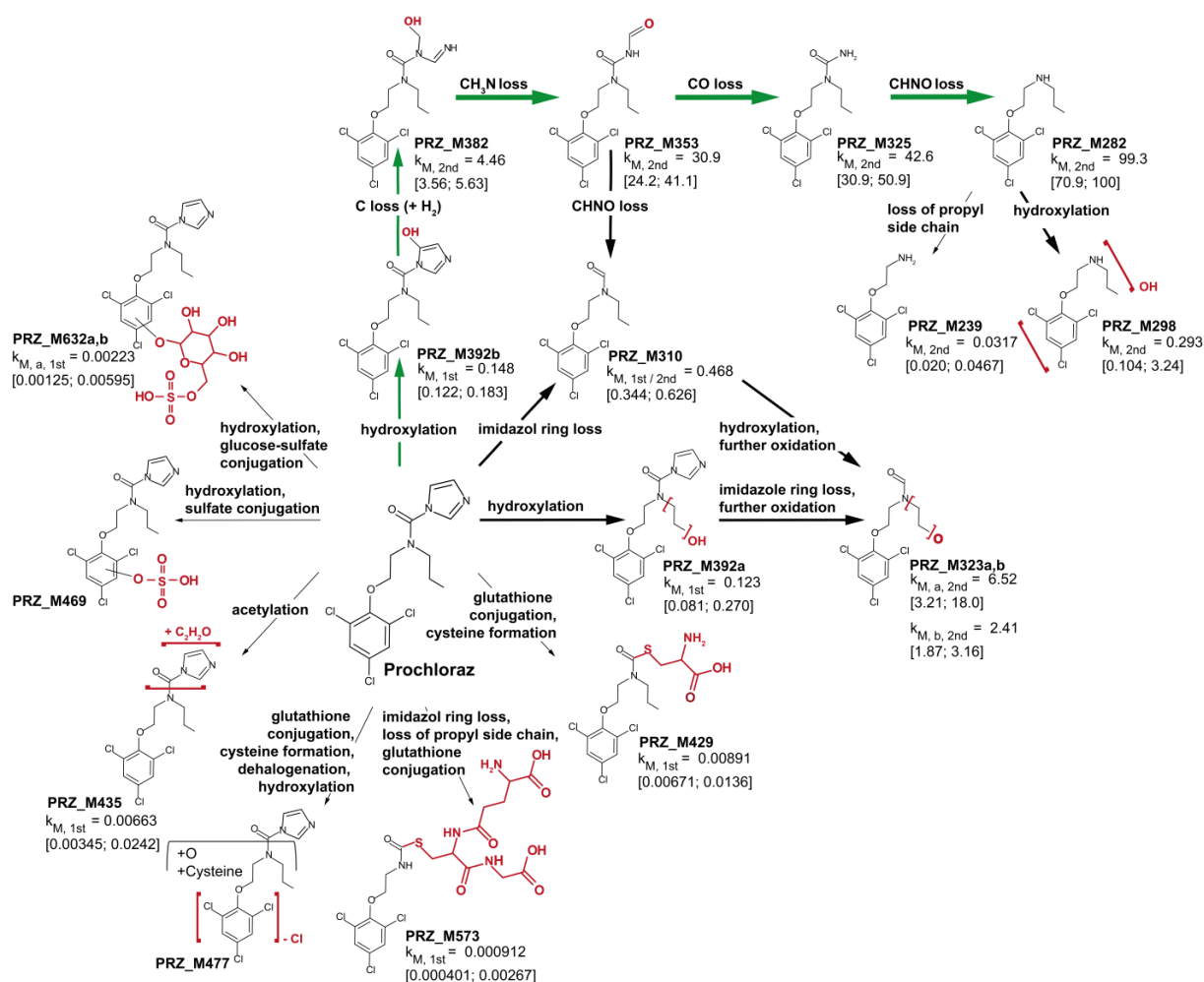


Figure 2-2: Proposed biotransformation pathway for prochloraz in *G. pulex*. Modeled biotransformation rate constants $k_{M,1st}$ and $k_{M,2nd}$ [d⁻¹] are displayed for all BTPs detected during the kinetic experiment. Limits of the 95% confidence interval are given in brackets. The structural changes of the BTPs are highlighted in red. Thin (k_M : 0 - 0.05 d⁻¹), middle (k_M : > 0.05 - 10 d⁻¹), and thick (k_M : > 10 - 100 d⁻¹) arrows differentiate between the magnitude of biotransformation. Green arrows display the pathway of imidazole ring oxidation that leads to the formation of the main BTP PRZ_M282 exhibiting the largest biotransformation rate k_M .

Significance of Azole Biotransformation: Toxicokinetics and Comparison of Internal Concentrations of Biotransformation Products and Parent Compounds

Despite the uncertainty of some model parameters, the one compartment first-order kinetic model was successfully fitted to the experimental data. Measured and modeled time courses of whole body internal concentrations of epoxiconazole, prochloraz, and their respective BTPs are represented in Figure 2-3. Internal concentrations stopped increasing after 17.5 h, indicating that steady state was reached. The much higher uptake rate k_u in comparison to the total elimination ($k_e + k_{M1, 1st} + \dots + k_{Mx, 1st}$) resulted in bioaccumulation for prochloraz and epoxiconazole. BAF_k s derived from the kinetic rate constants are in good agreement with BAF s based on steady state calculated from the internal concentration of the parent compound and the concentration of the exposure medium after 24 h exposure (see Table 2-1). If the assumption of steady state was inaccurate, rather lower BAF s based on internal concentrations would be expected compared to BAF_k s. Our kinetic and steady state BAF s (approximately $9 - 50 \text{ L kg}_{ww}^{-1}$) are in the same range to BAF s obtained in gammarids in previous studies (approximately $1 - 400 \text{ L kg}_{ww}^{-1}$) for micropollutants with similar $\log K_{ow}$ values.^{6, 30-31, 63} As defined in REACH, Annex XIII compounds are considered as bioaccumulative with BAF s $> 2000 \text{ L kg}^{-1}$.⁶⁴ Thus, azoles showed low bioaccumulation compared to the REACH criteria. Azoles potentially adsorbed to the exoskeleton of gammarids can influence the determination of BAF s by overestimating internal concentrations and uptake rates. Miller et al. (2016)⁶⁵ analyzed the exoskeletons of gammarids that molted during the exposure period. They observed that the percentage of the adsorbed fraction on the total chemical mass in the animal was between 3 and 24% for five out of eight pharmaceuticals studied. As these pharmaceuticals are ionic, they will more easily adsorb to the animal cuticle composed of calcium carbonate and chitin than the neutral azole fungicides. Consequently, we believe that the amount of adsorbed azoles does not significantly influence our determined BAF s. At the end of the 5 d depuration phase both parent compounds were almost completely eliminated to 1-2% of the highest internal concentration measured.

For epoxiconazole biotransformation contributed little to the elimination of the parent compound and thus to the reduction of bioaccumulation. This is expressed by around 3 orders of magnitude smaller biotransformation rate constants $k_{Mx, 1st}$ in comparison to the direct elimination k_e of epoxiconazole (for exact values refer to SI H).

For prochloraz a different pattern was observed. Primary biotransformation rate constants $k_{Mx, 1st}$ of BTPs that are not transformed further were also around three orders of magnitude smaller than the direct elimination k_e of prochloraz. However, especially the secondary BTPs PRZ_282, PRZ_M325, and PRZ_M353, each characterized by ring cleavage, were formed with biotransformation rate constants $k_{Mx, 2nd}$ that are 1 order of magnitude higher than the direct elimination of prochloraz. The major BTP PRZ_M282 reached mean internal concentrations of approximately 40% of those of the parent compound after 24 h exposure.

For the remaining studied azoles, where no kinetic study was performed, internal concentrations of the parent compound and their corresponding BTPs were compared after 24 h. Internal BTP concentrations of cyproconazole, propiconazole, tebuconazole, and ketoconazole were up to 3 orders of magnitude lower than the concentrations of the appropriate parent compounds ($2 \cdot 10^3$ - $2 \cdot 10^4$ nmol kg_{ww}⁻¹). These low internal concentrations indicate that biotransformation only plays a minor role regarding bioaccumulation and the elimination of the parent compounds. Consequently, prochloraz is the only studied azole fungicide where biotransformation (mainly hydroxylation and ring loss) adds to the reduction of bioaccumulation.

Only one study on toxicokinetics including biotransformation of azole fungicides in aquatic organisms was found. Konwick et al. (2006)⁶⁶ have shown that biotransformation highly contributes to the elimination of selected azoles in rainbow trout.

Biotransformation of azoles resulted in more polar compounds (see log D_{ow} values in Table 2-1) that were mostly retained longer in the organism in comparison with the parent compound (see $t_{1/2}$ depicted in Figure 2-3; for details on polarity of BTPs refer to SI J). These findings are in agreement with the results of other studies, that did not observe a simple relationship between elimination kinetics and hydrophobicity either.^{30-31, 63, 66} The slower elimination of hydrophilic molecules can be explained by the impaired transport across hydrophobic cell membranes, although their intracellular mobility is increased.⁶⁷

Biotransformation kinetics of organic compounds in gammarids differ widely among compounds. Ashauer et al. (2012)³⁰ have observed that biotransformation dominated toxicokinetics (log K_{ow} of the 15 studied compounds from 0.33-5.18). Richter and Nagel (2007)⁶⁸ have also found higher BTP concentrations compared to the two investigated parent compounds (log K_{ow} 2.9 and 5.3, respectively), whereas our results are comparable with the findings of Jeon et al. (2013)³¹ for irgarol (log D_{ow}: 2.9).

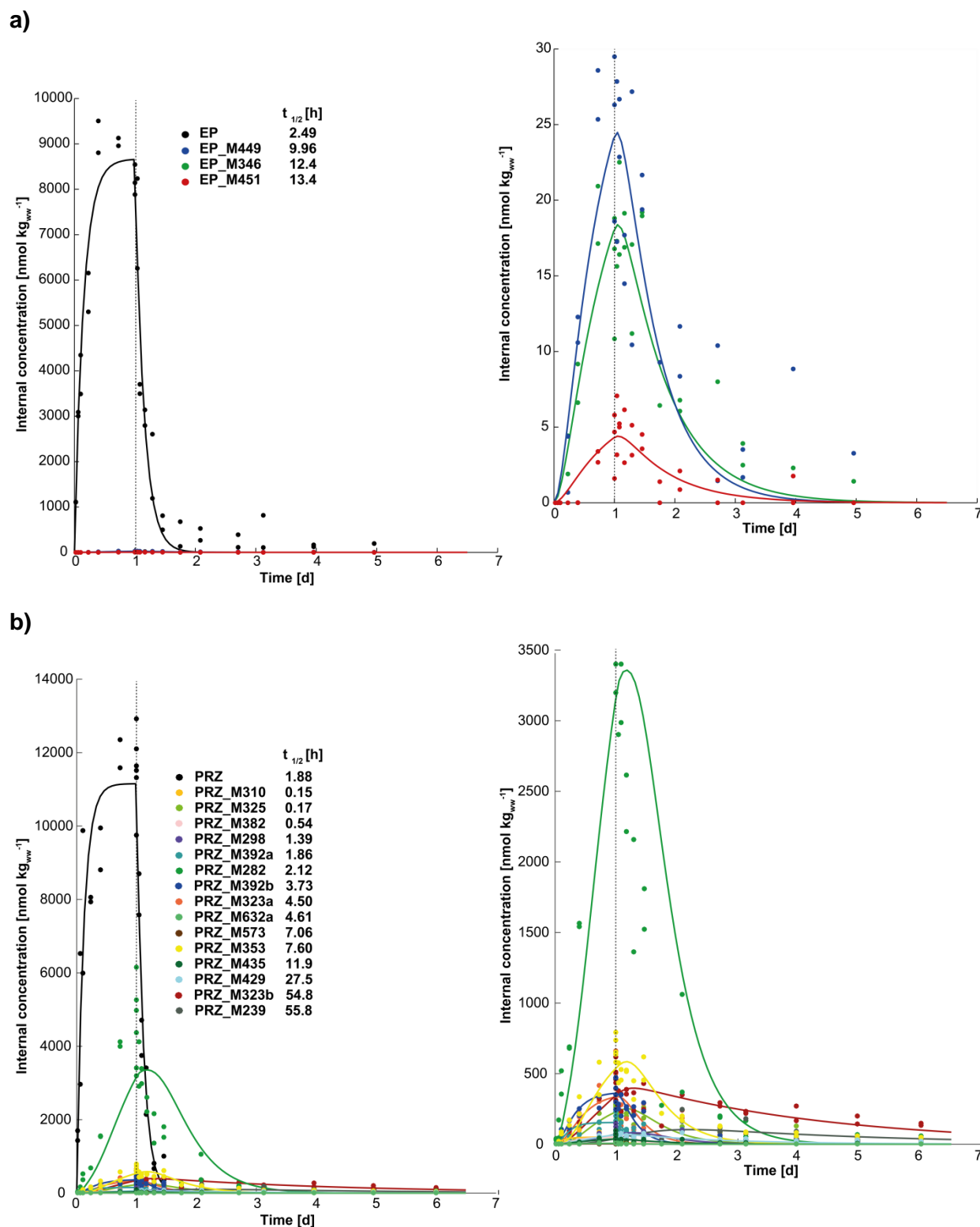


Figure 2-3: Measured (dots) and modeled (lines) time series of internal concentrations of epoxiconazole (a) and prochloraz (b) and their biotransformation products in *G. pullex* in the uptake and depuration phase as well as modeled elimination half-lives ($t_{1/2}$). The dashed vertical line indicates the change from uptake (1 d) to depuration (5 d). In the panels on the right the y-axis has been expanded to show the kinetics of the less concentrated BTPs.

2.3.3 Environmental Relevance

Our results confirm that the extent of biotransformation of organic xenobiotics is highly substance- and species-specific.^{30-31, 42, 69-70} Predicting BTPs based on common drug biotransformation reactions such as oxidations by CYP enzymes is feasible and was successfully applied in this study, assuming CYPs to be present among different organismal levels and species.^{42, 61, 71-72} However, toxicokinetic processes that determine the internal concentration quantitatively and thus the effect of a chemical are extremely difficult to predict. Uptake rate constants for small aquatic invertebrates seem to be mainly diffusion driven and dependent on the physicochemical properties as well as on the individual test species, whereas no simple relationship exists between elimination rate constants and hydrophobicity.^{30-31, 63, 66, 73-74}

We have shown that aside from prochloraz, azole BTPs were formed at low concentrations and most biotransformation reactions did not take place at the active moiety, indicating that the antifungal activity as well as the CYP inhibitory capacity of azoles is preserved. This can be of concern for organisms that are exposed to chemical mixtures containing an azole fungicide, as azoles might influence the bioaccumulation potential of other chemicals by inhibiting the CYP-catalyzed biotransformation reactions. Therefore, a better understanding of inhibition, induction, expression, and activity of CYPs towards chemicals in aquatic organisms is necessary to improve the link between exposure concentration, internal concentration at the target site, and effects – also in terms of environmental risk assessment.

Acknowledgment

Special thanks go to Tjalling Jager (DEBtox Research) for helpful discussion and assistance with toxicokinetic modeling and programming, and to Emma Schymanski (Eawag) for help in computational MS/MS spectra annotation. Furthermore, we thank Birgit Beck (Eawag) for support in field sampling and chemical analysis, Andreas Scheidegger (Eawag) for advise with statistics, and Jennifer Schollée (Eawag) for reading the manuscript. This research was funded by the Swiss National Science Foundation, grant number 315230141190.

References

- [1] IUPAC International Union of Pure and Applied Chemistry. Pesticide Properties Database. <http://sitem.herts.ac.uk/aeru/iupac/>.
- [2] Kahle, M.; Buerge, I. J.; Hauser, A.; Müller, M. D.; Poiger, T., Azole Fungicides: Occurrence and Fate in Wastewater and Surface Waters. *Environmental Science & Technology* **2008**, *42* (19), 7193-7200.
- [3] Battaglin, W.; Sandstrom, M.; Kuivila, K.; Kolpin, D.; Meyer, M., Occurrence of Azoxystrobin, Propiconazole, and Selected Other Fungicides in US Streams, 2005–2006. *Water Air Soil Pollut* **2011**, *218* (1-4), 307-322.
- [4] Kuzmanović, M.; Ginebreda, A.; Petrović, M.; Barceló, D., Risk assessment based prioritization of 200 organic micropollutants in 4 Iberian rivers. *Sci. Total Environ.* **2015**, *503-504*, 289-299.
- [5] Moschet, C.; Wittmer, I.; Simovic, J.; Junghans, M.; Piazzoli, A.; Singer, H.; Stamm, C.; Leu, C.; Hollender, J., How a complete pesticide screening changes the assessment of surface water quality. *Environ. Sci. Technol.* **2014**, *48* (10), 5423-5432.
- [6] Nyman, A. M.; Schirmer, K.; Ashauer, R., Toxicokinetic-toxicodynamic modelling of survival of *Gammarus pulex* in multiple pulse exposures to propiconazole: Model assumptions, calibration data requirements and predictive power. *Ecotoxicology* **2012**, *21* (7), 1828-1840.
- [7] Adam, O.; Badot, P. M.; Degiorgi, F.; Crini, G., Mixture toxicity assessment of wood preservative pesticides in the freshwater amphipod *Gammarus pulex* (L.). *Ecotoxicology and Environmental Safety* **2009**, *72* (2), 441-449.
- [8] Estimation Programs Interface Suite™ for Microsoft® Windows, v 4.11. United States Environmental Protection Agency, Washington, DC, USA. 2013.
- [9] Beketov, M. A.; Liess, M., Potential of 11 pesticides to initiate downstream drift of stream macroinvertebrates. *Arch. Environ. Contam. Toxicol.* **2008**, *55* (2), 247-53.
- [10] Haeba, M. H.; Hilscherova, K.; Mazurova, E.; Blaha, L., Selected endocrine disrupting compounds (vinclozolin, flutamide, ketoconazole and dicofol): Effects on survival, occurrence of males, growth, molting and reproduction of *Daphnia magna*. *Environ Sci Pollut Res* **2008**, *15* (3), 222-227.
- [11] Henry, M. J.; Sisler, H. D., Effects of sterol biosynthesis-inhibiting (SBI) fungicides on cytochrome P-450 oxygenations in fungi. *Pestic. Biochem. Physiol.* **1984**, *22* (3), 262-275.
- [12] Copping, L. G.; Hewitt, H. G., Chemistry and Mode of Action of Crop Protection agents. *Royal Society of Chemistry Cambridge, UK* **1998**.
- [13] Cedergreen, N., Quantifying synergy: A systematic review of mixture toxicity studies within environmental toxicology. *PLoS ONE* **2014**, *9* (5), e96580.
- [14] Bjergager, M.-B. A.; Hanson, M. L.; Lissemore, L.; Henriquez, N.; Solomon, K. R.; Cedergreen, N., Synergy in microcosms with environmentally realistic concentrations of prochloraz and esfenvalerate. *Aquat. Toxicol.* **2011**, *101* (2), 412-422.
- [15] Bjergager, M.-B. A.; Hanson, M. L.; Solomon, K. R.; Cedergreen, N., Synergy between prochloraz and esfenvalerate in *Daphnia magna* from acute and subchronic exposures in the laboratory and microcosms. *Aquatic toxicology* **2012**, *110-111* (0), 17-24.
- [16] Cedergreen, N.; Kamper, A.; Streibig, J. C., Is prochloraz a potent synergist across aquatic species? A study on bacteria, daphnia, algae and higher plants. *Aquat. Toxicol.* **2006**, *78* (3), 243-252.
- [17] Nørgaard, K. B.; Cedergreen, N., Pesticide cocktails can interact synergistically on aquatic crustaceans. *Environ Sci Pollut Res* **2010**, *17* (4), 957-967.
- [18] Von Der Ohe, P. C.; Liess, M., Relative sensitivity distribution of aquatic invertebrates to organic and metal compounds. *Environ. Toxicol. Chem.* **2004**, *23* (1), 150-156.
- [19] Kunz, P. Y.; Kienle, C.; Gerhardt, A., *Gammarus* spp. in aquatic ecotoxicology and water quality assessment: toward integrated multilevel tests. *Rev. Environ. Contam. Toxicol.* **2010**, *205*, 1-76.

- [20] Maltby, L.; Clayton, S. A.; Wood, R. M.; McLoughlin, N., Evaluation of the *Gammarus pulex* in situ feeding assay as a biomonitor of water quality: Robustness, responsiveness, and relevance. *Environ. Toxicol. Chem.* **2002**, *21* (2), 361-368.
- [21] Macneil, C.; Dick, J. T. A.; Elwood, R. W., The trophic ecology of freshwater *Gammarus* spp. (Crustacea: Amphipoda): Problems and perspectives concerning the functional feeding group concept. *Biological Reviews of the Cambridge Philosophical Society* **1997**, *72* (3), 349-364.
- [22] Ashauer, R.; Escher, B. I., Advantages of toxicokinetic and toxicodynamic modelling in aquatic ecotoxicology and risk assessment. *J. Environ. Monit.* **2010**, *12* (11), 2056-2061.
- [23] Landrum, P. F.; Lee li, H.; Lydy, M. J., Toxicokinetics in aquatic systems: Model comparisons and use in hazard assessment. *Environ. Toxicol. Chem.* **1992**, *11* (12), 1709-1725.
- [24] Ladewig, V.; Jungmann, D.; Koehler, A.; Schirling, M.; Triebkorn, R.; Nagel, R., Intersexuality in *Gammarus fossarum* Koch, 1835 (Amphipoda). *Crustaceana* **2002**, *75*, 1289-1299.
- [25] Naylor, C.; Maltby, L.; Calow, P., Scope for growth in *Gammarus pulex*, a freshwater benthic detritivore. *Hydrobiologia* **1989**, *188-189* (1), 517-523.
- [26] Jeon, J.; Kurth, D.; Hollender, J., Biotransformation pathways of biocides and pharmaceuticals in freshwater crustaceans based on structure elucidation of metabolites using high resolution mass spectrometry. *Chem. Res. Toxicol.* **2013**, *26* (3), 313-24.
- [27] Meringer, M.; Reinker, S.; Zhang, J.; Muller, A., MS/MS Data Improves Automated Determination of Molecular Formulas by Mass Spectrometry. *Match-Communications in Mathematical and in Computer Chemistry* **2011**, *65* (2), 259-290.
- [28] Kukkonen, J.; Oikari, A., Sulphate conjugation is the main route of pentachlorophenol metabolism in *Daphnia magna*. *Comparative Biochemistry and Physiology - C Pharmacology Toxicology and Endocrinology* **1988**, *91* (2), 465-468.
- [29] Schymanski, E. L.; Jeon, J.; Gulde, R.; Fenner, K.; Ruff, M.; Singer, H. P.; Hollender, J., Identifying Small Molecules via High Resolution Mass Spectrometry: Communicating Confidence. *Environmental Science & Technology* **2014**, *48* (4), 2097-2098.
- [30] Ashauer, R.; Hintermeister, A.; O'Connor, I.; Elumelu, M.; Hollender, J.; Escher, B. I., Significance of xenobiotic metabolism for bioaccumulation kinetics of organic chemicals in *gammarus pulex*. *Environ. Sci. Technol.* **2012**, *46* (6), 3498-3508.
- [31] Jeon, J.; Kurth, D.; Ashauer, R.; Hollender, J., Comparative toxicokinetics of organic micropollutants in freshwater crustaceans. *Environ. Sci. Technol.* **2013**, *47* (15), 8809-17.
- [32] European Mass Bank Server (NORMAN MassBank) www.massbank.eu.
- [33] Gubbins, P. O.; Amsden, J. R., Drug-drug interactions of antifungal agents and implications for patient care. *Expert Opin. Pharmacother.* **2005**, *6* (13), 2231-2243.
- [34] Peng, X.; Huang, Q.; Zhang, K.; Yu, Y.; Wang, Z.; Wang, C., Distribution, behavior and fate of azole antifungals during mechanical, biological, and chemical treatments in sewage treatment plants in China. *Sci. Total Environ.* **2012**, *426*, 311-317.
- [35] Brammer, K. W.; Coakley, A. J.; Jezequel, S. G.; Tarbit, M. H., The disposition and metabolism of C-14 fluconazole in humans. *Drug Metabolism and Disposition* **1991**, *19* (4), 764-767.
- [36] Ikenaka, Y.; Eun, H.; Ishizaka, M.; Miyabara, Y., Metabolism of pyrene by aquatic crustacean, *Daphnia magna*. *Aquat. Toxicol.* **2006**, *80* (2), 158-165.
- [37] Ikenaka, Y.; Ishizaka, M.; Eun, H.; Miyabara, Y., Glucose-sulfate conjugates as a new phase II metabolite formed by aquatic crustaceans. *Biochem. Biophys. Res. Commun.* **2007**, *360* (2), 490-495.
- [38] Sinsheimer, J. E.; Van Den Eeckhout, E.; Hooberman, B. H.; Beylin, V. G., Detoxication of aliphatic epoxides by diol formation and glutathione conjugation. *Chem. Biol. Interact.* **1987**, *63* (1), 75-90.
- [39] Quistad, G. B., Novel Polar Xenobiotic Conjugates. *ACS Symp. Ser.* **1986**, *299*, 221-241.
- [40] Wilkinson, C. F., Xenobiotic Conjugation in Insects. *ACS Symp. Ser.* **1986**, *299*, 48-61.

- [41] Testa, B.; Kraemer, S. D., The Biochemistry of Drug Metabolism - An Introduction Part 4. Reactions of Conjugation and Their Enzymes. *Chemistry & Biodiversity* **2008**, *5* (11), 2171-2336.
- [42] Katagi, T., Bioconcentration, Bioaccumulation, and Metabolism of Pesticides in Aquatic Organisms. In *Reviews of Environmental Contamination and Toxicology, Vol 204*, Whitacre, D. M., Ed. 2010; Vol. 204, pp 1-132.
- [43] Gulde, R.; Meier, U.; Schymanski, E. L.; Kohler, H.-P. E.; Helbling, D. E.; Derrer, S.; Rentsch, D.; Fenner, K., Systematic Exploration of Biotransformation Reactions of Amine-Containing Micropollutants in Activated Sludge. *Environmental Science & Technology* **2016**, *50* (6), 2908-2920.
- [44] Dalvie, D. K.; Kalgutkar, A. S.; Khojasteh-Bakht, S. C.; Obach, R. S.; O'Donnell, J. P., Biotransformation reactions of five-membered aromatic heterocyclic rings. *Chem. Res. Toxicol.* **2002**, *15* (3), 269-299.
- [45] Obach, R. S., Functional Group Biotransformations. In *Handbook of Metabolic Pathways of Xenobiotics*, John Wiley & Sons, Ltd: 2014.
- [46] Kraemer, S. D.; Testa, B., The Biochemistry of Drug Metabolism - An Introduction Part 7. Intra-Individual Factors Affecting Drug Metabolism. *Chemistry & Biodiversity* **2009**, *6* (10), 1477-1660.
- [47] Bjergager, M. B.; Hanson, M. L.; Solomon, K. R.; Cedergreen, N., Synergy between prochloraz and esfenvalerate in *Daphnia magna* from acute and subchronic exposures in the laboratory and microcosms. *Aquat. Toxicol.* **2012**, *110-111*, 17-24.
- [48] Gottardi, M.; Kretschmann, A.; Cedergreen, N., Measuring cytochrome P450 activity in aquatic invertebrates: a critical evaluation of in vitro and in vivo methods. *Ecotoxicology* **2015**, *25* (2), 419-430.
- [49] Needham, D.; Challis, I. R., The metabolism and excretion of prochloraz, an imidazole-based fungicide, in the rat. *Xenobiotica* **1991**, *21* (11), 1473-1482.
- [50] Laignelet, L.; Riviere, J. L.; Lhuguenot, J. C., Metabolism of an imidazole fungicide (prochloraz) in the rat after oral administration. *Food Chem. Toxicol.* **1992**, *30* (7), 575-583.
- [51] Debrauwer, L.; Rathahao, E.; Boudry, G.; Baradat, M.; Cravedi, J. P., Identification of the major metabolites of prochloraz in rainbow trout by liquid chromatography and tandem mass spectrometry. *J. Agric. Food. Chem.* **2001**, *49* (8), 3821-3826.
- [52] Roberts, T. R.; Hutson, D. H., Metabolic Pathways of Agrochemicals: Part 2, Insecticides and fungicides. *Royal Society of Chemistry* **1999**.
- [53] James, M. O., Conjugation of organic pollutants in aquatic species. *Environ. Health Perspect.* **1987**, *Vol. 71*, 97-103.
- [54] Venkatakrishnan, K.; von Moltke, L. L.; Greenblatt, D. J., Effects of the antifungal agents on oxidative drug metabolism - Clinical relevance. *Clin. Pharmacokinet.* **2000**, *38* (2), 111-180.
- [55] Whitehouse, L. W.; Menzies, A.; Dawson, B.; Cyr, T. D.; By, A. W.; Black, D. B.; Zamecnik, J., Mouse hepatic metabolites of ketoconazole - isolation and structure elucidation. *J. Pharm. Biomed. Anal.* **1994**, *12* (11), 1425-1441.
- [56] Whitehouse, L. W.; Menzies, A.; Dawson, B.; Zamecnik, J.; Sy, W. W., Deacetylated ketoconazole - a major ketoconazole metabolite isolated from mouse-liver. *J. Pharm. Biomed. Anal.* **1990**, *8* (7), 603-606.
- [57] Fitch, W. L.; Tran, T.; Young, M.; Liu, L.; Chen, Y., Revisiting the metabolism of ketoconazole using accurate mass. *Drug metabolism letters* **2009**, *3* (3), 191-8.
- [58] Obanda, D. N.; Shupe, T. F., Biotransformation of tebuconazole by microorganisms: Evidence of a common mechanism. *Wood and Fiber Science* **2009**, *41* (2), 157-167.
- [59] Obanda, D. N.; Shupe, T. F.; Catallo, W. J., Resistance of *Trichoderma harzianum* to the biocide tebuconazol - Proposed biodegradation pathways. *Holzforschung* **2008**, *62* (5), 613-619.
- [60] Mercadante, R.; Polledri, E.; Scurati, S.; Moretto, A.; Fustinoni, S., Identification and quantification of metabolites of the fungicide tebuconazole in human urine. *Chem. Res. Toxicol.* **2014**, *27* (11), 1943-1949.

- [61] Mazur, C. S.; Kenneke, J. F., Cross-species comparison of conazole fungicide metabolites using rat and rainbow trout (*Onchorhynchus mykiss*) hepatic microsomes and purified human CYP 3A4. *Environmental Science & Technology* **2008**, *42* (3), 947-954.
- [62] INCHEM IPCS International Program on Chemical Safety. <http://www.inchem.org/documents/jmpr/jmpmono/v94pr10.htm>.
- [63] Ashauer, R.; Caravatti, I.; Hintermeister, A.; Escher, B. I., Bioaccumulation kinetics of organic xenobiotic pollutants in the freshwater invertebrate *Gammarus pulex* modeled with prediction intervals. *Environ. Toxicol. Chem.* **2010**, *29* (7), 1625-36.
- [64] EC. Regulation No. 1907/2006 of the European Parliament and of the Council Concerning the Registration, Evaluation, Authorization and Restriction of Chemicals. 2006.
- [65] Miller, T. H.; McEneff, G. L.; Stott, L. C.; Owen, S. F.; Bury, N. R.; Barron, L. P., Assessing the reliability of uptake and elimination kinetics modelling approaches for estimating bioconcentration factors in the freshwater invertebrate, *Gammarus pulex*. *Sci. Total Environ.* **2016**, *547*, 396-404.
- [66] Konwick, B. J.; Garrison, A. W.; Avants, J. K.; Fisk, A. T., Bioaccumulation and biotransformation of chiral triazole fungicides in rainbow trout (*Oncorhynchus mykiss*). *Aquat. Toxicol.* **2006**, *80* (4), 372-81.
- [67] Gobas, F. A. P. C.; Opperhuizen, A.; Hutzinger, O., Bioconcentration of hydrophobic chemicals in fish: Relationship with membrane permeation. *Environ. Toxicol. Chem.* **1986**, *5* (7), 637-646.
- [68] Richter, S.; Nagel, R., Bioconcentration, biomagnification and metabolism of 14C-terbutryn and 14C-benzo[a]pyrene in *Gammarus fossarum* and *Asellus aquaticus*. *Chemosphere* **2007**, *66* (4), 603-610.
- [69] Livingstone, D. R., The fate of organic xenobiotics in aquatic ecosystems: Quantitative and qualitative differences in biotransformation by invertebrates and fish. *Comparative Biochemistry and Physiology - A Molecular and Integrative Physiology* **1998**, *120* (1), 43-49.
- [70] Nuutinen, S.; Landrum, P. F.; Schuler, L. J.; Kukkonen, J. V. K.; Lydy, M. J., Toxicokinetics of organic contaminants in *Hyalella azteca*. *Archives of Environmental Contamination and Toxicology* **2003**, *44* (4), 467-475.
- [71] Sole, M.; Livingstone, D. R., Components of the cytochrome P450-dependent monooxygenase system and 'NADPH-independent benzo a pyrene hydroxylase' activity in a wide range of marine invertebrate species. *Comparative Biochemistry and Physiology C-Toxicology & Pharmacology* **2005**, *141* (1), 20-31.
- [72] Snyder, M. J., Cytochrome P450 enzymes in aquatic invertebrates: Recent advances and future directions. *Aquat. Toxicol.* **2000**, *48* (4), 529-547.
- [73] Rubach, M. N.; Ashauer, R.; Maund, S. J.; Baird, D. J.; Van den Brink, P. J., Toxicokinetic variation in 15 freshwater arthropod species exposed to the insecticide chlorpyrifos. *Environ. Toxicol. Chem.* **2010**, *29* (10), 2225-34.
- [74] Meredith-Williams, M.; Carter, L. J.; Fussell, R.; Raffaelli, D.; Ashauer, R.; Boxall, A. B., Uptake and depuration of pharmaceuticals in aquatic invertebrates. *Environ. Pollut.* **2012**, *165*, 250-8.

Chapter S2. Supporting Information:
How Biotransformation influences Toxicokinetics of Azole Fungicides in the Aquatic Invertebrate *Gammarus pulex*

Andrea Rösch^{1,2}, Sabine Anliker^{1,2}, Juliane Hollender^{1,2*}

¹ Eawag, Swiss Federal Institute of Aquatic Science and Technology, 8600 Dübendorf, Switzerland

² Institute of Biogeochemistry and Pollutant Dynamics, ETH Zürich, 8092 Zürich, Switzerland

* Corresponding Author: Phone: +41 58 765 5493. e-mail: juliane.hollender@eawag.ch

Published in *Environmental Science and Technology*, DOI: 10.1021/acs.est.6b01301

SI.A Chemicals and Solutions

Table S2-1: Azole fungicides. All standard solutions were prepared in MeOH.

Substance	CAS number	Supplier	Quality
Cyproconazole	94361-06-5	Dr. Ehrenstorfer	96%
Epoxiconazole	135319-73-2	Dr. Ehrenstorfer	99%
Fluconazole	86386-73-4	Dr. Ehrenstorfer	99%
Fluconazole-d4		Toronto Research Chemicals	
Ketoconazole	65277-42-1	Sigma-Aldrich	98%
Propiconazole	60207-90-1	Dr. Ehrenstorfer	96.7%
Propiconazole-d5		Dr. Ehrenstorfer	
Prochloraz	67747-09-5	Dr. Ehrenstorfer	98.5%
Prochloraz-d7		Dr. Ehrenstorfer	
Tebuconazole	107534-96-3	Dr. Ehrenstorfer	98.5%
Tebuconazole-d6		Dr. Ehrenstorfer	

Table S2-2: Other chemicals and solutions.

Substance	CAS number	Supplier	Quality
Acetic acid	64-19-7	Merck	100%
Acetonitrile	75-05-8	Acros Organics	HPLC-grade
Ammonium acetate	631-61-8	Sigma-Aldrich	> 98%
Bovine Serum Albumin	9048-46-8	Sigma	> 96%
Calcium chloride	10035-04-8	Sigma-Aldrich	> 99%
Ethanol	64-17-5	Merck	Analytical grade
Formic acid	64-18-6	Merck	98-100%
Magnesium sulfate	10034-99-8	Sigma-Aldrich	> 99%
Isopropanol	67-63-0	Fisher Chemicals	
Methanol Optima	67-56-1	Fisher Chemicals	LC-MS grade
Potassium chloride	7447-40-7	Sigma-Aldrich	> 99%
Sodium acetate trihydrate	6131-90-4	Fluka	> 99.5%
Sodium hydrogen carbonate	144-55-8	Merck	
Sulfatase from patella vulgata	9016-17-5	Sigma	

SI.B Analytical Method

To minimize contamination of the MS with matrix components and to enrich the compounds of interest, gammarid extracts and medium samples were analyzed with an automated online-SPE procedure, as described in Jeon et al. (2013)¹. Directly before sample analysis 100 μL (BTP screening experiment) and 200 μL (toxicokinetic experiment) extract, respectively, were added to 20 mL headspace amber glass vials and filled up with 20 mL nanopure water.

The hardware used for the online-SPE LC-HRMS/MS analysis consisted of a tri-directional autosampler (HTC PAL, CTC Analytics), a dispenser syringe, a 20 mL sample loop, three LC pumps, two six-port valves, an empty online extraction cartridge (BGB Analytics), a mixer with a low volume mixing-chamber (Portmann Instruments AG) and a column oven (Portmann Instruments AG). A binary LC pump (Surveyor LC, Finnigan) was used for the sample loading, a quaternary low-pressure mixing gradient pump (Rheos 2200, Flux Instruments) for the SPE, an isocratic pump (Rehos 2000, Flux Instruments) for the water gradient.

The online-SPE process consists of three steps, loading, enrichment and elution.² The sample was loaded into the 20 mL sample loop via dual injection of 10 mL sample with the dispenser syringe. An in-house prepared mixed bed multilayer cartridge was used to enrich compounds of a broad range of different polarities and molecular sizes. The cartridge was filled with Oasis HLB (8-9 mg, 15 μm , Waters, USA) as first material and with a mixture (9-10 mg) of anion exchanger Strata X-AW, cation exchanger Strata X-CW (30 μm , Phenomenex, UK) and Env+ (Biotage, Sweden) in a ratio of 1:1:1.5 (X-AW : X-CW : ENV+) as second material.³ The sample was enriched together with the loading solution with a flow rate of 2 mL min^{-1} on the SPE cartridge. The loading solution consisted of nanopure water containing 2 mM ammonium acetate. The elution of the analytes from the SPE cartridge was performed with methanol (MeOH) containing 0.1% (vol.) formic acid in back-flush mode with a flow rate of 40 $\mu\text{L min}^{-1}$. To establish the initial conditions for the LC, the MeOH formic acid SPE eluate was mixed with water containing 0.1% formic acid in the mixing chamber prior to the analytical column. After every sample the loop and the SPE cartridge were rinsed with acetonitrile and then reconditioned with the loading solution (see Table S2-3). The use of two six-port valves enabled to load and extract the next sample (n+1) on the SPE cartridge during SPE and LC elution of a given sample (n).

Chromatographic separation was achieved on a XBridge C18 column (3.5 μm , 2.1x50 mm, Waters). The LC eluents were water and MeOH, both acidified with 0.1% (vol.) formic acid. LC was performed at 30 $^{\circ}\text{C}$ at a flow rate of 300 $\mu\text{L min}^{-1}$. The eluent composition and the applied gradient is shown in Table S2-4.

Detection of analytes was performed by using a quadrupole-orbitrap mass spectrometer (Q Exactive, Thermo Fisher Scientific Inc.) with electrospray ionization (ESI) in either positive or negative mode. Full scan acquisition for a mass range of 100 – 1000 m/z with a resolution of 70 000 (at m/z 200) was performed in polarity-switching mode followed by five (positive

mode) and two (negative mode) data-dependent MS/MS scans with a resolution of 17 500 (at m/z 200), an isolation window of 1 m/z and a “dynamic exclusion” of 3 sec.

For both ESI modes nitrogen was used as sheat gas at a flow rate of 40 L min^{-1} , as auxiliary gas at a flow rate of 10 L min^{-1} and a temperature of 40 °C and as collision gas. To obtain a more constant spray the sheat gas flow was set to 50 L min^{-1} , the auxiliary gas flow to 20 L min^{-1} and the auxiliary gas temperature was increased to 100 °C for the measurement sequence of the toxicokinetic experiment. Analyses were performed at a spray voltage of + 4 kV (positive mode) and – 3 kV (negative mode), a capillary temperature of 350 °C and S-lens level set at 50.

External mass calibration resulted in mass accuracies < 1 ppm for 11 amino acids with m/z between 116-997. For the MS/MS acquisition the resolving power was set to 17500 at m/z 200.

Specific compounds were remeasured in targeted mode with higher collision energies to get further fragment information for MS/MS spectra interpretation. Similar parameters to the above mentioned were used except for the resolving power in the MS/MS scan, which was set to 35 000 (at 200 m/z).

For triggering data-dependent MS/MS acquisition a mass list with suspected BTPs was set up. Three different approaches were used to predict possible BTPs which are (i) *in silico* pathway prediction (Eawag-PPS, formerly UM-PPS, <http://eawag-bbd.ethz.ch/predict/>, Eawag-PPS predicts microbial catabolic reactions based on biotransformation rules for reactions found in the Eawag-Biocatalysis/Biodegradation Database), (ii) manual prediction at which the most common enzymatic biotransformation reactions were considered including ring losses as well as all possible ring cleavages, and (iii) BTPs of azoles in any organism described in scientific literature were included as well. *In silico* pathway prediction using Eawag-PPS, which was developed for microbial biotransformation, was less successful. Particularly, Eawag-PPS does not include conjugation reactions and does not predict reactions taking place at the azole functional moiety.

Table S2-3: Time schedule of online-SPE. Gradient of the loading pump with ammonium acetate solution (2 mM in nanopure H₂O) and acetonitrile. Elution of the sample was performed via the elution pump, whereas loading of the sample was performed via the dispenser syringe. Acetonitrile was used to flush the sample loop and the SPE cartridge after every sample.

Time [min]	Ammonium acetate solution (2 mM) [$\mu\text{L min}^{-1}$]	Acetonitrile [$\mu\text{L min}^{-1}$]	SPE step
0.00	200		
0.10	0	2000	
0.60	0	2000	
0.65	2000		Elution of the sample from the cartridge (with elution pump) and washing of the loop
5.60	2000		
5.65	400		
6.20	400		
6.30		400	
13.9		400	Loading of the new sample into the loop and conditioning of the cartridge
14.00	400		
20.60	400		
20.70	2000		Enrichment of the new sample
32.00	2000		

Table S2-4: Time schedule of the LC gradient used for reversed-phase liquid chromatography (LC). Water and methanol were both acidified with 0.1% (vol.) formic acid.

Time [min]	H ₂ O [$\mu\text{L min}^{-1}$]	MeOH [$\mu\text{L min}^{-1}$]	Isopropanol [$\mu\text{L min}^{-1}$]
0.0	260	40	
0.4	260	40	
20.0	20	280	
20.2	20		280
26.0	20		280
26.2	260	40	
32.3	260	40	

SI.C Quality Control

Quantification was based on internal standard calibration. Isotopically labeled internal standards (ISTDs) were available for four (FLU, PRP, PRZ, TEB) out of the seven selected azoles. For the remaining three azoles the closest matching ISTD was used based on the structure and the retention time (tebuconazole-d6 was used for CP, EP and KET). A calibration curve in the concentration range of 0.5 – 3000 ng L⁻¹ with 16 calibration points was acquired at the beginning and the end of each measurement sequence. Concentrations were calculated by comparing the peak area ratio of the analyte and its internal standard to the corresponding ratio in the calibration standard curve. Calibration curves were obtained by linear least square regression using a weighting factor of 1/x. Calibration curves were linear ($R^2 > 0.99$) except for ketoconazole ($R^2 = 0.96$), where the least matching ISTD concerning structure and molecular weight was available. Amounts of BTPs were estimated based on the calibration curve of their parent compound since no reference standards could be obtained. Doing that relies on the assumption that the parent compound and its BTPs have similar ionization efficiencies what is obviously not necessarily the case. Jeon et al. (2013)⁴ tried to correct for the different ionization efficiencies of BTPs compared to the parent compounds by using physicochemical properties. Thereby quantification can be improved slightly, but still remains an approximation. Therefore, we did not calculate any conversion factors and the calculated sample amounts of the BTPs have to be regarded as an estimate.

The sulfate-containing BTPs can be detected more sensitively in negative ionization mode. But since all parent compounds and thereby the calibration curves were measured in positive ionization mode, the sulfate-containing BTPs were quantified in their less sensitive positive ionization mode.

Limits of quantification (LOQ) were calculated for the parent compounds in the gammarid extracts. Therefore, matrix correction factors were determined which reflect matrix effects resulting from sample preparation as well as from sample analysis (e.g., ion suppression) (see Table S2-5). Average matrix factors for all substances were below one (0.5-0.9), indicating that the sample matrix decreased the detector response of the analytes *i.e.*, leading to ionization suppression. LOQs were then derived by referencing the molar amount of the parent compound in the lowest calibration standard (0.01 ng absolute) to the average wet weight of the gammarids exposed to the corresponding parent compound and finally dividing this value by the calculated matrix factor.³ LOQs for all azoles were $< 0.5 \text{ nmol kg}_{\text{ww}}^{-1}$.¹ No LOQs could be calculated for the identified BTPs but since the quantification of the BTPs is based on the calibration curve of the corresponding parent compound it is assumed that LOQs of the BTPs are comparable to those of the corresponding parent compound.

¹ LOQs for gammarid extracts were recalculated, such that the molar amount of the parent compounds in the lowest calibration standard was adjusted to the average sample wet weight per injection, instead of the average sample wet weight per sample, as was previously done. Recalculation resulted in LOQs which were 10x higher than reported. This recalculation did not change the quantification and interpretation of the results however, since all reported values were still above the recalculated LOQs.

To report internal concentrations the measured amount of each substance was finally referred to the wet weight of the corresponding *G. pulex* sample.

Relative recoveries for the whole sample preparation and analytical procedure are displayed in Table S2-6 and the carry-over during the analytical measurement for parent compounds and isotopically labeled internal standards (ISTDs) is reported in Table S2-7.

Table S2-5: Calculated matrix factors for gammarid extracts and limits of quantification (LOQ) for the parent compounds in the exposure medium and in *G. pulex* extracts. Duplicate samples (prespike 1 and 2) were spiked before gammarid extraction with $50 \mu\text{g L}^{-1}$ (i.e., 5 ng absolute in $100 \mu\text{L}$ measured extract) and $100 \mu\text{g L}^{-1}$ (i.e., 10 ng absolute in $100 \mu\text{L}$ measured extract) of the parent compounds, respectively.

Compound	Matrix factors					LOQ ⁺	LOQ ⁺⁺
	Prespike 1 5 ng	Prespike 2 5 ng	Prespike 1 10 ng	Prespike 2 10 ng	Average	[ng L^{-1}]	[$\text{nmol kg}_{\text{ww}}^{-1}$]
Cyproconazole	0.8	0.7	0.6	0.6	0.7	0.8	0.4
Epoxiconazole	0.8	0.8	0.7	0.6	0.7	0.7	0.4
Fluconazole	1.0	1.0	0.8	0.7	0.9	0.6	0.3
Ketoconazole	0.5	0.5	0.5	0.5	0.5	1.0	0.3
Propiconazole	0.8	0.8	0.7	0.6	0.7	0.7	0.4
Prochloraz	0.8	0.8	0.7	0.7	0.8	0.7	0.3
Tebuconazole	0.8	0.8	0.7	0.6	0.7	0.7	0.3

⁺: LOQ for the exposure medium. No matrix factors have to be considered since the matrix of the artificial pond water did not lead to ion suppression compared to the calibration standards prepared in nanopure water (verified by comparing the peak areas of the internal standards). Therefore the LOQ of all azoles in the exposure medium is 0.5 ng L^{-1} .

⁺⁺: LOQ for gammarid extracts. Please refer to the footnote.

Table S2-6: Relative recoveries for the whole sample preparation and analytical procedure. Duplicate samples (prespike 1 and 2) spiked before the gammarid extraction with $50 \mu\text{g L}^{-1}$ (i.e., 5 ng absolute in $100 \mu\text{L}$ measured extract) and $100 \mu\text{g L}^{-1}$ (i.e., 10 ng absolute in $100 \mu\text{L}$ measured extract) of the parent compounds, respectively, were used to determine the recovery of the whole procedure of sample preparation and chemical analysis. Azoles without matching ISTD are marked with an asterisk.

Compound	Relative recovery [%]			
	Prespike 1 5 ng	Prespike 2 5 ng	Prespike 1 10 ng	Prespike 2 10 ng
Cyproconazole *	97	98	80	78
Epoxiconazole *	104	109	86	84
Fluconazole	116	116	104	100
Ketoconazole *	55	62	68	65
Propiconazole	116	115	102	95
Prochloraz	99	104	92	90
Tebuconazole	106	106	93	89

Table S2-7: Carry-over during the analytical measurement of the parent compounds and isotopically labeled internal standards (ISTDs). Blind 1 was measured directly after the 50 ng L⁻¹ calibration standard and blind 2 was measured after the 900 ng L⁻¹ calibration standard at the beginning of the measurement sequence. Blind 1 and 2: nanopure water spiked with 100 µL isotopically labeled internal standard solution (100 µg L⁻¹). Blank 1 was measured after a 50 ng L⁻¹ calibration standard. Blank 2 and Blank 3 were measured after gammarid extract samples. Blank 1, 2 and 3: nanopure water.

Compound	Carry-over [%]		
	Blind 1	Blind 2	
Cyproconazole	0.8	0.2	
Epoxiconazole	1.6	0.4	
Fluconazole	Not found	0.2	
Ketoconazole	16.0	6.4	
Propiconazole	0.4	0.3	
Prochloraz	2.9	1.9	
Tebuconazole	0.2	0.4	
	Blank 1	Blank 2	Blank 3
Fluconazole-d4	Not found	Not found	Not found
Prochloraz-d7	1.1	1.6	2.7
Propiconazole-d5	Not found	0.02	0.2
Tebuconazole-d6	0.1	0.2	0.2

SI.D SIEVE Settings

SIEVE software version 2.1 and 2.2 (Thermo Scientific) for differential expression analysis was used to compare treatment and control samples. Thereby peaks of suspected and nontarget BTPs can be identified that only occur in the treatment samples. As control samples we used the exposure medium and a chemical negative sample containing only gamma-irradiated matrix. The SIEVE software was operated in three steps: chromatographic alignment, framing, and identification by comparison with a generated mass list of suspected BTPs. Framing describes the process of building regions in the m/z versus retention time plane, whereby all peaks above a given threshold are collected until the maximum number of frames to be built is reached.

For suspect and nontarget screening approaches SIEVE software was run separately in positive ionization mode ($[M+H]^+$) and negative ionization mode ($[M-H]^-$) to identify possible BTPs.

Table S2-8: Settings used for suspect and nontarget screening with SIEVE (Thermo Scientific, version 2.1 and 2.2).

Retention time window:	5-20 min
m/z window:	100-1000
Frame time width:	1 min
m/z width:	10 ppm
Maximum number of frames:	15000
Peak intensity threshold:	10^6

SI.E Exposure Medium Concentrations

Screening Experiment

Table S2-9: Concentrations of parent compounds in the exposure medium of the biotransformation screening experiment. To quantify the aqueous concentrations 150 μL exposure medium were sampled at the beginning (t_0) and 24 h later at the end of the experiment (t_{24}). Subsequently 100 μL ISTD mix solution and 750 μL MeOH were added. Azoles without matching ISTD are marked with an asterisk.

Compound	Concentration in exposure medium [$\mu\text{g L}^{-1}$]			
	Medium 1 t_0	Medium 1 t_{24}	Medium 2 t_0	Medium 2 t_{24}
Cyproconazole *	164	155	170	165
Epoxiconazole *	164	170	172	156
Fluconazole	210	205	202	208
Ketoconazole *	134	854	880	Not measured
Propiconazole	188	182	190	174
Prochloraz	190	Not found	193	168
Tebuconazole	178	195	189	183

Toxicokinetic Experiment

Table S2-10: Concentrations of the parent compounds in the exposure medium of the biotransformation kinetic experiment. To quantify the aqueous concentrations, 150 μL medium was sampled at the beginning and the end of both the exposure and depuration phase. Subsequently, 200 μL of ISTD mix solution and 650 μL MeOH were added. Azoles without matching ISTD are marked with an asterisk.

Compound	Concentration in exposure medium [$\mu\text{g L}^{-1}$]			
	Medium 1 t_0	Medium 1 t_{24}	Medium 2 t_0	Medium 2 t_{24}
Epoxiconazole *	80	66	99	107
Prochloraz	98	73	93	72

SI.F Sampling during the Kinetic Experiment

Table S2-11: Sampled time-points during the kinetic experiment.

Uptake (U) / Depuration (D)	t [h]	t [d]	compound
U	0.5	0.02	EP / PRZ
U	1.5	0.06	EP / PRZ
U	2.5	0.10	EP / PRZ
U	5.5	0.23	EP / PRZ
U	9.5	0.40	EP / PRZ
U	17.5	0.73	EP / PRZ
U	24	1.00	EP / PRZ
D	24	1.00	EP / PRZ
D	25	1.04	EP / PRZ
D	26	1.08	EP / PRZ
D	28	1.17	EP / PRZ
D	31	1.29	EP / PRZ
D	35	1.46	EP / PRZ
D	42	1.75	EP / PRZ
D	50	2.08	EP / PRZ
D	65	2.71	EP / PRZ
D	75	3.13	EP / PRZ
D	95	3.96	EP / PRZ
D	119	4.96	EP / PRZ
D	144	6.00	PRZ

SI.G Sulfate Deconjugation Experiment

For further confirmation of possible sulfate conjugation products an enzyme deconjugation experiment was carried out. The experimental setup closely followed the method described by Kukkonen and Oikari (1988)⁵. Briefly, the remaining gammarid extracts of the duplicate samples where sulfate conjugation products were tentatively identified, were combined. 300 μL of 0.1 M sodium acetate buffer (pH 5) was added as a keeper and the MeOH of the gammarid extracts was evaporated under a gentle stream of nitrogen. In a further step, the samples were split into one treatment and one control sample each containing approx. 150 μL . Sulfatase was dissolved in 0.1 M sodium acetate buffer (pH 5) to a concentration of 20 units mL^{-1} . 700 μL of sulfatase solution was added to the treatment samples, whereas 700 μL 0.1 M acetate buffer (pH 5) and 1 mg of bovine serum albumin were added to the control samples. Samples were incubated overnight on a shaker at 37 °C and the reaction was stopped after approximately 8 h by adding 1 mL MeOH. Finally, the samples were filtered through 0.45 μm regenerated cellulose filters and analyzed by online-SPE LC-HRMS/MS.

SI.H Toxicokinetics and Bayesian Statistics

Table S2-12: Kinetic rate constants for epoxiconazole and prochloraz with lower and upper 95% confidence intervals, kinetic bioaccumulation factors (BAF_ks) and elimination half-lives ($t_{1/2}$). Results are rounded to three significant digits. Two replicate internal concentrations were used per time point. Confidence intervals are marked in red that hit the limits of the parameter values. Large confidence intervals, where the limits of the parameter values ranged up to four orders of magnitude, are marked in blue.

Compound	k_u [L kg _{ww} ⁻¹ d ⁻¹]	k_e [d ⁻¹]	k_{Mx} [d ⁻¹]	k_{eMx} [d ⁻¹]	$t_{1/2}$ [h]
EP	217	6.66			2.49
BAF _k : 32.5 [L kg _{ww} ⁻¹]	[179; 237]	[5.52; 7.33]			
EP_M346 (1 st BTP)			0.00415 [0.00332; 0.00561]	1.34 [0.935; 2.02]	12.4
EP_M449 (1 st BTP)			0.00624 [0.00444; 0.00920]	1.67 [0.9596; 2.736]	9.96
EP_M451 (1 st BTP)			0.000958 [0.000717; 0.00138]	1.24 [0.759; 2.09]	13.4
PRZ	439	8.07			1.88
BAF _k : 49.7 [L kg _{ww} ⁻¹]	[352; 526]	[6.37; 9.87]			
PRZ_M282 (2 nd BTP)			99.3 [70.9; 100]	7.52 [4.97; 9.43]	2.12
PRZ_M353 (2 nd BTP)			30.9 [24.2; 41.1]	1.72 [1.07; 2.55]	7.60
PRZ_M323b (2 nd BTP)			2.41 [1.87; 3.16]	0.304 [0.158; 0.548]	54.8
PRZ_M323a (2 nd BTP)			6.52 [3.21; 18.0]	3.70 [1.59; 10.0]	4.50
PRZ_M392b (1 st BTP)			0.148 [0.122; 0.183]	0.0001 [0.0001; 1.21]	3.73
PRZ_M392a (1 st BTP)			0.123 [0.081; 0.270]	0.000101 [0.0001; 18.4]	1.86
PRZ_M325 (2 nd BTP)			42.6 [30.9; 50.9]	0.000128 [0.0001; 100]	0.168
PRZ_M298 (2 nd BTP)			0.293 [0.104; 3.24]	11.9 [3.79; 100]	1.39
PRZ_M429 (1 st BTP)			0.00891 [0.00671; 0.0136]	0.604 [0.280; 1.45]	27.52
PRZ_M239 (2 nd BTP)			0.0317 [0.020; 0.0467]	0.298 [0.0837; 0.636]	55.7
PRZ_M435 (1 st BTP)			0.00663 [0.00345; 0.0242]	1.40 [0.399; 6.89]	11.9
PRZ_M382 (2 nd BTP)			4.46 [3.56; 5.63]	0.0001 [0.0001; 9.52]	0.539
PRZ_M632a (1 st BTP)			0.00223 [0.00125; 0.00595]	3.611 [1.91; 9.71]	4.61
PRZ_M310 (1 st / 2 nd BTP)			0.468 [0.344; 0.626]	0.0001 [0.0001; 100]	0.154
PRZ_M573 (1 st BTP)			0.000912 [0.000401; 0.00267]	2.36 [0.695; 7.98]	7.06

Calculation of kinetic BAF for PRZ:

Equation S2-1

$$\text{BAF}_k(\text{PRZ}) \left[\text{L} \cdot \text{kg}_{\text{ww}}^{-1} \right] = \frac{k_u}{k_e + k_{\text{M1},1\text{st}} + \dots + k_{\text{Mx},1\text{st}}} = \frac{k_u}{k_e + k_{\text{M392b}} + k_{\text{M392a}} + k_{\text{M429}} + k_{\text{M435}} + k_{\text{M632a}} + k_{\text{M310}} + k_{\text{M573}}}$$

Calculation of kinetic BAF for EP:

Equation S2-2

$$\text{BAF}_k(\text{EP}) \left[\text{L} \cdot \text{kg}_{\text{ww}}^{-1} \right] = \frac{k_u}{k_e + k_{\text{M1},1\text{st}} + \dots + k_{\text{Mx},1\text{st}}} = \frac{k_u}{k_e + k_{\text{M346}} + k_{\text{M449}} + k_{\text{M451}}}$$

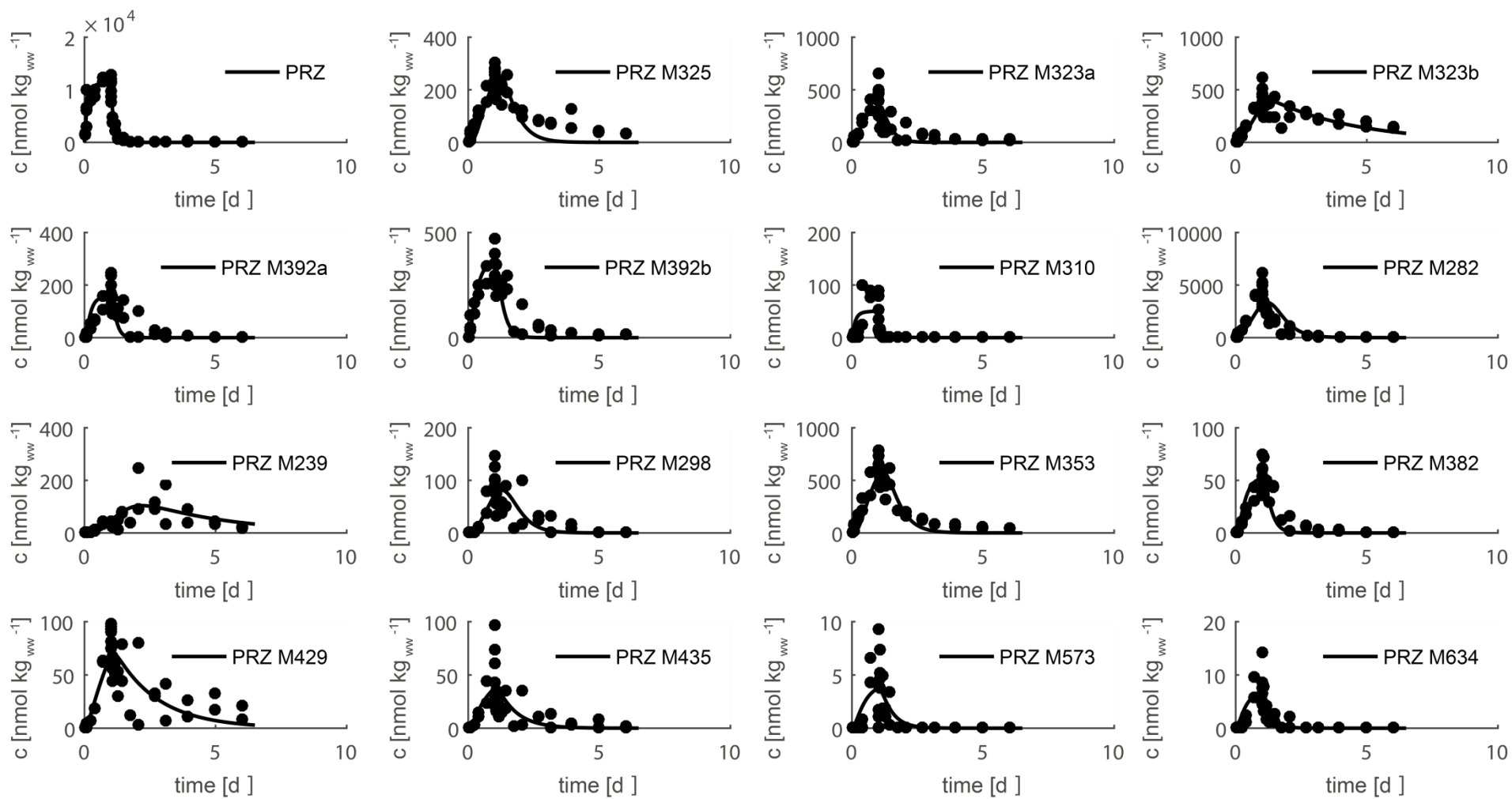
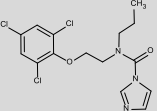


Figure S2-1: Measured (dots) and modeled (lines) time-series of internal concentrations of prochloraz and its biotransformation products in *G. pulex* in the uptake (1 d) and depuration phase (5 d).

SI.I Identified Biotransformation Products

Imidazole Fungicides

Table S2-14: Overview of prochloraz and identified biotransformation products formed in the aquatic invertebrate *G. pulex*. Biotransformation products are listed according to their relative peak intensity. Information about mass error, retention time (RT), and bioaccumulation factors (BAFs) are given for both replicate samples. CE stands for collision energy applied for fragmentation in the MS/MS experiment. Below each biotransformation product the abbreviation (S) stands for “identified by suspect screening (S)”, whereas (N) stands for “identified by nontarget” screening. The asterisk marks biotransformation products where the active azole moiety was altered.

Compound MassBank ID of displayed MS/MS spectrum	Formula [M] Exact mass of [M+H] ⁺ / [M-H] ⁻	Mass error [ppm]	RT [min]	Polarity	Elemental change ⁱⁱ⁾	Log D _{ow} ⁱⁱⁱ⁾	Identification confidence ^{iv)} /level according to Schymanski et al. (2014) ^{6/ v)}	Description	CE [eV]	MS/MS confirmatory ions ^{vi)}
Prochloraz (PRZ) ET20002 	C ₁₅ H ₁₆ Cl ₃ N ₃ O ₂ 376.0381	2.0 2.0	16.2 16.2	+		3.6	/1/	parent compound	30	308.0007 70.0288 265.9538
BAF [L kg_{ww}⁻¹] at t₂₄ ⁱ⁾: 54; 59										
PRZ_M282 * ET200103 (N)	C ₁₁ H ₁₄ Cl ₃ NO 282.0214	-0.6 -0.2	13.2 13.2	+	- C ₄ H ₂ N ₂ O	2.4	D p /2b/	loss of imidazole ring and CO	30	282.0212 86.0964 72.0807
PRZ_M353 * ET200203 (S)	C ₁₃ H ₁₅ Cl ₃ N ₂ O ₃ 353.0221	-0.6 -0.5	16.9 16.9	+	- C ₂ HN + O	3.4	D p l ⁷⁻⁹ m ⁷ /2b/	partial loss of hydroxylated imidazole ring, aldehyde formation	30	308.0005 70.0651 265.9536
PRZ_M323b * ET200302 (S)	C ₁₂ H ₁₂ Cl ₃ NO ₃ 323.9956	-0.9 -0.2	16.0 16.0	+	- C ₃ H ₄ N ₂ + O	2.6-3.2	d for keto group at propyl side chain /3/, 3 positional isomers	imidazole ring loss, aliphatic hydroxylation and further oxidation to a ketone	30	251.9752 84.0808 128.0707

Compound MassBank ID of displayed MS/MS spectrum	Formula [M] Exact mass of [M+H] ⁺ / [M-H] ⁻	Mass error [ppm]	RT [min]	Polarity	Elemental change ⁱⁱ⁾	Log D _{ow} ⁱⁱⁱ⁾	Identification confidence ^{iv)} /level according to Schymanski et al. (2014) ^{6/ v)}	Description	CE [eV]	MS/MS confirmatory ions ^{vi)}
PRZ_M323a * ET200402 (S)	C ₁₂ H ₁₂ Cl ₃ NO ₃ 323.9956	-0.7 -0.3	15.7 15.7	+	- C ₃ H ₄ N ₂ + O	2.3-2.6	d for keto group at propyl side chain /3/, 3 positional isomers	imidazole ring loss, aliphatic hydroxylation and further oxidation to a ketone	30	251.9744 128.0706 100.0393
PRZ_M392b * ET200502 (S)	C ₁₅ H ₁₆ Cl ₃ N ₃ O ₃ 392.0330	-1.1 -1.3	15.3 15.3	+	+ O	2.3	d, p for hydro- xylation at C-5 in imidazole ring (possible epoxide formation at C4- C5 as intermediate) /3/, most likely structure	imidazole ring hydroxylation	30	308.0006 265.9537 280.0057
PRZ_M392a ET200602 (S)	C ₁₅ H ₁₆ Cl ₃ N ₃ O ₃ 392.0330	-0.6 -0.8	13.9 13.9	+	+ O	2.1-2.5	d for hydro- xylation at propyl side chain /3/, 3 positional isomers	aliphatic hydroxylation	30	251.9746 69.0448 128.0707
PRZ_M325 * ET200702 (S)	C ₁₂ H ₁₅ Cl ₃ N ₂ O ₂ 325.0272	-1.0 -1.0	17.1 17.1	+	- C ₃ HN	3.4	D I ⁸⁻¹⁰ p /2b/	partial loss of imidazole ring	35	282.0213 325.0272 129.1022
PRZ_M298 * ET200804 (N)	C ₁₁ H ₁₄ Cl ₃ NO ₂ 298.0163	-2.0 -1.5	12.9 12.9	+	- C ₄ H ₂ N ₂ O + O	1.4-2.9	/3/, 6 positional isomers	loss of imidazole ring and CO, hydroxylation	50	70.0651 56.0495 85.0886
PRZ_M429 * ET200902 (S)	C ₁₅ H ₁₉ Cl ₃ N ₂ O ₄ S 429.0204	-0.7 -0.4	16.6 16.6	+	- C ₃ H ₂ N ₂ + C ₃ H ₅ NO ₂ S	1.4	D /2b/	loss of imidazole ring, cysteine product	20	308.0006 383.0149 429.0203
PRZ_M239 * ET201003 (N)	C ₈ H ₆ Cl ₃ NO 239.9744	-1.2 -1.0	12.6 12.6	+	- C ₇ H ₈ N ₂ O	1.4	D /2b/	remaining chlorophenyl moiety and C ₂ H ₅ NO	30	239.9746 119.0493 222.9480

Compound MassBank ID of displayed MS/MS spectrum	Formula [M] Exact mass of [M+H] ⁺ / [M-H] ⁻	Mass error [ppm]	RT [min]	Polarity	Elemental change ⁱⁱ⁾	Log D _{ow} ⁱⁱⁱ⁾	Identification confidence ^{iv)} /level according to Schymanski et al. (2014) ^{6/ v)}	Description	CE [eV]	MS/MS confirmatory ions ^{vi)}
PRZ_M435 * (NH₄⁺ adduct) ET201102 (S)	C ₁₇ H ₂₁ Cl ₃ N ₄ O ₃ 435.0752	-1.3 -1.1	14.9 14.9	+	+ C ₂ H ₂ O	-	d for acetylation at CO-imidazole ring moiety /3/, acetylation most likely at keto group	acetylation at CO-imidazole ring moiety; NH ₄ ⁺ adduct	20	282.0215 435.0753 154.0611
PRZ_M382 * ET201202 (S)	C ₁₄ H ₁₈ Cl ₃ N ₃ O ₃ 382.0487	-2.1 -2.8	16.6 16.6	+	- CH ₂ + °O	3.02	d, p for C-4 loss at hydroxylated (at C-5) imidazole ring /3/, most likely structure	partial loss of hydroxylated imidazole ring	20	308.0006 365.0221 337.0270
PRZ_M632a ET201352 (N)	C ₂₁ H ₂₆ Cl ₃ N ₃ O ₁₁ S 632.0281	0.1 -0.3	10.4 10.4	- ^(vii)	+ O + C ₆ H ₁₀ O ₈ S	-1.3	D for conjugation at the chlorophenyl moiety e , /2b/	aromatic hydroxylation, glucose and sulfate conjugation	40	209.9053 96.9600 241.0029
PRZ_M469 ET201452 (S)	C ₁₅ H ₁₆ Cl ₃ N ₃ O ₆ S 469.9753	0.0 -0.1	11.1 11.0	- ^(vii)	+ O + SO ₃	0.5	D for sulfate conjugation at the chlorophenyl moiety e /2b/	aromatic hydroxylation, sulfate conjugation	30	209.9047 390.0185 67.0295
PRZ_M310 * ET201502 (S)	C ₁₂ H ₁₄ Cl ₃ NO ₂ 310.0163	-0.7 -0.6	16.8/17.5 16.8/17.5	+	- C ₃ H ₂ N ₂	3.7	D /2b/	loss of imidazole ring	20	310.0164 114.0914 282.0215
PRZ_M632b ET201652 (N)	C ₂₁ H ₂₆ Cl ₃ N ₃ O ₁₁ S 632.0281	-0.1 -0.4	11.1 11.1	- ^(vii)	+ O + C ₆ H ₁₀ O ₈ S	-1.3	D for conjugation at the chlorophenyl moiety e /2b/	aromatic hydroxylation, glucose and sulfate conjugation	40	209.9047 241.0028 96.9600

Compound MassBank ID of displayed MS/MS spectrum	Formula [M] Exact mass of [M+H] ⁺ / [M-H] ⁻	Mass error [ppm]	RT [min]	Polarity	Elemental change ⁱⁱ⁾	Log D _{ow} ⁱⁱⁱ⁾	Identification confidence ^{iv)} /level according to Schymanski et al. (2014) ^{vi)} ^{v)}	Description	CE [eV]	MS/MS confirmatory ions ^{vi)}
PRZ_M477	C ₁₈ H ₂₂ Cl ₂ N ₄ O ₅ S	-0.6	11.2	+	+ C ₃ H ₆ NO ₂ S	-	d for no	cysteine product,	10	381.0440
ET201701 (S)	477.0761	-0.6	11.1		+ O - Cl		conjugation at the CO-imidazole ring moiety /3/, structural possibilities unclear	hydroxylation, dehalogenation		409.0387 477.0760
PRZ_M573 *	C ₁₉ H ₂₃ Cl ₃ N ₄ O ₅ S	-0.3	13.8	+	- C ₃ H ₂ N ₂	-1.9	/3/, most likely	loss of imidazole ring,	10	443.9949
ET201801 (S)	573.0375	-0.9	13.8		- C ₃ H ₆ +C ₁₀ H ₁₅ N ₃ O ₆ S		structure, glutathione con- jugation at epoxy group	loss of propyl side chain, glutathione conjugation		340.9681 573.0373

ⁱ⁾ See Equation 4 in section *Modeling Bioaccumulation and Biotransformation Kinetics* in the corresponding publication for the calculation of BAFs at steady state.

ⁱⁱ⁾ The elemental change refers to the change in the molecular formula of the biotransformation product in comparison with the parent compound.

ⁱⁱⁱ⁾ Log D_{ow} values were predicted by MarvinSketch version 14.10.20.0 at pH 7.9 and 25 °C. Log D_{ow} values correspond to corrected log K_{ow} values to account for pH-dependent dissociation. At pH 7.9 all selected target compounds are neutral thus log D_{ow} is equal to log K_{ow}. If different positional isomers are possible for one BTP, a range of log D_{ow} values is given.

^{iv)} D: diagnostic fragment for one structure; d: diagnostic fragment for positional isomers; e: enzyme deconjugation; l: structure reported in literature; m: MS/MS data from literature; p: biotransformation pathway information; d, p: diagnostic fragment for positional isomers (d) in combination with pathway information (p) give evidence for one possible structure.

^{v)} Levels are defined as follows: 5 (*exact mass*), 4 (*unequivocal molecular formula*), 3 (*tentative candidates: e.g., positional isomers*), 2 (*probable structure: library spectrum match (a) or diagnostic evidence for one structure (b)*) and 1 (*confirmed structure*).

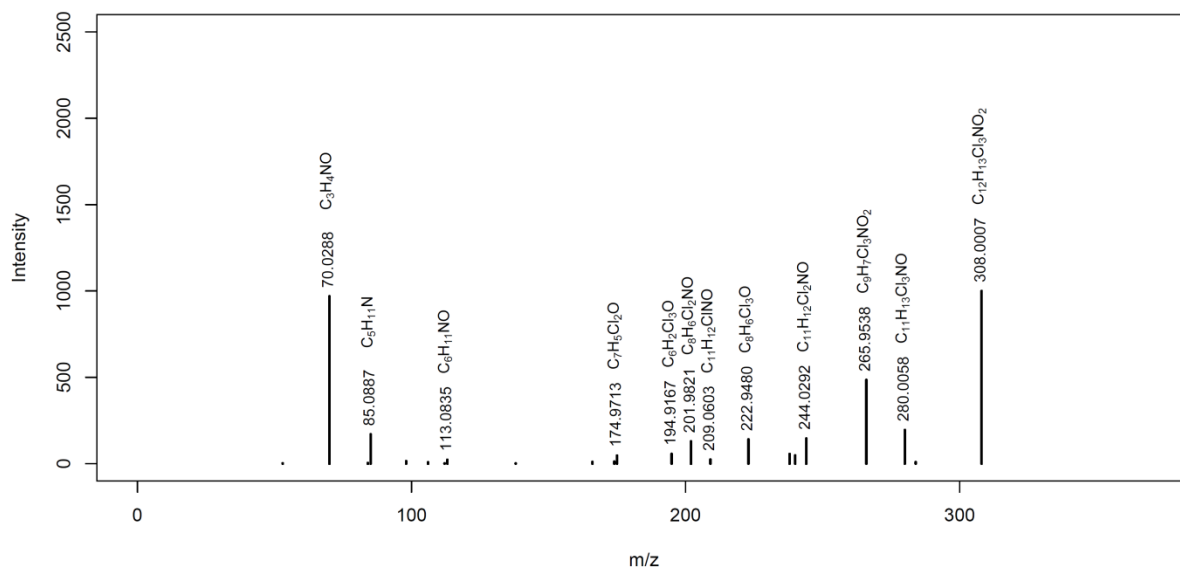
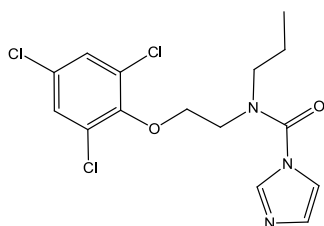
^{vi)} Diagnostic fragments (d, D) are listed first and are represented in bold in the table, other characteristic fragments are then presented according to their relative abundance. Only fragments where a chemical formula and structure could be attributed are considered.

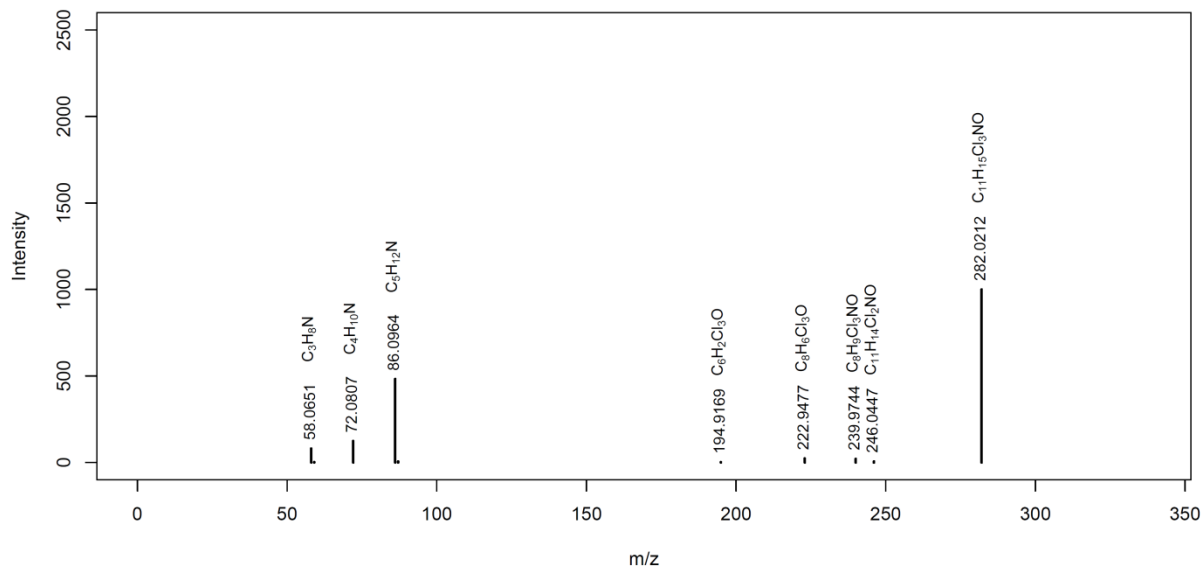
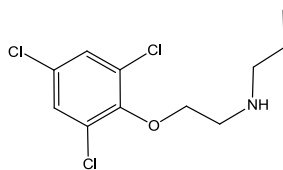
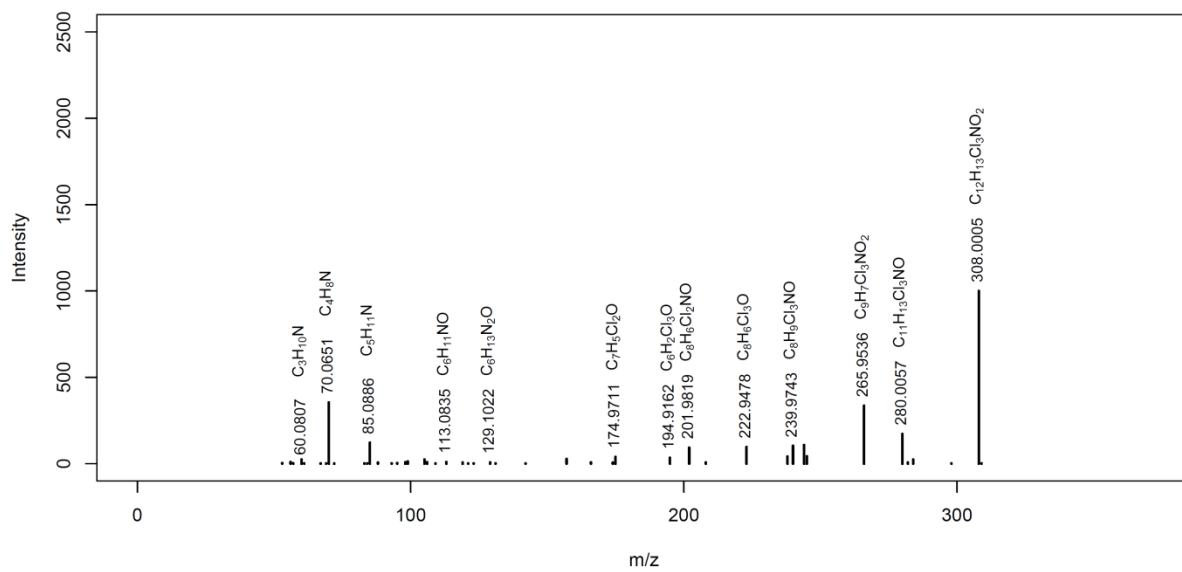
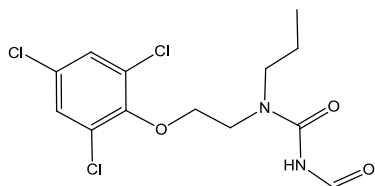
^{vii)} The sulfate-containing BTPs are more sensitive in negative ionization mode. However, they were quantified in positive ionization mode because the respective parent compounds were also detected in positive ionization mode.

The different MassBank IDs for one compound refer to different collision energies applied during MS/MS fragmentation. The MassBank ID displayed in bold indicates the depicted MS/MS spectrum.

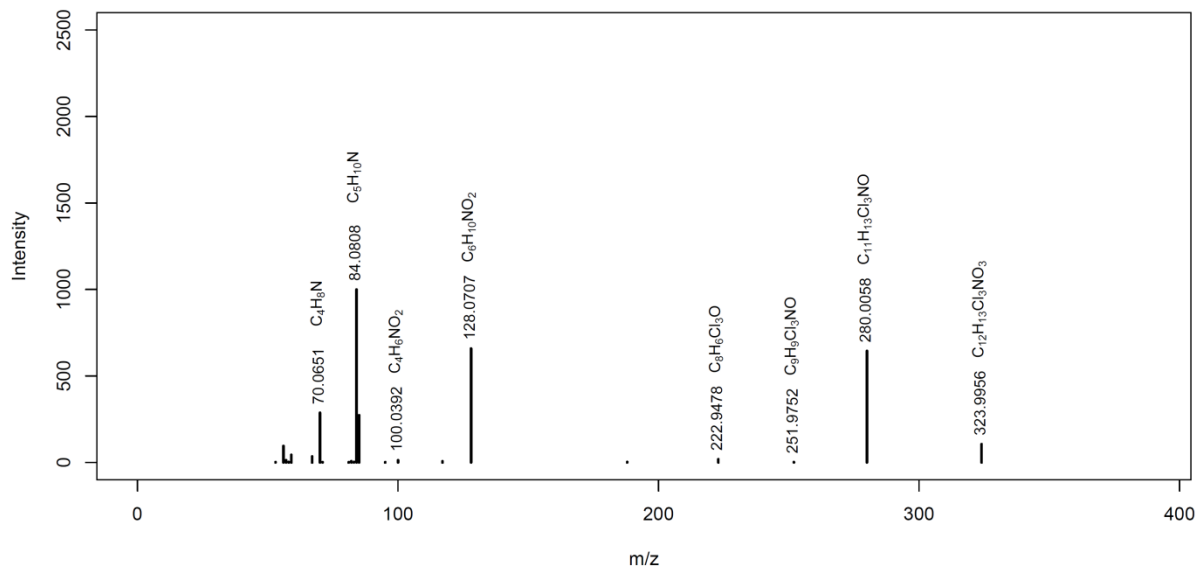
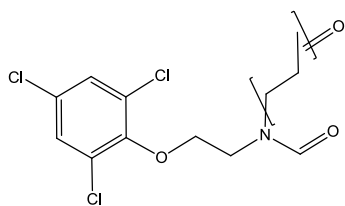
Prochloraz (PRZ)

MassBank ID: ET200001, **ET200002**, ET200003, ET200004

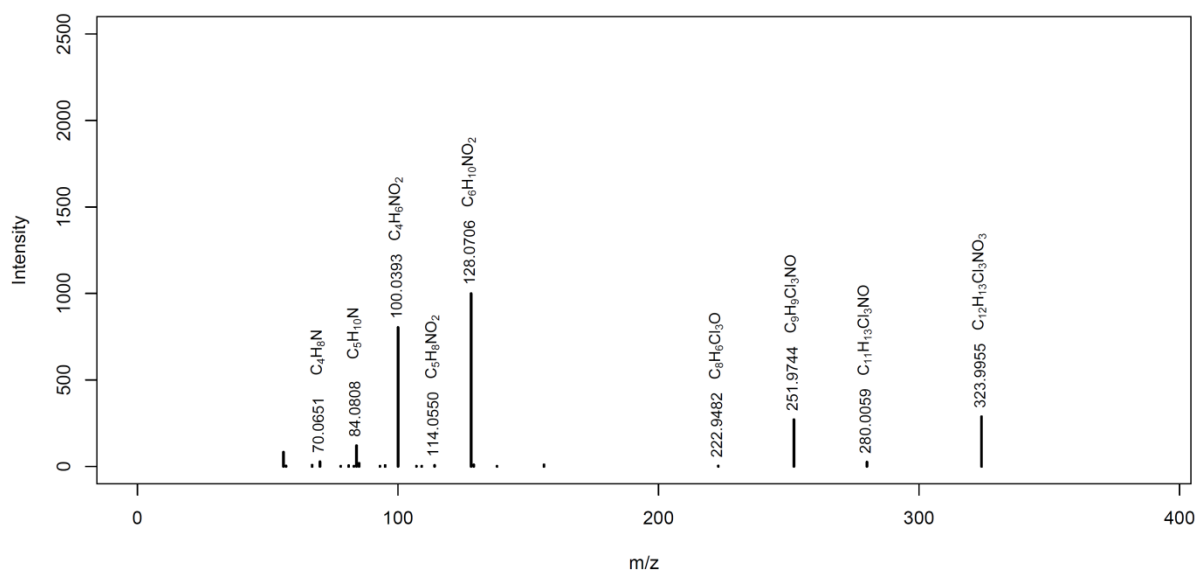
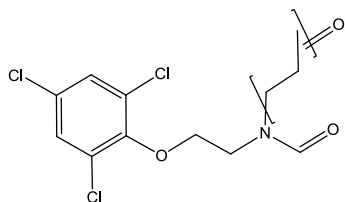


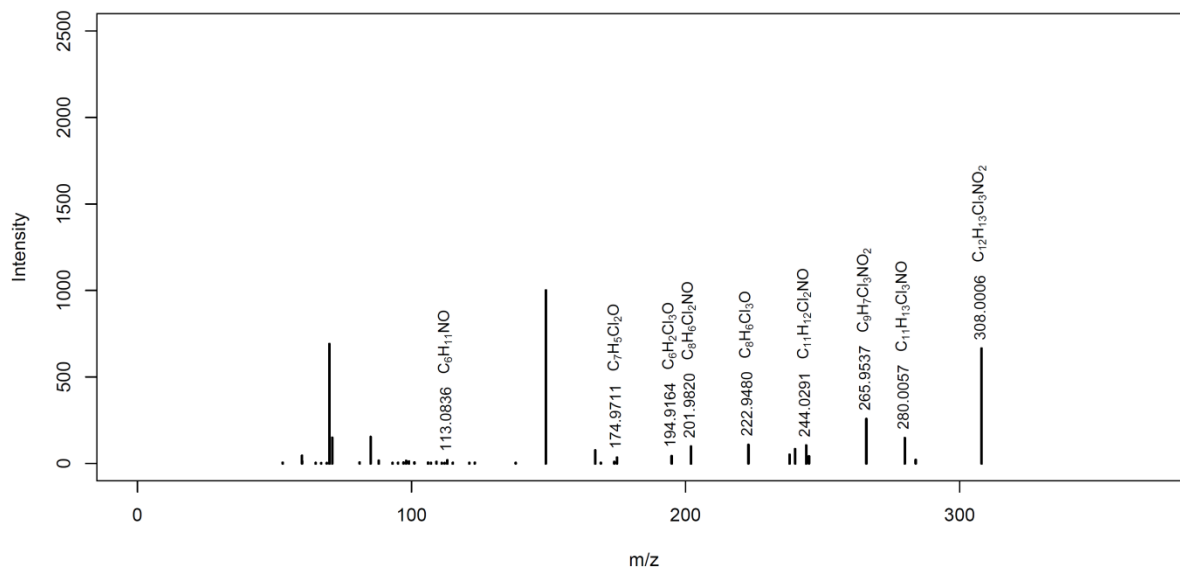
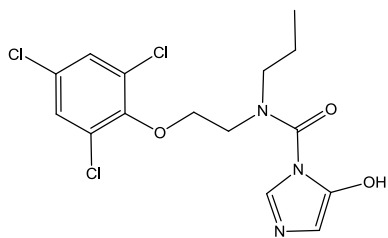
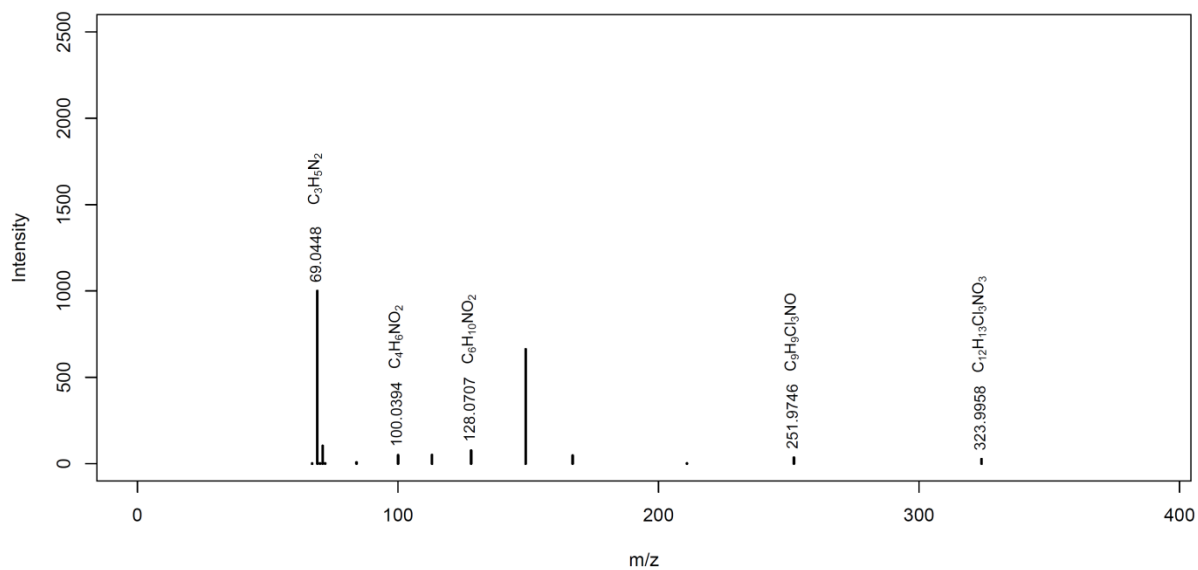
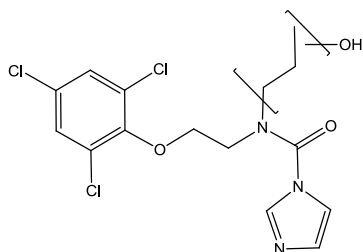
PRZ_M282MassBank ID: ET200101, ET200102, **ET200103**, ET200104, ET200105**PRZ_M353**MassBank ID: ET200201, ET200202, **ET200203**, ET200204, ET200205

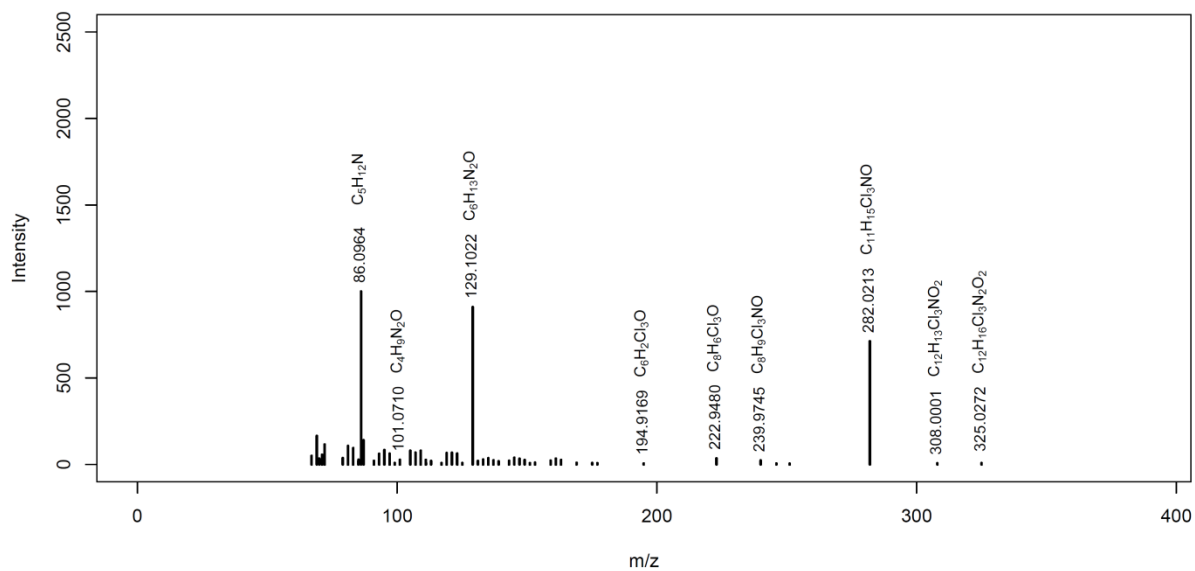
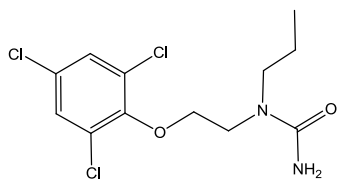
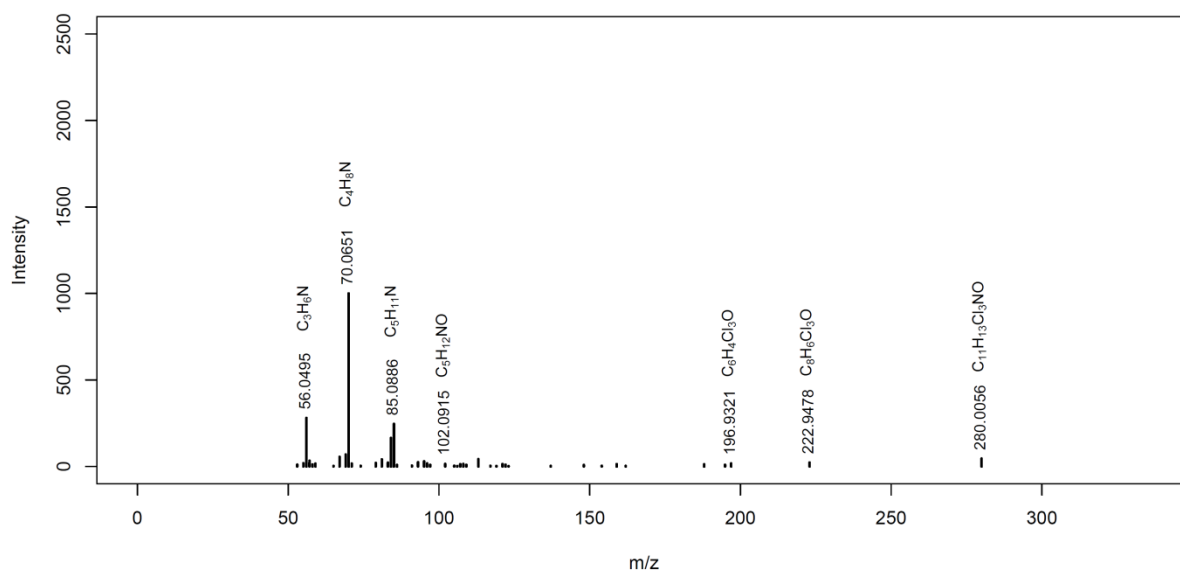
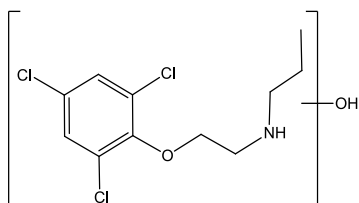
PRZ_M323b

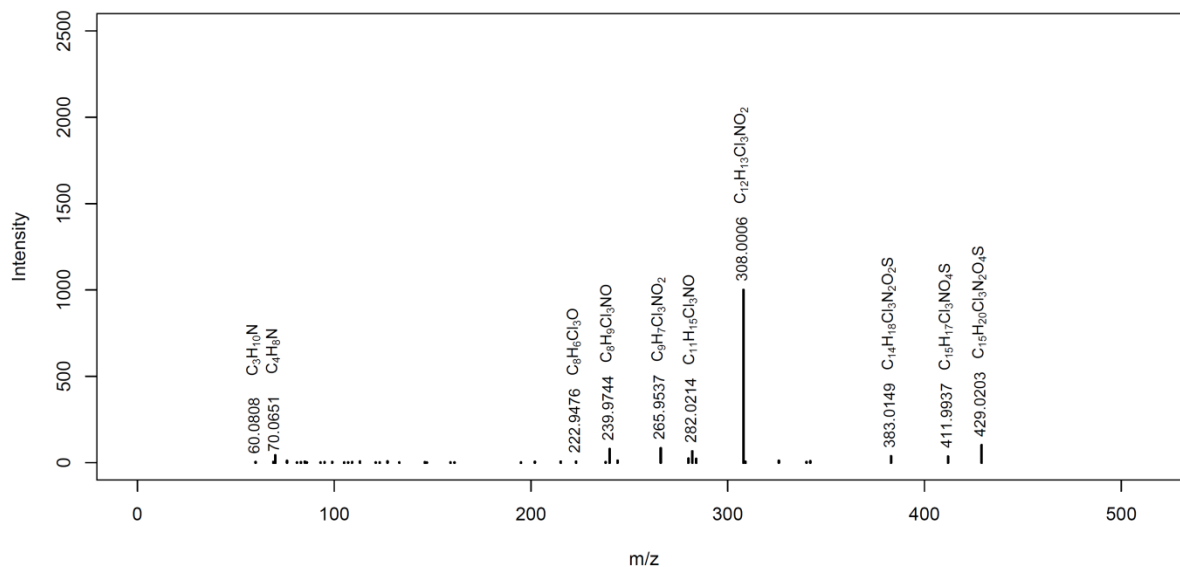
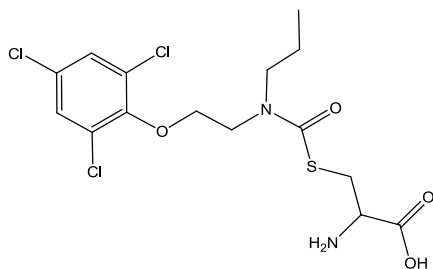
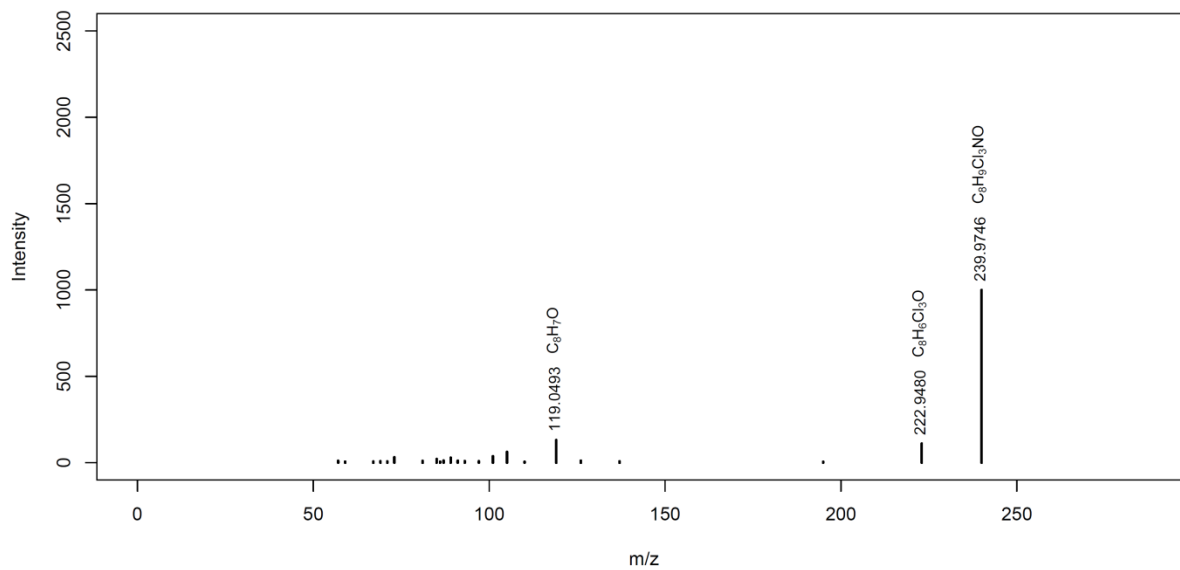
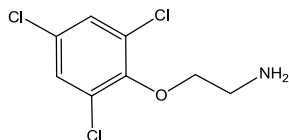
MassBank ID: ET200301, **ET200302**, ET200303, ET200304

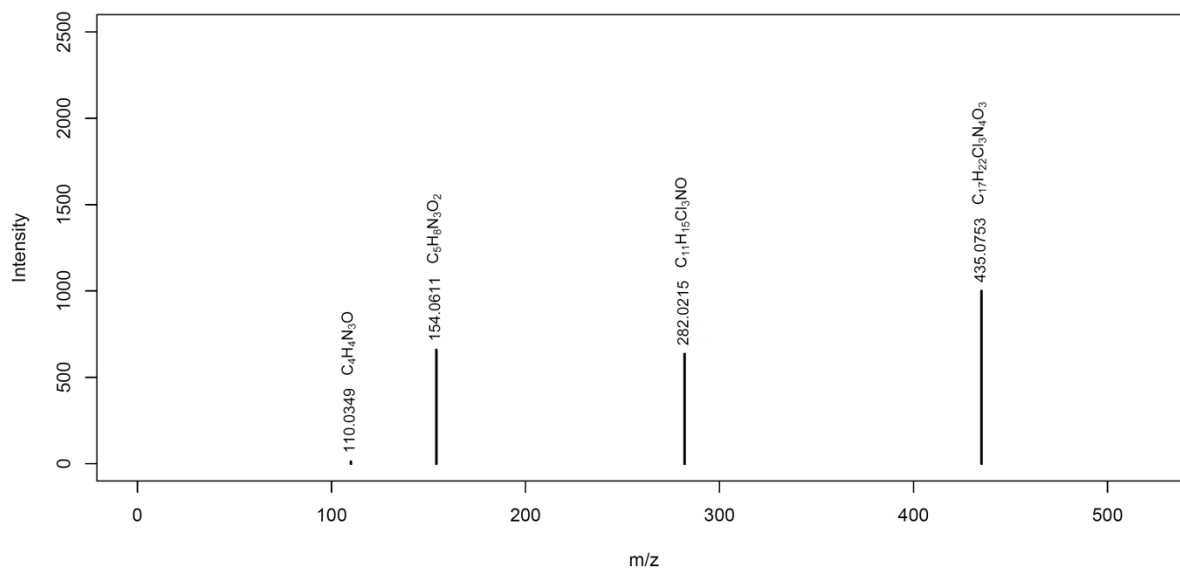
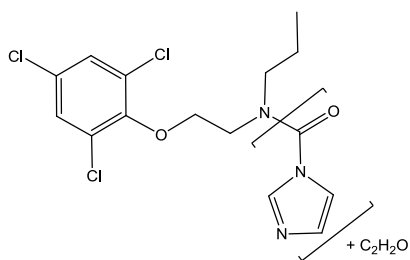
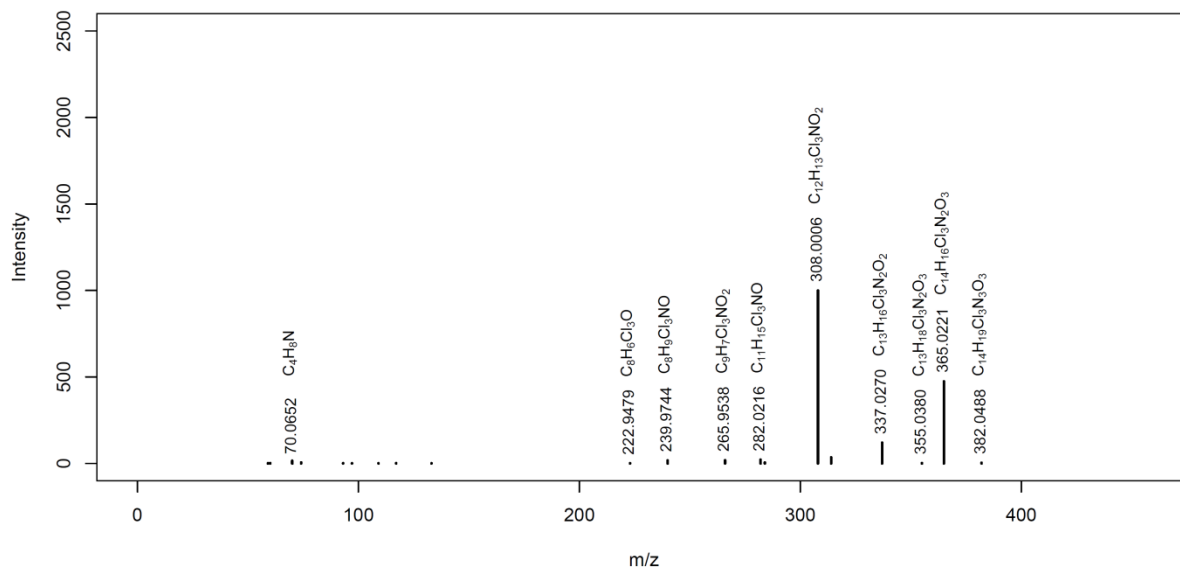
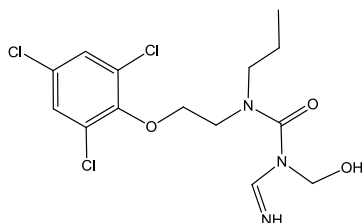
PRZ_M323a

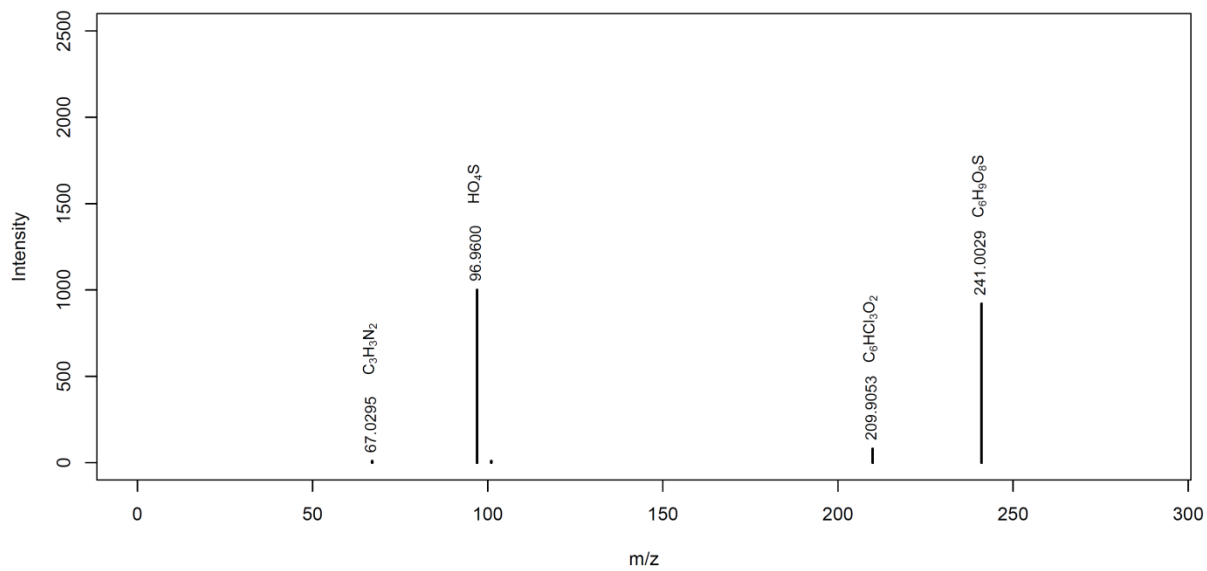
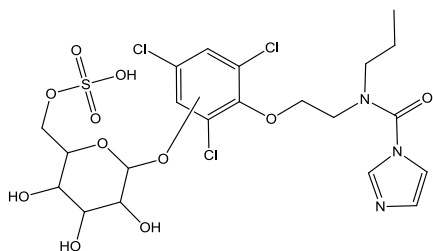
MassBank ID: ET200401, **ET200402**, ET200403, ET200404

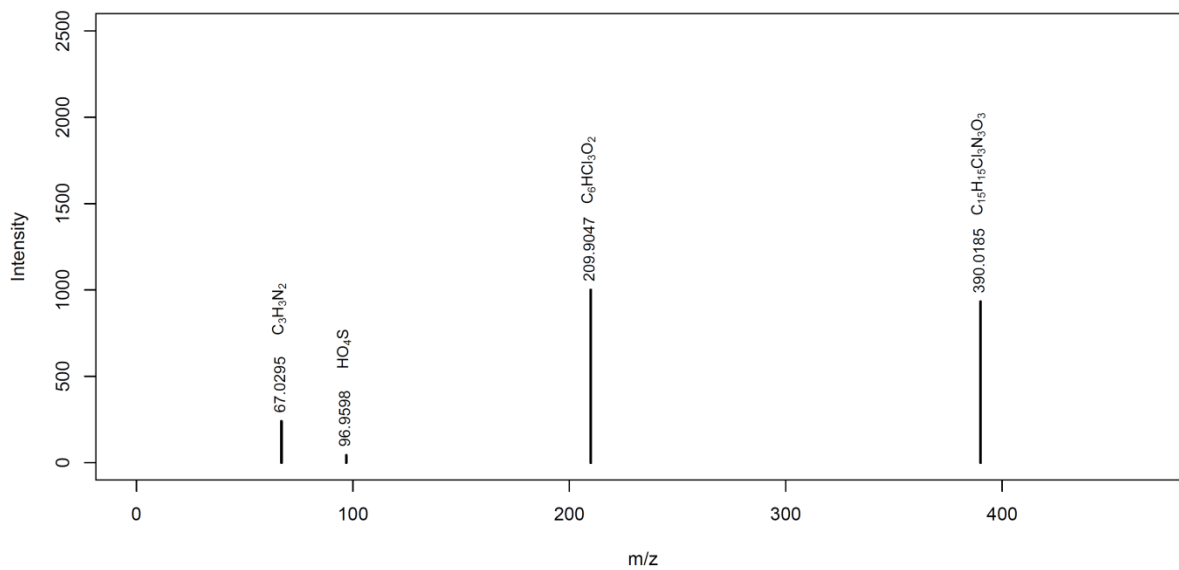
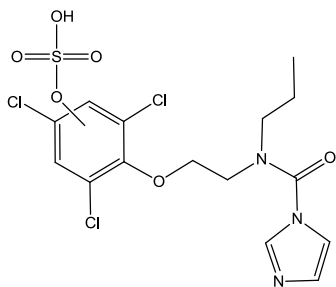
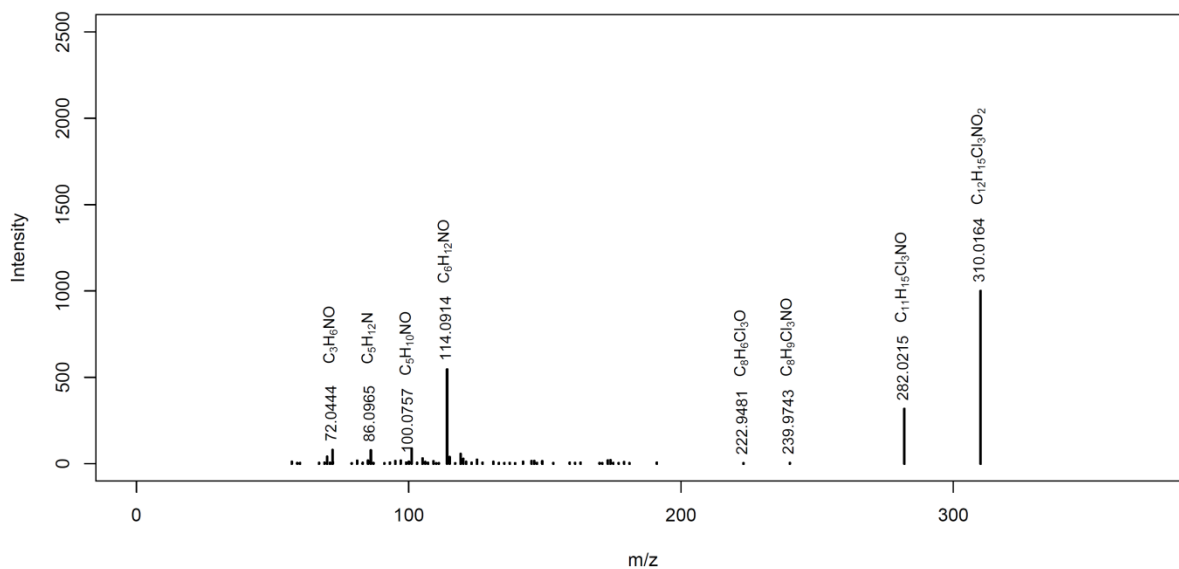
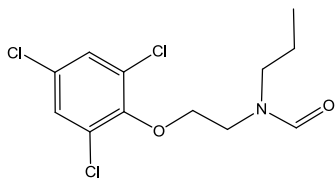
PRZ_M392bMassBank ID: ET200501, **ET200502**, ET200503, ET200504**PRZ_M392a**MassBank ID: ET200601, **ET200602**, ET200603, ET200604

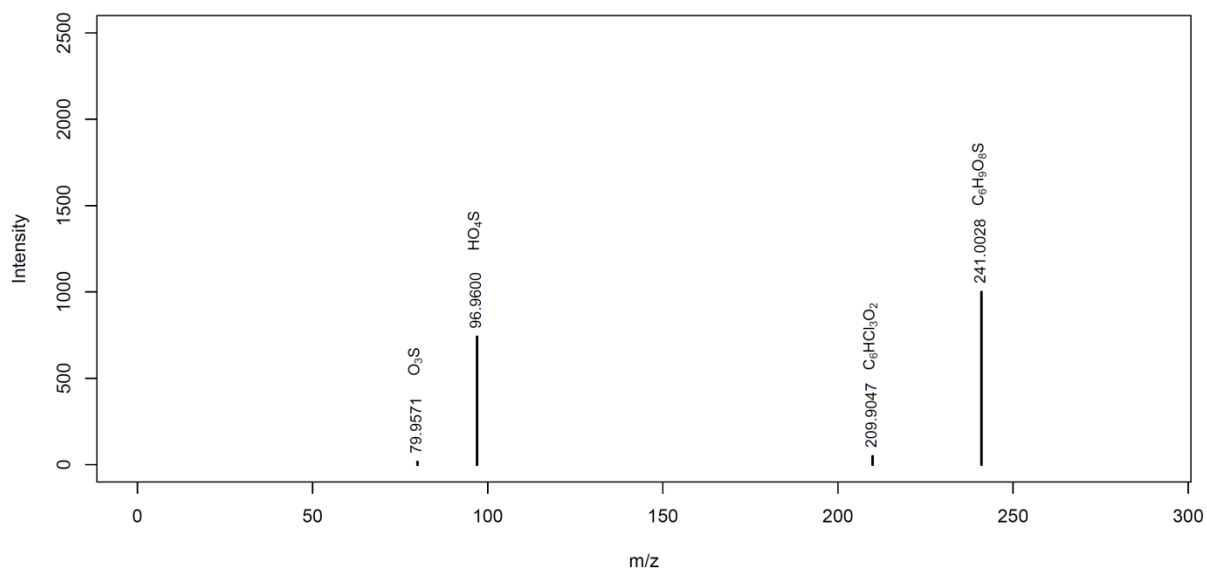
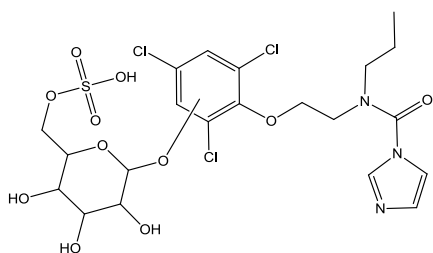
PRZ_M325MassBank ID: ET200701, **ET200702**, ET200703, ET200704**PRZ_M298**MassBank ID: ET200801, ET200802, ET200803, **ET200804**, ET200805

PRZ_M429MassBank ID: ET200901, **ET200902**, ET200903, ET200904, ET200905**PRZ_M239**MassBank ID: ET201001, ET201002, **ET201003**, ET201004, ET201005

PRZ_M435MassBank ID: ET201101, ET201102, **ET201103**, ET201104, ET201105**PRZ_M382**MassBank ID: ET201201, **ET201202**, ET201203, ET201204, ET201205

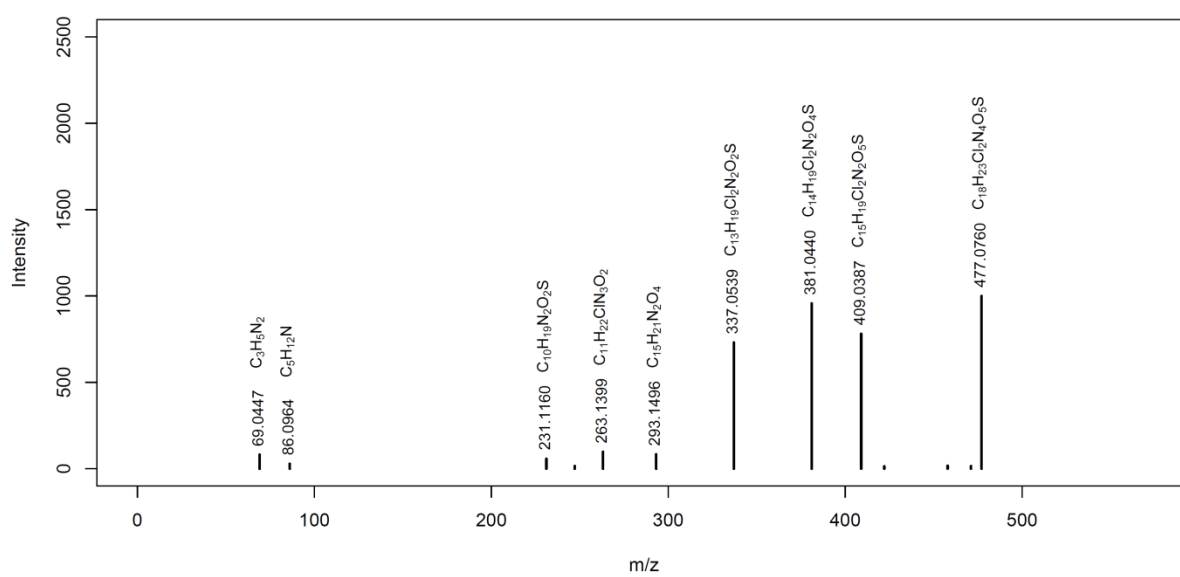
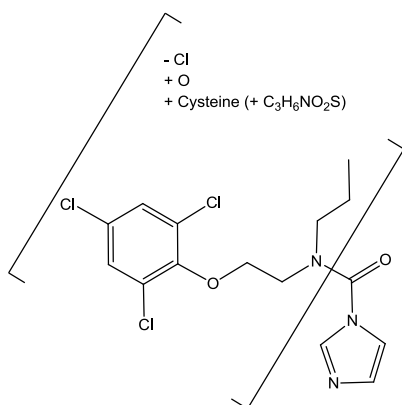
PRZ_M632aMassBank ID: ET201351, **ET201352**, ET201353, ET201354, ET201355

PRZ_M469MassBank ID: ET201451, **ET201452**, ET201453, ET201454**PRZ_M310**MassBank ID: ET201501, **ET201502**, ET201503, ET201504, ET201505

PRZ_M632bMassBank ID: ET201651, **ET201652**, ET201653, ET201654, ET201655

PRZ_M477

MassBank ID: ET201701, ET201702, ET201703, ET201704, ET201705



PRZ_M573

MassBank ID: ET201801, ET201802, ET201803, ET201804, ET201805

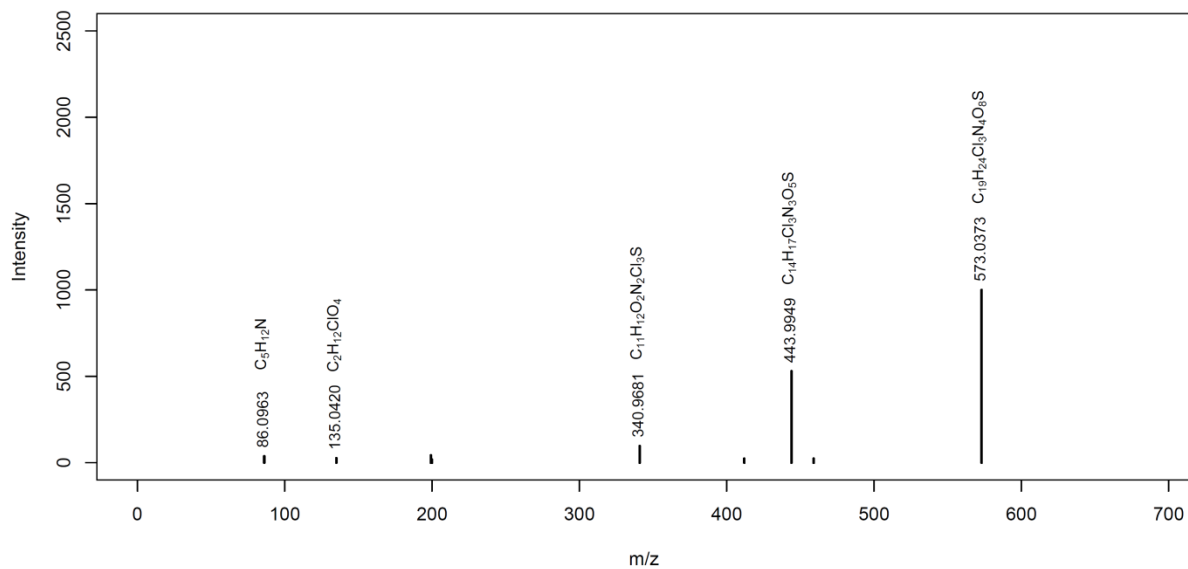
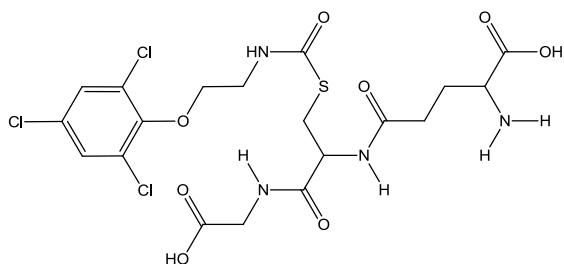
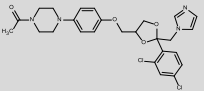


Table S2-15: Overview of ketoconazole and identified biotransformation products formed in the aquatic invertebrate *G. pulex*. Biotransformation products are listed according to their relative peak intensity. Information about mass error, retention time (RT), and bioaccumulation factors (BAFs) are given for both replicate samples. CE stands for collision energy applied for fragmentation in the MS/MS experiment. Below each biotransformation product the abbreviation (S) stands for “identified by suspect screening (S)”, whereas (N) stands for “identified by nontarget” screening. The asterisk marks biotransformation products where the activeazole moiety was altered.

Compound MassBank ID of displayed MSMS spectrum	Formula [M] Exact mass of [M+H] ⁺ / [M-H] ⁻	Mass error [ppm]	RT [min]	Polarity	Elemental change ⁱⁱ⁾	Log D _{ow} ⁱⁱⁱ⁾	Identification confidence ^{iv)} /level according to Schymanski et al. (2014) ^{6/ v)}	Description	CE [eV]	MS/MS confirmatory ions ^{vi)}
KET ET260003	C ₂₆ H ₂₈ Cl ₂ N ₄ O ₄ 531.1560	0.2 0.3	13.6 13.6	+		4.2	/1/	parent compound	40	531.1558 82.0525 489.1452
 <p>BAF [L kg_{ww}⁻¹] at t₂₄ⁱ⁾: 1.4/ 9.2^{vii)}; 3.0</p>										
KET_M565 * ET260102 (S)	C ₂₆ H ₃₀ Cl ₂ N ₄ O ₆ 565.1615	-2.7 -0.8	14.6 14.6	+	+ H ₂ O ₂	2.2	d for both extra oxygens at the opened imidazole ring l ¹¹⁻¹² m ¹¹ /3/, 2 positional isomers	imidazole ring oxidation	30	463.1188 219.1128 247.1441

ⁱ⁾ See Equation 4 in section *Modeling Bioaccumulation and Biotransformation Kinetics* for the calculation of BAFs at steady state.

ⁱⁱ⁾ The elemental change refers to the change in the molecular formula of the biotransformation product in comparison with the parent compound.

ⁱⁱⁱ⁾ Log D_{ow} values were predicted by MarvinSketch version 14.10.20.0 at pH 7.9 and 25 °C. Log D_{ow} values correspond to corrected log K_{ow} values to account for pH-dependent dissociation. At pH 7.9 all selected target compounds are neutral thus log D_{ow} is equal to log K_{ow}. If different positional isomers are possible for one BTP, a range of log D_{ow} values is given.

^{iv)} D: diagnostic fragment for one structure; d: diagnostic fragment for positional isomers; e: enzyme deconjugation; l: structure reported in literature; m: MS/MS data from literature; p: biotransformation pathway information; d, p: diagnostic fragment for positional isomers (d) in combination with pathway information (p) give evidence for one possible structure.

^{v)} Levels are defined as follows: 5 (*exact mass*), 4 (*unequivocal molecular formula*), 3 (*tentative candidates: e.g., positional isomers*), 2 (*probable structure: library spectrum match (a) or diagnostic evidence for one structure (b)*) and 1 (*confirmed structure*).

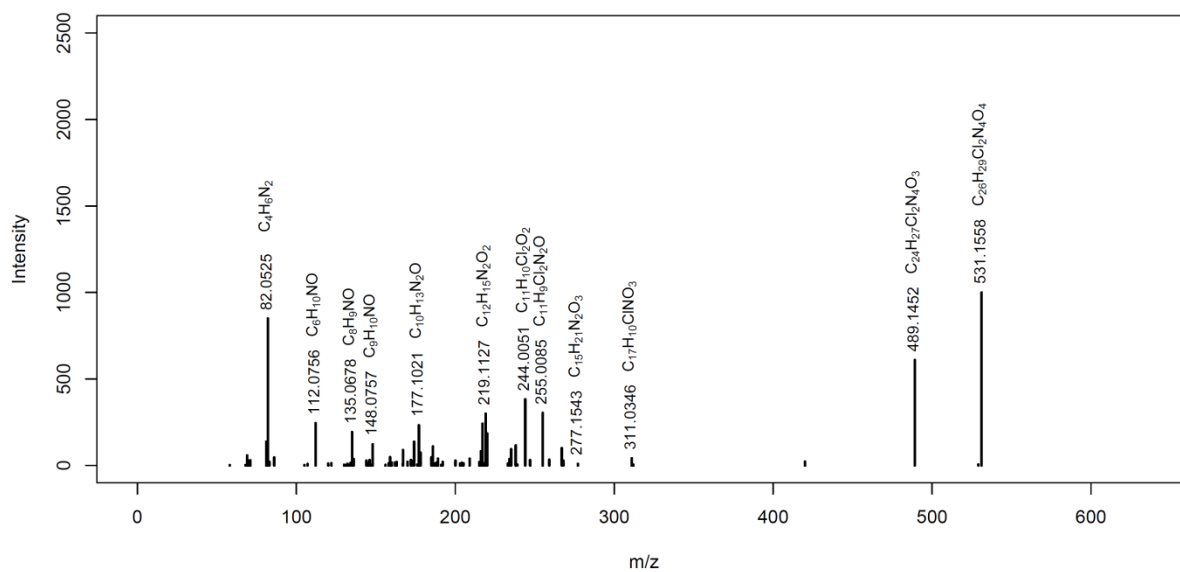
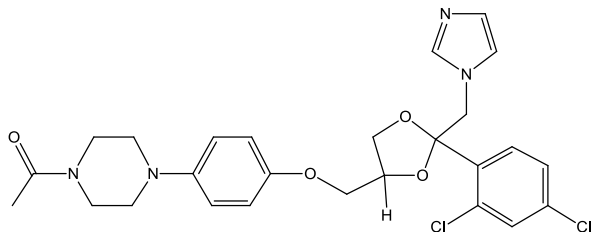
^{vi)} Diagnostic fragments (d, D) are listed first and are represented in bold in the table, other characteristic fragments are then presented according to their relative abundance. Only fragments where a chemical formula and structure could be attributed are considered.

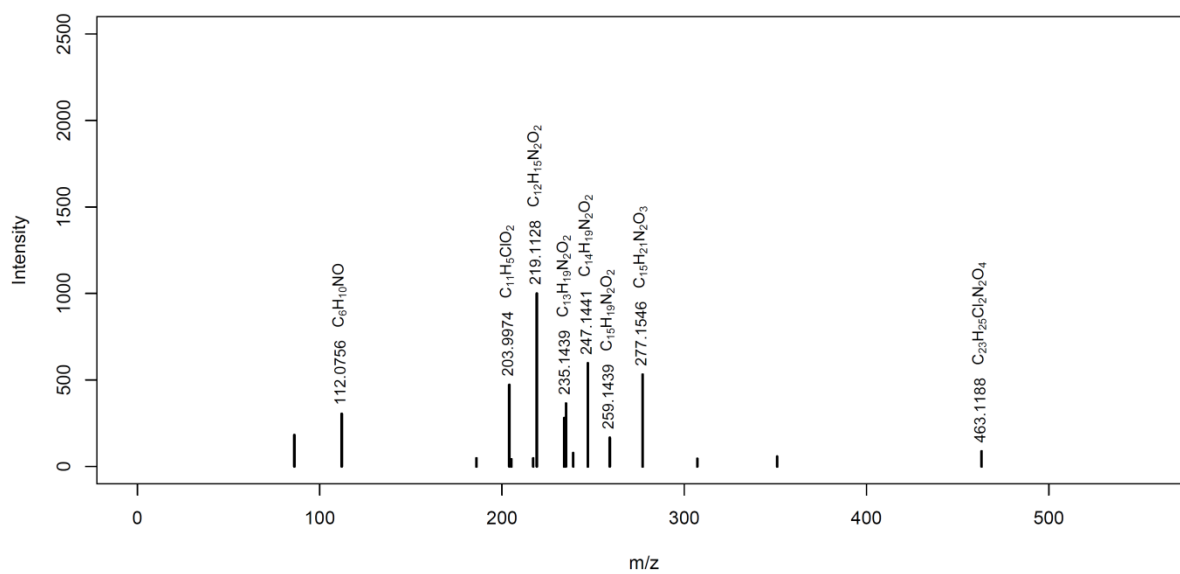
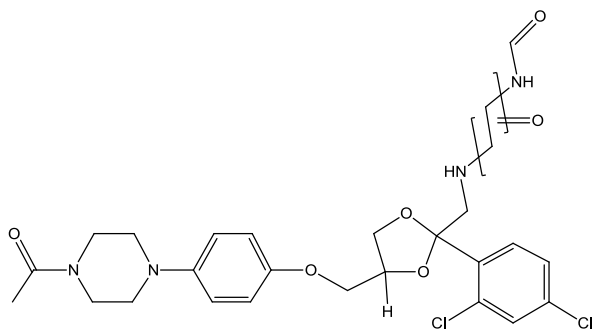
^{vii)} Due to inconsistent medium concentration measurements, different BAF resulted for medium concentrations measured at t₀ and t₂₄, respectively.

The different MassBank IDs for one compound refer to different collision energies applied during MS/MS fragmentation. The MassBank ID displayed in bold indicates the depicted MS/MS spectrum.

Ketoconazole (KET)

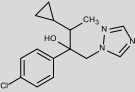
MassBank ID: ET260001, ET260002, **ET260003**, ET260004



KET_M565MassBank ID: ET260101, **ET260102**, ET260103, ET260104

Triazole Fungicides

Table S2-16: Overview of cyproconazole and identified biotransformation products formed in the aquatic invertebrate *G. pulex*. Biotransformation products are listed according to their relative peak intensity. Information about mass error, retention time (RT), and bioaccumulation factors (BAFs) are given for both replicate samples. CE stands for collision energy applied for fragmentation in the MS/MS experiment. Below each biotransformation product the abbreviation (S) stands for “identified by suspect screening (S)”, whereas (N) stands for “identified by nontarget” screening. The asterisk marks biotransformation products where the activeazole moiety was altered.

Compound MassBank ID of displayed MSMS spectrum	Formula [M] Exact mass of [M+H] ⁺ / [M-H] ⁻	Mass error [ppm]	RT [min]	Polarity	Elemental change ⁱⁱ⁾	Log D _{ow} ⁱⁱⁱ⁾	Identification confidence ^{iv)} /level according to Schymanski et al. (2014) ^{6/ v)}	Description	CE [eV]	MS/MS confirmatory ions ^{vi)}
Cyproconazole (CP) ET210001	C ₁₅ H ₁₈ ClN ₃ O 292.1211	0.9 0.4	15.7 15.7	+		2.9	/1/	parent compound	40	70.0400 125.0152 138.9945
										
BAF [L kg_{ww}⁻¹] at t₂₄ ⁱ⁾: 13; 11										
CP_M308a ET210101 (S)	C ₁₅ H ₁₈ ClN ₃ O ₂ 308.1160	-0.4 -0.5	13.5 13.5	+	+ O	1.5-1.9	1 ⁹ /3/, 6 positional isomers	aliphatic hydroxylation	35	70.0400 125.0152 308.1159
CP_M308b * ET210201 (S)	C ₁₅ H ₁₈ ClN ₃ O ₂ 308.1160	0.3 -0.4	14.1 14.1	+	+ O	3.1	d for hydroxylation at the triazole ring /3/, 2 positional isomers	triazole ring hydroxylation	35	86.0349 125.0152 308.1154
CP_M308c * ET210301 (S)	C ₁₅ H ₁₈ ClN ₃ O ₂ 308.1160	0.2 -0.3	14.7 14.7	+	+ O	3.2	d for hydroxylation at the triazole ring /3/, 2 positional isomers	triazole ring hydroxylation	35	86.0349 125.0152 138.1157

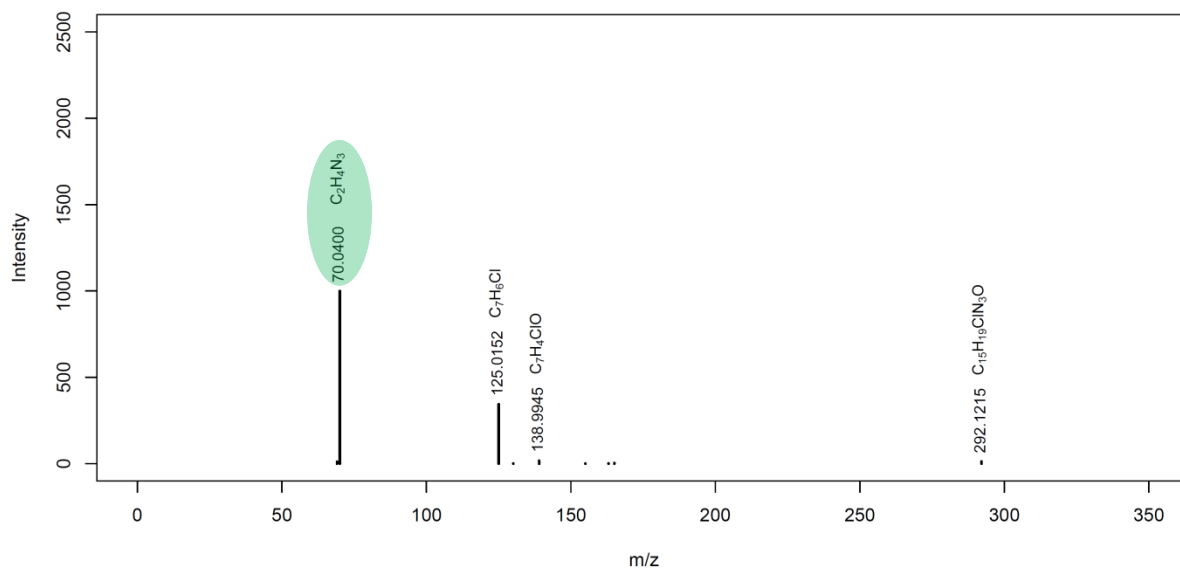
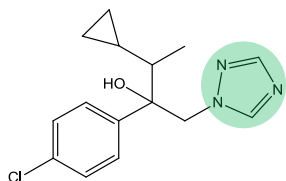
Explanation to Table S2-16:

- ⁱ⁾ See Equation 4 in section *Modeling Bioaccumulation and Biotransformation Kinetics* for the calculation of BAFs at steady state.
- ⁱⁱ⁾ The elemental change refers to the change in the molecular formula of the biotransformation product in comparison with the parent compound.
- ⁱⁱⁱ⁾ Log D_{ow} values were predicted by MarvinSketch version 14.10.20.0 at pH 7.9 and 25 °C. Log D_{ow} values correspond to corrected log K_{ow} values to account for pH-dependent dissociation. At pH 7.9 all selected target compounds are neutral thus log D_{ow} is equal to log K_{ow} . If different positional isomers are possible for one BTP, a range of log D_{ow} values is given.
- ^{iv)} D: diagnostic fragment for one structure; d: diagnostic fragment for positional isomers; e: enzyme deconjugation; l: structure reported in literature; m: MS/MS data from literature; p: biotransformation pathway information; d, p: diagnostic fragment for positional isomers (d) in combination with pathway information (p) give evidence for one possible structure.
- ^{v)} Levels are defined as follows: 5 (*exact mass*), 4 (*unequivocal molecular formula*), 3 (*tentative candidates: e.g., positional isomers*), 2 (*probable structure: library spectrum match (a) or diagnostic evidence for one structure (b)*) and 1 (*confirmed structure*).
- ^{vi)} Diagnostic fragments (d, D) are listed first and are represented in bold in the table, other characteristic fragments are then presented according to their relative abundance. Only fragments where a chemical formula and structure could be attributed are considered.

The different MassBank IDs for one compound refer to different collision energies applied during MS/MS fragmentation. The MassBank ID displayed in bold indicates the depicted MS/MS spectrum.

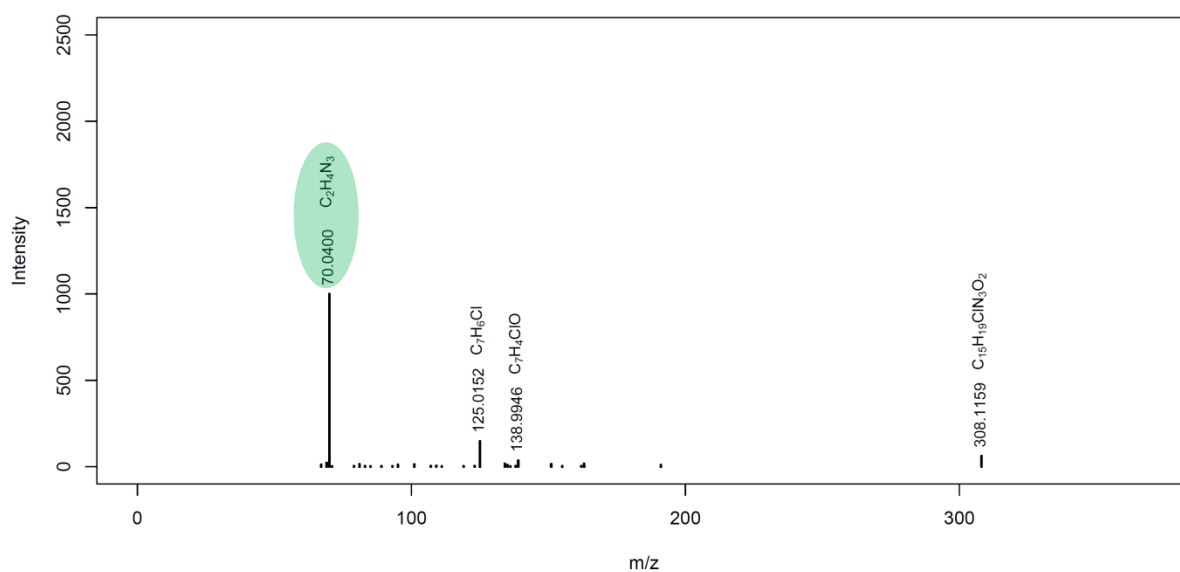
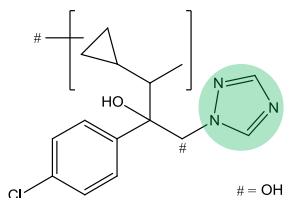
Cyproconazole (CP): The ionized triazole moiety is marked in green.

MassBank ID: **ET210001**



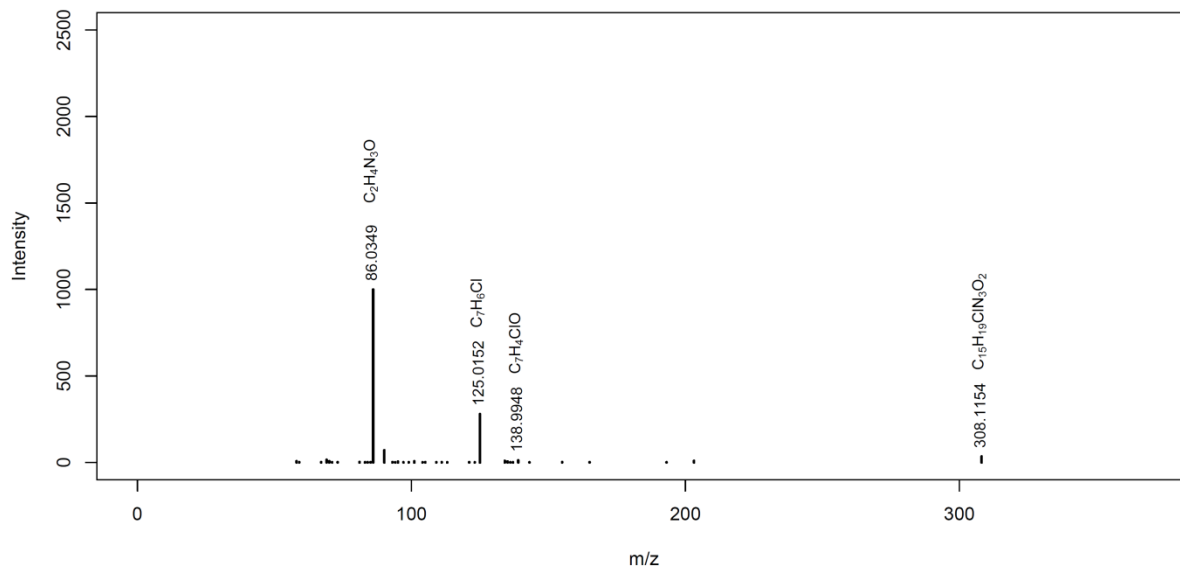
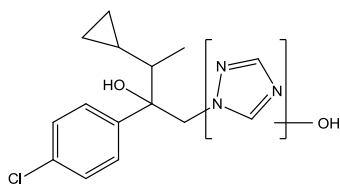
CP_M308a

MassBank ID: **ET210101:** The ionized triazole moiety is marked in green.



CP_M308b

MassBank ID: ET210201



CP_M308c

MassBank ID: ET210301

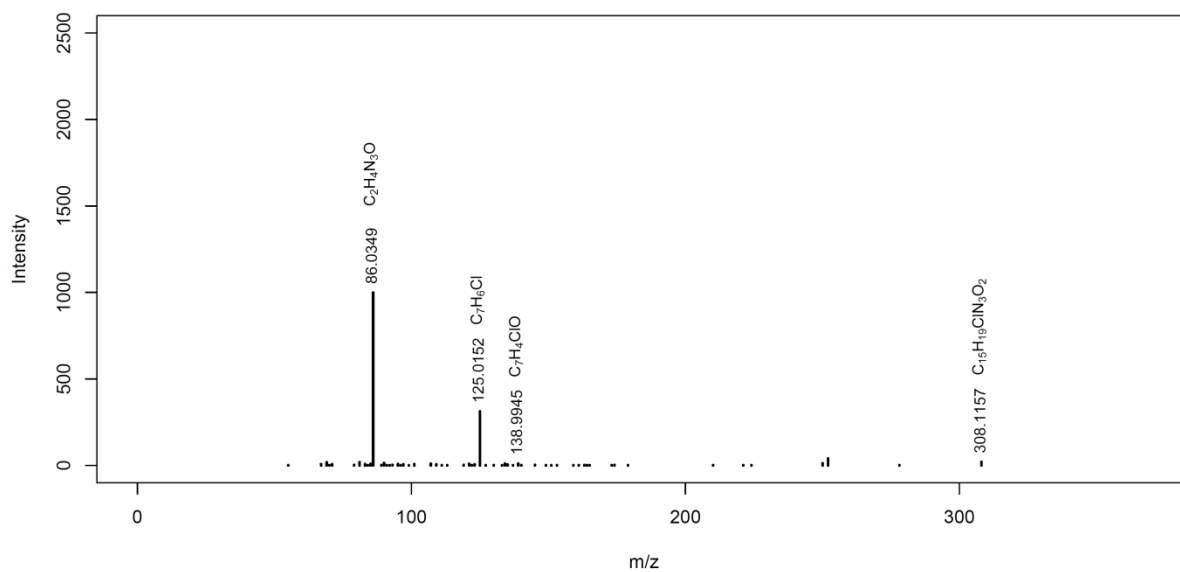
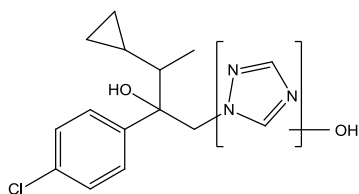
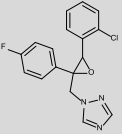


Table S2-17: Overview of epoxiconazole and identified biotransformation products formed in the aquatic invertebrate *G. pulex*. Biotransformation products are listed according to their relative peak intensity. Information about mass error, retention time (RT), and bioaccumulation factors (BAFs) are given for both replicate samples. CE stands for collision energy applied for fragmentation in the MS/MS experiment. Below each biotransformation product the abbreviation (S) stands for “identified by suspect screening (S)”, whereas (N) stands for “identified by nontarget” screening. The asterisk marks biotransformation products where the active azole moiety was altered.

Compound MassBank ID of displayed MSMS spectrum	Formula [M] Exact mass of [M+H] ⁺ / [M-H] ⁻	Mass error [ppm]	RT [min]	Polarity	Elemental change ⁱⁱ⁾	Log D _{ow} ⁱⁱⁱ⁾	Identification confidence ^{iv)} /level according to Schymanski et al. (2014) ^{6/ v)}	Description	CE [eV]	MS/MS confirmatory ions ^{vi)}
Epoxiconazole (EP) ET220001	C ₁₇ H ₁₃ ClFN ₃ O 330.0804	1.4 1.3	16.0 16.0	+		3.7	/1/	parent compound	25	121.0447 330.0803 141.0101
										
BAF [L kg_{ww}⁻¹] at t₂₄ ⁱ⁾: 57; 41										
EP_M346 * ET220101 (S)	C ₁₇ H ₁₃ ClFN ₃ O ₂ 346.0753	-0.5 -0.6	15.0 15.0	+	+ O	4.0-4.1	d for hydroxylation at the triazole ring /3/, 2 positional isomers	triazole ring hydroxylation	30	86.0349 121.0448 123.0241
EP_M449 ET220202 (S)	C ₂₀ H ₁₈ ClFN ₄ O ₃ S 449.0845	-1.3 0.2	13.9 13.9	+	+ C ₃ H ₇ NO ₂ S - H ₂	0.8	/3/, most likely structure, glutathione conjugation at epoxy group	glutathione conjugation and cysteine formation, further oxidation	30	404.0632 388.0684 70.0400
EP_M451 ET220302 (S)	C ₂₀ H ₂₀ ClFN ₄ O ₃ S 451.1001	-1.3 0.7	12.6 12.5	+	+ C ₃ H ₇ NO ₂ S	0.4	D for glutathione conjugation and cysteine formation at epoxy group /2b/	cysteine product	30	330.0804 120.0114 243.0372

Compound MassBank ID of displayed MSMS spectrum	Formula [M] Exact mass of [M+H] ⁺ / [M-H] ⁻	Mass error [ppm]	RT [min]	Polarity	Elemental change ⁱⁱ⁾	Log D _{ow} ⁱⁱⁱ⁾	Identification confidence ^{iv)} /level according to Schymanski et al. (2014) ⁶⁾ ^{v)}	Description	CE [eV]	MS/MS confirmatory ions ^{vi)}
EP_M467 ET220401 (S)	C ₂₀ H ₂₀ ClFN ₄ O ₄ S 467.0951	-0.4 -0.7	11.6 11.4	+	+ O + C ₃ H ₇ NO ₂ S	-0.01-0.6	D for glutathione conjugation and cysteine formation at epoxy group; d for no hydroxylation at fluorinated phenyl ring and triazole ring /3/, 5 positional isomers	hydroxylation, cysteine product	15	330.0803 120.0113 149.0389
EP_M424 ET220553 (S)	C ₁₇ H ₁₃ ClFN ₃ O ₅ S 424.0176	0.7 1.1	12.0 12.4	- ^(vii)	+ O + SO ₃	0.8	e /3/, 5 positional isomers but most likely structure; hydroxylation at C1 next to triazole ring	hydroxylation, sulfate conjugation	40	239.0515 68.0248 344.0610
EP_637 ET220601 (S)	C ₂₇ H ₃₀ ClFN ₆ O ₇ S 637.1642	-	12.4	+	+ C ₁₀ H ₁₇ N ₃ O ₆ S		D for glutathione conjugation at epoxy group /2b/	glutathione conjugation	20	330.0808 508.1218 562.1323

ⁱ⁾ See Equation 4 in section *Modeling Bioaccumulation and Biotransformation Kinetics* for the calculation of BAFs at steady state.

ⁱⁱ⁾ The elemental change refers to the change in the molecular formula of the biotransformation product in comparison with the parent compound.

ⁱⁱⁱ⁾ Log D_{ow} values were predicted by MarvinSketch version 14.10.20.0 at pH 7.9 and 25 °C. Log D_{ow} values correspond to corrected log K_{ow} values to account for pH-dependent dissociation. At pH 7.9 all selected target compounds are neutral thus log D_{ow} is equal to log K_{ow}. If different positional isomers are possible for one BTP, a range of log D_{ow} values is given.

^{iv)} D: diagnostic fragment for one structure; d: diagnostic fragment for positional isomers; e: enzyme deconjugation; l: structure reported in literature; m: MS/MS data from literature; p: biotransformation pathway information; d, p: diagnostic fragment for positional isomers (d) in combination with pathway information (p) give evidence for one possible structure.

^{v)} Levels are defined as follows: 5 (exact mass), 4 (unequivocal molecular formula), 3 (tentative candidates: e.g., positional isomers), 2 (probable structure: library spectrum match (a) or diagnostic evidence for one structure (b)) and 1 (confirmed structure).

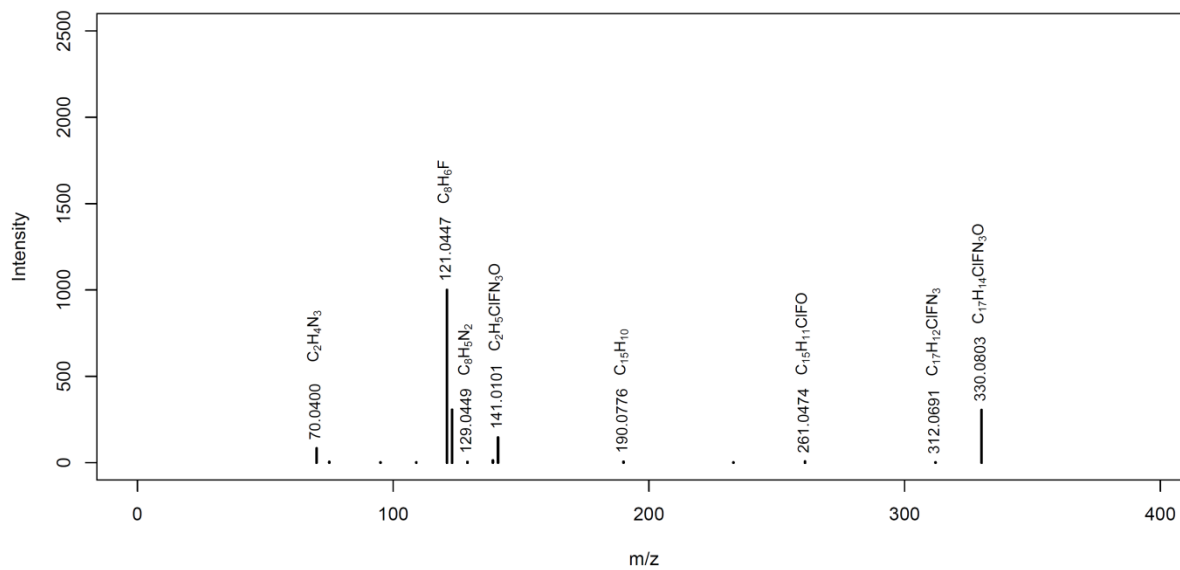
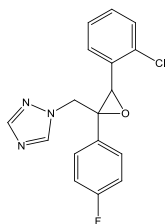
^{vi)} Diagnostic fragments (d, D) are listed first and are represented in bold in the table, other characteristic fragments are then presented according to their relative abundance. Only fragments where a chemical formula and structure could be attributed are considered.

^{vii)} The sulfate-containing BTPs are more sensitive in negative ionization mode. However, they were quantified in positive ionization mode because the respective parent compounds were also detected in positive ionization mode.

The different MassBank IDs for one compound refer to different collision energies applied during MS/MS fragmentation. The MassBank ID displayed in bold indicates the depicted MS/MS spectrum.

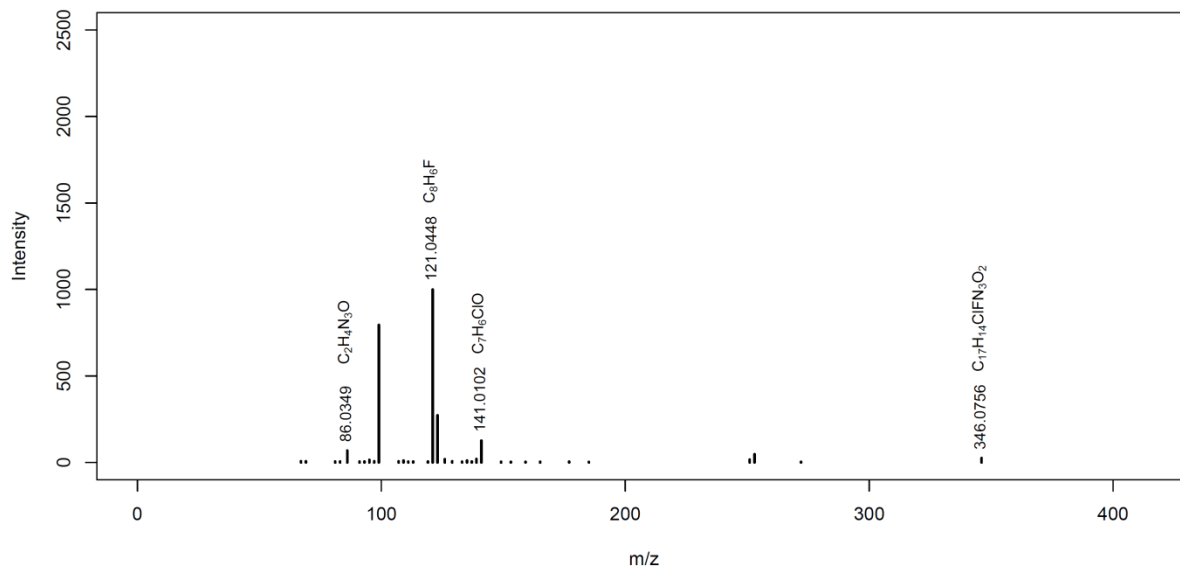
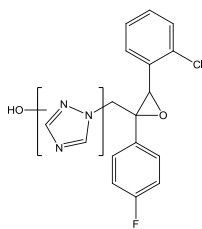
Epoxiconazole (EP)

MassBank ID: **ET220001**



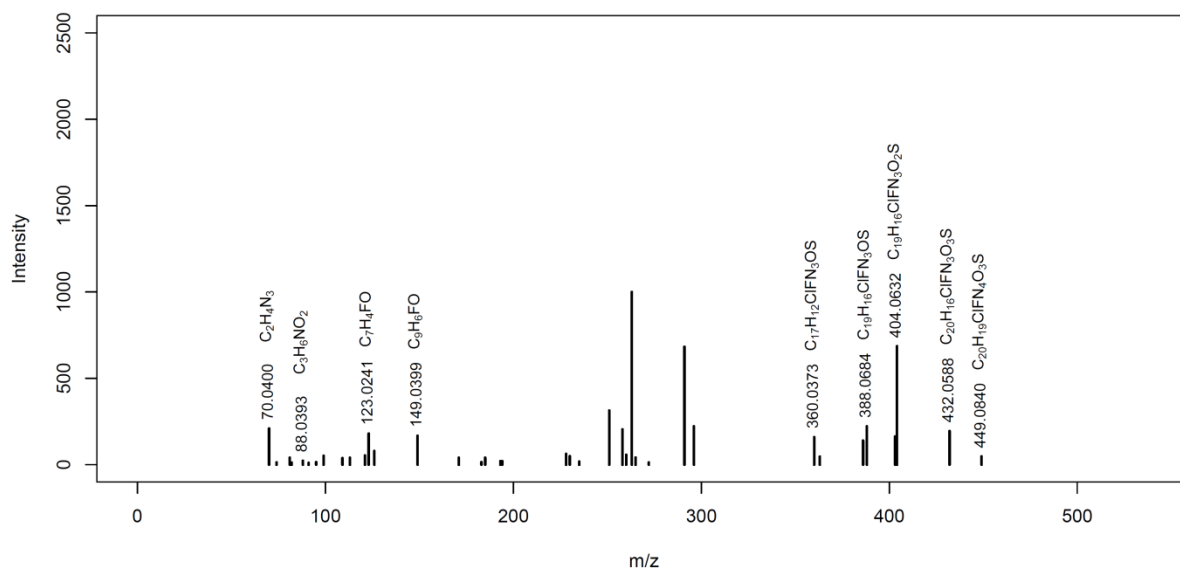
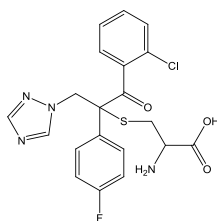
EP_M346

MassBank ID: ET220101, ET220102, ET220103, ET220104

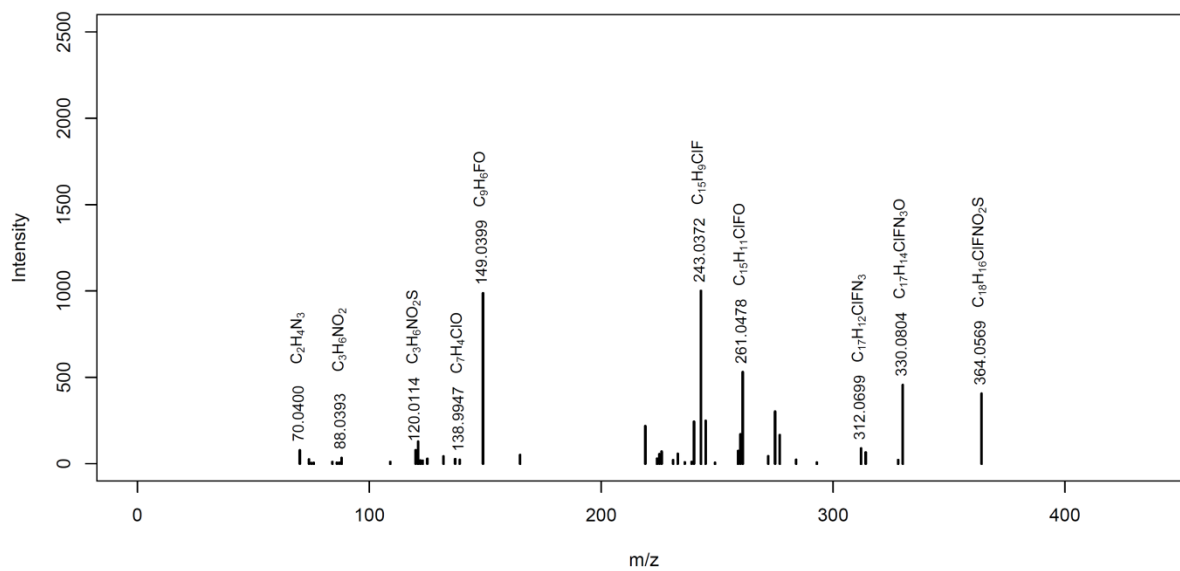
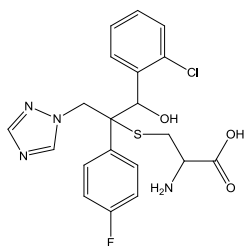


EP_M449

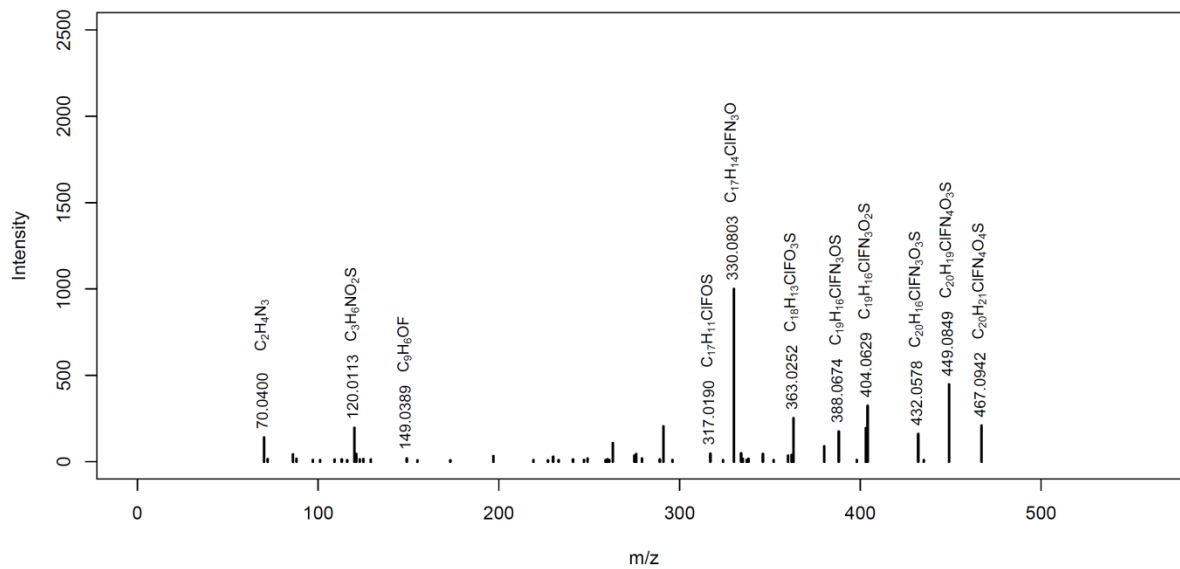
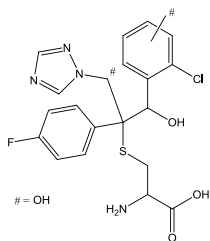
MassBank ID: ET220201, ET220202, ET220203, ET220204



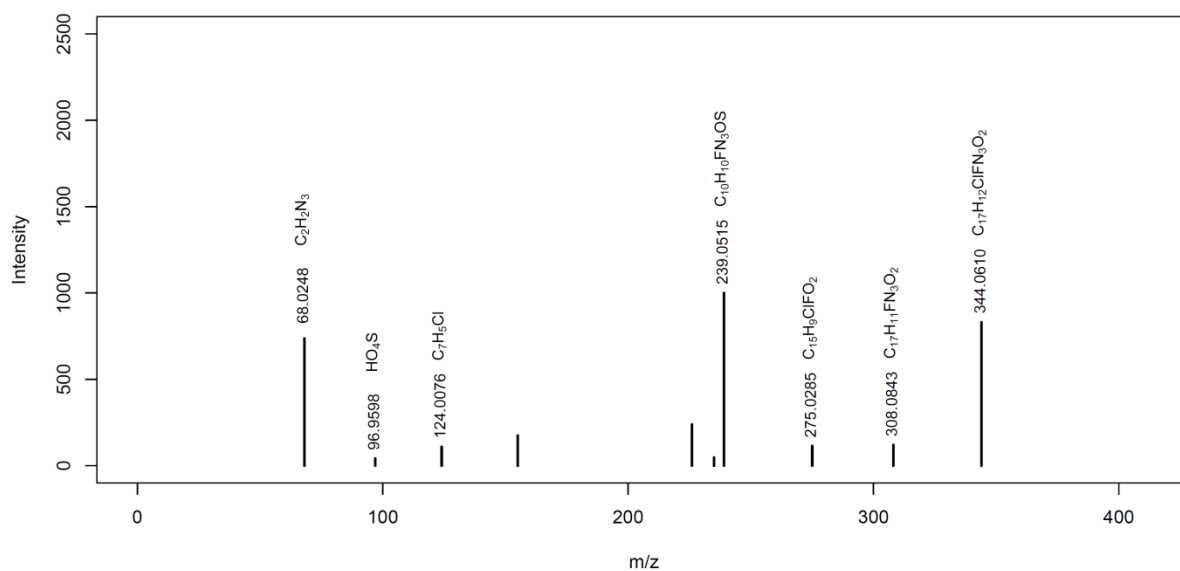
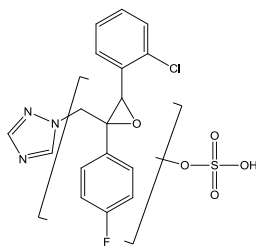
EP_M451

MassBank ID: ET220301, **ET220302**, ET220303, ET220304

EP_M467

MassBank ID: **ET220401**

EP_M424

MassBank ID: ET220551, ET220552, **ET220553**, ET220554

EP_M637

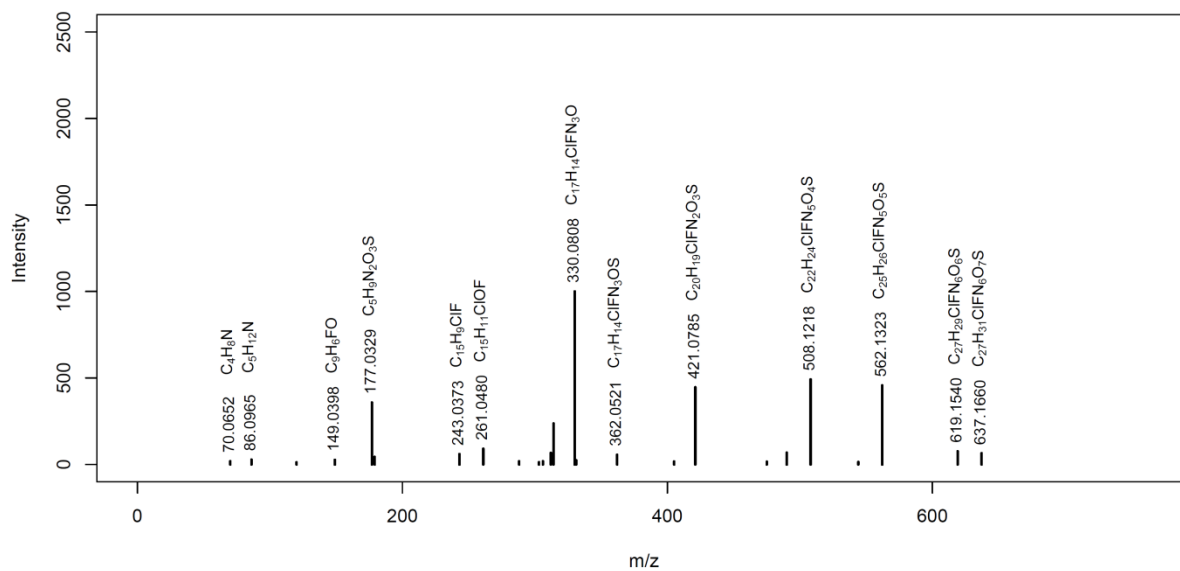
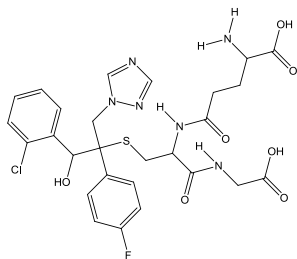
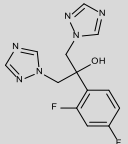
MassBank ID: **ET220601**, ET220602, ET220603, ET220604, ET220605

Table S2-18: Overview of fluconazole. Information about mass error, retention time (RT), and bioaccumulation factors (BAFs) are given for both replicate samples. CE stands for collision energy applied for fragmentation in the MS/MS experiment.

Compound MassBank ID of displayed MSMS spectrum	Formula [M] Exact mass of [M+H] ⁺ / [M-H] ⁻	Mass error [ppm]	RT [min]	Polarity	Elemental change ⁱⁱ⁾	Log D _{ow} ⁱⁱⁱ⁾	Identification confidence ^{iv)} /level according to Schymanski et al. (2014) ^{v)}	Description	CE [eV]	MS/MS confirmatory ions ^{vi)}
Fluconazole	C ₁₃ H ₁₂ F ₂ N ₆ O	-0.5	7.4	+		0.6	/1/	parent compound	35	220.0679
(FLU)	307.1113	-0.8	7.5							238.0784
ET230001										169.0458



BAF [L kg_{ww}⁻¹] at t₂₄ ⁱ⁾:
0.40; 0.38

ⁱ⁾ See Equation 4 in section *Modeling Bioaccumulation and Biotransformation Kinetics* for the calculation of BAFs at steady state.

ⁱⁱ⁾ The elemental change refers to the change in the molecular formula of the biotransformation product in comparison with the parent compound.

ⁱⁱⁱ⁾ Log D_{ow} values were predicted by MarvinSketch version 14.10.20.0 at pH 7.9 and 25 °C. Log D_{ow} values correspond to corrected log K_{ow} values to account for pH-dependent dissociation. At pH 7.9 all selected target compounds are neutral thus log D_{ow} is equal to log K_{ow}. If different positional isomers are possible for one BTP, a range of log D_{ow} values is given.

^{iv)} D: diagnostic fragment for one structure; d: diagnostic fragment for positional isomers; e: enzyme deconjugation; l: structure reported in literature; m: MS/MS data from literature; p: biotransformation pathway information; d, p: diagnostic fragment for positional isomers (d) in combination with pathway information (p) give evidence for one possible structure.

^{v)} Levels are defined as follows: 5 (*exact mass*), 4 (*unequivocal molecular formula*), 3 (*tentative candidates: e.g., positional isomers*), 2 (*probable structure: library spectrum match (a) or diagnostic evidence for one structure (b)*) and 1 (*confirmed structure*).

^{vi)} Diagnostic fragments (d, D) are listed first and are represented in bold in the table, other characteristic fragments are then presented according to their relative abundance. Only fragments where a chemical formula and structure could be attributed are considered.

The MassBank ID displayed in bold indicates the depicted MS/MS spectrum.

Fluconazole (FLU)

MassBank ID: **ET230001**

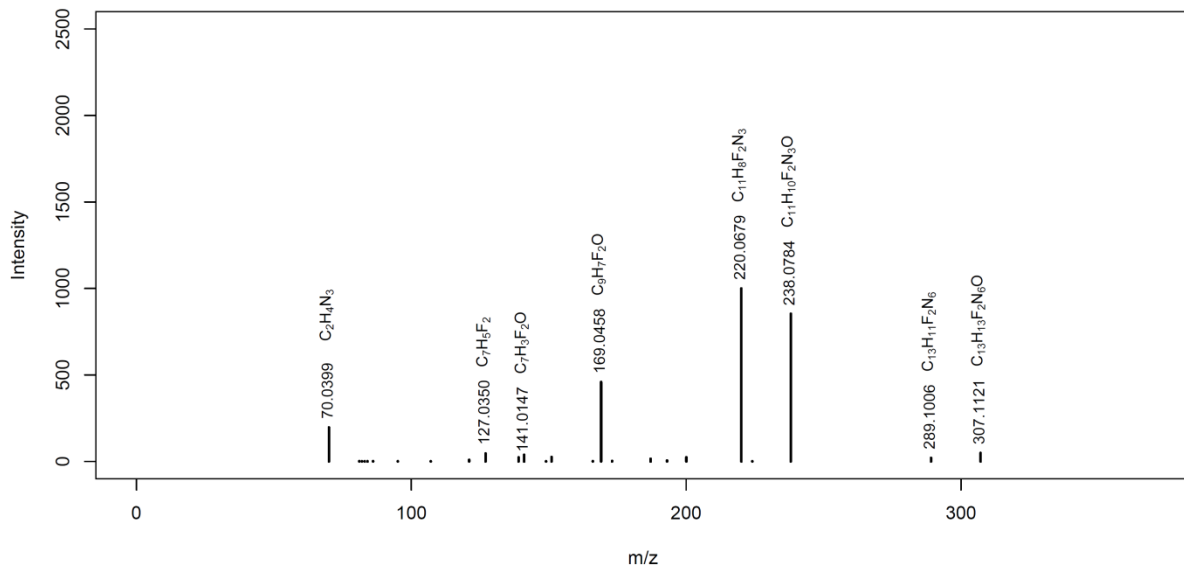
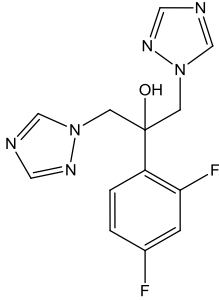
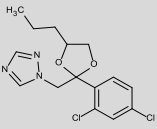


Table S2-19: Overview of propiconazole and identified biotransformation products formed in the aquatic invertebrate *G. pulex*. Biotransformation products are listed according to their relative peak intensity. Information about mass error, retention time (RT), and bioaccumulation factors (BAFs) are given for both replicate samples. CE stands for collision energy applied for fragmentation in the MS/MS experiment. Below each biotransformation product the abbreviation (S) stands for “identified by suspect screening (S)”, whereas (N) stands for “identified by nontarget” screening. The asterisk marks biotransformation products where the active azole moiety was altered.

Compound MassBank ID of displayed MSMS spectrum	Formula [M] Exact mass of [M+H] ⁺ / [M-H] ⁻	Mass error [ppm]	RT [min]	Polarity	Elemental change ⁱⁱ⁾	Log D _{ow} ⁱⁱⁱ⁾	Identification confidence ^{iv)} /level according to Schymanski et al. (2014) ^{6/ v)}	Description	CE [eV]	MS/MS confirmatory ions ^{vi)}
Propiconazole (PRP) ET240001	C ₁₅ H ₁₇ Cl ₂ N ₃ O ₂ 342.0771	2.0 1.9	17.0 17.0	+		4.3	/1/	parent compound	30	158.9762 69.0699 342.0768
 <p>BAF [L kg_{ww}⁻¹] at t₂₄ ⁱ⁾: 24; 29</p>										
PRP_M358a ET240103 (S)	C ₁₅ H ₁₇ Cl ₂ N ₃ O ₃ 358.0720	-0.5 -0.5	13.8 14.0	+	+ O	2.8-3.3	d for aliphatic hydroxylation l ¹³ m ¹³ /3/, 6 positional isomers	aliphatic hydroxylation	40	158.9762 70.0399 256.0036
PRP_M358b ET240203 (S)	C ₁₅ H ₁₇ Cl ₂ N ₃ O ₃ 358.0720	-0.5 0.2	14.5 14.5	+	+ O	2.8-3.3	d for aliphatic hydroxylation l ¹³ m ¹³ /3/, 6 positional isomers	aliphatic hydroxylation	40	158.9762 70.0400 256.0037
PRP_M258 ET240302 (N)	C ₁₀ H ₉ Cl ₂ N ₃ O 258.0195	-0.2 -0.2	12.3 12.3	+	- C ₅ H ₈ O	2.0	D l ⁹ /2b/	partial loss of dioxolane containing the propyl moiety (ether cleavage)	30	258.0196 70.0399 188.9868

Compound MassBank ID of displayed MSMS spectrum	Formula [M] Exact mass of [M+H] ⁺ / [M-H] ⁻	Mass error [ppm]	RT [min]	Polarity	Elemental change ⁱⁱ⁾	Log D _{ow} ⁱⁱⁱ⁾	Identification confidence ^{iv)} /level according to Schymanski et al. (2014) ^{6/ v)}	Description	CE [eV]	MS/MS confirmatory ions ^{vi)}
PRP_M256	C ₁₀ H ₇ Cl ₂ N ₃ O	-0.5	11.5	+	-C ₅ H ₁₀ O	2.2	D	partial loss of dioxolane	50	256.0036
ET240401 (S)	256.0039	0.1	11.6				I ⁹ /2b/	containing the propyl moiety (ether cleavage), further oxidation		158.9762 186.9710

ⁱ⁾ See Equation 4 in section *Modeling Bioaccumulation and Biotransformation Kinetics* for the calculation of BAFs at steady state.

ⁱⁱ⁾ The elemental change refers to the change in the molecular formula of the biotransformation product in comparison with the parent compound.

ⁱⁱⁱ⁾ Log D_{ow} values were predicted by MarvinSketch version 14.10.20.0 at pH 7.9 and 25 °C. Log D_{ow} values correspond to corrected log K_{ow} values to account for pH-dependent dissociation. At pH 7.9 all selected target compounds are neutral thus log D_{ow} is equal to log K_{ow}. If different positional isomers are possible for one BTP, a range of log D_{ow} values is given.

^{iv)} D: diagnostic fragment for one structure; d: diagnostic fragment for positional isomers; e: enzyme deconjugation; I: structure reported in literature; m: MS/MS data from literature ; p: biotransformation pathway information; d, p: diagnostic fragment for positional isomers (d) in combination with pathway information (p) give evidence for one possible structure.

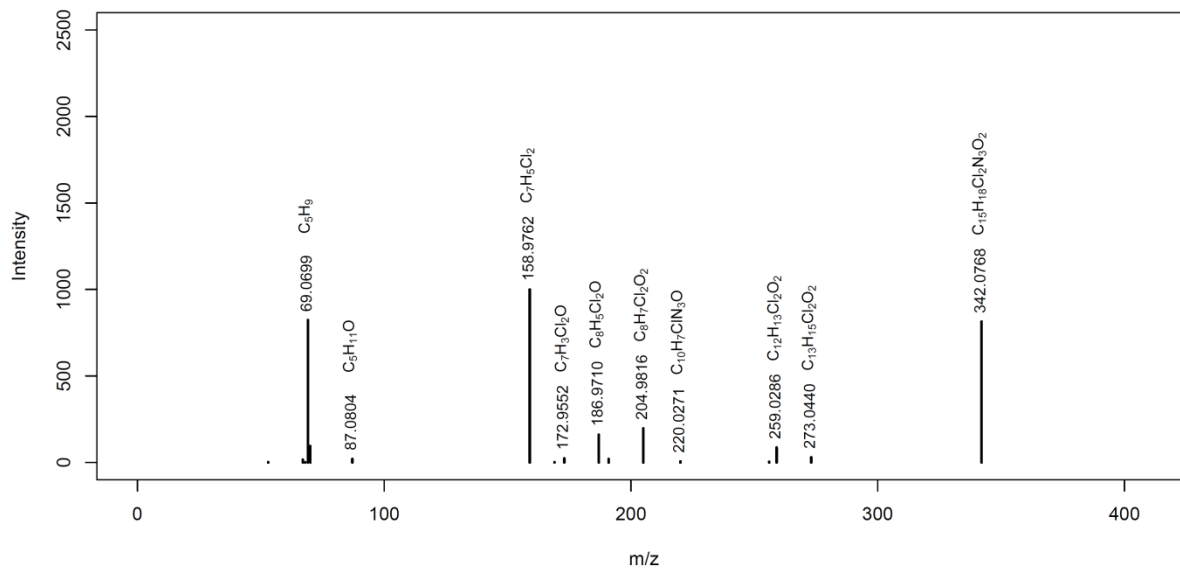
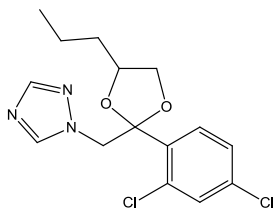
^{v)} Levels are defined as follows: 5 (*exact mass*), 4 (*unequivocal molecular formula*), 3 (*tentative candidates: e.g., positional isomers*), 2 (*probable structure: library spectrum match (a) or diagnostic evidence for one structure (b)*) and 1 (*confirmed structure*).

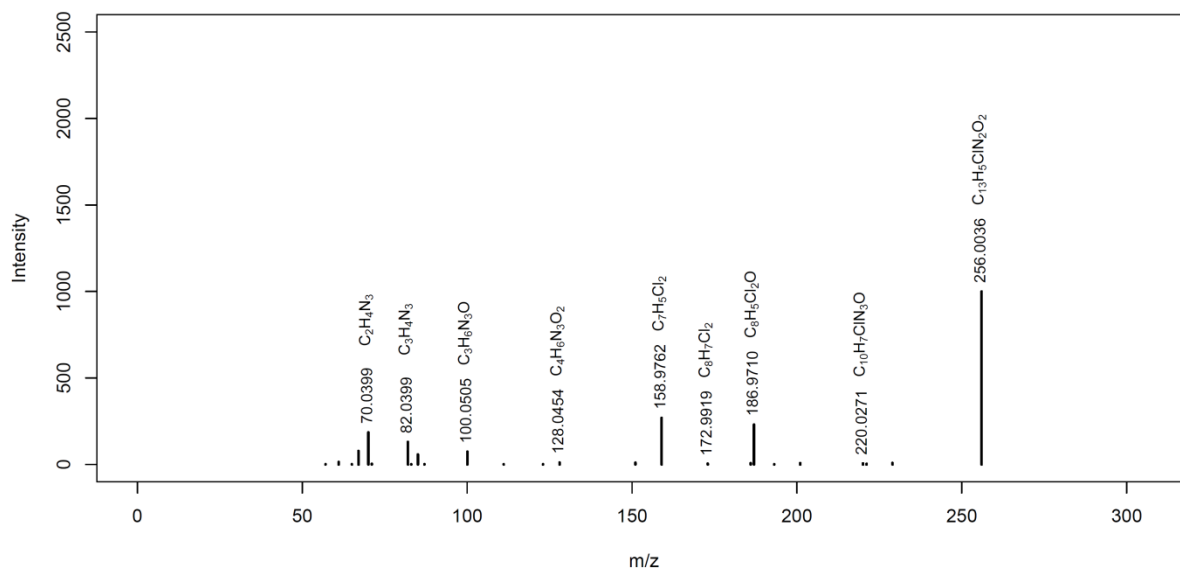
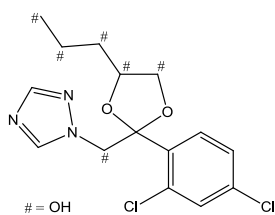
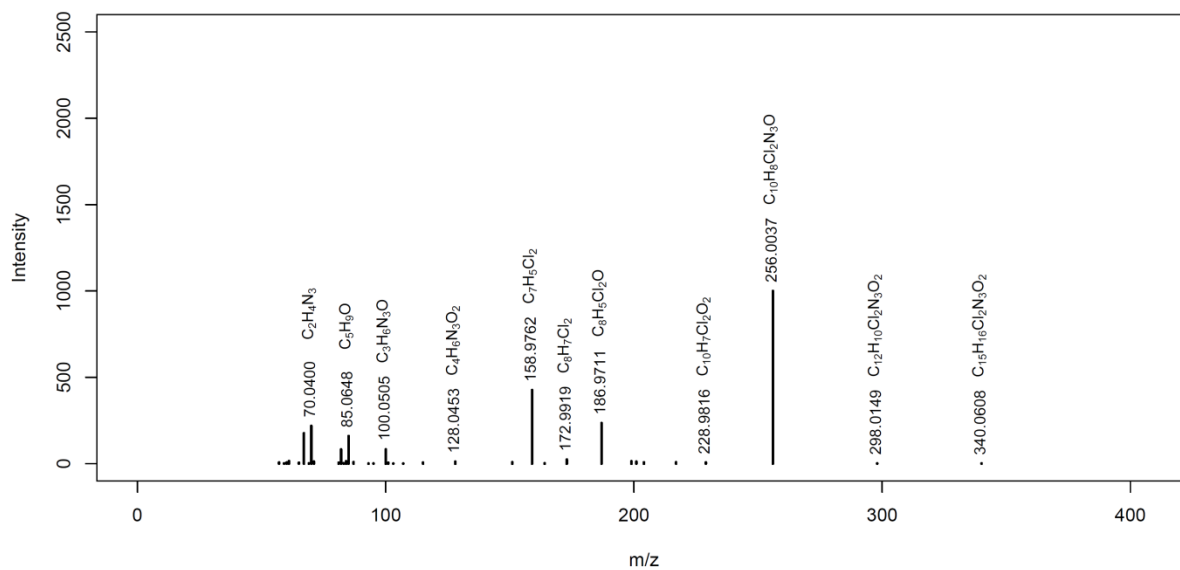
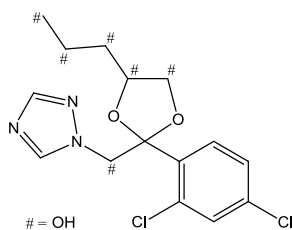
^{vi)} Diagnostic fragments (d, D) are listed first and are represented in bold in the table, other characteristic fragments are then presented according to their relative abundance. Only fragments where a chemical formula and structure could be attributed are considered.

The different MassBank IDs for one compound refer to different collision energies applied during MS/MS fragmentation. The MassBank ID displayed in bold indicates the depicted MS/MS spectrum.

Propiconazole (PRP)

MassBank ID: **ET240001**, ET240002, ET240003, ET240004



PRP_M358aMassBank ID: ET240101, ET240102, **ET240103**, ET240104**PRP_M358b**MassBank ID: ET240201, ET240202, **ET240203**, ET240204

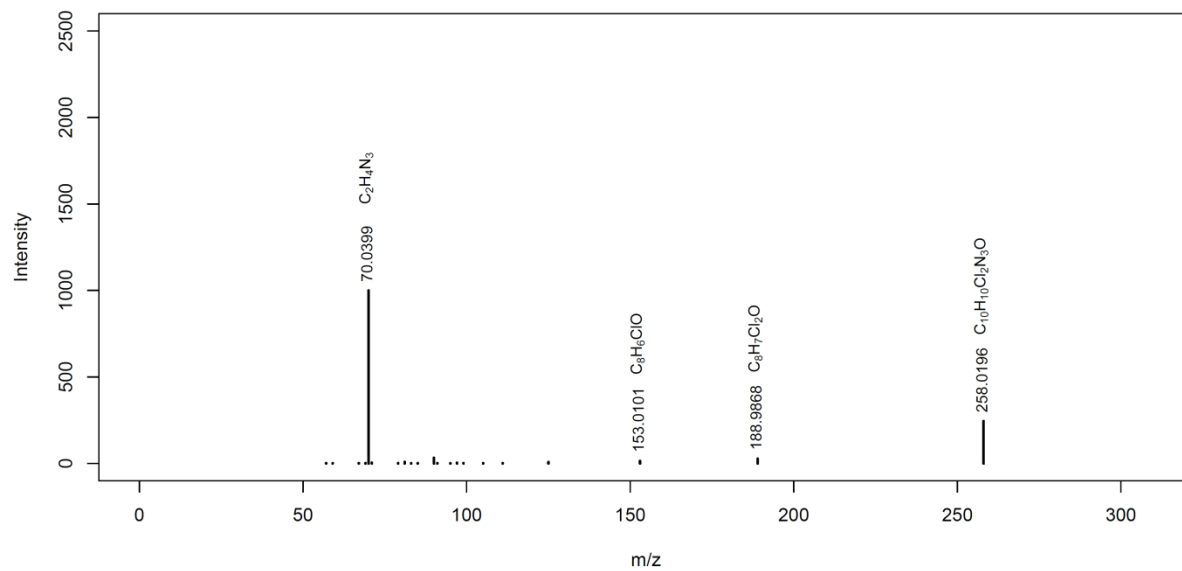
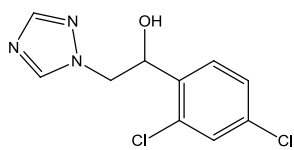
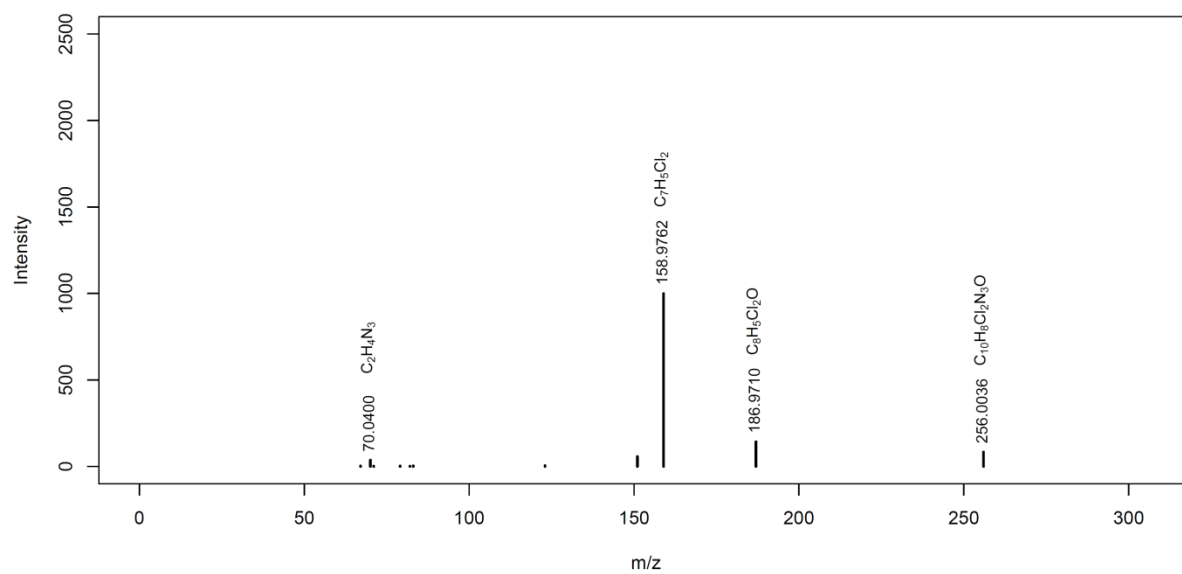
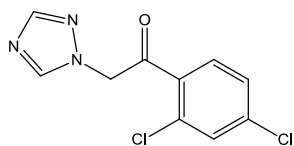
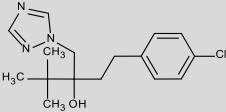
PRP_M258MassBank ID: ET240301, **ET240302**, ET240303, ET240304, ET240305**PRP_M256**MassBank ID: **ET240401**, ET240402, ET240403, ET240404

Table S2-20: Overview of tebuconazole and identified biotransformation products formed in the aquatic invertebrate *G. pulex*. Biotransformation products are listed according to their relative peak intensity. Information about mass error, retention time (RT), and bioaccumulation factors (BAFs) are given for both replicate samples. CE stands for collision energy applied for fragmentation in the MS/MS experiment. Below each biotransformation product the abbreviation (S) stands for “identified by suspect screening (S)”, whereas (N) stands for “identified by nontarget” screening. The asterisk marks biotransformation products where the active azole moiety was altered.

Compound MassBank ID of displayed MSMS spectrum	Formula [M] Exact mass of [M+H] ⁺ / [M-H] ⁻	Mass error [ppm]	RT [min]	Polarity	Elemental change ⁱⁱ⁾	Log D _{ow} ⁱⁱⁱ⁾	Identification confidence ^{iv)} /level according to Schymanski et al. (2014) ^{6/ v)}	Description	CE [eV]	MS/MS confirmatory ions ^{vi)}
Tebuconazole (TEB) ET250001	C ₁₆ H ₂₂ ClN ₃ O 308.1524	1.6 1.2	16.8 16.8	+		3.7	/1/	parent compound	35	70.0400 308.1524 125.0153
 <p>BAF [L kg_{ww}⁻¹] at t₂₄ ⁱ⁾: 31; 30</p>										
TEB_M324a ET250101 (S)	C ₁₆ H ₂₂ ClN ₃ O ₂ 324.1473	0.1 0.5	15.0 15.1	+	+ O	2.4	D for hydroxylation at <i>tert</i> -butyl group I ¹⁴ /2b/	aliphatic hydroxylation	30	165.0467 70.0399 324.1472
TEB_M388 ET250203 (N)	C ₁₆ H ₂₃ ClN ₃ O ₄ P 388.1187	-0.1 -0.1	15.7 15.8	+	+ HPO ₃	-0.2	D for phosphate conjugation at OH group /2b/	phosphate conjugation	30	290.1419 83.0855 105.0699
TEB_M404 ET250303 (N)	C ₁₆ H ₂₃ ClN ₃ O ₅ P 404.1137	-1.1 -0.3	12.6 12.6	+	+ O + HPO ₃	-1.5	D for phosphate conjugation at OH group and for hydroxylation at <i>tert</i> -butyl group /2b/	aliphatic hydroxylation, phosphate conjugation	30	306.1368 165.0466 288.1263

Compound MassBank ID of displayed MSMS spectrum	Formula [M] Exact mass of [M+H] ⁺ / [M-H] ⁻	Mass error [ppm]	RT [min]	Polarity	Elemental change ⁱⁱ⁾	Log D _{ow} ⁱⁱⁱ⁾	Identification confidence ^{iv)} /level according to Schymanski et al. (2014) ^{6/ v)}	Description	CE [eV]	MS/MS confirmatory ions ^{vi)}
TEB_M324b * ET250401 (S)	C ₁₆ H ₂₂ ClN ₃ O ₂ 324.1473	-0.4 0.3	15.8 15.9	+	+ O	4.0-4.1	d for hydroxylation at the triazole ring /3/, 2 positional isomers	triazole ring hydroxylation	30	86.0349 324.1474 151.0309
TEB_M324c ET250501 (S)	C ₁₆ H ₂₂ ClN ₃ O ₂ 324.1473	-0.1 -0.3	16.3 16.3	+	+ O	2.4	d for hydroxylation at the <i>tert</i> -butyl group, at the chlorophenyl moiety or at C1 next to the chlorophenyl moiety I ¹⁴ /3/, 5 positional isomers	hydroxylation	30	70.0400 324.1478 207.0934

ⁱ⁾ See Equation 4 in section *Modeling Bioaccumulation and Biotransformation Kinetics* for the calculation of BAFs at steady state.

ⁱⁱ⁾ The elemental change refers to the change in the molecular formula of the biotransformation product in comparison with the parent compound.

ⁱⁱⁱ⁾ Log D_{ow} values were predicted by MarvinSketch version 14.10.20.0 at pH 7.9 and 25 °C. Log D_{ow} values correspond to corrected log K_{ow} values to account for pH-dependent dissociation. At pH 7.9 all selected target compounds are neutral thus log D_{ow} is equal to log K_{ow}. If different positional isomers are possible for one BTP, a range of log D_{ow} values is given.

^{iv)} D: diagnostic fragment for one structure; d: diagnostic fragment for positional isomers; e: enzyme deconjugation; l: structure reported in literature; m: MS/MS data from literature; p: biotransformation pathway information; d, p: diagnostic fragment for positional isomers (d) in combination with pathway information (p) give evidence for one possible structure.

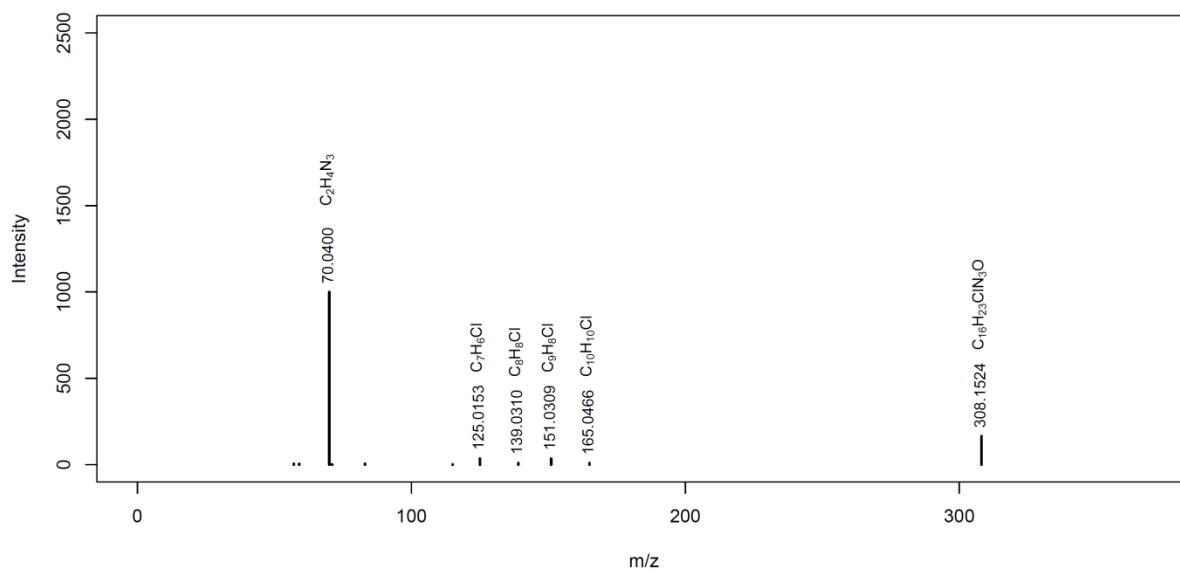
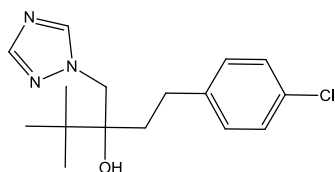
^{v)} Levels are defined as follows: 5 (*exact mass*), 4 (*unequivocal molecular formula*), 3 (*tentative candidates: e.g., positional isomers*), 2 (*probable structure: library spectrum match (a) or diagnostic evidence for one structure (b)*) and 1 (*confirmed structure*).

^{vi)} Diagnostic fragments (d, D) are listed first and are represented in bold in the table, other characteristic fragments are then presented according to their relative abundance. Only fragments where a chemical formula and structure could be attributed are considered.

The different MassBank IDs for one compound refer to different collision energies applied during MS/MS fragmentation. The MassBank ID displayed in bold indicates the depicted MS/MS spectrum.

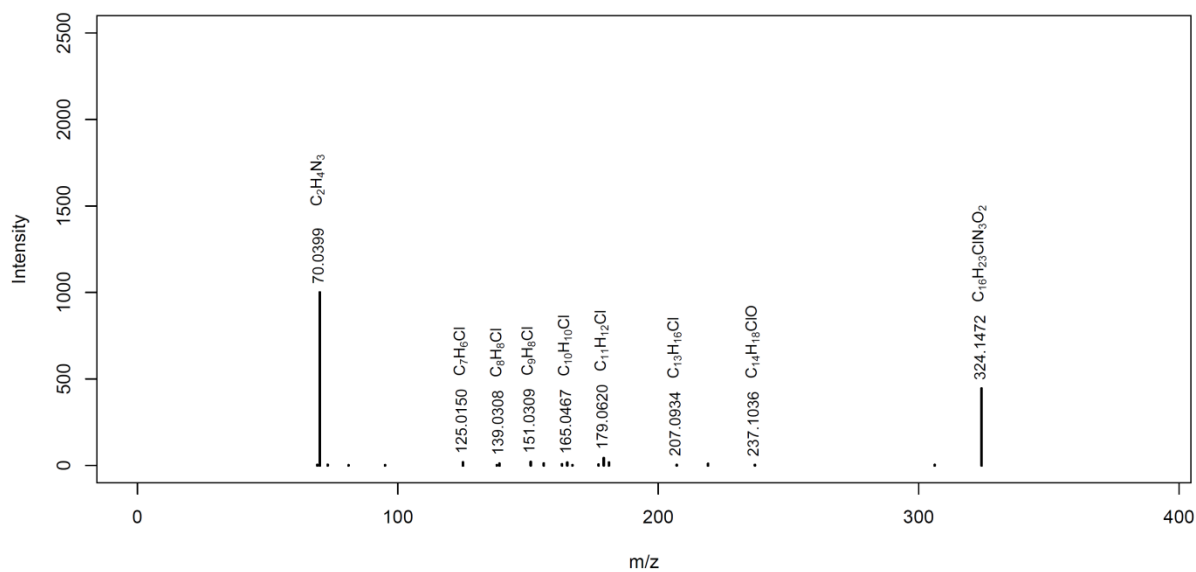
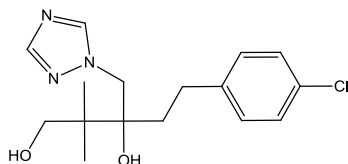
Tebuconazole (TEB)

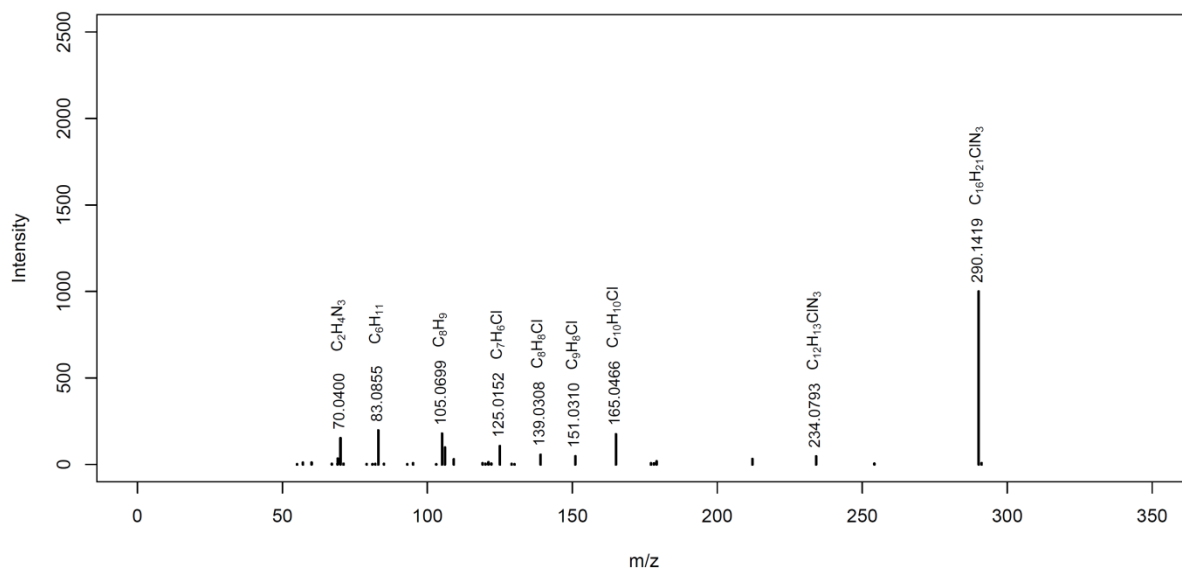
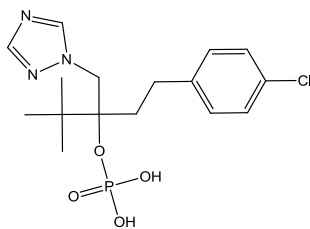
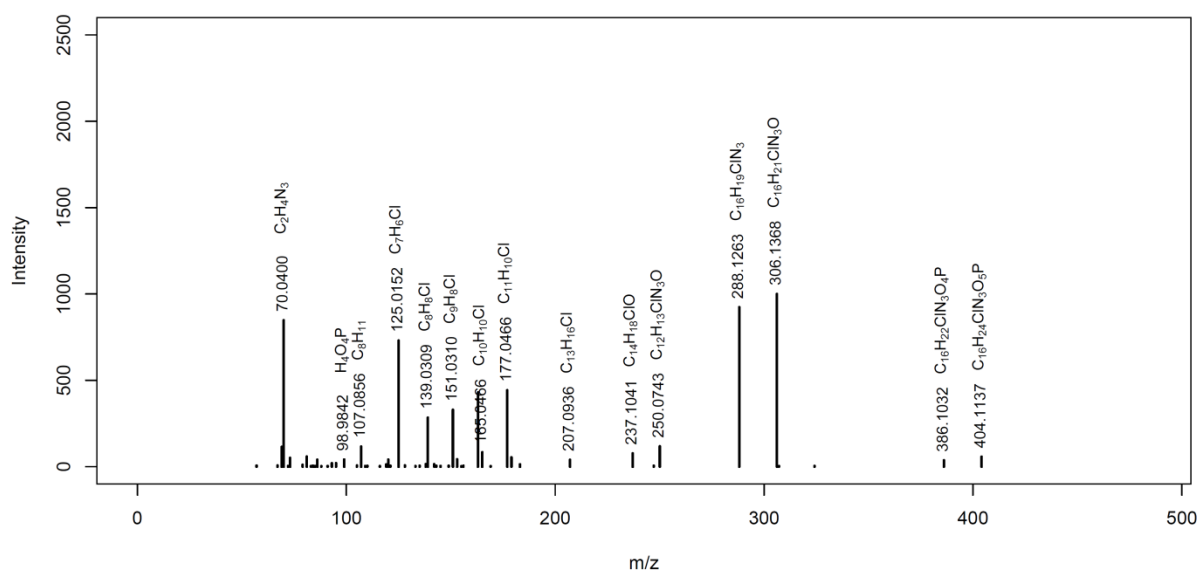
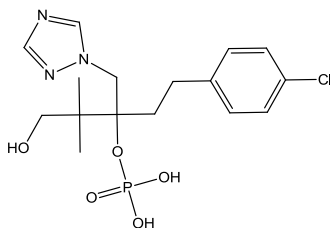
MassBank ID: **ET250001**



TEB_M324a

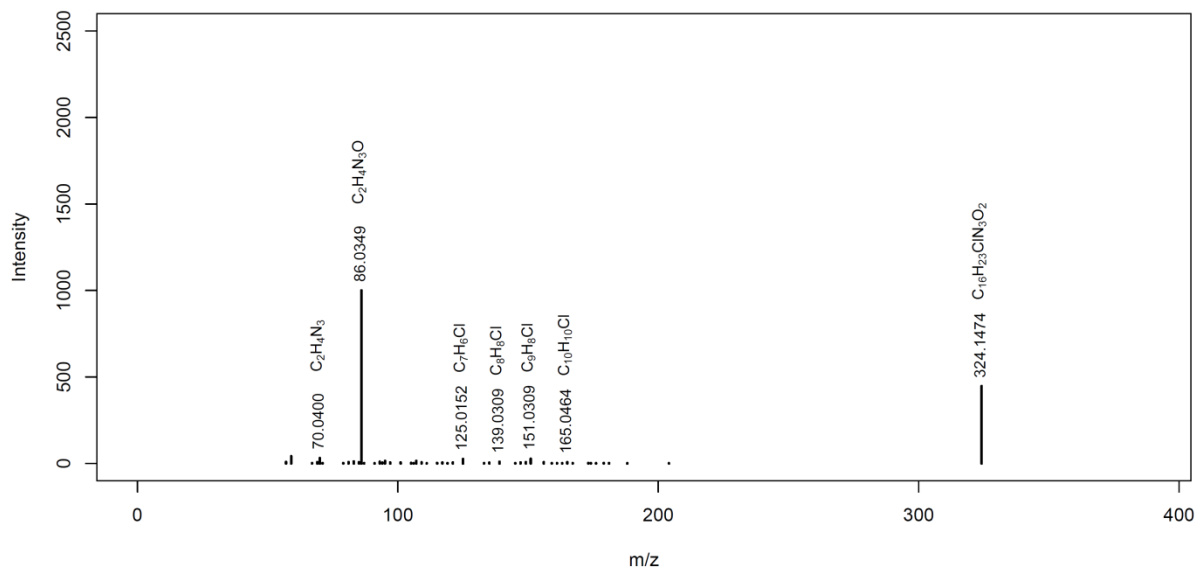
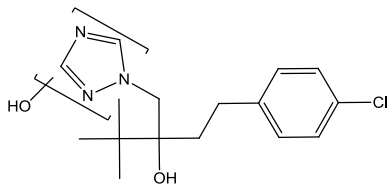
MassBank ID: **ET250101**



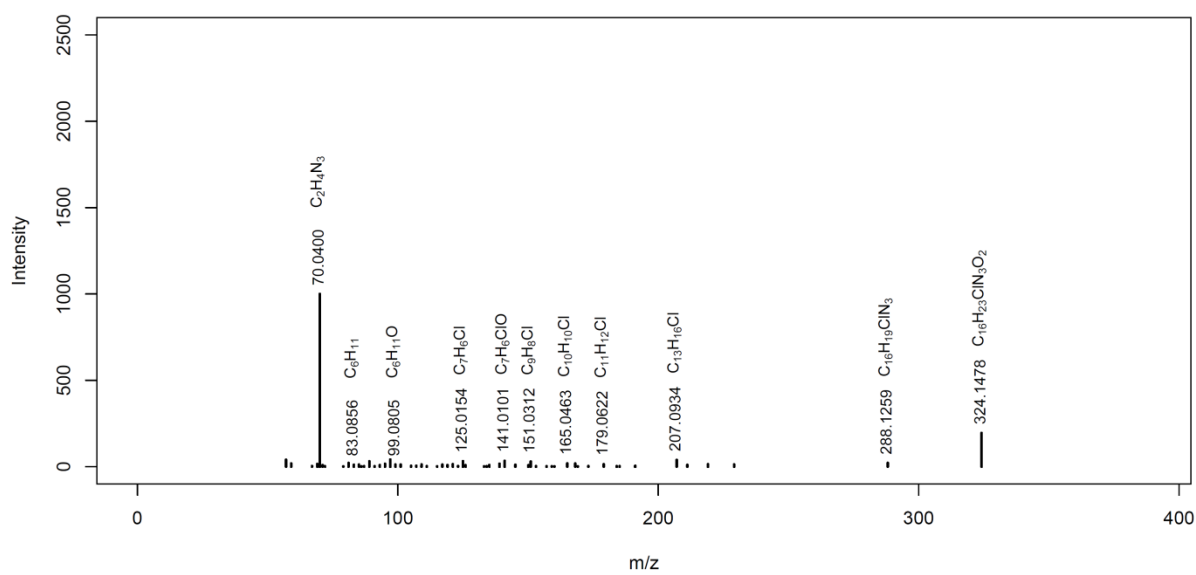
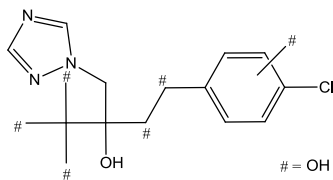
TEB_M388MassBank ID: ET250201, ET250202, **ET250203**, ET250204, ET250205**TEB_M404**MassBank ID: ET250301, ET250302, **ET250303**, ET250304, ET250305

TEB_M324b

MassBank ID: ET250401

**TEB_M324c**

MassBank ID: ET250501



SI.J Effects of Biotransformation on the Polarity of Biotransformation Products

Most of the identified BTPs displayed smaller chromatographic retention times on the reverse phase column than the parent compounds, except for all imidazole ring cleavage products (PRZ_M325, PRZ_M353, PRZ_M382, KET_M565) and the cysteine product PRZ_M429. This observation is in line with the general theory that biotransformation leads to more polar compounds and has also been found in other studies about biotransformation of xenobiotics in aquatic crustaceans^{1, 15}, and biotransformation of azole fungicides in other organism classes.^{7, 11, 16-17}

Log D_{ow} values were predicted for the parent compounds and their BTPs based on the molecules' atomic increments (MarvinSketch software version 14.10.20.0). Interestingly, the log D_{ow} values of the ring cleavage products are smaller than the corresponding value of the parent compound (see SI I). This is in agreement with the structural changes but in contrast to their higher chromatographic retention times.

References

- [1] Jeon, J.; Kurth, D.; Hollender, J., Biotransformation pathways of biocides and pharmaceuticals in freshwater crustaceans based on structure elucidation of metabolites using high resolution mass spectrometry. *Chem. Res. Toxicol.* **2013**, *26* (3), 313-24.
- [2] Stoob, K.; Singer, H. P.; Goetz, C. W.; Ruff, M.; Mueller, S. R., Fully automated online solid phase extraction coupled directly to liquid chromatography-tandem mass spectrometry - Quantification of sulfonamide antibiotics, neutral and acidic pesticides at low concentrations in surface waters. *Journal of Chromatography A* **2005**, *1097* (1-2), 138-147.
- [3] Huntscha, S.; Singer, H. P.; McArdell, C. S.; Frank, C. E.; Hollender, J., Multiresidue analysis of 88 polar organic micropollutants in ground, surface and wastewater using online mixed-bed multilayer solid-phase extraction coupled to high performance liquid chromatography-tandem mass spectrometry. *J. Chromatogr. A* **2012**, *1268*, 74-83.
- [4] Jeon, J.; Kurth, D.; Ashauer, R.; Hollender, J., Comparative toxicokinetics of organic micropollutants in freshwater crustaceans. *Environ. Sci. Technol.* **2013**, *47* (15), 8809-17.
- [5] Kukkonen, J.; Oikari, A., Sulphate conjugation is the main route of pentachlorophenol metabolism in *Daphnia magna*. *Comparative Biochemistry and Physiology - C Pharmacology Toxicology and Endocrinology* **1988**, *91* (2), 465-468.
- [6] Schymanski, E. L.; Jeon, J.; Gulde, R.; Fenner, K.; Ruff, M.; Singer, H. P.; Hollender, J., Identifying Small Molecules via High Resolution Mass Spectrometry: Communicating Confidence. *Environmental Science & Technology* **2014**, *48* (4), 2097-2098.
- [7] Debrauwer, L.; Rathahao, E.; Boudry, G.; Baradat, M.; Cravedi, J. P., Identification of the major metabolites of prochloraz in rainbow trout by liquid chromatography and tandem mass spectrometry. *J. Agric. Food. Chem.* **2001**, *49* (8), 3821-3826.
- [8] Needham, D.; Challis, I. R., The metabolism and excretion of prochloraz, an imidazole-based fungicide, in the rat. *Xenobiotica* **1991**, *21* (11), 1473-1482.
- [9] Roberts, T. R.; Hutson, D. H., Metabolic Pathways of Agrochemicals: Part 2, Insecticides and fungicides. *Royal Society of Chemistry* **1999**.
- [10] Laignelet, L.; Riviere, J. L.; Lhuguenot, J. C., Metabolism of an imidazole fungicide (prochloraz) in the rat after oral administration. *Food Chem. Toxicol.* **1992**, *30* (7), 575-583.
- [11] Fitch, W. L.; Tran, T.; Young, M.; Liu, L.; Chen, Y., Revisiting the metabolism of ketoconazole using accurate mass. *Drug metabolism letters* **2009**, *3* (3), 191-8.
- [12] Whitehouse, L. W.; Menzies, A.; Dawson, B.; Cyr, T. D.; By, A. W.; Black, D. B.; Zamecnik, J., Mouse hepatic metabolites of ketoconazole - isolation and structure elucidation. *J. Pharm. Biomed. Anal.* **1994**, *12* (11), 1425-1441.
- [13] Mazur, C. S.; Kenneke, J. F., Cross-species comparison of conazole fungicide metabolites using rat and rainbow trout (*Onchorhynchus mykiss*) hepatic microsomes and purified human CYP 3A4. *Environmental Science & Technology* **2008**, *42* (3), 947-954.
- [14] INCHEM IPCS International Program on Chemical Safety. <http://www.inchem.org/documents/jmpr/jmpmono/v94pr10.htm>.
- [15] Ikenaka, Y.; Ishizaka, M.; Eun, H.; Miyabara, Y., Glucose-sulfate conjugates as a new phase II metabolite formed by aquatic crustaceans. *Biochem. Biophys. Res. Commun.* **2007**, *360* (2), 490-495.
- [16] Chen, P. J.; Moore, T.; Nesnow, S., Cytotoxic effects of propiconazole and its metabolites in mouse and human hepatoma cells and primary mouse hepatocytes. *Toxicology in Vitro* **2008**, *22* (6), 1476-1483.
- [17] Obanda, D. N.; Shupe, T. F., Biotransformation of tebuconazole by microorganisms: Evidence of a common mechanism. *Wood and Fiber Science* **2009**, *41* (2), 157-167.

Chapter 3. Mechanistic Understanding of the Synergistic Potential of Azole Fungicides in the Aquatic Invertebrate *Gammarus pulex*

Andrea Rösch^{1,2}, Michele Gottardi³, Caroline Vignet¹, Nina Cedergreen³, Juliane Hollender^{1,2*}

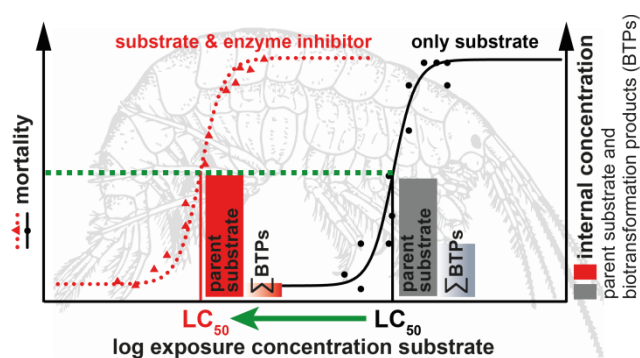
¹ Eawag, Swiss Federal Institute of Aquatic Science and Technology, 8600 Dübendorf, Switzerland

² Institute of Biogeochemistry and Pollutant Dynamics, ETH Zürich, 8092 Zürich, Switzerland

³ Department of Plant and Environmental Sciences, University of Copenhagen, 1871 Frederiksberg C, Denmark

* Corresponding Author: Phone: +41 58 765 5493. e-mail: juliane.hollender@eawag.ch

Published in *Environmental Science and Technology*, DOI: 10.1021/acs.est.7b03088



Abstract

Azole fungicides are known inhibitors of the important enzyme class cytochrome P450 monooxygenases (CYPs), thereby influencing the detoxification of co-occurring substances via biotransformation. This synergism in mixtures containing an azole has mostly been studied by effect measurements, while the underlying mechanism has been less well investigated. In this study, six azole fungicides (cyproconazole, epoxiconazole, ketoconazole, prochloraz, propiconazole and tebuconazole) were selected to investigate their synergistic potential and their CYP inhibition strength in the aquatic invertebrate *Gammarus pulex*. The strobilurin fungicide azoxystrobin was chosen as co-occurring substrate, and the synergistic potential was measured in terms of internal concentrations of azoxystrobin and associated biotransformation products (BTPs). Azoxystrobin is biotransformed by various reactions, and 18 BTPs were identified. By measuring internal concentrations of azoxystrobin and its BTPs with high resolution tandem mass spectrometry in the presence and absence of azole fungicides followed by toxicokinetic modeling, we showed that inhibition of CYP-catalyzed biotransformation reactions indeed played a role for the observed synergism. However, synergism was only observed for prochloraz at environmentally realistic concentrations. Increased uptake rate constants, an increase in the total internal concentration of azoxystrobin and its BTPs, *in vivo* assays for measuring CYP activities, and *G. pulex* video-tracking suggested that the 2-fold increase in bioaccumulation, and, thereby, the raised toxicity of azoxystrobin in the presence of prochloraz is not only caused by inhibited biotransformation but even more by increased azoxystrobin uptake induced by hyperactivity.

3.1 Introduction

Mixture effects of environmental contaminants, such as pesticides, have been discussed for a long time, and a better understanding of the mechanisms behind these mixture effects is often desired.¹⁻³ Recently, the inclusion of mixtures into risk assessment in the framework of the European REACH regulation and the Water Framework Directive (WFD) has been proposed.⁴⁻⁵ Within the European Legislation on Plant Protection Products (EC 1107/2009)⁶, only intentional mixtures of co-formulated products are considered in risk assessment. Concentration addition and independent action models have been developed to estimate the toxicity of mixtures on the basis of the toxicity of the single compounds. Often these models give accurate estimations of the toxicity of mixtures.⁷ However, synergistic interactions do occur, *i.e.*, some compounds can enhance the toxicity of other compounds. Two reviews reported that in approximately 5% of pesticide mixtures that were investigated, the observed effects were more than 2-fold greater than estimated from concentration addition.⁷⁻⁸ In general, the underlying mechanisms causing synergy are diverse, and interactions between chemicals can influence several processes such as bioavailability, uptake, internal transport, biotransformation, binding at the target site, and excretion.⁸

According to a recent review by Cedergreen (2014)⁸, one of the most relevant processes causing synergy is altered enzyme activity that subsequently affects biotransformation. Cytochrome P450 monooxygenases (CYPs) are one of the most important enzyme classes present in all kingdoms of life⁹⁻¹² and play a significant role in the detoxification of xenobiotics, their main function being oxidation of a large number of endogenous and exogenous compounds. Increased biotransformation usually leads to decreased toxicity if the toxicity stems from the parent compound. However, in some cases, biotransformation leads to bioactivation by enzymatically introducing an active group or by modifying an inactive molecule to an active molecule.¹³

Strobilurin and azole fungicides are two of the most important fungicide classes that are frequently applied worldwide against various fungal diseases.¹⁴⁻¹⁵ In aquatic ecosystems, azole and strobilurin fungicides have been measured at concentrations between few nanograms per liter and few micrograms per liter.¹⁶⁻²² One representative of strobilurin fungicides is the broad-spectrum agricultural fungicide azoxystrobin. It acts by inhibiting mitochondrial respiration in fungi^{15, 23} and exhibits a generally high toxicity towards aquatic invertebrates with median-lethal concentrations (LC₅₀S) ranging between 150 and 350 µg L⁻¹, determined in short-term acute toxicity tests.²⁴⁻²⁷ Copepods and cladocerans have been shown to be the most sensitive species towards azoxystrobin.²⁸⁻³⁰ The maximum allowable concentration environmental quality standard (MAC-EQS) for azoxystrobin proposed by the Swiss Centre for Applied Ecotoxicology is 0.55 µg L⁻¹.³¹ No environmental quality standards (EQSs) for azoxystrobin and azole fungicides are given in the WFD, which only lists EQSs for a limited number of priority substances.³² Azole fungicides, including the triazoles and the imidazoles, are frequently applied in agriculture as well as in human and veterinary medicine and are well-known to interfere with the fungal cell membrane by inhibiting CYPs.¹⁵ They belong to the class of ergosterol biosynthesis inhibitors which inhibit the specific CYP isoform

(the lanosterol-14 α -demethylase) that catalyzes the reaction from lanosterol to ergosterol, which is an essential constituent of fungal cell membranes.³³⁻³⁴ Azoles can interact with the CYP in the following ways: as a substrate via hydrophobic interactions in the binding cavity of the enzyme and by strongly coordinating to the active site (the heme-iron), thereby hindering the binding of molecular oxygen and interrupting the CYP catalytic cycle.³⁵⁻³⁷ Thus, azole fungicides can affect the biotransformation and bioaccumulation of other chemicals by inhibiting CYP-catalyzed biotransformation reactions. As single compounds, they exhibit moderate acute toxicity towards small aquatic organisms (LC₅₀s: few milligrams per liter).^{24, 38-41} MAC-EQSs proposed by the Ecotox Centre Eawag-EPFL are in the low $\mu\text{g L}^{-1}$ range (0.24-1.4 $\mu\text{g L}^{-1}$) for selected azole fungicides (cyproconazole, epoxiconazole, and tebuconazole). For prochloraz only an ad hoc MAC-EQS of 1.6 $\mu\text{g L}^{-1}$ is available (see Supporting Information (SI) Q).³¹ Several studies have shown that azole fungicides can enhance the toxicity of other pesticides, such as of pyrethroids, towards aquatic species.⁴²⁻⁴⁶ One study by Cedergreen et al. (2006)⁴⁵ has shown that prochloraz strongly synergized the effect of azoxystrobin towards *Daphnia magna*. It is likely that a threshold for synergistic interactions exists for most synergists, below which no effects on the metabolic processes are observed.⁸ Whether such a threshold is above or below environmental realistic concentrations (nanograms per liter to few micrograms per liter) is not always clear. To date, most studies have been conducted at concentrations much higher than what is observed in the environment, and only the effect, such as mortality or immobilization, has been documented. Studies with lower exposure concentrations^{1, 44} and that include the measurement of internal concentrations of parent compounds and associated biotransformation products (BTPs) are rare (one example is Belden and Lydy (2000)⁴⁷) and are needed to further understand the proposed mechanism of synergism.

In this study, we mechanistically investigated whether the observed synergism of azoles in mixtures is caused by the inhibition of CYPs and, thus, by the inhibition of biotransformation reactions. A total of six azole fungicides including four triazoles (cyproconazole, epoxiconazole, propiconazole, tebuconazole) and two imidazoles (ketoconazole, prochloraz) were selected to test their synergizing potential at a range of concentrations by measuring the internal concentrations of azoxystrobin and its biotransformation products (BTPs) in the test species *Gammarus pulex*. Gammarids are small aquatic invertebrates that as shredders are of great relevance in freshwater ecosystems and they exhibit a high sensitivity towards a vast range of stressors.⁴⁸⁻⁵¹ Azoxystrobin was selected because it was strongly biotransformed to various products, and CYPs were most probably responsible for several but not for all biotransformation reactions. To enable the detection of BTPs present at low concentrations, azoxystrobin concentrations were chosen in the μM range, located within 1 order of magnitude below acute LC₅₀s. Additionally, we aimed to determine the strengths of CYP inhibition of the selected azoles in terms of half maximal inhibitory concentrations (IC₅₀s) to determine and compare their CYP inhibition potencies, also in terms of relevance of synergism at environmentally realistic concentrations. Because it was recognized throughout

the study that uptake might be influenced by specific prochloraz concentrations, video-tracking of gammarids was used to test whether prochloraz can induce hyperactivity.

3.2 Material and Methods

3.2.1 Chemicals, Solutions and Test Organisms

Detailed information about all chemicals and solutions used during experiments and instrumental analysis are provided in SI A. Depending on the experiment, male and female gammarids (length: 1.5 ± 0.5 cm) were collected at uncontaminated creeks in Switzerland and Denmark (see SI B). Gammarids were kept in aerated artificial pond water (APW)⁵² at a pH of ~ 7.9 (11 ± 1 °C, 12 h light/12 h dark cycle) and were fed with horse chestnut (*Aesculus hippocastanum*) leaves inoculated with *Cladosporium herbarum*⁵² or degraded leaves collected at the sampling site. Experiments were performed at the above-mentioned conditions, and organisms were acclimatized to these test conditions for at least 3 days.

3.2.2 Whole Body Internal Concentration Measurements

General Design of Exposure Experiments to Determine Whole Body Internal Concentrations

If not stated otherwise in the experimental description, the following specifications are valid for all experiments dealing with internal concentration measurements of parent substrates (azoxystrobin, 7-ethoxycoumarin and tramadol) and associated BTPs. Experiments were performed in 600 mL glass beakers filled with 500 mL exposure medium prepared in APW at test conditions. Duplicate samples were prepared for each treatment. A total of four gammarids and four horse chestnut leaf discs inoculated with *C. herbarum* (diameter: 2 cm) were added to each beaker. Leaf discs provided food and shelter during the experiment. Different controls were performed during each experiment, *i.e.*, “organism controls” (chemical-negative, organism- and food-positive), “chemical controls” (organism- and food-negative, chemical-positive), and “food controls” (organism-negative, food- and chemical-positive). Exposure media were sampled at the beginning and end of the experiments to determine exposure concentrations.

At the end of the exposure phase, organisms were shortly rinsed with nanopure water, blotted dry on tissue, transferred to 2 mL-microcentrifuge tubes, and weighed. The homogenization and extraction was carried out with a FastPrep bead beater (MP Biomedicals, Switzerland) in two cycles of 15 s at 6 m s^{-1} (cooling on ice in between). Prior to that, 500 μL of methanol, 100 μL of isotopically labeled internal standard mix solution composed of azoxystrobin-d4, propiconazole-d5, prochloraz-d7, tebuconazole-d6, 7-ethoxycoumarin-d5 and tramadol-d6 (each $100 \mu\text{g L}^{-1}$), and 300 mg of 1 mm zirconia/silica beads (BioSpec Products, Inc.) were added. Subsequently, samples were centrifuged (6 min, 10 000 rpm, 20 °C), filtered (0.45 μm regenerated cellulose filters, BGB Analytic AG, Switzerland), and the filters were washed with 400 μL methanol. Filtrate and wash solution were merged, and the samples were stored at -20 °C until chemical analysis.

Biotransformation Product Identification of Azoxystrobin

To screen for BTPs of azoxystrobin, gammarids were exposed for 24 h to 0.5 μM of azoxystrobin. SIEVE software version 2.2 (Thermo Scientific) was used for conducting a suspect screening of predicted BTP candidates (see SI C) and a nontarget screening. Details about the criteria, such as (i) peak intensity thresholds, (ii) peak shape, (iii) the kinetic pattern of increase and decrease in the uptake and depuration phase, respectively, and (iv) the integrated intensity ratio between treatment and control samples that had to be fulfilled for both screening approaches, are found in SI E.

Structure elucidation of azoxystrobin BTPs was carried out in a manner similar to the procedure described in our previous publication⁵³ based on (1) the exact mass and isotopic pattern analysis to propose molecular formulas and on (2) the interpretation of tandem mass (MS/MS) spectra to identify diagnostic fragments and losses either specific for only one structure or for several positional isomers.

Biotransformation pathway information, sulfate and glucose enzymatic deconjugation experiments according to Kukkonen and Oikari (1988)⁵⁴ (see SI G), as well as MS/MS spectra reported in scientific literature provided additional evidence for some tentatively identified BTPs.

Exposure to Binary Mixtures

To investigate the effect of the selected azole fungicides on the internal azoxystrobin concentrations, gammarids were exposed to binary mixtures. Each mixture was composed of the substrate azoxystrobin (0.1 or 0.2 $\mu\text{M} \pm 40$ or 80 $\mu\text{g L}^{-1}$) and of similar molar concentration of the selected azole fungicide. Gammarids were pre-exposed separately for 4 h to each azole fungicide until azoxystrobin was added for a 24 h exposure phase. For prochloraz, which had the largest detected effect on the internal azoxystrobin concentration, additional exposure concentrations (0.15 and 0.5 μM of azoxystrobin and similar molar concentrations of prochloraz) and pre-exposure times (12 and 18 h) were tested. For comparison, piperonyl butoxide (1.5 μM , pre-exposure 4 h), a known CYP inhibitor, was also tested in combination with azoxystrobin (0.5 μM).

To test the effect of prochloraz on further substrates and to provide a link to CYP activities described in section 3.2.4, 7-ethoxycoumarin (0.5 μM) and tramadol (0.4 μM) were used in combination with two different prochloraz concentrations (0.1 and 1 μM) and two different pre-exposure times (4 and 18 h). For each treatment, triplicates were prepared, and incubation with the substrate lasted 24 h.

Toxicokinetics of Azoxystrobin With and Without Prochloraz

To determine internal concentrations over time, gammarids were exposed to 0.2 μM azoxystrobin for up to 24 h and were sampled at 7 time points during the uptake phase. For the 120 h depuration phase, gammarids were exposed for 24 h to 0.2 μM azoxystrobin, were subsequently transferred to clean medium, and were sampled at 13 time points. Simultaneously, in a separate uptake experiment, gammarids were pre-exposed to 0.2 μM

prochloraz for 4 h before the substrate azoxystrobin (0.2 μM) was added. After substrate addition, gammarids were sampled at 7 time points during 24 h. Exact sampling time points are given in SI F.

Modeling Bioaccumulation and Biotransformation Kinetics

Toxicokinetic rate constants for azoxystrobin, alone and in the presence of prochloraz, were estimated with a first-order compartment model using Matlab R2015b (BYOM: Build Your Own Model, <http://www.debtox.nl/about.html>). The toxicokinetic model is described by ordinary differential equations (ODEs), with which we differentiate between the time course of the parent compound, the time courses of primary BTPs (1st BTPs) that are directly formed from the parent compound, and the time courses of secondary BTPs (2nd BTPs), in which a direct precursor BTP was detected. All parameters were fitted simultaneously.

Bioaccumulation factors were either calculated at a specific time point based on the ratio of the concentration of the parent compound in the organisms and of the concentration of the parent compound in the exposure medium with the requirement of steady state (BAF), or kinetically based on the ratio of the uptake rate constant and of the total elimination rate constant of the parent compound (BAF_k). Full details including ODEs, equations to calculate BAF_(k)s and elimination half-lives ($t_{1/2}$) are described in SI H.

Half Maximal Inhibitory Concentrations of Prochloraz (IC_{50, PRZ, AZS}) Based on Internal Concentrations of Azoxystrobin and Associated BTPs

To investigate at what point synergism starts, IC_{50, PRZ, AZS} were determined by pre-exposing gammarids for 18 h to varying prochloraz concentrations (0 (control), 0.0005, 0.001, 0.002, 0.01, 0.02, 0.06, 0.1, 0.2 and 1 μM) before the substrate azoxystrobin (0.1 μM) was added and gammarids were exposed to the substrate for 24 h. The internal concentrations of azoxystrobin and associated BTPs in the treatment samples were compared with those in the control samples and the IC_{50, PRZ, AZS} were determined by fitting a four-parameter log-logistic model (see SI L) available in the R⁵⁵ package “drc” from Ritz and Streibig (2005)⁵⁶.

Chemical Analysis

Directly before analysis, 200 μL (100 μL for BTP screening experiment) gammarid extract or exposure medium was added to 20 mL headspace glass amber vials filled with 20 mL nanopure water. For chemical analysis, automated online solid-phase extraction reverse-phase liquid chromatography coupled to a high resolution quadrupole-orbitrap mass spectrometer (Q Exactive, Thermo Fisher Scientific Inc.) was used (online-SPE-LC-HRMS/MS).⁵³ Full-scan data were acquired in polarity switching mode (electrospray ionization) for a mass range of 100-1000 m/z with a resolution of 70000 (at m/z 200). For triggering data-dependent MS/MS scans with a resolution of 17500 (at m/z 200) a mass list with suspected BTPs for azoxystrobin was included that was based on *in silico* pathway prediction and scientific literature (see SI C). Internal standard calibration was used for quantification (Trace Finder software 3.1 and 3.3, Thermo Scientific). Due to the lack of reference standards, most BTPs were semi-quantified based on the calibration curve of the

parent compound. Further details about chemical analysis, quantification, and quality control can be found in SI C and SI D.

3.2.3 Median-Lethal Concentrations of Azoxystrobin (LC₅₀s) in the Presence and the Absence of Prochloraz

LC₅₀s (24 h) were determined for azoxystrobin alone and in the presence of two different prochloraz concentrations (0.001 and 0.2 µM) in APW at test conditions. Azoxystrobin concentrations were chosen on the basis of a range-defining test (see SI O). Each concentration was tested in duplicate by adding 10 organisms and one leaf collected at the sampling site to each beaker. Gammarids were pre-exposed for 18 h to one of the selected prochloraz concentrations or to APW until azoxystrobin was added. Mortality was monitored 24 h after substrate addition. If no moving of any appendices was observed by prodding immobile gammarids with a glass rod, gammarids were defined as dead. To determine the aqueous concentrations, the exposure medium was sampled at the beginning and at the end of the experiment. “Organism controls”, “chemical controls”, “food controls” (see section *General Design of Exposure Experiments to Determine Whole Body Internal Concentrations*), “solvent controls” (APW plus maximal ethanol concentration of 0.04% used in the treatments due to chemical spiking), and “prochloraz controls” (prochloraz-, organisms- and food-positive) were performed. For estimating LC₅₀s, a two-parameter log-logistic model available in the R⁵⁵ package “drc”⁵⁶ was applied (see SI L), assuming binomially distributed data.

3.2.4 Half Maximal Inhibitory Concentrations based on ECOD *in vivo* Activity (IC_{50, ECOD}s)

To determine CYP activities and their inhibition by azoles in a fast way, the transformation of the substrate 7-ethoxycoumarin to its fluorescent product 7-hydroxycoumarin (ECOD: 7-ethoxycoumarin-O-dealkylation) was measured spectrophotometrically. Therefore, IC₅₀s for ECOD *in vivo* activity (IC_{50, ECOD}s) were determined according to Gottardi et al. (2015)⁵⁷ at test conditions. Two azole concentrations (1 and 10 µM, 3 replicates with 2 organisms in 3 mL substrate-azole solution) were tested for all selected azoles in initial experiments, and the resulting 7-hydroxycoumarin fluorescence in the medium was compared to the fluorescence in the medium of the control samples.

More detailed investigations were conducted for 0 (control), 0.02, 0.1, 0.2, 1, 2 and 10 µM prochloraz, and 0 (control), 0.1, 0.2, 1, 2, 10 and 20 µM epoxiconazole in 250 mL glass flasks filled with 200 mL exposure solution (prepared in APW) and 23 gammarids. Gammarids were pre-exposed to the different prochloraz and epoxiconazole concentrations for 18 h and were fed with degraded leaves collected at the sampling site. For prochloraz, additional pre-exposure times of 0 and 4 h were investigated. After pre-exposure, 7-ethoxycoumarin was added to a final concentration of 20 µM (3.8 mg L⁻¹). A total of five replicates per concentration were prepared by filling 5 mL of substrate-azole solution into 10 mL glass vials and by each adding four gammarids. During an incubation period of 6 h, 100 µL aliquots were sampled hourly from the exposure media and were directly added to a

black microwell plate (BRANDplates pureGrade, Brand). The fluorescence of 7-hydroxycoumarin (excitation: 380 nm, emission: 480 nm) was measured with a multimode microplate reader (SpectraMax M5 Microplate Reader, Molecular Devices) at room temperature. The exposure media were sampled at the beginning and end of the pre-exposure phase to determine the azole concentration.

Treatment samples were compared to the control samples (see SI M for details) and $IC_{50, ECODS}$ were determined by applying a Brain-Cousens⁵⁸ four parameter hormesis model (see SI L), which is a modification of the three-parameter log-logistic model accounting for hormesis available in the R⁵⁵ package “drc”.⁵⁶

3.2.5 Video-Tracking of the Locomotory Behavior of Gammarids in the Presence of Prochloraz

Locomotion was recorded at 12 °C with the Noldus software (Media recorder and analyzed with Ethovision XT10) and the camera was placed above the infrared floor. Gammarids were individually placed in glass Petri dishes filled with 40 mL APW and acclimated overnight. The next morning, prochloraz was added in 10 mL APW to obtain the targeted concentrations (0 (control), 0.02, 0.1, 0.2, 1 and 2 μ M). After 30 min, gammarids were recorded for 18 h with constant light. A total of 3 runs of 18 gammarids were performed (3 gammarids per treatment in each run). Exposure media were sampled at the beginning and end of the experiment. Distance moved was analyzed with a general linear model in Statistica 9.0 with treatment and time as fixed factors, and run and gammarid number as random one.

3.3 Results and Discussion

3.3.1 Bioaccumulation and Biotransformation of the Substrate Azoxystrobin

Bioaccumulation of azoxystrobin with BAFs and BAF_{ks} of $5 \text{ L kg}_{\text{wet weight (ww)}}^{-1}$ on average (see Figure 3-2a, for exact values refer to SI H and SI I) was low in gammarids compared to the threshold of 2000 L kg^{-1} given in the European REACH regulation, Annex XIII for bioaccumulative substances.⁵⁹ Azoxystrobin medium concentrations, important for the calculation of BAFs, varied on average by 10% from nominal concentrations and declined during the 24 h exposure phase on average by 6% (see SI I).

In total, 18 BTPs were tentatively identified for azoxystrobin with the suspect and nontarget screening approaches, revealing a complex biotransformation pathway. Figure 3-1 shows the structures of the single BTPs and displays the proposed biotransformation pathway. Because no reference standards were available for most BTPs, their structures are mainly based on the identification of diagnostic fragments to propose one specific structure or to propose tentative candidates in which several positional isomers exist. The identification confidence of each BTP is stated in detail in SI R. Biotransformation predominantly took place via oxidation and/or conjugation reactions, and all BTPs (except AZ_M214 and AZ_M328a,b) were characterized by changes at the active (*E*)-methyl β -methoxyacrylate group. These changes mainly included demethylation, hydrolysis, hydroxylation, different conjugations, reduction of the acrylate double bond, or combinations of these. The hydrolysis of the methyl ester resulting in the acid derivative (AZ_M390b) is well-known and has been detected in natural aquatic environments,⁶⁰ at varying abiotic laboratory conditions,⁶¹⁻⁶² as well as during biotransformation across different organismal levels.⁶³⁻⁶⁵ Because the ester structure of strobilurins is required to maintain their antifungal activity, ester hydrolysis contributes to the detoxification of azoxystrobin.^{64, 66} The major BTP AZ_M392, which is formed via reduction of the acrylate double bond of the ester hydrolysis product AZ_M390b, reached mean internal concentration of around 35% of those of the parent compound after 24 h exposure (see SI H). This unusual reduction of azoxystrobin acid has been previously detected in plants.⁶⁴ Conjugation reactions with glutathione (resulting in cysteine products), with sulfate, or with glucose-sulfate were detected for azoxystrobin, confirming the importance of conjugation reactions for aquatic invertebrates.^{53-54, 67-70}

Primary biotransformation rate constants $k_{Mx, 1st}$ that directly contributed to the reduction of bioaccumulation of the parent compound were between 1 and 3 orders of magnitude lower than the direct elimination k_e of the parent compound (see SI H). Therefore, the percentage of the sum of $k_{Mx, 1st}$ on the total elimination ($k_e + \text{sum of } k_{Mx, 1st}$) was only approximately 10%. Thus, biotransformation contributed to the elimination of the parent compound azoxystrobin but did not play a major role in terms of reduction in the bioaccumulation of azoxystrobin.

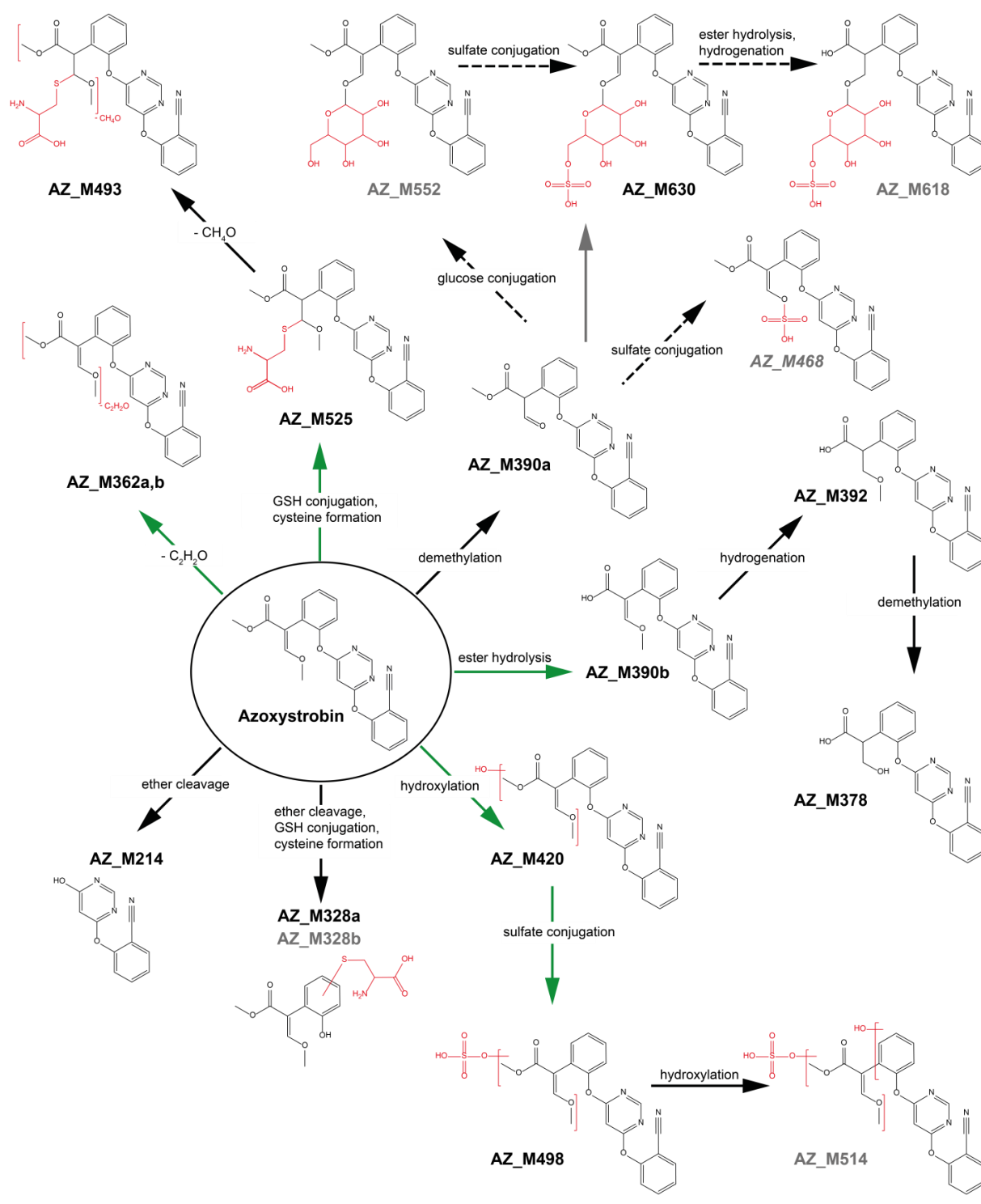


Figure 3-1: Proposed biotransformation pathway of azoxystrobin in *G. pulex*. Structural modifications of the BTPs are highlighted in red. The color and shape of the arrows distinguishes between biotransformation reaction types: black and continuous, reactions influenced by prochloraz; black and dashed, secondary reactions influenced by prochloraz only due to previous reactions being influenced by prochloraz; green, reactions not influenced by prochloraz; gray, alternative pathway used for the kinetic comparison of single exposure to azoxystrobin and mixture exposure to azoxystrobin and prochloraz because, for the mixture exposure, AZ_M552 was not detected.

BTPs marked in gray were not included in the kinetic model for comparing the kinetic rate constant in the presence and absence of prochloraz because they were not detected in the mixture exposure or only in the screening experiment using a higher exposure concentration (italic).

3.3.2 Influence of Co-occurring Azoles on the Bioaccumulation and Biotransformation of Azoxystrobin

Out of the six tested binary fungicide mixtures composed of 0.1 or 0.2 μM (\cong 40 or 80 $\mu\text{g L}^{-1}$) azoxystrobin and similar molar concentrations of one of the selected azoles, only prochloraz showed a strong inhibitory effect measured in terms of internal concentrations of the substrate azoxystrobin and associated BTPs (see SI J). Therefore, only the synergistic potential of prochloraz was investigated in more detail. The increase in the internal azoxystrobin concentration of approximately 50% in the presence of prochloraz was similar to the increase observed in the presence of the known CYP inhibitor piperonyl butoxide (see SI J).

Pre-exposure to the inhibitor instead of simultaneous exposure to the inhibitor and the substrate facilitates the investigation of single processes, such as binding to the enzyme, and ensures that azoles can display their synergistic potential. Different pre-exposure times to prochloraz (4, 12 and 18 h) were tested for the binary mixtures composed of prochloraz and azoxystrobin, but no differences were observed in internal concentrations of azoxystrobin (see SI J). In previous work,⁵³ it was determined that prochloraz is taken up fast and that steady state is reached after 24 h. After 5.5 h and 17.5 h exposure, 65% and nearly 100% of the maximal internal concentration after 24 h exposure were reached, respectively. Apparently, the internal concentration reached after 4 h pre-exposure is sufficient to cause distinct inhibition.

All tested prochloraz concentrations in the binary mixtures (0.1, 0.15, 0.2 and 0.5 μM) lead to clear CYP inhibition. Nevertheless, 100% inhibition was not reached with any of the prochloraz concentrations tested because low concentrations of azoxystrobin BTPs (< limit of quantification (LOQ) up to 5% compared to the control) likely to be CYP-catalyzed were still detected after 24h exposure. These detections were a result of the high sensitivity of the LC-HRMS/MS method with LOQs for azoxystrobin and associated BTPs of < 3 $\text{nmol kg}_{\text{ww}}^{-1}$ (see SI D). In addition, the azoxystrobin and prochloraz concentrations used were mostly below the levels of acute toxicity, therefore still enabling biotransformation in the organisms. Since the substrate azoxystrobin is highly toxic towards *G. pulex* (LC_{50} (24 h): $0.4 \pm 0.02 \mu\text{M} \cong 157 \pm 3 \mu\text{g L}^{-1}$; see below), the applied azoxystrobin and prochloraz concentrations are a compromise to avoid visible synergistic effects, such as mortality, while having sufficiently detectable internal concentrations.

3.3.3 Toxicokinetics of Azoxystrobin With and Without Prochloraz and Changed Toxicity

Due to the observed CYP inhibition with prochloraz, a kinetic experiment was performed for azoxystrobin alone and in combination with prochloraz for the determination of toxicokinetic rate constants. The implemented model equations were based on the depicted biotransformation pathway in Figure 3-1. For consistency, the same biotransformation path-

way was used for single and mixture exposure, focusing on BTPs still present in the mixture exposure (see Figure 3-1).

Figure 3-2a shows the internal concentrations over time of the substrate azoxystrobin during the 24 h uptake phase. There are significant differences concerning the internal concentrations of azoxystrobin between single and mixture exposure. The internal concentration of azoxystrobin after 24 h exposure was approximately twice as high in gammarids being co-exposed to prochloraz compared to the internal concentration of gammarids being exposed to azoxystrobin only.

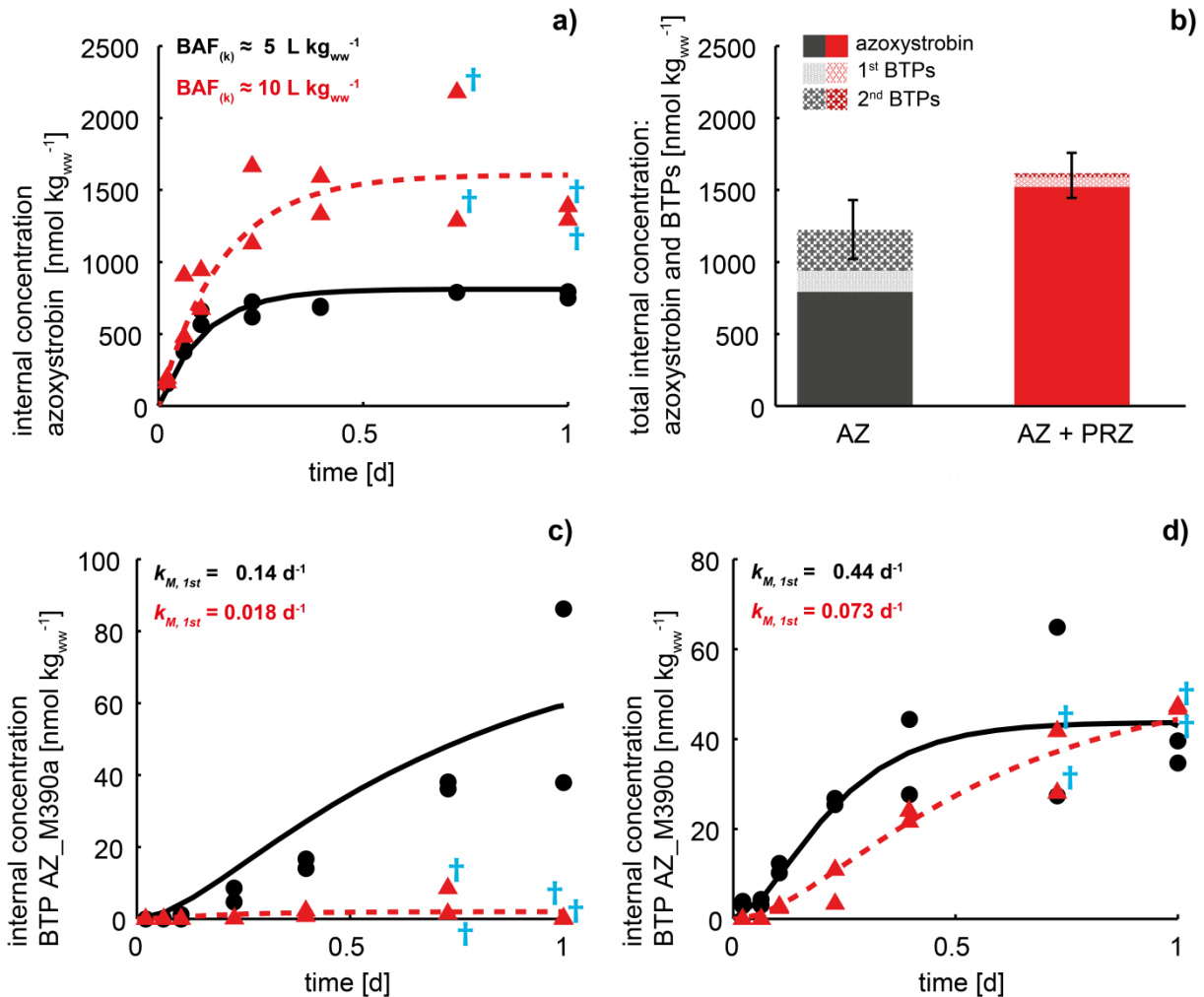


Figure 3-2: Panels (a), (c) and (d): 24 h uptake kinetic for the single exposure to 0.2 μM azoxystrobin (black) and for the 4 h pre-exposure to 0.2 μM prochloraz and the subsequent addition of 0.2 μM azoxystrobin (red). Shown are the measured (symbols) and modeled (lines) time courses for (a) the parent compound azoxystrobin, (c) the BTP AZ_M390a, and (d) the BTP AZ_M390b. Blue crosses mark sampled time points at which all gammarids died during exposure. In panel (a), bioaccumulation factors ($BAF_{(k)}$ s) are listed for the single exposure to azoxystrobin and for the mixture exposure to azoxystrobin and prochloraz in black and red, respectively, whereas in panels (c) and (d), primary biotransformation rate constants ($k_{M,1st}$) are displayed. Panel (b) shows the total internal concentration of azoxystrobin and associated BTPs after 24 h exposure in black for the single exposure to 0.2 μM azoxystrobin (AZ) and in red for the 4 h pre-exposure to 0.2 μM prochloraz and the subsequent addition of 0.2 μM azoxystrobin (AZ + PRZ). Standard deviations are given for the total internal concentrations.

This result is also reflected in the calculated BAFs and BAF_k s for azoxystrobin that double in the presence of prochloraz (see Figure 3-2a as well as SI H and SI I for exact values). Consequently, co-exposure to prochloraz leads to increased mortality (see blue crosses in Figure 3-2), indicating a higher concentration of azoxystrobin at the target site and, thus, raised toxicity around three times higher than what is expected from the model of concentration addition (see SI K). Because the organisms started to die after steady state was reached, toxicokinetic rate constants should not be strongly affected by the observed mortality. In separate toxicity tests, LC_{50} s were determined for azoxystrobin alone and in combination with prochloraz (0.2 μM), confirming the increased toxicity because the LC_{50} was reduced by a factor of 4.5 (see Figure 3-3).

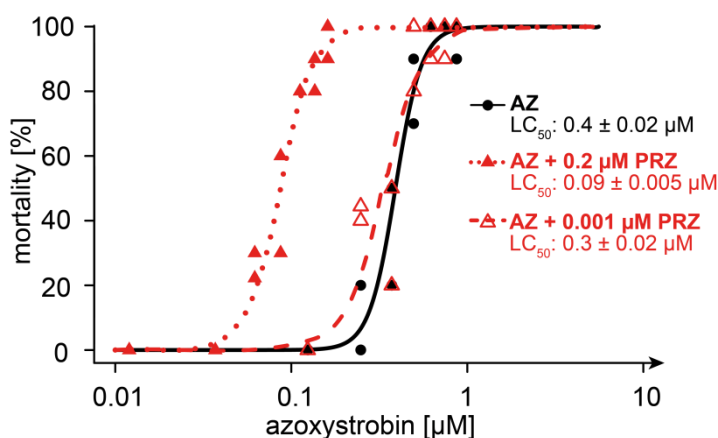


Figure 3-3: Concentration-response (mortality) curves for the LC_{50} determination of azoxystrobin (AZ) alone and in combination with two different prochloraz (PRZ) concentrations (0.2 and 0.001 μM , respectively) after 18 h pre-exposure to prochloraz.

As expected, mainly oxidative biotransformation reactions likely to be CYP-catalyzed were influenced by prochloraz (see Figure 3-1). This result is also illustrated in Figure 3-2c which shows exemplary the internal concentration over time of the demethylation product AZ_M390a during the 24 h uptake phase. In the presence of prochloraz, nearly no demethylation product ($< \text{LOQ}$) was formed after 24 h, pointing towards the inhibition of the respective CYP isoform. In contrast, no inhibitory effect was observed for direct conjugation reactions and ester hydrolyses such as azoxystrobin acid (AZ_M390b) (see Figure 3-2d; reactions are shown in Figure 3-1), for which similar internal concentrations were reached after 24 h. These observations fit within expectations because conjugation reactions and ester hydrolyses are catalyzed by different enzymes, such as transferases or esterases. Moreover, these differences in the amount of BTPs formed between single and mixture exposure are also visible in the estimated biotransformation rate constants $k_{Mx, 1st \text{ or } 2nd}$ (see $k_{Mx, 1st}$ displayed in Figure 3-2c and Figure 3-2d as well as in Table 3-1). Rate constants for the single exposure and for the mixture exposure were defined as significantly different when their respective 95% confidence intervals (CIs) did not overlap (see Table 3-1). In general, biotransformation rate constants influenced by prochloraz showed 2 to 70 times smaller $k_{Mx, 1st \text{ or } 2nd}$ (true for 6 out of 7 reactions) and non-influenced reactions exhibited similar $k_{Mx, 1st \text{ or } 2nd}$ (true for 4 out of 6 reactions) compared to the $k_{Mx, 1st \text{ or } 2nd}$ estimated from the single

exposure to azoxystrobin (see Table 3-1). However, there are some exceptions, such as the modeled $k_{M, 1st}$ for azoxystrobin acid (AZ_M390b), which is significantly lower in the presence of prochloraz. This difference might be due to the lack of isotopically labeled internal standards for BTPs and/or slightly different biological activity of gammarids (see Figure 3-2d and Table 3-1).

Surprisingly, the hydroxylation product AZ_M420 was not influenced by prochloraz (see Figure 3-1), although hydroxylation is a typically CYP-catalyzed biotransformation reaction. Different enzyme classes apart from CYPs might be involved in this hydroxylation reaction, such as flavin-containing monooxygenases (FMOs). However, FMOs are more likely to catalyze the formation of N- and S-oxides, whereas C-hydroxylations are rarely reported.⁷¹ Several secondary reactions are indirectly influenced by prochloraz, such as the glucose (AZ_M552) or glucose-sulfate (AZ_M630, AZ_M618) conjugation products. Only their precursor (AZ_M390a) is influenced, and the actual conjugation reaction is unaffected.

Using a mass balance after 24 h, the difference in the internal concentrations of the parent compound azoxystrobin in the single and mixture exposure (see Figure 3-2a) can only partially be explained by inhibited biotransformation reactions that lead to an accumulation of azoxystrobin. Contrary to expectations, most BTPs were not excreted faster compared to the parent compound azoxystrobin (see the elimination half-lives in Table 3-1). Therefore, the sum of the internal concentrations of the parent compound azoxystrobin and its formed BTPs should stay constant, if prochloraz only affects biotransformation. However, the total internal concentration increased in the presence of prochloraz (see Figure 3-2b), pointing towards additional processes being influenced. This effect varied in its potency among the different tested prochloraz concentrations. The strongest increase in the total internal concentration compared to the control sample was observed with a concentration of 0.1 μM ($\pm 37 \mu\text{g L}^{-1}$) prochloraz (see SI J).

This effect was confirmed by the simultaneous fitted kinetic rate constants. The sum of the primary biotransformation rate constants $k_{Mx, 1st}$ decreased by approximately 80% in the presence of prochloraz. However, the sum of $k_{Mx, 1st}$ only contributed to about 10% to the total elimination in the single exposure to azoxystrobin and was reduced to 2% in the mixture exposure. In contrast, the fitted uptake rate constant k_u increased by a factor of about 1.4 in the presence of prochloraz (see SI H). When first only fitting the uptake rate k_u and one elimination rate k_e to the total internal concentration, and, in a second step, fitting all other parameters for the single BTPs, more weight is given to the uptake rate. Thereby, the difference in the uptake rates becomes even more distinct as the uptake rate increases by a factor of 3.2 in the presence of prochloraz (see SI H).

Table 3-1: Elimination half-lives ($t_{1/2}$) and biotransformation rate constants (k_{Mx}) for azoxystrobin and associated BTPs for the single exposure to azoxystrobin and for the mixture exposure to azoxystrobin and prochloraz, listed with increasing $t_{1/2}$. Lower and upper 95% confidence intervals for k_{Mx} are given in brackets. If two confidence intervals are displayed, then the confidence interval from the likelihood profile is a broken set. $t_{1/2}$ and k_{Mx} are based on the reduced azoxystrobin biotransformation pathway for comparing rate constants between single and mixture exposure displayed in Figure 3-1. Toxicokinetic rate constants for uptake and elimination are reported in SI H.

	$t_{1/2}$ [h]	k_{Mx} [d ⁻¹] single exposure to azoxystrobin	k_{Mx} [d ⁻¹] mixture exposure to azoxystrobin and prochloraz
azoxystrobin	1.9		
AZ_M525 (1 st BTP)	2.0	0.037 [0.030; 0.060]	0.0067 [0.0051; 0.0089] [0.011; 0.021]
AZ_M390b (1 st BTP)	2.1	0.44 [0.38; 0.61]	0.073 [0.061; 0.087]
AZ_M498 (2 nd BTP)	3.1	1.9 [1.4; 3.0]	1.0 [0.30; 2.7]
AZ_M378 (2 nd BTP)	5.8	0.79 [0.19; 0.44] [0.62; 1.3]	0.46 [0.33; 0.66] 0.97; 4.8]
AZ_M420 (1 st BTP)	8.9	0.045 [0.036; 0.069]	0.039 [0.030; 0.062]
AZ_M630 (2 nd BTP)	12	1.4 [1.1; 1.8]	15 [4.8; 94]
AZ_M390a (1 st BTP)	12	0.14 [0.12; 0.19]	0.018 [0.0054; 0.049]
AZ_M214 (1 st BTP)	13	0.052 [0.040; 0.081]	0.0011 [0.00082; 0.0014]
AZ_M328a (1 st BTP)	14	0.063 [0.049; 0.090]	0.00095 [0.00062; 0.0096]
AZ_M493 (2 nd BTP)	18	8.3 [6.3; 18]	0.93 [0.45; 1.7]
AZ_M392 (2 nd BTP)	21	8.1 [6.8; 13]	2.2 [1.7; 2.7]
AZ_M362a (1 st BTP)	16000	0.0015 [0.00055; 0.0026]	0.00096 [0.00039; 0.0016] [0.0019; 0.095]
AZ_M362b (1 st BTP)	16000	0.032 [0.025; 0.052]	0.014 [0.0083; 0.023]

3.3.4 Azole CYP Inhibition Strength Determined via the ECOD Assay and by Internal Concentration Measurements

The ECOD assay according to Gottardi et al. (2015)⁵⁷ has been applied because it is described as a fast tool for measuring CYP activities in various aquatic invertebrates,⁵⁷ mammals,⁷²⁻⁷⁴ fish,⁷⁵ molluscs,⁷⁶ nematodes,⁷⁷ and insects⁷⁸⁻⁷⁹ *in vivo* and *in vitro*. In a range-defining test on the selected azoles using up to 10 μM , only prochloraz and epoxiconazole inhibited CYP activity in *G. pulex*. Because the concentrations tested were well-above environmentally realistic concentrations, 10 μM equates to 2.9 (cyproconazole) to 5.3 (ketoconazole) mg L^{-1} , further experiments were only done with prochloraz. For epoxiconazole no $\text{IC}_{50, \text{ECOD}}$ could be determined as the organisms started to die at 20 μM before ECOD activity was severely inhibited.

Figure 3-4a shows the concentration-response curve for the $\text{IC}_{50, \text{ECOD}}$ determination of prochloraz (18 h pre-exposure) based on the ECOD assay ($\text{IC}_{50, \text{PRZ, ECOD}}$). The determined $\text{IC}_{50, \text{PRZ, ECOD}}$ was approximately $0.5 \pm 0.1 \mu\text{M}$ ($200 \pm 60 \mu\text{g L}^{-1}$). The relatively large variations among the sample replicates (coefficient of variation: 0.23-0.85) are most likely caused by biological diversity among the single gammarids which were collected in the field. At low prochloraz concentrations (0.02 μM and 0.1 μM) increased ECOD activity was observed, being statistically significant for 0.1 μM prochloraz ($p < 0.05$) compared to the control (see SI M). Different pre-exposure times (0, 4 and 18 h) all revealed the same pattern of stimulated ECOD activity at low doses (see SI M). Hormesis, a stimulation of response at low doses and inhibition of response at high doses, is well-known and can be induced by organic or inorganic compounds as well as by radiation across different organismal levels.⁸⁰⁻⁸² This hormetic effect of increased ECOD activity can be caused by the following processes: the induction of specific CYP isoforms responsible for the deethylation reaction of 7-ethoxycoumarin or the influence of prochloraz on other processes, such as on the uptake of 7-ethoxycoumarin.

As was reported, the O-deethylation reaction of 7-ethoxycoumarin is catalyzed by a broad spectrum of CYP isoforms⁷³⁻⁷⁴ in various organisms,^{57, 72-79} it seems likely that some of these CYP isoforms can also catalyze oxidative biotransformation reactions of azoxystrobin. Therefore, we expected to observe the same pattern with the ECOD assay as well as with the internal concentration measurements, *i.e.*, that low concentrations of prochloraz increase the response (ECOD activity and amount of oxidative formed azoxystrobin BTPs, respectively), and that high doses inhibit the response. However, hormesis was not found for the substrate azoxystrobin because no BTP of azoxystrobin that is likely to be CYP-catalyzed showed a higher internal concentration compared to the control in the presence of low prochloraz concentrations (see Figure 3-4b, exemplary BTP_M390a).

To address this discrepancy, internal concentrations of 7-ethoxycoumarin and its BTPs were measured with LC-HRMS/MS in the presence of two prochloraz concentrations, one in which clearly increased ECOD activity was observed (0.1 μM) and one in which clearly decreased ECOD activity was observed (1 μM). Surprisingly, 7-hydroxycoumarin (7-Etc_M161), which is the deethylation product measured in the ECOD assay, was hardly detectable in gammarids.

Instead, two conjugation products were identified that were formed via sulfate (7-Etc_M240) or glucose-sulfate (7-Etc_M403) conjugation of 7-Etc_M161 (see SI J). 7-Ethoxycoumarin was mainly present in its unchanged form after 24 h exposure and total BTP concentrations of 7-ethoxycoumarin were low, reaching at maximum 6% of those of the parent compound. However, low prochloraz concentrations (0.1 μM) lead to slightly higher concentrations of 7-Etc_M240 compared to the control, confirming the hormesis observed in the ECOD assay (see Figure 3-4a). Moreover, significantly higher ($p < 0.05$) internal 7-ethoxycoumarin concentrations (approximately 20%) were obtained in the presence of low prochloraz concentrations (0.1 μM) compared to the controls (see SI J). This increase in the total internal concentrations of the parent compounds 7-ethoxycoumarin and azoxystrobin (see section 3.3.2 and 3.3.3) in the presence of low prochloraz concentrations indicates that uptake is influenced and no induction of specific CYP isoforms occurs. For further confirmation, internal concentrations of tramadol and its BTPs were measured in the presence and absence of prochloraz (0.1 and 1 μM). Tramadol, a pharmaceutical with known BTPs and corresponding elimination half-lives in *G. pulex*,⁶⁷ showed the same trend in increasing total internal concentrations for the 0.1 μM exposure to prochloraz as the substrates azoxystrobin and 7-ethoxycoumarin (see SI J).

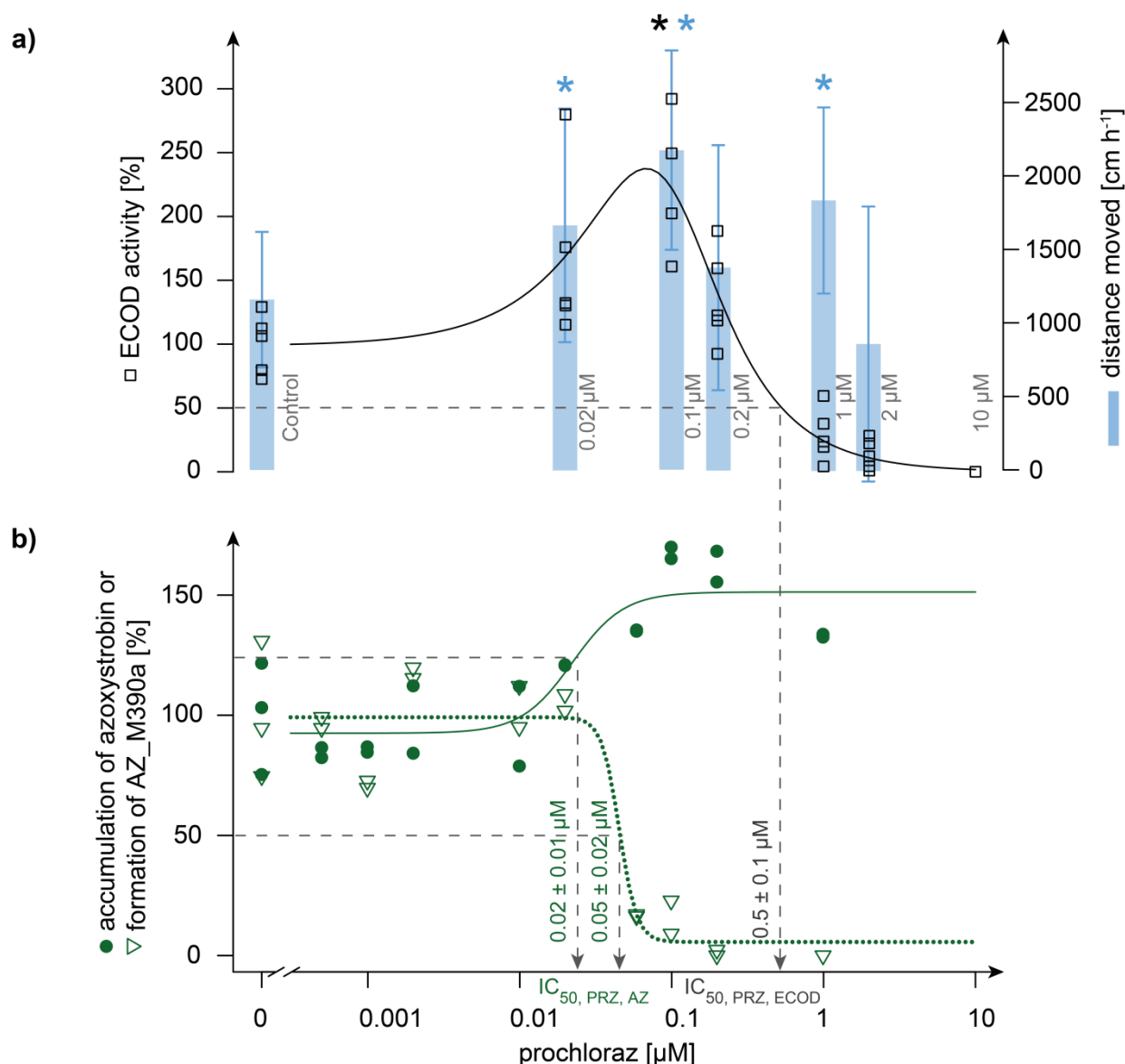


Figure 3-4: Dose-response curves for the IC₅₀ determination based on ECOD activity (a), or based on internal concentration measurements of azoxystrobin and associated BTPs (exemplary AZ_M390a is shown) (b) with 18 h pre-exposure to prochloraz. The dashed lines mark the determined and displayed IC₅₀s. The bar plot in panel (a) shows the results of the video-tracking experiment and displays the effect of varying prochloraz concentrations on the locomotor behavior, *i.e.*, on the distance gammarids moved per hour during 18 h exposure. Asterisks (black, ECOD activity; blue, video-tracking) mark treatment samples that are significantly different from the control.

Overall, the *in vivo* ECOD assay does not only include primary biotransformation reactions, such as the formation of 7-hydroxycoumarin, which would be desired if we want to compare CYP activities across different species. Secondary biotransformation reactions including conjugation reactions as observed in this study, uptake, and excretion can strongly affect the actual concentration of the measured fluorescent BTP 7-hydroxycoumarin. Because toxicokinetic processes are extremely difficult to predict and can differ strongly among species, CYP activities based on the detection of only one primary BTP should only be compared across different species with great care. Nevertheless, the ECOD assay is suitable

to compare the potencies of different chemicals, e.g., azoles in one species. However, transferring the IC_{50} for prochloraz determined via ECOD activity ($IC_{50, PRZ, ECOD}$: $0.5 \pm 0.1 \mu M \cong 200 \pm 60 \mu g L^{-1}$) to another substrate is not feasible since we have seen considerable inhibition already at much lower prochloraz concentrations (see section 3.3.2 and 3.3.3 as well as Figure 3-4b) when measuring internal concentrations of azoxystrobin and associated BTPs. These differences indicate that 7-ethoxycoumarin is not as broad a CYP substrate as it is described in humans.⁷³⁻⁷⁴ To identify when synergism actually starts between azoxystrobin and prochloraz, an additional IC_{50} for prochloraz was determined via internal concentration measurements using azoxystrobin as a substrate ($IC_{50, PRZ, AZ}$). Figure 3-4b depicts the accumulation of the parent compound azoxystrobin and the formation of one exemplary BTP, its demethylation product AZ_M390a, in the presence of different prochloraz concentrations. The $IC_{50, PRZ, AZ}$ was $0.02 \pm 0.01 \mu M$ ($8 \pm 3 \mu g L^{-1}$), and the $IC_{10, PRZ, AZ}$ was $0.009 \pm 0.005 \mu M$ ($4 \pm 2 \mu g L^{-1}$) based on the dose-response curve of the parent compound azoxystrobin. The $IC_{50/10, PRZ, AZ}$ s based on the dose-response curves of the associated primary CYP-catalyzed BTPs were in the same range (see SI N). It is likely that the $IC_{50/10, PRZ, AZ}$ s determined via the substrate azoxystrobin are transferable to other environmental contaminants because several different biotransformation reactions were observed for azoxystrobin, with many reactions probably catalyzed by CYPs (see Figure 3-1). Moreover, one of the structural features of azoxystrobin, the alkyl group attached to an oxygen, is widespread among chemicals, and CYP-catalyzed O-dealkylation reactions are frequent reactions in drug metabolism.⁷¹

3.3.5 Locomotory Behavior of Gammarids in the Presence of Prochloraz

To test whether increased uptake is caused by increased movement of pleopods due to hyperactivity, which results in increased ventilation, the locomotory behavior of gammarids in the presence of different prochloraz concentrations was investigated by video-tracking. Hyperactivity has been reported for gammarids being exposed to sublethal insecticide concentrations and has been shown to be linked to drift behavior.⁸³⁻⁸⁴ In *Chironomus* larvae, increased uptake rates have been observed in the presence of pesticide mixtures.⁴⁷ Figure 3-4a shows the results of the video-tracking experiment and displays the effect of prochloraz on gammarids' locomotory behavior. At $0.1 \mu M$ prochloraz, the total distance gammarids moved during 18 h was greatest (almost double compared to control) and significantly different from the control (see SI P). The behavioral data are in line with the increase in total internal concentrations of several different substrates, the *in vivo* ECOD assay, and the modeled uptake rate constants k_u (see section 3.3.3), thereby providing strong evidence for elevated uptake induced by hyperactivity.

3.3.6 Environmental Relevance

All six azoles apart from prochloraz showed no synergistic effects measured in terms of internal azoxystrobin concentrations and ECOD activity using exposure concentrations in the low μM range (40 and 80 $\mu\text{g L}^{-1}$). Azole concentrations measured in Swiss surface waters are between approximately 0.06-0.3 $\mu\text{g L}^{-1}$, suggesting that synergism is not relevant at environmental concentrations in Swiss surface waters.^{19, 22} However, the $\text{IC}_{10, \text{PRZ, AZ}}$ for prochloraz ($4 \pm 2 \mu\text{g L}^{-1}$) is only around 10 times higher than what was found in Swiss monitoring data.²² Strobilurin and azole fungicides are two of the most important fungicide classes applied worldwide¹⁴⁻¹⁵ and are detected in considerably higher concentrations in surface waters strongly influenced by agriculture and/or wastewater.^{17, 23, 85} The LC_{50} of azoxystrobin in the presence of Swiss environmental prochloraz concentrations ($0.001 \mu\text{M} \pm 0.37 \mu\text{g L}^{-1}$) was not significantly reduced (see Figure 3-3). However, LC_{50} s refer to acute toxicity, and no conclusions can be made about chronic effects over a longer time period. In addition, further investigations are needed to determine whether species that are more sensitive towards azoxystrobin, such as copepods and cladocerans, show synergistic effects already at lower exposure concentrations.²⁸⁻³⁰

We showed that the synergism by prochloraz is caused not only by CYP inhibition but also by increased substrate uptake. Independent simulations of both processes with the developed toxicokinetic model showed that increased substrate uptake contributed significantly more to the observed synergism compared to CYP inhibition (see SI H). The combination of both processes might be the reason why, out of the selected azoles, only the co-exposure to prochloraz produced such a pronounced increase in internal azoxystrobin concentrations, leading to increased toxicity. This is in line with other studies in which prochloraz was also found to be a strong synergist.⁴²⁻⁴⁶ Moreover, hydrophobic interactions of the azole ring substituents of the selected azoles most likely differ, which thereby influence the complex formation of azole and CYP. Needing to account for both processes, CYP inhibition and increased uptake, further complicates mechanistic-based toxicokinetic and toxicodynamic modeling that would allow for the prediction of internal concentrations of a chemical and its effect, also in the presence of varying inhibitor-to-substrate ratios, for a proper risk assessment of mixture. In the future, hopefully more information will be gathered about chemical induced behavioral changes as well as about the enzyme composition and kinetics in invertebrates. This would support the more accurate predictive modeling of synergistic effects and thereby enable a better evaluation of the importance of synergy.

Acknowledgment

We give special thanks to Emma Schymanski (Eawag) for assistance with computational MS/MS spectra annotation. Furthermore, we thank Roman Ashauer (University of York) and Tjalling Jager (DEBtox Research) for helpful discussion and advice with toxicokinetic modeling, Rebecka Hischer (Eawag) for acute toxicity testing, Jennifer Schollée (Eawag) for discussion. This research was funded by the Swiss National Science Foundation, grant numbers 315230141190 and 205320165935.

References

- [1] Laetz, C. A.; Baldwin, D. H.; Collier, T. K.; Hebert, V.; Stark, J. D.; Scholz, N. L., The Synergistic Toxicity of Pesticide Mixtures: Implications for Risk Assessment and the Conservation of Endangered Pacific Salmon. *Environ. Health Perspect.* **2009**, *117* (3), 348-353.
- [2] Borgert, C. J.; Quill, T. F.; McCarty, L. S.; Mason, A. M., Can mode of action predict mixture toxicity for risk assessment? *Toxicol. Appl. Pharmacol.* **2004**, *201* (2), 85-96.
- [3] Altenburger, R.; Ait-Aissa, S.; Antczak, P.; Backhaus, T.; Barceló, D.; Seiler, T. B.; Brion, F.; Busch, W.; Chipman, K.; de Alda, M. L.; de Aragão Umbuzeiro, G.; Escher, B. I.; Falciani, F.; Faust, M.; Focks, A.; Hilscherova, K.; Hollender, J.; Hollert, H.; Jäger, F.; Jahnke, A.; Kortenkamp, A.; Krauss, M.; Lemkine, G. F.; Munthe, J.; Neumann, S.; Schymanski, E. L.; Scrimshaw, M.; Segner, H.; Slobodnik, J.; Smedes, F.; Kughathas, S.; Teodorovic, I.; Tindall, A. J.; Tollefsen, K. E.; Walz, K. H.; Williams, T. D.; Van den Brink, P. J.; van Gils, J.; Vrana, B.; Zhang, X.; Brack, W., Future water quality monitoring - Adapting tools to deal with mixtures of pollutants in water resource management. *Sci. Total Environ.* **2015**, *512-513*, 540-551.
- [4] Backhaus, T.; Faust, M., Predictive Environmental Risk Assessment of Chemical Mixtures: A Conceptual Framework. *Environmental Science & Technology* **2012**, *46* (5), 2564-2573.
- [5] European Commission, COM(2012) 252 final - Communication from The Commission to The Council, The combination effects of chemicals - Chemical mixtures. 2012.
- [6] EU Regulation (EC) No 1107/2009 of the European Parliament and of the Council of 21 October 2009 concerning the placing of plant protection products on the market and repealing Council Directives 79/117/EEC and 91/414/EEC.
- [7] Belden, J. B.; Gilliom, R. J.; Lydy, M. J., How well can we predict the toxicity of pesticide mixtures to aquatic life? *Integrated environmental assessment and management* **2007**, *3* (3), 364-372.
- [8] Cedergreen, N., Quantifying synergy: A systematic review of mixture toxicity studies within environmental toxicology. *PLoS ONE* **2014**, *9* (5), e96580.
- [9] Guengerich, F. P., Common and uncommon cytochrome P450 reactions related to metabolism and chemical toxicity. *Chem. Res. Toxicol.* **2001**, *14* (6), 611-650.
- [10] Katagi, T., Bioconcentration, Bioaccumulation, and Metabolism of Pesticides in Aquatic Organisms. In *Reviews of Environmental Contamination and Toxicology, Vol 204*, Whitacre, D. M., Ed. 2010; Vol. 204, pp 1-132.
- [11] Snyder, M. J., Cytochrome P450 enzymes in aquatic invertebrates: Recent advances and future directions. *Aquat. Toxicol.* **2000**, *48* (4), 529-547.
- [12] Sole, M.; Livingstone, D. R., Components of the cytochrome P450-dependent monooxygenase system and 'NADPH-independent benzo a pyrene hydroxylase' activity in a wide range of marine invertebrate species. *Comparative Biochemistry and Physiology C-Toxicology & Pharmacology* **2005**, *141* (1), 20-31.
- [13] Sijm, D. T. H. M.; Rikken, M. G. J.; Rorije, E.; Traas, T. P.; Mclachlan, M. S.; Peijnenburg, W. J. G. M., Transport, Accumulation and Transformation Processes. In *Risk Assessment of Chemicals: An Introduction*, Leeuwen, C. J. v.; Vermeire, T. G., Eds. Springer Netherlands: Dordrecht, 2007; pp 73-158.
- [14] Global Fungicides Market (Type, Crop Type and Geography - Size, Share, Global Trends, Company Profiles, Analysis, Segmentation and Forecast, 2013 - 2020. http://www.researchandmarkets.com/research/7dtjwc/global_fungicides.
- [15] IUPAC International Union of Pure and Applied Chemistry. Pesticide Properties Database. <http://sitem.herts.ac.uk/aeru/iupac/>.
- [16] Kahle, M.; Buerge, I. J.; Hauser, A.; Müller, M. D.; Poiger, T., Azole Fungicides: Occurrence and Fate in Wastewater and Surface Waters. *Environmental Science & Technology* **2008**, *42* (19), 7193-7200.

- [17] Battaglin, W.; Sandstrom, M.; Kuivila, K.; Kolpin, D.; Meyer, M., Occurrence of Azoxystrobin, Propiconazole, and Selected Other Fungicides in US Streams, 2005–2006. *Water Air Soil Pollut* **2011**, *218* (1-4), 307-322.
- [18] Kuzmanović, M.; Ginebreda, A.; Petrović, M.; Barceló, D., Risk assessment based prioritization of 200 organic micropollutants in 4 Iberian rivers. *Sci. Total Environ.* **2015**, *503-504*, 289-299.
- [19] Moschet, C.; Wittmer, I.; Simovic, J.; Junghans, M.; Piazzoli, A.; Singer, H.; Stamm, C.; Leu, C.; Hollender, J., How a complete pesticide screening changes the assessment of surface water quality. *Environ. Sci. Technol.* **2014**, *48* (10), 5423-5432.
- [20] Berenzen, N.; Hümmer, S.; Liess, M.; Schulz, R., Pesticide Peak Discharge from Wastewater Treatment Plants into Streams During the Main Period of Insecticide Application: Ecotoxicological Evaluation in Comparison to Runoff. *Bull. Environ. Contam. Toxicol.* **2003**, *70* (5), 0891-0897.
- [21] Rasmussen, J. J.; Baattrup-Pedersen, A.; Wiberg-Larsen, P.; McKnight, U. S.; Kronvang, B., Buffer strip width and agricultural pesticide contamination in Danish lowland streams: Implications for stream and riparian management. *Ecol. Eng.* **2011**, *37* (12), 1990-1997.
- [22] Doppler, T.; Mangold, S.; Wittmer, I.; Spycher, S.; Comte, R.; Stamm, C.; Singer, H., Hohe PSM-Belastung in schweizer Bächen. *Aqua und Gas* **2017**, *4*, 46-56.
- [23] Rodrigues, E. T.; Lopes, I.; Pardal, M. A., Occurrence, fate and effects of azoxystrobin in aquatic ecosystems: a review. *Environment international* **2013**, *53*, 18-28.
- [24] Beketov, M. A.; Liess, M., Potential of 11 pesticides to initiate downstream drift of stream macroinvertebrates. *Arch. Environ. Contam. Toxicol.* **2008**, *55* (2), 247-53.
- [25] Zubrod, J. P.; Baudy, P.; Schulz, R.; Bundschuh, M., Effects of current-use fungicides and their mixtures on the feeding and survival of the key shredder *Gammarus fossarum*. *Aquat. Toxicol.* **2014**, *150*, 133-143.
- [26] Warming, T. P.; Mulderu, G.; Christoffersen, K. S., Clonal variation in physiological responses of *Daphnia magna* to the strobilurin fungicide azoxystrobin. *Environ. Toxicol. Chem.* **2009**, *28* (2), 374-380.
- [27] Ochoa-Acuna, H. G.; Bialkowski, W.; Yale, G.; Hahn, L., Toxicity of soybean rust fungicides to freshwater algae and *Daphnia magna*. *Ecotoxicology* **2009**, *18* (4), 440-446.
- [28] Gustafsson, K.; Blidberg, E.; Elfgrén, I. K.; Hellström, A.; Kylin, H.; Gorokhova, E., Direct and indirect effects of the fungicide azoxystrobin in outdoor brackish water microcosms. *Ecotoxicology* **2010**, *19* (2), 431-444.
- [29] Zafar, M. I.; Belgers, J. D. M.; Van Wijngaarden, R. P. A.; Matser, A.; Van den Brink, P. J., Ecological impacts of time-variable exposure regimes to the fungicide azoxystrobin on freshwater communities in outdoor microcosms. *Ecotoxicology* **2012**, *21* (4), 1024-1038.
- [30] van Wijngaarden, R. P. A.; Belgers, D. J. M.; Zafar, M. I.; Matser, A. M.; Boerwinkel, M.-C.; Arts, G. H. P., Chronic aquatic effect assessment for the fungicide azoxystrobin. *Environ. Toxicol. Chem.* **2014**, *33* (12), 2775-2785.
- [31] Oekotoxzentrum, Vorschläge für akute und chronische Qualitätskriterien für ausgewählte schweizrelevante Substanzen. **2017**.
- [32] European Commission, Common Implementation Strategy for the Water Framework Directive (2000/60/EC). 2011.
- [33] Henry, M. J.; Sisler, H. D., Effects of sterol biosynthesis-inhibiting (SBI) fungicides on cytochrome P-450 oxygenations in fungi. *Pestic. Biochem. Physiol.* **1984**, *22* (3), 262-275.
- [34] Copping, L. G.; Hewitt, H. G., Chemistry and Mode of Action of Crop Protection agents. *Royal Society of Chemistry Cambridge, UK* **1998**.
- [35] Kraemer, S. D.; Testa, B., The Biochemistry of Drug Metabolism - An Introduction Part 7. Intra-Individual Factors Affecting Drug Metabolism. *Chemistry & Biodiversity* **2009**, *6* (10), 1477-1660.
- [36] Ortiz De Montellano, P. R.; Almira Correia, M., *Inhibition of cytochrome P450 enzymes*. 1995; p 305-364.
- [37] Badyal, D. K.; Dadhich, A. P., Cytochrome P450 and drug interactions. *Indian Journal of Pharmacology* **2001**, *33* (4), 248-259.

- [38] Nyman, A. M.; Schirmer, K.; Ashauer, R., Toxicokinetic-toxicodynamic modelling of survival of *Gammarus pulex* in multiple pulse exposures to propiconazole: Model assumptions, calibration data requirements and predictive power. *Ecotoxicology* **2012**, *21* (7), 1828-1840.
- [39] Adam, O.; Badot, P. M.; Degiorgi, F.; Crini, G., Mixture toxicity assessment of wood preservative pesticides in the freshwater amphipod *Gammarus pulex* (L.). *Ecotoxicology and Environmental Safety* **2009**, *72* (2), 441-449.
- [40] Estimation Programs Interface Suite™ for Microsoft® Windows, v 4.11. United States Environmental Protection Agency, Washington, DC, USA. 2013.
- [41] Haeba, M. H.; Hilscherova, K.; Mazurova, E.; Blaha, L., Selected endocrine disrupting compounds (vinclozolin, flutamide, ketoconazole and dicofol): Effects on survival, occurrence of males, growth, molting and reproduction of *Daphnia magna*. *Environ Sci Pollut Res* **2008**, *15* (3), 222-227.
- [42] Nørgaard, K. B.; Cedergreen, N., Pesticide cocktails can interact synergistically on aquatic crustaceans. *Environ Sci Pollut Res* **2010**, *17* (4), 957-967.
- [43] Bjergager, M. B.; Hanson, M. L.; Solomon, K. R.; Cedergreen, N., Synergy between prochloraz and esfenvalerate in *Daphnia magna* from acute and subchronic exposures in the laboratory and microcosms. *Aquat. Toxicol.* **2012**, *110-111*, 17-24.
- [44] Bjergager, M.-B. A.; Hanson, M. L.; Lissemore, L.; Henriquez, N.; Solomon, K. R.; Cedergreen, N., Synergy in microcosms with environmentally realistic concentrations of prochloraz and esfenvalerate. *Aquat. Toxicol.* **2011**, *101* (2), 412-422.
- [45] Cedergreen, N.; Kamper, A.; Streibig, J. C., Is prochloraz a potent synergist across aquatic species? A study on bacteria, daphnia, algae and higher plants. *Aquat. Toxicol.* **2006**, *78* (3), 243-252.
- [46] Kretschmann, A.; Gottardi, M.; Dalhoff, K.; Cedergreen, N., The synergistic potential of the azole fungicides prochloraz and propiconazole toward a short α -cypermethrin pulse increases over time in *Daphnia magna*. *Aquat. Toxicol.* **2015**, *162*, 94-101.
- [47] Belden, J. B.; Lydy, M. J., Impact of atrazine on organophosphate insecticide toxicity. *Environ. Toxicol. Chem.* **2000**, *19* (9), 2266-2274.
- [48] Kunz, P. Y.; Kienle, C.; Gerhardt, A., *Gammarus* spp. in aquatic ecotoxicology and water quality assessment: toward integrated multilevel tests. *Rev. Environ. Contam. Toxicol.* **2010**, *205*, 1-76.
- [49] Gerhardt, A.; Bloor, M.; Mills, C. L., *Gammarus*: Important Taxon in Freshwater and Marine Changing Environments. *International Journal of Zoology* **2011**.
- [50] Maltby, L.; Clayton, S. A.; Wood, R. M.; McLoughlin, N., Evaluation of the *Gammarus pulex* in situ feeding assay as a biomonitor of water quality: Robustness, responsiveness, and relevance. *Environ. Toxicol. Chem.* **2002**, *21* (2), 361-368.
- [51] Macneil, C.; Dick, J. T. A.; Elwood, R. W., The trophic ecology of freshwater *Gammarus* spp. (Crustacea: Amphipoda): Problems and perspectives concerning the functional feeding group concept. *Biological Reviews of the Cambridge Philosophical Society* **1997**, *72* (3), 349-364.
- [52] Naylor, C.; Maltby, L.; Calow, P., Scope for growth in *Gammarus pulex*, a freshwater benthic detritivore. *Hydrobiologia* **1989**, *188-189* (1), 517-523.
- [53] Rösch, A.; Anliker, S.; Hollender, J., How Biotransformation Influences Toxicokinetics of Azole Fungicides in the Aquatic Invertebrate *Gammarus pulex*. *Environmental Science & Technology* **2016**, *50* (13), 7175-7188.
- [54] Kukkonen, J.; Oikari, A., Sulphate conjugation is the main route of pentachlorophenol metabolism in *Daphnia magna*. *Comparative Biochemistry and Physiology - C Pharmacology Toxicology and Endocrinology* **1988**, *91* (2), 465-468.
- [55] R Core Team *A language and environment for statistical computing*, R Foundation for Statistical Computing: 2016.
- [56] Ritz, C.; Streibig, J. C., Bioassay analysis using R. *Journal of Statistical Software* **2005**, *12*, 1-22.

- [57] Gottardi, M.; Kretschmann, A.; Cedergreen, N., Measuring cytochrome P450 activity in aquatic invertebrates: a critical evaluation of in vitro and in vivo methods. *Ecotoxicology* **2015**, *25* (2), 419-430.
- [58] Brain, P.; Cousens, R., An equation to describe dose responses where there is stimulation of growth at low doses. *Weed Research* **1989**, *29* (2), 93-96.
- [59] EC. Regulation No. 1907/2006 of the European Parliament and of the Council Concerning the Registration, Evaluation, Authorization and Restriction of Chemicals. 2006.
- [60] Kern, S.; Fenner, K.; Singer, H. P.; Schwarzenbach, R. P.; Hollender, J., Identification of transformation products of organic contaminants in natural waters by computer-aided prediction and high-resolution mass spectrometry. *Environ. Sci. Technol.* **2009**, *43* (18), 7039-7046.
- [61] Boudina, A.; Emmelin, C.; Baaliouamer, A.; Païssé, O.; Chovelon, J. M., Photochemical transformation of azoxystrobin in aqueous solutions. *Chemosphere* **2007**, *68* (7), 1280-1288.
- [62] Singh, N.; Singh, S. B.; Mukerjee, I.; Gupta, S.; Gajbhiye, V. T.; Sharma, P. K.; Goel, M.; Dureja, P., Metabolism of ¹⁴C-azoxystrobin in water at different pH. *Journal of Environmental Science and Health Part B-Pesticides Food Contaminants and Agricultural Wastes* **2010**, *45* (2), 123-127.
- [63] Laird, W. J. D.; Gledhill, A. J.; Lappin, G. J., Metabolism of methyl-(E)-2-{2- 6-(2-cyanophenoxy)pyrimidin-4-yloxy phenyl}-3-methoxyac rylate (azoxystrobin) in rat. *Xenobiotica* **2003**, *33* (6), 677-690.
- [64] Roberts, T. R.; Hutson, D. H., Metabolic Pathways of Agrochemicals: Part 2: Insecticides and Fungicides. *Royal Society of Chemistry* **2006**.
- [65] Clinton, B.; Warden, A. C.; Haboury, S.; Easton, C. J.; Kotsonis, S.; Taylor, M. C.; Oakeshott, J. G.; Russell, R. J.; Scott, C., Bacterial degradation of strobilurin fungicides: a role for a promiscuous methyl esterase activity of the subtilisin proteases? *Biocatal. Biotransform.* **2011**, *29* (4), 119-129.
- [66] EFSA, Conclusion on the peer review of the pesticide risk assessment of the active substance azoxystrobin. *EFSA Journal* **2010**, *8* (4).
- [67] Jeon, J.; Kurth, D.; Hollender, J., Biotransformation pathways of biocides and pharmaceuticals in freshwater crustaceans based on structure elucidation of metabolites using high resolution mass spectrometry. *Chem. Res. Toxicol.* **2013**, *26* (3), 313-24.
- [68] Ashauer, R.; Hintermeister, A.; O'Connor, I.; Elumelu, M.; Hollender, J.; Escher, B. I., Significance of xenobiotic metabolism for bioaccumulation kinetics of organic chemicals in *gammarus pulex*. *Environ. Sci. Technol.* **2012**, *46* (6), 3498-3508.
- [69] Ikenaka, Y.; Eun, H.; Ishizaka, M.; Miyabara, Y., Metabolism of pyrene by aquatic crustacean, *Daphnia magna*. *Aquat. Toxicol.* **2006**, *80* (2), 158-165.
- [70] Ikenaka, Y.; Ishizaka, M.; Eun, H.; Miyabara, Y., Glucose-sulfate conjugates as a new phase II metabolite formed by aquatic crustaceans. *Biochem. Biophys. Res. Commun.* **2007**, *360* (2), 490-495.
- [71] Testa, B.; Kramer, S. D., The biochemistry of drug metabolism - An introduction - Part 2. Redox reactions and their enzymes. *Chemistry & Biodiversity* **2007**, *4* (3), 257-405.
- [72] Moon, J. Y.; Lee, D. W.; Park, K. H., Inhibition of 7-ethoxycoumarin O-deethylase activity in rat liver microsomes by naturally occurring flavonoids: structure-activity relationships. *Xenobiotica* **1998**, *28* (2), 117-126.
- [73] Waxman, D. J.; Chang, T. K. H., Use of 7-ethoxycoumarin to monitor multiple enzymes in the human CYP1, CYP2, and CYP3 families. *Methods in molecular biology (Clifton, N.J.)* **2006**, *320*, 153-6.
- [74] Yamazaki, H.; Inoue, K.; Mimura, M.; Oda, Y.; Guengerich, F. P.; Shimada, T., 7-ethoxycoumarin O-deethylation catalyzed by cytochromes P450 1A2 and 2E1 in human liver microsomes. *Biochem. Pharmacol.* **1996**, *51* (3), 313-319.
- [75] Bach, J.; Snegaroff, J., Effects of the fungicide prochloraz on xenobiotic metabolism in rainbow trout: inhibition in vitro and time course of induction in vivo. *Xenobiotica* **1989**, *19* (3), 255-267.

- [76] Gagnaire, B.; Geffard, O.; Noury, P.; Garric, J., In vivo Indirect Measurement of Cytochrome P450-Associated Activities in Freshwater Gastropod Molluscs. *Environmental Toxicology* **2010**, *25* (6), 545-553.
- [77] Kotze, A. C., Oxidase activities in macrocyclic-resistant and -susceptible *Haemonchus contortus*. *Journal of Parasitology* **2000**, *86* (4), 873-876.
- [78] Fisher, T.; Crane, M.; Callaghan, A., Induction of cytochrome P-450 activity in individual *Chironomus riparius* Meigen larvae exposed to xenobiotics. *Ecotoxicology and Environmental Safety* **2003**, *54* (1), 1-6.
- [79] Sturm, A.; Hansen, P. D., Altered cholinesterase and monooxygenase levels in *Daphnia magna* and *Chironomus riparius* exposed to environmental pollutants. *Ecotoxicology and Environmental Safety* **1999**, *42* (1), 9-15.
- [80] Calabrese, E. J.; Baldwin, L. A., Toxicology rethinks its central belief - Hormesis demands a reappraisal of the way risks are assessed. *Nature* **2003**, *421* (6924), 691-692.
- [81] Calabrese, E. J., Overcompensation stimulation: A mechanism for hormetic effects. *Crit. Rev. Toxicol.* **2001**, *31* (4-5), 425-470.
- [82] Stebbing, A. R. D., A mechanism for hormesis - A problem in the wrong discipline. *Crit. Rev. Toxicol.* **2003**, *33* (3-4), 463-467.
- [83] Norum, U.; Frederiksen, M. A. T.; Bjerregaard, P., Locomotory behaviour in the freshwater amphipod *Gammarus pulex* exposed to the pyrethroid cypermethrin. *Chemistry and Ecology* **2011**, *27* (6), 569-577.
- [84] Norum, U.; Friberg, N.; Jensen, M. R.; Pedersen, J. M.; Bjerregaard, P., Behavioural changes in three species of freshwater macroinvertebrates exposed to the pyrethroid lambda-cyhalothrin: Laboratory and stream microcosm studies. *Aquat. Toxicol.* **2010**, *98* (4), 328-335.
- [85] Riise, G.; Lundekvam, H.; Wu, Q. L.; Haugen, L. E.; Mulder, J., Loss of pesticides from agricultural fields in SE Norway - runoff through surface and drainage water. *Environ. Geochem. Health* **2004**, *26* (2-3), 269-276.

Chapter S3. Supporting Information:
The Synergistic Potential of Azole Fungicides in the Aquatic Invertebrate *Gammarus pulex*

Andrea Rösch^{1,2}, Michele Gottardi³, Caroline Vignet¹, Nina Cedergreen³, Juliane Hollender^{1,2*}

¹ Eawag, Swiss Federal Institute of Aquatic Science and Technology, 8600 Dübendorf, Switzerland

² Institute of Biogeochemistry and Pollutant Dynamics, ETH Zürich, 8092 Zürich, Switzerland

³ Department of Plant and Environmental Sciences, University of Copenhagen, 1871 Frederiksberg C, Denmark

* Corresponding Author: Phone: +41 58 765 5493. e-mail: juliane.hollender@eawag.ch

Published in *Environmental Science and Technology*, DOI: 10.1021/acs.est.7b03088

SI.A Chemicals and Solutions

Table S3-1: Fungicides. All standard solutions were prepared in methanol.

Substance	CAS number	Supplier	Quality
Azoxystrobin	131860-33-8	Dr. Ehrenstorfer	99.5%
Azoxystrobin acid	1185255-09-7	HPC Standards GmbH	99%
Azoxystrobin-d4	1346606-39-0	Sigma-Aldrich	98%
Cyproconazole	94361-06-5	Dr. Ehrenstorfer	96%
Cyproconazole ¹⁾	94361-06-5	Sigma Aldrich	99.6%
Epoxiconazole	135319-73-2	Dr. Ehrenstorfer	99%
Epoxiconazole ¹⁾	135319-73-2	Sigma Aldrich	99%
Ketoconazole	65277-42-1	Sigma-Aldrich	98%
Propiconazole	60207-90-1	Dr. Ehrenstorfer	96.7%
Propiconazole-d5		Dr. Ehrenstorfer	100%
Prochloraz	67747-09-5	Dr. Ehrenstorfer	98.5%
Prochloraz ¹⁾	67747-09-5	Sigma Aldrich	98.6%
Prochloraz-d7		Dr. Ehrenstorfer	97%
Tebuconazole	107534-96-3	Dr. Ehrenstorfer	98.5%
Tebuconazole ¹⁾	107534-96-3	Sigma Aldrich	99.3%
Tebuconazole-d6		Dr. Ehrenstorfer	100%

¹⁾: Used for experiments dealing with ECOD (7-ethoxycoumarin-O-dealkylation) activity.

Table S3-2: Other chemicals and solutions.

Substance	CAS number	Supplier	Quality
Acetic acid	64-19-7	Merck	100%
Acetonitrile	75-05-8	Acros Organics	HPLC-grade
Ammonium acetate	631-61-8	Sigma-Aldrich	> 98%
Bovine Serum Albumin	9048-46-8	Sigma-Aldrich	> 96%
Calcium chloride	10035-04-8	Sigma-Aldrich	> 99%
Ethanol	64-17-5	Merck	Analytical grade
Formic acid	64-18-6	Merck	98-100%
β -Glucosidase from almonds	9001-22-3	Sigma-Aldrich	
Magnesium sulfate	10034-99-8	Sigma-Aldrich	> 99%
Isopropanol	67-63-0	Fisher Chemicals	> 99%
Methanol Optima	67-56-1	Fisher Chemicals	LC-MS grade
Potassium chloride	7447-40-7	Sigma-Aldrich	> 99%
Sodium acetate trihydrate	6131-90-4	Fluka	> 99.5%
Sodium hydrogen carbonate	144-55-8	Merck	> 99%
Sulfatase from patella vulgata	9016-17-5	Sigma	

SI.B Test Organisms

Experimental Design, Sections “*Whole Body Internal Concentration Measurements of the Substrate Azoxystrobin and associated BTPs*”, “*Median-Lethal Concentrations of Azoxystrobin (LC_{50} s) in the Presence and Absence of Prochloraz*” and “*Video-Tracking of the Locomotory Behavior of *Gammarus pulex* in the Presence of Prochloraz*” of the present publication:

Male and female adult *Gammarus pulex* were collected between October 2014 and November 2016 from a small creek near Zürich, Switzerland (47°16'29.0" N 8°47'21.4" E), located in a small nature reserve. Organisms were kept in aerated artificial pond water (APW)¹ and were fed with horse chestnut (*Aesculus hippocastanum*) leaves inoculated with *Cladosporium herbarum*¹.

Experimental Design, Section “*Half Maximal Inhibitory Concentrations based on ECOD in vivo Activity (IC_{50} , $ECODs$)*” of the present publication:

Male and female adult *G. pulex* were collected north of Copenhagen, Denmark (55° 48' 58" N 12° 18' 45" E) from a small uncontaminated creek in January and June 2016. Organisms were kept in aerated APW and were fed with degraded leaves collected at the sampling site.

SI.C Analytical Method

Source Parameters

Table S3-3: Source parameters used for HRMS/MS measurement. (Quadrupole-orbitrap mass spectrometer: Q Exactive, Thermo Fisher Scientific Inc.).

sheat gas (nitrogen) flow rate	40 L min ⁻¹
auxiliary gas (nitrogen) flow rate	10 L min ⁻¹
auxiliary gas heater temperature	40 °C
capillary temperature	350 °C
S-Lens RF level	50
external mass calibration	mass calibration with an in-house prepared amino acid solution (11 amino acids with m/z between 116-997) in positive and negative ionization mode
spray voltage	4 kV (positive ionization mode) 3 kV (negative ionization mode)

MS Parameters

Full scan acquisition was performed for a mass range of 100-1000 m/z with a resolution of 70 000 (at m/z 200) in polarity switching mode followed by data-dependent MS/MS scans with a resolution of 17 000 (at m/z 200) and an isolation window of 1 m/z (loop count for MS/MS acquisition: positive ionization mode: 2 to 5, negative ionization mode: 1 to 2, dynamic exclusion: 1 to 7 s) with a quadrupole-orbitrap mass spectrometer (Q Exactive, Thermo Fisher Scientific Inc.). The number of data-dependent MS/MS scans varied depending on the scope of the experiment. For BTP screening of azoxystrobin a mass list of suspected BTPs was set up based on (i) *in silico* pathway prediction (Eawag-PPS, <http://eawag-bbd.ethz.ch/predict/>, Eawag-PPS predicts microbial degradation of chemicals based on biotransformation rules), (ii) *in silico* manual prediction of BTPs considering most common enzymatic biotransformation reactions, and (iii) identified BTPs of azoxystrobin reported in any organisms in scientific literature. The final mass list used for triggering data-dependent MS/MS scans and for BTP screening with SIEVE software (see SI E) contained 1325 suspected BTP masses. Additionally, targeted MS/MS spectra were acquired using different collision energies for BTPs tentatively identified to get further fragmentation information for MS/MS spectra interpretation. After identification of BTPs, the mass list for

triggering data-dependent MS/MS scans in the following experiments was shortened to the number of identified BTPs. Thereby, BTPs were confirmed in each experiment by MS/MS acquisition.

Online-SPE-LC (automated online solid phase extraction reverse-phase liquid chromatography)

For sample enrichment and sample clean-up online-SPE was used. An empty stainless steel SPE cartridge (20 mm x 2.1 mm, BGB) was filled with ca. 9 mg Oasis HLB (15 μm particle size, Waters, USA) and ca. 9 mg of a mixture of anion exchanger Strata X-AW, cation exchanger Strata X-CW (both ion exchangers: 30 μm , Phenomenex, UK) and Env+ (70 μm , Biotage, Sweden) in a ratio of 1:1:1.5 (X-AW : X-CW : Env+).

Table S3-4: Time schedule of the online-SPE procedure. Gradient of the loading pump with ammonium acetate solution (2 mM in nanopure water) and acetonitrile. Elution of the sample was performed via the elution pump, whereas loading of the sample was performed via the dispenser syringe. Acetonitrile was used to flush the sample loop and the SPE cartridge after every sample.

Time [min]	Ammonium acetate solution (2 mM) [$\mu\text{L min}^{-1}$]	Acetonitrile [$\mu\text{L min}^{-1}$]	SPE step
0.00	200		
0.10	0	2000	
0.60	0	2000	Elution of the sample from the cartridge (with elution pump) and washing of the loop
0.65	2000		
5.60	2000		
5.65	400		
6.20	400		
6.30		400	
13.9		400	Loading of the new sample into the loop and conditioning of the cartridge
14.00	400		
20.60	400		
20.70	2000		Enrichment of the new sample
32.00	2000		

Table S3-5: Time schedule of the LC gradient. Chromatographic separation was achieved with a reversed-phase column (XBridge C18 column, 3.5 μm , 2.1 x 50 mm, Waters).¹⁾ Water and methanol were both acidified with 0.1% (vol.) formic acid.

Time [min]	Water [$\mu\text{L min}^{-1}$]	Methanol [$\mu\text{L min}^{-1}$]	Isopropanol ²⁾ [$\mu\text{L min}^{-1}$]
0.0	260	40	
0.4	260	40	
20.0	20	280	
20.2	20		280
26.0	20		280
26.2	260	40	
32.3	260	40	

¹⁾ For the internal concentration measurements of 7-ethoxycoumarin and associated BTPs an acetonitrile-water (both acidified with 0.1% (vol.) formic acid) gradient with above shown flow rates was used on an Atlantis C18 column (3 μm , 3 x 150 mm, Waters).

²⁾ If only medium samples were measured no isopropanol was used as a matrix cleaning step of the column.

SI.D Quality Control

Quantification was based on internal standard calibration (Trace Finder software 3.1 and 3.3, Thermo Scientific) in a calibration range of 0.5 – 3000 ng L^{-1} with 16 calibration points at the beginning and end of each experiment if low concentrated BTPs and parent compounds were quantified. For targeted analysis of exposure medium samples, the calibration range was reduced to 8 calibration points (5 – 500 ng L^{-1}). Isotopically labeled internal standards (ISTDs) were available for 7-ethoxycoumarin, azoxystrobin, prochloraz, propiconazole, tebuconazole and tramadol. For the remaining azoles, the closest matching ISTD based on the structure and retention time was used (tebuconazole-d6 for cyproconazole, epoxiconazole and ketoconazole). Calibration curves were obtained by linear least square regression using a weighing factor of 1/x. Calibration curves were linear with $R^2 > 0.99$. Linearity was slightly reduced if no matching ISTD was available. Due to the lack of BTP reference standards, quantification of BTPs was based on the calibration curve of the parent compound azoxystrobin except for azoxystrobin acid (AZ_M390b), where a reference standard was available.

The limit of quantification (LOQ) of azoxystrobin in the gammarid extract was calculated by referencing the amount of azoxystrobin (AZ) in the lowest measured calibration standard per injection (0.01 ng AZ in 20 mL nanopure water) to the average sample wet weight per injection (mg wet weight in 20 mL nanopure water) and finally dividing this value by the calculated matrix factor. This wet weight varies depending on the volume of spiked gammarid extract in 20 mL and thereby influences the calculation of LOQs. 100 or 200 μL of gammarid extract were added to 20 mL nanopure water for sample analysis during different experiments. The LOQ calculation is based on 100 μL gammarid extract. However, 200 μL

gammarid extract would rather lower the LOQ as long as ion suppression does not increase substantially due to an increased matrix load. No LOQs could be calculated for the identified BTPs in the gammarid extracts; however, since the quantification of the BTPs is based on the calibration curve of azoxystrobin, it is assumed that LOQs of the BTPs are comparable to the LOQ of azoxystrobin.

For exposure medium samples, the lowest measured calibration standard was used since the matrix of the artificial pond water did not lead to ion suppression compared to calibration standards prepared in nanopure water (verified by comparing the peak areas of the internal standard azoxystrobin-d4). LOQs of the selected azole fungicides can be found in our previous publication.²

Table S3-6: Calculated matrix factors for gammarid extracts and limit of quantification (LOQ) for azoxystrobin in *G. pulex* extracts and in the exposure medium. Duplicate samples (prespike 1 and 2) were spiked before gammarid extraction with 50 µg L⁻¹ (i.e., 5 ng absolute in 100 µL measured extract) and 100 µg L⁻¹ (i.e., 10 ng absolute in 100 µL measured extract) of azoxystrobin, respectively.

Compound	Matrix factors					LOQ*	LOQ**
	Pre-spike 1 5 ng	Pre-spike 2 5 ng	Pre-spike 1 10 ng	Pre-spike 2 10 ng	Average	[nmol kg _{ww} ⁻¹]	[ng L ⁻¹]
Azoxystrobin	0.7	0.7	0.7	0.6	0.7	2.9	0.5

*: LOQ for gammarid extract samples

**: LOQ for medium samples

Table S3-7: Relative recoveries for the whole sample preparation and analytical procedure. Duplicate samples (prespike 1 and 2) spiked before the gammarid extraction with 50 µg L⁻¹ (i.e., 5 ng absolute in 100 µL measured extract) and 100 µg L⁻¹ (i.e., 10 ng absolute in 100 µL measured extract) of the parent compounds, respectively, were used to determine the recovery of the whole procedure of sample preparation and chemical analysis.

Compound	Relative recovery [%]			
	Prespike 1 5 ng	Prespike 2 5 ng	Prespike 1 10 ng	Prespike 2 10 ng
Azoxystrobin	127	129	119	121

SI.E Biotransformation Product Identification with SIEVE Software

Similar to our previous publication² SIEVE software version 2.2 (Thermo Scientific) for differential expression analysis was used to compare treatment and control samples. Thereby peaks of suspected and nontarget BTPs could be identified that only occurred in the treatment samples. As control samples, the exposure medium and “organism controls” (chemical negative, organism and food positive, *i.e.*, organism matrix) were used. The SIEVE software was operated in the following three steps: chromatographic alignment, framing, and identification by either comparison with a generated mass list of predicted BTPs (suspect screening, for the generated mass list refer to SI C) or by filtering the whole frame list (nontarget screening). Framing describes the process of building regions in the *m/z* versus retention time plane, whereby all peaks above a given threshold are collected until the user-defined maximum number of frames is reached.

For suspect and nontarget screening approaches SIEVE software was run separately in positive ionization mode ($[M+H]^+$) and negative ionization mode ($[M-H]^-$) to identify potential BTPs. Only peaks with an intensity $\geq 10^6$ in at least one replicate sample and at minimum three scans in the extracted ion chromatograms were considered as potential BTPs. Furthermore, intensities of potential BTPs had to increase in the uptake phase and decrease in the depuration phase.

For the nontarget screening, the whole generated frame lists of positive and negative ionization modes were filtered with an integrated intensity (*i.e.*, peak area) threshold. An integrated intensity threshold of 0.1% of the integrated intensity of the parent compound azoxystrobin was used. Additionally, the intensity ratio between treatment and control samples was set to be > 10 .

Table S3-8: Settings used for suspect and nontarget screening with SIEVE (Thermo Scientific, version 2.2).

Retention time window:	5-20 min
<i>m/z</i> window:	100-1000
Frame time width:	1 min
<i>m/z</i> tolerance:	10 ppm
Maximum number of frames:	15000
Peak intensity threshold:	10^6

SI.F Sampling During the Kinetic Experiment

Table S3-9: Sampled time-points during the kinetic experiments.

Uptake (U) / Depuration (D)	Time [h]	Time [d]	Kinetic
U	0.5	0.02	AZ / AZ + PRZ
U	1.5	0.06	AZ / AZ + PRZ
U	2.5	0.10	AZ / AZ + PRZ
U	5.5	0.23	AZ / AZ + PRZ
U	9.5	0.40	AZ / AZ + PRZ
U	17.5	0.73	AZ / AZ + PRZ
U	24	1.00	AZ / AZ + PRZ
D	24	1.00	AZ
D	25	1.04	AZ
D	26	1.08	AZ
D	28	1.17	AZ
D	31	1.29	AZ
D	35	1.46	AZ
D	42	1.75	AZ
D	50	2.08	AZ
D	65	2.71	AZ
D	75	3.13	AZ
D	95	3.96	AZ
D	119	4.96	AZ
D	144	6.00	AZ

SI.G Sulfate and Glucose Deconjugation Experiment

An enzyme deconjugation experiment was carried out for further confirmation of possible azoxystrobin glucose and sulfate conjugation products. The experimental setup closely followed the method described by Kukkonen and Oikari (1988)³. Briefly, the remaining gammarid extracts (from previous experiments with gammarid exposure to azoxystrobin) were combined and 900 μL of 0.1 M sodium acetate buffer (pH 5) was added as a keeper. The methanol in the gammarid extracts was evaporated under a gentle stream of nitrogen. Next, the samples were split into treatment and control samples, each containing approximately 150 μL . Sulfatase / glucosidase was dissolved in 0.1 M sodium acetate buffer (pH 5) to a concentration of 20 / 28 units mL^{-1} . To the treatment samples 700 μL of sulfatase or glucosidase solution was added, whereas 700 μL 0.1 M acetate buffer (pH 5) and 1 mg of bovine serum albumin were added to the control samples. Treatment and control samples were prepared in duplicate. Samples were incubated overnight on a shaker at 37 °C and the reaction was stopped after approximately 8 h by adding 1 mL methanol. Finally, the samples

were filtered through 0.45 µm regenerated cellulose filters and analyzed by online-SPE LC-HRMS/MS.

SI.H Modeling Bioaccumulation and Biotransformation Kinetics

The Model

Toxicokinetic rate constants for azoxystrobin - alone and in the presence of prochloraz - were estimated using a first-order compartment model. Therefore, we used the scripts and functions built in the BYOM (Build Your Own Model) modeling platform programmed by Tjalling Jager (<http://www.debtox.nl/about.html>) to simulate biotransformation and bioaccumulation kinetics with Matlab R2015b.

The toxicokinetic model is described by the following ordinary differential equations (ODEs), where we differentiate between primary BTPs (1st BTPs) that are directly formed out of the parent compound, and secondary BTPs (2nd BTPs), where a direct precursor BTP was detected:

Time course for the parent compound:

$$\frac{dC_{in,p}(t)}{dt} = C_{water}(t) \cdot k_u - C_{in,p}(t) \cdot k_e - C_{in,p}(t) \cdot (k_{M1,1st} + \dots + k_{Mx,1st}) \quad \text{Equation S3-1}$$

Time courses for the primary BTPs:

$$\frac{dC_{in,M1,1st}(t)}{dt} = C_{in,p}(t) \cdot k_{M1,1st} - C_{in,M1,1st}(t) \cdot k_{eM1,1st} - C_{in,M1,1st}(t) \cdot (k_{M1,2nd} + \dots + k_{Mx,2nd}) \quad \text{Equation S3-2}$$

Time courses for the secondary BTPs:

$$\frac{dC_{in,M1,2nd}(t)}{dt} = C_{in,M1,1st}(t) \cdot k_{M1,2nd} - C_{in,M1,2nd}(t) \cdot k_{eM1,2nd} - C_{in,M1,2nd}(t) \cdot (k_{M1,further} + \dots + k_{Mx,further}) \quad \text{Equation S3-3}$$

where $C_{in,p}(t)$, $C_{in,Mx,1st}(t)$ and $C_{in,Mx,2nd}(t)$ [nmol kg_{ww}⁻¹] are the whole body internal concentrations in *G. pulex* of the parent compound, the primary BTPs and the secondary BTPs, respectively, and $C_{water}(t)$ [nmol L⁻¹] describes the time course of the parent compound in the exposure medium. k_u [L kg_{ww}⁻¹ d⁻¹] denotes the uptake rate constant of the parent compound from the medium by food, respiratory surfaces, and dermal absorption, whereas k_e [d⁻¹] is the direct elimination of the parent compound via passive (respiratory surfaces) and active (excretion of faeces) processes. The biotransformation rate constants [d⁻¹] and elimination rate constants [d⁻¹] for primary and secondary BTPs are described by $k_{Mx,1st}$ and $k_{Mx,2nd}$ and $k_{eMx,1st}$ and $k_{eMx,2nd}$, respectively. In case no successor BTPs were identified, $k_{eMx,1st}$ or $k_{eMx,2nd}$ are lumped rate constants that include direct excretion as well as elimination due to further biotransformation, otherwise further biotransformation is considered separately.

Model Calibration and Parameter Estimation

ODEs were solved numerically (Runge-Kutta algorithm) and fitted to the measured internal concentrations of the parent compound and its BTPs. Parameters were obtained by minimizing the sum of squares (Nelder-Mead Simplex method) between measured and simulated internal concentration. All parameters were fitted simultaneously and were constrained to positive values. The best fit parameters were used to simulate the internal concentrations of the parent compound and of its BTPs. The exposure medium was measured during both the uptake and depuration phase and the values were used as input for C_{water} . 95% confidence intervals were calculated using profile likelihoods.

Bioaccumulation Factors

Bioaccumulation factors (BAFs) [$L\ kg^{-1}$] were either calculated at a specific time point based on the ratio of the concentration of the parent compound in the organisms and of the concentration of the parent compound in the exposure medium with the requirement of steady state:

$$BAF = \frac{C_{in,p}(t)}{C_{water}(t)} \quad \text{Equation S3-4}$$

or kinetically based on the ratio of the uptake of the parent compound and of its total elimination:

$$\text{kinetic BAF (BAF}_k) = \frac{k_u}{k_e + k_{M1,1st} + \dots + k_{Mx,1st}} \quad \text{Equation S3-5}$$

Elimination Half-lives

Elimination half-lives ($t_{1/2}$) [h] were calculated for the parent compound azoxystrobin and its BTPs based on the total elimination. Details are described in our previous publication.²

Elimination half-life for the parent compound azoxystrobin:

$$t_{1/2,p} = \frac{\ln 2}{k_e + k_{M1,1st} + \dots + k_{Mx,1st}} \quad \text{Equation S3-6}$$

Elimination half-lives for BTPs where one or more direct successor is known:

$$t_{1/2,M1,1stor2nd} = \frac{\ln 2}{k_{eM1,1stor2nd} + k_{M1,2ndor\ further} + \dots + k_{Mx,2ndor\ further}} \quad \text{Equation S3-7}$$

Elimination half-lives for BTPs where no direct successor is known:

$$t_{1/2,M1,1stor2nd} = \frac{\ln 2}{k_{eM1,1stor2nd}} \quad \text{Equation S3-8}$$

Table S3-10: Kinetic rate constants for azoxystrobin (lower and upper 95% confidence intervals are given in brackets), kinetic bioaccumulation factor (BAF_k) and elimination half-lives ($t_{1/2}$). The ordinary differential equations used for fitting the kinetic rate constants are based on the azoxystrobin biotransformation pathway displayed in Figure 1 in the present publication. The kinetic rate constants for azoxystrobin are based on uptake and depuration data. 1st and 2nd BTPs refer to primary and secondary BTPs, respectively. Results are rounded to three significant digits. Two replicate internal concentrations were used per time point. Confidence intervals are marked in red that hit the limits of the parameter values. Large confidence intervals, where the limits of the parameter values ranged up to four orders of magnitude, are marked in blue.

Compound	k_u [L kg _{ww} ⁻¹ d ⁻¹]	k_e [d ⁻¹]	k_{Mx} [d ⁻¹]	k_{eMx} [d ⁻¹]	$t_{1/2}$ [h]
AZ BAF _k : 4.91 [L kg _{ww} ⁻¹]	37.2 [32.8; 57.8]	6.68 [5.72; 10.8]			2.19
AZ_M392 (2 nd BTP)			8.96 [7.17; 12.0]	0.0001 [0.0001; 3.95]	19.3
AZ_M390a (1 st BTP)			0.165 [0.135; 0.202]	0.0001 [0.0001; 0.739]	10.2
AZ_M630 (2 nd BTP)			20.9 [13.9; 44.1]	1.63 [0.0001; 0.324] [0.858; 2.48]	9.20
AZ_M328a (1 st BTP)			0.0678 [0.0518; 0.0892]	1.30 [0.868; 1.91]	12.8
AZ_M378 (2 nd BTP)			0.864 [0.674; 1.30]	3.36 [2.33; 6.02]	4.96
AZ_M214 (1 st BTP)			0.0570 [0.0413; 0.0791]	1.39 [0.855; 2.18]	12.0
AZ_M390b (1 st BTP)			0.472 [0.397; 0.609]	0.0001 [0.0001; 100]	1.86
AZ_M328b (1 st BTP)			0.0126 [0.00921; 0.0185]	1.00 [0.585; 1.78]	16.6
AZ_M498 (2 nd BTP)			2.34 [1.43; 3.19]	6.552 [0.0001; 0.495] [3.01; 10.3]	2.38
AZ_M525 (1 st BTP)			0.0420 [0.0320; 0.0585]	0.0001 [0.0001; 9.40]	1.71
AZ_M362a (1 st BTP)			0.00142 [0.000494; 0.00257]	0.0001 [0.0001; 100]	166355
AZ_M552 (2 nd BTP)			1.63 [1.20; 2.09]	0.0001 [0.0001; 13.7]	0.80
AZ_M514 (2 nd BTP)			0.432 [0.256; 7.63]	1.82 [0.874; 48.2]	9.13
AZ_M618 (2 nd BTP)			0.180 [0.0896; 2.05]	2.79 [1.08; 43.9]	5.96
AZ_M420 (1 st BTP)			0.0548 [0.0359; 0.0737]	0.0001 [0.0001; 2.26]	7.11
AZ_M493 (2 nd BTP)			9.74 [6.96; 17.0]	1.04 [0.669; 1.74]	15.9
AZ_M362b (1 st BTP)			0.0351 [0.0264; 0.0490]	0.0001 [0.0001; 100]	166355

Calculation of BAF_k for azoxystrobin:

Equation S3-9

$$BAF_k(AZ) \left[L \cdot kg_{ww}^{-1} \right] = \frac{k_u}{k_e + k_{M1,1st} + \dots + k_{Mx,1st}}$$

$$= \frac{k_u}{k_e + k_{M390a} + k_{M328a} + k_{M328b} + k_{M214} + k_{M390b} + k_{M525} + k_{M362a} + k_{M420} + k_{M362b}}$$

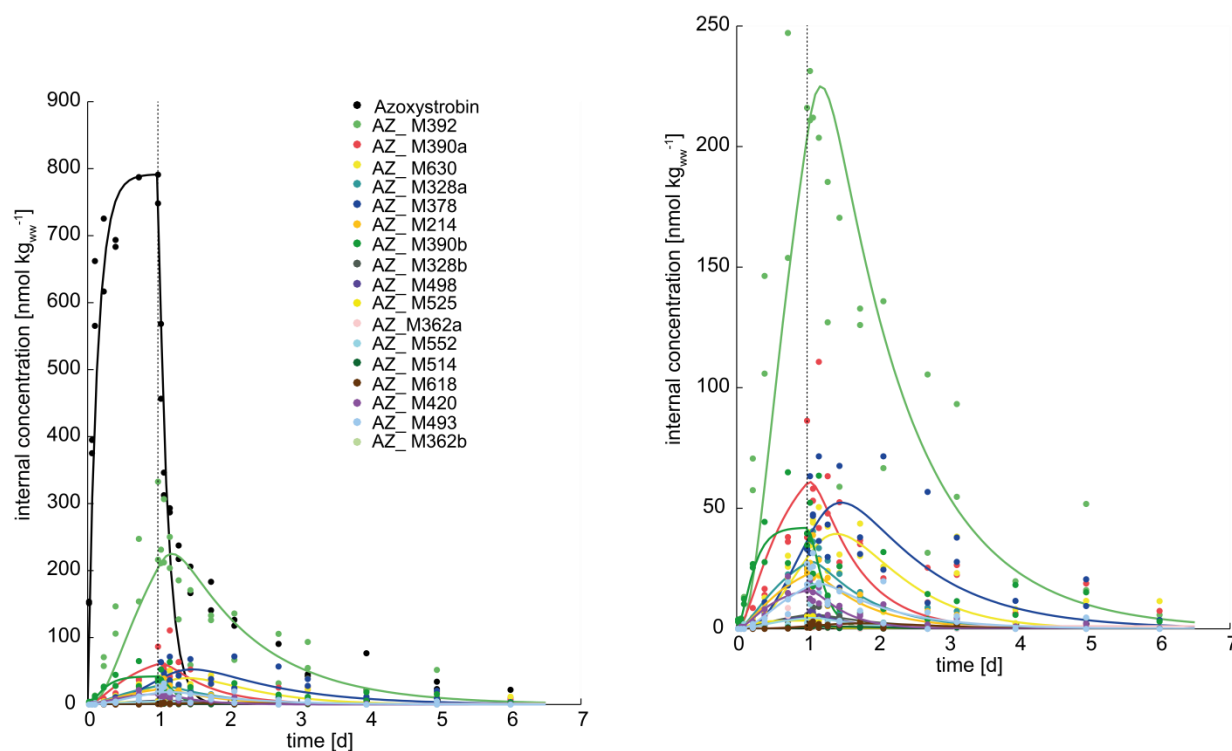


Figure S3-1: Uptake and depuration kinetic for azoxystrobin in *G. pulex*. Shown are the measured (dots) and modeled (lines) time courses for azoxystrobin and associated BTPs. Dashed vertical lines indicate the change from uptake (1 d) to depuration (5 d). In the panels on the right the y-axis has been expanded to show the kinetics of the less concentrated BTPs.

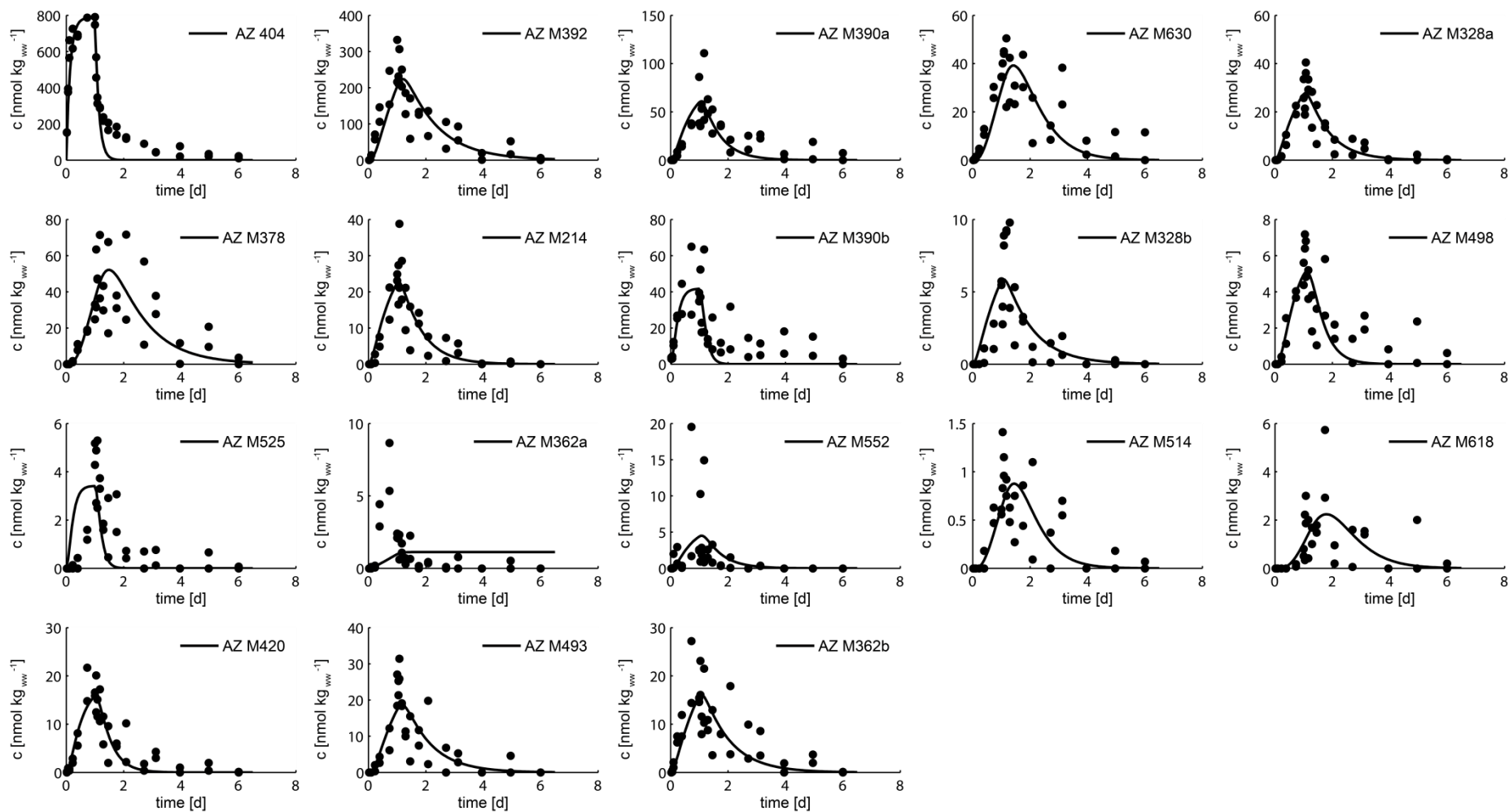


Figure S3-2: Measured (dots) and modeled (lines) time-series of internal concentrations of azoxystrobin and its BTPs in *G. pulex* in the uptake (1 d) and deuration phase (5 d) shown in separate panels.

Table S3-11: Kinetic rate constants for azoxystrobin alone and in combination with prochloraz (lower and upper 95% confidence intervals are given in brackets) and kinetic bioaccumulation factors (BAF_ks). The ordinary differential equations used for fitting the kinetic rate constants are based on the reduced azoxystrobin biotransformation pathway for comparing rate constants between single and mixture exposure displayed in Figure 1 in the present publication. The kinetic rate constants for the single exposure to azoxystrobin are based on uptake and depuration data, whereas the kinetic rate constants for the mixture exposure are only based on uptake data. 1st and 2nd BTPs refer to primary and secondary BTPs, respectively. Results are rounded to three significant digits. Two replicate internal concentrations were used per time point. Confidence intervals are marked in red that hit the limits of the parameter values. Large confidence intervals, where the limits of the parameter values ranged up to four orders of magnitude, are marked in blue.

Compound	k_u [L kg _{ww} ⁻¹ d ⁻¹]	k_e [d ⁻¹]	k_{Mx} [d ⁻¹]	k_{eMx} [d ⁻¹]
<u>Azoxystrobin</u>				
AZ	44.2	8.02		
BAF _k : 5.00 [L kg _{ww} ⁻¹]	[34.4; 59.3]	[5.94; 11.4]		
AZ + PRZ	63.6	6.26		
BAF _k : 9.92 [L kg _{ww} ⁻¹]	[44.1; 88.0]	[4.01; 9.19]		
<u>AZ M392 (2nd BTP)</u>				
AZ			8.08	0.0138
			[6.84; 12.6]	[0.0001; 3.83]
AZ + PRZ			2.19	0.000138
			[1.70; 2.68]	[0.0001; 6.35]
<u>AZ M390a (1st BTP)</u>				
AZ			0.144	0.000101
			[0.121; 0.191]	[0.0001; 0.762]
AZ + PRZ			0.0180	0.000113
			[0.00539; 0.0486]	[0.0001; 100]
<u>AZ M630 (2nd BTP)</u>				
AZ			1.37	1.44
			[1.06; 1.79]	[0.977; 2.26]
AZ + PRZ			14.6	46.2
			[4.84; 93.6]	[13.2; 100]
<u>AZ M328a (1st BTP)</u>				
AZ			0.0629	1.21
			[0.0485; 0.0901]	[0.792; 1.92]
AZ + PRZ			0.000945	0.000166
			[0.000617; 0.00956]	[0.0001; 18.0]
<u>AZ M378 (2nd BTP)</u>				
AZ			0.786	2.86
			[0.191; 0.442]	[0.270; 1.69]
			[0.615; 1.33]	[2.05; 6.19]
AZ + PRZ			0.457	0.000146
			[0.332; 0.655]	[0.0001; 26.1]
			[0.973; 4.76]	
<u>AZ M214 (1st BTP)</u>				
AZ			0.0521	1.28
			[0.0398; 0.0805]	[0.796; 2.17]
AZ + PRZ			0.00110	0.000160
			[0.000815; 0.00141]	[0.0001; 1.06]

Compound	k_u [L kg _{ww} ⁻¹ d ⁻¹]	k_e [d ⁻¹]	k_{Mx} [d ⁻¹]	k_{eMx} [d ⁻¹]
AZ M390b (1st BTP)				
AZ			0.436 [0.381; 0.611]	0.000117 [0.0001; 100]
AZ + PRZ			0.073 [0.0614; 0.0867]	0.000141 [0.0001; 1.57]
AZ M498 (2nd BTP)				
AZ			1.87 [1.37; 3.01]	5.32 [3.56; 9.46]
AZ + PRZ			1.031 [0.304; 2.70]	21.2 [5.27; 56.7]
AZ M525 (1st BTP)				
AZ			0.0369 [0.0298; 0.060]	0.0001 [0.0001; 11.0]
AZ + PRZ			0.00674 [0.00508; 0.00892] [0.0107; 0.0214]	0.000803 [0.0001; 3.85]
AZ M362a (1st BTP)				
AZ			0.00146 [0.000545; 0.00264]	0.000163 [0.0001; 100]
AZ + PRZ			0.000955 [0.000388; 0.00155] [0.00187; 0.0954]	0.000125 [0.0001; 100]
AZ M420 (1st BTP)				
AZ			0.0447 [0.0358; 0.0685]	0.0001 [0.0001; 2.37]
AZ + PRZ			0.0394 [0.0296; 0.0624]	0.000105 [0.0001; 1.46]
AZ M493 (2nd BTP)				
AZ			8.26 [6.28; 17.9]	0.902 [0.614; 1.78]
AZ + PRZ			0.933 [0.453; 1.71]	1.87 [0.0727; 4.27]
AZ M362b (1st BTP)				
AZ			0.0319 [0.0253; 0.0516]	0.000143 [0.0001; 100]
AZ + PRZ			0.0137 [0.00832; 0.0233]	0.000128 [0.0001; 100]

Calculation of BAF_k for azoxystrobin in the presence of prochloraz (AZ + PRZ):

$$BAF_k(AZ + PRZ) \left[L \cdot kg_{ww}^{-1} \right] = \frac{k_u}{k_e + k_{M1,1st} + \dots + k_{Mx,1st}} \quad \text{Equation S3-10}$$

$$= \frac{k_u}{k_e + k_{M390a} + k_{M328a} + k_{M214} + k_{M390b} + k_{M525} + k_{M362a} + k_{M420} + k_{M362b}}$$

Table S3-12: Kinetic rate constants for azoxystrobin based on only uptake data (U) or based on uptake and depuration data (U+D) (lower and upper 95% confidence intervals given in brackets) and kinetic bioaccumulation factors (BAF_k s). The ordinary differential equations used for fitting the kinetic rate constants are based on the reduced azoxystrobin biotransformation pathway for comparing rate constants between single and mixture exposure displayed in Figure 1 in the present publication. 1st and 2nd BTPs refer to primary and secondary BTPs, respectively. Results are rounded to three significant digits. Two replicate internal concentrations were used per time point. Confidence intervals are marked in red that hit the limits of the parameter values. Large confidence intervals, where the limits of the parameter values ranged up to four orders of magnitude, are marked in blue.

Compound	k_u [L kg _{ww} ⁻¹ d ⁻¹]	k_e [d ⁻¹]	k_{Mx} [d ⁻¹]	k_{eMx} [d ⁻¹]
<u>Azoxystrobin</u>				
AZ (U+D)	44.2	8.02		
BAF_k : 5.00 [L kg _{ww} ⁻¹]	[34.4; 59.3]	[5.94; 11.4]		
AZ (U)	52.4	9.96		
BAF_k : 4.75 [L kg _{ww} ⁻¹]	[40.2; 64.6]	[6.98; 12.8]		
<u>AZ M392 (2nd BTP)</u>				
AZ (U+D)			8.08	0.0138
			[6.84; 12.6]	[0.0001; 3.83]
AZ (U)			13.36	0.0001009
			[10.6; 17.0]	[0.0001; 4.46]
<u>AZ M390a (1st BTP)</u>				
AZ (U+D)			0.144	0.000101
			[0.121; 0.191]	[0.0001; 0.762]
AZ (U)			0.205	0.000101
			[0.167; 0.244]	[0.0001; 6.19]
<u>AZ M630 (2nd BTP)</u>				
AZ (U+D)			1.37	1.44
			[1.06; 1.79]	[0.977; 2.26]
AZ (U)			3.14	3.604
			[2.58; 3.92]	[2.70; 4.54]
<u>AZ M328a (1st BTP)</u>				
AZ (U+D)			0.0629	1.21
			[0.0485; 0.0901]	[0.792; 1.92]
AZ (U)			0.0417	0.000120
			[0.0353; 0.0361]	[0.0001; 1.02]
			[0.0375; 0.0460]	
			[0.0497; 0.0607]	
<u>AZ M378 (2nd BTP)</u>				
AZ (U+D)			0.786	2.86
			[0.191; 0.442]	[0.270; 1.69]
			[0.615; 1.33]	[2.05; 6.19]
AZ (U)			1.18	10.8
			[0.694; 1.83]	[5.59; 17.7]

Compound	k_u [L kg _{ww} ⁻¹ d ⁻¹]	k_e [d ⁻¹]	k_{Mx} [d ⁻¹]	k_{eMx} [d ⁻¹]
<u>AZ M214 (1st BTP)</u>				
AZ (U+D)			0.0521 [0.0398; 0.0805]	1.28 [0.796; 2.17]
AZ (U)			0.0336 [0.0296; 0.0379] [0.0384; 0.0399]	0.000142 [0.0001; 1.24]
<u>AZ M390b (1st BTP)</u>				
AZ (U+D)			0.436 [0.381; 0.611]	0.000117 [0.0001; 100]
AZ (U)			0.685 [0.577; 0.824]	0.0001 [0.0001; 100]
<u>AZ M498 (2nd BTP)</u>				
AZ (U+D)			1.87 [1.37; 3.01]	5.32 [3.56; 9.46]
AZ (U)			1.71 [1.16; 2.39]	5.16 [2.84; 7.95]
<u>AZ M525 (1st BTP)</u>				
AZ (U+D)			0.0369 [0.0298; 0.060]	0.0001 [0.0001; 11.0]
AZ (U)			0.0308 [0.0252; 0.0361]	0.000157 [0.0001; 100]
<u>AZ M362a (1st BTP)</u>				
AZ (U+D)			0.00146 [0.000545; 0.00264]	0.000163 [0.0001; 100]
AZ (U)			0.00743 [0.00411; 0.495]	0.000608 [0.0001; 100]
<u>AZ M420 (1st BTP)</u>				
AZ (U+D)			0.0447 [0.0358; 0.0685]	0.0001 [0.0001; 2.37]
AZ (U)			0.0500 [0.0410; 0.0611]	0.0001006 [0.0001; 3.45]
<u>AZ M493 (2nd BTP)</u>				
AZ (U+D)			8.26 [6.28; 17.9]	0.902 [0.614; 1.78]
AZ (U)			10.8 [6.84; 23.1]	0.0001 [0.0001; 3.83]
<u>AZ M362b (1st BTP)</u>				
AZ (U+D)			0.0319 [0.0253; 0.0516]	0.000143 [0.0001; 100]
AZ (U)			0.0300 [0.0221; 0.0424] [0.0494; 0.0921]	0.000214 [0.0001; 100]

Table S3-13: Kinetic rate constants for azoxystrobin alone and in combination with prochloraz (lower and upper 95% confidence intervals are given in brackets) and kinetic bioaccumulation factors (BAF_s) based on total internal concentrations. The kinetic rate constants k_u and k_e were determined by applying the simplest one compartment model (see equation S3-11) to the total internal concentrations (sum of parent compound and of all BTPs). The kinetic rate constants for the single exposure to azoxystrobin are based on uptake and depuration data, whereas the kinetic rate constants for the mixture exposure are only based on uptake data. Results are rounded to three significant digits. Two replicate total internal concentrations were used per time point.

	k_u [L kg _{ww} ⁻¹ d ⁻¹]	k_e [d ⁻¹]
<u>Total internal concentration</u>		
AZ	23.2	2.55
	[17.3; 29.5]	[1.84; 3.35]
AZ + PRZ	75.0	7.32
	[49.7; 117]	[4.46; 12.3]

Simplest one compartment model:

$$\frac{dC_{in,total}(t)}{dt} = C_{water}(t) \cdot k_u - C_{in,total}(t) \cdot k_e$$

Equation S3-11

where $dC_{in,total}(t)$ is the total internal concentration and k_e is in this case the total elimination comprising direct elimination and elimination due to biotransformation.

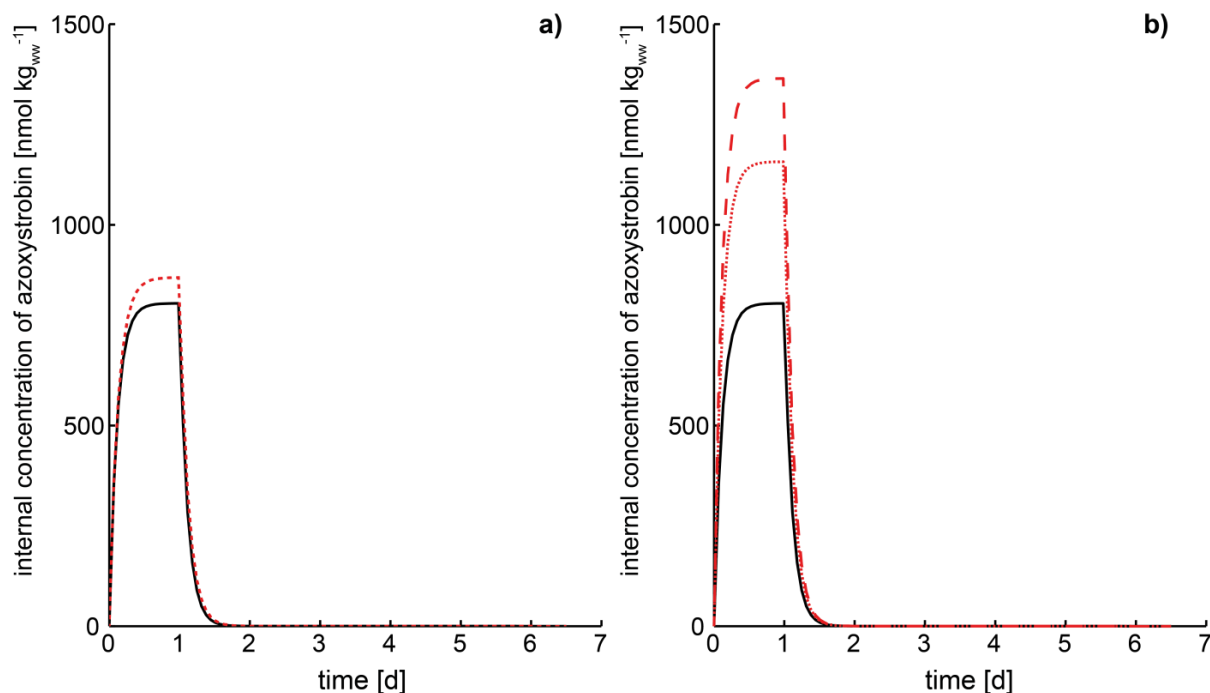


Figure S3-3: Simulations of internal azoxystrobin concentrations with the best fit parameters from the developed toxicokinetic model testing (a) impact of inhibited primary biotransformation rate constants $k_{Mx,1st}$ whereby all parameters were kept constant except for $k_{Mx,1st}$ and (b) impact of increased uptake rate constants k_u , whereby all parameters were kept constant except for k_u . The ordinary differential equations used for fitting the kinetic rate constants are based on the reduced azoxystrobin biotransformation pathway for comparing rate constants between single and mixture exposure displayed in Figure 3-1 of the present publication.

Panel a: straight line: simulation with best fit parameters for the single exposure to azoxystrobin, red dashed line: simulation with best fit parameters but decreased $k_{Mx,1st}$ by 80% in the presence of prochloraz.

Panel b: straight line: simulation with best fit parameters for the single exposure to azoxystrobin ($k_u=44.2 \text{ L kg}_{ww}^{-1} \text{ d}^{-1}$), narrow dashed red line: simulation with best fit parameters but increased k_u in the presence of prochloraz ($k_u=63.6 \text{ L kg}_{ww}^{-1} \text{ d}^{-1}$), wide dashed red line: simulation with best fit parameters but increased k_u in the presence of prochloraz ($k_u=75.0 \text{ L kg}_{ww}^{-1} \text{ d}^{-1}$ when fitted to the total internal concentration of azoxystrobin).

SI.I Exposure Medium Concentrations, Internal Concentrations and Bioaccumulation Factors (BAFs)

Tables in this section are sorted according to the order of the experiments in the *Material and Methods* section in the present publication. BAFs reported in this section are based on the ratio of the concentration of the parent compound in the organisms and of the concentration of the parent compound in the exposure medium with the requirement of steady state (see equation S3-4 in SI H *Modeling Bioaccumulation and Biotransformation Kinetics*). t_0 refers to the addition of the substrate and t_{10}/t_{24} to the end of the exposure phase.

The following abbreviations are valid for all tables located in this section:

m: medium samples

C+ L-: "chemical controls" (organisms and food negative, chemical positive)

C+ L+: "food controls" (organism negative, food and chemical positive)

AZ: azoxystrobin

PRZ: prochloraz

PBO: piperonyl butoxide

7-Etc: 7-ethoxycoumarin

TRM: tramadol

CP: cyproconazole

EP: epoxiconazole

TEB: tebuconazole

KET: ketoconazole

PRP: propiconazole

Table S3-14: Binary mixtures composed of 200 µg L⁻¹ AZ and equimolar PRZ concentration of 186 µg L⁻¹ (4 h pre-exposure to PRZ). In the control samples nominal concentrations of 200 µg L⁻¹ were used for AZ and PRZ. In the binary mixture composed of 200 µg L⁻¹ AZ and 500 µg L⁻¹ PBO, PBO could not be quantified with the used analytical method.

Exposure medium			
	AZ [µg L ⁻¹]	AZ [nmol L ⁻¹]	PRZ [µg L ⁻¹]
m_C+ L+ t0_1	200		182
m_C+ L+ t0_2	201		177
m_C+ L+ t24_1	201		177
m_C+ L- t0_1	208		183
m_C+ L- t0_2	199		186
m_C+ L- t24_1	205		186
m_AZ t0_1	212	526	
m_AZ t24_1	201	500	
m_AZ + PBO t0_1	207	513	
m_AZ + PBO t24_1	189	468	
m_AZ + PRZ t0_1	200	497	176
m_AZ + PRZ t24_1	208	515	171

Whole body internal concentrations 24 h after substrate addition and corresponding BAFs			
	AZ [nmol kg _{ww} ⁻¹]	BAF AZ [L kg _{ww} ⁻¹]	PRZ [nmol kg _{ww} ⁻¹]
AZ_1	1768	3	
AZ_2	1281	2	
AZ + PBO_1	3140	6	
AZ + PBO_2	3024	6	
AZ + PRZ_1	4426	9	19930

Table S3-15: Binary mixtures composed of AZ (40 and 80 $\mu\text{g L}^{-1}$) and equimolar concentrations of one of the selected azole fungicides (4 h pre-exposure to the selected azole fungicide). Mixtures were composed of 40 / 80 $\mu\text{g L}^{-1}$ AZ + 37 / 74 $\mu\text{g L}^{-1}$ PRZ, + 34 / 68 $\mu\text{g L}^{-1}$ PRP, + 31 / 61 $\mu\text{g L}^{-1}$ TEB, + 33 / 65 $\mu\text{g L}^{-1}$ EP, + 29 / 58 $\mu\text{g L}^{-1}$ CP and + 53 / 105 $\mu\text{g L}^{-1}$ KET, respectively. In the control samples nominal concentrations of 40 and 80 $\mu\text{g L}^{-1}$ were used for AZ and all selected azole fungicides.

Exposure medium	AZ [$\mu\text{g L}^{-1}$]	AZ [nmol L ⁻¹]	PRZ [$\mu\text{g L}^{-1}$]	PRP [$\mu\text{g L}^{-1}$]	TEB [$\mu\text{g L}^{-1}$]	EP [$\mu\text{g L}^{-1}$]	CP [$\mu\text{g L}^{-1}$]	KET [$\mu\text{g L}^{-1}$]
m_C+ L- t0_1 (40)	41		n. s.	n. s.	n. s.	n. s.	n. s.	n. s.
m_C+ L- t0_2 (40)	36		32	31	33	29	29	25
m_C+ L- t24_1 (40)	35		33	32	35	30	32	25
m_C+ L- t24_2 (40)	38		34	34	36	30	31	28
m_C+ L+ t0_1 (40)	38		36	34	37	32	32	28
m_C+ L+ t0_2 (40)	36		34	32	34	30	31	27
m_C+ L+ t24_1 (40)	37		35	33	35	32	32	37
m_C+ L+ t24_2 (40)	37		35	32	37	31	32	27
m_C+ L- t0_1 (80)	n. a.		n. a.	n. a.	n. a.	n. a.	n. a.	n. a.
m_C+ L- t0_2 (80)	70		66	64	66	59	59	51
m_C+ L- t24_1 (80)	72		70	67	74	62	64	60
m_C+ L- t24_2 (80)	68		64	62	68	61	62	61
m_C+ L+ t0_1 (80)	71		69	64	71	61	63	52
m_C+ L+ t0_2 (80)	70		67	65	68	61	62	54
m_C+ L+ t24_1 (80)	72		70	66	74	63	68	41
m_C+ L+ t24_2 (80)	67		64	62	69	58	62	50
m_AZ t0_1 (40)	35	86						
m_AZ t0_2 (40)	34	85						
m_AZ t24_1 (40)	34	85						
m_AZ t24_2 (40)	33	82						
m_AZ + PRZ t0_1 (40)	n. a.		n. a.					
m_AZ + PRZ t0_2 (40)	41	103	32					
m_AZ + PRZ t24_1 (40)	41	101	33					
m_AZ + PRZ t24_2 (40)	36	89	26					

Exposure medium								
	AZ [$\mu\text{g L}^{-1}$]	AZ [nmol L^{-1}]	PRZ [$\mu\text{g L}^{-1}$]	PRP [$\mu\text{g L}^{-1}$]	TEB [$\mu\text{g L}^{-1}$]	EP [$\mu\text{g L}^{-1}$]	CP [$\mu\text{g L}^{-1}$]	KET [$\mu\text{g L}^{-1}$]
m_AZ + PRP t0_1 (40)	36	90		25				
m_AZ + PRP t0_2 (40)	38	94		28				
m_AZ + PRP t24_1 (40)	39	96		27				
m_AZ + PRP t24_2 (40)	34	84		26				
m_AZ + TEB t0_1 (40)	37	91			26			
m_AZ + TEB t0_2 (40)	36	89			25			
m_AZ + TEB t24_1 (40)	36	90			27			
m_AZ + TEB t24_2 (40)	36	89			26			
m_AZ + EP t0_1 (40)	35	87				23		
m_AZ + EP t0_2 (40)	34	85				24		
m_AZ + EP t24_1 (40)	34	85				23		
m_AZ + EP t24_2 (40)	31	78				23		
m_AZ + CP t0_1 (40)	35	87					21	
m_AZ + CP t0_2 (40)	33	82					22	
m_AZ + CP t24_1 (40)	34	85					23	
m_AZ + CP t24_2 (40)	36	90					10	
m_AZ + KET t0_1 (40)	n. a.	n. a.						n. a.
m_AZ + KET t0_2 (40)	40	98						57
m_AZ + KET t24_1 (40)	39	97						54
m_AZ + KET t24_2 (40)	36	89						39
m_AZ t0_1 (80)	74	184						
m_AZ t0_2 (80)	74	184						
m_AZ t24_1 (80)	71	176						
m_AZ t24_2 (80)	71	176						
m_AZ + PRZ t0_1 (80)	78	193	68					
m_AZ + PRZ t0_2 (80)	86	214	73					
m_AZ + PRZ t24_1 (80)	75	185	62					

Exposure medium								
	AZ [$\mu\text{g L}^{-1}$]	AZ [nmol L^{-1}]	PRZ [$\mu\text{g L}^{-1}$]	PRP [$\mu\text{g L}^{-1}$]	TEB [$\mu\text{g L}^{-1}$]	EP [$\mu\text{g L}^{-1}$]	CP [$\mu\text{g L}^{-1}$]	KET [$\mu\text{g L}^{-1}$]
m_AZ + PRZ t24_2 (80)	75	186	60					
m_AZ + PRP t0_1 (80)	65	161		48				
m_AZ + PRP t0_2 (80)	82	202		61				
m_AZ + PRP t24_1 (80)	71	177		54				
m_AZ + PRP t24_2 (80)	73	180		55				
m_AZ + TEB t0_1 (80)	67	166			51			
m_AZ + TEB t0_2 (80)	85	211			63			
m_AZ + TEB t24_1 (80)	67	166			51			
m_AZ + TEB t24_2 (80)	75	186			54			
m_AZ + EP t0_1 (80)	69	172				49		
m_AZ + EP t0_2 (80)	72	179				49		
m_AZ + EP t24_1 (80)	70	174				48		
m_AZ + EP t24_2 (80)	74	185				49		
m_AZ + CP t0_1 (80)	69	172					40	
m_AZ + CP t0_2 (80)	79	197					42	
m_AZ + CP t24_1 (80)	68	168					38	
m_AZ + CP t24_2 (80)	69	170					42	
m_AZ + KET t0_1 (80)	n. a.	n. a.						n. a.
m_AZ + KET t0_2 (80)	68	168						80
m_AZ + KET t24_1 (80)	72	177						81
m_AZ + KET t24_2 (80)	68	170						79

Whole body internal concentrations 24 h after substrate addition and corresponding BAFs

	AZ [nmol kg _{ww} ⁻¹]	BAF AZ [L kg _{ww} ⁻¹]	PRZ [nmol kg _{ww} ⁻¹]	PRP [nmol kg _{ww} ⁻¹]	TEB [nmol kg _{ww} ⁻¹]	EP [nmol kg _{ww} ⁻¹]	CP [nmol kg _{ww} ⁻¹]	KET [nmol kg _{ww} ⁻¹]
AZ_1 (40)	591	7						
AZ_2 (40)	752	9						
AZ + PRZ_1 (40)	1149	12	3125					
AZ + PRZ_2 (40)	1154	12	3401					
AZ + PRP_1 (40)	742	8		2102				
AZ + PRP_2 (40)	681	7		1872				
AZ + TEB_1 (40)	740	8			3298			
AZ + TEB_2 (40)	700	8			2959			
AZ + EP_1 (40)	689	8				4734		
AZ + EP_2 (40)	746	9				4888		
AZ + CP_1 (40)	663	8					1325	
AZ + CP_2 (40)	739	9					1027	
AZ + KET_1 (40)	643	7						2224
AZ + KET_2 (40)	637	7						1494
AZ_1 (80)	727	4						
AZ_2 (80)	838	5						
AZ + PRZ_1 (80)	1615	8	7828					
AZ + PRZ_2 (80)	1408	7	5983					
AZ + PRP_1 (80)	733	4		3226				
AZ + PRP_2 (80)	881	5		3277				
AZ + TEB_1 (80)	781	4			5368			
AZ + TEB_2 (80)	856	5			5604			
AZ + EP_1 (80)	943	5				7419		
AZ + EP_2 (80)	1166	7				7960		
AZ + CP_1 (80)	943	5					2122	
AZ + CP_2 (80)	832	5					2282	

Whole body internal concentrations 24 h after substrate addition and corresponding BAFs								
	AZ [nmol kg _{ww} ⁻¹]	BAF AZ [L kg _{ww} ⁻¹]	PRZ [nmol kg _{ww} ⁻¹]	PRP [nmol kg _{ww} ⁻¹]	TEB [nmol kg _{ww} ⁻¹]	EP [nmol kg _{ww} ⁻¹]	CP [nmol kg _{ww} ⁻¹]	KET [nmol kg _{ww} ⁻¹]
AZ + KET_1 (80)	1039	6						1512
AZ + KET_2 (80)	812	5						3074

n. s.: not spiked.

n. a.: not analyzed.

Table S3-16: Binary mixtures composed of 60 µg L⁻¹ AZ and equimolar PRZ concentration of 56 µg L⁻¹ (4 h pre-exposure to PRZ). In the control samples nominal concentrations of 40 µg L⁻¹ AZ and 37 µg L⁻¹ PRZ were used.

Exposure medium			
	AZ [µg L ⁻¹]	AZ [nmol L ⁻¹]	PRZ [µg L ⁻¹]
m_C+ L+ t0_1	39		36
m_C+ L+ t0_2	39		37
m_C+ L+ t18_1	37		33
m_C+ L+ t18_2	36		32
m_C+ L+ t28_1	37		33
m_C+ L+ t28_2	37		33
m_AZ t0_1	58	145	
m_AZ t0_2	55	137	
m_AZ t24_1	52	129	
m_AZ t24_2	57	142	
m_AZ + PRZ_1 (t0 PRZ)			52
m_AZ + PRZ_2 (t0 PRZ)			53
m_AZ + PRZ t0_1	62	153	48
m_AZ + PRZ t0_2	67	166	50
m_AZ + PRZ t24_1	57	141	45
m_AZ + PRZ t24_2	57	141	49
Whole body internal concentrations 24 h after substrate addition and corresponding BAFs			
	AZ [nmol kg _{ww} ⁻¹]	BAF AZ [L kg _{ww} ⁻¹]	PRZ [nmol kg _{ww} ⁻¹]
AZ_1	844	6	
AZ_2	692	5	
AZ + PRZ_1	1425	9	4202
AZ + PRZ_2	1900	13	6095

Table S3-17: Binary mixtures composed of 40 µg L⁻¹ AZ and equimolar PRZ concentrations of 37 µg L⁻¹. Different pre-exposure times to PRZ (4, 12 and 18 h) were tested. In the control samples nominal concentrations of 40 µg L⁻¹ AZ and 37 µg L⁻¹ PRZ were used.

Exposure medium	AZ [µg L ⁻¹]	AZ [nmol L ⁻¹]	PRZ [µg L ⁻¹]
m_C+ L+ _1 (t0 PRZ)	39		36
m_C+ L+ _2 (t0 PRZ)	39		37
m_C+ L+ t0_1	37		33
m_C+ L+ t0_2	36		32
m_C+ L+ t10_1	37		33
m_C+ L+ t10_2	37		33
m_AZ t0_1	39	96	
m_AZ t0_2	37	93	
m_AZ t10_1	37	92	
m_AZ t10_2	39	97	
m_AZ + PRZ-4h _1 (t0 PRZ)			34
m_AZ + PRZ-4h _2 (t0 PRZ)			35
m_AZ + PRZ-4h t0_1	44	110	33
m_AZ + PRZ-4h t0_2	39	97	33
m_AZ + PRZ-4h t10_1	37	93	32
m_AZ + PRZ-4h t10_2	37	92	31
m_AZ + PRZ-12h _1 (t0 PRZ)			38
m_AZ + PRZ-12h _2 (t0 PRZ)			37
m_AZ + PRZ-12h t0_1	43	108	33
m_AZ + PRZ-12h t0_2	41	102	32
m_AZ + PRZ-12h t10_1	37	92	30
m_AZ + PRZ-12h t10_2	36	89	30
m_AZ + PRZ-18h _1 (t0 PRZ)			37
m_AZ + PRZ-18h _2 (t0 PRZ)			36
m_AZ + PRZ-18h t0_1	43	108	33

Exposure medium			
	AZ [$\mu\text{g L}^{-1}$]	AZ [nmol L^{-1}]	PRZ [$\mu\text{g L}^{-1}$]
m_AZ + PRZ-18h t0_2	41	102	32
m_AZ + PRZ-18h t10_1	38	94	31
m_AZ + PRZ-18h t10_2	38	94	32

Whole body internal concentrations 10 h after substrate addition and corresponding BAFs			
	AZ [$\text{nmol kg}_{\text{ww}}^{-1}$]	BAF AZ [$\text{L kg}_{\text{ww}}^{-1}$]	PRZ [$\text{nmol kg}_{\text{ww}}^{-1}$]
AZ_1	617	7	
AZ_2	777	8	
AZ_3	629	7	
AZ + PRZ-4h_1	1002	10	3814
AZ + PRZ-4h_2	935	10	3272
AZ + PRZ-4h_3	870	9	3658
AZ + PRZ-12h_1	784	8	3252
AZ + PRZ-12h_2	896	9	3702
AZ + PRZ-12h_3	1050	11	4730
AZ + PRZ-18h_1	967	10	3848
AZ + PRZ-18h_2	1156	12	4621
AZ + PRZ-18h_3	920	9	4248

Table S3-18: Binary mixtures with the substrates 7-Etc ($100 \mu\text{g L}^{-1}$) and TRM ($100 \mu\text{g L}^{-1}$), respectively, in combination with two different PRZ concentrations (38 and $375 \mu\text{g L}^{-1}$). Gammarids were pre-exposed for 4 h and 18 h to PRZ, respectively. In the control samples nominal concentrations of $100 \mu\text{g L}^{-1}$ 7-Etc, $100 \mu\text{g L}^{-1}$ TRM and $375 \mu\text{g L}^{-1}$ PRZ were used.

Exposure medium	7-Etc [$\mu\text{g L}^{-1}$]	7-Etc [nmol L^{-1}]	TRM [$\mu\text{g L}^{-1}$]	TRM [nmol L^{-1}]	PRZ [$\mu\text{g L}^{-1}$]
m_C+ L+_1 (t0 PRZ)					294
m_C+ L+ t0_1	108		107		299
m_C+ L+ t24_1	96		101		281
m_7-Etc t0_1	118	621			
m_7-Etc t24_1	102	535			
m_7-Etc + PRZ(38)-4h_1 (t0 PRZ)					42
m_7-Etc + PRZ(38)-4h t0_1	121	635			49
m_7-Etc + PRZ(38)-4h t24_1	103	543			40
m_7-Etc + PRZ(38)-18h_1 (t0 PRZ)					43
m_7-Etc + PRZ(38)-18h t0_1	111	582			46
m_7-Etc + PRZ(38)-18h t24_1	100	527			38
m_7-Etc + PRZ(375)-4h_1 (t0 PRZ)					427
m_7-Etc + PRZ(375)-4h t0_1	126	664			353
m_7-Etc + PRZ(375)-4h t24_1	113	595			276
m_7-Etc + PRZ(375)-18h_1 (t0 PRZ)					293
m_7-Etc + PRZ(375)-18h t0_1	115	606			299
m_7-Etc + PRZ(375)-18h t24_1	106	559			274
m_TRM t0_1			102	388	
m_TRM t24_1			95	361	
m_TRM + PRZ(38)-4h_1 (t0 PRZ)					37
m_TRM + PRZ(38)-4h t0_1			119	451	49
m_TRM + PRZ(38)-4h t24_1			102	387	48
m_TRM + PRZ(38)-18h_1 (t0 PRZ)					35
m_TRM + PRZ(38)-18h t0_1			106	404	45
m_TRM + PRZ(38)-18h t24_1			106	404	42

Exposure medium					
	7-Etc [$\mu\text{g L}^{-1}$]	7-Etc [nmol L^{-1}]	TRM [$\mu\text{g L}^{-1}$]	TRM [nmol L^{-1}]	PRZ [$\mu\text{g L}^{-1}$]
m_TRM + PRZ(375)-4h_1 (t0 PRZ)					306
m_TRM + PRZ(375)-4h t0_1			119	451	334
m_TRM + PRZ(375)-4h t24_1			107	408	287
m_TRM + PRZ(375)-18h_1 (t0 PRZ)					300
m_TRM + PRZ(375)-18h t0_1			125	476	315
m_TRM + PRZ(375)-18h t24_1			108	412	284
Whole body internal concentrations 24 h after substrate addition and corresponding BAFs					
	7-Etc [$\text{nmol kg}_{\text{ww}}^{-1}$]	BAF 7-Etc [$\text{L kg}_{\text{ww}}^{-1}$]	TRM [$\text{nmol kg}_{\text{ww}}^{-1}$]	BAF TRM [$\text{L kg}_{\text{ww}}^{-1}$]	PRZ [$\text{nmol kg}_{\text{ww}}^{-1}$]
7-Etc_1	3562	6			
7-Etc_2	3218	6			
7-Etc_3	3211	6			
7-Etc + PRZ(38)-4h_1	3787	6			4220
7-Etc + PRZ(38)-4h_2	3964	7			4188
7-Etc + PRZ(38)-4h_3	4285	7			4175
7-Etc + PRZ(38)-18h_1	4264	8			3672
7-Etc + PRZ(38)-18h_2	3697	7			3880
7-Etc + PRZ(38)-18h_3	4247	8			4514
7-Etc + PRZ(375)-4h_1	3028	5			28082
7-Etc + PRZ(375)-4h_2	3224	5			26469
7-Etc + PRZ(375)-4h_3	2862	5			26327
7-Etc + PRZ(375)-18h_1	2976	5			37862
7-Etc + PRZ(375)-18h_2	3720	6			33366
7-Etc + PRZ(375)-18h_3	3105	5			26504
TRM_1			770	2	
TRM_2			1268	3	
TRM_3			871	2	

Whole body internal concentrations 24 h after substrate addition and corresponding BAFs					
	7-Etc [nmol kg _{ww} ⁻¹]	BAF 7-Etc [L kg _{ww} ⁻¹]	TRM [nmol kg _{ww} ⁻¹]	BAF TRM [L kg _{ww} ⁻¹]	PRZ [nmol kg _{ww} ⁻¹]
TRM + PRZ(38)-4h_1			1460	3	3915
TRM + PRZ(38)-4h_2			1145	3	4965
TRM + PRZ(38)-4h_3			1409	3	4340
TRM + PRZ(38)-18h_1			1944	5	4842
TRM + PRZ(38)-18h_2			897	2	5252
TRM + PRZ(38)-18h_3			2234	6	5319
TRM + PRZ(375)-4h_1			762	2	38479
TRM + PRZ(375)-4h_2			1579	4	35141
TRM + PRZ(375)-4h_3			798	2	33419
TRM + PRZ(375)-18h_1			1177	3	39779
TRM + PRZ(375)-18h_2			594	1	32027
TRM + PRZ(375)-18h_3			1740	4	39457

Table S3-19: Toxicokinetic experiment: single exposure to 80 µg L⁻¹ AZ and mixture exposure to 80 µg L⁻¹ AZ and equimolar PRZ concentrations of 74 µg L⁻¹ (4 h pre-exposure to PRZ). In the control samples nominal concentrations of 80 µg L⁻¹ AZ and 100 µg L⁻¹ PRZ were used.

Exposure medium			
	AZ [µg L ⁻¹]	AZ [nmol L ⁻¹]	PRZ [µg L ⁻¹]
m_C+ L- t0_1	68		74
m_C+ L- t0_2	74		87
m_C+ L- t24_1	70		84
m_C+ L- t24_2	78		85
m_C+ L+ t0_1	96		92
m_C+ L+ t0_2	92		89
m_C+ L+ t24_1	63		80
m_C+ L+ t24_2	72		83
m_AZ t0_1	68	169	
m_AZ t0_2	62	154	
m_AZ t24_1	60	150	
m_AZ t24_2	67	166	
m_AZ + PRZ t0_1	65	161	59
m_AZ + PRZ t0_2	64	159	53
m_AZ + PRZ t24_1	67	165	56
m_AZ + PRZ t24_2	68	168	56

Whole body internal concentrations 24 h after substrate addition and corresponding BAFs			
	AZ [nmol kg _{ww} ⁻¹]	BAF AZ [L kg _{ww} ⁻¹]	PRZ [nmol kg _{ww} ⁻¹]
AZ_1	791	5	
AZ_2	748	5	
AZ + PRZ_1	1293	8	4876
AZ + PRZ_2	1388	8	4886

Table S3-20: Half maximal inhibitory concentration of PRZ using AZ as a substrate ($IC_{50, PRZ, AZ}$). Exposure to $40 \mu\text{g L}^{-1}$ AZ and varying PRZ concentrations of $c1 = 0.19 \mu\text{g L}^{-1}$, $c2 = 0.37 \mu\text{g L}^{-1}$, $c3 = 0.74 \mu\text{g L}^{-1}$, $c4 = 3.7 \mu\text{g L}^{-1}$, $c5 = 7.4 \mu\text{g L}^{-1}$, $c6 = 22 \mu\text{g L}^{-1}$, $c7 = 37 \mu\text{g L}^{-1}$, $c8 = 74 \mu\text{g L}^{-1}$ and $c9 = 372 \mu\text{g L}^{-1}$ (18 h pre-exposure to PRZ).

Exposure medium	AZ [$\mu\text{g L}^{-1}$]	AZ [nmol L^{-1}]	PRZ [$\mu\text{g L}^{-1}$]
m_AZ + PRZ c1_1 (t0 PRZ)			n.q.
m_AZ + PRZ c2_1 (t0 PRZ)			n.q.
m_AZ + PRZ c3_1 (t0 PRZ)			n.q.
m_AZ + PRZ c4_1 (t0 PRZ)			3
m_AZ + PRZ c5_1 (t0 PRZ)			6
m_AZ + PRZ c6_1 (t0 PRZ)			18
m_AZ + PRZ c7_1 (t0 PRZ)			29
m_AZ + PRZ c8_1 (t0 PRZ)			65
m_AZ + PRZ c9_1 (t0 PRZ)			321
m_AZ t0_1	34	85	
m_AZ + PRZ c1 t0_1	36	89	n.q.
m_AZ + PRZ c2 t0_1	35	86	n.q.
m_AZ + PRZ c3 t0_1	34	86	n.q.
m_AZ + PRZ c4 t0_1	34	84	2
m_AZ + PRZ c5 t0_1	35	86	4
m_AZ + PRZ c6 t0_1	34	85	14
m_AZ + PRZ c7 t0_1	34	85	24
m_AZ + PRZ c8 t0_1	34	85	53
m_AZ + PRZ c9 t0_1	40	100	317
m_AZ t24_1	32	78	
m_AZ + PRZ c1 t24_1	33	81	n.q.
m_AZ + PRZ c2 t24_1	32	80	n.q.
m_AZ + PRZ c3 t24_1	33	83	n.q.
m_AZ + PRZ c4 t24_1	31	77	2
m_AZ + PRZ c5 t24_1	32	80	4

Exposure medium			
	AZ [$\mu\text{g L}^{-1}$]	AZ [nmol L^{-1}]	PRZ [$\mu\text{g L}^{-1}$]
m_AZ + PRZ c6 t24_1	34	85	13
m_AZ + PRZ c7 t24_1	33	83	22
m_AZ + PRZ c8 t24_1	35	86	49
m_AZ + PRZ c9 t24_1	39	96	262
Whole body internal concentrations 24 h after substrate addition and corresponding BAFs			
	AZ [$\text{nmol kg}_{\text{ww}}^{-1}$]	BAF AZ [$\text{L kg}_{\text{ww}}^{-1}$]	PRZ [$\text{nmol kg}_{\text{ww}}^{-1}$]
AZ_1	990	12	
AZ_2	840	10	
AZ_3	613	8	
AZ + PRZ c1_1	705	8	18
AZ + PRZ c1_2	671	8	20
AZ + PRZ c2_1	689	8	39
AZ + PRZ c2_2	708	9	35
AZ + PRZ c3_1	686	8	102
AZ + PRZ c3_2	915	11	104
AZ + PRZ c4_1	643	8	250
AZ + PRZ c4_2	912	11	446
AZ + PRZ c5_1	985	12	786
AZ + PRZ c5_2	983	12	773
AZ + PRZ c6_1	1100	13	2101
AZ + PRZ c6_2	1103	13	2082
AZ + PRZ c7_1	1385	17	4361
AZ + PRZ c7_2	1346	16	4411
AZ + PRZ c8_1	1267	15	6535
AZ + PRZ c8_2	1371	16	7639
AZ + PRZ c9_1	1089	11	38606
AZ + PRZ c9_2	1079	11	48859

Table S3-21: Half maximal inhibitory concentration of PRZ based on ECOD activity ($IC_{50, PRZ, ECOD}$) using different pre-exposure times to PRZ (4 and 18 h). 0.02, 0.1, 0.2, 1, 2 and 10 μ M PRZ refer to 8, 38, 75, 375, 750 and 3750 μ g L⁻¹ PRZ.

Exposure medium	PRZ [μ g L ⁻¹]
m_PRZ_01uM t0	34
m_PRZ_01uM t18	16
m_PRZ_1uM t0	272
m_PRZ_1uM t18	165
m_PRZ_002uM t0	7
m_PRZ_002uM t18	4
m_PRZ_02uM t0	60
m_PRZ_02uM t18	34
m_PRZ_2uM t0	762
m_PRZ_2uM t18	835
m_PRZ_10uM t0	4943
m_PRZ_10uM t18	3891
m_PRZ_01uM t0	26
m_PRZ_01uM t4	24
m_PRZ_1uM t0	254
m_PRZ_1uM t4	231
m_PRZ_002uM t0	5
m_PRZ_002uM t4	5
m_PRZ_02uM t0	52
m_PRZ_02uM t4	42
m_PRZ_2uM t0	494
m_PRZ_2uM t4	409
m_PRZ_10uM t0	3260
m_PRZ_10uM t4	3541

Table S3-22: Median-lethal concentrations of AZ (LC₅₀s) in the presence and absence of PRZ. For LC₅₀ determination in the presence of PRZ gammarids were pre-exposed for 18 h to 74 µg L⁻¹ and 0.37 µg L⁻¹ PRZ, respectively. In the control samples 50 µg L⁻¹ AZ and 74 µg L⁻¹ PRZ were used. For the treatment samples always the lowest and the highest AZ concentrations were sampled (50 µg L⁻¹ and 350 µg L⁻¹ for the single exposure to AZ and the co-exposure to 0.37 µg L⁻¹ PRZ, 5 µg L⁻¹ and 65 µg L⁻¹ AZ for the co-exposure to 74 µg L⁻¹ PRZ).

Exposure medium	AZ [µg L ⁻¹]	PRZ [µg L ⁻¹]
m_C+ L- _1 (t0 PRZ)		10 ^{*)}
m_C+ L- _2 (t0 PRZ)		28 ^{*)}
m_C+ L- t0_1	50	69
m_C+ L- t0_2	45	69
m_C+ L- t24_1	49	74
m_C+ L- t24_2	50	70
m_C+ L+ _1 (t0 PRZ)		256 ^{*)}
m_C+ L+ _2 (t0 PRZ)		558 ^{*)}
m_C+ L+ t0_1	49	94
m_C+ L+ t0_2	48	78
m_C+ L+ t24_1	58	81
m_C+ L+ t24_2	46	72
m_AZ_50 t0_1	39	
m_AZ_50 t0_2	37	
m_AZ_50 t24_1	40	
m_AZ_50 t24_2	40	
m_AZ_350 t0_1	416 ^{*)}	
m_AZ_350 t0_2	519 ^{*)}	
m_AZ_350 t24_1	267	
m_AZ_350 t24_2	266	
m_AZ 50 + PRZ(0.37)_1 (t0 PRZ)		n. q.
m_AZ 50 + PRZ(0.37)_2 (t0 PRZ)		n. q.
m_AZ 50 + PRZ(0.37) t0_1	34	n. q.
m_AZ 50 + PRZ(0.37) t0_2	46	n. q.

Exposure medium	AZ [$\mu\text{g L}^{-1}$]	PRZ [$\mu\text{g L}^{-1}$]
m_AZ 50 + PRZ(0.37) t24_1	38	n. q.
m_AZ 50 + PRZ(0.37) t24_2	41	n. q.
m_AZ 350 + PRZ(0.37)_1 (t0 PRZ)		n. q.
m_AZ 350 + PRZ(0.37)_2 (t0 PRZ)		n. q.
m_AZ 350 + PRZ(0.37) t0_1	320	n. q.
m_AZ 350 + PRZ(0.37) t0_2	n. d.	n. q.
m_AZ 350 + PRZ(0.37) t24_1	264	n. q.
m_AZ 350 + PRZ(0.37) t24_2	276	n. q.
m_AZ 5 + PRZ(74)_1 (t0 PRZ)		91
m_AZ 5 + PRZ(74)_2 (t0 PRZ)		76
m_AZ 5 + PRZ(74) t0_1	20 ^{*)}	67
m_AZ 5 + PRZ(74) t0_2	14 ^{*)}	68
m_AZ 5 + PRZ(74) t24_1	5	66
m_AZ 5 + PRZ(74) t24_2	4	65
m_AZ 65 + PRZ(74)_1 (t0 PRZ)		74
m_AZ 65 + PRZ(74)_2 (t0 PRZ)		67
m_AZ 65 + PRZ(74) t0_1	83 ^{*)}	68
m_AZ 65 + PRZ(74) t0_2	99 ^{*)}	59
m_AZ 65 + PRZ(74) t24_1	61	62
m_AZ 65 + PRZ(74) t24_2	59	45

*) Exposure medium was most likely sampled before complete mixing of spiked analyte and artificial pond water was achieved.

n. q.: not quantifiable. PRZ amount too little in sampled volume of exposure medium.

n. d.: not detected.

Table S3-23: Video-tracking of the locomotory behavior of gammarids in the presence of different PRZ concentrations. 0.02, 0.1, 0.2, 1 and 2 μM PRZ refer to 8, 38, 75, 375 and 750 $\mu\text{g L}^{-1}$ PRZ.

Exposure medium	PRZ [$\mu\text{g L}^{-1}$]
m_PRZ_002uM_t0_1	7
m_PRZ_002uM_t0_2	6
m_PRZ_002uM_t24_1	8
m_PRZ_01uM_t0_1	33
m_PRZ_01uM_t0_2	33
m_PRZ_01uM_t24_1	36
m_PRZ_01uM_t24_2	38
m_PRZ_02uM_t0_1	61
m_PRZ_02uM_t0_2	66
m_PRZ_02uM_t24_1	74
m_PRZ_02uM_t24_2	82
m_PRZ_1uM_t0_1	320
m_PRZ_1uM_t0_2	329
m_PRZ_1uM_t24_1	423
m_PRZ_1uM_t24_2	455
m_PRZ_2uM_t0_1	682
m_PRZ_2uM_t0_2	628
m_PRZ_2uM_t24_1	758
m_PRZ_2uM_t24_2	804

SI.J Internal Concentration Measurements of Binary Mixtures

The Substrate Azoxystrobin

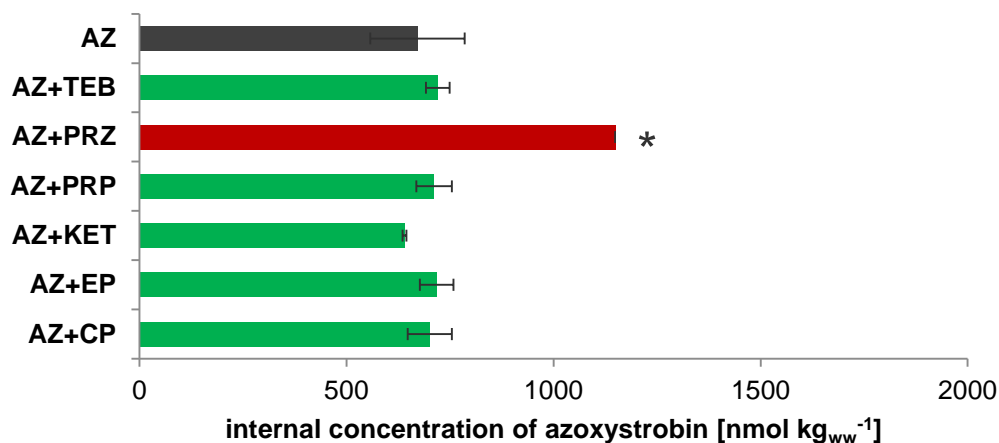


Figure S3-4: Whole body internal concentration of azoxystrobin after 24 h exposure to 40 µg L⁻¹ azoxystrobin. Shown are the single exposure to azoxystrobin (AZ) in black (sample replicates n=2) and the mixture exposure to azoxystrobin and equimolar concentrations of one of the selected azole fungicides (n=2) (CP: cyproconazole, EP: epoxiconazole, KET: ketoconazole, PRP: propiconazole and TEB: tebuconazole) with the respective standard deviation of the internal azoxystrobin concentration. Internal azoxystrobin concentrations of each mixture were compared to those of the controls (single exposure to azoxystrobin) with a t-test (two tailed distribution, two-sample equal variance). Mixtures displayed in green showed no statistical difference from the control, whereas the mixture composed of prochloraz and azoxystrobin displayed in red was significantly different from the control ($p < 0.05$) and is marked with an asterisk.

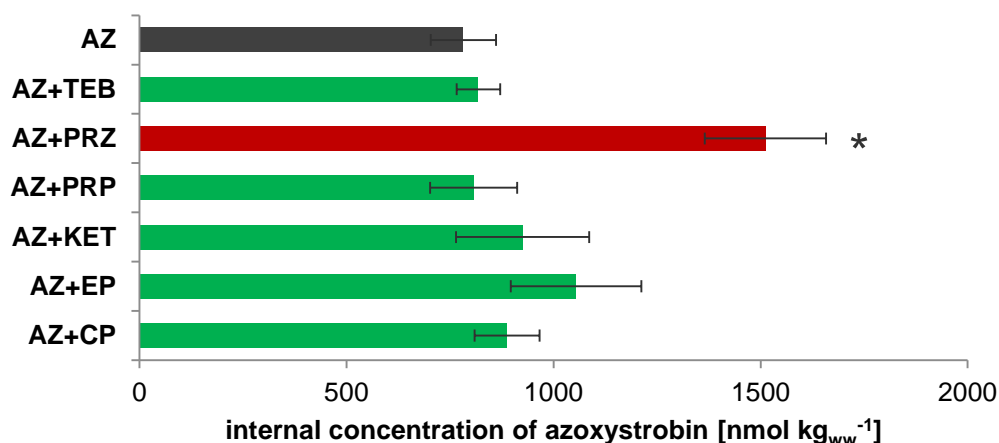


Figure S3-5: Whole body internal concentration of azoxystrobin after 24 h exposure to 80 µg L⁻¹ azoxystrobin. Shown are the single exposure to azoxystrobin (AZ) in black (sample replicates n=2) and the mixture exposure to azoxystrobin and equimolar concentrations of one of the selected azole fungicides (n=2) (CP: cyproconazole, EP: epoxiconazole, KET: ketoconazole, PRP: propiconazole and TEB: tebuconazole) with the respective standard deviation of the internal azoxystrobin concentration. Internal azoxystrobin concentrations of each mixture were compared to those of the controls (single exposure to azoxystrobin) with a t-test (two tailed distribution, two-sample equal variance). Mixtures displayed in green showed no statistical difference from the control, whereas the mixture composed of prochloraz and azoxystrobin displayed in red was significantly different from the control ($p < 0.05$) and is marked with an asterisk.

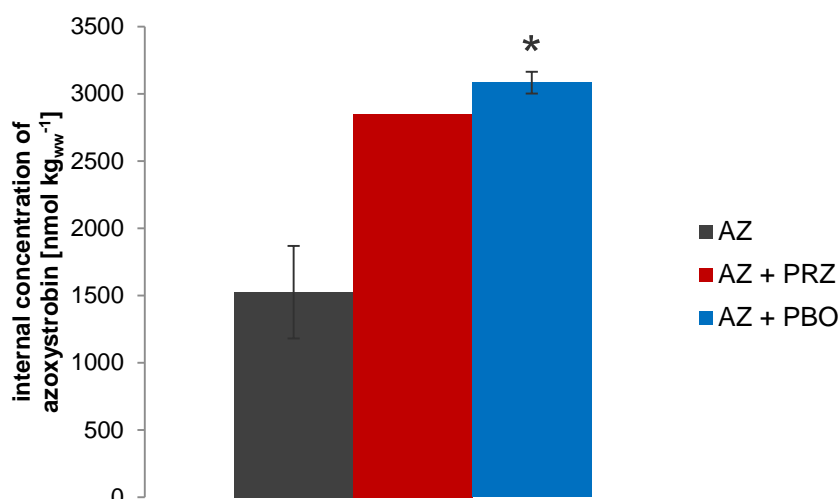


Figure S3-6: Whole body internal concentration of azoxystrobin (AZ) after 24 h exposure to $200 \mu\text{g L}^{-1}$ azoxystrobin: 4 h pre-exposure without chemical in black, 4 h pre-exposure to $186 \mu\text{g L}^{-1}$ prochloraz (PRZ) in red, and 4 h pre-exposure to piperonyl butoxide (PBO) in blue. Duplicates were prepared for each treatment and treatments are displayed with the respective standard deviation of the internal azoxystrobin concentration. However, for one of the AZ-PRZ mixtures, the internal standard was spiked wrongly why the sample was excluded. Internal azoxystrobin concentrations of the mixtures containing PBO were compared to those of the controls (single exposure to azoxystrobin) with a t-test (two tailed distribution, two-sample equal variance) and were significantly different from the control ($p < 0.05$) which is displayed with an asterisk.

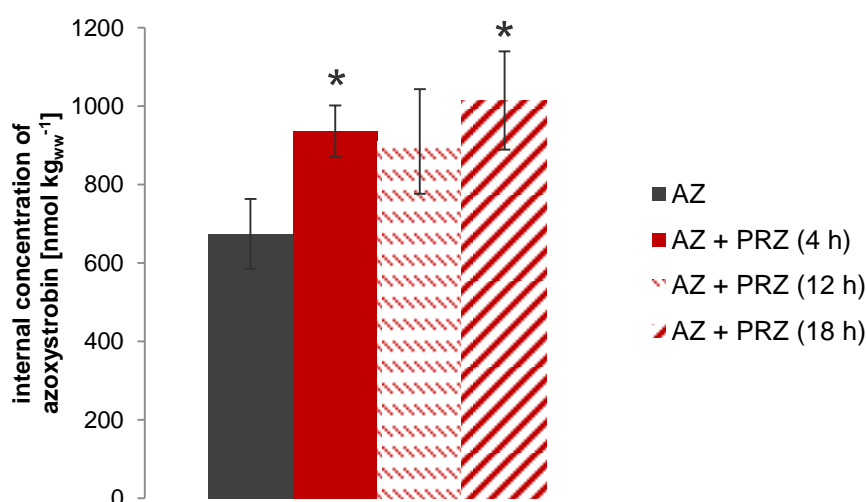


Figure S3-7: Whole body internal concentration of azoxystrobin (AZ) after 24 h exposure to $40 \mu\text{g L}^{-1}$ azoxystrobin: 4 h pre-exposure without chemical in black and pre-exposure to $37 \mu\text{g L}^{-1}$ prochloraz (PRZ) in red (4, 12 and 18 h pre-exposure). Triplicates were prepared for each treatment and treatments are displayed with the respective standard deviation of the internal azoxystrobin concentration. Internal azoxystrobin concentrations of each mixture were compared to those of the controls (single exposure to azoxystrobin) with a t-test (two tailed distribution, two-sample equal variance). Asterisks mark treatment samples that are significantly different from the control ($p < 0.05$).

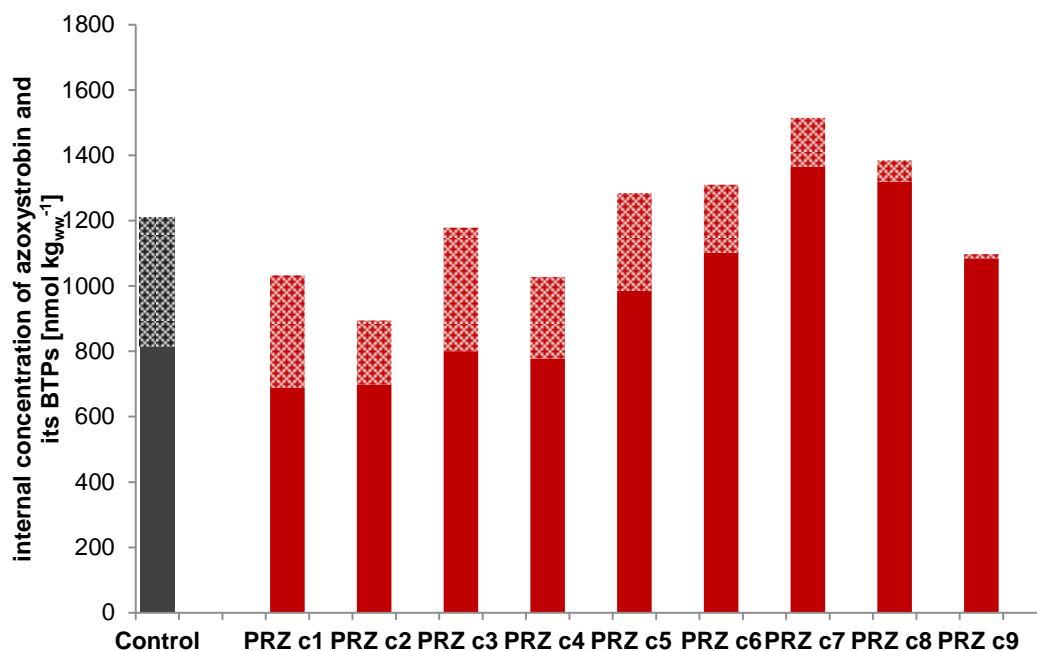


Figure S3-8: Whole body internal concentration of azoxystrobin and its BTPs after 24 h exposure to $40 \mu\text{g L}^{-1}$ azoxystrobin: 18 h pre-exposure without chemical in black (sample replicates $n=3$) and 18 h pre-exposure to varying prochloraz (PRZ) concentrations ($n=2$) (c1: 0.19, c2: 0.37, c3: 0.74, c4: 3.7, c5: 7.4, c6: 22, c7: 37, c8: 74 and c9: $372 \mu\text{g L}^{-1}$) in red. The filled areas mark the parent compound azoxystrobin, whereas the hatched areas mark the sum of all detected BTPs.

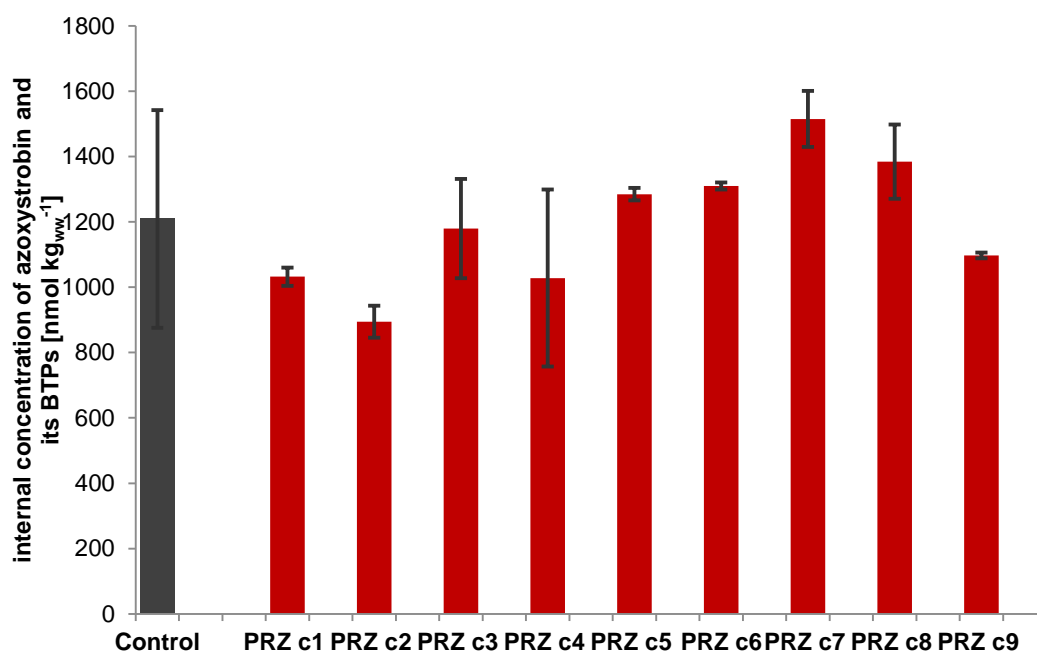


Figure S3-9: Whole body internal concentration of azoxystrobin and its BTPs after 24 h exposure to $40 \mu\text{g L}^{-1}$ azoxystrobin: 18 h pre-exposure without chemical in black and 18 h pre-exposure to varying prochloraz (PRZ) concentrations (c1: 0.19, c2: 0.37, c3: 0.74, c4: 3.7, c5: 7.4, c6: 22, c7: 37, c8: 74 and c9: $372 \mu\text{g L}^{-1}$) in red. Controls (single exposure to azoxystrobin) (sample replicates $n=3$) and treatments ($n=2$) are displayed with the standard deviation of the total internal concentration (azoxystrobin and the sum of all BTPs). Total internal concentrations in each mixture were compared to those of the controls (single exposure to azoxystrobin) with a t-test (two tailed distribution, two-sample equal variance) and showed no statistical difference ($p > 0.05$) and only an increasing trend in total internal concentrations was observed.

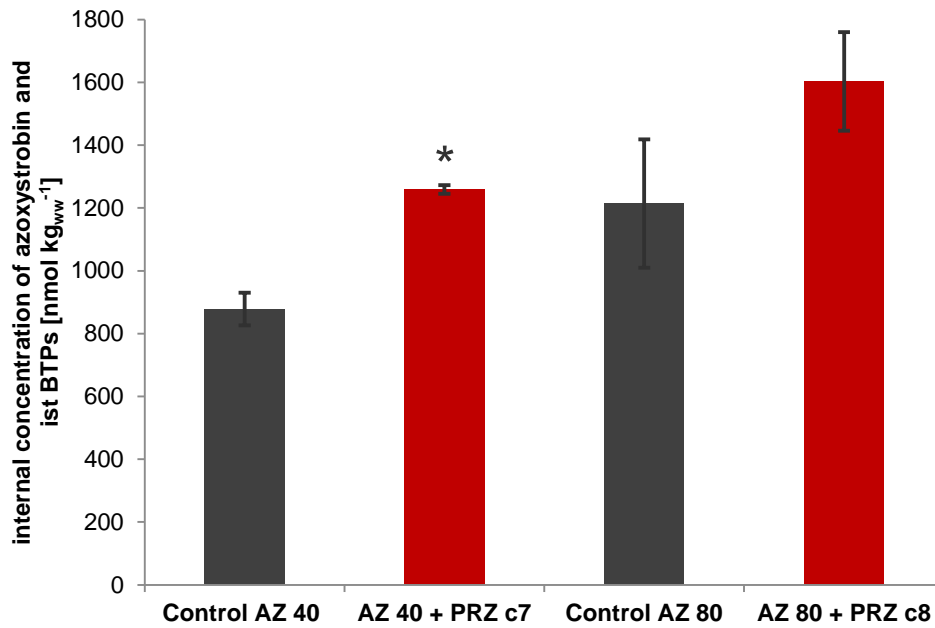


Figure S3-10: Whole body internal concentration of azoxystrobin and its BTPs after 24 h exposure to 40 and 80 $\mu\text{g L}^{-1}$ azoxystrobin, respectively: 4 h pre-exposure without chemical in black (sample replicates $n=2$) and 4 h pre-exposure to equimolar prochloraz (PRZ) concentrations (c7: 37 $\mu\text{g L}^{-1}$ and c8: 74 $\mu\text{g L}^{-1}$) ($n=2$) in red. Standard deviations are shown for the total internal concentrations (azoxystrobin and the sum of all BTPs). Total internal concentrations in each mixture were compared to those of the corresponding controls (single exposure to azoxystrobin) with a t -test (two tailed distribution, two-sample equal variance). Asterisks mark treatment samples that are significantly different from the corresponding control ($p < 0.05$).

The Substrate 7-Ethoxycoumarin

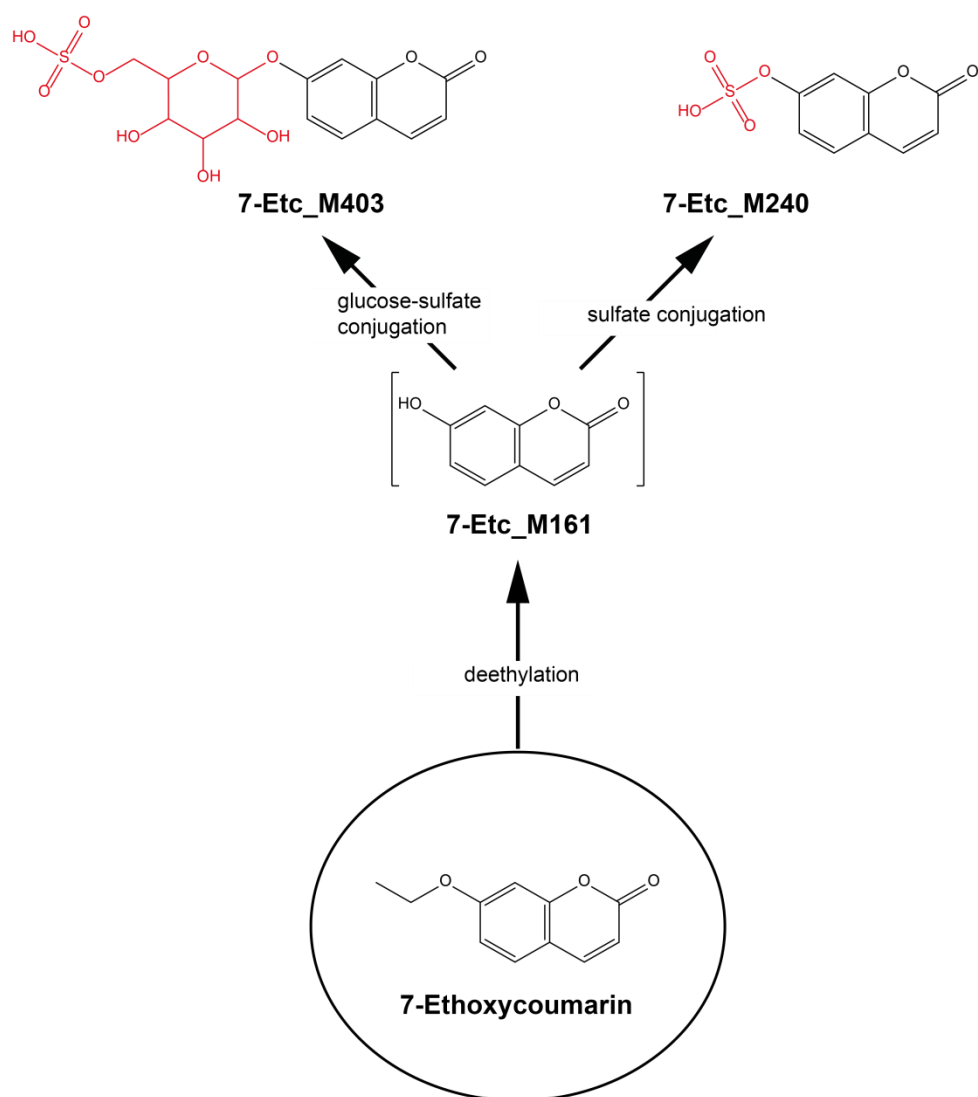


Figure S3-11: Proposed biotransformation pathway of 7-ethoxycoumarin in *G. pulex*. The BTP 7-Etc_M161 was not detected but is required as precursor for the two identified conjugation products 7-Etc_M240 and 7-Etc_M403.

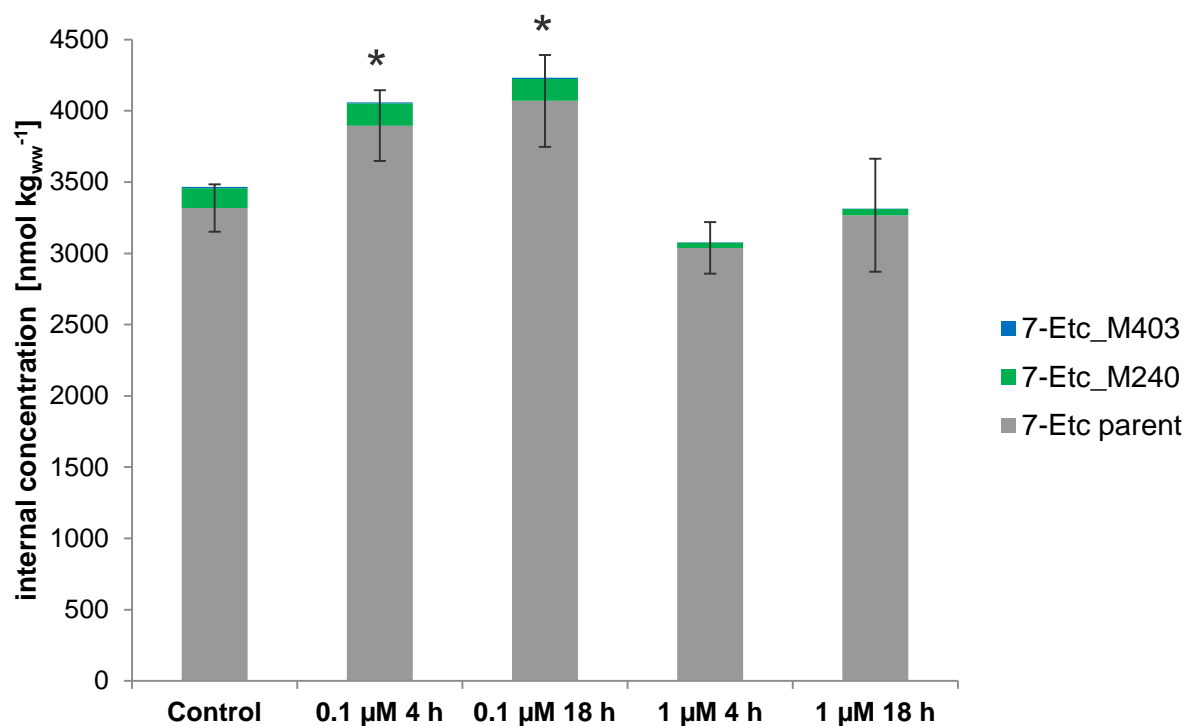


Figure S3-12: Whole body internal concentration of 7-ethoxycoumarin (7-Etc) and associated BTPs after 24 h exposure to 7-ethoxycoumarin ($100 \mu\text{g L}^{-1}$) in the presence and absence of prochloraz (0.1 and $1 \mu\text{M}$) with 4 and 18 h pre-exposure, respectively. Triplicates were prepared for each treatment and treatments are displayed with the respective standard deviation of the internal 7-ethoxycoumarin concentration. Internal 7-ethoxycoumarin concentrations and total internal concentrations (7-ethoxycoumarin and the sum of all BTPs) of each mixture were compared to those of the controls (pre-exposure without chemical and subsequent addition of 7-ethoxycoumarin) with a t-test (two tailed distribution, two-sample equal variance). 0.1 μM treatment samples were different from the control ($p < 0.05$) for internal 7-ethoxycoumarin concentrations as well as for total internal concentrations and are marked with an asterisk.

The Substrate Tramadol

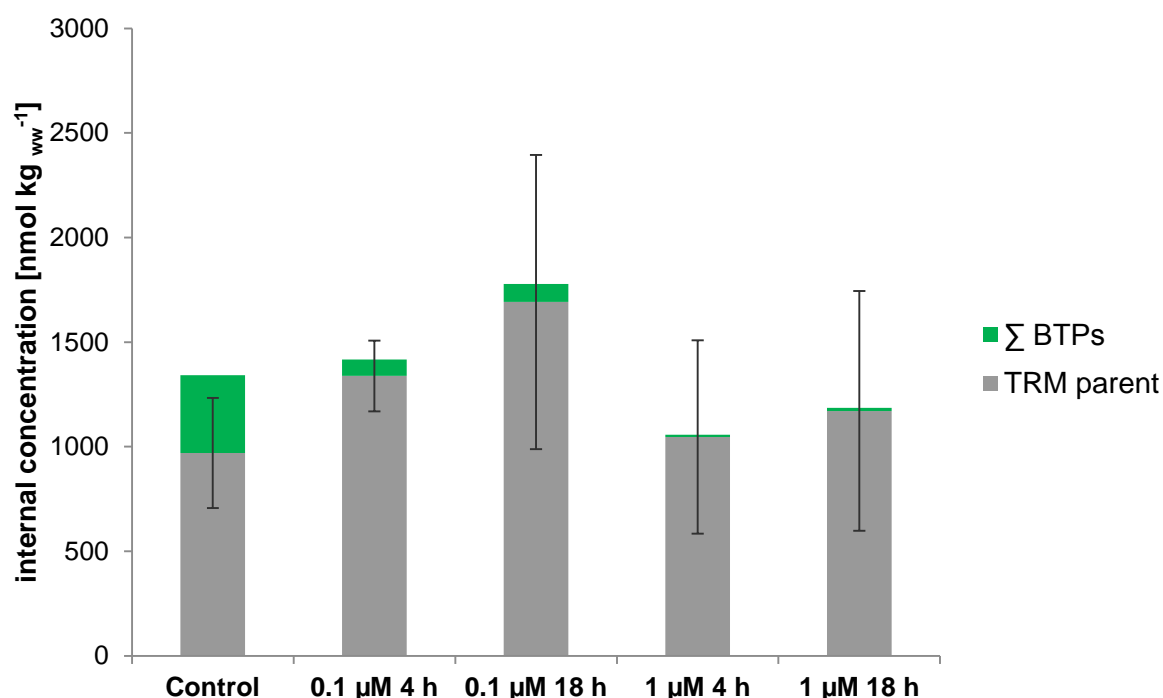


Figure S3-13: Whole body internal concentration of tramadol (TRM) and associated BTPs after 24 h exposure to tramadol ($100 \mu\text{g L}^{-1}$) in the presence and absence of prochloraz (0.1 and $1 \mu\text{M}$) with 4 and 18 h pre-exposure, respectively. Triplicates were prepared for each treatment and treatments are displayed with the respective standard deviation of the internal tramadol concentrations. Internal tramadol concentrations and total internal concentrations (tramadol and the sum of all BTPs) of each mixture were compared to those of the controls (pre-exposure without chemical and subsequent addition of tramadol) with a t-test (two tailed distribution, two-sample equal variance) but did not show significant difference from the control ($p > 0.05$) and only an increasing trend in total internal concentrations was observed.

SI.K Toxicity Prediction based on Concentration Addition (CA)

same site of action and similar mode of action:

$$\frac{d_1}{EC_{x,1}} + \frac{d_2}{EC_{x,2}} = 1 \rightarrow CA \quad \text{Equation S3-12}$$

d_1 and d_2 : concentration of chemical 1 and 2 in a mixture

$EC_{x,1}$ and $EC_{x,2}$: effect concentration of chemical 1 and 2 when tested separately

Binary mixture of azoxystrobin and prochloraz in the kinetic experiment:

d_1 : $80 \mu\text{g L}^{-1}$ azoxystrobin (AZ)

d_2 : $74 \mu\text{g L}^{-1}$ prochloraz (PRZ)

LC_{50} (AZ, 96 h)⁴: $270 \mu\text{g L}^{-1}$

LC_{50} (PRZ, 96 h)⁴: $2200 \mu\text{g L}^{-1}$

$$\frac{d_1}{LC_{50,1}} + \frac{d_2}{LC_{50,2}} = \frac{80}{270} + \frac{74}{2200} = 0.33 < 1 \rightarrow \text{synergism}$$

SI.L Dose-Response Fitting

All functions used for the fitting of dose-response curves are available in the R⁵ package “drc” from Ritz and Streibig (2005)⁶ and are described by the following equations:

Log-logistic four-parameter model (LL.4):

$$f(x) = c + \frac{d - c}{1 + \exp(b(\log(x) - \log(e)))}$$

Equation S 3-13

Log-logistic two-parameter model (LL.2):

$$f(x) = \frac{1}{1 + \exp(b(\log(x) - \log(e)))}$$

Equation S 3-14

Brain-Cousens⁷ four-parameter hormesis model with lower limit $c = 0$ (BC.4):

$$f(x) = \frac{d + fx}{1 + \exp(b(\log(x) - \log(e)))}$$

Equation S 3-15

where d and c are the upper and lower limits of response, respectively, and b denotes the relative slope in the inflection point for symmetric dose-response curves (the two- and four-parameter log-logistic model), whereas for non-symmetric dose-response curves b has no direct interpretation. For symmetric dose-response curves, e is the inflection point and thereby the EC_{50} , whereas for non-symmetric dose-response curves, such as the Brain-Cousens model, it marks the inflection point of the decreasing part. x is the azole concentration and f the potential size of the hormesis effect.

SI.M Half Maximal Inhibitory Concentrations based on *in vivo* ECOD Activity ($IC_{50, ECODS}$)

For $IC_{50, ECOD}$ determination based on ECOD (7-ethoxycoumarin-O-dealkylation) *in vivo* activity the measured fluorescence over time (one sample every hour during an incubation period of 6 h) was corrected for background fluorescence by subtracting the average fluorescence that was measured in the blank samples (0.02 mM 7-ethoxycoumarin in artificial pond water without organisms). Additionally, the measured fluorescence was corrected for the differing gammarid biomass by referencing the fluorescence to the organism wet weight per sample. For each tested azole concentration a linear curve was fitted to the corrected fluorescence values over time and thereby the slope was determined. The slopes of the treatment samples were compared to the slopes of the control samples and $IC_{50, ECODS}$ were determined by applying a Brain-Cousens⁷ four parameter hormesis model (equation S3-15, SI L) which is a modification of the three-parameter log-logistic model accounting for hormesis available in the R⁵ package “drc”⁶.

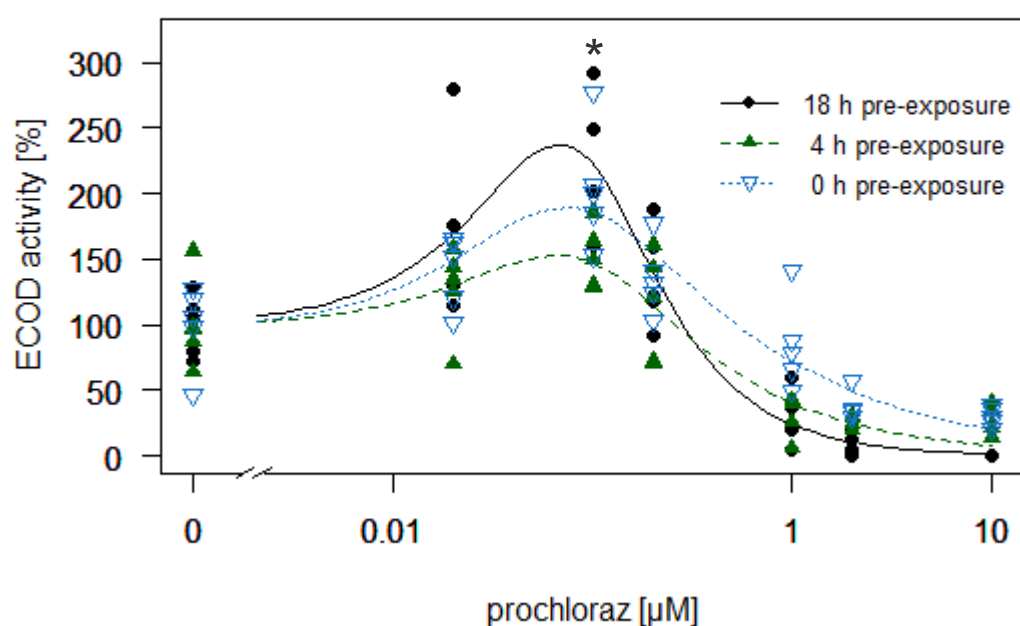


Figure S3-14: Dose-response curves for the IC_{50} determination of prochloraz based on ECOD activity with 0 h, 4 h and 18 h pre-exposure to prochloraz. Fluorescence was measured hourly during an incubation time of 6 h. ECOD activities of the different prochloraz treatments (0.02 μ M, 0.1 μ M and 0.2 μ M for the different pre-exposure scenarios, replicates per treatment: $n=5$) were compared to those of the controls (pre-exposure without chemical) with a t-test (two tailed distribution, two-sample equal variance). Asterisks mark treatment samples that are significantly different from the control ($p < 0.05$).

Table S3-24: Estimated parameters (b: no direct interpretation; d: upper limit of response; e: inflection point of the decreasing part; f: size of the hormesis effect) and determined $EC_{50,ECOD}$ s with the Brain-Cousens model. Parameters are reported with the corresponding standard errors.

	b	d	e	f	$EC_{50,ECOD}$ [μ M]	$EC_{50,ECOD}$ [μ g L ⁻¹]
18 h pre-exposure	2.14 ± 0.25	98.7 ± 15.5	0.093 ± 0.020	3828 ± 1232	0.54 ± 0.16	201 ± 61.4
4 h pre-exposure	1.69 ± 0.15	98.4 ± 11.5	0.097 ± 0.035	2026 ± 1018	0.76 ± 0.24	283 ± 90.1
0 h pre-exposure	1.54 ± 0.09	95.7 ± 13.3	0.078 ± 0.022	3626 ± 1248	2.09 ± 0.88	789 ± 335

SI.N Inhibitory Concentrations based on Internal Concentration Measurements ($IC_{50/10, PRZ, AZ}$)

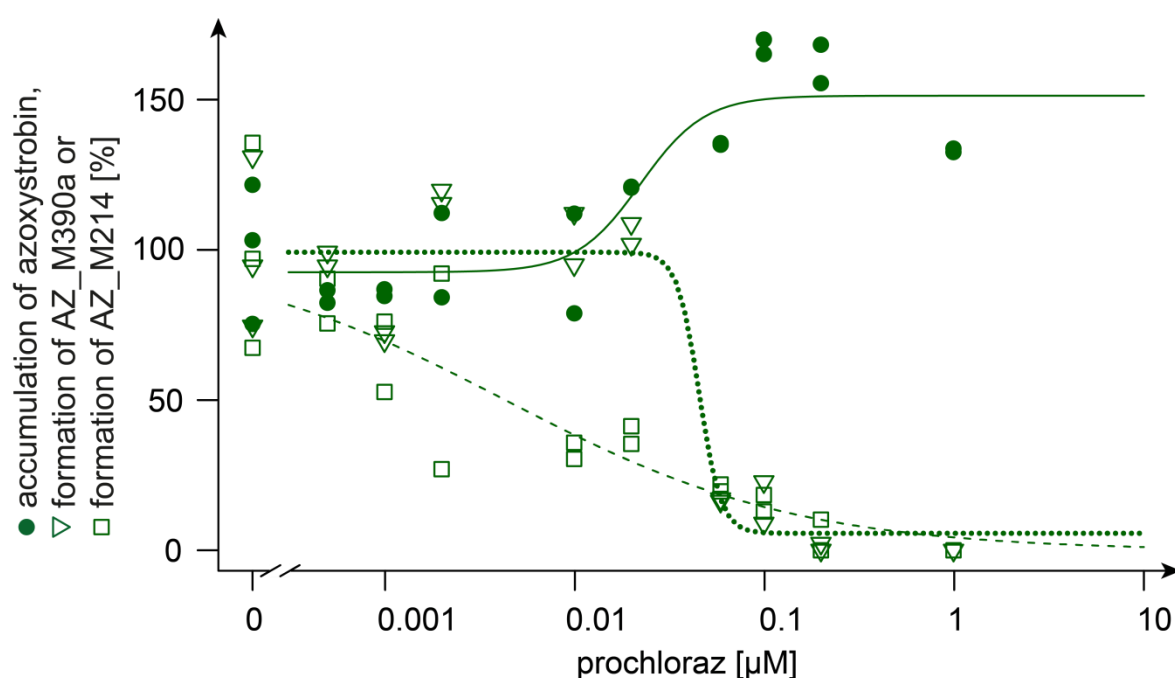


Figure S3-15: Dose-response curves for the $IC_{50/10, PRZ, AZ}$ determination based on whole body internal concentration measurements of azoxystrobin and its BTPs (shown are the two primary BTPs AZ_M390a and AZ_M214). Internal concentrations of azoxystrobin and its BTPs were measured after 24 h exposure to $40 \mu\text{g L}^{-1}$ azoxystrobin. Controls were pre-exposed without chemical for 18 h, whereas treatments were pre-exposed for 18 h to varying prochloraz concentrations (c1: 0.19, c2: 0.37, c3: 0.74, c4: 3.7, c5: 7.4, c6: 22, c7: 37, c8: 74 and c9: $372 \mu\text{g L}^{-1}$). For AZ_M214 no sigmoidal dose-response curve could be fitted.

Table S3-25: Estimated parameters (d: upper limit of response; c: lower limit of response; b: relative slope in the inflection point; e: inflection point and thereby the $IC_{50, PRZ, AZ}$) and determined $IC_{50/10, PRZ, AZ}$ s for azoxystrobin and primary BTPs with the four-parameter log-logistic model. Parameters and $IC_{50/10, PRZ, AZ}$ s are reported with the corresponding standard errors. For AZ_M214 no sigmoidal dose response curve could be fitted (see Figure S15 above). Therefore, $IC_{50/10, AZ, PRZ}$ s based on the dose response curve of AZ_M214 have to be treated with care.

	b	c	d	e, $IC_{50, PRZ, AZ}$ [μM]	e, $IC_{50, PRZ, AZ}$ [$\mu g L^{-1}$]	$IC_{10, PRZ, AZ}$ [μM]	$IC_{10, PRZ, AZ}$ [$\mu g L^{-1}$]
Azoxystrobin	-2.58 ± 1.70	92.5 ± 5.23	151 ± 7.04	0.0222 ± 0.00816	8.32 ± 3.06	0.009 ± 0.005	3.5 ± 1.8
AZ_M390b	7.58 ± 14.7	5.64 ± 6.97	99.2 ± 4.58	0.0452 ± 0.0213	16.9 ± 7.16	0.03 ± 0.03	12.5 ± 11.6
AZ_M214	0.564 ± 0.219	-0.155 ± 15.7	100 ± 10.1	0.00429 ± 0.00404	1.61 ± 1.52	0.0001 ± 0.0001	0.03 ± 0.05

SI.O Lethal Concentrations of Azoxystrobin (LC_{50} s) in the Presence and Absence of Prochloraz

Table S3-26: Used azoxystrobin concentration [$\mu g L^{-1}$] for the determination of LC_{50} s of azoxystrobin in the presence and absence of prochloraz based on a range defining test.

AZ	50, 100, 150, 200, 250, 300, 350
AZ + 0.37 $\mu g L^{-1}$ PRZ	50, 100, 150, 200, 250, 300, 350
AZ + 74 $\mu g L^{-1}$ PRZ	5, 15, 25, 35, 45, 55, 65

SI.P Data Evaluation of the Video-Tracking of Gammarids

Statistica 9.0 was used for data analysis. Distance moved was analyzed with a general linear model (GLM). If GLM analysis showed significant differences, a Dunnett post hoc test was applied. Treatments (five concentrations + control) and time (per hour) were tested as fixed factors, and replicate ($n=3$) and subject (gammarid; $n=3$ per replicate and per treatment) as random ones. Interactions between treatment and time were also investigated. Treatments that contained exoskeletons due to molting of gammarids were not included in data analysis because video-tracking was affected ($n=3$: 1 from treatment $0.02 \mu\text{M}$, 1 from treatment $0.2 \mu\text{M}$, and 1 from treatment $2 \mu\text{M}$).

For data analysis the average distance moved during different time windows (15 min and 1 h) was tested and both time windows showed the same pattern.

After 4 hours exposure, no time or treatment effect was observed.

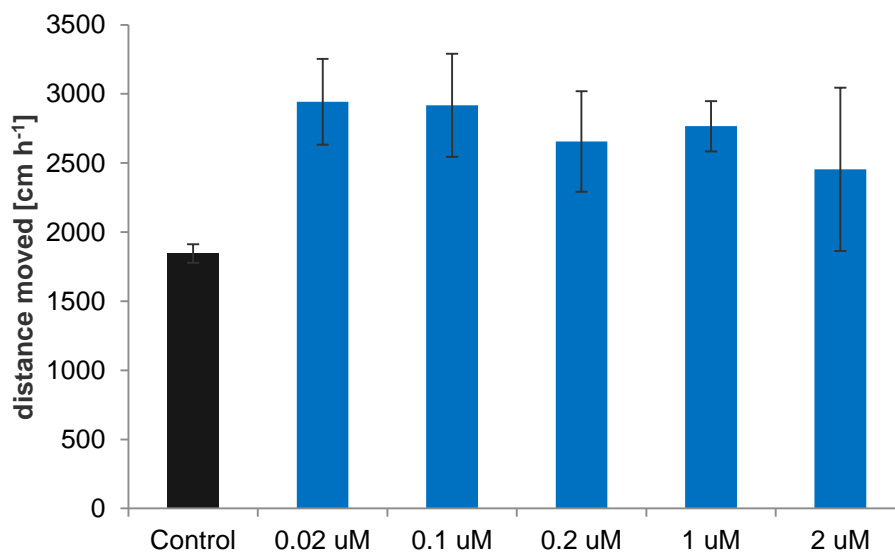


Figure S3-16: Distance moved in cm h^{-1} during 0 to 4 h exposure to different prochloraz concentrations ($n=9$ for control, 0.1 and $1 \mu\text{M}$ and $n=8$ for 0.02, 0.2 and $2 \mu\text{M}$).

After 9 hours exposure, time ($F = 6.52$; $p < 0.001$) and treatment ($F = 5.28$; $p < 0.001$) effects were observed but no interaction effects. Dunnett post hoc test showed that the effect of time started to be different after 4 hours (4 h: $p = 0.04$; 5 h: $p = 0.005$; 6 h: $p = 0.001$; 7 and 8 h: $p < 0.001$) and that the 0.1 μM ($p < 0.001$) and 1 μM ($p = 0.009$) treatments were significantly different from the control.

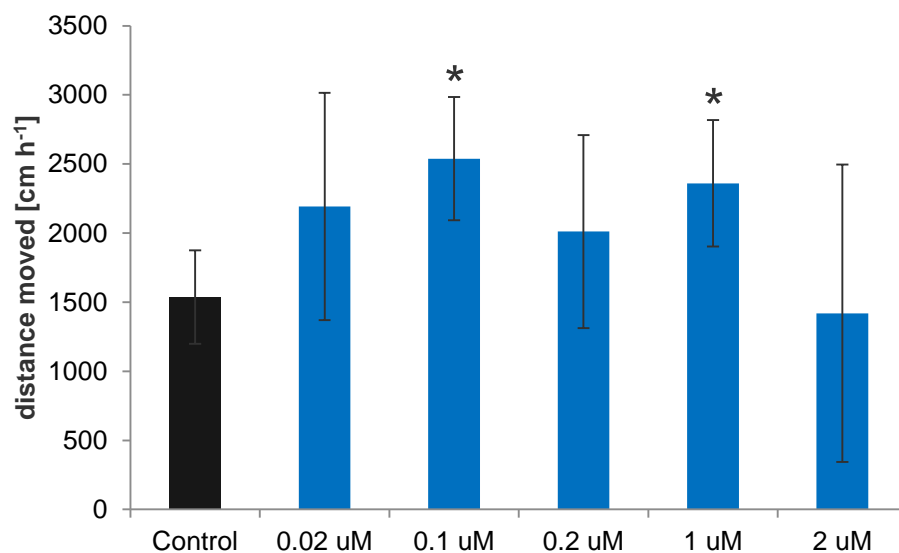


Figure S3-17: Distance moved in cm h^{-1} during 0 to 9 h exposure to different prochloraz concentrations ($n=9$ for control, 0.1 and 1 μM and $n=8$ for 0.02, 0.2 and 2 μM). Asterisks mark treatment samples that are significantly different from the control.

After 18 hours exposure, time ($F = 11.91$; $p < 0.001$) and treatment ($F = 16.98$; $p < 0.001$) effects were observed but no interaction effects. Dunnett post hoc test showed that the effect of time started to be different after 4 hours (4 h: $p = 0.01$; 5 to 18 h $p < 0.001$) and that the 0.02 μM ($p = 0.007$), 0.1 μM ($p < 0.001$) and 1 μM ($p < 0.001$) treatments were different from the control.

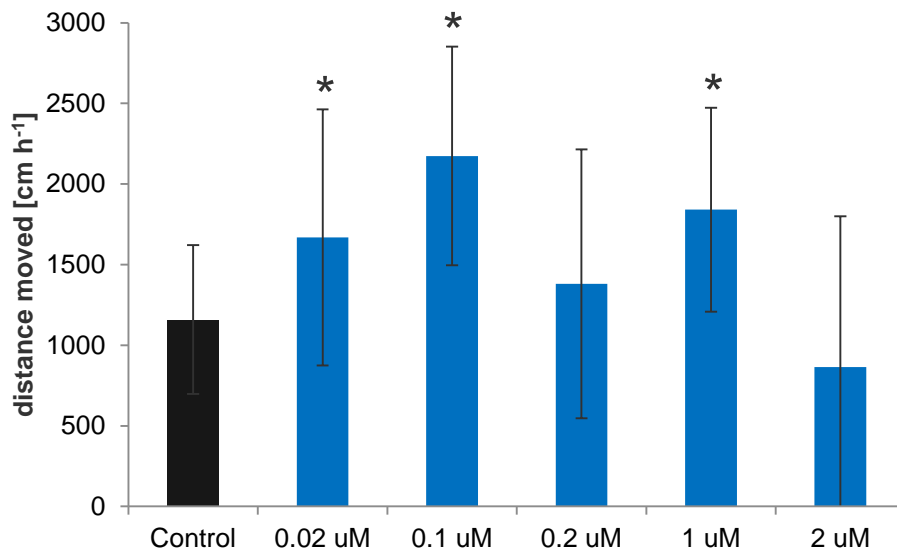


Figure S3-18: Distance moved in cm h^{-1} during 0 to 18 h exposure to different prochloraz concentrations ($n=9$ for control, 0.1 and 1 μM and $n=8$ for 0.02, 0.2 and 2 μM). Asterisks mark treatment samples that are significantly different from the control.

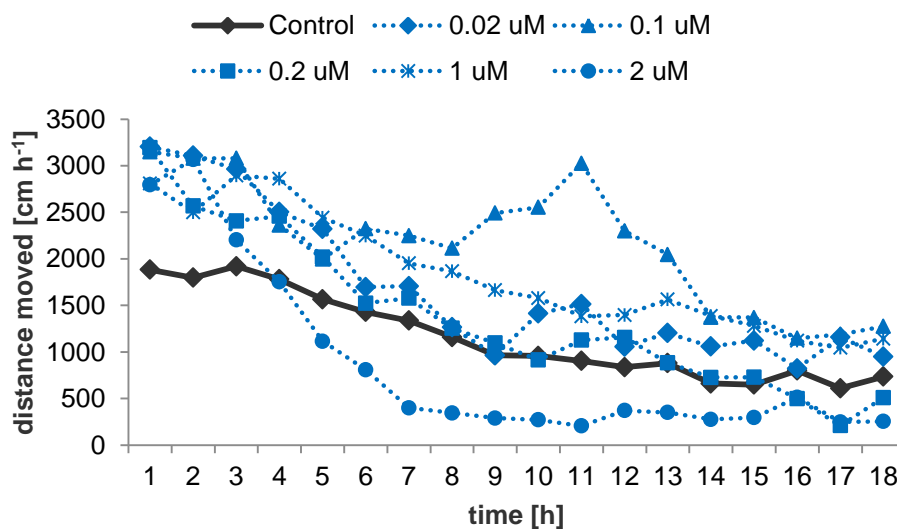
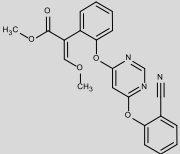


Figure S3-19: Distance moved in cm h^{-1} during 0 to 18 h exposure to different prochloraz concentrations ($n=9$ for control, 0.1 and 1 μM and $n=8$ for 0.02, 0.2 and 2 μM).

SI.Q Identified Biotransformation Products for Azoxystrobin

Table S3-27: Overview of azoxystrobin and identified biotransformation products formed in the aquatic invertebrate *G. pulex*. Biotransformation products are listed according to their relative peak intensity. Information about mass error and retention time (RT) are given for both replicate samples. CE stands for collision energy applied for fragmentation in the MS/MS experiment. All biotransformation product were identified with the suspect screening approach.

Compound	Formula [M]	Mass error [ppm]	RT [min] ⁱⁱⁱ⁾	Polarity	Elemental change ^{iv)}	Log D _{ow} ^{v)}	Identification confidence ^{vi)} /level according to Schymanski et al. (2014) ^{6/ vii)}	Description	CE [eV]	MS/MS confirmatory ions ^{viii)}
MassBank ID of displayed MS/MS spectrum	Exact mass of [M+H] ⁺ / [M-H] ⁻									
Azoxystrobin (AZ)	C ₂₂ H ₁₇ N ₃ O ₅	-0.3	14.4	+		4.2	/1/	parent compound	30	372.0977
ET270001	404.1241	0.2	14.6							344.1029 329.0792
 <p>BAF [L kg_{ww}⁻¹] at t₂₄ⁱ⁾: 5 BAF_k [L kg_{ww}⁻¹] ii): 5</p>										
AZ_M392	C ₂₁ H ₁₇ N ₃ O ₅	-0.7	13.2	+	- CH ₂	0.1	I ⁸	ester hydrolysis,	20	342.0873
ET271102	392.1241	-0.2	13.4		+ H ₂		p /3/, most likely structure	hydrogenation		314.0923 374.1137
AZ_M390b	C ₂₁ H ₁₅ N ₃ O ₅	-0.3	13.3	+	- CH ₂	0.4	I ⁸⁻¹⁰	ester hydrolysis	30	372.0980
ET270203	390.1084	0.1	13.6				/1/			344.1030 329.0794

Compound MassBank ID of displayed MS/MS spectrum	Formula [M] Exact mass of [M+H] ⁺ / [M-H] ⁻	Mass error [ppm]	RT [min] ⁱⁱⁱ⁾	Polarity	Elemental change ^{iv)}	Log D _{ow} ^{v)}	Identification confidence ^{vi)} /level according to Schymanski et al. (2014) ^{6/ vii)}	Description	CE [eV]	MS/MS confirmatory ions ^{viii)}
AZ_M378	C ₂₀ H ₁₅ N ₃ O ₅	-0.5	12.1	+	+ H ₂	-0.5	D	hydrogenation,	10	378.1086
ET270501	378.1084	-0.1	12.4		- C ₂ H ₄		/2b/	didemethylation		342.0875 360.0980
AZ_M630	C ₂₇ H ₂₅ N ₃ O ₁₃ S	-0.9	11.5	- ^{ix)}	- CH ₂	-0.5	d, p	demethylation,	20	241.0025
ET271552	630.1035	-0.8	11.7		+ C ₆ H ₁₀ O ₅ + SO ₃		/3/, most likely structure	glucose conjugation, sulfate conjugation		630.1050 96.9603
AZ_M390a	C ₂₁ H ₁₅ N ₃ O ₅	0.1	11.7	+	- CH ₂	3.5	D	demethylation	30	372.0979
ET270103	390.1084	-0.4	11.8				/2b/			344.1028 329.0793
AZ_M362b	C ₂₀ H ₁₅ N ₃ O ₄	-0.1	14.2	+	- C ₂ H ₂ O	0.8-2.8	d for C ₂ H ₂ O loss at the (<i>E</i>)-methyl β- methoxyacrylate group	- C ₂ H ₂ O	20	362.1137
ET270902	362.1135	-0.3	14.5				/3/, ≥ 3 positional isomers			302.0925 330.0874
AZ_M493	C ₂₄ H ₂₀ N ₄ O ₆ S	-1.0	12.2-13.8	+	- CH ₄ O	1.2-1.3	d, p	- CH ₄ O,	20	132.0111
ET270702	493.1176	-0.8	12.5-14.1		+ C ₃ H ₇ NO ₂ S		/3/, most likely structures	cysteine product		330.0866 461.0906

Compound MassBank ID of displayed MS/MS spectrum	Formula [M] Exact mass of [M+H] ⁺ / [M-H] ⁻	Mass error [ppm]	RT [min] ⁱⁱⁱ⁾	Polarity	Elemental change ^{iv)}	Log D _{ow} ^{v)}	Identification confidence ^{vi)} /level according to Schymanski et al. (2014) ^{6/ vii)}	Description	CE [eV]	MS/MS confirmatory ions ^{viii)}
AZ_M362a ET270802	C ₂₀ H ₁₅ N ₃ O ₄ 362.1135	-0.9 0.5	13.3 13.5	+	- C ₂ H ₂ O	0.8-2.8	d for C ₂ H ₂ O loss at the (<i>E</i>)-methyl β- methoxyacrylate group /3/, ≥ 3 positional isomers	- C ₂ H ₂ O	20	362.1137 330.0874 302.0925
AZ_M420 ET271004	C ₂₂ H ₁₇ N ₃ O ₆ 420.1190	-0.5 -0.2	11.1-14.2 11.3-14.4	+	+ O	3.6-3.7	p for hydroxylation at the (<i>E</i>)-methyl β- methoxyacrylate group /3/, 3 positional isomers	aliphatic hydroxylation	50	345.0741 199.0500 360.0975
AZ_M328a ET271202	C ₁₄ H ₁₇ NO ₆ S 328.0849	-0.6 0.2	8.4 8.8	+	- C ₁₁ H ₇ N ₃ O + C ₃ H ₇ NO ₂ S	-1.3 to -1.4	d for glutathione conjugation and cysteine formation at the aromatic ring /3/, 4 positional isomers	ether cleavage, cysteine product	20	164.0165 264.0325 296.0588
AZ_M525 ET270402	C ₂₅ H ₂₄ N ₄ O ₇ S 525.1438	-0.2 -0.1	12.5-12.8 12.8-13.1	+	+ C ₃ H ₇ NO ₂ S	1.1	d, p /3/, most likely structure	cysteine product	20	132.0113 372.0981 461.0915

Compound MassBank ID of displayed MS/MS spectrum	Formula [M] Exact mass of [M+H] ⁺ / [M-H] ⁻	Mass error [ppm]	RT [min] ⁱⁱⁱ⁾	Polarity	Elemental change ^{iv)}	Log D _{ow} ^{v)}	Identification confidence ^{vi)} /level according to Schymanski et al. (2014) ^{6/ vii)}	Description	CE [eV]	MS/MS confirmatory ions ^{viii)}
AZ_M498	C ₂₂ H ₁₇ N ₃ O ₉ S	-0.1	11.2	- ^{ix)}	+ O	1.3-1.7	p for hydroxylation and sulfate conjugation at the (<i>E</i>)- methyl β- methoxyacrylate group	aliphatic hydroxylation, sulfate conjugation	30	418.1042
ET271453	498.0613	0.1	11.4		+ SO ₃		e /3/, 3 positional isomers			284.0432 403.0806
AZ_M214	C ₁₁ H ₇ N ₃ O ₂	-0.5	5.8	+	- C ₁₁ H ₁₀ O ₃	2.3	D	ether cleavage	40	214.0607
ET270602	214.0611	-0.2	6.2				I ⁸ /2b/			187.0499 120.0442
AZ_M552	C ₂₇ H ₂₅ N ₃ O ₁₀	-1.1	12.0	+	- CH ₂	1.8	d, p	demethylation,	20	145.0496
ET270302	552.1613	1.9	12.3		+ C ₆ H ₁₀ O ₅		e /3/, most likely structure	glucose conjugation		358.0823 213.1234
AZ_M328b	C ₁₄ H ₁₇ NO ₆ S	0.2	9.4	+	- C ₁₁ H ₇ N ₃ O	-1.3 to	d for glutathione conjugation and cysteine formation at the aromatic ring	ether cleavage, cysteine product	20	164.0166
ET271302	328.0849	0.7	9.8		+ C ₃ H ₇ NO ₂ S	-1.4	 /3/, 4 positional isomers			264.0325 296.0588

Compound MassBank ID of displayed MS/MS spectrum	Formula [M] Exact mass of [M+H] ⁺ / [M-H] ⁻	Mass error [ppm]	RT [min] ⁱⁱⁱ⁾	Polarity	Elemental change ^{iv)}	Log D _{ow} ^{v)}	Identification confidence ^{vi)} /level according to Schymanski et al. (2014) ^{6/ vii)}	Description	CE [eV]	MS/MS confirmatory ions ^{viii)}
AZ_M618	C ₂₆ H ₂₅ N ₃ O ₁₃ S	-0.5	10.9	- ^{ix)}	- CH ₂	-4.6	d, p	demethylation,	20	241.0017
ET271852	618.1032	-0.3	11.2		+ C ₆ H ₁₀ O ₅ + SO ₃ - CH ₂ + H ₂		/3/, most likely structure	glucose conjugation, sulfate conjugation, ester hydrolysis, hydrogenation		618.1029 96.9600
AZ_M514	C ₂₂ H ₁₇ N ₃ O ₁₀ S	-0.5	10.9	- ^{ix)}	+ O	-0.8-2.0	d for only one hydroxylation at the (<i>E</i>)-methyl β-methoxy- acrylate group	aliphatic hydroxylation, sulfate conjugation, hydroxylation	30	359.0546
ET271753	514.0562	-0.3	11.2		+ SO ₃ + O		p for hydroxylation and sulfate conjugation at the (<i>E</i> - methyl β- methoxyacrylate group e /3/, many positional isomers			434.0993 300.0385
AZ_M468	C ₂₁ H ₁₅ N ₃ O ₈ S	-0.4	11.6	- ^{ix)}	- CH ₂	1.3	p	demethylation,	20	328.0724
ET271652	468.0507	-0.8	11.8		+ SO ₃		e /3/, most likely structure	sulfate conjugation		360.0987 388.0938

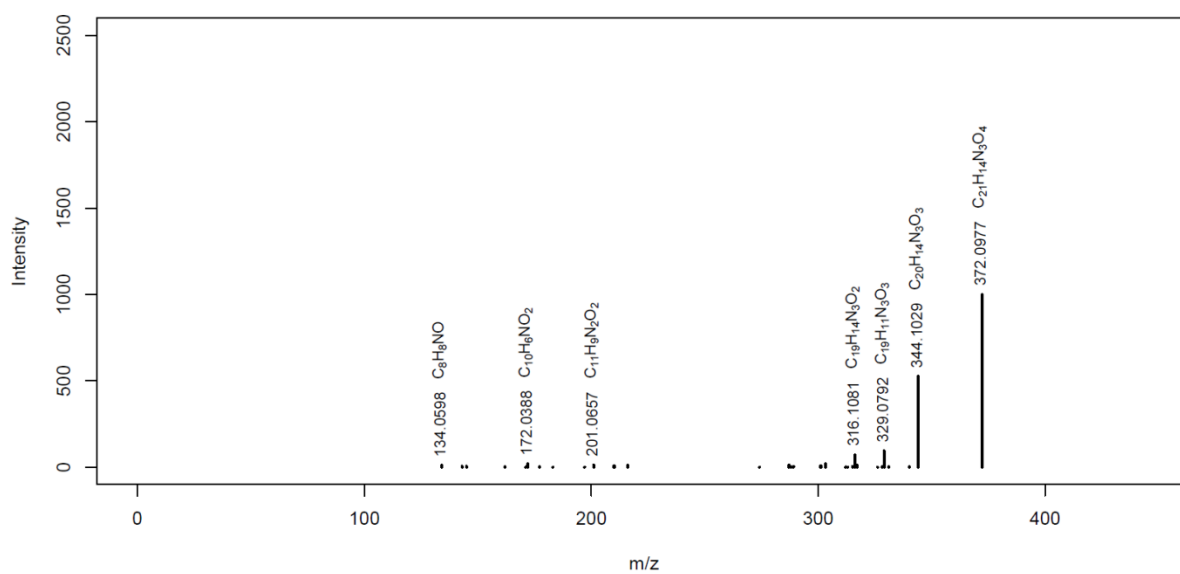
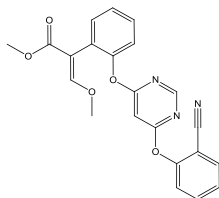
Explanation to Table-S3-27:

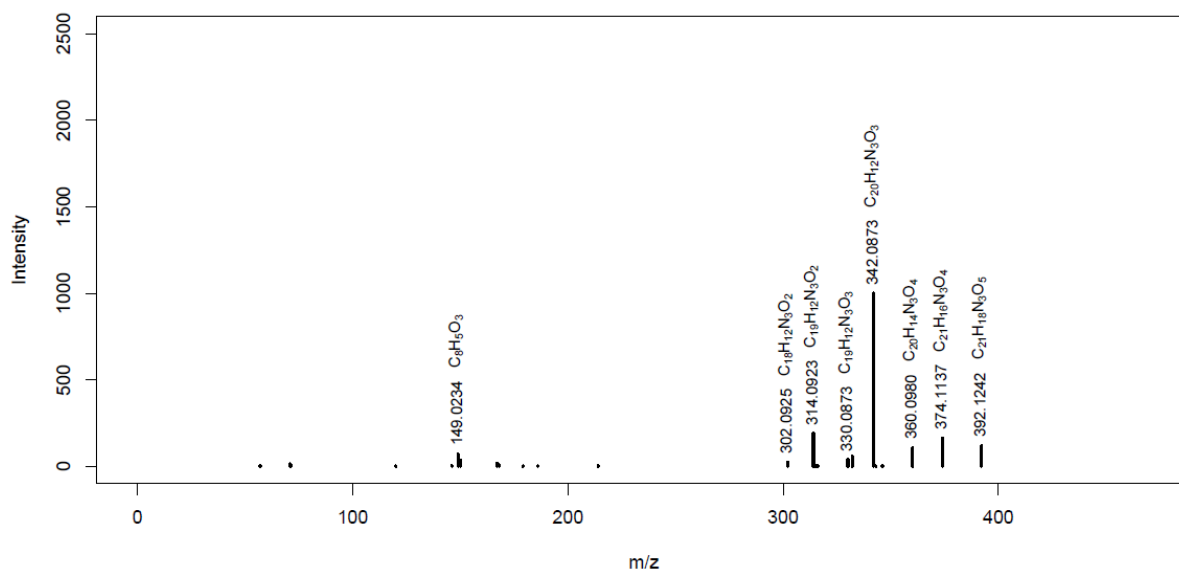
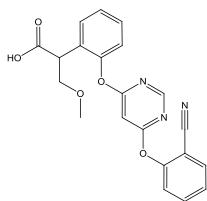
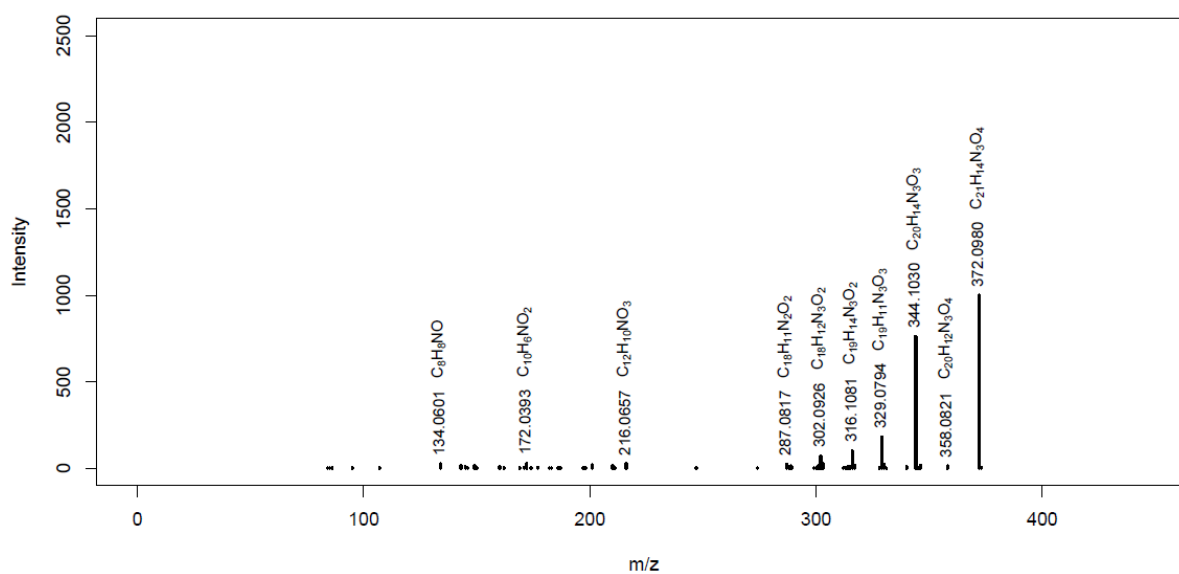
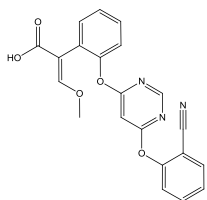
- ⁱ⁾ See Equation S3-4 in SI H *Modeling Bioaccumulation and Biotransformation Kinetics* for the calculation of BAFs at steady state and SI I. The reported BAF is based on the same azoxystrobin exposure concentration of $80 \mu\text{g L}^{-1}$ as used in the kinetic experiment.
- ⁱⁱ⁾ See Equation S3-5 in SI H *Modeling Bioaccumulation and Biotransformation Kinetics* for the calculation of kinetic BAF_{k,s}.
- ⁱⁱⁱ⁾ In case of a retention time range, several possibly positional isomers were integrated as one peak, due to bad peak separation.
- ^{iv)} The elemental change refers to the change in the molecular formula of the biotransformation product in comparison with the parent compound.
- ^{v)} Log D_{ow} values were predicted by MarvinSketch version 14.10.20.0 at pH 7.9 and 25 °C. Log D_{ow} values correspond to corrected log K_{ow} values to account for pH-dependent dissociation. At pH 7.9 azoxystrobin is neutral thus log D_{ow} is equal to log K_{ow}. If different positional isomers are possible for one BTP, a range of log D_{ow} values is given.
- ^{vi)} D: diagnostic fragment/evidence for one structure; d: diagnostic fragment/evidence for positional isomers; e: enzyme deconjugation; l: structure reported in literature; m: MS/MS data from literature; p: biotransformation pathway information; d, p: diagnostic fragment for positional isomers (d) in combination with pathway information (p) give evidence for one possible structure.
- ^{vii)} Levels are defined as follows: 5 (*exact mass*), 4 (*unequivocal molecular formula*), 3 (*tentative candidates: e.g., positional isomers*), 2 (*probable structure: library spectrum match (a) or diagnostic evidence for one structure (b)*) and 1 (*confirmed structure*).
- ^{viii)} Diagnostic fragments (d, D) are listed first and are represented in bold in the table, other characteristic fragments are then presented according to their relative abundance. Only fragments where a chemical formula and structure could be attributed are considered.
- ^{ix)} The sulfate-containing BTPs are more sensitive in negative ionization mode. However, they were quantified in positive ionization mode because azoxystrobin was detected and quantified in positive ionization mode.

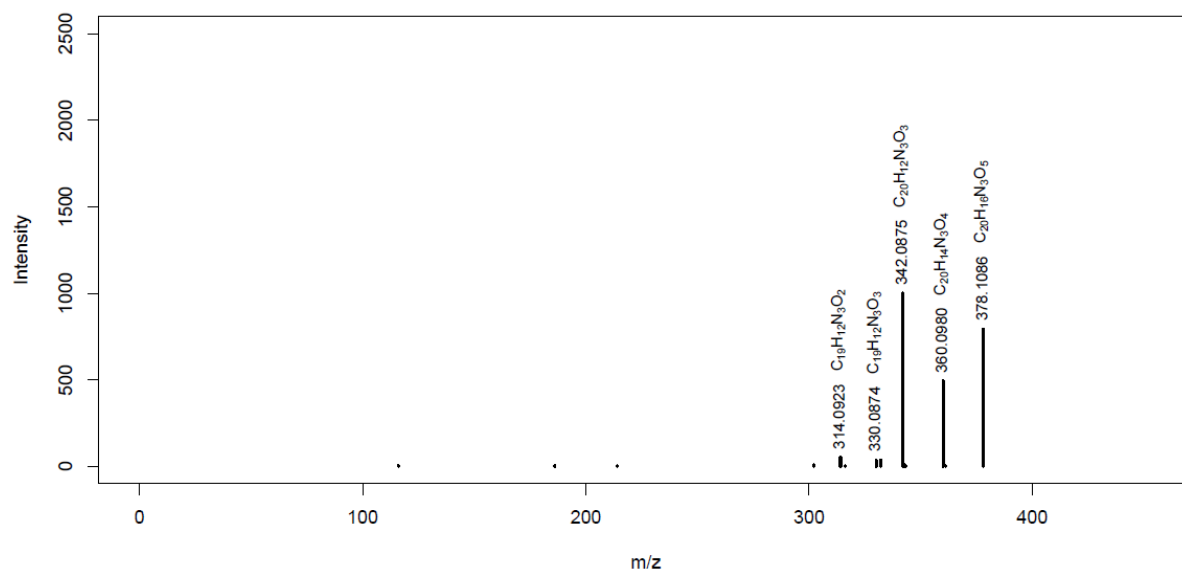
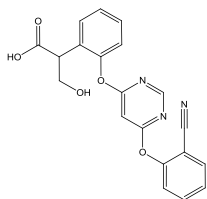
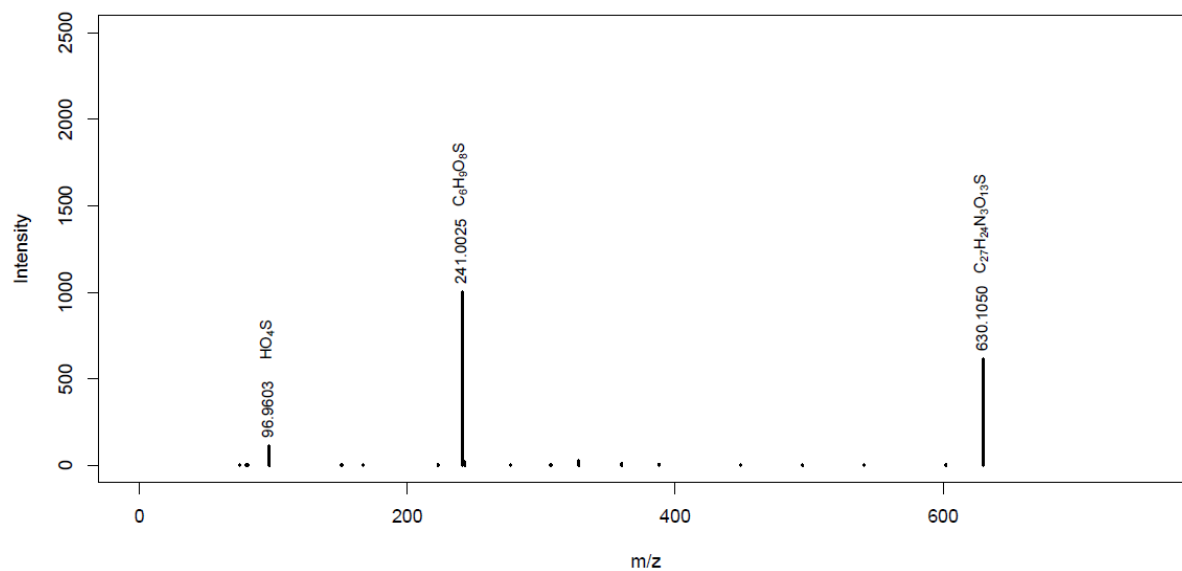
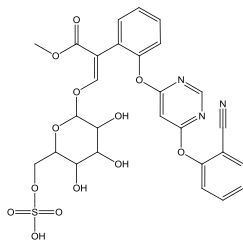
The different MassBank IDs for one compound refer to different collision energies applied during MS/MS fragmentation. The MassBank ID displayed in bold indicates the depicted MS/MS spectrum. Spectra are also available electronically in the MassBank database.¹¹

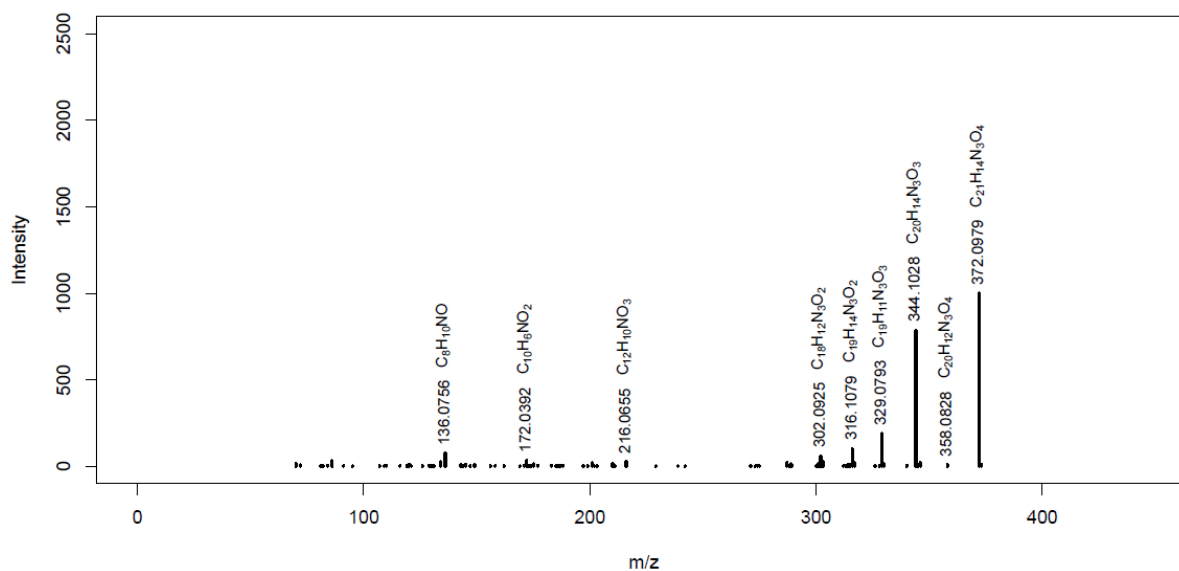
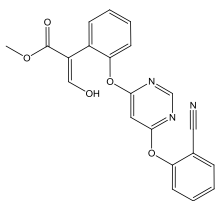
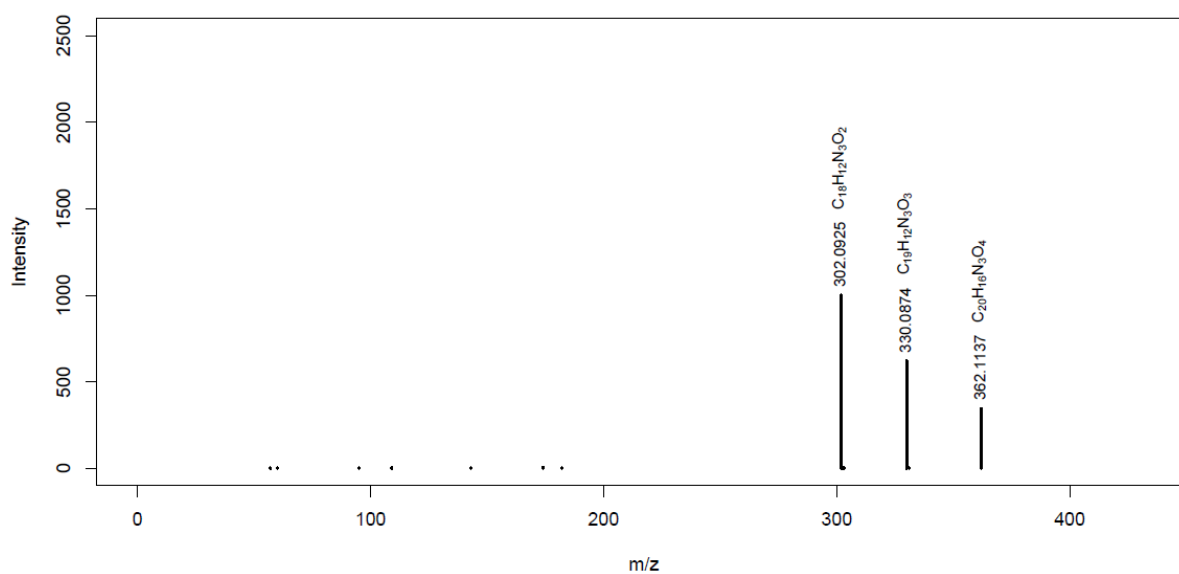
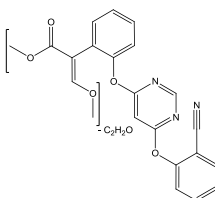
Azoxystrobin (AZ)

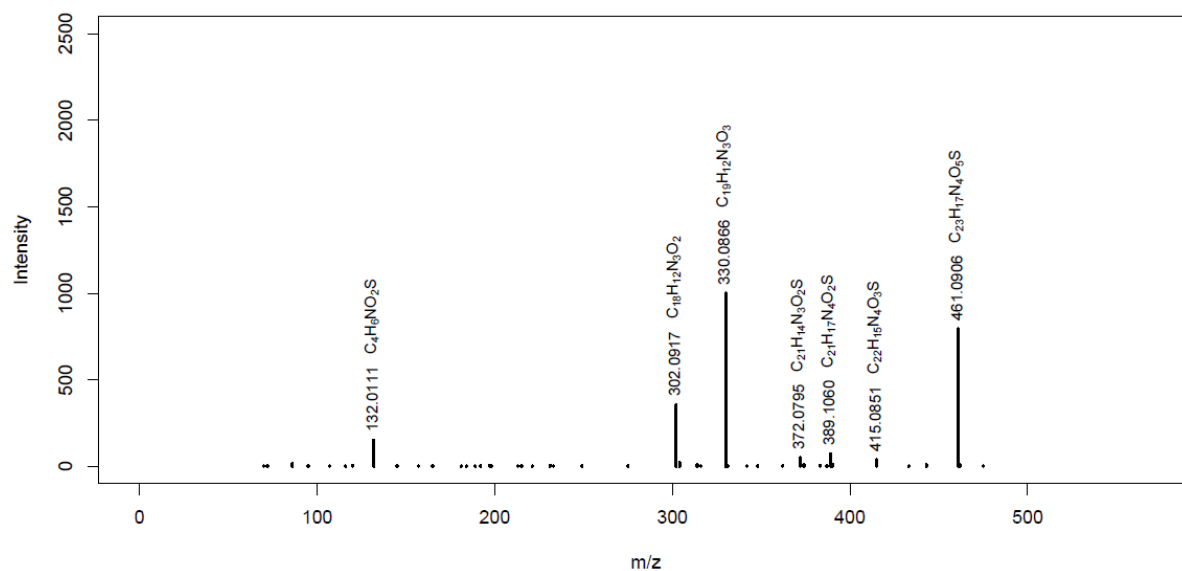
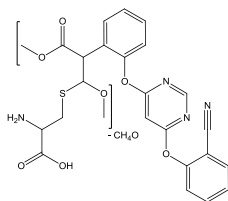
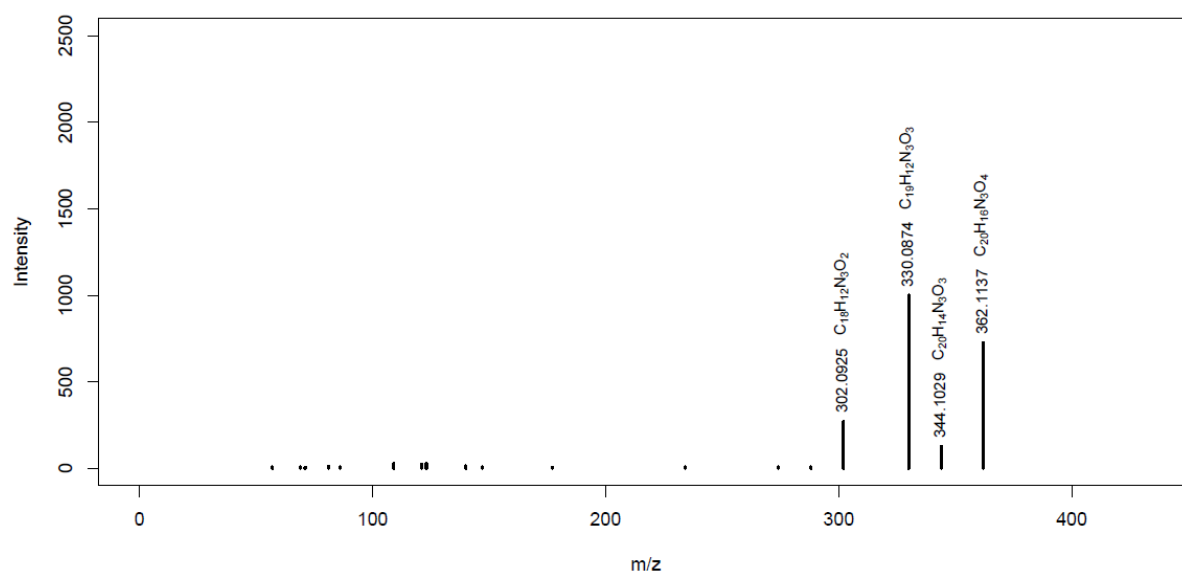
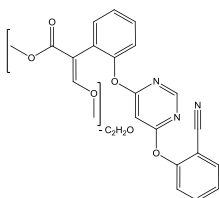
MassBank ID: **ET270001**

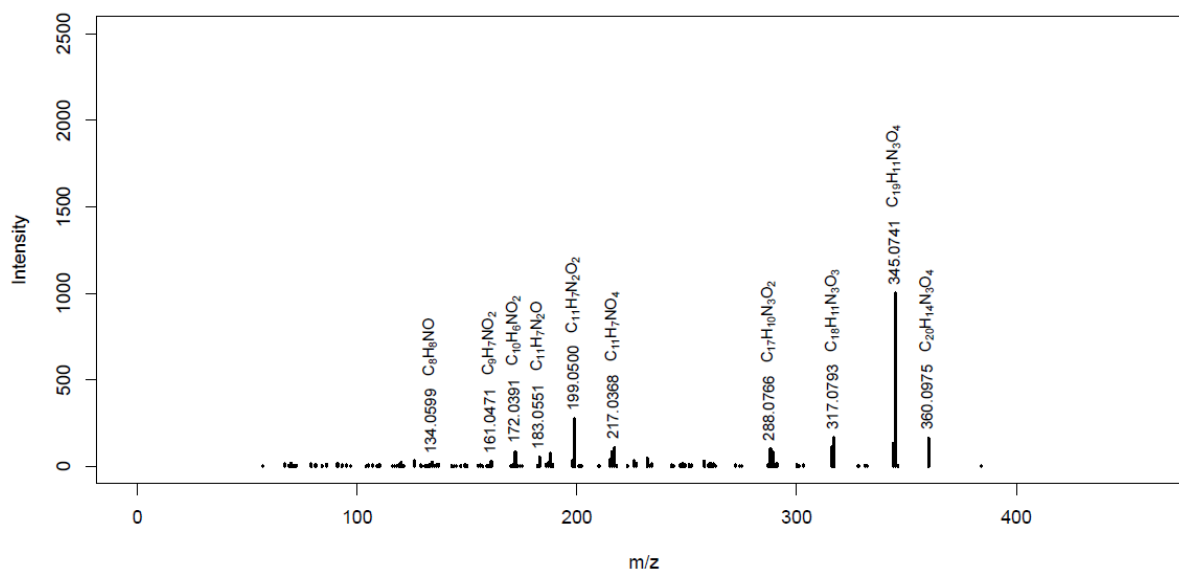
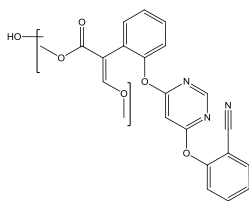
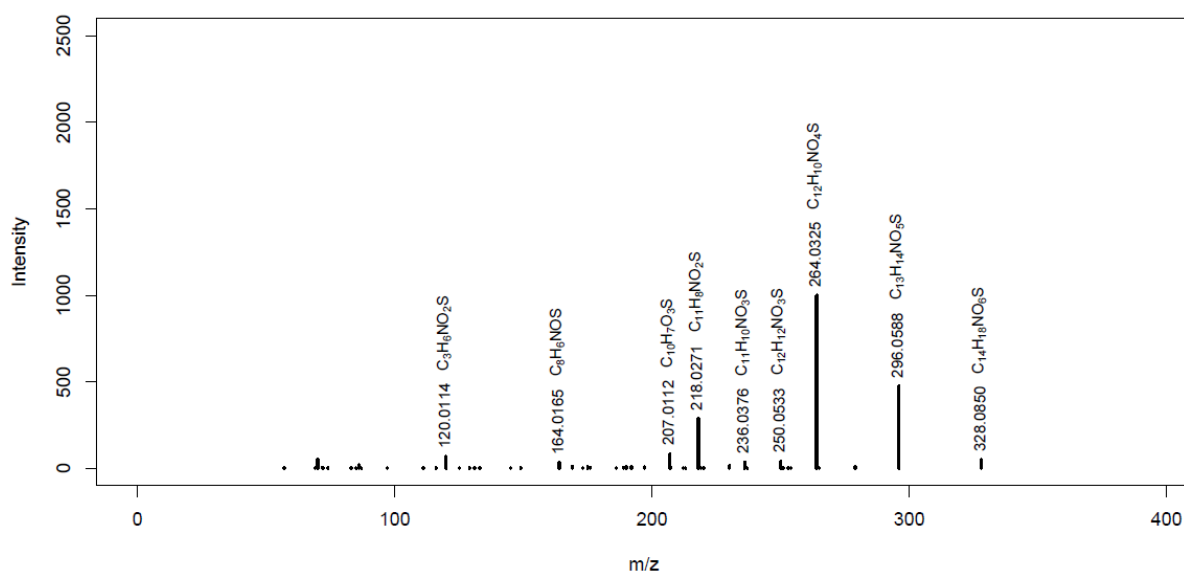
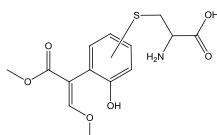


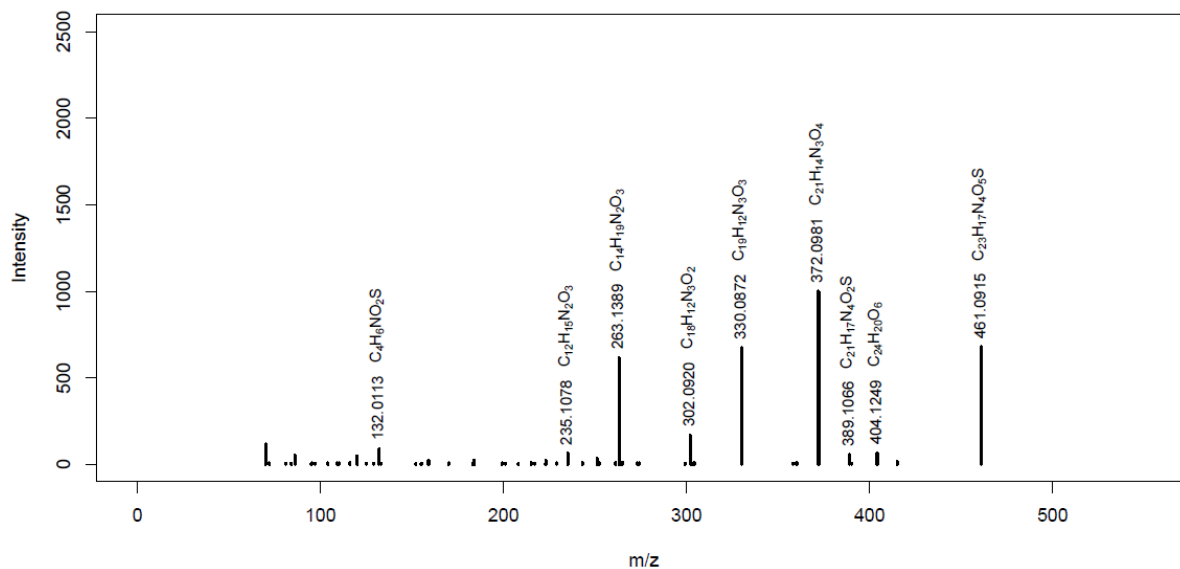
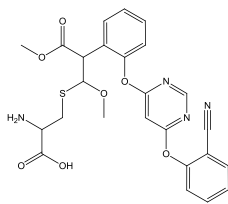
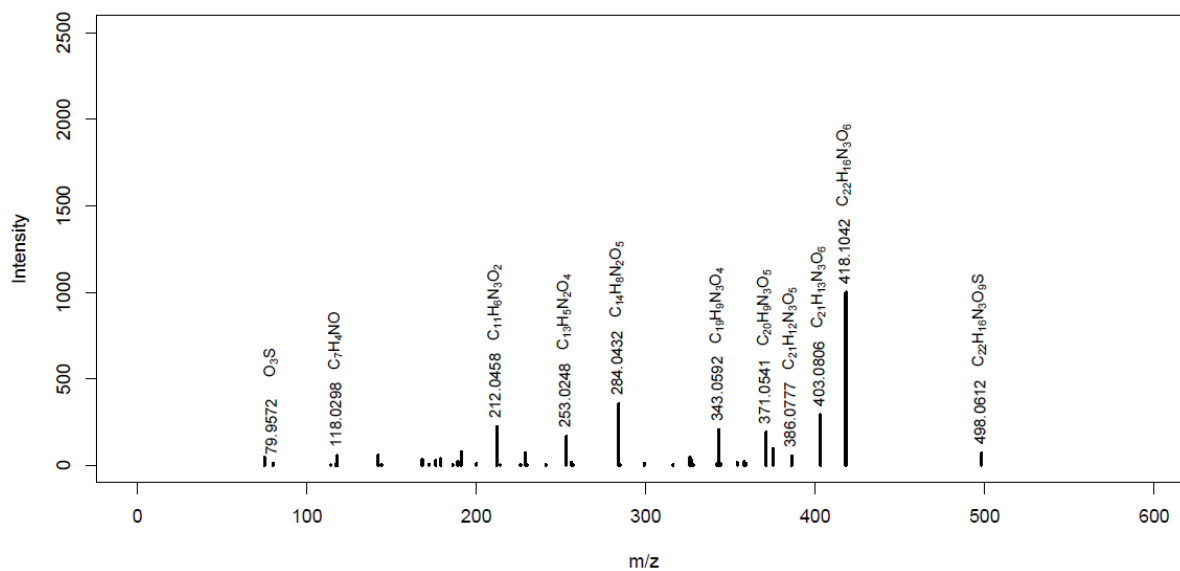
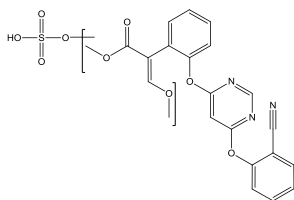
AZ_M392MassBank ID: ET271101, **ET271102**, ET271103, ET271104, ET271105**AZ_M390b**MassBank ID: ET270201, ET270202, **ET270203**, ET270204, ET270205

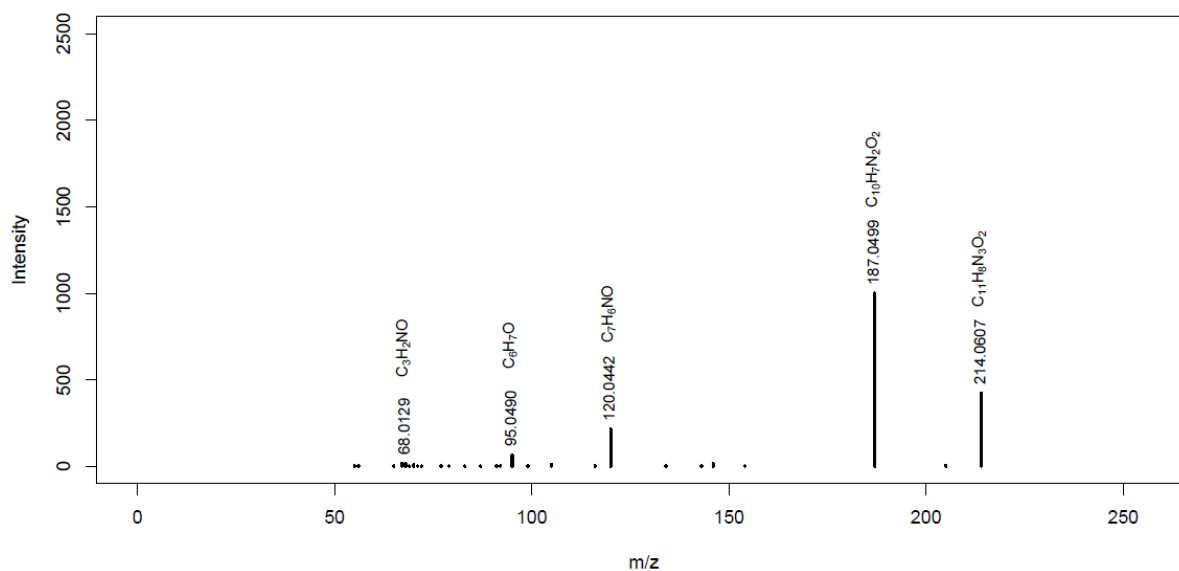
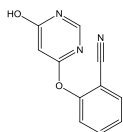
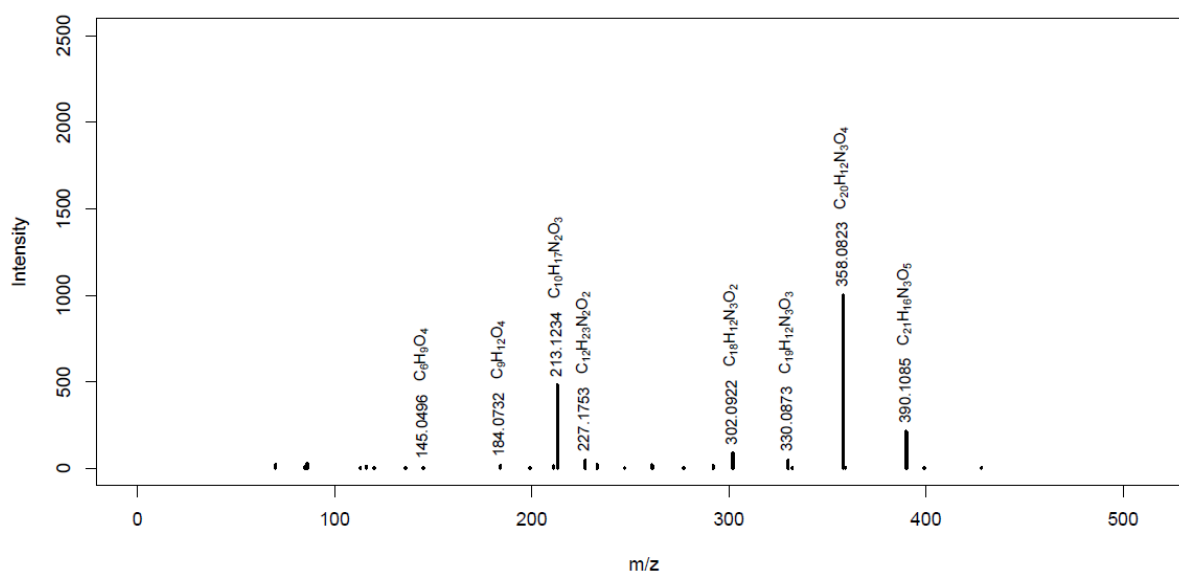
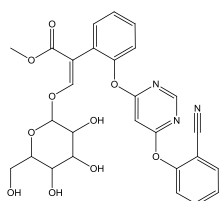
AZ_M378MassBank ID: **ET270501**, ET270502, ET270503, ET270504, ET270505**AZ_M630**MassBank ID: ET271551, **ET271552**, ET271553, ET271554, ET271555

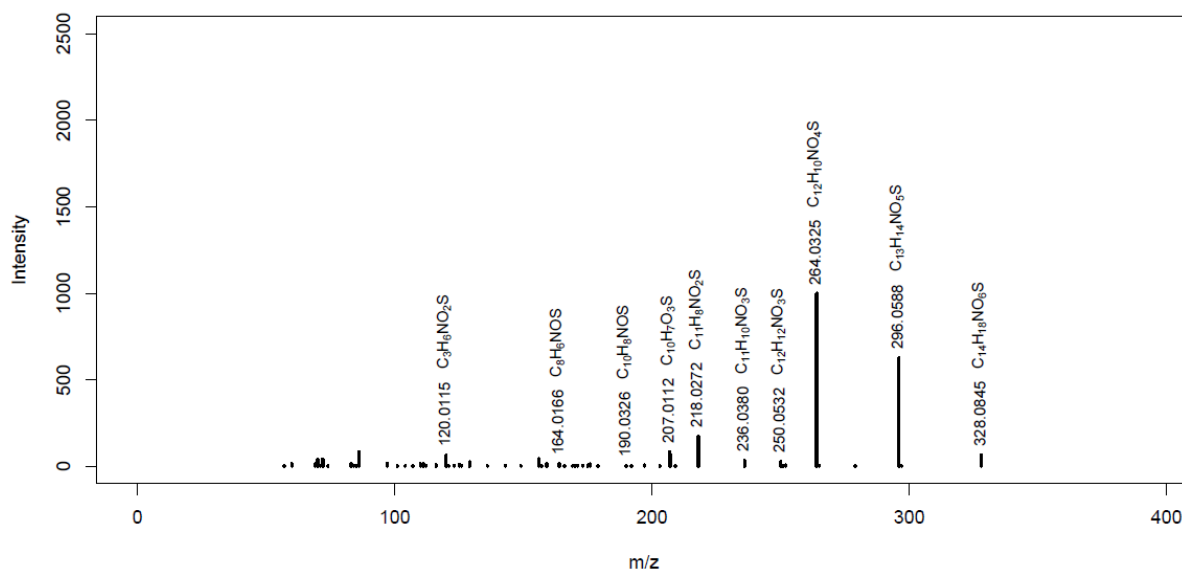
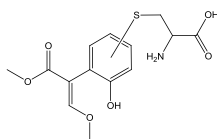
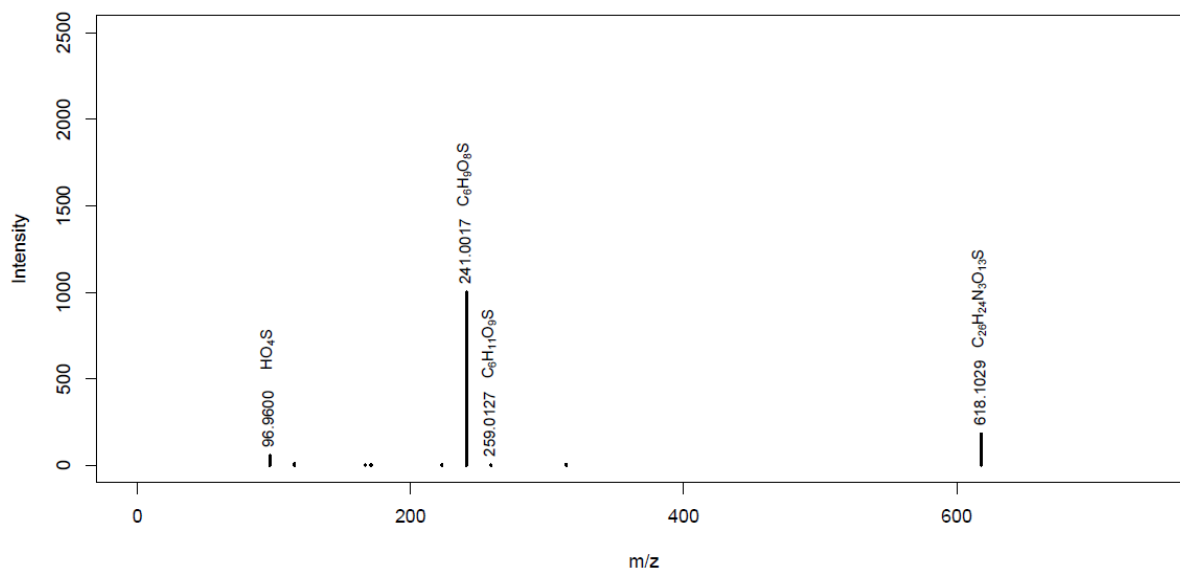
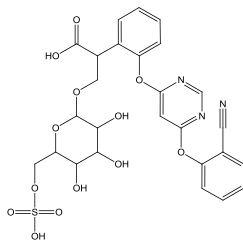
AZ_M390aMassBank ID: ET270101, ET270102, **ET270103**, ET270104, ET270105**AZ_M362b**MassBank ID: ET270901, **ET270902**, ET270903, ET270904, ET270905

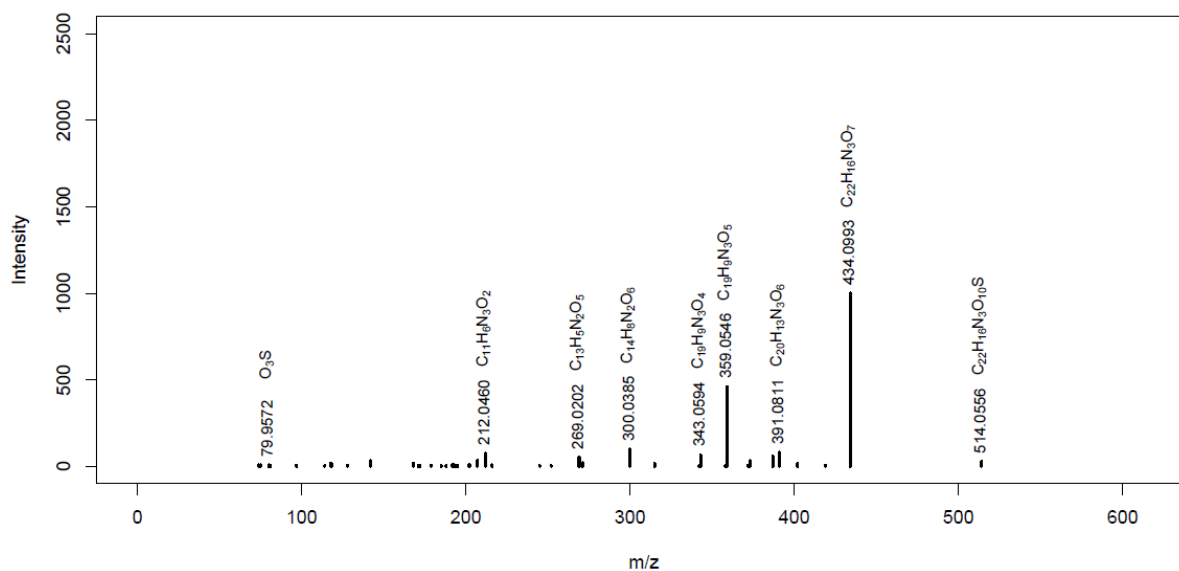
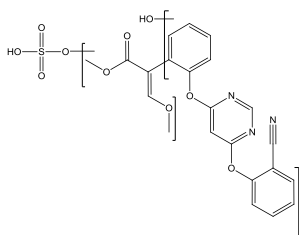
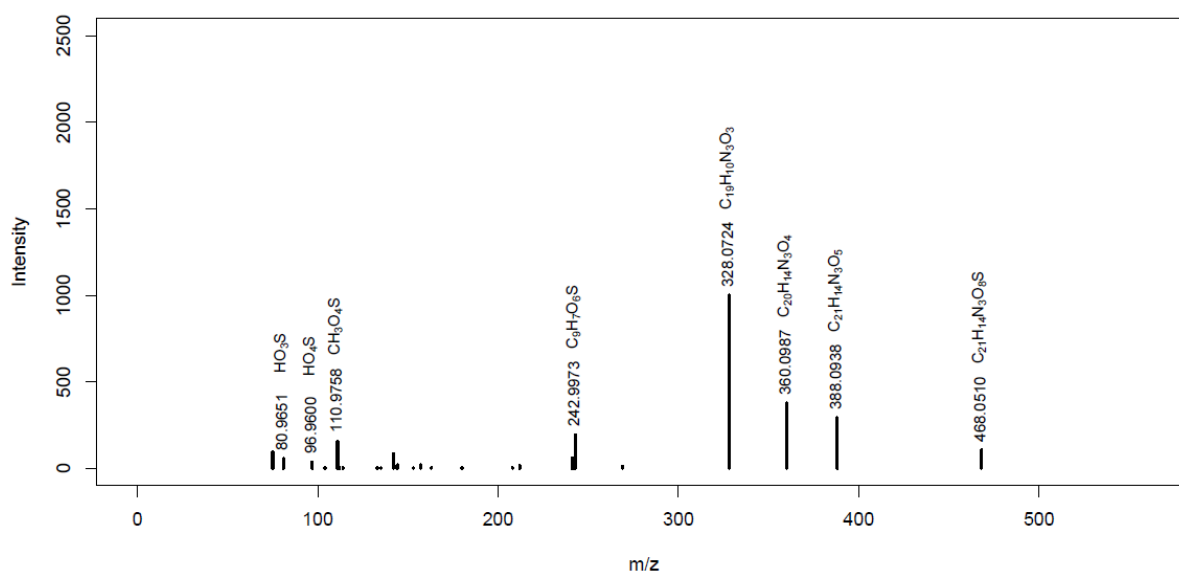
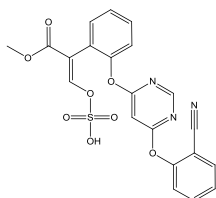
AZ_M493MassBank ID: ET270701, **ET270702**, ET270703, ET270704, ET270705**AZ_M362a**MassBank ID: ET270801, **ET270802**, ET270803, ET270804, ET270805

AZ_M420MassBank ID: ET271001, ET271002, ET271003, **ET271004**, ET271005**AZ_M328a**MassBank ID: ET271201, **ET271202**, ET271203, ET271204, ET271205

AZ_M525MassBank ID: ET270401, **ET270402**, ET270403, ET270404, ET270405**AZ_M498**MassBank ID: ET271451, ET271452, **ET271453**, ET271454, ET271455

AZ_M214MassBank ID: ET270601, **ET270602**, ET270603, ET270604, ET270605**AZ_M552**MassBank ID: ET270301, **ET270302**, ET270303, ET270304, ET270305

AZ_M328bMassBank ID: ET271301, **ET271302**, ET271303, ET271304, ET271305**AZ_M618**MassBank ID: ET271851, **ET271852**, ET271853, ET271854, ET271855

AZ_M514MassBank ID: ET271751, ET271752, **ET271753**, ET271754, ET271755**AZ_M468**MassBank ID: ET271651, **ET271652**, ET271653, ET271654, ET271655

References

- [1] Naylor, C.; Maltby, L.; Calow, P., Scope for growth in *Gammarus pulex*, a freshwater benthic detritivore. *Hydrobiologia* **1989**, 188-189 (1), 517-523.
- [2] Rösch, A.; Anliker, S.; Hollender, J., How Biotransformation Influences Toxicokinetics of Azole Fungicides in the Aquatic Invertebrate *Gammarus pulex*. *Environmental Science & Technology* **2016**, 50 (13), 7175-88.
- [3] Kukkonen, J.; Oikari, A., Sulphate conjugation is the main route of pentachlorophenol metabolism in *Daphnia magna*. *Comparative Biochemistry and Physiology - C Pharmacology Toxicology and Endocrinology* **1988**, 91 (2), 465-468.
- [4] Beketov, M. A.; Liess, M., Potential of 11 pesticides to initiate downstream drift of stream macroinvertebrates. *Arch. Environ. Contam. Toxicol.* **2008**, 55 (2), 247-53.
- [5] R Core Team *A language and environment for statistical computing*, R Foundation for Statistical Computing: 2016.
- [6] Ritz, C.; Streibig, J. C., Bioassay analysis using R. *Journal of Statistical Software* **2005**, 12, 1-22.
- [7] Brain, P.; Cousens, R., An equation to describe dose responses where there is stimulation of growth at low doses. *Weed Research* **1989**, 29 (2), 93-96.
- [8] Roberts, T. R.; Hutson, D. H., Metabolic Pathways of Agrochemicals: Part 2: Insecticides and Fungicides. *Royal Society of Chemistry* **2006**.
- [9] Clinton, B.; Warden, A. C.; Haboury, S.; Easton, C. J.; Kotsonis, S.; Taylor, M. C.; Oakeshott, J. G.; Russell, R. J.; Scott, C., Bacterial degradation of strobilurin fungicides: a role for a promiscuous methyl esterase activity of the subtilisin proteases? *Biocatal. Biotransform.* **2011**, 29 (4), 119-129.
- [10] Laird, W. J. D.; Gledhill, A. J.; Lappin, G. J., Metabolism of methyl-(E)-2-{2- 6-(2-cyanophenoxy)pyrimidin-4-yloxy phenyl}-3-methoxyacrylate (azoxystrobin) in rat. *Xenobiotica* **2003**, 33 (6), 677-690.
- [11] European Mass Bank Server (NORMAN MassBank) www.massbank.eu.

Chapter 4. Comparing Biotransformation of two Fungicides and the Potential of Cytochrome P450 Inhibition in two Aquatic Invertebrates

Andrea Rösch^{1,2}, Qiuguo Fu¹, Juliane Hollender^{1,2}

¹ Eawag, Swiss Federal Institute of Aquatic Science and Technology, 8600 Dübendorf, Switzerland

² Institute of Biogeochemistry and Pollutant Dynamics, ETH Zürich, 8092 Zürich, Switzerland

Abstract

To understand differences in species sensitivity towards chemicals a detailed understanding of toxicokinetics (uptake, internal distribution, biotransformation, elimination) and toxicodynamics (interactions at biological target sites) is necessary. Within this study, we compared the biotransformation potential of two fungicides (the strobilurin azoxystrobin and the imidazole prochloraz) in two invertebrate species, *Hyaella azteca* and *Gammarus pulex* after 24 h exposure. By measuring internal concentrations of parent compounds and associated biotransformation products (BTPs) with the use of high resolution tandem mass spectrometry, similar BTPs were identified in *H. azteca* and *G. pulex*. BTPs were mainly formed by oxidation and conjugation reactions in both species, indicating a conservation of enzymes across the two invertebrate species. However, differences were observed and new routes of conjugation with taurine and malonyl were identified in *H. azteca*. Estimated kinetic rate constants confirmed the importance of secondary BTPs, such as conjugation products, for both species and suggested that biotransformation might be more important in *H. azteca* for the reduction of parent compound bioaccumulation. However, compared to REACH criteria, bioaccumulation of both fungicides was low and comparable in the two species. Mixture experiments with azoxystrobin and prochloraz showed that *H. azteca* was about five times less sensitive towards cytochrome P450 monooxygenase inhibition by prochloraz compared to *G. pulex*, indicating a lower potential for synergistic effects.

4.1 Introduction

A large variety of chemicals from industry, agriculture and households enters aquatic ecosystems. The complex mixture of these chemicals present in the environment may exert acute or chronic toxic effects if they are taken up by organisms and reach the target site and can thereby pose a threat to aquatic organisms.¹⁻² Bioconcentration describes the accumulation of water-borne chemicals in aquatic organisms through nondietary uptake routes, such as uptake via dermal or respiratory surfaces, whereas bioaccumulation also considers dietary exposure routes.³⁻⁴ Both processes are fundamental in terms of risk assessment and required in a regulatory context including the European REACH regulation (EC no. 1907/2006)⁵. Bioconcentration factors (BCF) of chemicals are usually determined by fish tests (OECD 305 guideline⁶) or, if the chemicals are more likely bound to sediments, bioaccumulation factors (BAF) are determined by benthic oligochaetes tests (OECD 315 guideline⁷). Fish bioconcentration tests are time-consuming and require the use of many test organisms. Thus, there is the need for alternative approaches that replace protected vertebrate species⁸ such as fish (replacement), that reduce the number of test animals (reduction), and that avoid unnecessary suffering of test animals (refinement), known as the principle of the 3Rs.⁹ Preliminary results suggest that the invertebrate species *Hyalella azteca* may be a suitable replacement organism for fish, since BCFs determined via *H. azteca* were comparable to BCFs obtained from fish.¹⁰

The freshwater epibenthic amphipod *H. azteca* inhabits lakes and streams and is distributed widely throughout North and Central America. As a result of its widespread occurrence, ease of culture, environmental relevance and sensitivity towards chemicals, *H. azteca* has been used as test organisms for sediment and water quality assessment predominantly in North America.¹¹⁻¹⁴ Amphipods from the genus *Gammarus*, the European relatives to *H. azteca*, are often used for biomonitoring or in lab experiments to examine the effect of stressors with endpoints such as mortality or feeding activity¹⁵⁻¹⁸, due to the high sensitivity of *Gammarus spp.* towards a wide range of contaminants.¹⁹⁻²¹ However, in most studies where *Gammarus spp.* were used as test organisms, organisms were collected from uncontaminated stream sites, since culturing of *Gammarus spp.* is challenging and only a few studies exist which have used lab-cultures.²²⁻²³ The ability to easily culture *H. azteca* is beneficial compared to field organisms such as *Gammarus pulex* since it offers a homogenous test population over the whole year. However, there is still more information needed if *H. azteca* and related native aquatic invertebrates exhibit similar sensitivities towards chemicals.

Assessing the impact of organic pollutants on different aquatic organisms requires fundamental understanding of many processes, in which (i) toxicokinetics (describes the uptake, internal distribution, biotransformation and elimination of a chemical within an organism) and (ii) toxicodynamics (describes the interaction of a chemical at the site of toxic action and thereby the effect) represent the two major ones.²⁴⁻²⁵ Toxicokinetics and toxicodynamics can be used to address the differences in species' sensitivity towards the same chemical and the differences in toxicity of different chemicals towards one species.

To date, most studies that either investigate toxicokinetic processes in one aquatic invertebrate species or that compare toxicokinetics among different aquatic invertebrate species are based on the uptake and elimination kinetics of the parent compound, or on total internal concentrations measured in terms of total radioactivity of radiolabeled parent compounds and any BTPs formed still carrying the radiolabeled moiety.²⁶⁻³² In these cases, no differentiation between different elimination routes of the parent compound, such as direct elimination and biotransformation, is possible. Only a few studies which investigated toxicokinetics of organic chemicals in aquatic invertebrate species have thoroughly assessed the role of biotransformation by using comprehensive BTP screening approaches and suitable analytical methods to identify BTPs.³³⁻³⁷

Knowledge on the biotransformation potential is needed to understand differences in species' sensitivity towards the same chemical, since biotransformation is a key process that can greatly influence bioaccumulation and thereby the toxicity of a chemical. Furthermore, the biotransformation potential of different organisms reflects their enzyme composition, which is crucial for a better understanding of conservation of enzymes, such as of cytochrome P450 monooxygenases (CYPs). CYPs are one of the most important enzyme classes present in all kingdoms of life that are active in the metabolization of endogenous and exogenous substrates, whereby they can detoxify xenobiotics via biotransformation.³⁸⁻⁴¹ Inhibition of CYPs by chemicals such as azole fungicides has been shown to influence the biotransformation of co-occurring substances in aquatic organisms, resulting in higher toxicity (synergism).^{33, 42-46}

The aim of this study was to compare routes of biotransformation in *H. azteca* and *G. pulex* and to assess the importance of biotransformation in terms of reducing bioaccumulation of the parent compound in these two species. Two fungicides (the strobilurin fungicide azoxystrobin and the imidazole fungicide prochloraz) with known biotransformation pathways and toxicokinetics in *G. pulex* were selected as test compounds.^{33, 36} Furthermore, we have shown in previous work³³ that out of six selected azole fungicides, which are known inhibitors of CYP, the imidazole prochloraz showed the strongest CYP inhibition potential in *G. pulex*. Therefore, it was of interest if prochloraz exhibits a comparable CYP inhibition capacity in *H. azteca* as observed in *G. pulex*.

4.2 Material and Methods

4.2.1 Chemicals, Solutions and Test Organisms

Detailed information about all chemicals and solutions used during experiments and instrumental analysis can be found in Supporting Information (SI) A.

H. azteca were kept in 1.5 L glass beakers filled with previously aerated Borgmann water⁴⁷ and were fed three times a week with approximately 30 mg ground fish food flakes. Each beaker contained approximately 100 organisms and a piece of cotton gauze as substrate to hold on to and hide. All beakers were placed in a water bath (23 ± 1 °C) with a 16 h light/8 h dark cycle. Borgmann water was changed weekly and juvenile *H. azteca* were separated from the adults and kept in separate beakers.

4.2.2 Experimental Design

All exposure media were prepared in 500 mL Borgmann water and one piece of cotton gauze was added to each 600 mL glass beaker. All samples were prepared in duplicate. Different controls were performed during each experiment, *i.e.*, “organism controls” (chemical negative, organism and cotton gauze positive), “chemical controls” (organism and cotton gauze negative, chemical positive), and “cotton gauze controls” (organism negative, cotton gauze and chemical positive). Exposure media were sampled at the beginning and end of the experiments to determine the aqueous concentration. Experiments were performed in a climate cabinet at 23 ± 1 °C and with a 16 h light/8 h dark cycle.

After exposure, organisms were shortly rinsed with nanopure water, blotted dry on tissue, transferred to 2 mL-microcentrifuge tubes, and weighed. 100 μ L isotopically labeled internal standard mix solution ($100 \mu\text{g L}^{-1}$), 500 μ L methanol, and 300 mg of 1 mm zirconia/silica beads (BioSpec Products, Inc., U.S.A.) were added before samples were homogenized and extracted with a FastPrep bead beater (MP Biomedicals, Switzerland) in two cycles of 15 s at 6 m s^{-1} (cooling on ice in between). Afterwards, samples were centrifuged (6 min, 10 000 rpm, 20 °C), and filtered through 0.45 μ m regenerated cellulose filters (BGB Analytic AG, Switzerland). Filters were washed with 400 μ L methanol and the filtrate was combined with the extract. All samples were stored at -20 °C until chemical analysis.

4.2.3 Chemical Analysis

H. azteca extracts and exposure medium samples were analyzed by online solid phase extraction coupled to reversed phase liquid chromatography high resolution tandem mass spectrometry (online-SPE-LC-HRMS/MS) (Q Exactive, Thermo Fisher Scientific Inc.). Detection was done by full scan acquisition with a resolution of 70000 (at m/z 200) in polarity switching mode (electrospray ionization) followed by five (positive mode) and two (negative mode) data-dependent MS/MS scans with a resolution of 17000 (at m/z 200) with an isolation window of 1 m/z . Information on the mass list used for triggering data-dependent MS/MS scans can be found in SI C. Several BTPs were remeasured in targeted mode with higher collision energies to get additional fragmentation information for MS/MS spectra

interpretation. Further details about chemical analysis are described in our previous studies³⁶ and details on quality control and quantification are reported in SI B.

4.2.4 Biotransformation Product Screening and Identification

Organisms were exposed separately to 100 µg L⁻¹ azoxystrobin and 100 µg L⁻¹ prochloraz for 24 h. Each exposure beaker contained 50 organisms. For the exposure to azoxystrobin, additional treatments containing 30 organisms were tested.

Acquired HRMS/MS data were analyzed with Compound Discoverer software version 2.0 (Thermo Scientific) and the software was used for suspect and nontarget screening by comparing treatment and control samples. Details about the applied criteria and parameter settings are found in SI C. Structure elucidation of BTPs was done according to our previous study.³⁶ In brief, structure elucidation was based on (1) the exact mass and the isotopic pattern to assign molecular formulas and on (2) MS/MS spectra information to identify diagnostic fragments or losses either specific for one structure or for several positional isomers.

4.2.5 Toxicokinetics of Azoxystrobin

Organisms were exposed to 80 µg L⁻¹ azoxystrobin in the 24 h uptake phase and were sampled at 7 different time points. For the 120 h depuration phase, organisms were transferred to clean medium and were sampled at 12 different time points (see SI D). Each beaker contained 30 organisms.

To estimate toxicokinetic rate constants of azoxystrobin a first-order compartment model was applied using Matlab R2015b (Build Your Own Model, <http://www.debttox.nl/about.html>). The model is based on the biotransformation pathway of azoxystrobin in *H. azteca* and is described by the following ordinary differential equations (ODEs), in which we distinguish between the time course of the parent compound, the time course of the sum of all primary BTPs that are directly formed from the parent compound, and the time course of the sum of all secondary BTPs, where a direct precursor BTP was detected:

Parent compound: (1)

$$\frac{dC_{in,p}(t)}{dt} = C_{water}(t) \cdot k_u - C_{in,p}(t) \cdot k_e - C_{in,p}(t) \cdot k_{M,1st,total}$$

Primary BTPs: (2)

$$\frac{dC_{in,M,1st,total}(t)}{dt} = C_{in,p}(t) \cdot k_{M,1st,total} - C_{in,M,1st,total}(t) \cdot k_{eM,1st,total} - C_{in,M,1st,total}(t) \cdot k_{M,2nd,total}$$

Secondary BTPs: (3)

$$\frac{dC_{in,M,2nd,total}(t)}{dt} = C_{in,M,1st,total}(t) \cdot k_{M,2nd,total} - C_{in,M,2nd,total}(t) \cdot k_{eM,2nd,total}$$

where $C_{in,p}(t)$, $C_{in,M,1st,total}(t)$ and $C_{in,M,2nd,total}(t)$ [$\text{nmol kg}_{\text{ww}}^{-1}$] are the whole body internal concentrations in *H. azteca* of the parent compound, the sum of all primary BTPs and the sum of all secondary BTPs, respectively. $C_{\text{water}}(t)$ [nmol L^{-1}] describes the time course of the parent compound in the exposure medium. Measured exposure medium concentrations during the uptake and depuration phase were used as input for C_{water} . Uptake of the parent compound via food, dermal and respiratory surfaces is described by the uptake rate constant k_u [$\text{L kg}_{\text{ww}}^{-1} \text{d}^{-1}$], whereas k_e [d^{-1}] is the direct elimination of the parent compound via passive (respiratory and dermal surfaces) and active (excretion of faeces) processes. $k_{M,1st,total}$ and $k_{M,2nd,total}$ and $k_{eM,1st,total}$ and $k_{eM,2nd,total}$ are the biotransformation rate constants [d^{-1}] and elimination rate constants [d^{-1}] for the sum of primary BTPs and the sum of secondary BTPs, respectively. $k_{eM,2nd,total}$ is a lumped rate constant that includes direct excretion of secondary BTPs as well as elimination due to further biotransformation. All parameters were fitted simultaneously.

The simplest compartment model (see equation 4) for simulating the time course of the parent compound was used to determine in a first step the uptake rate constant k_u [$\text{L kg}_{\text{ww}}^{-1} \text{d}^{-1}$] and k_e [d^{-1}] of the parent compound. In this case k_e is a lumped rate constant covering direct elimination of the parent compound as well as further elimination due to biotransformation. In a second step this k_u was fixed and primary BTPs and secondary BTPs were included into the model, to simultaneously fit their kinetic rate constants and the direct elimination rate k_e of the parent compound.

$$\frac{dC_{in,p}(t)}{dt} = C_{\text{water}}(t) \cdot k_u - C_{in,p}(t) \cdot k_e \quad (4)$$

ODEs were solved numerically (Runge-Kutta algorithm) and fitted to the measured internal concentrations of the parent compound, the sum of primary BTPs, and the sum of secondary BTPs. Best fit parameters were obtained by minimizing the sum of squares (Nelder-Mead Simplex method) between measured and simulated internal concentration. Calculation of 95% confidence intervals for kinetic rate constants was done by profiling likelihoods.

Bioaccumulation factors (BAFs) were either calculated based on the ratio of the internal concentration of the parent compound in the organisms and the concentration of the parent compound in the exposure medium with the requirement of steady-state:

$$\text{BAF} = \frac{C_{in,p}(t)}{C_{\text{water}}(t)} \quad (5)$$

or based on the kinetic rate constants:

$$\text{kinetic BAF}(\text{BAF}_k) = \frac{k_u}{k_e + k_{M,1st,total}} \quad (6)$$

Elimination half-lives ($t_{1/2}$) were calculated based on the total elimination for azoxystrobin, primary BTPs and secondary BTPs:

Parent compound:

$$t_{1/2,p} = \frac{\ln 2}{k_e + k_{M,1st,total}} \quad (7)$$

Primary BTPs:

$$t_{1/2,M,1st,total} = \frac{\ln 2}{k_{eM,1st,total} + k_{M,2nd,total}} \quad (8)$$

Secondary BTPs:

$$t_{1/2,M,2nd,total} = \frac{\ln 2}{k_{eM,2nd,total}} \quad (9)$$

4.2.6 Half Maximal Inhibitory Concentrations of Prochloraz ($IC_{50, PRZ, AZS}$)

To determine the CYP inhibition potency of prochloraz in terms of $IC_{50, PRZ, AZS}$, 30 organisms per beaker were pre-exposed for 18 h to varying prochloraz concentrations (0 (control), 0.19, 0.37, 0.74, 3.7, 7.4, 22, 37, 74 and 372 $\mu\text{g L}^{-1}$). Afterwards, azoxystrobin was added to reach a final substrate concentration of 40 $\mu\text{g L}^{-1}$. Incubation with the substrate lasted 24 h. Control samples were prepared in triplicate.

Internal concentrations of azoxystrobin and associated BTPs in the treatment samples were compared to those in the control samples and the $IC_{50, PRZ, AZS}$ were determined by fitting a four-parameter log-logistic model (see SI H) available in the R⁴⁸ package “drc” from Ritz and Streibig (2005)⁴⁹.

4.3 Results and Discussion

4.3.1 Identified Biotransformation Products of Azoxystrobin and Prochloraz in *H. azteca* compared to *G. pulex*

Both compounds showed complex biotransformation patterns in *H. azteca*. For azoxystrobin, 29 mostly tentatively identified BTPs were detected (see Figure 4-2 and SI J), whereas for prochloraz 34 (including 7 minor BTPs with unclear structure) mostly tentatively identified BTPs were detected (see SI J and selected BTPs displayed in Figure 4-1). Similar to *G. pulex*, most BTPs were formed by oxidation and/or conjugation reactions. Nearly all BTPs that had been identified in our previous work in *G. pulex* for azoxystrobin (18 BTPs)³³ and prochloraz (18 BTPs)³⁶ were also identified in *H. azteca*. The exposure concentration in the *H. azteca* screening was half of that used in the *G. pulex* screening. However, for *G. pulex* no substantial differences in the number of detected BTPs were observed either using exposure concentrations of 200 or 100 $\mu\text{g L}^{-1}$ ($\sim 300\text{-}500 \text{ nmol L}^{-1}$)^{33, 36} since the limits of quantification (LOQs) for azoxystrobin, prochloraz and their BTPs were less than 2.5 $\text{nmol kg}_{\text{ww}}^{-1}$ in the LC-HRMS/MS method used (see SI B). *G. pulex* BTPs that were not detected in *H. azteca* were predominantly related to glutathione conjugation products and their enzymatic degradation products; additionally, one sulfate conjugation product of azoxystrobin (AZ_M468) that was found only at low concentrations was also not detected. One cysteine product of prochloraz (PRZ_M429) as well as cysteine products of azoxystrobin resulting from glutathione conjugation at the aromatic ring (AZ_M328a,b) identified in *G. pulex* were not detected in *H. azteca*, partially due to their role as precursor for further transformations in *H. azteca*. Instead, additional BTPs resulting from the breakdown of glutathione were identified in *H. azteca* such as PRZ_M558, characterized by a loss of glycine (see Figure 4-1). As already observed in *G. pulex*, most biotransformation reactions of prochloraz lead to a change at the active imidazole ring moiety, through either imidazole ring cleavages or a loss of the imidazole ring (see SI J, and Figure 4-3c and d).

In addition to conjugation reactions with glucose, sulfate, glucose-sulfate, and glutathione resulting in cysteine products, which were identified in *G. pulex*, new conjugation reactions with taurine and glucose-malonyl were identified in *H. azteca* (see Figure 4-1, Figure 4-2 and SI J). Taurine conjugation is catalyzed by bile acid-CoA:amino acid N-acyltransferase (BAT) and BAT activities have been reported for numerous species, such as humans, fish and rat.⁵⁰⁻⁵¹ Taurine conjugations have been identified for xenobiotic carboxylic acids in crayfish⁵², lobster⁵³ and fish⁵⁴⁻⁵⁶, whereas no taurine conjugation products have been described so far in small aquatic invertebrates. In many species, predominately in vertebrates, the main physiological function of taurine together with glycine is the conjugation of biliary acids to increase their aqueous solubility.⁵⁰⁻⁵¹ Substrates for taurine and glycine conjugations are carboxylic acids, such as the ester hydrolysis product AZ_M390b of azoxystrobin, which is most likely the reason why taurine conjugations were only identified for azoxystrobin and not for prochloraz. Whether taurine conjugation is specific for biotransformation in *H. azteca* compared to *G. pulex* needs to be confirmed by testing more substrates that contain a carboxylic acid moiety as parent substance or substrates where biotransformation leads to a

carboxylic acid BTP. In addition to glucose-sulfate conjugations detected in *G. pulex* and *H. azteca*, glucose-malonyl conjugations were identified for azoxystrobin and prochloraz in *H. azteca*. Malonyl transfer to a glucoside is a known biotransformation reaction in plants⁵⁷⁻⁵⁹ but only one study identified 6-O-malonyl-glucosides in terrestrial invertebrates.⁶⁰ In plants, malonylation is assumed to act as a signal for the translocation into the vacuole or extracellular space.⁵⁷⁻⁵⁸

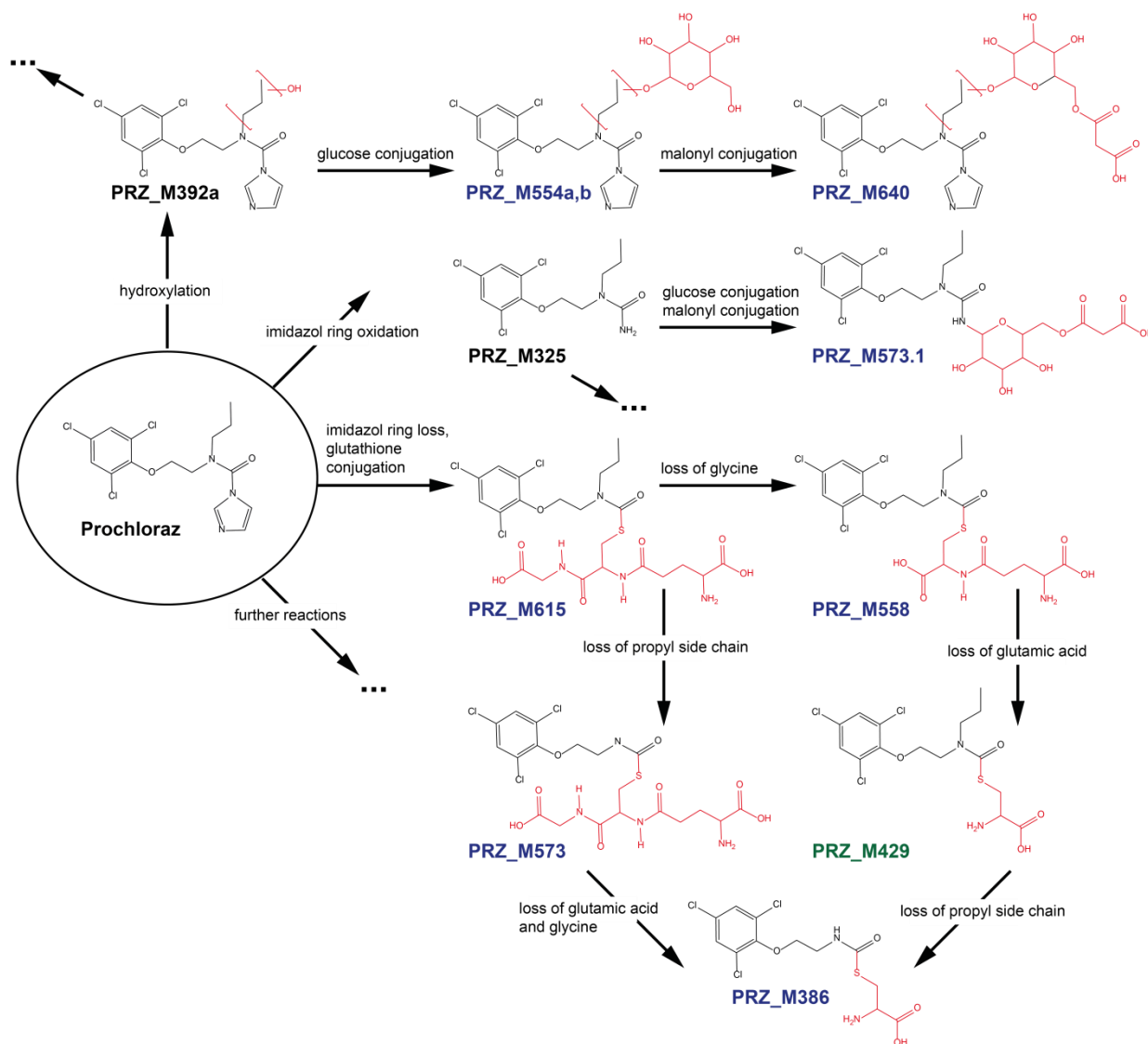


Figure 4-1: Detail of the proposed biotransformation pathway of prochloraz in *H. azteca* and *G. pulex* with focus on the newly identified conjugation products in *H. azteca* compared to *G. pulex*. Shown are the biotransformation reactions leading to glucose-malonyl conjugation products as well as to glutathione conjugation products and their enzymatic degradation products. BTPs written in black were detected in both species, whereas BTPs written in green are specific for *G. pulex* and BTPs written in blue are specific for *H. azteca*. Structural modifications of the BTPs are highlighted in red.

In general, we hereby confirmed the conservation of enzymes such as CYPs and transferases across different invertebrate species^{40-41, 61} and the relevance of conjugation reactions as important routes of biotransformation in aquatic invertebrates.^{33-34, 36, 62-65} However, two aquatic invertebrate species from the same taxonomic order of *Amphipoda* already showed differences concerning their transferase activities and/or presence of transferases. Most observed conjugation reactions add a negative charge to the molecule making the BTPs more water soluble and increasing their mobility inside the organism compared to the parent compound. However, cell membranes are passively permeable for neutral compounds, whereas charged molecules cannot pass easily.⁶⁶ Clarification is needed as to whether glucosides that are further conjugated with sulfate or malonyl have a specific function as signals for sequestration (as it is described in plants) or if these conjugates, present as anions at physiological pH (~5-8, dependent on the subcellular compartment)⁶⁷, are substrates for active carrier mediated transport.^{65, 68-69}

Figure 4-2: Proposed biotransformation pathway of azoxystrobin in *G. pulex* and *H. azteca* based on the validated biotransformation pathway of *G. pulex*.³³ Structural modifications of the BTPs are highlighted in red. BTPs written in black were detected in both species, whereas BTPs written in green are specific for *G. pulex* and BTPs written in blue are specific for *H. azteca*. Superscript text after italic written BTPs marks BTPs that were either not detected in the kinetic experiments (k) or not detected in the inhibition experiments (i, IC₅₀, PRZ, AZ) of *G. pulex* (G) or *H. azteca* (H) but in the BTP screening experiment.

The color and shape of the arrows distinguishes between biotransformation reaction types and test species (blue: *H. azteca*, green: *G. pulex*): continuous: reaction influenced by prochloraz; dashed: reaction influenced by prochloraz only due to previous reactions being influenced by prochloraz; continuous with circle: reaction not influenced by prochloraz; continuous light blue: no information on influence of prochloraz for *H. azteca*. The small blue stars located at the arrowhead of the prochloraz influenced biotransformation reaction towards the BTPs AZ_M392 and AZ_M378 for *H. azteca* mark the unexpected increase in internal concentrations of AZ_M392 and AZ_M378 with increasing prochloraz concentration.

†) AZ_M554 is actually characterized by two low intensity peaks but it is unclear whether AZ_M554 is addition-ally formed out of AZ_M390b.

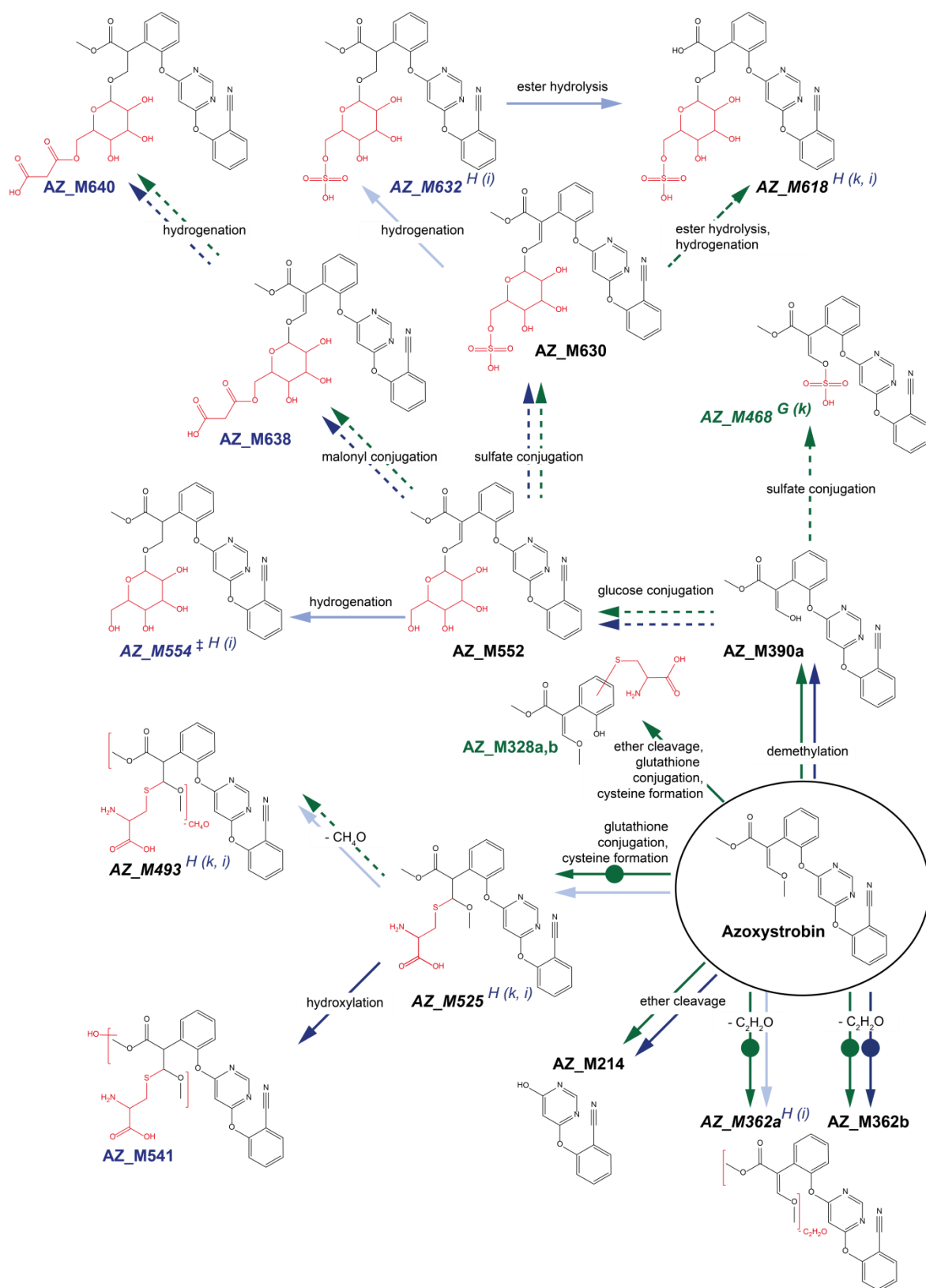


Figure 4-2: For figure caption refer to page 223.

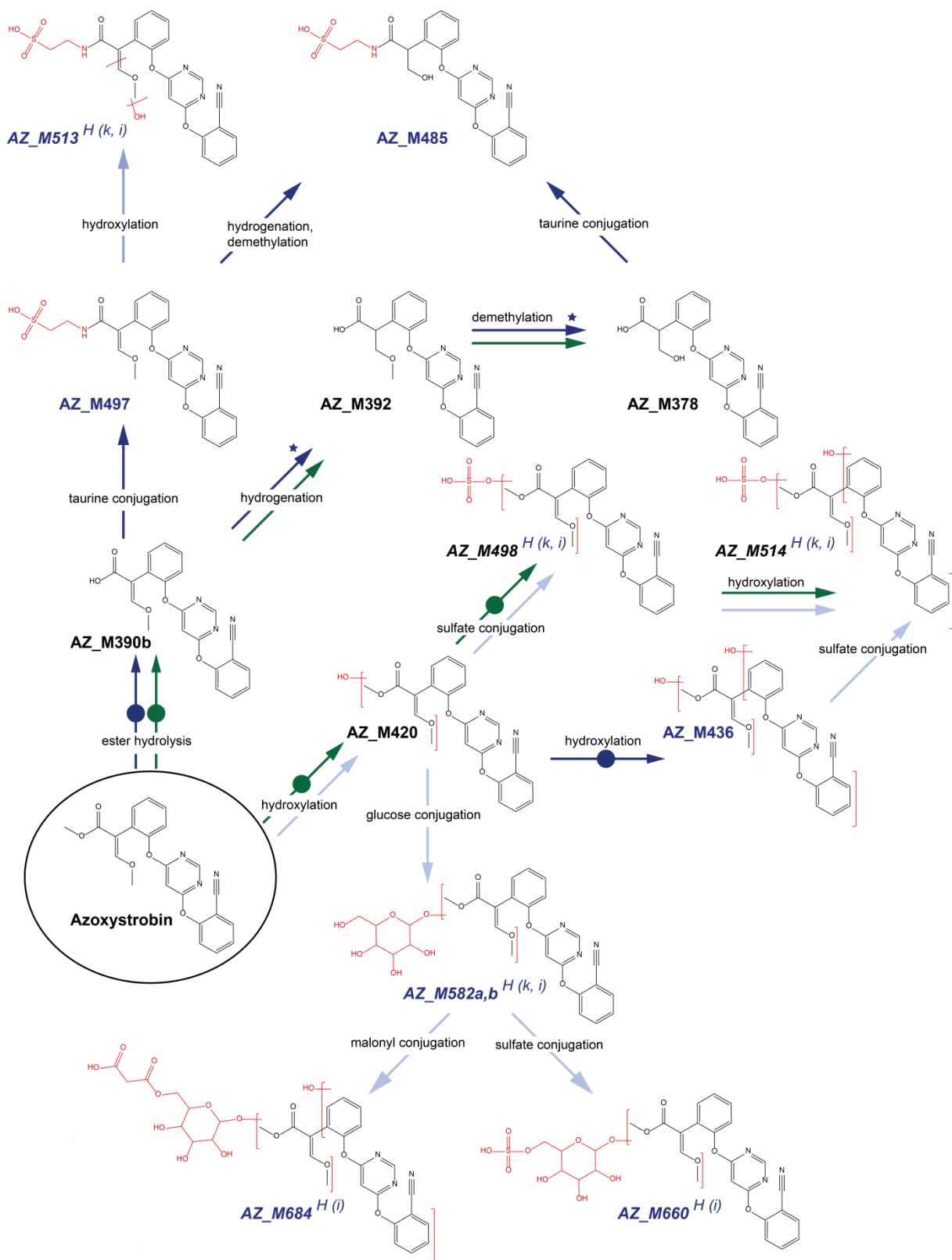


Figure 4-2 continued: For figure caption refer to page 223.

4.3.2 Influence of Biotransformation on Bioaccumulation in *H. azteca* and *G. pulex*

BAFs were calculated based on the internal concentrations and the exposure medium concentrations after 24 h exposure. Bioaccumulation of azoxystrobin was similar in *H. azteca* and *G. pulex* with BAFs of approximately $5 \text{ L kg}_{\text{ww}}^{-1}$, whereas bioaccumulation of prochloraz was by a factor of three higher in *H. azteca* ($\approx 163 \text{ L kg}_{\text{ww}}^{-1}$) compared to *G. pulex* ($\approx 57 \text{ L kg}_{\text{ww}}^{-1}$) (see Figure 4-3). It was assumed that prochloraz and azoxystrobin were at steady state after 24 h, although for prochloraz no kinetic experiment was performed in *H. azteca* to confirm this assumption. However, for *G. pulex* steady state was reached for prochloraz after 24 h. Exposure concentrations of azoxystrobin and prochloraz, important for the calculation of BAFs, varied from nominal concentrations on average by 3% to 7% for azoxystrobin and prochloraz, respectively. Exposure concentrations did not decline during the 24 h exposure phase of the azoxystrobin kinetic experiment and declined during the screening experiment by 6% for azoxystrobin and by 17% for prochloraz (see SI F).

Overall, bioaccumulation of azoxystrobin and prochloraz was low in both species according to the REACH criteria⁵, which designated compounds as bioaccumulative when BAFs exceed 2000 L kg^{-1} .

Comparison of Internal Concentrations of Azoxystrobin, Prochloraz and their associated BTPs after 24 h Exposure

Figure 4-3 shows a comparison of the internal concentrations of the parent compounds azoxystrobin and prochloraz and their BTPs in *H. azteca* and *G. pulex* after 24 h exposure. Comparing internal concentrations at one time point is of limited value since it is only a snapshot, and does not contain information on the toxicokinetics such as on how rapidly BTPs are further biotransformed or excreted from the organism. Only toxicokinetic rate constants provide a more profound understanding of the relative importance of biotransformation. However, in the case of steady state, single time points allow for the calculation of BAFs and give a first impression on ongoing biotransformation processes.

For both compounds and species, the unchanged parent compounds dominated the total internal concentration after 24 h and secondary BTPs represented the second big proportion of the total internal concentration after 24 h exposure. The proportion of azoxystrobin BTPs formed was very similar for both species and represented around 50% of the total internal concentration. Major primary BTPs of azoxystrobin in *G. pulex* and *H. azteca* were the ester hydrolysis (AZ_M390b) and the demethylation product (AZ_M390b). Secondary BTPs of azoxystrobin in *G. pulex* were predominantly characterized by changes at the (*E*)-methyl β -methoxyacrylate group (AZ_M392 and AZ_M378), whereas in *H. azteca* the glucose-malonyl (AZ_M638 and AZ_M640) and taurine (AZ_M497) conjugation products comprised the biggest portion.

For prochloraz, the percentage of the total internal concentration after 24 h attributed to BTPs differed in the two species (40% in *G. pulex* and 25% in *H. azteca*). Assuming that the proportions of BTPs formed after 24 h approximately reflect the biotransformation rate constants, as observed for *G. pulex* (PRZ_M282 and PRZ_M353 had the largest estimated

biotransformation rate constants in our previous study³⁶), biotransformation seems to be less important in *H. azteca* resulting in higher bioaccumulation of prochloraz compared to *G. pulex*. Primary BTPs of prochloraz only contributed $\approx 2\%$ to the total internal concentration in both species, whereas secondary BTPs of prochloraz resulting from imidazole ring oxidation (PRZ_M353 \rightarrow PRZ_M325 \rightarrow PRZ_M282) represented the highest proportion of the total internal concentration in both *G. pulex* and *H. azteca*. However, PRZ_M353 was most prevalent in *H. azteca*, while PRZ_M282 was most prevalent in *G. pulex*, pointing towards imidazole ring oxidations at different rates. Although primary BTPs of prochloraz for both species only represented a small portion of the total internal concentration, they contribute to the elimination of the parent compound and are often precursors of secondary BTPs. Obviously, the rate of further biotransformation to secondary BTPs was high in both species.

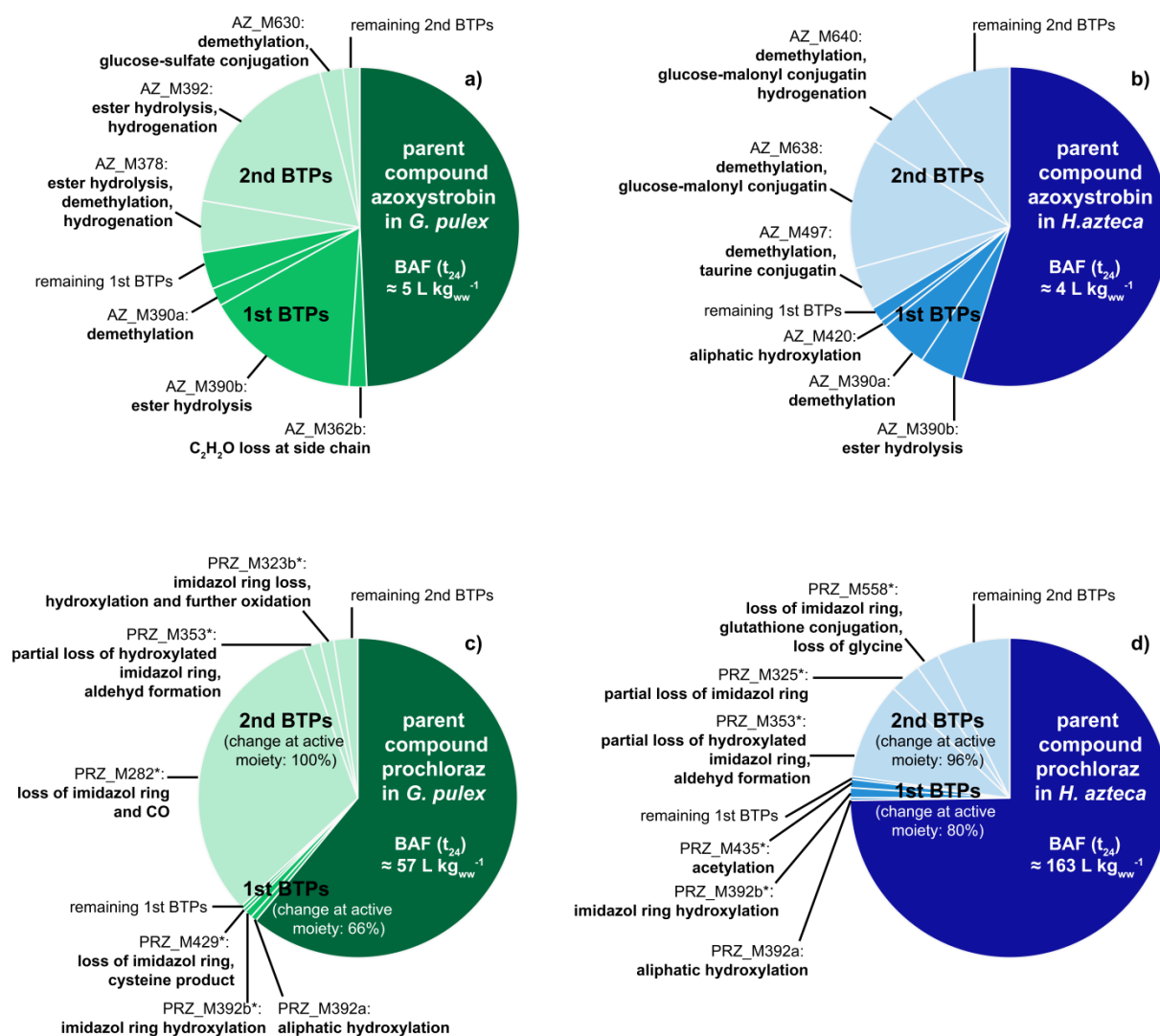


Figure 4-3: Comparison of internal concentrations of parent compounds and associated BTPs after 24 h exposure to either prochloraz or azoxystrobin (exposure concentrations of $100 \mu\text{g L}^{-1}$ (*H. azteca*) and $200 \mu\text{g L}^{-1}$ (*G. pulex*), respectively) in *G. pulex* (green, panel (a) and (c)) and *H. azteca* (blue, panel (b) and (d)) normalized to the total internal concentration (sum of parent compound and associated BTPs). Each panel shows the proportions of the parent compound, the sum of primary BTPs (1st BTPs) and the sum of secondary BTPs (2nd BTPs). For primary and secondary BTPs, the three BTPs that reached the highest internal concentrations after 24 h exposure are displayed separately. An asterisk for PRZ BTPs marks BTPs where the active azole moiety was altered during biotransformation. BAFs are reported based on the ratio of the concentration of the parent compound in the organism and of the concentration of the parent compound in the exposure medium with the assumption of steady state.

Comparing Toxicokinetic Processes of Azoxystrobin

To understand the importance of biotransformation on bioaccumulation more comprehensively, an additional kinetic experiment was performed for azoxystrobin. Azoxystrobin exposure concentrations during the uptake phase were the same as during the *G. pulex* kinetic experiment ($80 \mu\text{g L}^{-1}$). Reducing the sample wet weight and thereby the number of test organisms (from 50 to 30 *H. azteca* per sample) required for measuring internal concentrations at many time points during the uptake and depuration phase was tested and regarded as acceptable (see SI I).

Seven low concentrated BTPs could not be included in the kinetic model (see Figure 4-2), either as a result of hindered quantification (lower sensitivity of sulfate-containing BTPs in positive electrospray ionization mode, see SI I) or as a result of only single detects after 24 h exposure, preventing the modeling of toxicokinetic processes.

The high number of detected BTPs made the toxicokinetic modeling challenging, since primary and secondary BTPs need to be defined, which requires a detailed knowledge on the biotransformation pathway. Using a not fully elucidated biotransformation pathway, in which precursors are not always clearly assigned, adds to model uncertainty. Moreover, the more BTPs included in the kinetic model, the more toxicokinetic rate constants have to be determined, which can add to parameter uncertainty, depending on the amount and quality of underlying data. Therefore, to compare toxicokinetics of azoxystrobin between *G. pulex* and *H. azteca* a reduced pathway was used, simultaneously modeling the time course of the internal concentration of the parent compound azoxystrobin, the time course of the internal concentration of the sum of all detected primary BTPs, and the time course of the internal concentration of the sum of all detected secondary BTPs. Consequently, no biotransformation rate constant of single BTPs ($k_{Mx, 1st \text{ or } 2nd}$) can be compared, but the model still allows for an estimation of the importance of biotransformation since $k_{M, 1st, total}$ indicates how much biotransformation adds to the reduction of parent compound bioaccumulation.

The reduced azoxystrobin kinetic model of *G. pulex* was compared to the detailed modeling of kinetic rate constants of single BTPs in *G. pulex* carried out in our previous study and similar results were obtained.³³ Both models indicate that the sum of primary biotransformation rate constants $k_{Mx, 1st}$ or the total primary biotransformation rate constant $k_{M, 1st, total}$ contribute approximately 10% to the total elimination of azoxystrobin. Uptake and elimination rate constants of azoxystrobin in both models were comparable resulting in BAF_{ks} of $\approx 5 \text{ L kg}_{ww}^{-1}$.

Figure 4-4 shows the measured and modeled time courses of whole body internal concentrations of azoxystrobin and the sum of associated primary BTPs and secondary BTPs in *H. azteca* (panel a) and *G. pulex* (panel b). In general, the first-order compartment kinetic model implemented with a reduced biotransformation pathway and simultaneous fitting of all parameters was able to describe the experimental data. However, especially the modeled time courses of the parent compound for both species did not perfectly reflect the measured internal concentrations. For *H. azteca*, the experimental data hinted at a more

rapid uptake than was predicted, whereas for *G. pulex* uptake was well captured by the model but simulated elimination during the depuration phase was much faster than proposed by the experimental data. This disparity between model and experimental data can strongly influence the interpretation of the relative importance of biotransformation, since it relies on the comparison of $k_{M, 1st, total}$ to the total elimination of the parent compound ($k_e + k_{M, 1st, total}$). As a result, biotransformation would be of minor relevance in *G. pulex*, only contributing approximately 10% to the total elimination, whereas in *H. azteca* biotransformation would play a major role as biotransformation represents more than 90% of the total elimination (see Figure 4-4).

In addition to simultaneously fitting of all rate constants, another modeling approach is to first determine the uptake and elimination rate of the parent compound by fitting the simplest compartment model (see equation 4) with only two parameters (k_u and $k_{e, total\ or\ parent}$), to either the total internal concentrations (if radioactivity measurement is used) or to the internal concentration of the parent compound. Then, in a second step, k_u is fixed, BTPs are included and the remaining rate constants are fitted simultaneously. This stepwise approach ensures that stronger weight is given to the uptake rate during the first step, since only two parameters are fitted at once.

According to this approach, uptake and elimination rates for azoxystrobin in *H. azteca* and *G. pulex* were first determined by modeling only the kinetics of the parent compound. With this stepwise approach, the mismatch between model and experimental data for *H. azteca* during the uptake phase decreased compared to the simultaneously fitting approach of all rate constants, as uptake is now simulated more rapidly; however, elimination of the parent compound is predicted too fast (see SI E). For *G. pulex*, the simulation did not change with this stepwise approach, since estimated uptake rates are almost the same with either of the models.

In general, the simultaneously fitting approach of all rate constants and the stepwise fitting approach showed the same result that for *H. azteca* $k_{M, 1st, total}$ seemed to contribute more to the total elimination of the parent compound compared to *G. pulex* (see Figure 4-4). Although especially for *G. pulex*, elimination of azoxystrobin was overpredicted by either of the models, elimination of azoxystrobin was faster in *G. pulex* compared to *H. azteca* (see SI E) and consequently the smaller $k_{M, 1st, total}$ of *G. pulex* compared to those of *H. azteca* contributed less to the total elimination. Reason for the discrepancy of actual and simulated elimination could be a longer retention of azoxystrobin in any biomass component of aquatic organisms such as lipids, which is not covered by the applied simple compartment model assuming well-mixed organisms. However, elimination of azoxystrobin was simulated much better in *H. azteca*, although both species do not significantly deviate in their total lipid content (1.3-1.8% of wet weight)^{28, 70}, indicating that the change to a more complex model such as a two-compartment model does not necessarily improve the match between experimental data and model and might be more important for more lipophilic compounds and more lipid rich organisms.⁷¹

The uptake rate in *G. pulex* was significantly higher (see Figure 4-4) compared to *H. azteca* independent of the fitting approach, which is contrary to expectations, since *H. azteca* exhibits a greater surface area to volume ratio compared to *G. pulex* and, with increasing body size, the ventilation volume and gill surface area per unit body weight usually decreases. This implies that smaller aquatic organisms exhibit higher uptake and elimination rates compared to larger aquatic organisms. This relationship has been shown for fish.^{4, 72-75} Nevertheless, the determined uptake rate for azoxystrobin in *H. azteca* was comparable to uptake rates from another study which determined uptake rates for neutral organic chemicals with similar $\log K_{ow}$ to azoxystrobin ($\log K_{ow} = 4.2$, predicted with MarvinSketch⁷⁶) in *H. azteca*.²⁹

Overall, both fitting approaches indicate a greater relevance of biotransformation measured in terms of $k_{M, 1st, total}$ in *H. azteca*. In addition, $k_{M, 2nd, total}$ of both species were five (*H. azteca*) and four (*G. pulex*) times higher than $k_{M, 1st, total}$ (see Figure 4-4), confirming the importance of secondary biotransformation reactions such as conjugation reactions.

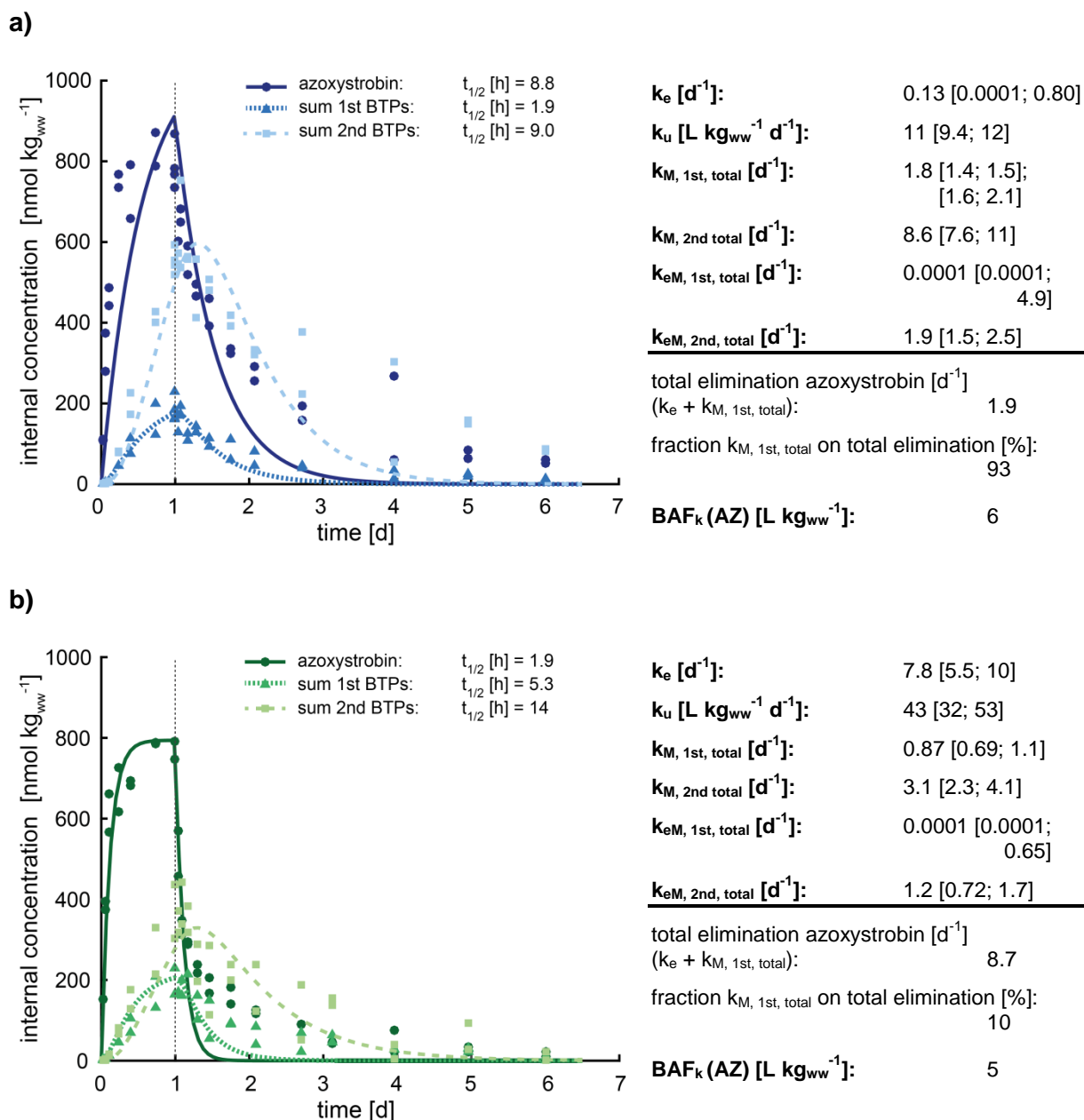


Figure 4-4: Measured (symbols) and modeled (lines) time courses of whole body internal concentrations of azoxystrobin and the sum of associated primary BTPs and secondary BTPs in *H. azteca* (panel a) and *G. pulex* (panel b), as well as modeled elimination half-lives ($t_{1/2}$). The dashed vertical line indicates the change from the uptake (1 d) to the depuration phase (5 d). Toxicokinetic rate constants with respective 95% confidence intervals given in brackets are displayed on the right side of both panels.

4.3.3 CYP Inhibition Strength of Prochloraz in *H. azteca* compared to *G. pulex*

Figure 4-5 shows the CYP inhibition potential of prochloraz towards *H. azteca*, measured in terms of internal concentrations of azoxystrobin and associated BTPs, in comparison to *G. pulex*. In the case of CYP inhibition, higher internal parent compound concentrations and lower internal BTP concentrations (for CYP-catalyzed biotransformation reactions) are expected. It depicts the dose response curves for the $IC_{50, PRZ, AZ}$ determination based on the accumulation of azoxystrobin and the formation of one exemplary BTP, the demethylation product AZ_M390a, in the presence of varying prochloraz concentrations. The $IC_{50, PRZ, AZ}$ for *H. azteca*, calculated based on the dose response curve of the parent compound, was $0.1 \pm 0.01 \mu\text{M}$ ($42 \pm 5 \mu\text{g L}^{-1}$), which is significantly different ($p\text{-value} < 0.05$, see SI H) and approximately five times higher than the $IC_{50, PRZ, AZ}$ determined in *G. pulex*.³³ However, more detailed investigations, such as testing more prochloraz concentrations in the concentration range of inhibition, should be done to confirm this result. $IC_{50, PRZ, AZ}$ s determined via the dose-response curve of the parent compound were comparable to $IC_{50, PRZ, AZ}$ s obtained via the dose-response curves of the primary CYP-catalyzed BTPs of azoxystrobin in both species (see Figure 4-5 and SI H).

Reason for species' sensitivity differences in terms of CYP inhibition are diverse. In general, the internal concentration and thereby the BAF of prochloraz determines the portion of inhibited CYP. As the imidazole ring represents the active part of the molecule by interacting with the heme iron of the CYP,⁷⁷ biotransformation reactions leading to a loss or cleavage of the ring functional moiety decrease the CYP inhibition capacity. In contrast, BTPs with unchanged imidazole ring would add to the CYP inhibition, if we assume that all other factors crucial for CYP inhibition, such as steric and electronic effects of the substituent, as well as hydrophobic interactions in the binding cavity of the CYP, are still present.⁷⁷⁻⁷⁸ Therefore, the total internal concentration of prochloraz, which is the sum of the parent compound and of all BTPs with active moiety, needs to be considered.

Bioaccumulation of prochloraz in *H. azteca* was by a factor of three higher compared to those in *G. pulex* (see Figure 4-3c and d, and SI F). CYPs are located primarily in the membrane of the endoplasmic reticulum, which is an organelle present in all eukaryotic cells, and CYP activity has been shown to be highest in the hepatopancreas, the digestive gland of amphipods.⁴¹ Assuming similar internal partitioning and lipid content of the hepatopancreas in both test species, whole-body internal concentrations are supposed to be suitable surrogates for target site concentrations. BTPs formed through imidazole ring oxidation dominated in both species (see Figure 4-3c and d), thereby reducing the CYP inhibitory capacity of prochloraz. However, toxicokinetic rate constants of prochloraz in *H. azteca* are needed to confirm the importance of BTPs formed by ring loss or cleavages. Furthermore, the composition of specific CYP isoforms within one CYP family or the presence of CYP families can be different in *H. azteca* and *G. pulex*. Consequently, both species can differ in their accessibility for prochloraz CYP inhibition and their ability for azoxystrobin biotransformation.

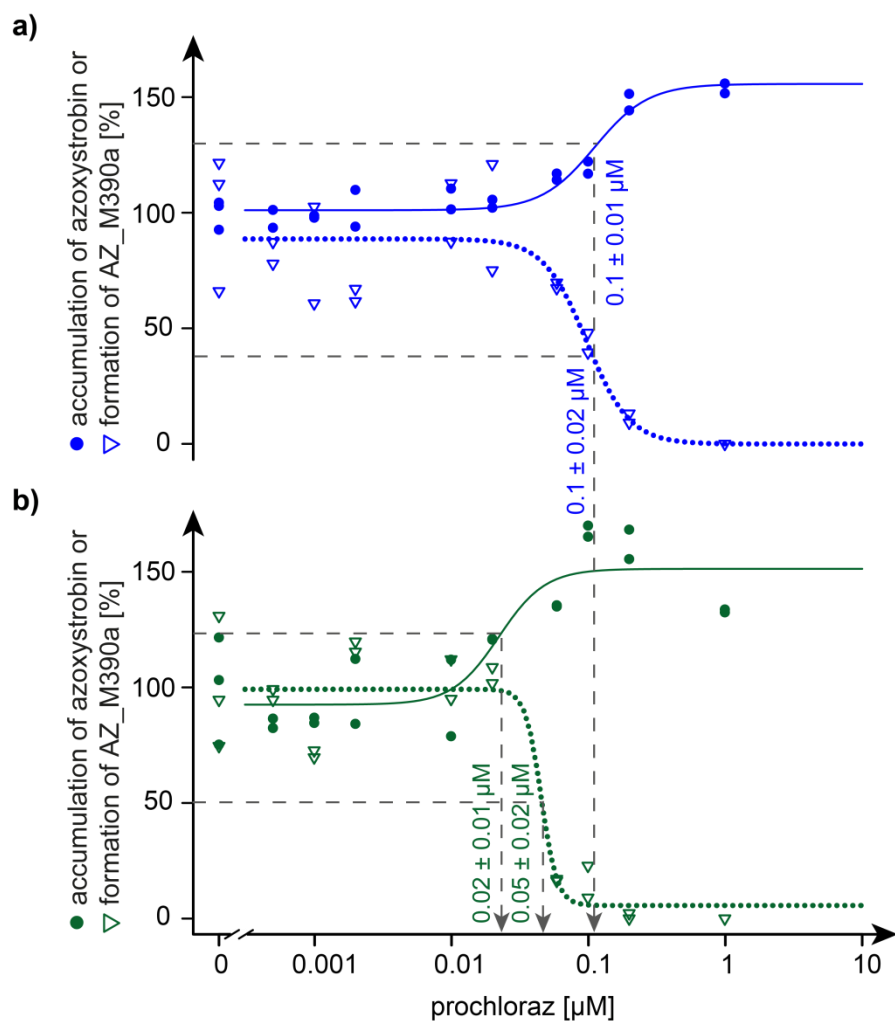


Figure 4-5: Dose-response curves for the $IC_{50, PRZ, AZ}$ determination for *H. azteca* (a) and *G. pulex* (b) based on internal concentration measurements of azoxystrobin and associated BTPs (exemplary AZ_M390a is shown). The dashed lines mark the determined and displayed $IC_{50, PRZ, AZ}$ s.

Regarding the biotransformation pathway of azoxystrobin in both *H. azteca* and *G. pulex*, a similar prochloraz inhibition pattern was observed (see Figure 4-2). Mainly oxidative biotransformation reactions likely to be CYP-catalyzed were influenced by prochloraz, and several secondary biotransformation reactions leading to conjugation products with glucose (AZ_M552), glucose-sulfate (AZ_M630, AZ_M618) or glucose-malonyl (AZ_M638, AZ_M640) were indirectly influenced by prochloraz, due to the inhibited biotransformation reaction of their precursor (AZ_M390a). However, it was not possible to determine the influence of prochloraz on some biotransformation reactions of azoxystrobin in *H. azteca*, since no toxicokinetic experiments were carried out in the presence and absence of one prochloraz concentration. The inhibition by prochloraz in *H. azteca* was determined through evaluation of the data collected for the $IC_{50, PRZ, AZ}$ determination, in which similar substrate concentrations of $40 \mu\text{g L}^{-1}$ azoxystrobin were used as in our previous study, for the $IC_{50, PRZ, AZ}$ determination in *G. pulex*.³³ Using exposure concentrations of $100 \mu\text{g L}^{-1}$ azoxystrobin (as in the BTP screening experiment) during the $IC_{50, PRZ, AZ}$ determination was not feasible due to the increasing accumulation and subsequent toxicity of azoxystrobin in the presence of increasing prochloraz concentrations.

Contrary to expectations, the reaction of taurine conjugation was influenced by prochloraz, even though biotransformation of the supposed precursor of the taurine conjugation product (AZ_M497), the esterase catalyzed azoxystrobin acid (AZ_M390b), showed no influence by prochloraz. Transferases catalyzing the taurine conjugation (BAT) should not be inhibited by prochloraz, pointing towards the inhibition of another process, possibly the inhibition of the taurine synthesis or adaptation of the taurine synthesis to the internal bile acid concentration, whose synthesis is CYP-catalyzed.⁷⁹ Steroid molecules are present in all invertebrate species but the presence and function of bile acids and their involvement in lipid digestion is much better understood in vertebrates than in invertebrates.^{50, 80-81} Additionally, one could argue that the precursor was assigned wrongly and that the taurine conjugation is actually formed out of the demethylation product (AZ_M390a), similar to the glucose conjugation (AZ_M552) and the subsequent sulfate (AZ_M630, AZ_M618) and malonyl (AZ_M638, AZ_M640) conjugations. However, substrates for taurine conjugation are known to be carboxylic acids, such as azoxystrobin acid (AZ_M390b). Furthermore, unexpected increases in internal concentrations of AZ_M392 and AZ_M378, which also have the acid AZ_M390b as a precursor, were observed with increasing prochloraz concentrations, probably because with a smaller biotransformation rate constant of AZ_M497 in the presence of prochloraz, a higher concentration of AZ_M390b is available as precursor for the formation of AZ_M392 and AZ_M378. Biotransformation rate constants $k_{Mx, 1st\ or\ 2nd}$ of single BTPs in the presence and absence of prochloraz are needed for further investigation of the inhibited taurine conjugation and its consequences for other biotransformation processes.

Total internal concentrations (the sum of parent compound and its formed BTPs) should remain constant independent of the presence of prochloraz, assuming that BTPs are not excreted faster than the parent compound and that prochloraz only affects biotransformation involving CYP-catalyzed reactions. Modeled elimination half-lives ($t_{1/2}$) (see Figure 4-4) show that the sum of primary BTPs is eliminated faster, whereas the sum of secondary BTPs exhibits longer $t_{1/2}$ in *H. azteca*. Biotransformation of azoxystrobin resulted in more polar compounds compared to the parent compound (see log D_{ow} values in SI J). However, especially secondary BTPs including conjugation products were retained longer in the organism compared to the parent compound. This finding is in line with other studies that have also observed a slow elimination of polar BTPs.^{29, 33-34, 36, 53, 63, 82} Yet, total internal concentrations increased in the presence of specific prochloraz concentrations ($74\ \mu\text{g L}^{-1}$ (0.1 μM) and $372\ \mu\text{g L}^{-1}$ (1 μM), see SI G), indicating the influence of prochloraz on other toxicokinetic processes such as uptake, similar to what we observed in *G. pulex*.³³

4.3.4 *H. azteca* as Alternative Test Organisms for Bioconcentration Studies?

BCFs are required in the European REACH regulation (EC no. 1907/2006)⁵ if chemicals exhibit log K_{ow} s ≥ 3 or if there is other evidence of bioaccumulation potential. However, there is the need for alternative non-vertebrate test species for BCF determination in the context of the 3R⁹ (replacement, reduction and refinement). Preliminary results of Schlechtriem et al. (2015)¹⁰ showed that comparable BCFs were obtained for lipophilic compounds (log K_{ow} > 5) in *H. azteca* and rainbow trout. For azoxystrobin, no fish BCFs for comparison are available

due to a log $K_{ow} < 3$ (according to IUPAC⁸³), whereas for prochloraz (log $K_{ow} > 3$) a rainbow trout BCF of $\approx 200 \text{ L kg}^{-1}$ was determined.⁸⁴ This value is close to the BAF of 163 L kg^{-1} determined in this study for prochloraz in *H. azteca*. Ashauer et al. (2012)³⁴ have shown that dietary uptake of selected organic chemicals (log K_{ow} from 0.33 to 5.15) in *G. pulex* contributed by less than 1% to the total uptake. Therefore, our measured BAFs should be close to BCFs, enabling a comparison of fish BCFs to *H. azteca* BAFs. Although the BCF for fish and the *H. azteca* BAF are not lipid normalized, both values are in the same range and are much lower than the threshold of 2000 L kg^{-1} given in the REACH regulation.⁵ Debrauwer et al. (2001)⁸⁵ identified the imidazole ring cleavage product PRZ_M353 as major BTP in rainbow trout similar to prochloraz biotransformation in *H. azteca*, confirming the importance of imidazole ring oxidation. Conjugation in rainbow trout took place via glucuronidation, which is in line with the finding by James (1987)⁵⁶ that glucuronidation is more common in fish, whereas invertebrates more often form glucose conjugation products. These first results point towards the suitability of *H. azteca* as alternative non-vertebrate test species for BCF determination, but more substances with different physicochemical properties will need to be investigated.

4.3.5 Environmental Relevance

By comparing biotransformation routes in *H. azteca* to those in the native invertebrate species *G. pulex*, we showed that enzymes, especially CYPs, seem to be predominantly conserved between the two invertebrate species, as nearly all BTPs previously identified in *G. pulex* were also detected in *H. azteca*. However, additional conjugation routes with taurine and malonyl were identified in *H. azteca*, suggesting differences in transferase activity and/or the presence of transferases compared to *G. pulex*. Toxicokinetic modeling of azoxystrobin indicated that biotransformation is more relevant in *H. azteca* compared to *G. pulex*. Certainly, toxicokinetic rate constants of additional compounds, especially of compounds which are more bioaccumulative, are required to further explore the significance of biotransformation in terms of reducing bioaccumulation in aquatic invertebrate species.

The determined $IC_{50, PRZ, AZ}$ suggests that *H. azteca* was at a factor of five less sensitive to prochloraz-induced CYP inhibition. However, these species' sensitivity differences seem to be of minor importance with regard to ecotoxicological risk assessment, since assessment factors are applied to account for interspecies variability.

In general, the use of test animals that can be easily cultured is always advantageous in that it provides a homogenous test population all over the year. Knowing the age and the life cycle stage of a test population reduces the animals' variability, for example in terms of enzyme composition. Due to the smaller size of *H. azteca* compared to *G. pulex*, more single organisms are needed to reach a sufficient sample wet weight, which reduces the intraspecies variability necessary for reliable results. In contrast to vertebrates, invertebrates are not protected in a legal context.⁸ From an ethical point of view, it is questionable if the use of more test animals per sample is really beneficial. However, *H. azteca* can be cultured easily and no collection of test animals from aquatic ecosystems is necessary.

Acknowledgment

Special thanks go to Emma Schymanski (Eawag) for all her support with computational MS/MS annotation. Furthermore, we thank Christian Schlechtriem and his group (Fraunhofer-Institut) for advice with culturing *H. azteca* and Jennifer Schollée (Eawag) for discussion.

References

- [1] Malaj, E.; von der Ohe, P. C.; Grote, M.; Kuehne, R.; Mondy, C. P.; Usseglio-Polatera, P.; Brack, W.; Schaefer, R. B., Organic chemicals jeopardize the health of freshwater ecosystems on the continental scale. *Proceedings of the National Academy of Sciences of the United States of America* **2014**, *111* (26), 9549-9554.
- [2] Schwarzenbach, R. P.; Escher, B. I.; Fenner, K.; Hofstetter, T. B.; Johnson, C. A.; Von Gunten, U.; Wehri, B., The challenge of micropollutants in aquatic systems. *Science* **2006**, *313* (5790), 1072-1077.
- [3] Arnot, J. A.; Gobas, F. A. P. C., A food web bioaccumulation model for organic chemicals in aquatic ecosystems. *Environ. Toxicol. Chem.* **2004**, *23* (10), 2343-2355.
- [4] Barron, M. G., Bioconcentration. Will water-borne organic chemicals accumulate in aquatic organisms? *Environmental Science & Technology* **1990**, *24* (11), 1612-1618.
- [5] EC. Regulation No. 1907/2006 of the European Parliament and of the Council Concerning the Registration, Evaluation, Authorization and Restriction of Chemicals. 2006.
- [6] OECD, *Test No. 305: Bioaccumulation in Fish: Aqueous and Dietary Exposure*. OECD Publishing.
- [7] OECD, *Test No. 315: Bioaccumulation in Sediment-dwelling Benthic Oligochaetes*. OECD Publishing.
- [8] Directive 2010/63/EU of the European Parliament and of the Council on the protection of animals used for scientific purposes. 2010.
- [9] Russell, W. M. S.; Burch, R. L., *The principles of humane experimental technique*. Methuen: London, 1959.
- [10] Schlechtriem, C.; Kampe, S.; Bruckert, H. J.; Schaefers, C.; L'Haridon, J. In *Bioconcentration tests with fish and the freshwater amphipod Hyalella azteca. Are the results comparable?*, SETAC Europe 25th Annual Meeting, Barcelona, Spain, Barcelona, Spain, 2015.
- [11] Borgmann, U.; Ralph, K. M.; Norwood, W. P., Toxicity test procedures for *Hyalella azteca*, and chronic toxicity of cadmium and pentachlorophenol to *H. azteca*, *Gammarus fasciatus*, and *Daphnia magna*. *Archives of Environmental Contamination and Toxicology* **1989**, *18* (5), 756-764.
- [12] EPA, Methods for measuring the toxicity and bioaccumulation of sediment-associated contaminants with freshwater invertebrates. **2000**.
- [13] Ingersoll, C. G.; Brunson, E. L.; Dwyer, F. J.; Ankley, G. T.; Benoit, D. A.; Norberg-King, T. J.; Burton, G. A.; Hoke, R. A.; Landrum, P. F.; Winger, P. V., Toxicity and bioaccumulation of sediment-associated contaminants using freshwater invertebrates: A review of methods and applications. *Environ. Toxicol. Chem.* **1995**, *14* (11), 1885-1894.
- [14] Bartlett, A. J.; Struger, J.; Grapentine, L. C.; Palace, V. P., Examining impacts of current-use pesticides in Southern Ontario using in situ exposures of the amphipod *Hyalella azteca*. *Environ. Toxicol. Chem.* **2016**, *35* (5), 1224-1238.
- [15] Kunz, P. Y.; Kienle, C.; Gerhardt, A., *Gammarus* spp. in aquatic ecotoxicology and water quality assessment: toward integrated multilevel tests. *Rev. Environ. Contam. Toxicol.* **2010**, *205*, 1-76.
- [16] Fässler, S.; Stöckli, A., Das Fehlen von Bachflohkrebsen. *Aqua und Gas* **2013**, *4*, 62-72.
- [17] Gerhardt, A.; Kienle, C.; Allan, I. J.; Greenwood, R.; Guigues, N.; Fouillac, A. M.; Mills, G. A.; Gonzalez, C., Biomonitoring with *Gammarus pulex* at the Meuse (NL), Aller (GER) and Rhine (F) rivers with the online Multispecies Freshwater Biomonitor®. *J. Environ. Monit.* **2007**, *9* (9), 979-985.
- [18] Bundschuh, M.; Pierstorf, R.; Schreiber, W. H.; Schulz, R., Positive effects of wastewater ozonation displayed by in situ bioassays in the receiving stream. *Environ. Sci. Technol.* **2011**, *45* (8), 3774-80.
- [19] Gerhardt, A.; Bloor, M.; Mills, C. L., *Gammarus*: Important Taxon in Freshwater and Marine Changing Environments. *International Journal of Zoology* **2011**.

- [20] Maltby, L.; Clayton, S. A.; Yu, H.; McLoughlin, N.; Wood, R. M.; Yin, D., Using single-species toxicity tests, community-level responses, and toxicity identification evaluations to investigate effluent impacts. *Environ. Toxicol. Chem.* **2000**, *19* (1), 151-157.
- [21] Macneil, C.; Dick, J. T. A.; Elwood, R. W., The trophic ecology of freshwater *Gammarus* spp. (Crustacea: Amphipoda): Problems and perspectives concerning the functional feeding group concept. *Biological Reviews of the Cambridge Philosophical Society* **1997**, *72* (3), 349-364.
- [22] Bloor, M. C.; Banks, C. J.; Krivtsov, V., Acute and sublethal toxicity tests to monitor the impact of leachate on an aquatic environment. *Environment International* **2005**, *31* (2), 269-273.
- [23] McCahon, C. P.; Pascoe, D., Culture techniques for three freshwater macroinvertebrate species and their use in toxicity tests. *Chemosphere* **1988**, *17* (12), 2471-2480.
- [24] McCarty, L. S.; Mackay, D., Enhancing ecotoxicological modeling and assessment. *Environ. Sci. Technol.* **1993**, *27* (9), 1719-1728.
- [25] Rozman, K. K.; Doull, J., Dose and time as variables of toxicity. *Toxicology* **2000**, *144* (1-3), 169-178.
- [26] Miller, T. H.; McEneff, G. L.; Stott, L. C.; Owen, S. F.; Bury, N. R.; Barron, L. P., Assessing the reliability of uptake and elimination kinetics modelling approaches for estimating bioconcentration factors in the freshwater invertebrate, *Gammarus pulex*. *Sci. Total Environ.* **2016**, *547*, 396-404.
- [27] Meredith-Williams, M.; Carter, L. J.; Fussell, R.; Raffaelli, D.; Ashauer, R.; Boxall, A. B., Uptake and depuration of pharmaceuticals in aquatic invertebrates. *Environ. Pollut.* **2012**, *165*, 250-8.
- [28] Ashauer, R.; Caravatti, I.; Hintermeister, A.; Escher, B. I., Bioaccumulation kinetics of organic xenobiotic pollutants in the freshwater invertebrate *Gammarus pulex* modeled with prediction intervals. *Environ. Toxicol. Chem.* **2010**, *29* (7), 1625-36.
- [29] Nuutinen, S.; Landrum, P. F.; Schuler, L. J.; Kukkonen, J. V. K.; Lydy, M. J., Toxicokinetics of organic contaminants in *Hyalella azteca*. *Archives of Environmental Contamination and Toxicology* **2003**, *44* (4), 467-475.
- [30] Ashauer, R.; Boxall, A.; Brown, C., Uptake and elimination of chlorpyrifos and pentachlorophenol into the freshwater amphipod *Gammarus pulex*. *Archives of Environmental Contamination and Toxicology* **2006**, *51* (4), 542-548.
- [31] Rubach, M. N.; Ashauer, R.; Maund, S. J.; Baird, D. J.; Van den Brink, P. J., Toxicokinetic variation in 15 freshwater arthropod species exposed to the insecticide chlorpyrifos. *Environ. Toxicol. Chem.* **2010**, *29* (10), 2225-34.
- [32] Schuler, L. J.; Wheeler, M.; Bailer, A. J.; Lydy, M. J., Toxicokinetics of sediment-sorbed benzo a pyrene and hexachlorobiphenyl using the freshwater invertebrates *Hyalella azteca*, *Chironomus tentans*, and *Lumbriculus variegatus*. *Environ. Toxicol. Chem.* **2003**, *22* (2), 439-449.
- [33] Rösch, A.; Gottardi, M.; Vignet, C.; Cedergreen, N.; Hollender, J., Mechanistic Understanding of the Synergistic Potential of Azole Fungicides in the Aquatic Invertebrate *Gammarus pulex*. *Environmental Science & Technology* **2017**, *51* (21), 12784-12795.
- [34] Ashauer, R.; Hintermeister, A.; O'Connor, I.; Elumelu, M.; Hollender, J.; Escher, B. I., Significance of xenobiotic metabolism for bioaccumulation kinetics of organic chemicals in *gammarus pulex*. *Environ. Sci. Technol.* **2012**, *46* (6), 3498-3508.
- [35] Jeon, J.; Kurth, D.; Ashauer, R.; Hollender, J., Comparative toxicokinetics of organic micropollutants in freshwater crustaceans. *Environ. Sci. Technol.* **2013**, *47* (15), 8809-17.
- [36] Rösch, A.; Anliker, S.; Hollender, J., How Biotransformation Influences Toxicokinetics of Azole Fungicides in the Aquatic Invertebrate *Gammarus pulex*. *Environmental Science & Technology* **2016**, *50* (13), 7175-7188.
- [37] Miller, T. H.; Bury, N. R.; Owen, S. F.; Barron, L. P., Uptake, biotransformation and elimination of selected pharmaceuticals in a freshwater invertebrate measured using liquid chromatography tandem mass spectrometry. *Chemosphere* **2017**, *183*, 389-400.

- [38] Guengerich, F. P., Common and uncommon cytochrome P450 reactions related to metabolism and chemical toxicity. *Chem. Res. Toxicol.* **2001**, *14* (6), 611-650.
- [39] Katagi, T., Bioconcentration, Bioaccumulation, and Metabolism of Pesticides in Aquatic Organisms. In *Reviews of Environmental Contamination and Toxicology, Vol 204*, Whitacre, D. M., Ed. 2010; Vol. 204, pp 1-132.
- [40] Snyder, M. J., Cytochrome P450 enzymes in aquatic invertebrates: Recent advances and future directions. *Aquat. Toxicol.* **2000**, *48* (4), 529-547.
- [41] Sole, M.; Livingstone, D. R., Components of the cytochrome P450-dependent monooxygenase system and 'NADPH-independent benzo a pyrene hydroxylase' activity in a wide range of marine invertebrate species. *Comparative Biochemistry and Physiology C-Toxicology & Pharmacology* **2005**, *141* (1), 20-31.
- [42] Nørgaard, K. B.; Cedergreen, N., Pesticide cocktails can interact synergistically on aquatic crustaceans. *Environ Sci Pollut Res* **2010**, *17* (4), 957-967.
- [43] Bjergager, M. B.; Hanson, M. L.; Solomon, K. R.; Cedergreen, N., Synergy between prochloraz and esfenvalerate in *Daphnia magna* from acute and subchronic exposures in the laboratory and microcosms. *Aquat. Toxicol.* **2012**, *110-111*, 17-24.
- [44] Bjergager, M.-B. A.; Hanson, M. L.; Lissemore, L.; Henriquez, N.; Solomon, K. R.; Cedergreen, N., Synergy in microcosms with environmentally realistic concentrations of prochloraz and esfenvalerate. *Aquat. Toxicol.* **2011**, *101* (2), 412-422.
- [45] Cedergreen, N.; Kamper, A.; Streibig, J. C., Is prochloraz a potent synergist across aquatic species? A study on bacteria, daphnia, algae and higher plants. *Aquat. Toxicol.* **2006**, *78* (3), 243-252.
- [46] Kretschmann, A.; Gottardi, M.; Dalhoff, K.; Cedergreen, N., The synergistic potential of the azole fungicides prochloraz and propiconazole toward a short α -cypermethrin pulse increases over time in *Daphnia magna*. *Aquat. Toxicol.* **2015**, *162*, 94-101.
- [47] Borgmann, U., Systematic analysis of aqueous ion requirements of *Hyalella azteca*: A standard artificial medium including the essential bromide ion. *Archives of Environmental Contamination and Toxicology* **1996**, *30* (3), 356-363.
- [48] R Core Team *A language and environment for statistical computing*, R Foundation for Statistical Computing: 2016.
- [49] Ritz, C.; Streibig, J. C., Bioassay analysis using R. *Journal of Statistical Software* **2005**, *12*, 1-22.
- [50] Shonsey, E. M.; Sfakianos, M.; Johnson, M.; He, D. N.; Falany, C. N.; Falany, J.; Merkler, D. J.; Barnes, S., Bile acid coenzyme A: Amino acid N-acyltransferase in the amino acid conjugation of bile acids. In *Phase II Conjugation Enzymes and Transport Systems*, Sies, H.; Packer, L., Eds. 2005; Vol. 400, pp 374-394.
- [51] Testa, B.; Kraemer, S. D., The Biochemistry of Drug Metabolism - An Introduction Part 4. Reactions of Conjugation and Their Enzymes. *Chemistry & Biodiversity* **2008**, *5* (11), 2171-2336.
- [52] Barron, M. G.; Hansen, S. C.; Ball, T., Pharmacokinetics and metabolism of triclopyr in the crayfish (*Procambarus clarki*). *Drug Metabolism and Disposition* **1991**, *19* (1), 163-167.
- [53] James, M. O., Disposition and taurine conjugation of 2,4-dichlorophenoxyacetic acid, 2,4,5-trichlorophenoxyacetic acid, bis(4-chlorophenyl)acetic acid, and phenylacetic acid in the spiny lobster, *Panulirus argus*. *Drug Metabolism and Disposition* **1982**, *10* (5), 516-522.
- [54] Brox, S.; Seiwert, B.; Haase, N.; Kuester, E.; Reemtsma, T., Metabolism of clofibric acid in zebrafish embryos (*Danio rerio*) as determined by liquid chromatography-high resolution-mass spectrometry. *Comparative Biochemistry and Physiology C-Toxicology & Pharmacology* **2016**, *185*, 20-28.
- [55] James, M. O.; Bend, J. R., Taurine conjugation of 2,4-dichlorophenoxyacetic acid and phenylacetic acid in two marine species. *Xenobiotica* **1976**, *6* (7), 393-398.
- [56] James, M. O., Conjugation of organic pollutants in aquatic species. *Environ. Health Perspect.* **1987**, Vol. 71, 97-103.
- [57] Sandermann, H., Plant metabolism of xenobiotics. *Trends Biochem. Sci* **1992**, *17* (2), 82-84.

- [58] Komossa, D.; Langebartels, C.; Sandermann, H., Jr., *Metabolic processes for organic chemicals in plants*. 1995; p 69-103.
- [59] Macherius, A.; Eggen, T.; Lorenz, W.; Moeder, M.; Ondruschka, J.; Reemtsma, T., Metabolization of the Bacteriostatic Agent Triclosan in Edible Plants and its Consequences for Plant Uptake Assessment. *Environmental Science & Technology* **2012**, *46* (19), 10797-10804.
- [60] Stroomborg, G. J.; Zappey, H.; Steen, R. J. C. A.; Van Gestel, C. A. M.; Ariese, F.; Velthorst, N. H.; Van Straalen, N. M., PAH biotransformation in terrestrial invertebrates - A new phase II metabolite in isopods and springtails. *Comparative Biochemistry and Physiology - C Toxicology and Pharmacology* **2004**, *138* (2), 129-137.
- [61] Álvarez-muñoz, D.; Sáez, M.; Gómez-Parra, A.; González-Mazo, E., Experimental determination of bioconcentration, biotransformation, and elimination of linear alkylbenzene sulfonates in *Solea senegalensis*. *Environ. Toxicol. Chem.* **2007**, *26* (12), 2579-2586.
- [62] Kukkonen, J.; Oikari, A., Sulphate conjugation is the main route of pentachlorophenol metabolism in *Daphnia magna*. *Comparative Biochemistry and Physiology - C Pharmacology Toxicology and Endocrinology* **1988**, *91* (2), 465-468.
- [63] Jeon, J.; Kurth, D.; Hollender, J., Biotransformation pathways of biocides and pharmaceuticals in freshwater crustaceans based on structure elucidation of metabolites using high resolution mass spectrometry. *Chem. Res. Toxicol.* **2013**, *26* (3), 313-24.
- [64] Ikenaka, Y.; Eun, H.; Ishizaka, M.; Miyabara, Y., Metabolism of pyrene by aquatic crustacean, *Daphnia magna*. *Aquat. Toxicol.* **2006**, *80* (2), 158-165.
- [65] Ikenaka, Y.; Ishizaka, M.; Eun, H.; Miyabara, Y., Glucose-sulfate conjugates as a new phase II metabolite formed by aquatic crustaceans. *Biochem. Biophys. Res. Commun.* **2007**, *360* (2), 490-495.
- [66] Gobas, F. A. P. C.; Opperhuizen, A.; Hutzinger, O., Bioconcentration of hydrophobic chemicals in fish: Relationship with membrane permeation. *Environ. Toxicol. Chem.* **1986**, *5* (7), 637-646.
- [67] Casey, J. R.; Grinstein, S.; Orlowski, J., Sensors and regulators of intracellular pH. *Nature Reviews Molecular Cell Biology* **2010**, *11* (1), 50-61.
- [68] Bard, S. M., Multixenobiotic resistance as a cellular defense mechanism in aquatic organisms. *Aquat. Toxicol.* **2000**, *48* (4), 357-389.
- [69] Kurelec, B., The multixenobiotic resistance mechanism in aquatic organisms. *Crit. Rev. Toxicol.* **1992**, *22* (1), 23-43.
- [70] Lotufo, G. R.; Landrum, P. F.; Gedeon, M. L.; Tigue, E. A.; Herche, L. R., Comparative toxicity and toxicokinetics of DDT and its major metabolites in freshwater amphipods. *Environ. Toxicol. Chem.* **2000**, *19* (2), 368-379.
- [71] Jager, T.; Øverjordet, I. B.; Nepstad, R.; Hansen, B. H., Dynamic Links between Lipid Storage, Toxicokinetics and Mortality in a Marine Copepod Exposed to Dimethylnaphthalene. *Environmental Science & Technology* **2017**.
- [72] Hoffman, D.; Rattner, B.; Allen Burton Jr, G.; Cairns Jr, J., In *Handbook of Ecotoxicology, Second Edition*, CRC Press: 2002.
- [73] Sijm, D. T. H. M.; Rikken, M. G. J.; Rorije, E.; Traas, T. P.; Mclachlan, M. S.; Peijnenburg, W. J. G. M., Transport, Accumulation and Transformation Processes. In *Risk Assessment of Chemicals: An Introduction*, Leeuwen, C. J. v.; Vermeire, T. G., Eds. Springer Netherlands: Dordrecht, 2007; pp 73-158.
- [74] Arnot, J. A.; Gobas, F. A. P. C., A review of bioconcentration factor (BCF) and bioaccumulation factor (BAF) assessments for organic chemicals in aquatic organisms. *Environmental Reviews* **2006**, *14* (4), 257-297.
- [75] Hayton, W. L.; Barron, M. G., Rate-limiting barriers to xenobiotic uptake by the gill. *Environ. Toxicol. Chem.* **1990**, *9* (2), 151-157.
- [76] MarvinSketch v14.10.20.0 from ChemAxon. Available at <https://www.chemaxon.com/products/marvin/marvinsketch/>

- [77] Kraemer, S. D.; Testa, B., The Biochemistry of Drug Metabolism - An Introduction Part 7. Intra-Individual Factors Affecting Drug Metabolism. *Chemistry & Biodiversity* **2009**, *6* (10), 1477-1660.
- [78] Ortiz De Montellano, P. R.; Almira Correia, M., *Inhibition of cytochrome P450 enzymes*. 1995; p 305-364.
- [79] Chiang, J. Y. L., Bile acids: regulation of synthesis. *J. Lipid Res.* **2009**, *50* (10), 1955-1966.
- [80] Lafont, R.; Mathieu, M., Steroids in aquatic invertebrates. *Ecotoxicology* **2007**, *16* (1), 109-130.
- [81] Vonk, H. J., Bile acids and fat resorption in invertebrates. *Recueil des Travaux Chimiques des Pays-Bas* **1945**, *64* (11), 320-320.
- [82] Konwick, B. J.; Garrison, A. W.; Avants, J. K.; Fisk, A. T., Bioaccumulation and biotransformation of chiral triazole fungicides in rainbow trout (*Oncorhynchus mykiss*). *Aquat. Toxicol.* **2006**, *80* (4), 372-81.
- [83] IUPAC International Union of Pure and Applied Chemistry. Pesticide Properties Database. <http://sitem.herts.ac.uk/aeru/iupac/>.
- [84] EFSA, Conclusion on the peer review of the pesticide risk assessment of the active substance prochloraz. *EFSA Journal* **2011**, *9* (7).
- [85] Debrauwer, L.; Rathahao, E.; Boudry, G.; Baradat, M.; Cravedi, J. P., Identification of the major metabolites of prochloraz in rainbow trout by liquid chromatography and tandem mass spectrometry. *J. Agric. Food. Chem.* **2001**, *49* (8), 3821-3826.

Chapter S4. Supporting Information:
**Comparing Biotransformation of two Fungicides and the
Potential of Cytochrome P450 Inhibition in two Aquatic
Invertebrates**

Andrea Rösch^{1,2}, Qiuguo Fu¹, Juliane Hollender^{1,2}

¹ Eawag, Swiss Federal Institute of Aquatic Science and Technology, 8600 Dübendorf, Switzerland

² Institute of Biogeochemistry and Pollutant Dynamics, ETH Zürich, 8092 Zürich, Switzerland

SI.A Chemicals and Solutions

Table S4-1: Fungicides. All standard solutions were prepared in methanol.

Substance	CAS number	Supplier	Quality
Azoxystrobin	131860-33-8	Dr. Ehrenstorfer	99.5%
Azoxystrobin acid	1185255-09-7	HPC Standards GmbH	99%
Azoxystrobin-d4	1346606-39-0	Sigma-Aldrich	98%
Prochloraz	67747-09-5	Dr. Ehrenstorfer	98.5%
Prochloraz-d7		Dr. Ehrenstorfer	97%

Table S4-2: Other chemicals and solutions.

Substance	CAS number	Supplier	Quality
Acetic acid	64-19-7	Merck	100%
Acetonitrile	75-05-8	Acros Organics	HPLC-grade
Ammonium acetate	631-61-8	Sigma-Aldrich	> 98%
Calcium chloride	10035-04-8	Sigma-Aldrich	> 99%
Ethanol	64-17-5	Merck	Analytical grade
Formic acid	64-18-6	Merck	98-100%
Magnesium sulfate	10034-99-8	Sigma-Aldrich	> 99%
Isopropanol	67-63-0	Fisher Chemicals	> 99%
Methanol Optima	67-56-1	Fisher Chemicals	LC-MS grade
Potassium chloride	7447-40-7	Sigma-Aldrich	> 99%
Sodium acetate trihydrate	6131-90-4	Fluka	> 99.5%
Sodium hydrogen carbonate	144-55-8	Merck	> 99%
Sodium bromide	7647-15-6	Sigma-Aldrich	> 99%

SI.B Quality Control

Internal standard calibration was used for quantification using Trace Finder software 3.1 and 3.3 (Thermo Scientific). 16 calibration points were prepared in a range of 0.5-3000 ng L⁻¹ and the calibration curves were obtained by linear least square regression using a weighing factor of 1/x. All BTPs were quantified based on the calibration curve of the corresponding parent compound except for azoxystrobin acid (AZ_M390b), for which a reference standard was available. Reference standards for two prochloraz BTPs (PRZ_M282 and PRZ_M325) were obtained after finishing the experiment and measurement and no calibration curve was acquired for PRZ_M282 and PRZ_M325. Reference standards were measured afterwards and only used for confirming the proposed structures.

Limits of Quantification (LOQ) and matrix factors were calculated according to our previous publications.¹

Table S4-3: Calculated matrix factors for *H. azteca* extracts and limits of quantification (LOQs) for azoxystrobin and prochloraz in *H. azteca* extracts and in the exposure medium. Duplicate samples (prespike 1 and 2) were spiked before *H. azteca* extraction with 25 µg L⁻¹ (i.e., 5 ng absolute in 200 µL measured extract) and 50 µg L⁻¹ (i.e., 10 ng absolute in 200 µL measured extract) of azoxystrobin (AZ) and prochloraz (PRZ), respectively.

Compound	Matrix factors					LOQ*	LOQ**
	Pre-spike 1 5 ng	Pre-spike 2 5 ng	Pre-spike 1 10 ng	Pre-spike 2 10 ng	Average	[nmol kg _{ww} ⁻¹]	[ng L ⁻¹]
AZ	0.4	0.4	0.4	0.4	0.4	2.4	0.5
PRZ	0.6	0.6	0.6	0.6	0.6	1.7	0.5

*: LOQ for gammarid extract samples

**: LOQ for medium samples

Table S4-4: Relative recoveries for the whole sample preparation and analytical procedure. Duplicate samples (prespike 1 and 2) spiked before *H. azteca* extraction with 25 µg L⁻¹ (i.e., 5 ng absolute in 200 µL measured extract) and 50 µg L⁻¹ (i.e., 10 ng absolute in 200 µL measured extract) of the parent compounds, respectively, were used to determine the recovery of the whole procedure of sample preparation and chemical analysis.

Compound	Relative recovery [%]			
	Prespike 1 5 ng	Prespike 2 5 ng	Prespike 1 10 ng	Prespike 2 10 ng
Azoxystrobin	101	101	104	98
Prochloraz	115	118	107	99

SI.C Biotransformation Product Identification in *H. azteca* by Suspect and Nontarget Screening using Compound Discoverer

Compound Discoverer small molecule identification software version 2.0 (Thermo Scientific) was used for suspect and nontarget screening by comparing treatment and control samples. As control samples “exposure medium controls”, “chemical controls” (chemical positive, cotton gauze and organism negative), “organism controls” (chemical negative, organism and food positive) and “standard controls” (calibration standard) were used. “Standard controls” and “chemical controls” were additionally selected as control samples compared to the screening conducted with SIEVE software (Thermo Scientific) in our previous publications.¹⁻² “Standard controls” account for impurities of the reference standards, and “chemical controls” provide in addition to the “exposure medium controls” evidence that BTPs are actually formed by the organisms and not due to *e.g.*, abiotic processes in the medium. Due to a high volume to organism ratio (500 mL exposure medium containing 50 organisms) and since no additional enrichment of the exposure medium besides online-SPE was conducted, no BTPs formed by the organisms can be detected in the medium. Thus, the detection of BTPs in the exposure medium would point towards additional formation processes.

For suspect screening, the generated frame list was compared to the mass list of predicted BTPs. BTPs were predicted based on (i) *in silico* pathway prediction (Eawag-PPS, <http://eawag-bbd.ethz.ch/predict/>, Eawag-PPS predicts microbial degradation of chemicals based on biotransformation rules.), (ii) *in silico* manual prediction of BTPs considering most common enzymatic biotransformation reactions, and (iii) identified BTPs of azoxystrobin and prochloraz reported in any organisms in scientific literature. The mass lists for azoxystrobin and prochloraz contained 1325 and 490 predicted BTPs masses, respectively.

Framing describes the process of building regions in the m/z versus retention time plane, whereby all peaks above a given threshold are collected.

For nontarget screening, the generated frame list was filtered with (i) an integrated intensity threshold of 0.1% of the parent compound and (ii) an integrated intensity ratio between treatment and control samples of 10 (with the exception of the ratio “treatment / organisms control”, which was adjusted individually, see below).

The workflow was validated with known low concentrated BTPs detected in previous work¹⁻² that were also detected in *H. azteca*. With the selected nontarget criteria the filtered frame list should still contain these low concentrated BTPs. The node “Fill Gaps”, included in the applied workflow, fills in areas for missing peaks or for peaks with intensities below the chosen threshold. This is done to avoid dividing by zero to be still able to form ratios with control samples, where no peak was detected. For some of these low concentrated BTPs the ratio “treatment / organisms control” was considerably smaller than 10 due to “Fill Gaps”. Therefore, the ratio “treatment / organisms control” was adopted to the observed conditions and reduced to 4 (AZ) and 3.8 (PRZ), respectively.

For both screening approaches, potential BTPs had to show increasing/decreasing intensities during the uptake/depuration phase. Moreover, Compound Discoverer allows to

screen for specific isotopic patterns. Therefore, the presence of the chlorophenyl moiety (chlorine isotopic pattern) in potential BTPs that after biotransformation still contain the chlorophenyl moiety, facilitated BTP screening for prochloraz.

Table S4-5: Settings used for suspect and nontarget screening with Compound Discoverer (Thermo Scientific, version 2.0).

Retention time window	5-20 min
m/z window	100-1000
Minimal number of scans per peak	3
Maximum peak width	1 min
m/z tolerance	5 ppm
Peak intensity threshold	10 ⁶

SI.D Sampling during the *H. azteca* Kinetic Experiment

Table S4-6: Sampled time-points during the azoxystrobin kinetic experiment.

Uptake (U) / Depuration (D)	Time [h]	Time [d]
U	0.5	0.02
U	1.5	0.06
U	2.5	0.10
U	5.5	0.23
U	9.5	0.40
U	17.5	0.73
U	24	1.00
D	24	1.00
D	25	1.04
D	26	1.08
D	28	1.17
D	31	1.29
D	35	1.46
D	42	1.75
D	50	2.08
D	65	2.71
D	95	3.96
D	119	4.96
D	144	6.00

SI.E Modeling Bioaccumulation and Biotransformation Kinetics

For simulating the parent compound azoxystrobin kinetic in *G. pulex* and *H. azteca* the simplest first-order compartment model (see equation S4-1) was used:

$$\frac{dC_{in,p}(t)}{dt} = C_{water}(t) \cdot k_u - C_{in,p}(t) \cdot k_e \quad \text{equation S4-1}$$

where $C_{in,p}(t)$ is whole body internal concentration of azoxystrobin, $C_{water}(t)$ [nmol L⁻¹] is the time course of azoxystrobin in the exposure medium and k_u [L kg_{ww}⁻¹ d⁻¹] and k_e [d⁻¹] are the uptake and elimination rate constant, respectively. In this case k_e covers direct elimination of the parent compound as well as further elimination due to biotransformation.

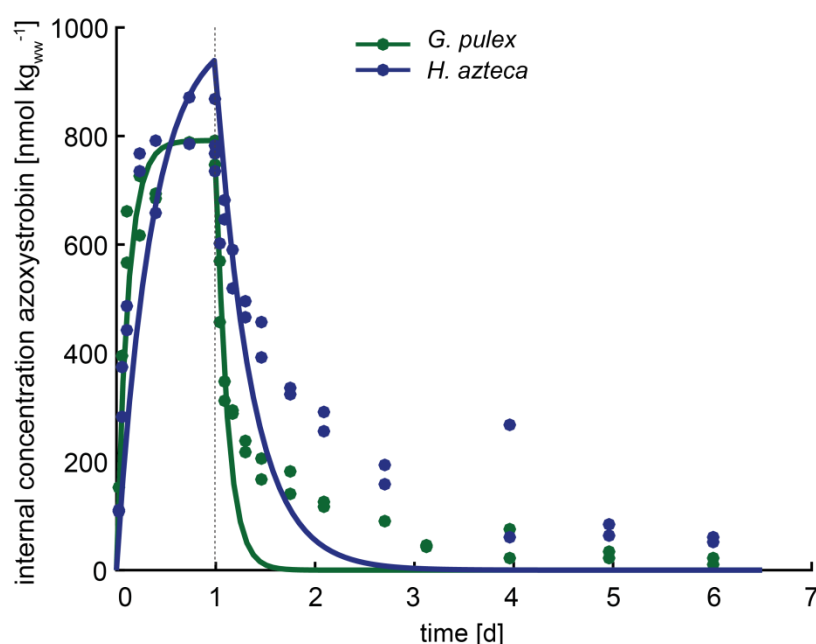


Figure S4-1: Uptake and depuration kinetic for azoxystrobin in *G. pulex* (green) and *H. azteca* (blue) modeled with the simplest first-order compartment model (see equation S4-1). Shown are the measured (dots) and modeled (lines) time courses for azoxystrobin in *G. pulex* and *H. azteca*. The dashed vertical line indicates the change from uptake (1 d) to depuration (5 d).

Table S4-7: Kinetic rate constants for azoxystrobin in the two species *G. pulex* and *H. azteca* (lower and upper 95% confidence intervals are given in brackets) and kinetic bioaccumulation factors (BAF_{k,s}). The simplest first-order compartment model (see equation S4-1) was used for fitting the kinetic rate constants. Results are rounded to three significant digits. Two replicate internal concentrations were used per time point.

	k_u [L kg _{ww} ⁻¹ d ⁻¹]	k_e [d ⁻¹]
<u>Azoxystrobin</u>		
<i>G. pulex</i>		
BAF _k AZ: 4.95 [L kg _{ww} ⁻¹]	42.2 [33.6; 55.7]	8.52 [6.81; 11.4]
<i>H. azteca</i>		
BAF _k AZ: 5.22 [L kg _{ww} ⁻¹]	14.7 [9.65; 20.3]	2.82 [1.68; 4.07]

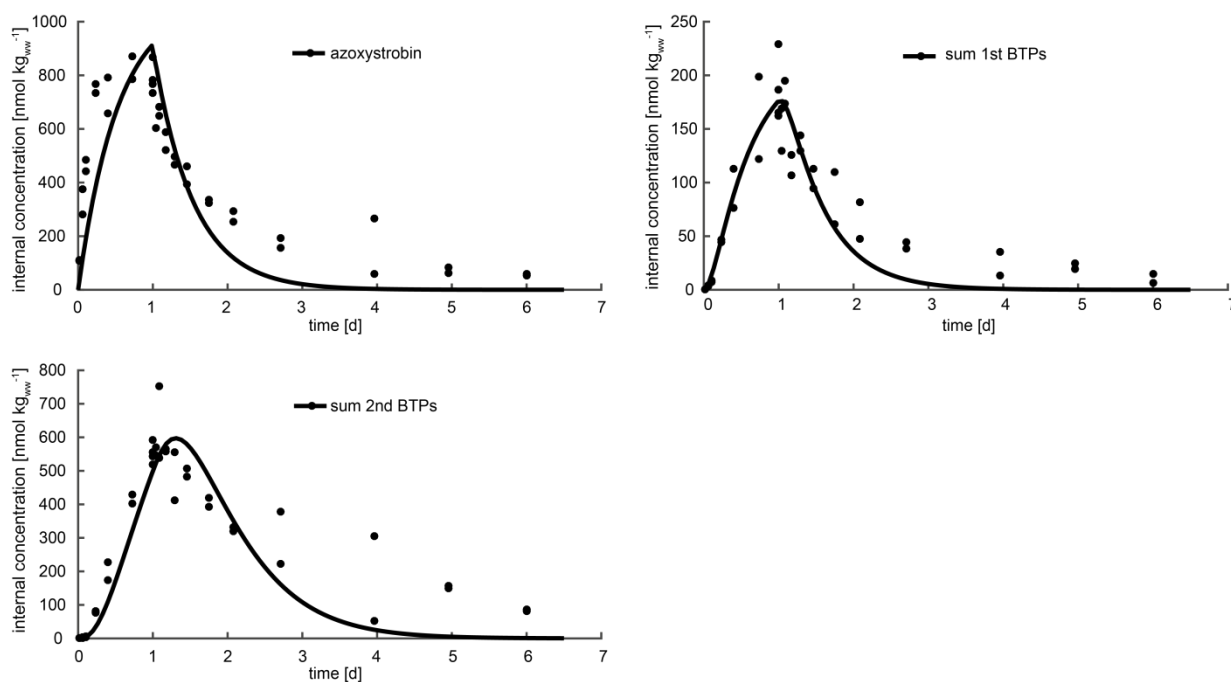


Figure S4-2: Measured (dots) and modeled (lines) time series of internal concentrations of azoxystrobin, the sum of 1st BTPs and the sum of 2nd BTPs in *H. azteca* in the uptake (1 d) and depuration phase (5 d) shown in separate panels. All parameters were fitted simultaneously.

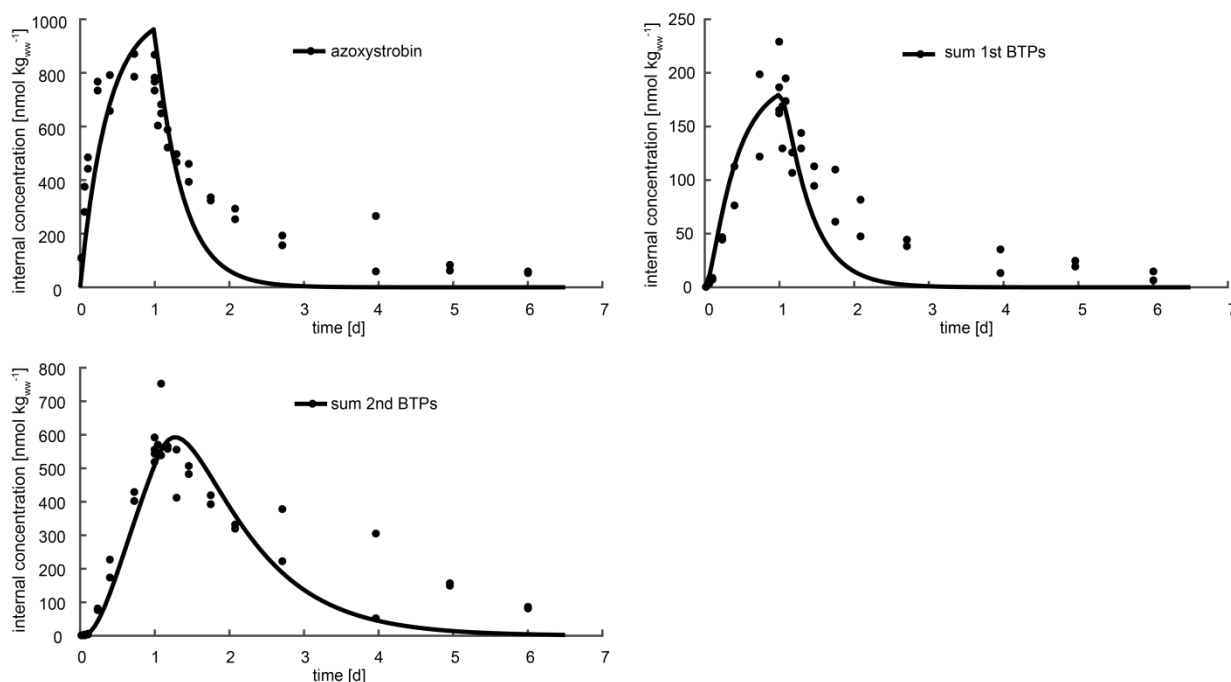


Figure S4-3: Measured (dots) and modeled (lines) time series of internal concentrations of azoxystrobin, the sum of 1st BTPs and the sum of 2nd BTPs in *H. azteca* in the uptake (1 d) and depuration phase (5 d) shown in separate panels. The uptake rate k_u [$\text{L kg}_{\text{ww}}^{-1} \text{d}^{-1}$] was determined in a first step by only fitting the azoxystrobin parent compound kinetic with two parameters (k_u and k_e , see equation S4-1) and in a second step fixing k_u ($14.7 \text{ L kg}_{\text{ww}}^{-1} \text{d}^{-1}$, see Table S4-7) and simultaneously fitting k_e and the kinetic rate constants of the sum of 1st BTPs and the sum of 2nd BTPs, respectively.

Table S4-8: Comparison of kinetic rate constants of azoxystrobin, the sum of 1st BTPs and the sum of 2nd BTPs in *H. azteca*. Kinetic rate constants were either determined by simultaneously fitting of all kinetic rate constants or with a stepwise approach, by first only fitting the azoxystrobin parent compound kinetic with two parameters (k_u and k_e , see equation S4-1) and in a second step fixing k_u ($14.7 \text{ L kg}_{\text{ww}}^{-1} \text{ d}^{-1}$, see Table S4-7) and simultaneously fitting k_e and the kinetic rate constants of the sum of 1st BTPs and the sum of 2nd BTPs, respectively.

	simultaneously fitting of all kinetic rate constants	fixed k_u ($14.7 \text{ L kg}_{\text{ww}}^{-1} \text{ d}^{-1}$, see Table S4-7) and simultaneously fitting of all remaining kinetic rate constants
k_e [d^{-1}]:	0.131 [0.0001; 0.804]	0.001 [0.001; 1.77]
k_u [$\text{L kg}_{\text{ww}}^{-1} \text{ d}^{-1}$]:	10.6 [9.40; 12.2]	-
$k_{M, 1\text{st, total}}$ [d^{-1}]:	1.75 [1.46; 1.48]; [1.57; 2.14]	2.74 [2.40; 3.05]
$k_{M, 2\text{nd, total}}$ [d^{-1}]:	8.62 [7.60; 11.0]	6.42 [4.94; 8.14]
$k_{eM, 1\text{st, total}}$ [d^{-1}]:	0.0001 [0.0001; 4.92]	7.97 [5.90; 9.78]
$k_{eM, 2\text{nd, total}}$ [d^{-1}]:	1.85 [1.50; 2.52]	1.14 [0.69; 1.73]
total elimination azoxystrobin $[\text{d}^{-1}] (k_e + k_{M, 1\text{st, total}})$:	1.88	2.74
fraction $k_{M, 1\text{st, total}}$ on total elimination [%]:	93.0	100
BAF_k AZ [$\text{L kg}_{\text{ww}}^{-1}$]:	5.63	5.37

SI.F Exposure Medium Concentrations, Internal Concentrations and Bioaccumulation Factors (BAFs) for *H. azteca*

Tables in this section are sorted according to the order of the experiments in the *Material and Methods* section in the corresponding manuscript. BAFs reported in this section are based on the ratio of the concentration of the parent compound in the organisms and of the concentration of the parent compound in the exposure medium with the requirement of steady state (see equation 5 in the corresponding manuscript). t_0 refers to the addition of the substrate and t_{24} to the end of the exposure phase.

The following abbreviations are valid for all tables located in this section:

m: medium samples

C+ cg-: "chemical controls" (organism and cotton gauze negative, chemical positive)

C+ cg+: "food controls" (organism negative, cotton gauze and chemical positive)

AZ: azoxystrobin

PRZ: prochloraz

Table S4-9: Biotransformation screening experiment in *H. azteca*: exposure to 100 µg L⁻¹ AZ and PRZ, respectively. In the control samples nominal concentrations of 100 µg L⁻¹ AZ and PRZ, respectively, were used.

Exposure medium	AZ [µg L ⁻¹]	AZ [nmol L ⁻¹]	PRZ [µg L ⁻¹]	PRZ [nmol L ⁻¹]
m_C+ cg- t0_1	98		96	
m_C+ cg- t0_2	96		95	
m_C+ cg- t24_1	102		98	
m_C+ cg- t24_2	102		100	
m_C+ cg+ t0_1	92		84	
m_C+ cg+ t0_2	100		93	
m_C+ cg+ t24_1	101		91	
m_C+ cg+ t24_2	98		89	
m_AZ t0_1	101	252		
m_AZ t0_2	96	239		
m_AZ t24_1	97	240		
m_AZ t24_2	89	222		
m_PRZ t0_1			101	269
m_PRZ t0_2			100	265
m_PRZ t24_1			81	216
m_PRZ t24_2			91	243
Whole body internal concentrations 24 h after substrate addition and corresponding BAFs				
	AZ [nmol kg _{ww} ⁻¹]	BAF AZ [L kg _{ww} ⁻¹]	PRZ [nmol kg _{ww} ⁻¹]	BAF PRZ [L kg _{ww} ⁻¹]
AZ_1	890	4		
AZ_2	901	4		
PRZ_1			37651	155
PRZ_2			43173	170

Table S4-10: Toxicokinetic experiment in *H. azteca*: exposure to 80 µg L⁻¹ AZ in the uptake phase. In the control samples nominal concentrations of 80 µg L⁻¹ AZ were used.

Exposure medium	AZ [µg L ⁻¹]	AZ [nmol L ⁻¹]
m_C+ cg- t0_1	77	
m_C+ cg- t0_2	77	
m_C+ cg- t24_1	78	
m_C+ cg- t24_2	80	
m_C+ cg+ t0_1	82	
m_C+ cg+ t0_2	78	
m_C+ cg+ t24_1	82	
m_C+ cg+ t24_2	75	
m_AZ t0_1	71	177
m_AZ t0_2	79	195
m_AZ t24_1	77	191
m_AZ t24_2	78	193
m_AZ t0_1 ⁾	76	189
m_AZ t0_2 ⁾	78	194
m_AZ t24_1 ⁾	80	199
m_AZ t24_2 ⁾	81	201
Whole body internal concentrations 24 h after substrate addition and corresponding BAFs		
	AZ [nmol kg _{ww} ⁻¹]	BAF AZ [L kg _{ww} ⁻¹]
AZ_Ut24_1	767	4
AZ_Ut24_2	782	4
AZ_Dt0_1	734	4
AZ_Dt0_2	868	5

⁾ Uptake phase for following depuration experiment.

Table S4-11: Half maximal inhibitory concentration of PRZ in *H. azteca* using AZ as a substrate ($IC_{50, PRZ, AZ}$). Exposure to $40 \mu\text{g L}^{-1}$ AZ and varying PRZ concentrations of $c1 = 0.19 \mu\text{g L}^{-1}$, $c2 = 0.37 \mu\text{g L}^{-1}$, $c3 = 0.74 \mu\text{g L}^{-1}$, $c4 = 3.7 \mu\text{g L}^{-1}$, $c5 = 7.4 \mu\text{g L}^{-1}$, $c6 = 22 \mu\text{g L}^{-1}$, $c7 = 37 \mu\text{g L}^{-1}$, $c8 = 74 \mu\text{g L}^{-1}$ and $c9 = 372 \mu\text{g L}^{-1}$ (18 h pre-exposure to PRZ). In the control samples nominal concentrations of $40 \mu\text{g L}^{-1}$ AZ and $37 \mu\text{g L}^{-1}$ PRZ were used.

Exposure medium	AZ [$\mu\text{g L}^{-1}$]	AZ [nmol L^{-1}]	PRZ [$\mu\text{g L}^{-1}$]
m_C+ cg-_1 (t0 PRZ)			36
m_C+ cg-_2 (t0 PRZ)			36
m_C+ cg- t0_1	39		35
m_C+ cg- t0_2	40		36
m_C+ cg- t24_1	38		34
m_C+ cg- t24_2	40		35
m_C+ cg+_1 (t0 PRZ)			37
m_C+ cg+_2 (t0 PRZ)			36
m_C+ cg+ t0_1	38		36
m_C+ cg+ t0_2	39		37
m_C+ cg+ t24_1	38		34
m_C+ cg+ t24_2	38		36
m_AZ + PRZ c1_1 (t0 PRZ)			0.2
m_AZ + PRZ c1_2 (t0 PRZ)			0.2
m_AZ + PRZ c2_1 (t0 PRZ)			0.4
m_AZ + PRZ c2_2 (t0 PRZ)			0.4
m_AZ + PRZ c3_1 (t0 PRZ)			0.7
m_AZ + PRZ c3_2 (t0 PRZ)			0.7
m_AZ + PRZ c4_1 (t0 PRZ)			3
m_AZ + PRZ c4_2 (t0 PRZ)			3
m_AZ + PRZ c5_1 (t0 PRZ)			7
m_AZ + PRZ c5_2 (t0 PRZ)			7
m_AZ + PRZ c6_1 (t0 PRZ)			20

Exposure medium	AZ [$\mu\text{g L}^{-1}$]	AZ [nmol L^{-1}]	PRZ [$\mu\text{g L}^{-1}$]
m_AZ + PRZ c7_1 (t0 PRZ)			34
m_AZ + PRZ c7_2 (t0 PRZ)			35
m_AZ + PRZ c8_1 (t0 PRZ)			68
m_AZ + PRZ c8_2 (t0 PRZ)			69
m_AZ + PRZ c9_1 (t0 PRZ)			358
m_AZ + PRZ c9_2 (t0 PRZ)			339
m_AZ t0_1	39	97	
m_AZ t0_2	40	99	
m_AZ + PRZ c1 t0_1	37	92	0.4
m_AZ + PRZ c1 t0_2	37	92	0.4
m_AZ + PRZ c2 t0_1	39	98	0.5
m_AZ + PRZ c2 t0_2	38	94	0.5
m_AZ + PRZ c3 t0_1	38	93	0.8
m_AZ + PRZ c3 t0_2	40	100	0.8
m_AZ + PRZ c4 t0_1	37	92	3
m_AZ + PRZ c4 t0_2	40	98	3
m_AZ + PRZ c5 t0_1	39	97	7
m_AZ + PRZ c5 t0_2	41	101	8
m_AZ + PRZ c6 t0_1	41	102	20
m_AZ + PRZ c6 t0_2	40	100	21
m_AZ + PRZ c7 t0_1	38	95	34
m_AZ + PRZ c7 t0_2	38	95	35
m_AZ + PRZ c8 t0_1	38	94	70
m_AZ + PRZ c8 t0_2	39	98	68
m_AZ + PRZ c9 t0_1	41	103	353

Exposure medium	AZ [$\mu\text{g L}^{-1}$]	AZ [nmol L^{-1}]	PRZ [$\mu\text{g L}^{-1}$]
m_AZ + PRZ c9 t0_2	41	102	348
m_AZ t24_1	37	92	
m_AZ t24_2	39	97	
m_AZ + PRZ c1 t24_1	38	94	0.3
m_AZ + PRZ c1 t24_2	38	94	0.3
m_AZ + PRZ c2 t24_1	39	98	0.4
m_AZ + PRZ c2 t24_2	39	96	0.4
m_AZ + PRZ c3 t24_1	38	94	0.8
m_AZ + PRZ c3 t24_2	41	101	0.8
m_AZ + PRZ c4 t24_1	37	91	3
m_AZ + PRZ c4 t24_2	41	101	3
m_AZ + PRZ c5 t24_1	38	95	7
m_AZ + PRZ c5 t24_2	40	99	7
m_AZ + PRZ c6 t24_1	40	100	19
m_AZ + PRZ c6 t24_2	39	98	19
m_AZ + PRZ c7 t24_1	38	95	33
m_AZ + PRZ c7 t24_2	39	97	33
m_AZ + PRZ c8 t24_1	38	93	65
m_AZ + PRZ c8 t24_2	40	98	67
m_AZ + PRZ c9 t24_1	38	94	338
m_AZ + PRZ c9 t24_2	42	104	355

Whole body internal concentrations 24 h after substrate addition and corresponding BAFs

	AZ [nmol kg _{ww} ⁻¹]	BAF AZ [L kg _{ww} ⁻¹]	PRZ [nmol kg _{ww} ⁻¹]
AZ_1	781	8	
AZ_2	703	7	
AZ_3	792	8	
AZ + PRZ c1_1	710	8	54
AZ + PRZ c1_2	769	8	52
AZ + PRZ c2_1	750	8	127
AZ + PRZ c2_2	743	8	113
AZ + PRZ c3_1	713	7	211
AZ + PRZ c3_2	834	9	221

Whole body internal concentrations 24 h after substrate addition and corresponding BAFs

	AZ [nmol kg _{ww} ⁻¹]	BAF AZ [L kg _{ww} ⁻¹]	PRZ [nmol kg _{ww} ⁻¹]
AZ + PRZ c4_1	770	8	1107
AZ + PRZ c4_2	838	9	1129
AZ + PRZ c5_1	802	8	3158
AZ + PRZ c5_2	776	8	2243
AZ + PRZ c6_1	888	9	6720
AZ + PRZ c6_2	867	9	6496
AZ + PRZ c7_1	927	10	10937
AZ + PRZ c7_2	887	9	11245
AZ + PRZ c8_1	1095	11	20921
AZ + PRZ c8_2	1149	12	22851
AZ + PRZ c9_1	1183	12	77899
AZ + PRZ c9_2	1151	11	67027

SI.G Determination of $IC_{50, PRZ, AZ}$ s in *H. azteca*

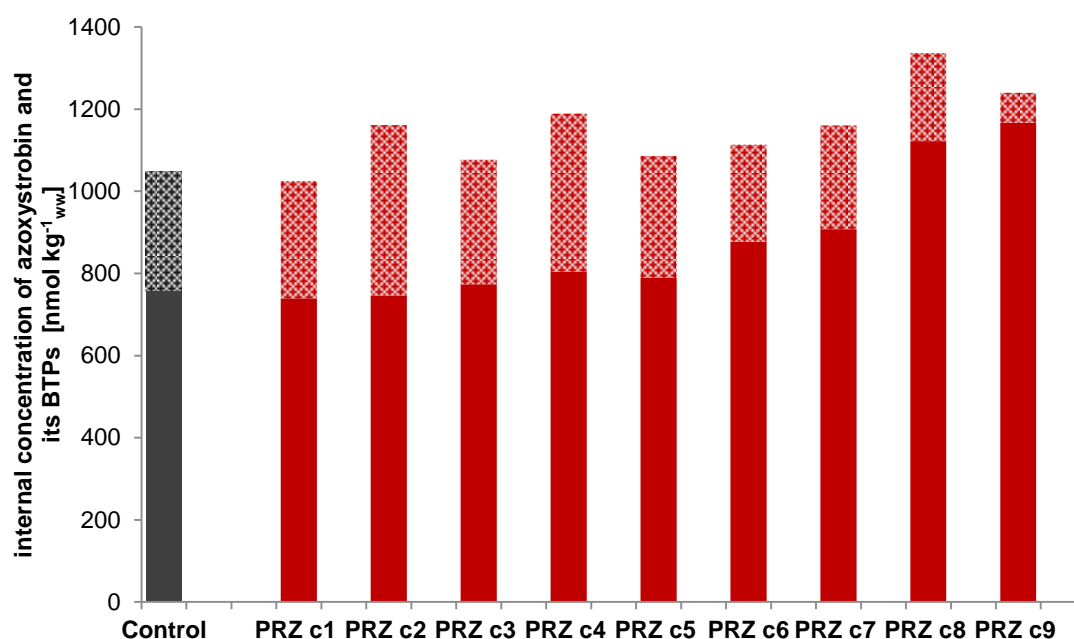


Figure S4-4: Whole body internal concentration of azoxystrobin and its BTPs after 24 h exposure to $40 \mu\text{g L}^{-1}$ azoxystrobin: 18 h pre-exposure without chemical in black (sample replicates $n=3$) and 18 h pre-exposure to varying prochloraz (PRZ) concentrations ($n=2$) (c1: 0.19, c2: 0.37, c3: 0.74, c4: 3.7, c5: 7.4, c6: 22, c7: 37, c8: 74 and c9: $372 \mu\text{g L}^{-1}$) in red. The filled areas mark the parent compound azoxystrobin, whereas the hatched areas mark the sum of all detected BTPs.

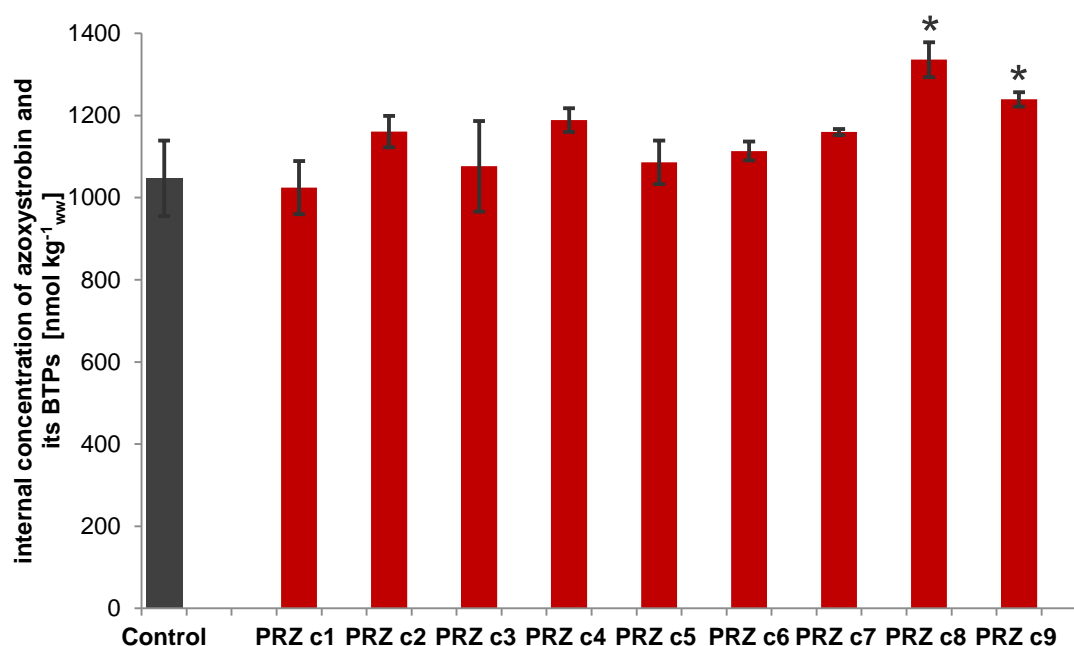


Figure S4-5: Whole body internal concentration of azoxystrobin and its BTPs after 24 h exposure to $40 \mu\text{g L}^{-1}$ azoxystrobin: 18 h pre-exposure without chemical in black and 18 h pre-exposure to varying prochloraz (PRZ) concentrations (c1: 0.19, c2: 0.37, c3: 0.74, c4: 3.7, c5: 7.4, c6: 22, c7: 37, c8: 74 and c9: $372 \mu\text{g L}^{-1}$) in red. Controls (single exposure to azoxystrobin) (sample replicates $n=3$) and treatments ($n=2$) are displayed with the standard deviation of the total internal concentration (azoxystrobin and the sum of all BTPs). Total internal concentrations in each mixture were compared to those of the controls (single exposure to azoxystrobin) with a t-test (two tailed distribution, two-sample equal variance) and showed statistical difference for treatment PRZ c8 and PRZ c9 ($p < 0.05$) marked with an asterisk.

SI.H Dose-Response Fitting of $IC_{50, PRZ, AZ}$ s in *H. azteca*

The log-logistic four-parameter model (LL.4) used for the fitting of dose-response curves is available in the R³ package “drc” from Ritz and Streibig (2005)⁴ and is described by the following equation:

Log-logistic four-parameter model (LL.4):

$$f(x) = c + \frac{d - c}{1 + \exp(b(\log(x) - \log(e)))} \quad \text{equation S4-2}$$

where d and c are the upper and lower limits of response, respectively, b denotes the relative slope in the inflection point, e is the inflection point and thereby the EC_{50} , and x is the prochloraz concentration.

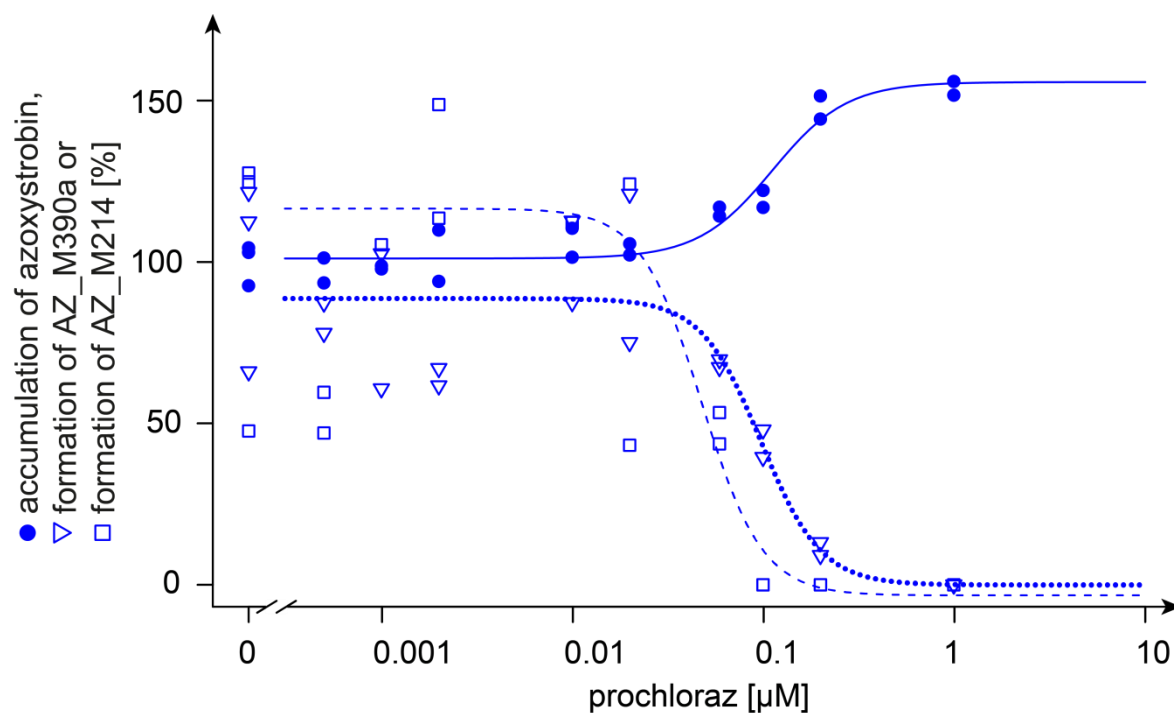


Figure S4-6: Dose-response curves for the $IC_{50/10, PRZ, AZ}$ determination based on whole body internal concentration measurements of azoxystrobin and its BTPs (shown are the two primary BTPs AZ_M390a and AZ_M214). Internal concentrations of azoxystrobin and its BTPs were measured after 24 h exposure to $40 \mu\text{g L}^{-1}$ azoxystrobin. Controls were pre-exposed without chemical for 18 h, whereas treatments were pre-exposed for 18 h to varying prochloraz concentrations (c1: 0.19, c2: 0.37, c3: 0.74, c4: 3.7, c5: 7.4, c6: 22, c7: 37, c8: 74 and c9: $372 \mu\text{g L}^{-1}$).

Table S4-12: Estimated parameters (d: upper limit of response; c: lower limit of response; b: relative slope in the inflection point; e: inflection point and thereby the $IC_{50, PRZ, AZ}$) and determined $IC_{50/10, PRZ, AZ}$ s for azoxystrobin and primary BTPs with the four-parameter log-logistic model in *H. azteca*. Parameters and $IC_{50/10, PRZ, AZ}$ s are reported with the corresponding standard errors. Measured internal concentrations of AZ_M214 exhibited large variations (see Figure S4-6 above). Therefore, $IC_{50/10, AZ, PRZ}$ s based on the dose response curve of AZ_M214 have to be treated with care.

	b	c	d	e, $IC_{50, PRZ, AZ}$ [μM]	e, $IC_{50, PRZ, AZ}$ [$\mu g L^{-1}$]	$IC_{10, PRZ, AZ}$ [μM]	$IC_{10, PRZ, AZ}$ [$\mu g L^{-1}$]
Azoxystrobin	-2.24 ± 0.686	101 ± 1.73	156 ± 4.09	0.111 ± 0.0144	41.7 ± 5.39	0.0416 ± 0.0134	15.6 ± 5.01
AZ_M390b	2.78 ± 1.41	-0.0557 ± 13.1	88.7 ± 5.43	0.0970 ± 0.0234	36.4 ± 8.76	0.0440 ± 0.0173	16.5 ± 6.47
AZ_M214	2.73 ± 2.28	-3.29 ± 24.1	117 ± 14.7	0.0472 ± 0.0264	17.7 ± 9.92	0.0211 ± 0.0217	7.91 ± 8.15

A “Lack-of-fit-F-test” with the “anova function” available in the R³ package “drc” from Ritz and Streibig (2005)⁴ was performed to test if there is statistical difference between the dose-response curves fitted to the internal concentrations of azoxystrobin and AZ_M390b, respectively, in *H. azteca* and *G. pulex*. It was tested if the reduction from a larger to a smaller model is statistically justified. Therefore, first, both datasets (data of azoxystrobin or AZ_M390b, respectively, of the two test species) are fitted into one model together but with individual parameters for the log-logistic four parameter model for each dataset. Second, both datasets are fitted into one model with similar parameters for the log-logistic four parameter model.

The calculated p-values showed that there is statistical difference between the dose response curves for azoxystrobin ($p < 0.0059$) and AZ_M390b ($p < 0.0130$), respectively, for the two test species.

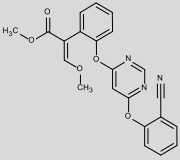
SI.I Comparison of different *H. azteca* Sample Wet Weights for Detection and Quantification of Biotransformation Products

Measuring internal concentrations at different time points during the uptake and depuration phase requires the use of plenty of test organisms (~2000 organisms if one sample is composed of 50 organisms). Therefore, reducing the amount of organisms was tried. For the *H. azteca* screening experiment (exposure to 100 $\mu g L^{-1}$ azoxystrobin) the same sample wet weight as applied in the *G. pulex* bioaccumulation and biotransformation experiments was used (~130 mg which relate to 4 *G. pulex* or 50 *H. azteca*). Additionally, a reduced wet weight of ~70 mg (30 *H. azteca*) with similar exposure concentrations was tested to evaluate if a decreased wet weight is sufficient in terms of LOQs of BTPs (see SI B). All BTPs of azoxystrobin were still detected in the extracts of the reduced sample wet weight. However, the sulfate-containing BTPs are more sensitive during negative electrospray ionization but have to be quantified in positive ionization mode since their quantification is based on the

parent compound, which is only detectable in positive ionization mode. Therefore, two sulfate-containing BTPs (AZ_M514 and AZ_M618) that already displayed very low intensities using ~130 mg wet weight, could no longer be quantified. The loss of two minor BTPs was considered acceptable in the light of reducing the number of test organisms. This is why the kinetic experiment was carried out with the reduced wet weight.

SI.J Identified Biotransformation Products for Azoxystrobin and Prochloraz in *H. azteca*

Table S4-13: Overview of azoxystrobin and identified biotransformation products formed in the aquatic invertebrate *H. azteca*. Biotransformation products are listed according to their relative peak intensity. Information about mass error and retention time (RT) are given for both replicate samples. CE stands for collision energy applied for fragmentation in the MS/MS experiment. Below each biotransformation product the abbreviation (S) stands for “identified by suspect screening (S)”, whereas (N) stands for “identified by nontarget” screening. The abbreviation (H) stands for BTPs that were only identified in *H. azteca* and not in *G. pulex*. (H‡) stands for BTPs that were afterward identified in *G. pulex*, but with intensities below the set threshold of 1E6. The mass error of all identified BTPs was < 3ppm.

Compound	Formula [M]	RT [min] ⁱⁱⁱ⁾	Polarity	Elemental change ^{iv)}	Log D _{ow} ^{v)}	Identification confidence ^{vi)}	Description	CE [eV]	MS/MS confirmatory ions ^{viii)}
MassBank ID of displayed MS/MS spectrum	Exact mass of [M+H] ⁺ / [M-H] ⁻					/level according to Schymanski et al. (2014) ^{6/ vii)}			
Azoxystrobin	C ₂₂ H ₁₇ N ₃ O ₅	14.6	+		4.2	/1/	parent compound	15	
ET270001	404.1241	14.6							
 <p>BAF [L kg_{ww}⁻¹] at t₂₄ⁱ⁾: 4; 4 BAF_k [L kg_{ww}⁻¹] ii): 6</p>									
AZ_M638 (H)	C ₃₀ H ₂₇ O ₁₃ N ₃	12.7	+	- CH ₂	-1.3	d, p	demethylation,	20	390.1083
ET273401	638.1617	12.7		+ C ₆ H ₁₀ O ₅		/3/, most likely structure	glucose conjugation,		358.0821
(N)				+ C ₃ H ₂ O ₃			malonyl conjugation		302.0916
AZ_M640 (H)	C ₃₀ H ₂₉ O ₁₃ N ₃	13.0	+	- CH ₂	-1.8	d, p	demethylation,	20	392.1239
ET273301	640.1773	13.0		+ H ₂		/3/, most likely structure	hydrogenation,		342.0872
(N)				+ C ₆ H ₁₀ O ₅			glucose conjugation,		360.0979
				+ C ₃ H ₂ O ₃			malonyl conjugation		

Compound MassBank ID of displayed MS/MS spectrum	Formula [M] Exact mass of [M+H] ⁺ / [M-H] ⁻	RT [min] ⁱⁱⁱ⁾	Polarity	Elemental change ^{iv)}	Log D _{ow} ^{v)}	Identification confidence ^{vi)} /level according to Schymanski et al. (2014) ^{6/ vii)}	Description	CE [eV]	MS/MS confirmatory ions ^{viii)}
AZ_M390a ET273701 (S)	C ₂₁ H ₁₅ N ₃ O ₅ 390.1084	11.9 11.7	+	- CH ₂	3.5	D /2b/	demethylation	30	372.0979 344.1031 329.0795
AZ_M390b ET273801 (S)	C ₂₁ H ₁₅ N ₃ O ₅ 390.1084	13.6 13.6	+	- CH ₂	0.4	I ⁵⁻⁷ /1/	ester hydrolysis	30	372.0981 344.1032 302.0927
AZ_M497 (H) ET271902 (S)	C ₂₃ H ₂₀ N ₄ O ₇ S 497.1125	11.5 11.4	+	- CH ₂ + C ₂ H ₅ NO ₂ S	-0.1	d (in negative ionization mode diagnostic taurine loss), p for conjugation of AZ_M390b /2b/	demethylation, taurine conjugation	40	344.1031 329.0795 372.0979
AZ_M392 ET274601 (S)	C ₂₁ H ₁₇ N ₃ O ₅ 392.1241	13.5 13.5	+	- CH ₂ + H ₂	0.1	I ⁵ p /3/, most likely structure	ester hydrolysis, hydrogenation	15	342.0871 392.1238 360.0977
AZ_M630 ET273251 (S)	C ₂₇ H ₂₅ N ₃ O ₁₃ S 630.1035	11.7 11.6	- ^{ix)}	- CH ₂ + C ₆ H ₁₀ O ₅ + SO ₃	-0.5	d, p /3/, most likely structure	demethylation, glucose conjugation, sulfate conjugation	20	241.0024 96.9601 630.1038
AZ_M420 ET274902 (S)	C ₂₂ H ₁₇ N ₃ O ₆ 420.1190	11.2-14.5 11.1-14.4	+	+ O	3.6-3.7	p for hydroxylation at the (<i>E</i>)-methyl β- methoxyacrylate group /3/, 3 positional isomers	aliphatic hydroxylation	40	329.0796 360.0979 316.1075

Compound MassBank ID of displayed MS/MS spectrum	Formula [M] Exact mass of [M+H] ⁺ / [M-H] ⁻	RT [min] ⁱⁱⁱ⁾	Polarity	Elemental change ^{iv)}	Log D _{ow} ^{v)}	Identification confidence ^{vi)} /level according to Schymanski et al. (2014) ^{6/ vii)}	Description	CE [eV]	MS/MS confirmatory ions ^{viii)}
AZ_M214 ET274201 (S)	C ₁₁ H ₇ N ₃ O ₂ 214.0611	7.9	+	- C ₁₁ H ₁₀ O ₃	2.3	D I ⁵	ether cleavage	40	214.0610 187.0501 120.0442
AZ_M362b ET274501 (S)	C ₂₀ H ₁₅ N ₃ O ₄ 362.1135	14.4	+	- C ₂ H ₂ O	0.8-2.8	d for C ₂ H ₂ O loss at the (<i>E</i>)-methyl β- methoxyacrylate group /3/, ≥ 3 positional isomers	- C ₂ H ₂ O	20	362.1135 302.0922 330.0872
AZ_M485 (H) ET272401 (S)	C ₂₂ H ₂₀ N ₄ O ₇ S 485.1125	10.9	+	- C ₂ H ₂ + H ₂ + C ₂ H ₅ NO ₂ S	-0.9	d, p for conjugation of AZ_M390b /3/ most likely structure	ester hydrolysis, demethylation, hydrogenation, taurine product	20	126.0220 342.0875 467.1022
AZ_M378 ET274102 (S)	C ₂₀ H ₁₅ N ₃ O ₅ 378.1084	12.4	+	- C ₂ H ₂	-0.5	D /2b/	hydrogenation, didemethylation,	15	378.1082 342.0872 360.0972
AZ_M552 ET273904 (S)	C ₂₇ H ₂₅ N ₃ O ₁₀ 552.1613	12.4	+	- CH ₂ + C ₆ H ₁₀ O ₅	1.8	d, p /3/, most likely structure	demethylation, glucose conjugation	15	358.0822 390.1085 552.1632
AZ_M541 (H) ET272201 (S)	C ₂₅ H ₂₄ N ₄ O ₈ S 541.1388	11.0	+	+ O + C ₃ H ₇ NO ₂ S	0.5	d, p /3/, 3 positional isomers	aliphatic hydroxylation, cysteine product	20	491.1020 388.0923 328.0852

Compound MassBank ID of displayed MS/MS spectrum	Formula [M] Exact mass of [M+H] ⁺ / [M-H] ⁻	RT [min] ⁱⁱⁱ⁾	Polarity	Elemental change ^{iv)}	Log D _{ow} ^{v)}	Identification confidence ^{vi)} /level according to Schymanski et al. (2014) ^{6/ vii)}	Description	CE [eV]	MS/MS confirmatory ions ^{viii)}
AZ_M513 (H) ET272701 (S)	C ₂₃ H ₂₀ N ₄ O ₈ S 513.1074	11.4 11.3	+	- CH ₂ + O + C ₂ H ₅ NO ₂ S	-0.7 to 0.1	d, p for taurine loss and conjugation of AZ_M390b /3/ 2 positional isomers	demethylation, aliphatic hydroxylation, taurine conjugation	20	356.0666 513.1076 481.0806
AZ_M554b (H) ET272101 (S)	C ₂₇ H ₂₇ N ₃ O ₁₀ 554.1769	12.8 12.8	+	- CH ₂ + H ₂ + C ₆ H ₁₀ O ₅	1.4	p /3/, most likely structure	demethylation, hydrogenation, glucose conjugation	20	392.1239 342.0875 360.0979
AZ_M582b (H) ET272604 (S)	C ₂₈ H ₂₇ N ₃ O ₁₁ 582.1718	13.2 13.2	+	+ O + C ₆ H ₁₀ O ₅	1.9-2.2	d, p for hydroxylation and glucose conjugation at the (<i>E</i> - methyl β- methoxyacrylate group /3/, 3 positional isomers	aliphatic hydroxylation, glucose conjugation	15	145.0492 334.1185 316.1089
AZ_M582a (H) ET272501 (S)	C ₂₈ H ₂₇ N ₃ O ₁₁ 582.1718	11.2 11.1	+	+ O + C ₆ H ₁₀ O ₅	1.9-2.2	p for hydroxylation and glucose conjugation at the (<i>E</i> - methyl β-meth- oxyacrylate group /3/, 3 positional isomers	aliphatic hydroxylation, glucose conjugation	15	550.1453 388.0932 420.1190

Compound MassBank ID of displayed MS/MS spectrum	Formula [M] Exact mass of [M+H] ⁺ / [M-H] ⁻	RT [min] ⁱⁱⁱ⁾	Polarity	Elemental change ^{iv)}	Log D _{ow} ^{v)}	Identification confidence ^{vi)} /level according to Schymanski et al. (2014) ^{6/ vii)}	Description	CE [eV]	MS/MS confirmatory ions ^{viii)}
AZ_M498 ET273152 (S)	C ₂₂ H ₁₇ N ₃ O ₉ S 498.0613	11.4 11.3	- ^{ix)}	+ O + SO ₃	1.3-1.7	p for hydroxylation and sulfate conjugation at the (<i>E</i> - methyl β- methoxyacrylate group /3/, 3 positional isomers	aliphatic hydroxylation, sulfate conjugation	15	498.0614 418.1045 358.0818
AZ_M493 ET274303 (S)	C ₂₄ H ₂₀ N ₄ O ₆ S 493.1176	12.9-14.0	+	- CH ₄ O + C ₃ H ₇ NO ₂ S	1.2-1.3	d, p /3/, most likely structures	- CH ₄ O, cysteine product	20	132.0115 330.0869 461.0911
AZ_M618 ET273052 (S)	C ₂₆ H ₂₅ N ₃ O ₁₃ S 618.1035	11.2 11.1	- ^{ix)}	- CH ₂ + C ₆ H ₁₀ O ₅ + SO ₃ - CH ₂ + H ₂	-4.6	d, p /3/, most likely structure	demethylation, glucose conjugation, sulfate conjugation, ester hydrolysis, hydrogenation	20	241.0025 618.1044 96.9601
AZ_M525 ET274005 (S)	C ₂₅ H ₂₄ N ₄ O ₇ S 525.1438	12.5-13.3 12.5-13.4	+	+ C ₃ H ₇ NO ₂ S	1.1	p /3/, most likely structure	cysteine product	20	372.0980 330.0870 461.0893

Compound MassBank ID of displayed MS/MS spectrum	Formula [M] Exact mass of [M+H] ⁺ / [M-H] ⁻	RT [min] ⁱⁱⁱ⁾	Polarity	Elemental change ^{iv)}	Log D _{ow} ^{v)}	Identification confidence ^{vi)} /level according to Schymanski et al. (2014) ^{6/ vii)}	Description	CE [eV]	MS/MS confirmatory ions ^{viii)}
AZ_M514	C ₂₂ H ₁₇ N ₃ O ₁₀ S	11.2	- ^{ix)}	+ O	-0.8-2.0	d for only one hydroxylation at the (<i>E</i>)-methyl β-methoxy- acrylate group	aliphatic hydroxylation,	20	359.0535
ET272851 (S)	514.0562	11.1		+ O + SO ₃		p for hydroxylation and sulfate conjugation at the (<i>E</i> - methyl β- methoxyacrylate group /3/ many positional isomers	hydroxylation, sulfate conjugation		434.1000 514.0580

ⁱ⁾ See Equation 5 in the manuscript for the calculation of BAFs at steady state.

ⁱⁱ⁾ See Equation 6 in the manuscript for the calculation of kinetic BAF_ks.

ⁱⁱⁱ⁾ In case of a retention time range, several possibly positional isomers were integrated as one peak, due to bad peak separation.

^{iv)} The elemental change refers to the change in the molecular formula of the biotransformation product in comparison with the parent compound.

^{v)} Log D_{ow} values were predicted by MarvinSketch version 14.10.20.0 at pH 7.9 and 25 °C. Log D_{ow} values correspond to corrected log K_{ow} values to account for pH-dependent dissociation. At pH 7.9 azoxystrobin is neutral thus log D_{ow} is equal to log K_{ow}. If different positional isomers are possible for one BTP, a range of log D_{ow} values is given.

^{vi)} D: diagnostic fragment/evidence for one structure; d: diagnostic fragment/evidence for positional isomers; l: structure reported in literature; m: MS/MS data from literature; p: biotransformation pathway information; d, p: diagnostic fragment for positional isomers (d) in combination with pathway information (p) give evidence for one possible structure.

^{vii)} Levels are defined as follows: 5 (*exact mass*), 4 (*unequivocal molecular formula*), 3 (*tentative candidates: e.g., positional isomers*), 2 (*probable structure: library spectrum match (a) or diagnostic evidence for one structure (b)*) and 1 (*confirmed structure*).

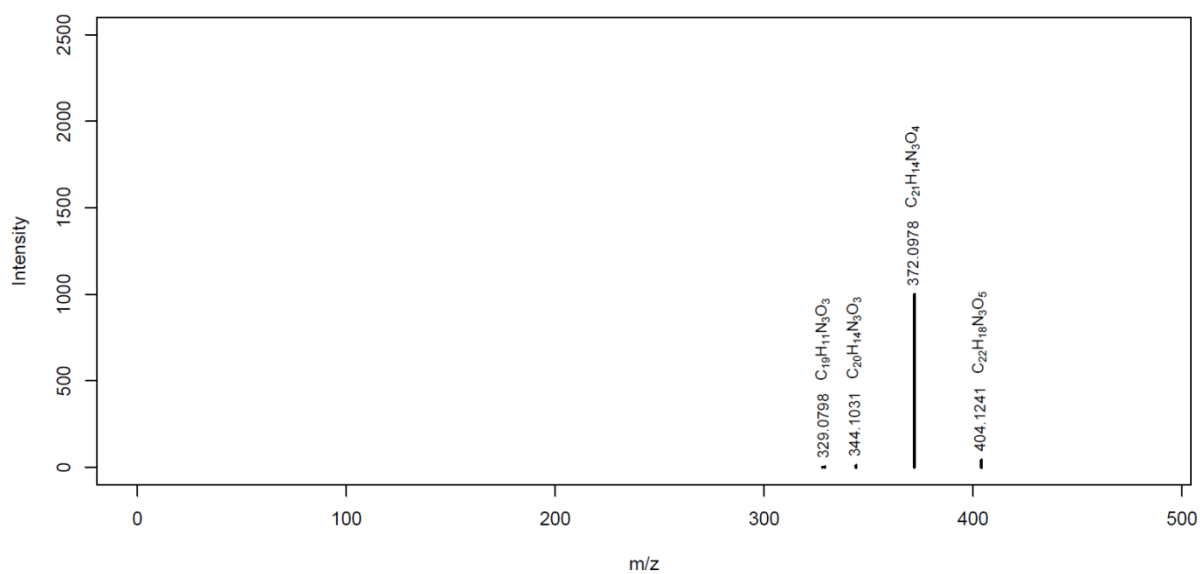
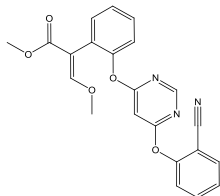
^{viii)} Diagnostic fragments (d, D) are listed first and are represented in bold in the table, other characteristic fragments are then presented according to their relative abundance. Only fragments where a chemical formula and structure could be attributed are considered.

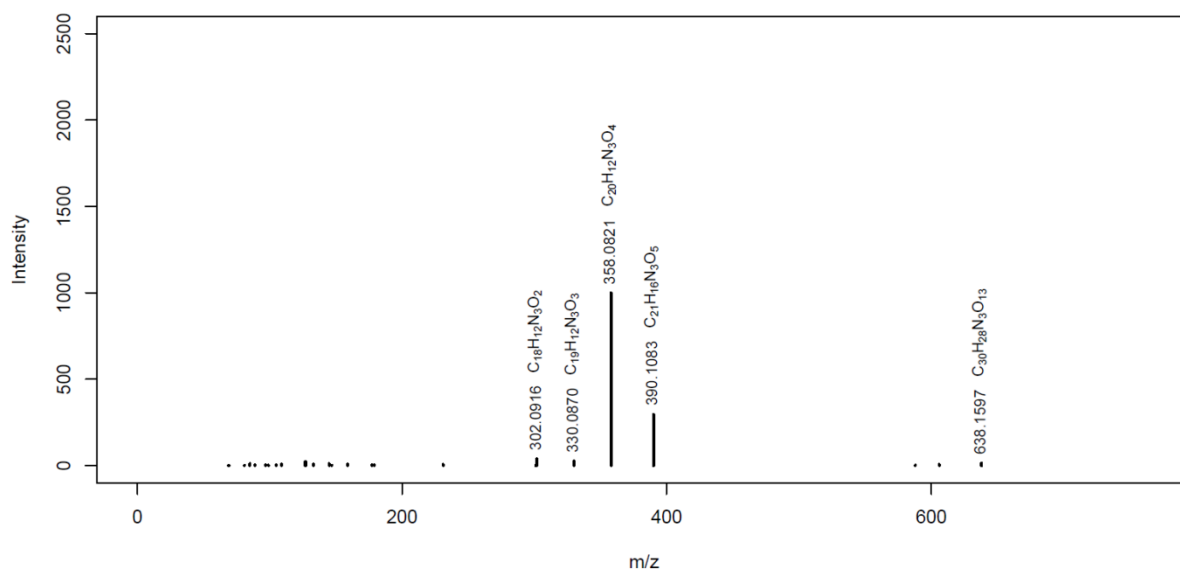
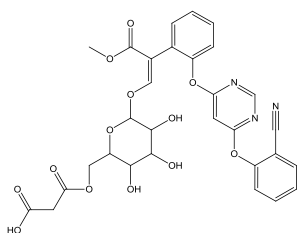
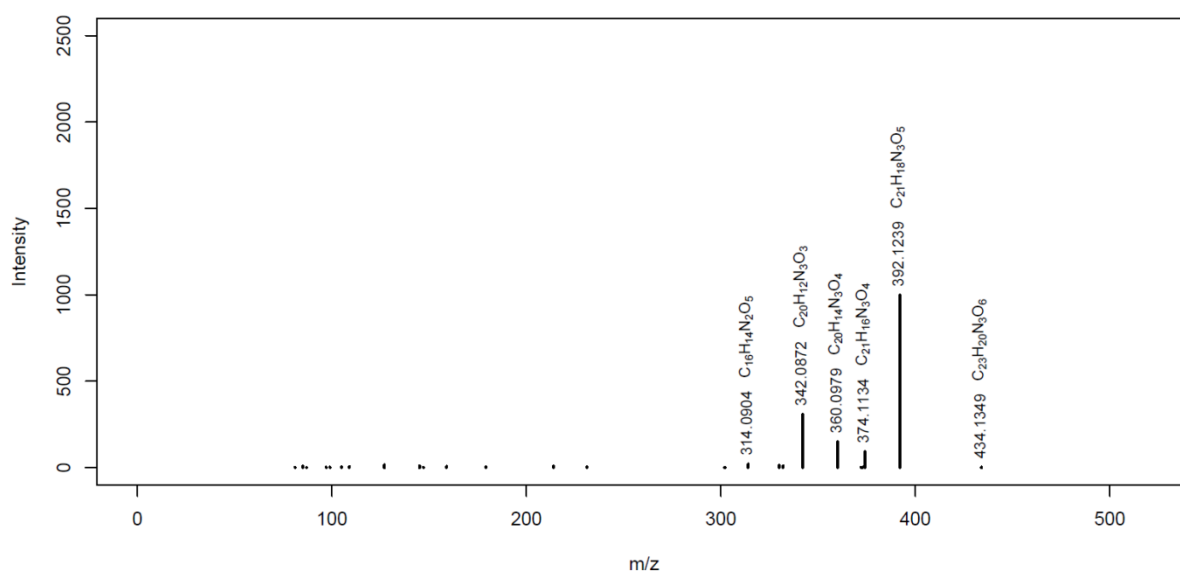
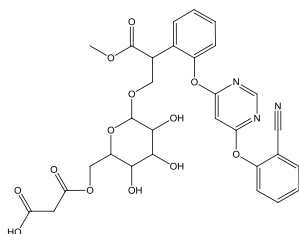
^{ix)} The sulfate-containing BTPs are more sensitive in negative ionization mode. However, they were quantified in positive ionization mode because azoxystrobin was detected and quantified in positive ionization mode.

The different MassBank IDs for one compound refer to different collision energies applied during MS/MS fragmentation. The MassBank ID displayed in bold indicates the depicted MS/MS spectrum. Spectra are also available electronically in the MassBank database.⁸

Azoxystrobin (AZ)

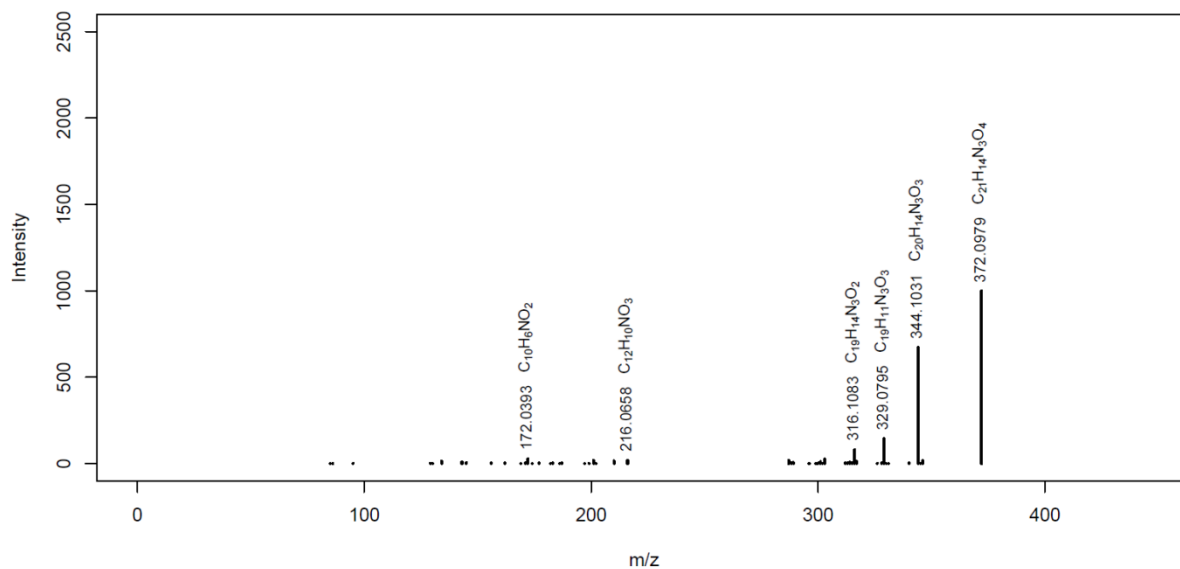
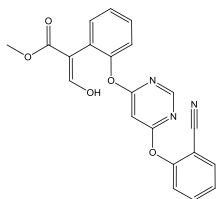
MassBank ID: **ET270001**



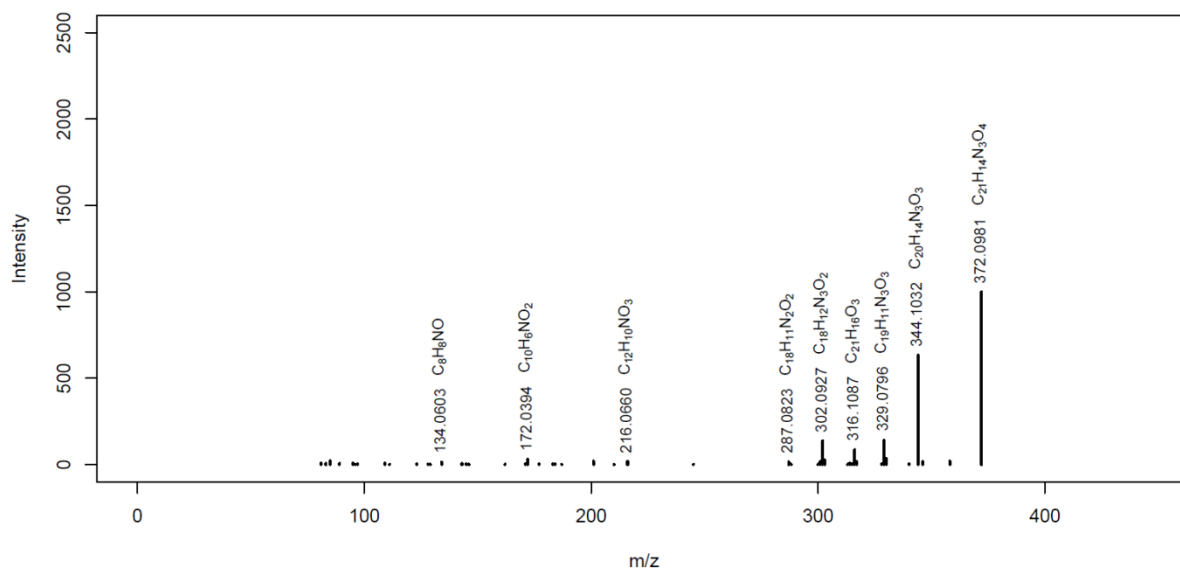
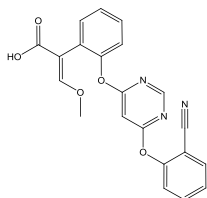
AZ_M638MassBank ID: **ET273401**, ET273402, ET273403, ET273404**AZ_M640**MassBank ID: **ET273501**, ET273502, ET273503, ET273504

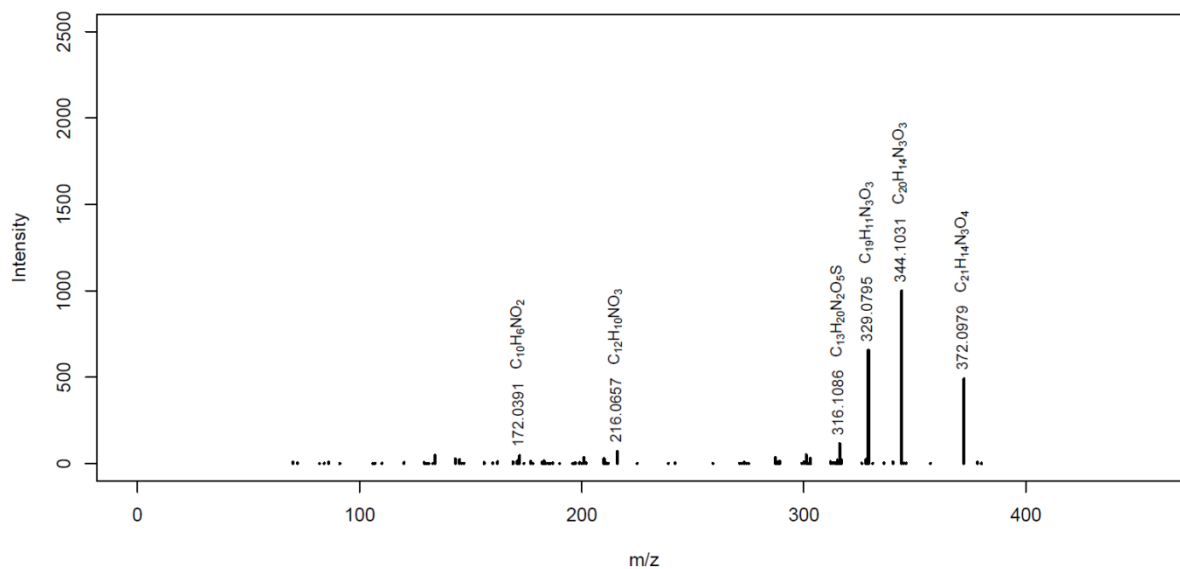
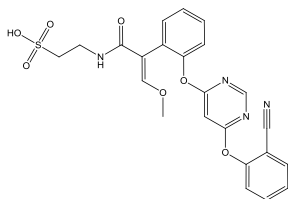
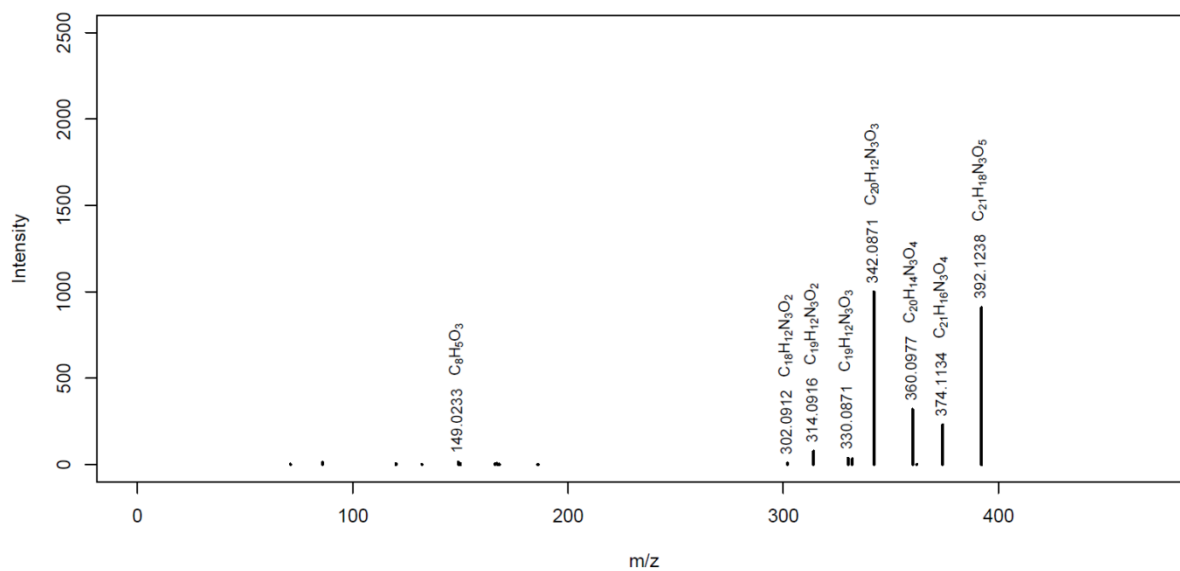
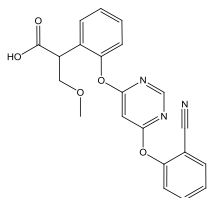
AZ_M390a

MassBank ID: ET273701

**AZ_M390b**

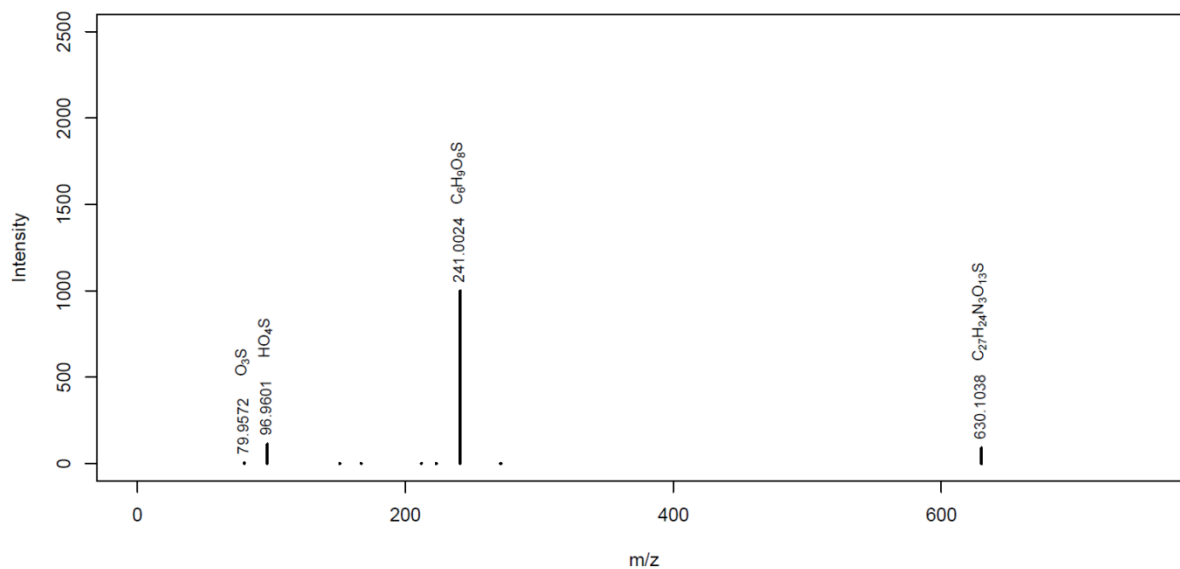
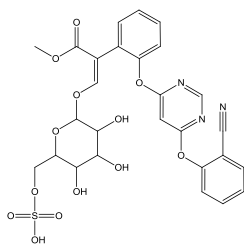
MassBank ID: ET273801



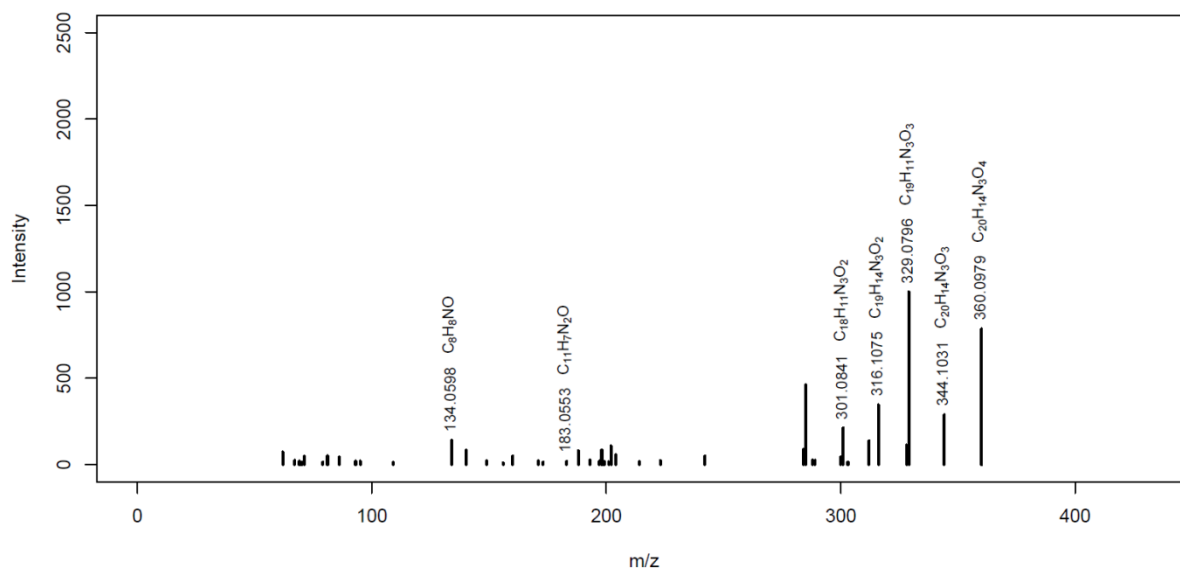
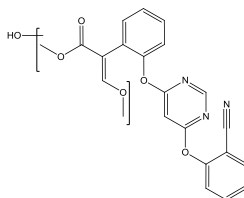
AZ_M497MassBank ID: ET271901, **ET271902**, ET271903, ET271904**AZ_M392**MassBank ID: **ET274601**

AZ_M630

MassBank ID: ET273251

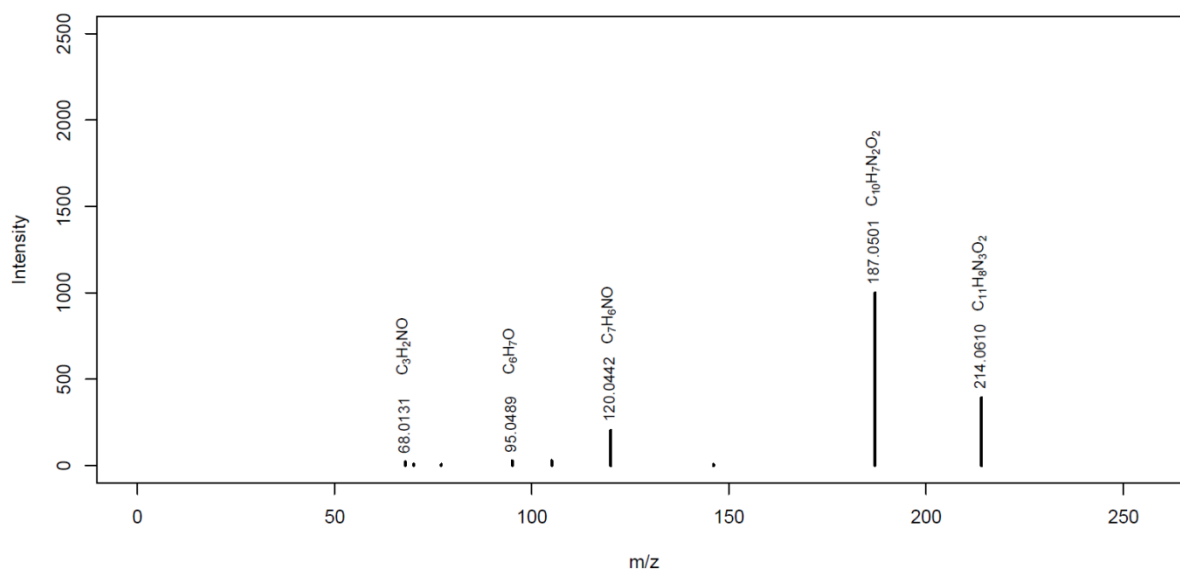
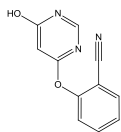
**AZ_M420**

MassBank ID: ET274902

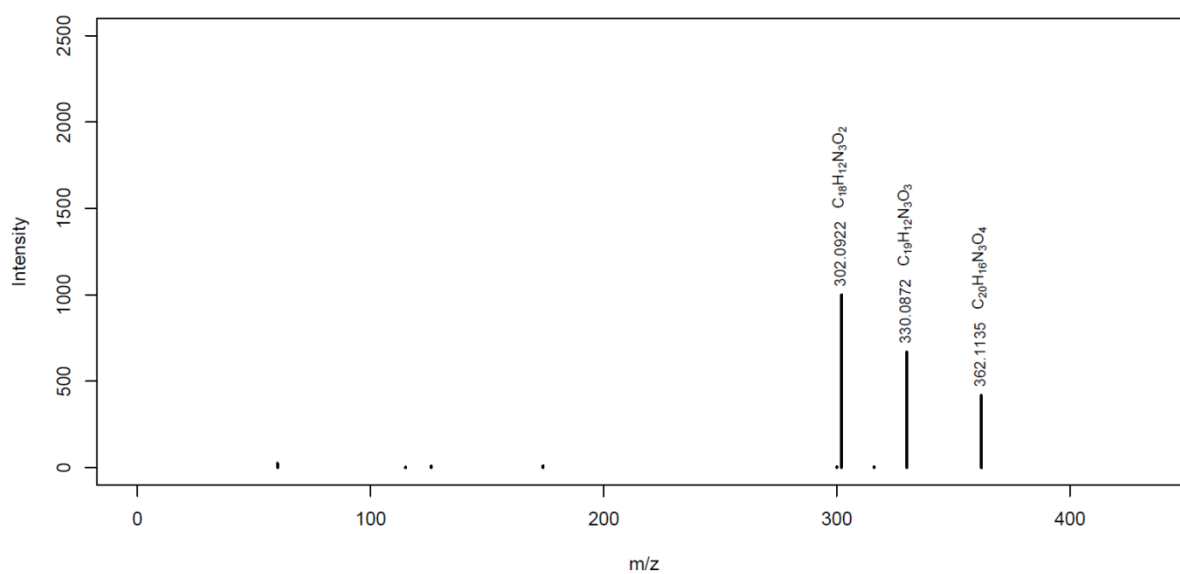
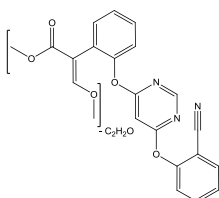


AZ_M214

MassBank ID: ET274201

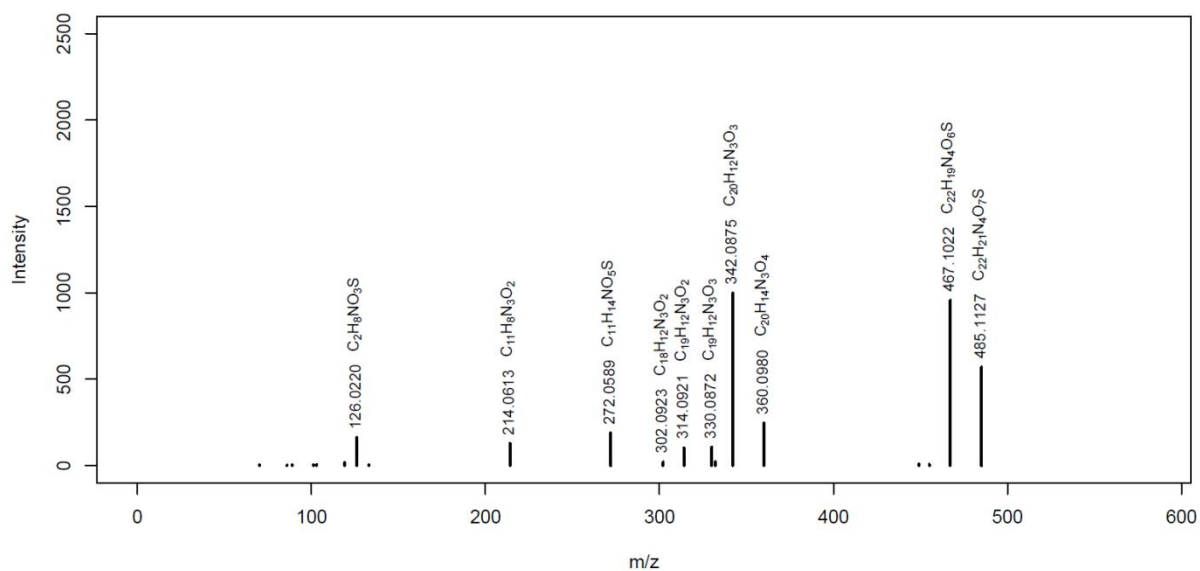
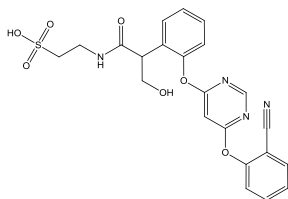
**AZ_M362b**

MassBank ID: ET274501

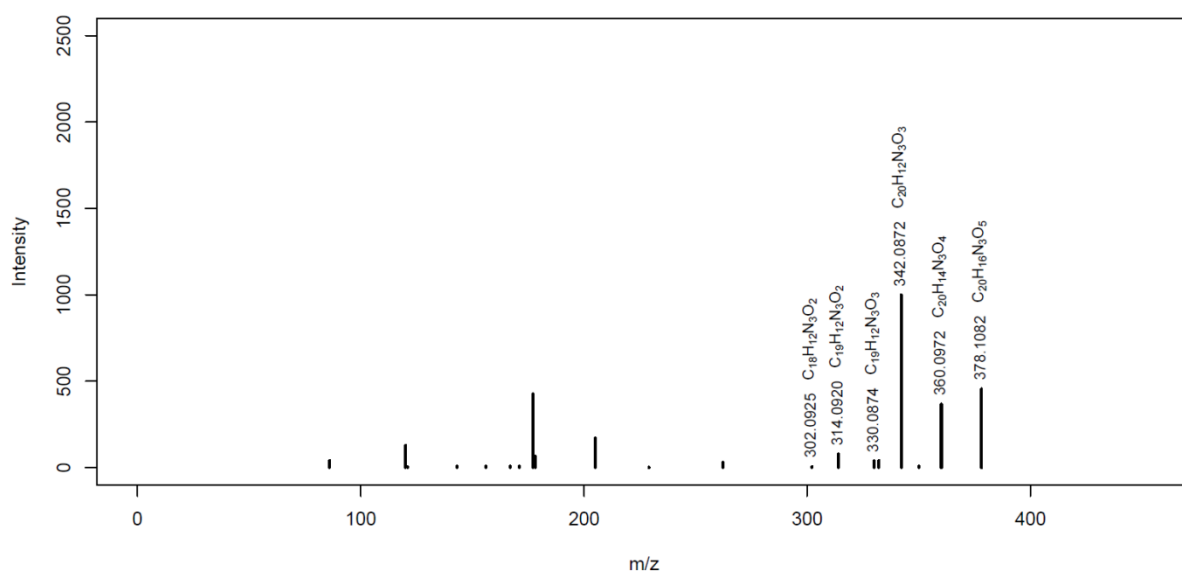
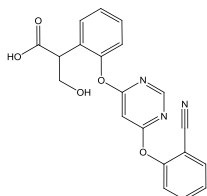


AZ_M485

MassBank ID: ET272401, ET272402, ET272403, ET272404

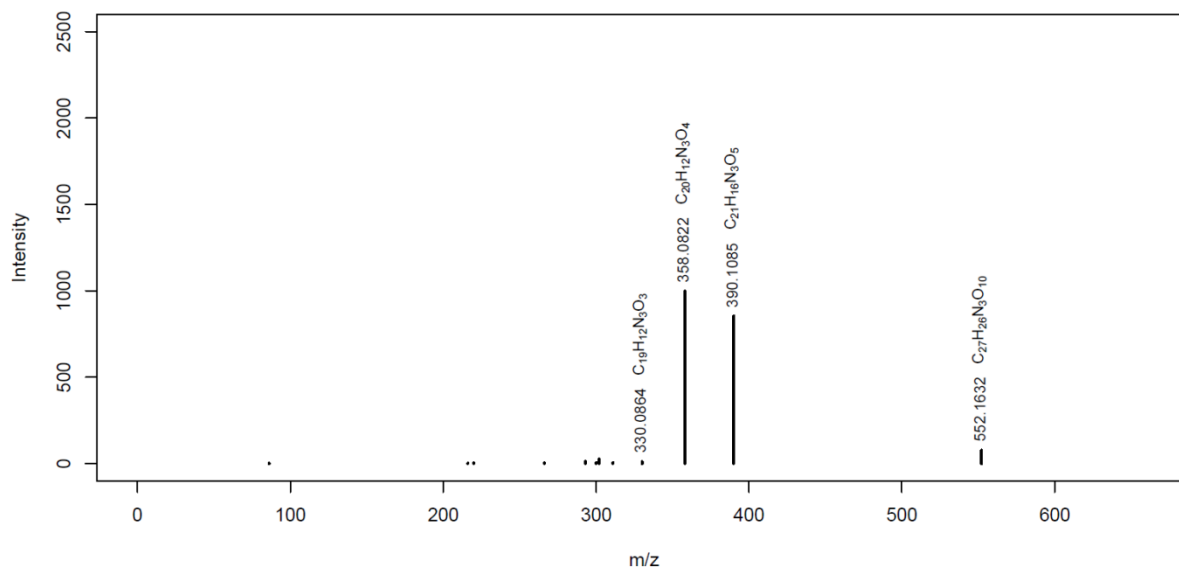
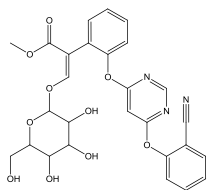
**AZ_M378**

MassBank ID: ET274102

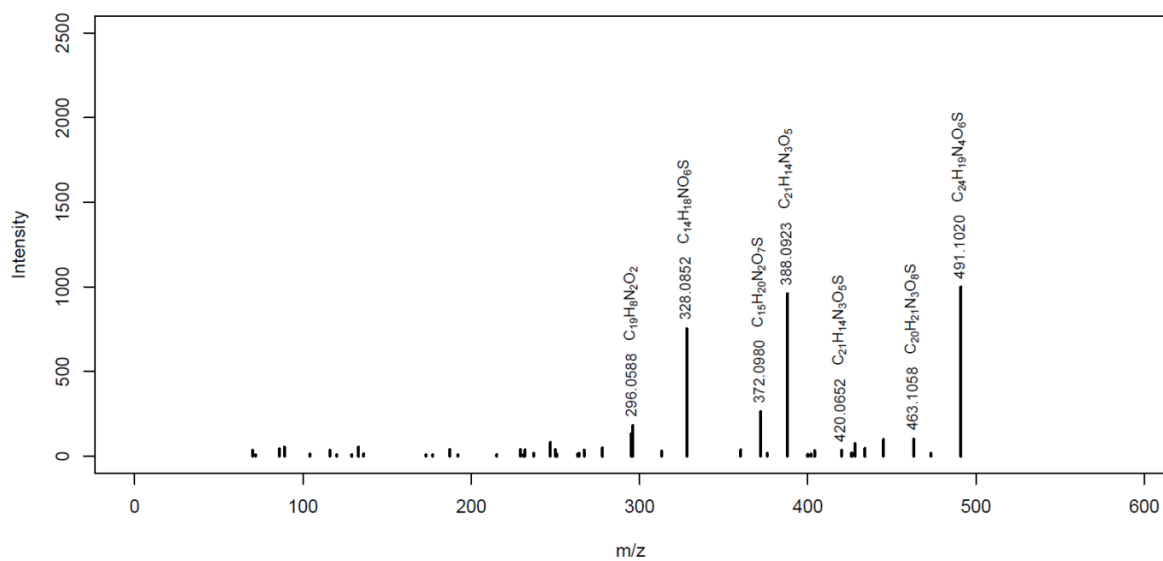
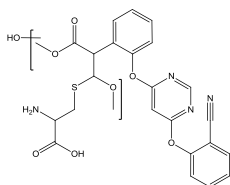


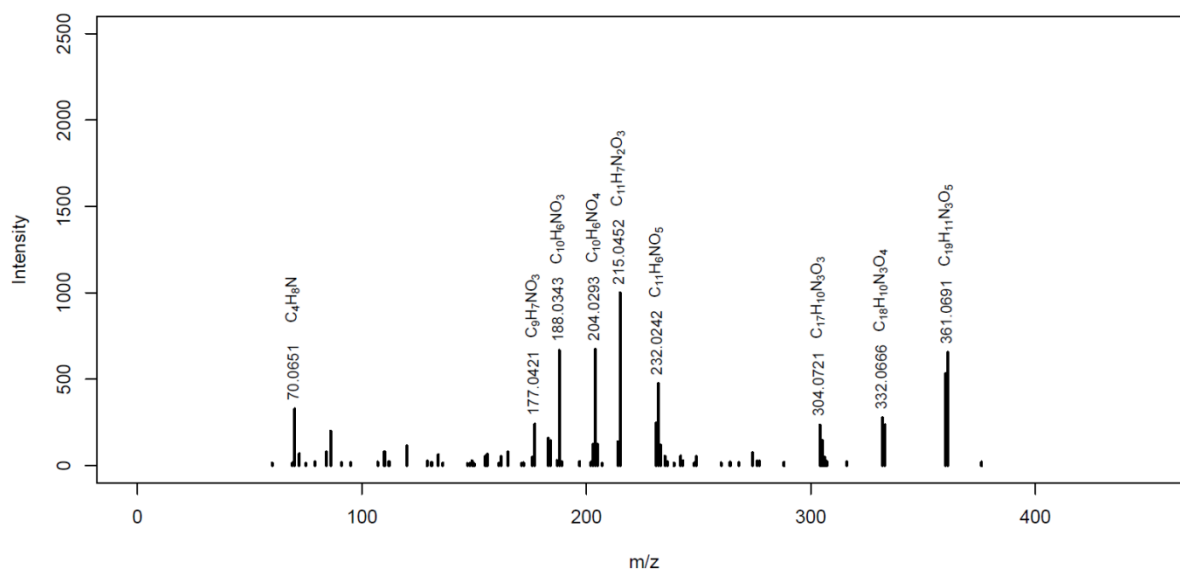
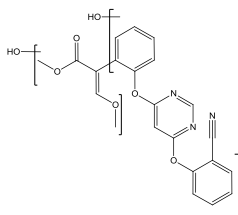
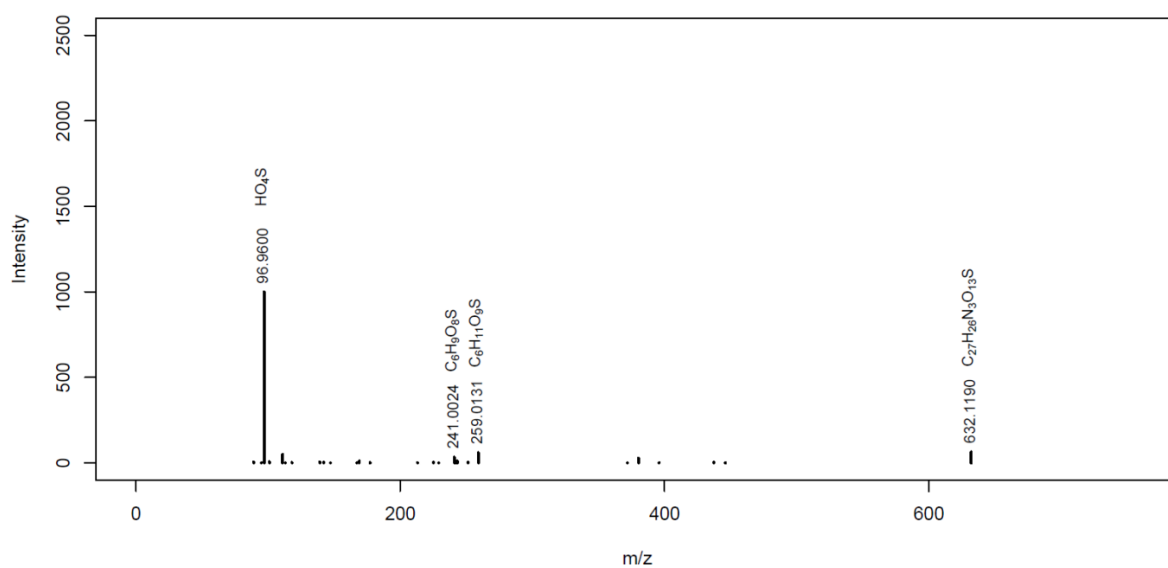
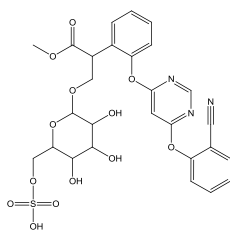
AZ_M552

MassBank ID: ET273904

**AZ_M541**

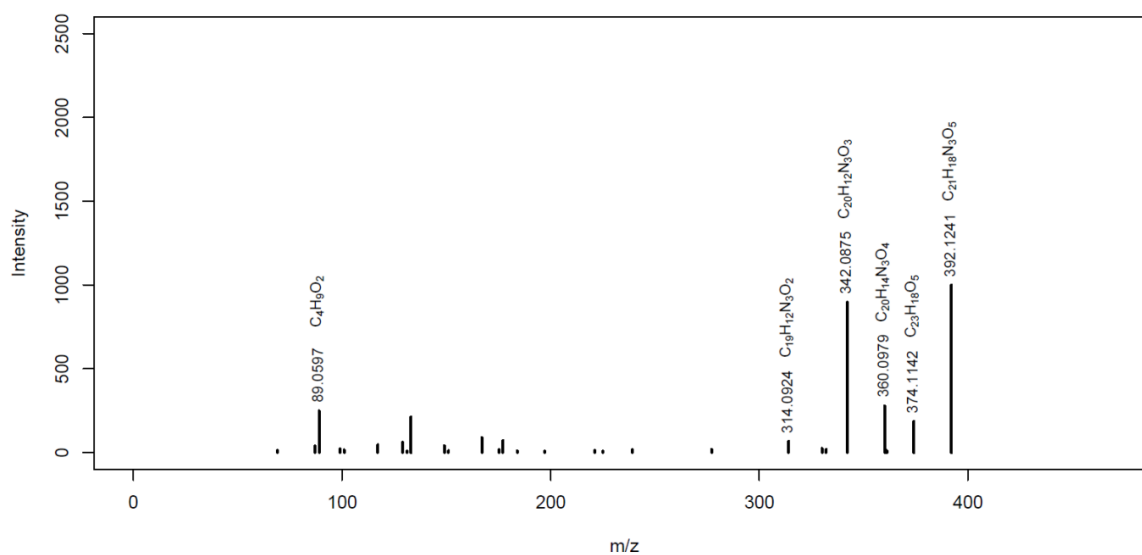
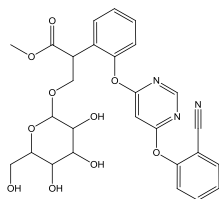
MassBank ID: ET272201, ET272202, ET272203, ET272204



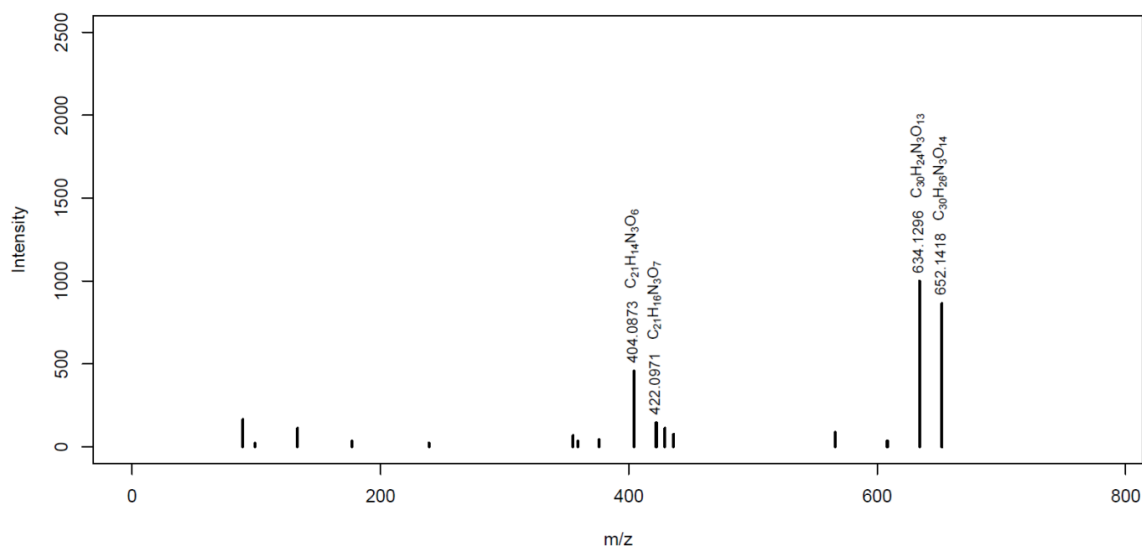
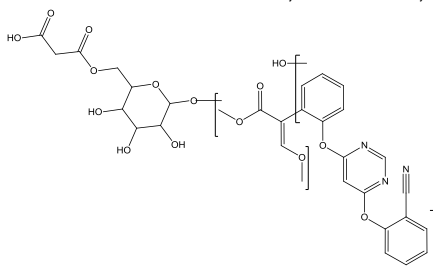
AZ_M436MassBank ID: ET272301, ET272302, **ET272303**, ET272304**AZ_M632**MassBank ID: ET272951, **ET272952**, ET272953, ET272954

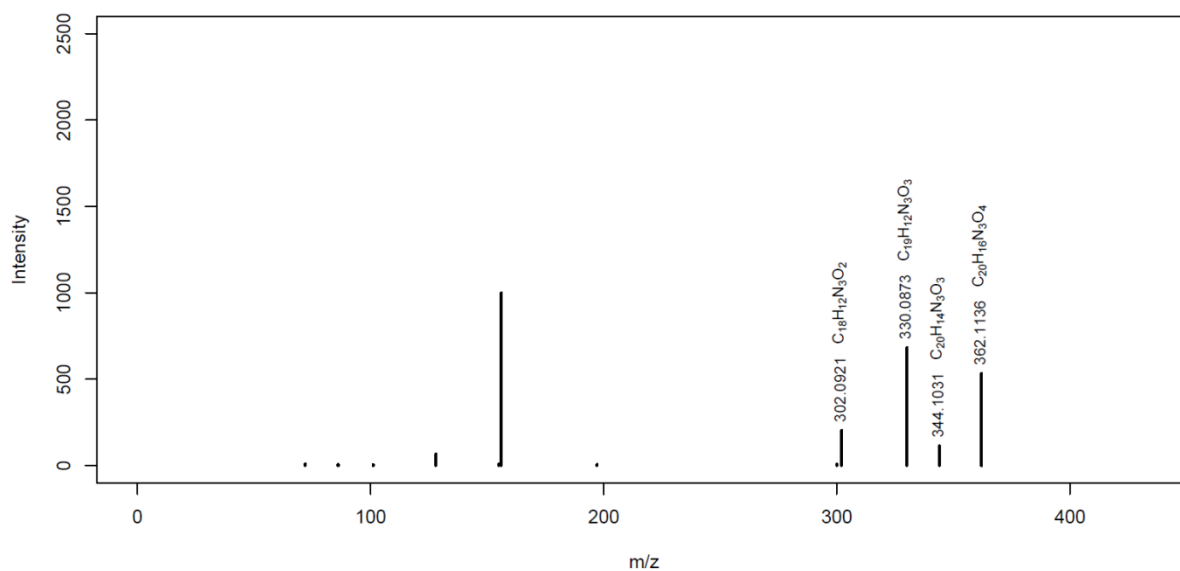
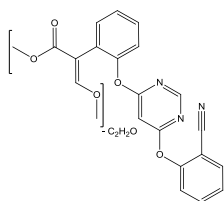
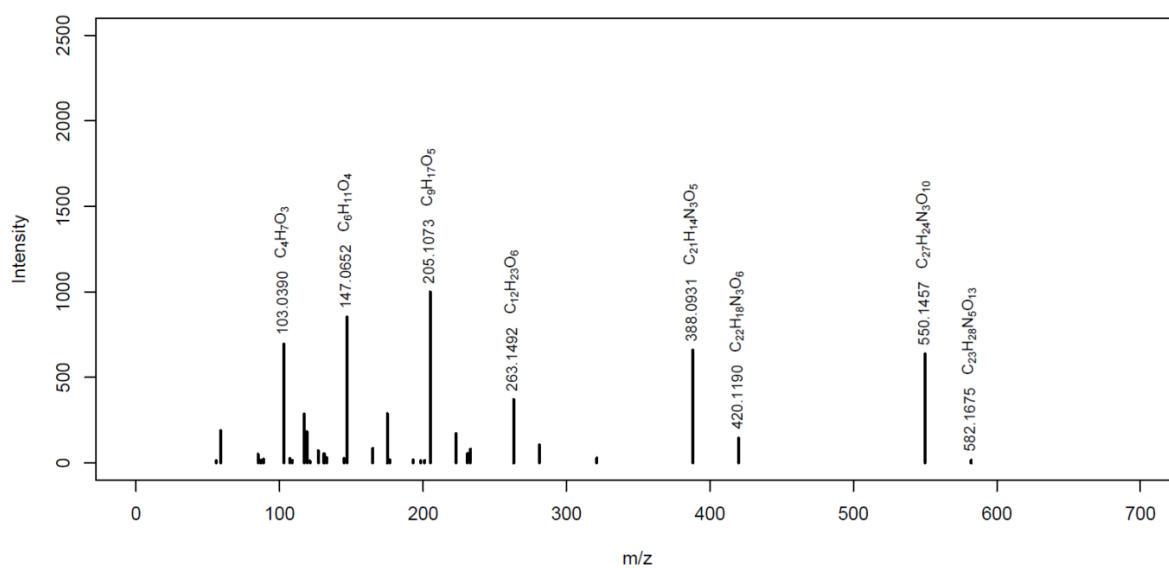
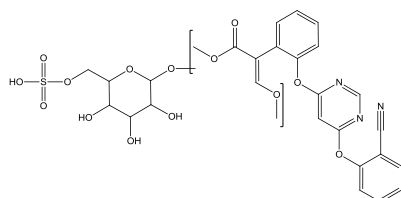
AZ_M554a

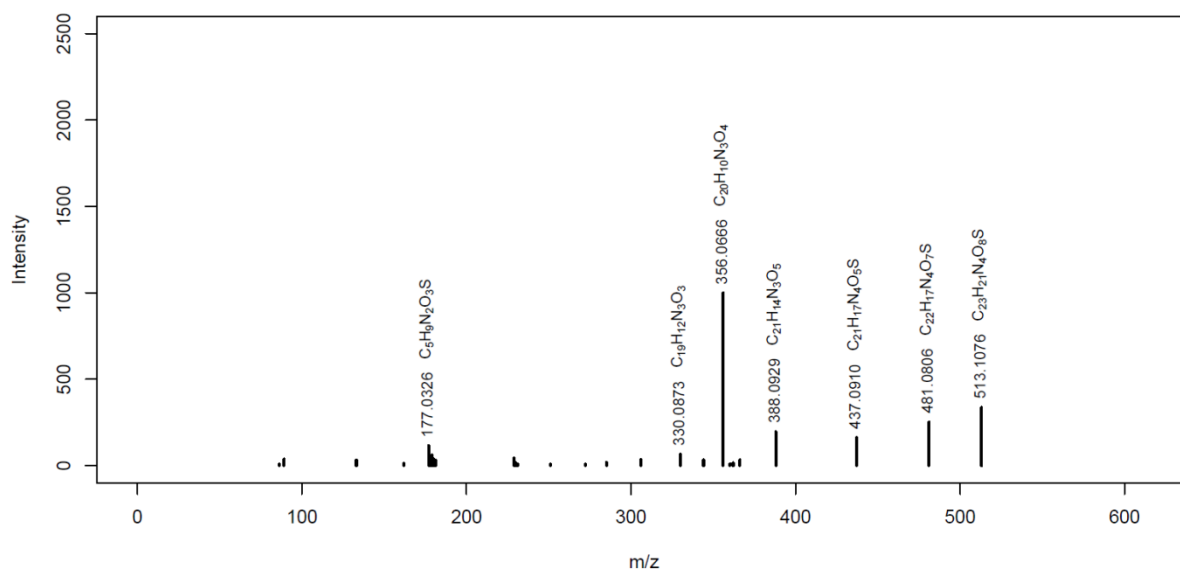
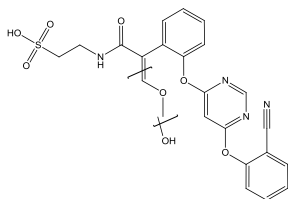
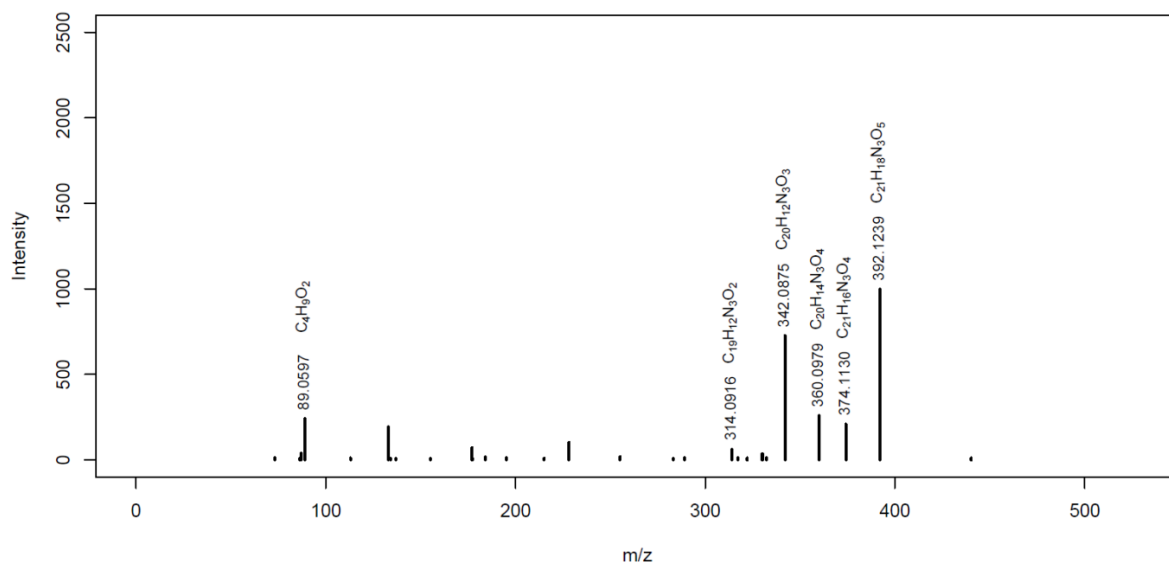
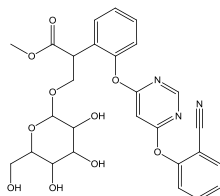
MassBank ID: ET272001, ET272002, ET272003, ET272004

**AZ_M684**

MassBank ID: ET273501, ET273502, ET273503, ET273504

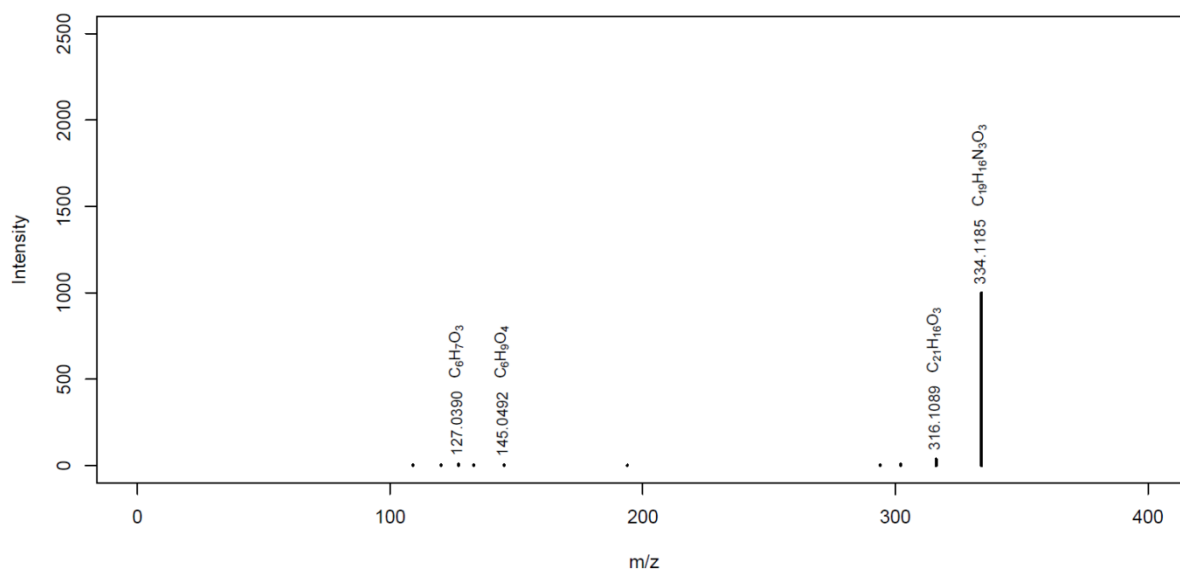
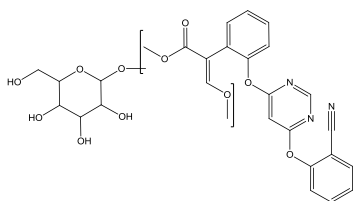


AZ_M362aMassBank ID: **ET274403****AZ_M660**MassBank ID: **ET273601**, ET273602, ET273603, ET273604

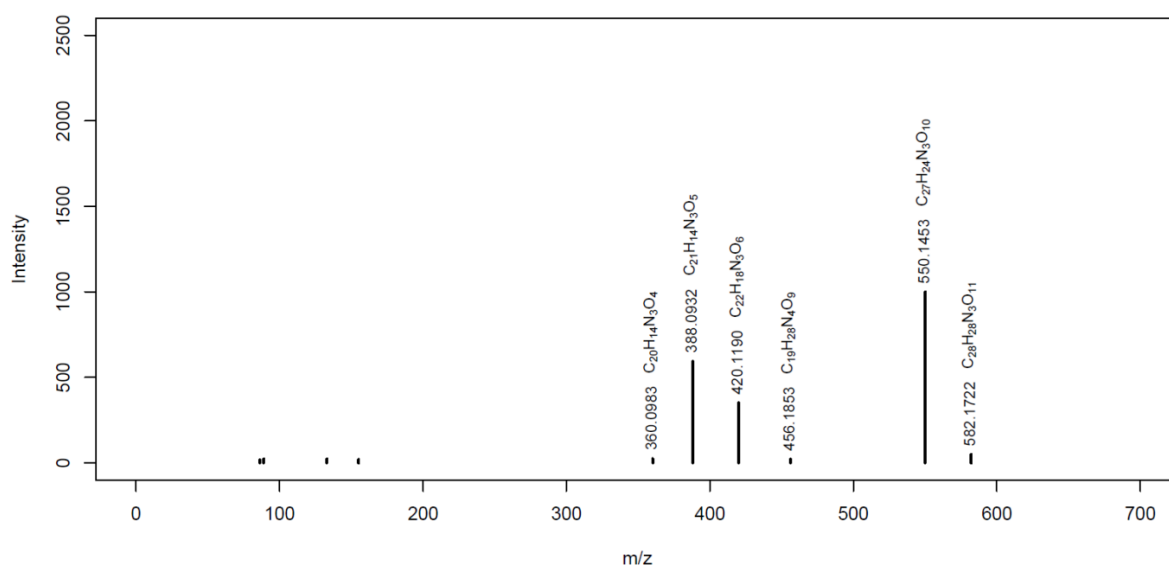
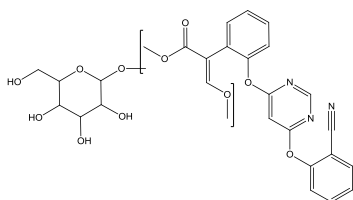
AZ_M513MassBank ID: **ET272701**, ET272702, ET272703, ET272704**AZ_M554b**MassBank ID: **ET272101**, ET272102, ET272103, ET272104

AZ_M582b

MassBank ID: ET272604

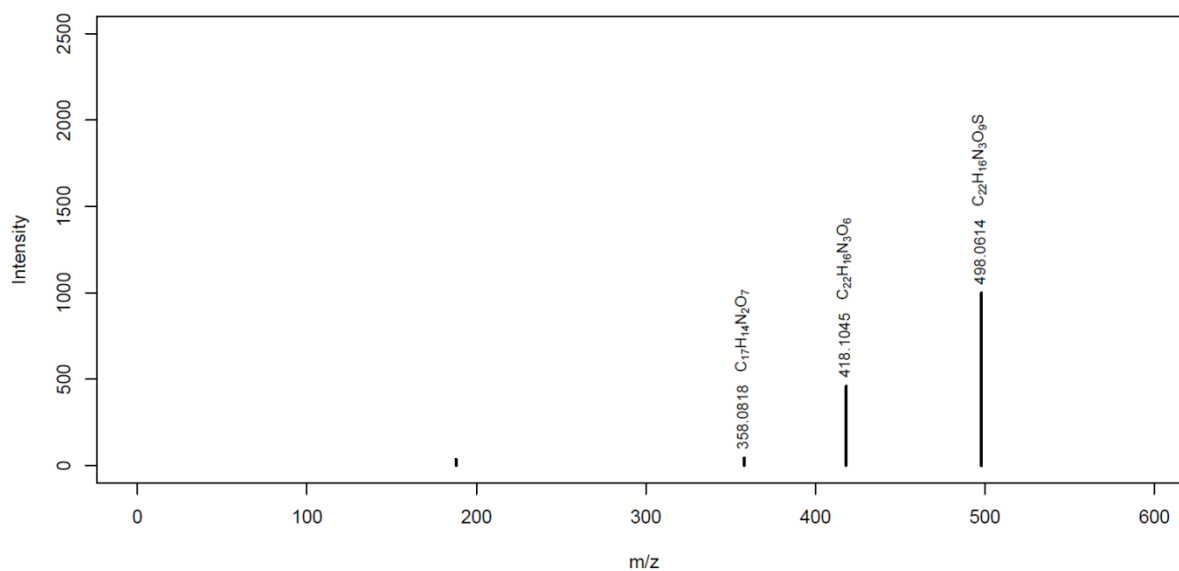
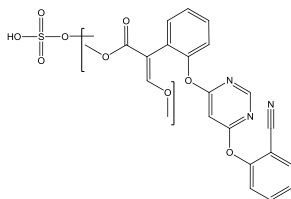
**AZ_M582a**

MassBank ID: ET272501

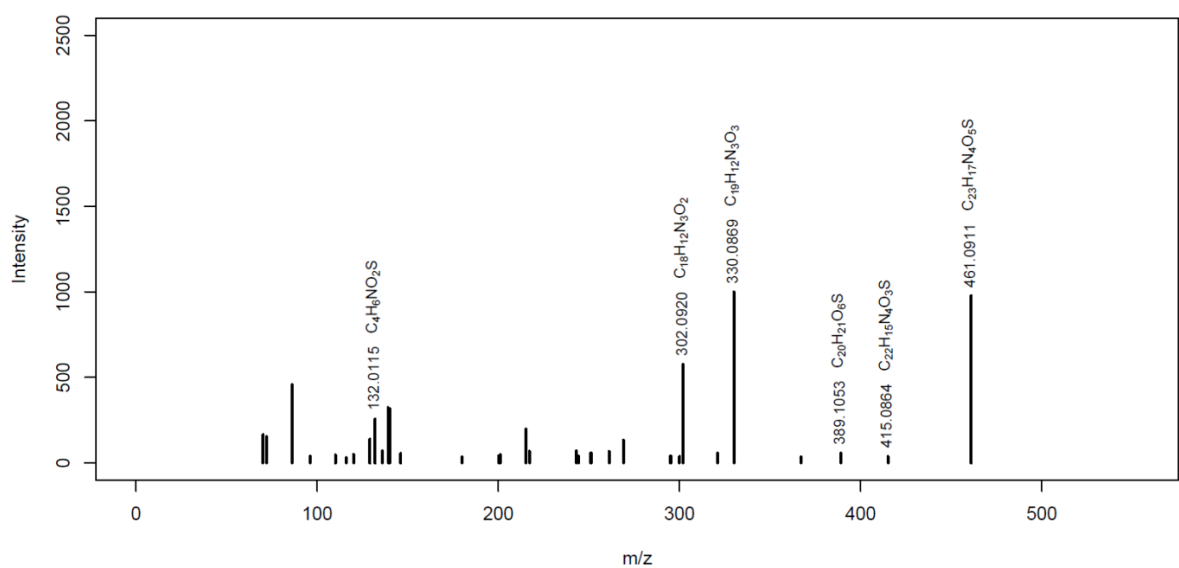
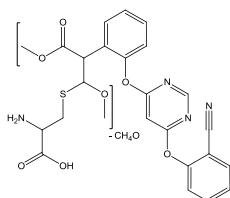


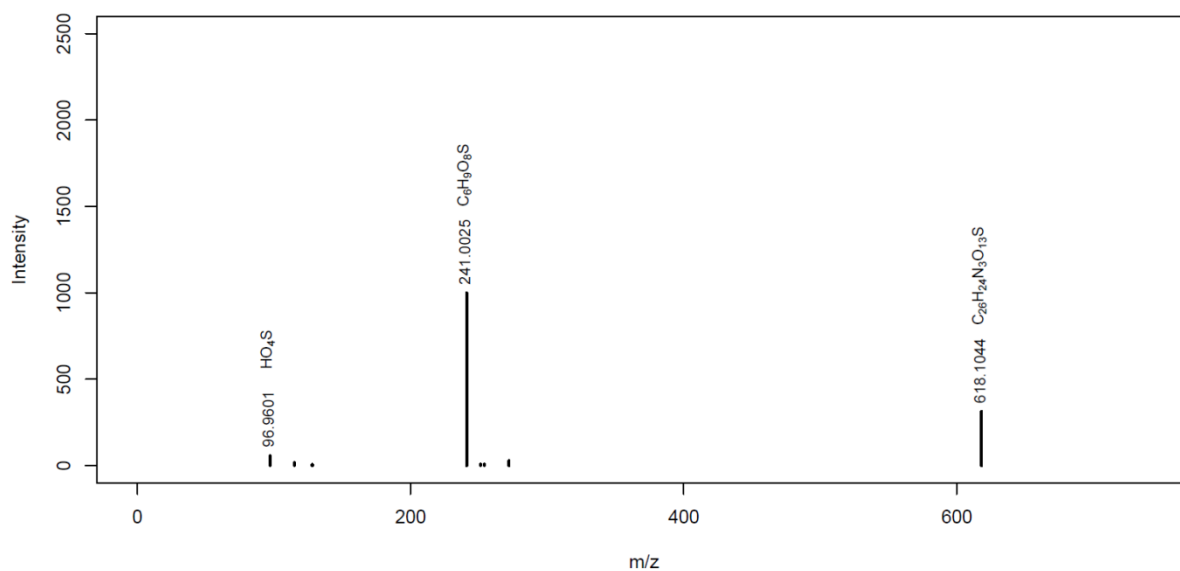
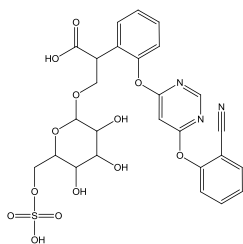
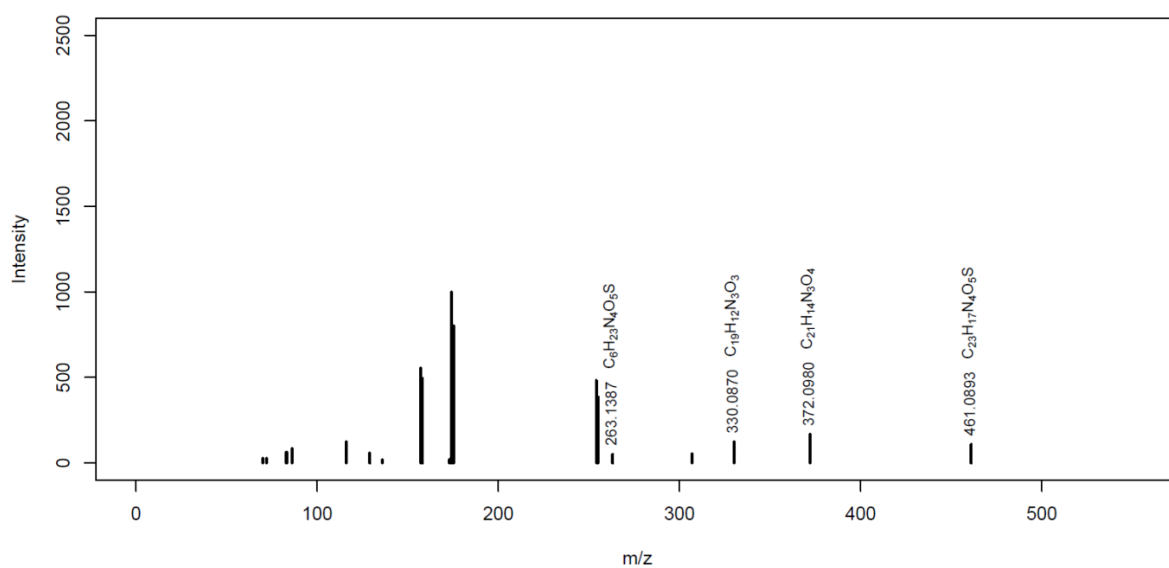
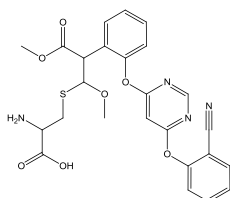
AZ_M498

MassBank ID: ET273152

**AZ_M493**

MassBank ID: ET274303



AZ_M618MassBank ID: ET273051, **ET273052**, ET273053, ET273054**AZ_M525**MassBank ID: **ET274005**

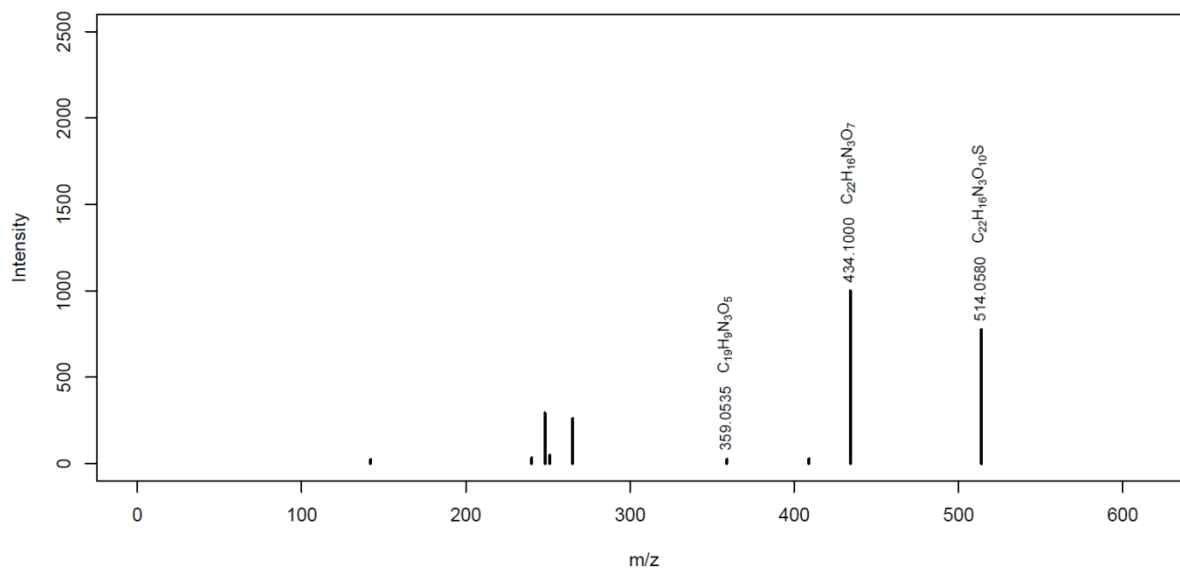
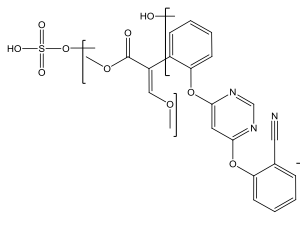
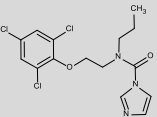
AZ_M514MassBank ID: **ET272851**, ET272852, ET272853, ET272854

Table S4-14: Overview of prochloraz and identified biotransformation products formed in the aquatic invertebrate *H. azteca*. Biotransformation products are listed according to their relative peak intensity. Information about mass error and retention time (RT) are given for both replicate samples. CE stands for collision energy applied for fragmentation in the MS/MS experiment. Below each biotransformation product the abbreviation (S) stands for “identified by suspect screening (S)”, whereas (N) stands for “identified by nontarget” screening. The abbreviation (H) stands for BTPs that were only identified in *H. azteca* and not in *G. pulex*. (H‡) stands for BTPs that were identified afterward in *G. pulex*, but with intensities below the set threshold of 1E6. The asterisk marks biotransformation products where the activeazole moiety was altered. The mass error of all identified BTPs was < 3ppm.

Compound	Formula [M]	RT [min] ⁱⁱ⁾	Polarity	Elemental change ⁱⁱⁱ⁾	Log D _{ow} ^{iv)}	Identification confidence ^{v)}	Description	CE [eV]	MS/MS confirmatory ions ^{vii)}
MassBank ID of displayed MS/MS spectrum	Exact mass of [M+H] ⁺ / [M-H] ⁻					/level according to Schymanski et al. (2014) ^{6/ vi)}			
Prochloraz (PRZ)	C ₁₅ H ₁₆ Cl ₃ N ₃ O ₂	16.3	+		3.6	/1/	parent compound	30	308.0006
ET200001	376.0381	16.3							70.0288
									265.9536
									
BAF [L kg_{ww}⁻¹] at t₂₄ⁱ⁾:									
155; 170									
PRZ_M353 *	C ₁₃ H ₁₅ Cl ₃ N ₂ O ₃	17.0	+	- C ₂ HN	3.4	D	partial loss of hydroxylated imidazole ring,	30	308.0007
ET202601	353.0221	17.0		+ O		p	aldehyde formation		70.0288
(S)						l ⁹⁻¹¹			265.9536
						m ⁹			
						/2b/			
PRZ_M325 *	C ₁₂ H ₁₅ Cl ₃ N ₂ O ₂	17.1	+	- C ₃ HN	3.4	D	partial loss of imidazole ring	35	282.0213
ET202701	325.0272	17.2				l ¹⁰⁻¹²			325.0273
(S)						p			129.1022
						/1/			

Compound MassBank ID of displayed MS/MS spectrum	Formula [M] Exact mass of [M+H] ⁺ / [M-H] ⁻	RT [min] ⁱⁱ⁾	Polarity	Elemental change ⁱⁱⁱ⁾	Log D _{ow} ^{iv)}	Identification confidence ^{v)} /level according to Schymanski et al. (2014) ⁶⁾ / ^{vi)}	Description	CE [eV]	MS/MS confirmatory ions ^{vii)}
PRZ_M558 * (H) ET204901 (S)	C ₂₀ H ₂₆ Cl ₃ N ₃ O ₇ S 558.0630	16.7 16.7	+	- C ₃ H ₂ N ₂ + C ₁₀ H ₁₅ N ₃ O ₆ S - C ₂ H ₅ NO ₂	-2.9	D p /2b/ most likely structure	loss of imidazole ring, glutathione conjugation, loss of glycine	20	308.0009 429.0207 558.0634
PRZ_M282 * ET203201 (S)	C ₁₁ H ₁₄ Cl ₃ NO 282.0214	13.7 13.7	+	- C ₄ H ₂ N ₂ O	2.4	D p /1/	loss of imidazole ring and CO	30	282.0212 86.0964 72.0807
PRZ_M323b * ET202301 (S)	C ₁₂ H ₁₂ Cl ₃ NO ₃ 323.9956	16.0 16.0	+	- C ₃ H ₄ N ₂ + O	2.6-3.2	d for keto group at propyl side chain (low intense diagnostic fragment in <i>G. pulex</i> , in <i>H. azteca</i> missing, most likely same position of aliphatic hydroxylation in <i>H. azteca</i> compared to <i>G. pulex</i>) /3/, 3 positional isomers	imidazole ring loss, aliphatic hydroxylation and further oxidation to a ketone	30	84.0808 128.0706 280.0057
PRZ_M239 * ET202501 (S)	C ₈ H ₆ Cl ₃ NO 239.9744	12.8 12.8	+	- C ₇ H ₈ N ₂ O	1.4	D /2b/	remaining chlorophenyl moiety and C ₂ H ₅ NO	30	239.9743 222.9481 196.9315
PRZ_M392b * ET202201 (S)	C ₁₅ H ₁₆ Cl ₃ N ₃ O ₃ 392.0330	15.4 15.4	+	+ O	2.3	d, p for hydroxylation at C-5 in imidazole ring (possible epoxide forma- tion at C4-C5 as intermediate) /3/, most likely structure	imidazole ring hydroxylation	30	308.0006 70.0287 265.9535

Compound MassBank ID of displayed MS/MS spectrum	Formula [M] Exact mass of [M+H] ⁺ / [M-H] ⁻	RT [min] ⁱⁱ⁾	Polarity	Elemental change ⁱⁱⁱ⁾	Log D _{ow} ^{iv)}	Identification confidence ^{v)} /level according to Schymanski et al. (2014) ^{6/ vi)}	Description	CE [eV]	MS/MS confirmatory ions ^{vii)}
PRZ_M435 * (NH ₄ ⁺ adduct) ET203301 (S)	C ₁₇ H ₂₁ Cl ₃ N ₄ O ₃ 435.0752	15.5 15.5	+	+ C ₂ H ₂ O	-	d for acetylation at CO- imidazole ring moiety /3/, acetylation most likely at keto group	acetylation at CO-imidazole ring moiety; NH ₄ ⁺ adduct	20	282.0212 435.0750 154.0610
PRZ_M640 (H‡) ET204101 (N)	C ₂₄ H ₂₈ Cl ₃ N ₃ O ₁₁ 640.0862	11.7-14.4 (4 partly separated peaks)	+	+ O + C ₆ H ₁₀ O ₅ + C ₃ H ₂ O ₃	-1.9 to -2.8	d, p /3/, most likely structure	hydroxylation at propyl side chain, glucose conjugation, malonyl conjugation	20	323.9958 69.0449 128.9958
PRZ_M323a * ET202401 (S)	C ₁₂ H ₁₂ Cl ₃ NO ₃ 323.9956	15.7 15.7	+	- C ₃ H ₄ N ₂ + O	2.6-3.2	d for keto group at propyl side chain (low intense diagnostic fragment in <i>G. pulex</i> , in <i>H. azteca</i> missing, most likely same position of aliphatic hydroxylation in <i>H. azteca</i> compared to <i>G. pulex</i>) /3/, 3 positional isomers	imidazole ring loss, aliphatic hydroxylation and further oxidation to a ketone	30	84.0808 128.0706 280.0057
PRZ_M382 * ET203401 (S)	C ₁₄ H ₁₈ Cl ₃ N ₃ O ₃ 382.0487	16.6 16.6	+	- CH ₂ + O	3.0	d, p for C-4 loss at hydroxylated (at C-5) imidazole ring /3/, most likely structure	partial loss of hydroxylated imidazole ring	20	308.0007 365.0225 337.0271
PRZ_M326 * (H) ET204201 (S)	C ₁₁ H ₁₀ Cl ₃ NO ₄ 325.9748	14.5 14.5	+	- C ₄ H ₂ N ₂ O + OH + O + O	-	d for at least two hydroxylations at the aliphatic part of the molecule /3/, several positional isomers	loss of imidazole ring and CO, hydroxylations and further oxidations to ketones	20	130.0501 265.9540 325.9751

Compound MassBank ID of displayed MS/MS spectrum	Formula [M] Exact mass of [M+H] ⁺ / [M-H] ⁻	RT [min] ⁱⁱ⁾	Polarity	Elemental change ⁱⁱⁱ⁾	Log D _{ow} ^{iv)}	Identification confidence ^{v)} /level according to Schymanski et al. (2014) ^{6/ vi)}	Description	CE [eV]	MS/MS confirmatory ions ^{vii)}
PRZ_M298 * ET202801 (S)	C ₁₁ H ₁₄ Cl ₃ NO ₂ 298.0163	13.3 13.3	+	- C ₄ H ₂ N ₂ O + O	1.4-2.9	/3/, 6 positional isomers	loss of imidazole ring and CO, hydroxylation	50	70.0651 280.0061 222.9483
PRZ_M392a ET202101 (S)	C ₁₅ H ₁₆ Cl ₃ N ₃ O ₃ 392.0330	14.2 14.2	+	+ O	2.1-2.5	d for hydroxylation at propyl side chain /3/, 3 positional isomers	aliphatic hydroxylation	30	251.9742 69.0447 128.0706
PRZ_M589 (H) ET204001 (N)	C ₂₄ H ₂₅ O ₈ N ₃ Cl ₃ 589.0780	14.8 14.7	+			/4/	unclear, most likely related to PRZ_M435*	20	282.0218 308.0646 264.0748
PRZ_M374 (H) ET205001 (S)	C ₁₅ H ₁₄ Cl ₃ N ₃ O ₂ 374.0224	17.0 17.0	+	- H ₂	3.5-3.7	/3/, 3 positional isomers	dehydrogenation	20	305.9851 277.9902 222.9478
PRZ_M397 *(H‡) ET204301 (S)	C ₁₅ H ₁₉ Cl ₃ N ₂ O ₄ 397.0483	17.5 17.6	+	+ O + O - NH ₄	1.9	d, p	N loss of dihydroxylated imidazole ring	20	308.0010 397.0488 265.9539
PRZ_M615 *(H) ET203701 (S)	C ₂₂ H ₂₉ Cl ₃ N ₄ O ₈ S 615.0844	16.5 16.4	+	- C ₃ H ₂ N ₂ + C ₁₀ H ₁₅ N ₃ O ₆ S	-4	d, p /3/, most likely structure	loss of imidazole ring, glutathione conjugation	15	486.0418 383.0152 615.0841
PRZ_M386 *(H‡) ET201902 (S)	C ₁₂ H ₁₃ Cl ₃ N ₂ O ₄ S 386.9734	14.2 14.2	+	- C ₃ H ₂ N ₂ - C ₃ H ₆ + C ₃ H ₅ NO ₂ S	0.3	D /2b/	loss of imidazole ring, loss of propyl side chain, cysteine product	15	122.0270 239.9739 386.9738

Compound MassBank ID of displayed MS/MS spectrum	Formula [M] Exact mass of [M+H] ⁺ / [M-H] ⁻	RT [min] ⁱⁱ⁾	Polarity	Elemental change ⁱⁱⁱ⁾	Log D _{ow} ^{iv)}	Identification confidence ^{v)} /level according to Schymanski et al. (2014) ^{6/ vi)}	Description	CE [eV]	MS/MS confirmatory ions ^{vii)}
PRZ_M683 (H) ET204501 (N)	C ₂₆ H ₃₃ Cl ₃ N ₄ O ₁₁ 683.1284	14.6 14.6	+			/4/	unclear	20	402.1148 282.0218 154.0613
PRZ_M573.1 * (H) ET204801 (N)	C ₂₄ H ₂₅ Cl ₃ N ₃ O ₇ 573.0830	16.1 16.2	+	- C ₃ HN + C ₆ H ₁₀ O ₅ + C ₃ H ₂ O ₃	-1.9	d, p /3/, most likely structure	partial loss of imidazole ring, glucose conjugation, malonyl conjugation	20	325.0276 308.0010 367.0383
PRZ_M632c (H) ET203152 (S)	C ₂₁ H ₂₆ Cl ₃ N ₃ O ₁₁ S 632.0281	12.7 12.7	- ^(viii)	+ O + C ₆ H ₁₀ O ₈ S		/4/	unclear, sulfate and glucose attached at different sites	40	194.9176 96.9601 436.1038
PRZ_M573 * ET203502 (S)	C ₁₉ H ₂₃ Cl ₃ N ₄ O ₆ S 573.0375	14.0 14.0	+	- C ₃ H ₂ N ₂ - C ₃ H ₆ + C ₁₀ H ₁₅ N ₃ O ₆ S	-1.9	/3/, most likely structure	loss of imidazole ring, loss of propyl side chain, glutathione conjugation	10	573.0375 443.9947 340.9676
PRZ_M310 * ET205202 (S)	C ₁₂ H ₁₄ O ₂ NCl ₃ 310.0163	16.9/17.5 16.9/17.5	+	- C ₃ H ₂ N ₂	3.7	/3/, most likely structure	loss of imidazole ring	20	136.0757 149.0234 114.0913
PRZ_M632a ET202952 (S)	C ₂₁ H ₂₆ Cl ₃ N ₃ O ₁₁ S 632.0281	10.8 10.7	- ^(viii)	+ O + C ₆ H ₁₀ O ₅ + SO ₃	-1.3	D for conjugation at the chlorophenyl moiety /2b/	aromatic hydroxylation, glucose conjugation, sulfate conjugation	40	209.9047 96.9601 241.0024
PRZ_M554a (H‡) ET203801 (S)	C ₂₁ H ₂₆ Cl ₃ N ₃ O ₈ 554.0858	13.6 13.6	+	+ O + C ₆ H ₁₀ O ₅	0.7-1.3	d for hydroxylation at propyl side chain /3/ 3 positional isomers	hydroxylation at propyl side chain, glucose conjugation	40	251.9749 69.0499 323.9959

Compound MassBank ID of displayed MS/MS spectrum	Formula [M] Exact mass of [M+H] ⁺ / [M-H] ⁻	RT [min] ⁱⁱ⁾	Polarity	Elemental change ⁱⁱⁱ⁾	Log D _{ow} ^{iv)}	Identification confidence ^{v)} /level according to Schymanski et al. (2014) ^{6/ vi)}	Description	CE [eV]	MS/MS confirmatory ions ^{vii)}
PRZ_M469 ET202051 (S)	C ₁₅ H ₁₆ Cl ₃ N ₃ O ₆ S 469.9753	11.2 11.2	- ^(viii)	+ O + SO ₃	0.5	D for sulfate conjugation at the chlorophenyl moiety /2b/	aromatic hydroxylation, sulfate conjugation	15	209.9043 96.9604 390.0185
PRZ_M477 ET203601 (S)	C ₁₈ H ₂₂ Cl ₂ N ₄ O ₅ S 477.0761	11.2 11.1	+	+ C ₃ H ₆ NO ₂ S + O - Cl		d for no conjugation at the CO-imidazole ring moiety /3/, structural possibilities unclear	cysteine product, hydroxylation, dehalogenation	10	381.0441 409.0380 477.0784
PRZ_M632b ET203051 (S)	C ₂₁ H ₂₆ Cl ₃ N ₃ O ₁₁ S 632.0281	11.4 11.3	- ^(viii)	+ O + C ₆ H ₁₀ O ₅ + SO ₃	-1.3	D for conjugation at the chlorophenyl moiety /2b/	aromatic hydroxylation, glucose conjugation, sulfate conjugation	40	209.9049 241.0024 96.9602
PRZ_M554b (H‡) ET203901 (S)	C ₂₁ H ₂₆ Cl ₃ N ₃ O ₈ 554.0858	14.1 14.1	+	+ O + C ₆ H ₁₀ O ₅	0.7-1.3	/3/ 3 positional isomers	most likely hydroxylation at propyl side chain similar to PRZ_M554a, glucose conjugation	40	69.0450 84.0810 280.0053
PRZ_M515 (H‡) ET204402 (N)	515.0418	15.1 15.1	+			/5/	unclear	20	282.0218 86.0967
PRZ_M661 (H‡) ET204601 (N)	661.3064	16.6 16.6	+			/5/	unclear	20	308.0009 376.0385 265.9538

Compound MassBank ID of displayed MS/MS spectrum	Formula [M] Exact mass of [M+H] ⁺ / [M-H] ⁻	RT [min] ⁱⁱ⁾	Polarity	Elemental change ⁱⁱⁱ⁾	Log D _{ow} ^{iv)}	Identification confidence ^{v)} /level according to Schymanski et al. (2014) ^{6/ vi)}	Description	CE [eV]	MS/MS confirmatory ions ^{vii)}
PRZ_M409 (H⁺)	409.9997	17.3	+			/5/	unclear	20	341.9621
ET204701		17.4							299.9150
(N)									70.0289
PRZ_M675 (H)	675.2829	16.4	+			/5/	unclear	20	308.0009
ET205101		16.4							376.0385
(N)									265.9539

ⁱ⁾ See Equation 5 in the manuscript for the calculation of BAFs at steady state.

ⁱⁱ⁾ In case of a retention time range, several possibly positional isomers were integrated as one peak, due to bad peak separation.

ⁱⁱⁱ⁾ The elemental change refers to the change in the molecular formula of the biotransformation product in comparison with the parent compound.

^{iv)} Log D_{ow} values were predicted by MarvinSketch version 14.10.20.0 at pH 7.9 and 25 °C. Log D_{ow} values correspond to corrected log K_{ow} values to account for pH-dependent dissociation. At pH 7.9 prochloraz is neutral thus log D_{ow} is equal to log K_{ow}. If different positional isomers are possible for one BTP, a range of log D_{ow} values is given.

^{v)} D: diagnostic fragment/evidence for one structure; d: diagnostic fragment/evidence for positional isomers; l: structure reported in literature; m: MS/MS data from literature; p: biotransformation pathway information; d, p: diagnostic fragment for positional isomers (d) in combination with pathway information (p) give evidence for one possible structure.

^{vi)} Levels are defined as follows: 5 (*exact mass*), 4 (*unequivocal molecular formula*), 3 (*tentative candidates: e.g., positional isomers*), 2 (*probable structure: library spectrum match (a) or diagnostic evidence for one structure (b)*) and 1 (*confirmed structure*).

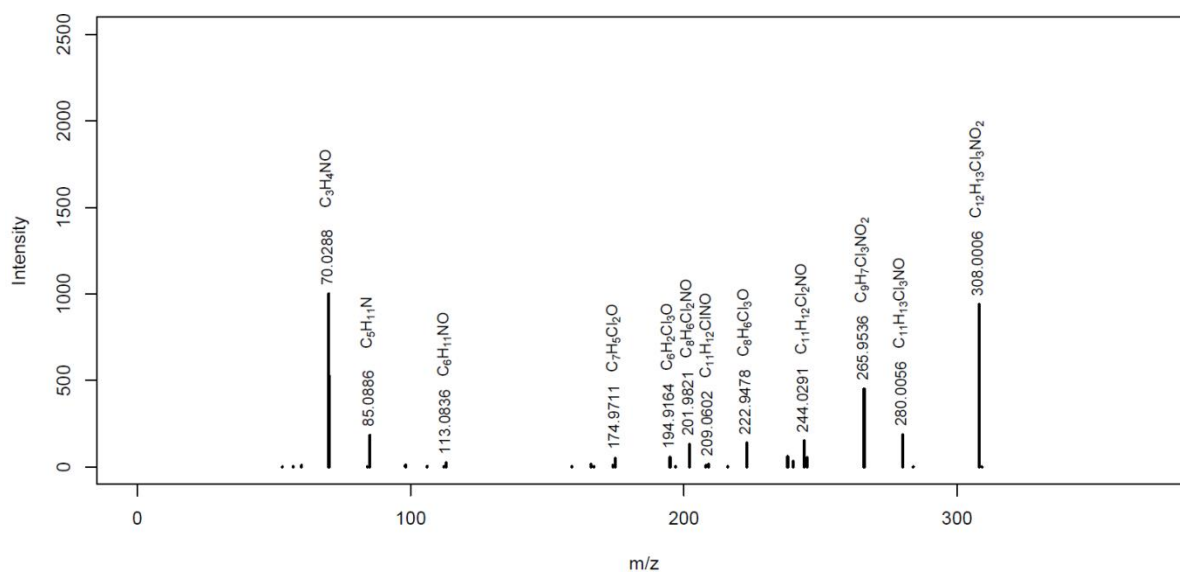
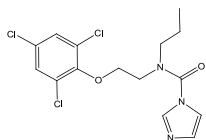
^{vii)} Diagnostic fragments (d, D) are listed first and are represented in bold in the table, other characteristic fragments are then presented according to their relative abundance. Only fragments where a chemical formula and structure could be attributed are considered.

^{viii)} The sulfate-containing BTPs are more sensitive in negative ionization mode. However, they were quantified in positive ionization mode because prochloraz was detected and quantified in positive ionization mode.

The different MassBank IDs for one compound refer to different collision energies applied during MS/MS fragmentation. The MassBank ID displayed in bold indicates the depicted MS/MS spectrum. Spectra are also available electronically in the MassBank database.⁸

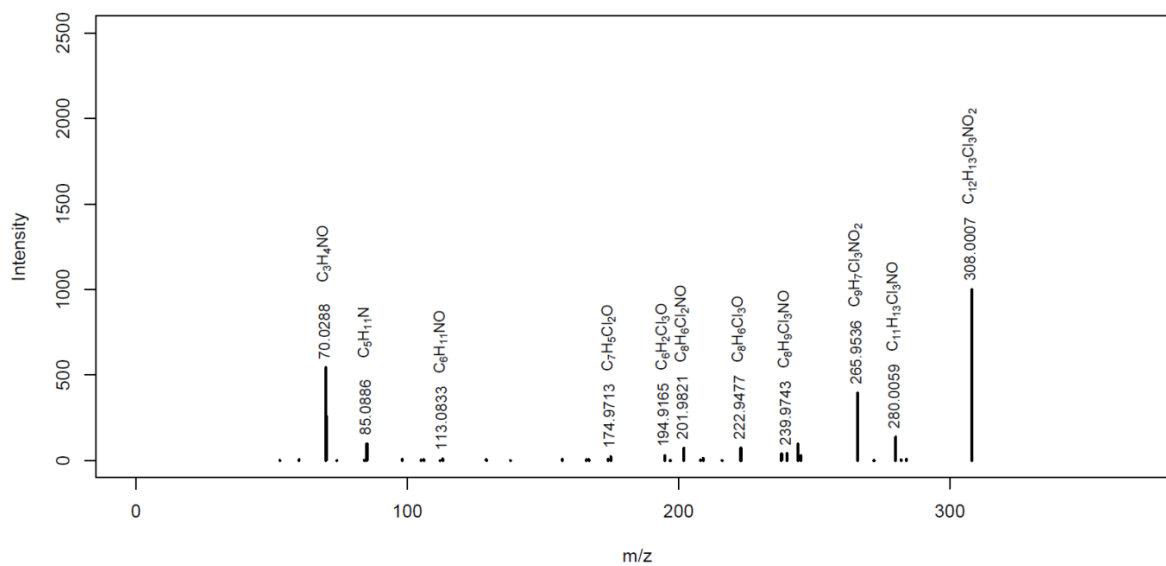
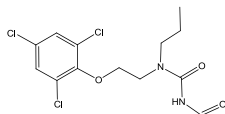
Prochloraz (PRZ)

MassBank ID: **ET200001**



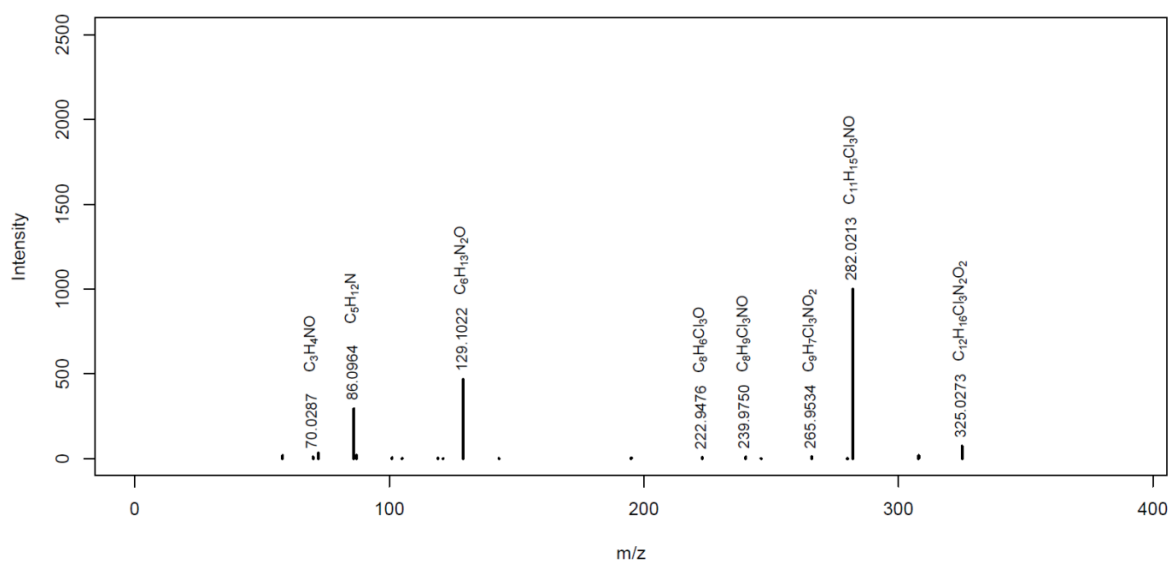
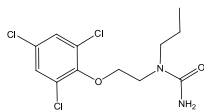
PRZ_M353 *

MassBank ID: ET202601



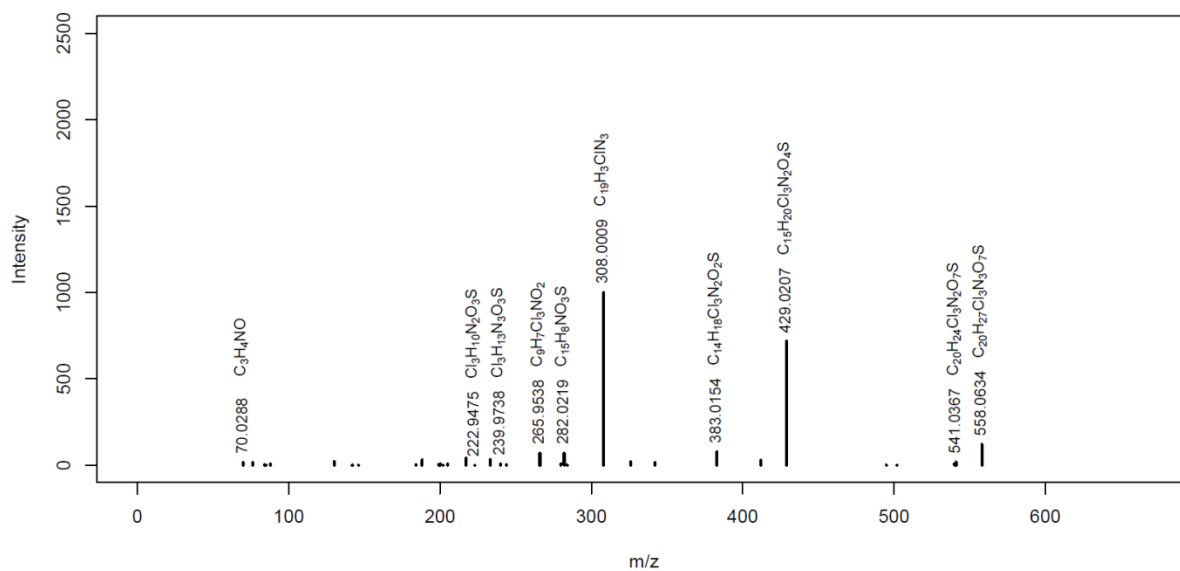
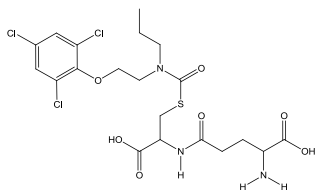
PRZ_M325 *

MassBank ID: ET202701



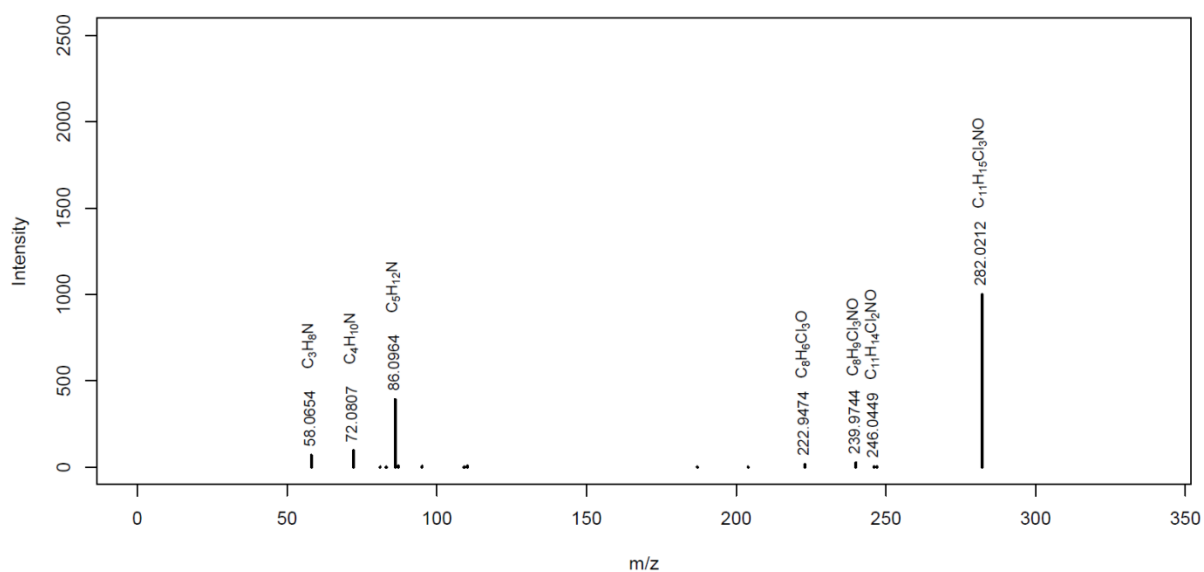
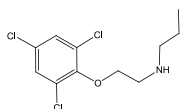
PRZ_M558 *

MassBank ID: ET204901



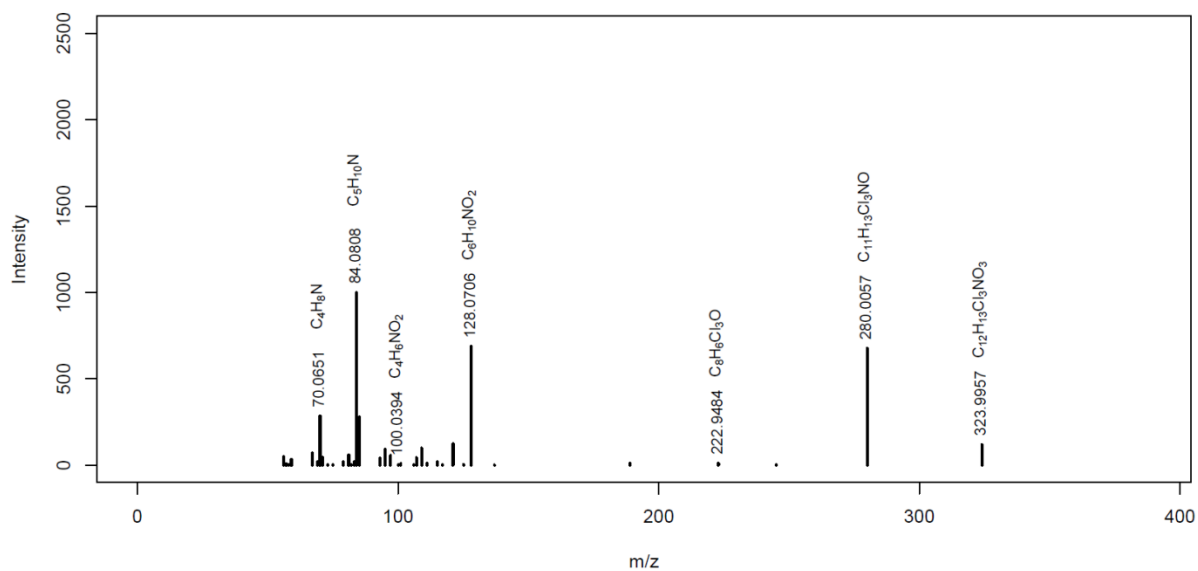
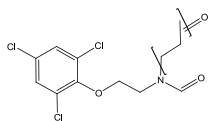
PRZ_M282 *

MassBank ID: ET203201



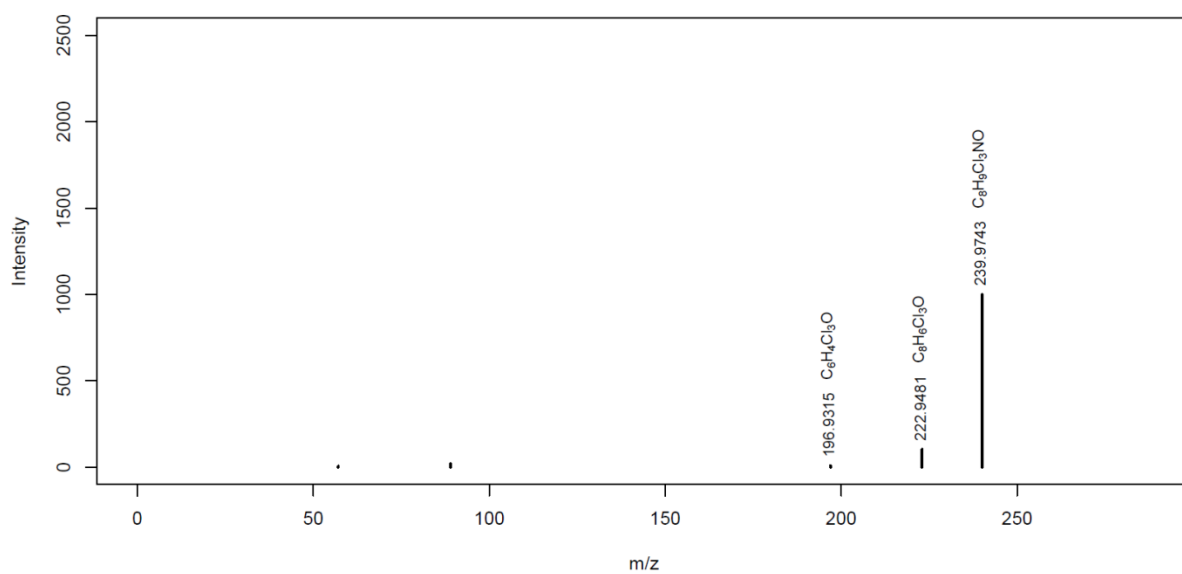
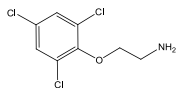
PRZ_M323b *

MassBank ID: ET202301



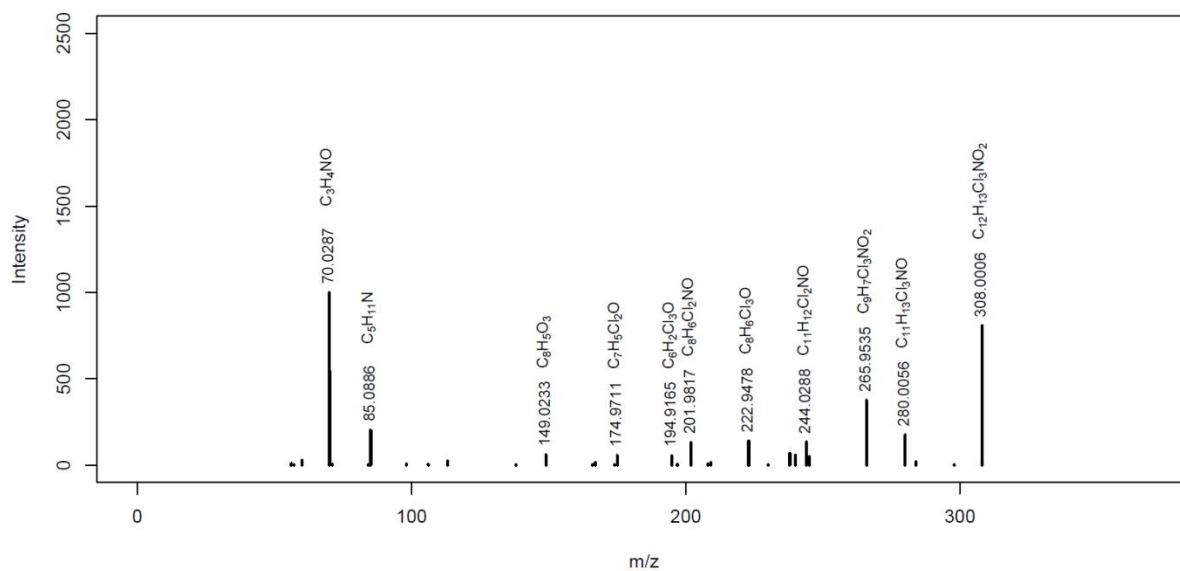
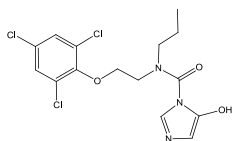
PRZ_M239 *

MassBank ID: ET202501



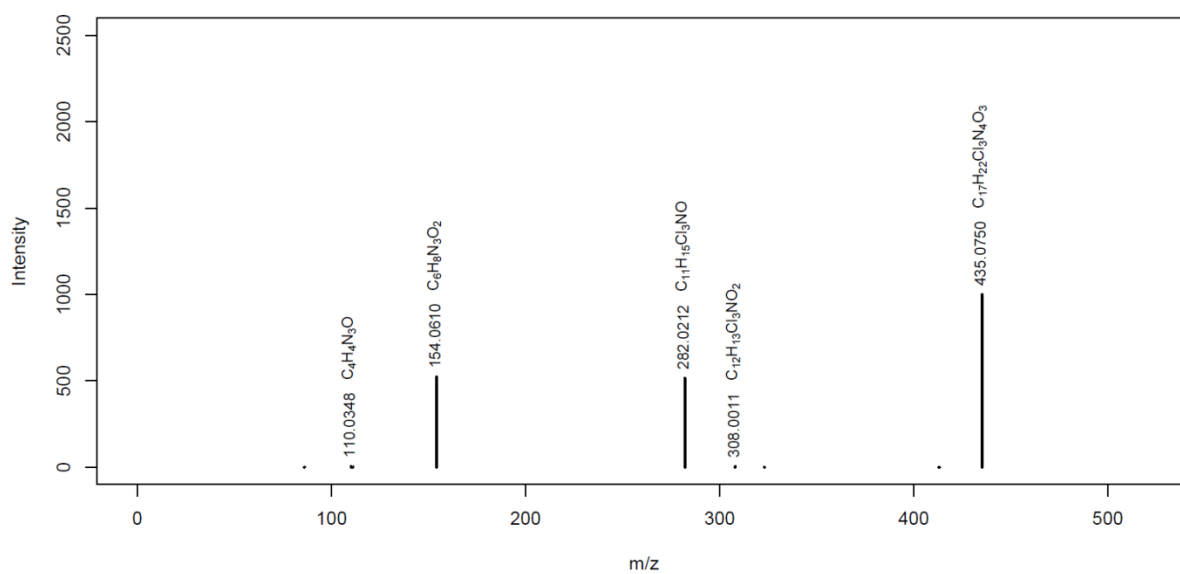
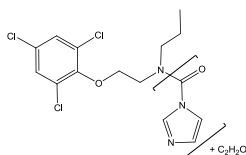
PRZ_M392b *

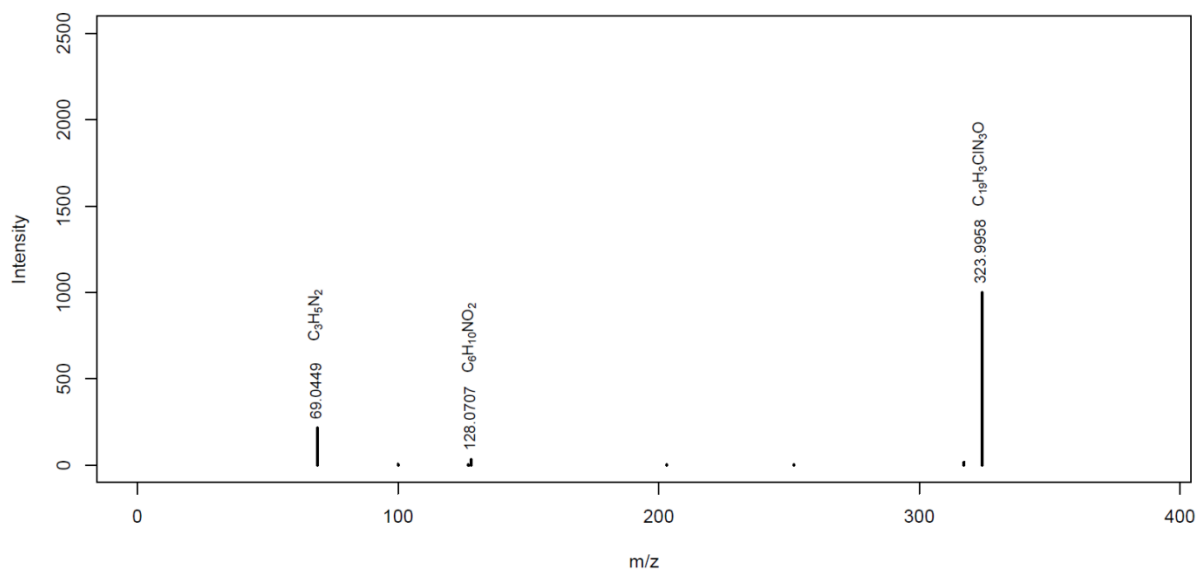
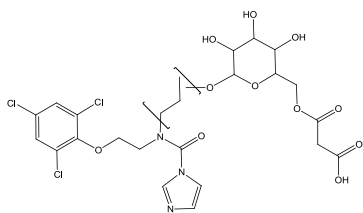
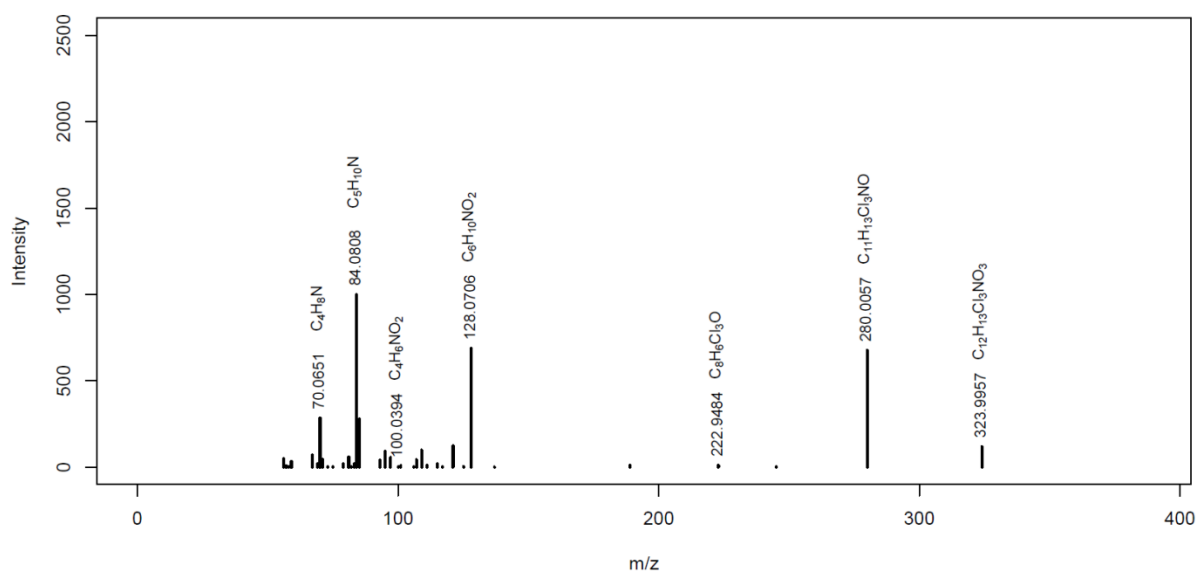
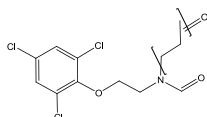
MassBank ID: ET202201



PRZ_M435 *

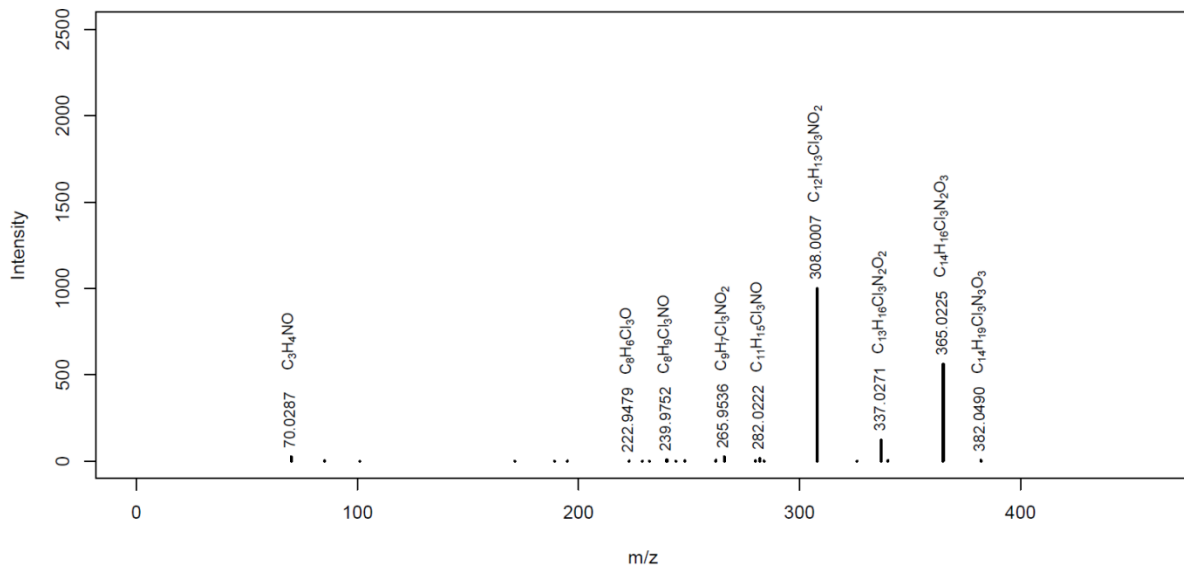
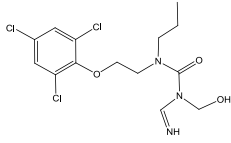
MassBank ID: ET203301



PRZ_M640MassBank ID: **ET204101****PRZ_M323a ***MassBank ID: **ET202401**

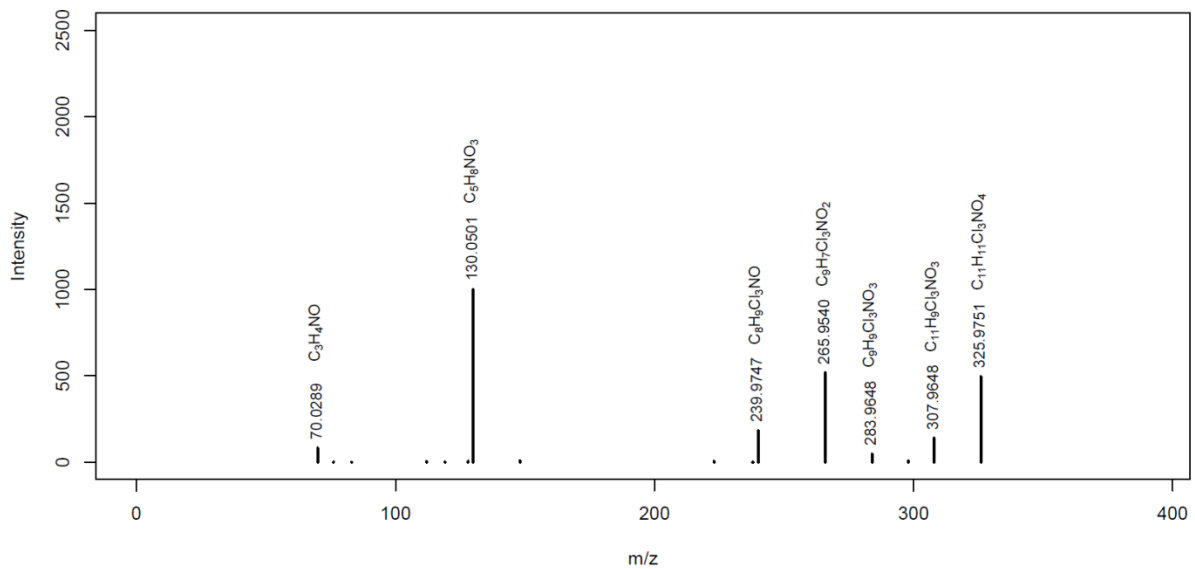
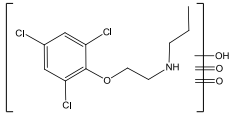
PRZ_M382 *

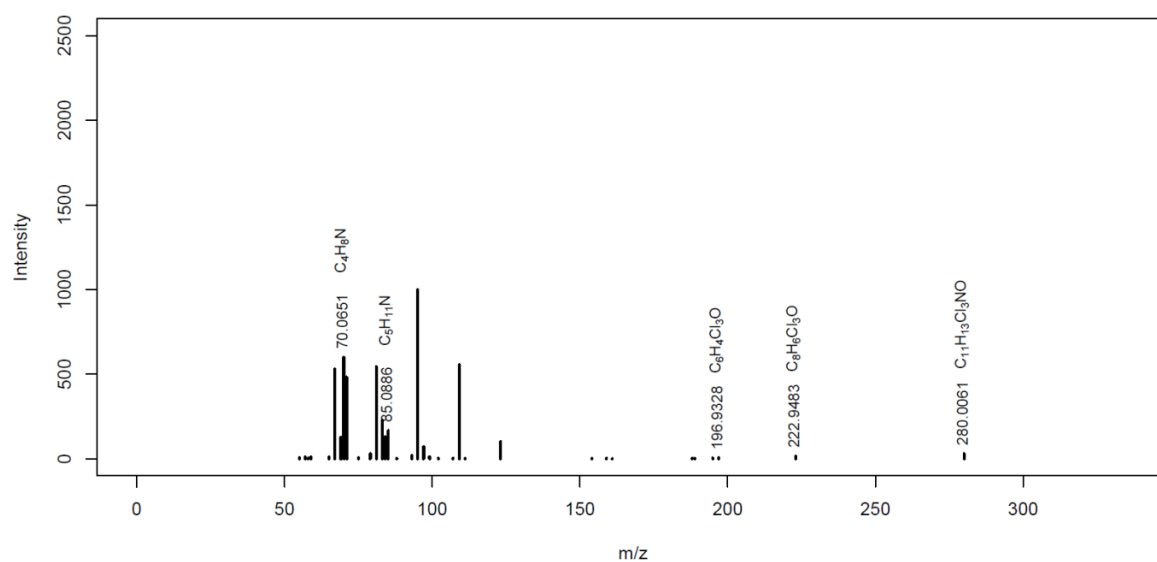
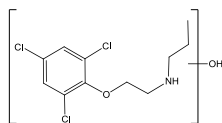
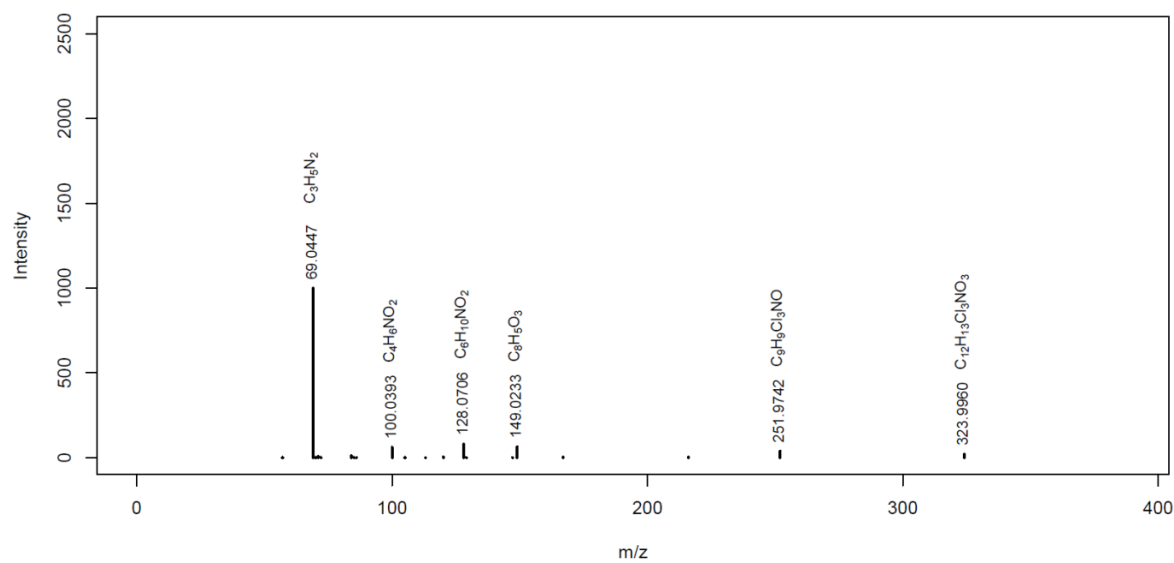
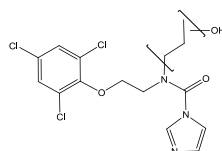
MassBank ID: ET203401

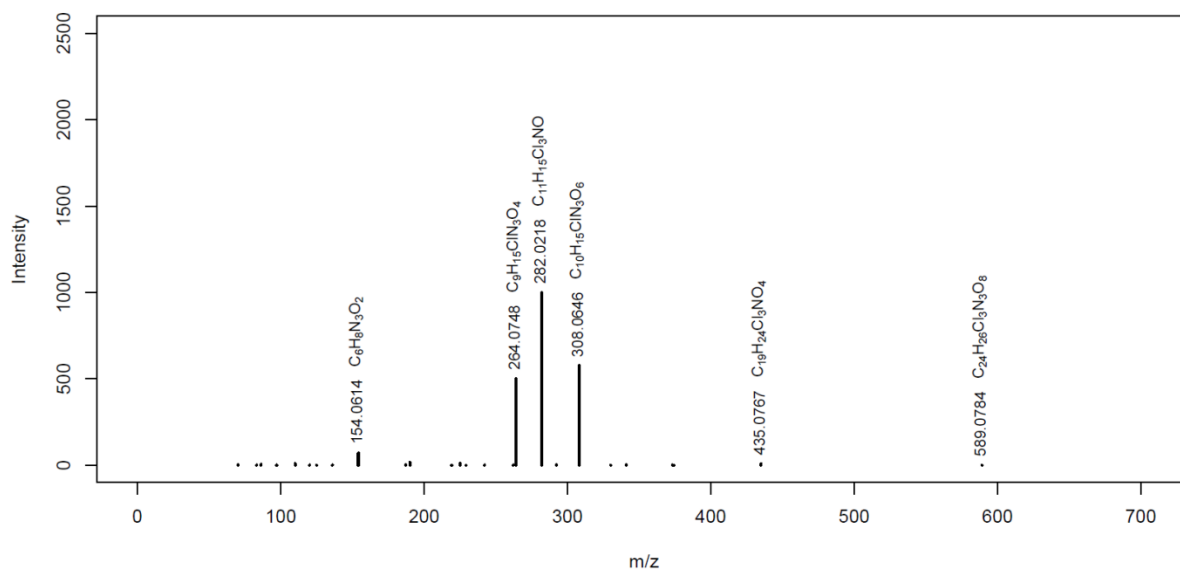
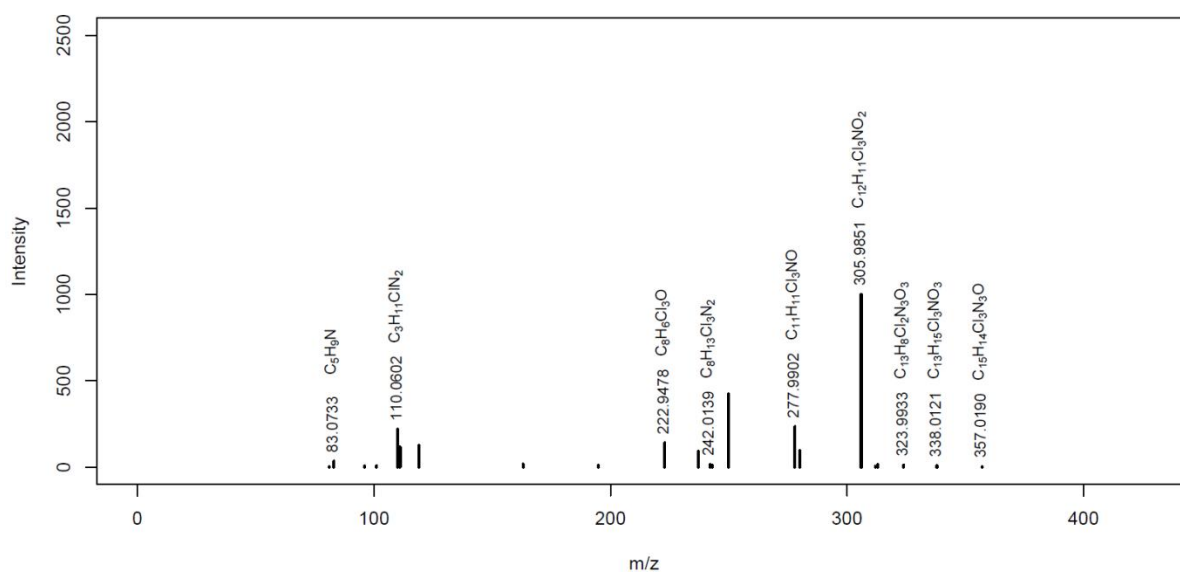
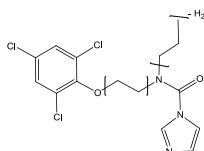


PRZ_M326 *

MassBank ID: ET204201

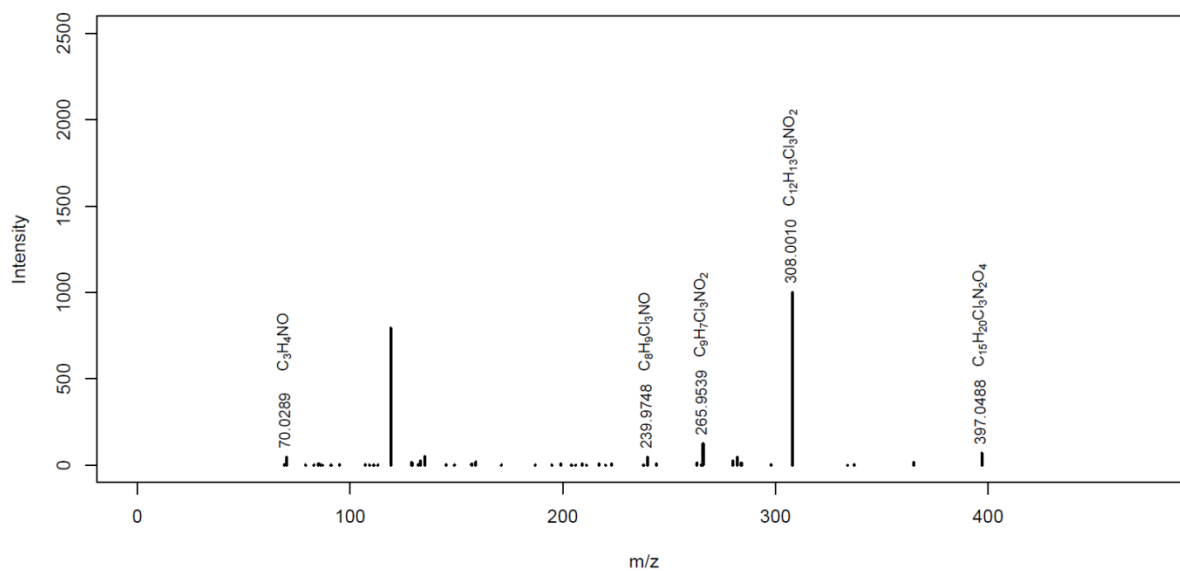
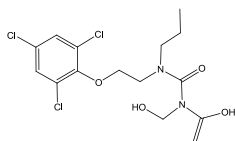


PRZ_M298 *MassBank ID: **ET202801****PRZ_M392a**MassBank ID: **ET202101**

PRZ_M589MassBank ID: **ET204001***unclear structure***PRZ_M374**MassBank ID: **ET205001**, ET205002, ET205003, ET205004

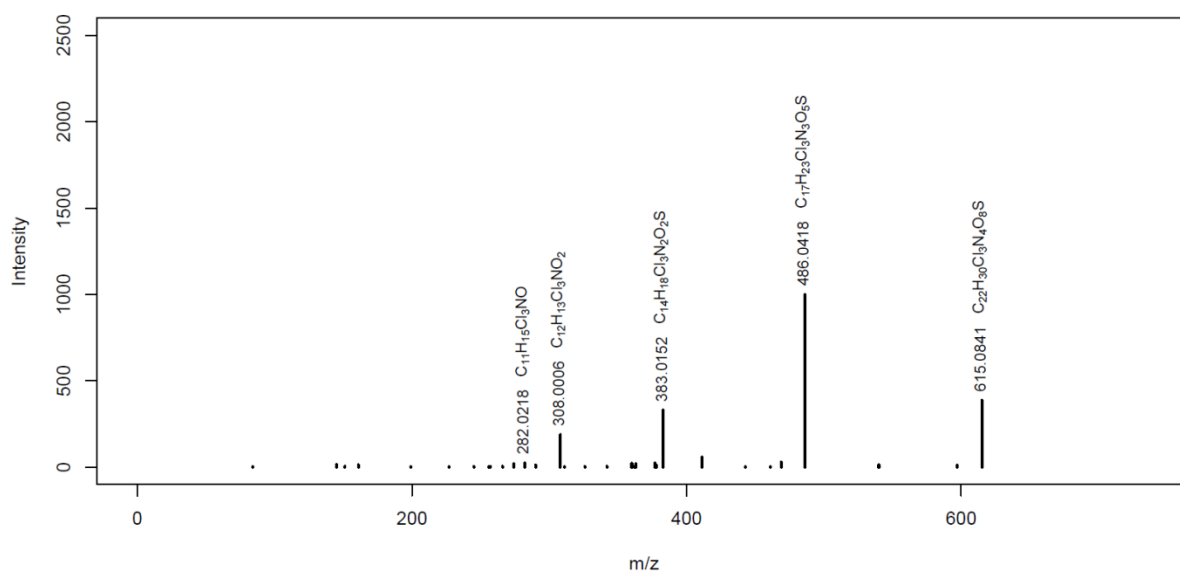
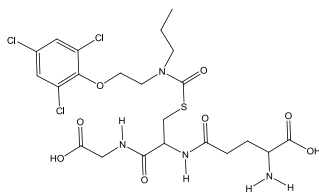
PRZ_M397 *

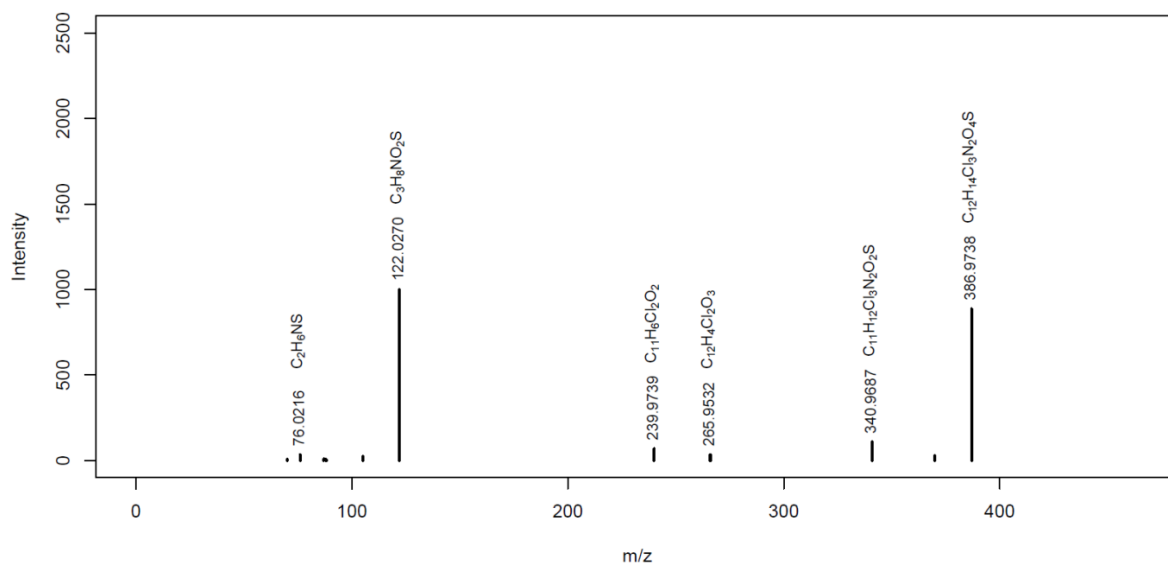
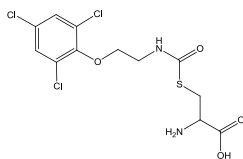
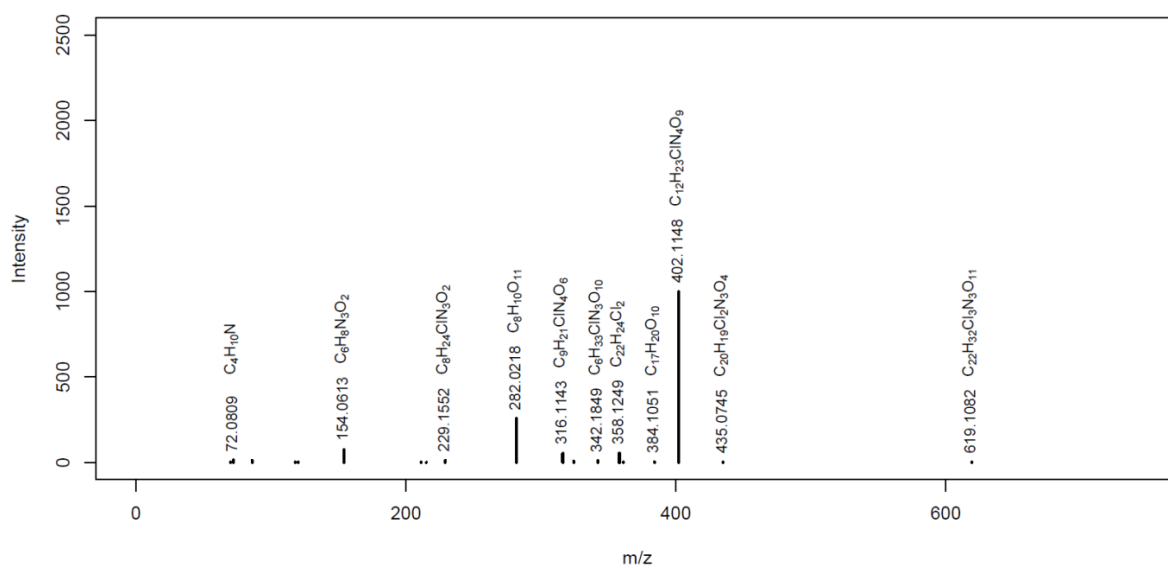
MassBank ID: ET204301

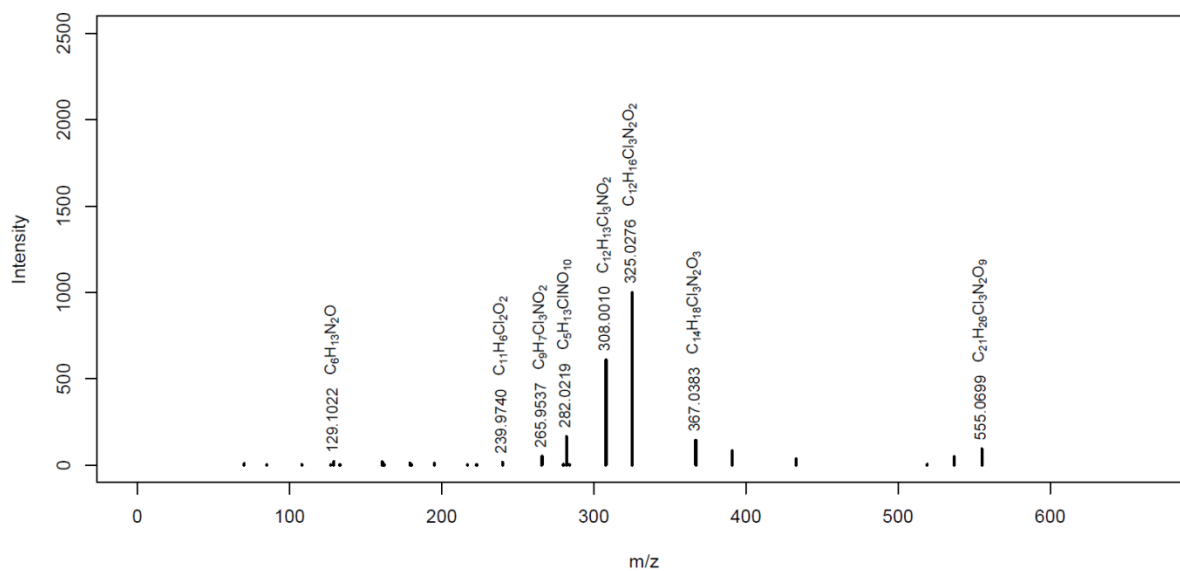
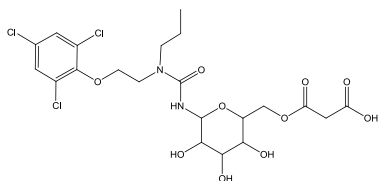
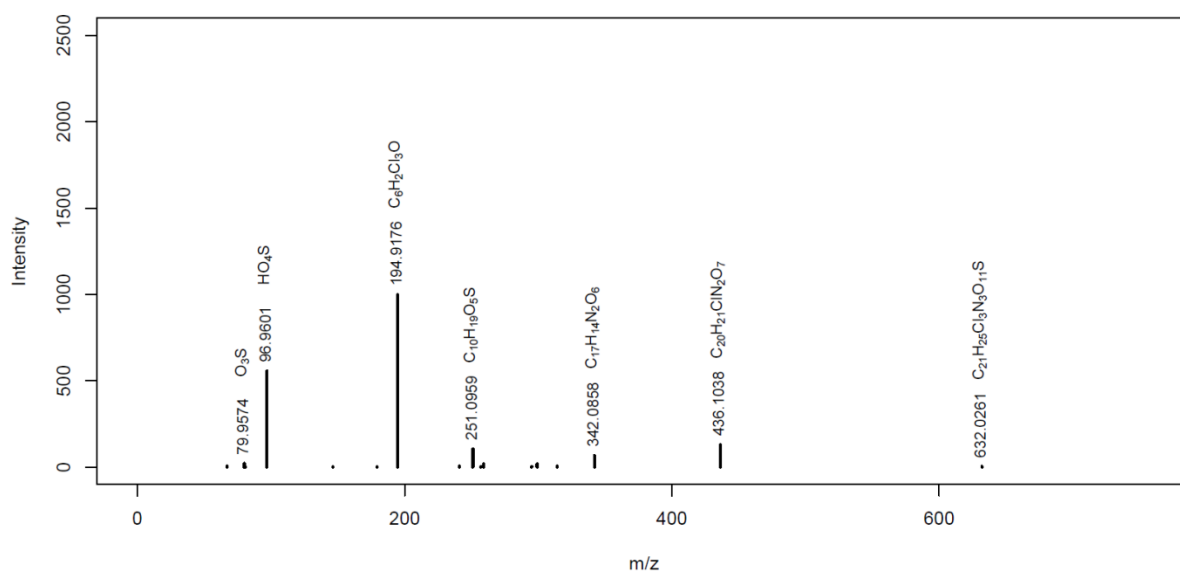


PRZ_M615 *

MassBank ID: ET203701

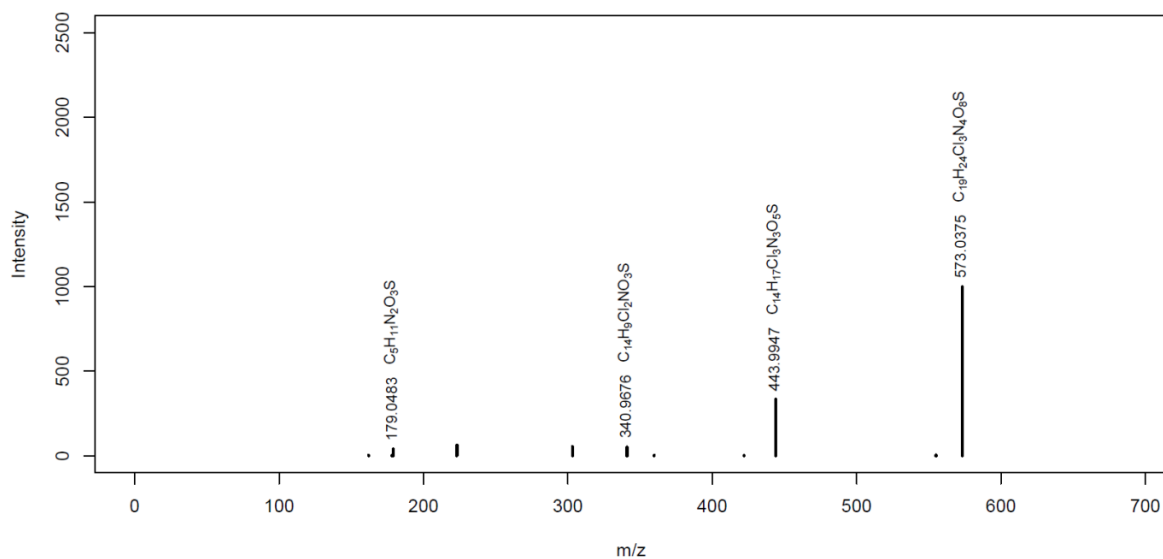
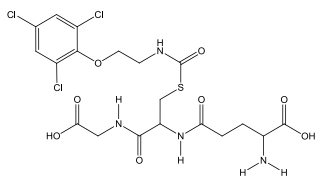


PRZ_M386 *MassBank ID: **ET201902****PRZ_M683**MassBank ID: **ET204501***unclear structure*

PRZ_M573.1 *MassBank ID: **ET204801****PRZ_M632c**MassBank ID: **ET203152***unclear structure*

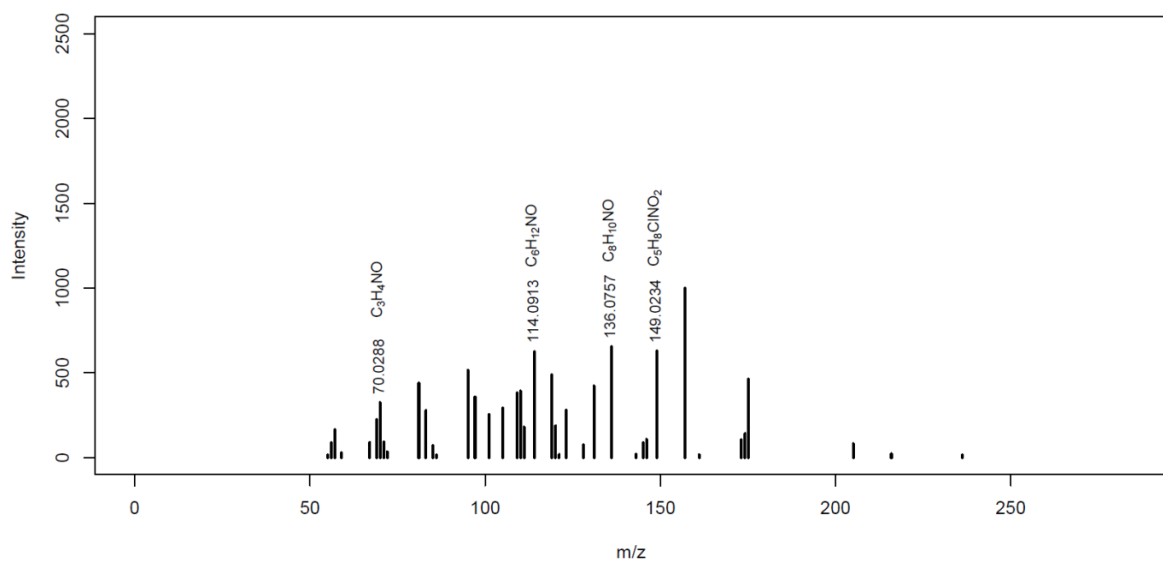
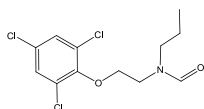
PRZ_M573 *

MassBank ID: ET203502



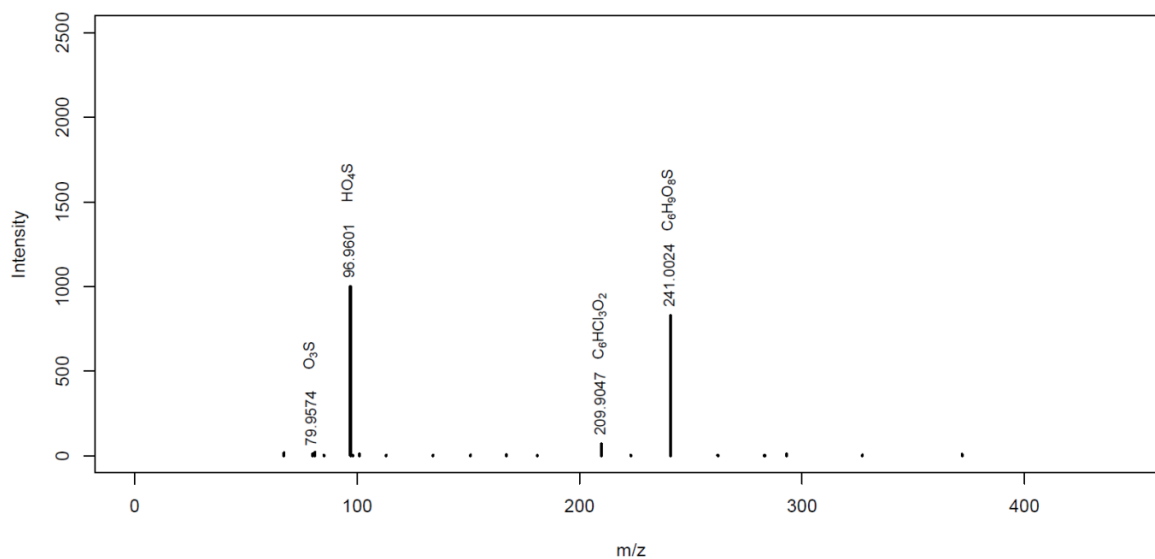
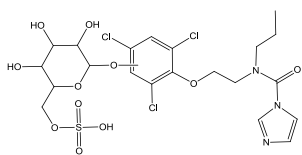
PRZ_M310 *

MassBank ID: ET205202



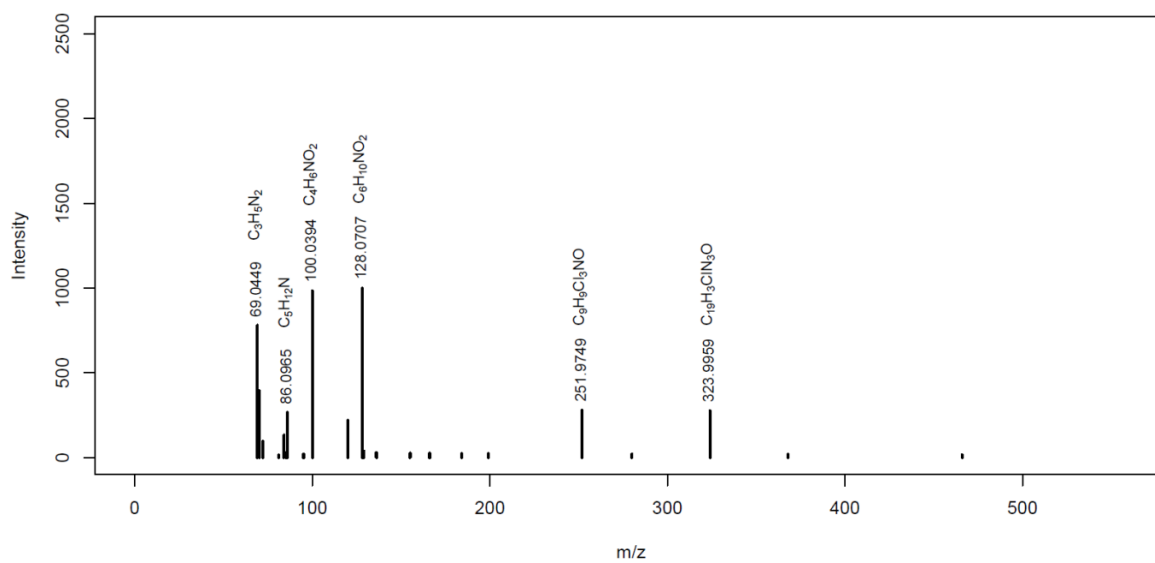
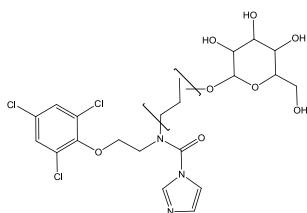
PRZ_M632a

MassBank ID: ET202952



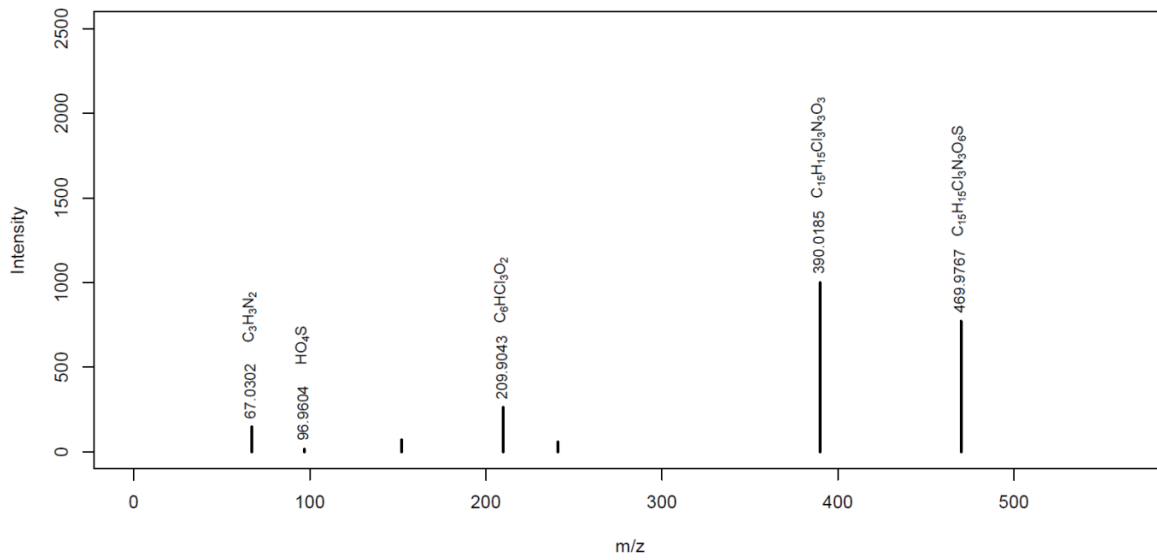
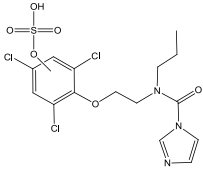
PRZ_M554a

MassBank ID: ET203801



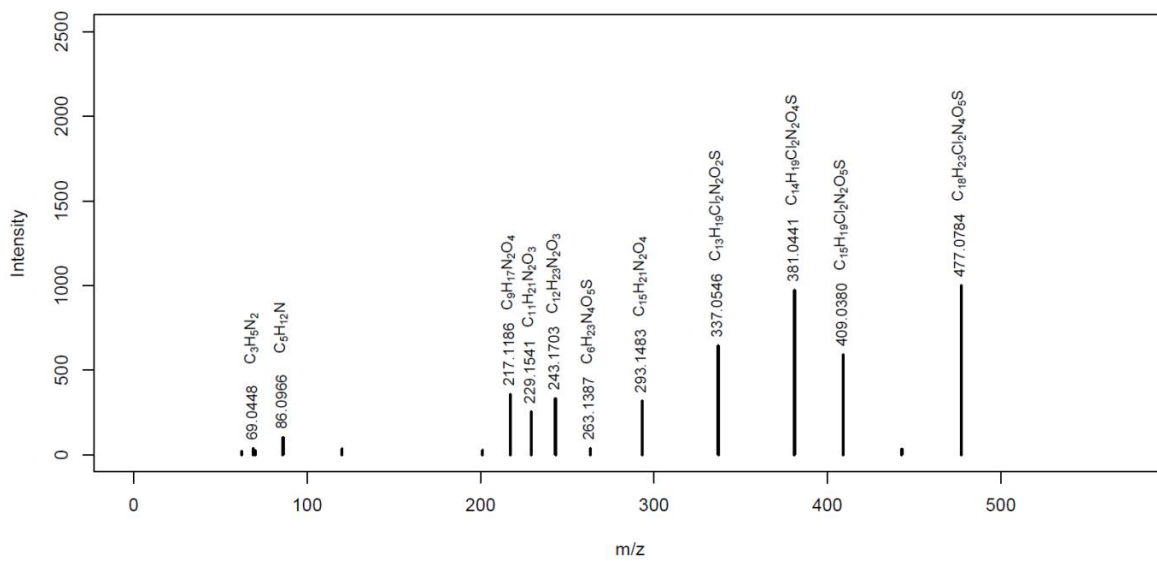
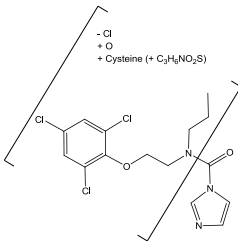
PRZ_M469

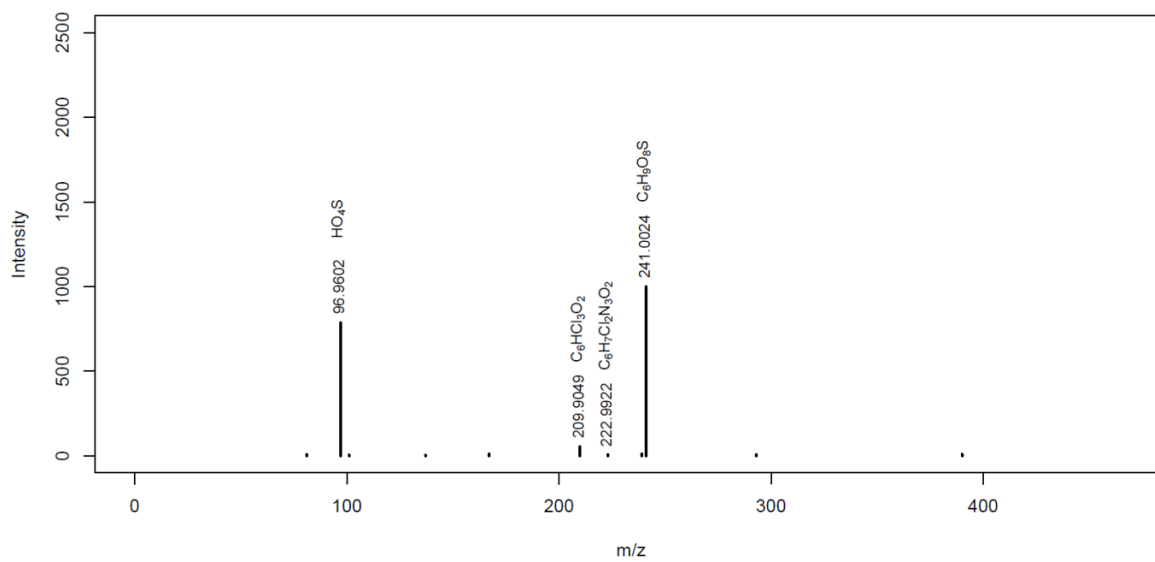
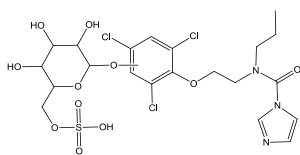
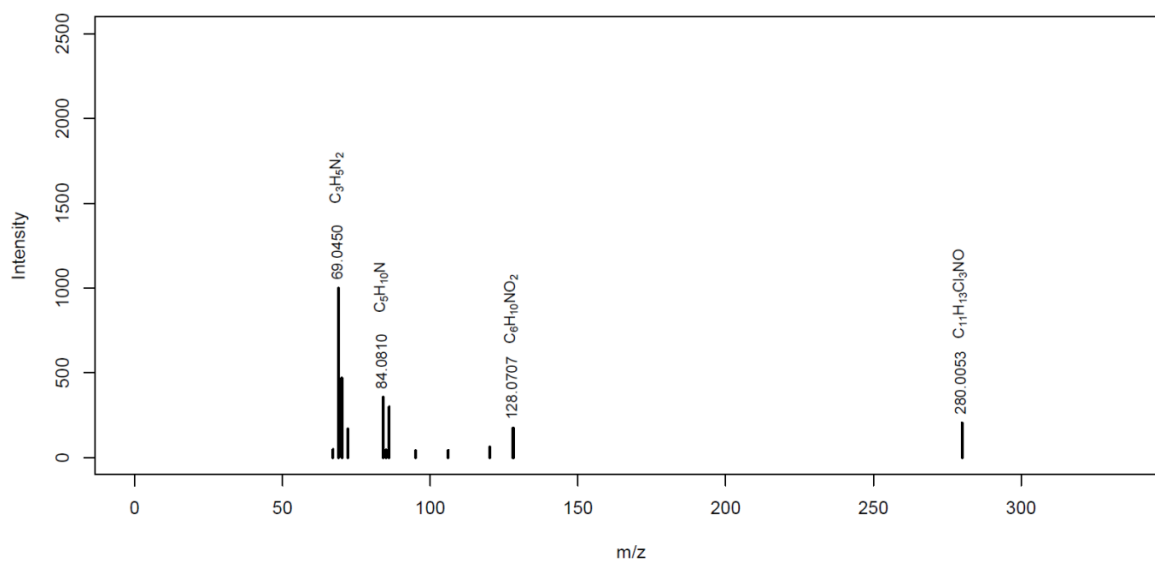
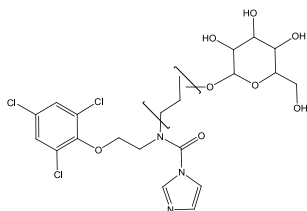
MassBank ID: ET202051

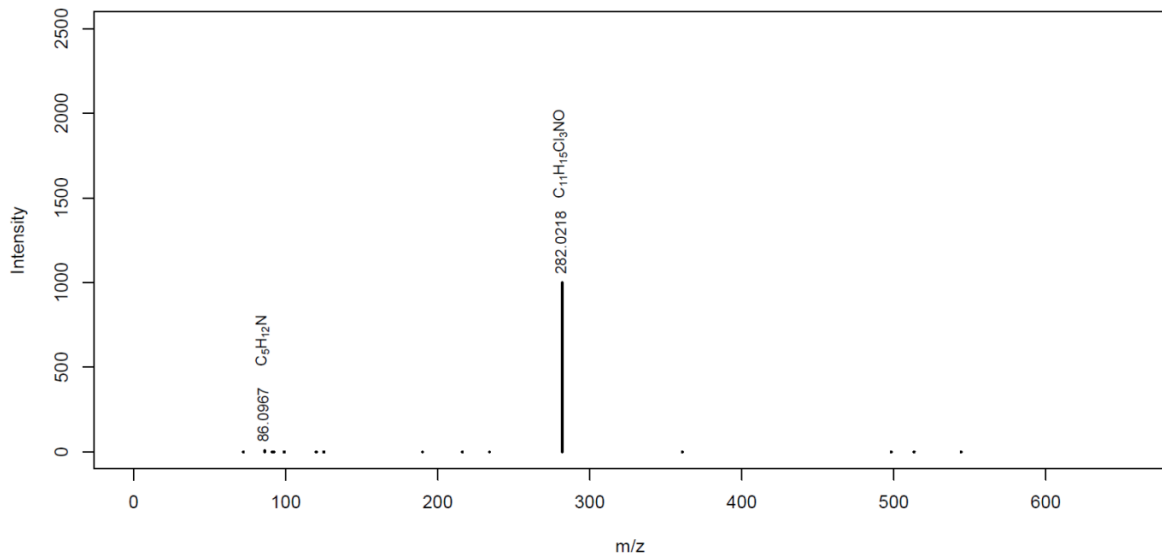
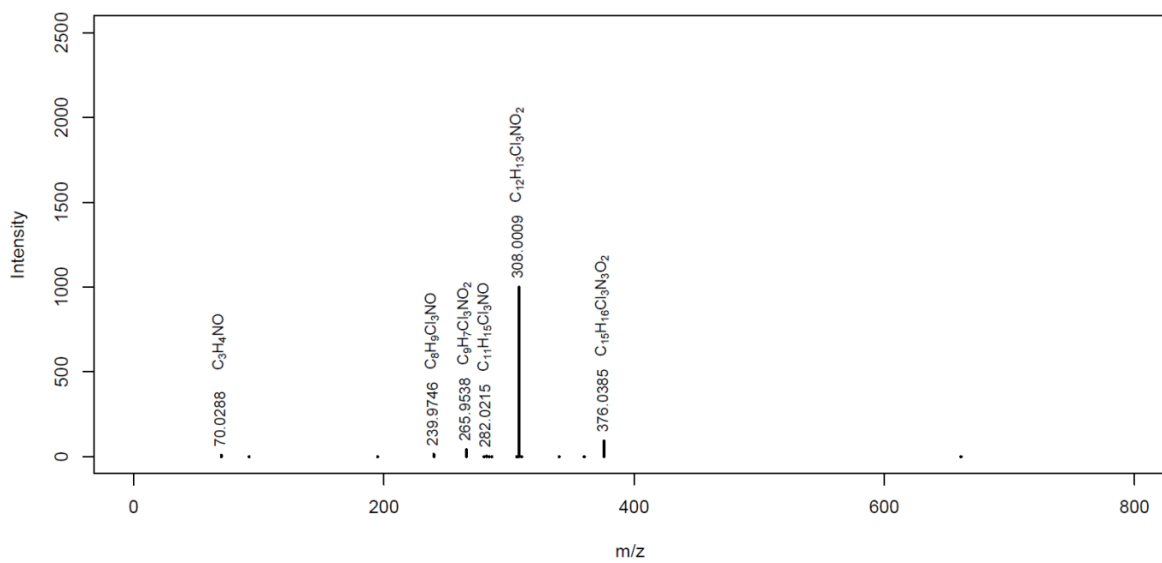


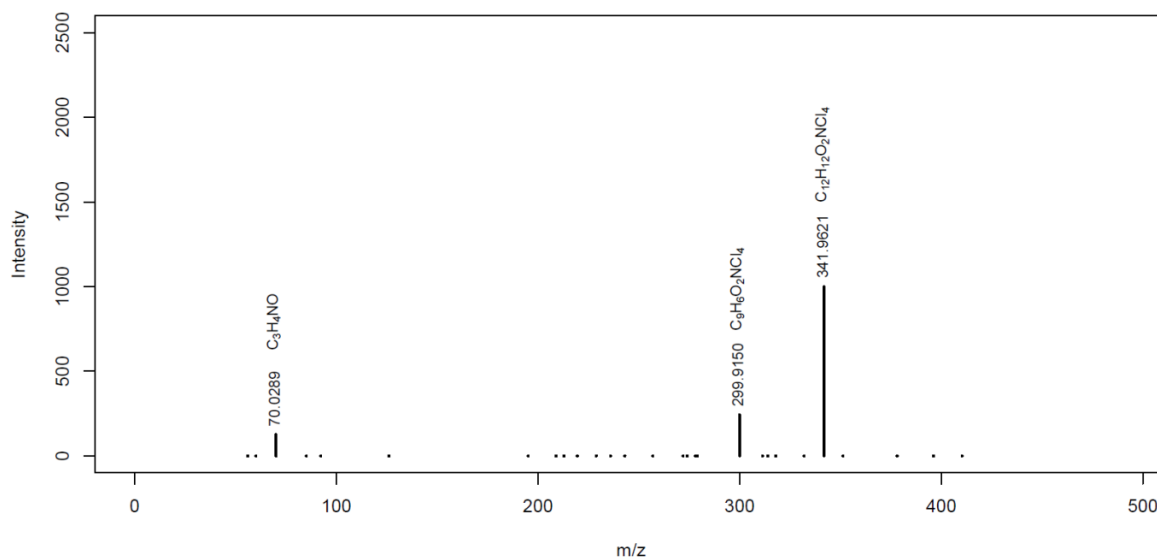
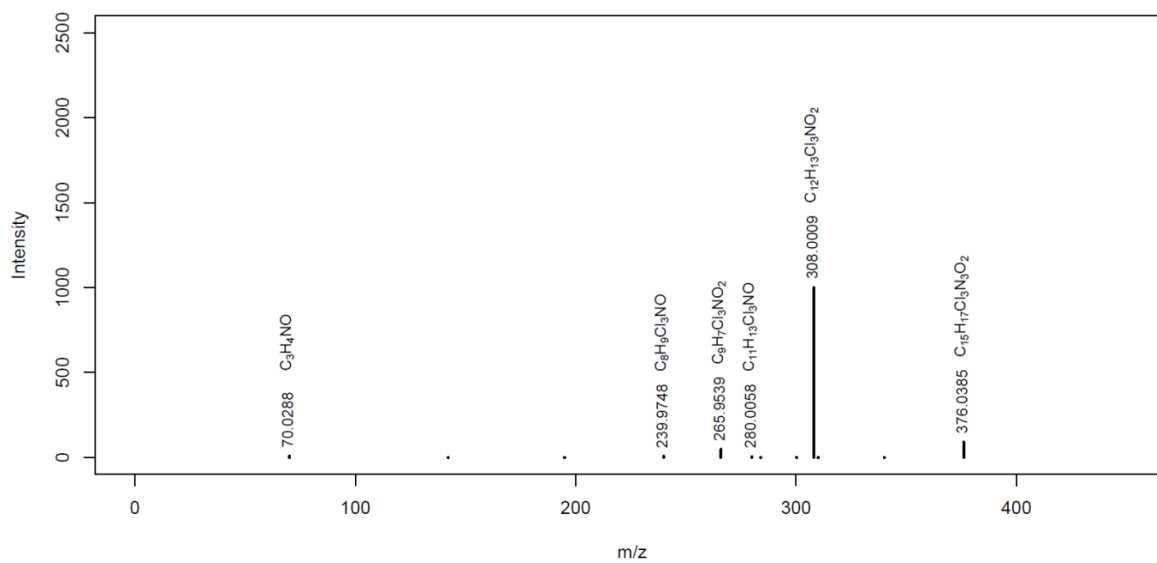
PRZ_M477

MassBank ID: ET203601



PRZ_M632bMassBank ID: **ET203051****PRZ_M554b**MassBank ID: **ET203901**

PRZ_M515MassBank ID: **ET204402***unclear structure***PRZ_M661**MassBank ID: **ET204601***unclear structure*

PRZ_M409MassBank ID: **ET204701***unclear structure***PRZ_M675**MassBank ID: **ET205101***unclear structure*

References

- [1] Rösch, A.; Anliker, S.; Hollender, J., How Biotransformation Influences Toxicokinetics of Azole Fungicides in the Aquatic Invertebrate *Gammarus pulex*. *Environmental Science & Technology* **2016**, *50* (13), 7175-7188.
- [2] Rösch, A.; Gottardi, M.; Vignet, C.; Cedergreen, N.; Hollender, J., Mechanistic Understanding of the Synergistic Potential of Azole Fungicides in the Aquatic Invertebrate *Gammarus pulex*. *Environmental Science & Technology* **2017**, *51* (21), 12784-12795.
- [3] R Core Team *A language and environment for statistical computing*, R Foundation for Statistical Computing: 2016.
- [4] Ritz, C.; Streibig, J. C., Bioassay analysis using R. *Journal of Statistical Software* **2005**, *12*, 1-22.
- [5] Roberts, T. R.; Hutson, D. H., Metabolic Pathways of Agrochemicals: Part 2: Insecticides and Fungicides. *Royal Society of Chemistry* **2006**.
- [6] Clinton, B.; Warden, A. C.; Haboury, S.; Easton, C. J.; Kotsonis, S.; Taylor, M. C.; Oakeshott, J. G.; Russell, R. J.; Scott, C., Bacterial degradation of strobilurin fungicides: a role for a promiscuous methyl esterase activity of the subtilisin proteases? *Biocatal. Biotransform.* **2011**, *29* (4), 119-129.
- [7] Laird, W. J. D.; Gledhill, A. J.; Lappin, G. J., Metabolism of methyl-(E)-2-{2- 6-(2-cyanophenoxy)pyrimidin-4-yloxy phenyl}-3-methoxyacrylate (azoxystrobin) in rat. *Xenobiotica* **2003**, *33* (6), 677-690.
- [8] European Mass Bank Server (NORMAN MassBank) www.massbank.eu.
- [9] Debrauwer, L.; Rathahao, E.; Boudry, G.; Baradat, M.; Cravedi, J. P., Identification of the major metabolites of prochloraz in rainbow trout by liquid chromatography and tandem mass spectrometry. *J. Agric. Food. Chem.* **2001**, *49* (8), 3821-3826.
- [10] Needham, D.; Challis, I. R., The metabolism and excretion of prochloraz, an imidazole-based fungicide, in the rat. *Xenobiotica* **1991**, *21* (11), 1473-1482.
- [11] Roberts, T. R.; Hutson, D. H., Metabolic Pathways of Agrochemicals: Part 2, Insecticides and fungicides. *Royal Society of Chemistry* **1999**.
- [12] Laignelet, L.; Riviere, J. L.; Lhuguenot, J. C., Metabolism of an imidazole fungicide (prochloraz) in the rat after oral administration. *Food Chem. Toxicol.* **1992**, *30* (7), 575-583.

Chapter 5. Conclusion, Outlook and Open Questions

The present work was carried out to extend the knowledge about biotransformation processes and their importance in aquatic invertebrate species. By using high resolution tandem mass spectrometry (HRMS/MS) to screen for fungicide biotransformation products (BTPs) and then including the identified BTPs into a kinetic model, the role of biotransformation on toxicokinetic processes was determined. Thereby, it was possible to differentiate between elimination routes, to evaluate the role of biotransformation in reducing parent compound bioaccumulation and to investigate the influence of fungicides on the biotransformation of co-occurring substances.

5.1 Prediction and Identification of Biotransformation Products

The suspect screening for predicted BTP exact masses was applied successfully (**Chapter 2, 3 and 4**). With predictions based on common drug biotransformation reactions such as cytochrome P450 monooxygenases (CYP)-catalyzed oxidation and conjugation reactions, most of the identified BTPs were covered. However, in **Chapter 2** we did not consider double conjugations, explaining why the glucose-sulfate conjugation products were not identified with the suspect screening but rather in the subsequent nontarget screening. Moreover, since malonyl conjugation is not a typical route of conjugation in aquatic organisms, it was not included in the prediction of suspected BTPs. It is assumed that with the applied comprehensive screening approaches we detected the majority of BTPs that were formed with concentrations above the set intensity threshold ($>10^6$). To test this assumption and to confirm that no relevant BTPs were missed, total internal concentrations (the sum of the parent compound and of all detected BTPs), determined via HRMS/MS, could be compared to total internal concentrations determined via radiolabeled parent compounds. Prerequisite for this comparison would be that the BTPs formed still contain the radiolabeled part of the molecule. However, radiolabeled compounds are not available for many compounds and its handling requires special precautions, therefore HRMS screening is regarded as a suitable alternative.

Several *in silico* BTP pathway prediction tools, such as *EAWAG-PPS* (<http://eawag-bbd.ethz.ch/predict/>), which is a rule-based system specialized in microbial biotransformation, or the knowledge-based mammalian prediction system *Meteor Nexus*¹ are available.² Additionally, there are tools predicting interactions of chemicals with biotransformation enzymes, such as CYPs (e.g., *ADMET Predictor*³). While enzymes such as CYPs seem to be conserved across all kingdoms of life⁴⁻⁸, especially conjugation reactions, which have been shown to be an important route of biotransformation in aquatic organisms, can differ among species.⁹⁻¹⁰ In general, no available BTP prediction system is specialized on biotransformation reactions in aquatic organisms, since most BTP prediction systems are based on mammalian or microbial metabolism. The diversity of identified BTPs in this work adds knowledge to possible biotransformation reactions in aquatic invertebrates, which could be used to extend an existing prediction system to better predict specific biotransformation reactions in aquatic invertebrates. Furthermore, including information about enzymes, such as CYPs, that are present in aquatic organisms and are involved in biotransformation reactions, would further improve the prediction of possible BTPs. The hepatopancreas

transcriptome for *Gammarus pulex* has been sequenced.¹¹ Further identification of genes and the encoded CYP proteins could improve the predictability of CYP-catalyzed biotransformation reactions in aquatic invertebrates such as in *G. pulex*.

All acquired BTP HRMS/MS spectra with various collision energies are available electronically in the MassBank High Resolution Spectral Database¹². In this way, HRMS/MS spectra of (tentatively) identified BTPs are available for the wider scientific community to assist in the discovery of relevant BTPs in environmental samples using computational mass spectrometric methods, even where reference standards are not available.

5.2 (Semi)-Quantification of Biotransformation Products

For most of the BTPs identified, no reference standards were commercially available. Therefore, peak area ratios of BTPs (area of the BTP divided by the area of the isotopically labeled internal standard of the parent compound) were compared to the calibration curve of the parent compound. However, ionization efficiencies during electrospray ionization can vary greatly between parent compound and BTPs. Jeon et al. (2013)¹³ applied a method based on estimated relative ionization efficiencies of BTPs to the parent compounds using physicochemical properties. Thereby, conversion factors can be obtained to calculate adjusted peak area ratios of the BTPs, which are then used for the quantification based on the calibration curve of the parent compound. With this method the accuracy of quantification could be slightly improved (~20%) for BTPs that are structurally similar to the parent compound, but quantification still remains an estimation. Especially for conjugation products, ionization efficiencies might be completely different due to their markedly higher molecular weights and different physicochemical properties caused by the addition of polar endogenous molecules. For example, sulfate-containing conjugation products are much more sensitive in negative electrospray ionization mode, but the corresponding parent compounds were only detectable in positive electrospray ionization mode. Therefore, the sulfate-containing conjugation products had to be quantified in their less sensitive mode, leading to higher limits of detection. More accurate quantification is prevented due to the lack of reference standards, and consequently, assessing the importance of biotransformation is hindered.

5.3 Prediction of Toxicokinetic Processes

Predicting BTPs based on common drug biotransformation reactions (see above) has been shown to be feasible, whereas predicting toxicokinetic processes quantitatively is challenging. Several methods for predicting fish **uptake rates** exist, e.g., based on the fish weight and/or log K_{ow} in a range of approximately 3.5 to 8.2 of neutral organic chemicals. However, uncertainty of estimated uptake rates is relatively large, even for the models that were found to perform best.¹⁴ Although for lipophilic compounds uptake is mainly fugacity driven, other parameters such as steric hindrance of chemicals, biological factors (respiration strategy, organism size and lipid content) and environmental conditions (e.g., temperature) can affect the actual uptake.¹⁵

We have shown that BTPs, especially secondary hydrophilic and/or charged BTPs were slowly **eliminated**, exhibiting considerably higher elimination half-lives compared to the parent compounds. Conjugation products with taurine, glucose-sulfate and glucose-malonyl are mainly present as anions at physiological pH (~5-8, dependent on the subcellular compartment)¹⁶, which impedes the crossing of cell membranes. Active carrier mediated transport is known as a cellular defense mechanism in aquatic organisms¹⁷⁻¹⁸; however, for amphipods it is unknown to what extent such active transporters contribute to the total elimination of chemicals. Overall, our results show that there is no clear relationship between physicochemical properties of a chemical and its total elimination (also considering further biotransformation) as well as its direct elimination.

Using elimination rates as a metric for the bioaccumulation potential has been discussed by Goss et al. (2013)¹⁹. They argue that elimination rates of chemicals are independent from exposure routes and can therefore be applied to dietary and non-dietary exposure scenarios. Furthermore, they state that both uptake and elimination rates are directly related to physicochemical properties of chemicals, but that uptake rates are additionally influenced by individual biological factors, making elimination rates a more reliable parameter. Yet, without considering biotransformation separately, an elimination rate covers all routes of elimination, such as direct elimination as well as biotransformation. Drawing a straight relationship between physicochemical properties and total elimination is critical, also in light of our results, which revealed no simple relationship between hydrophobicity and elimination half-lives or direct elimination rates. But if the only goal is to determine BAFs or BCFs of parent compounds, there is no need to separate different elimination routes by identifying BTPs, because all routes of elimination, including biotransformation are summed up into one rate constant, which represents the overall elimination of the parent compound and is necessary for calculating kinetic BAFs or BCFs.

However, the ecotoxicological risk might be underestimated when neglecting BTPs, because BTPs which still contain the toxicophore most likely add to the parent compound toxicity. This underestimation may be especially true for toxic BTPs that are retained longer in the organism than the parent compound.

Predicting **biotransformation rates** of neutral organic chemicals has been proposed using different approaches such as mass balance, quantitative structure activity relationships, and internal partitioning.²⁰⁻²³ However, among all toxicokinetic rate constants, biotransformation seems to be the rate constant that is most difficult to predict, since biotransformation does not follow a simple quantitative structure activity relationship and depends on factors such as the chemical distribution within the organism, structural and thereby physicochemical properties of the chemical, the presence of specific enzymes, and the enzymes' capacity to bind to and biotransform a chemical.²⁴

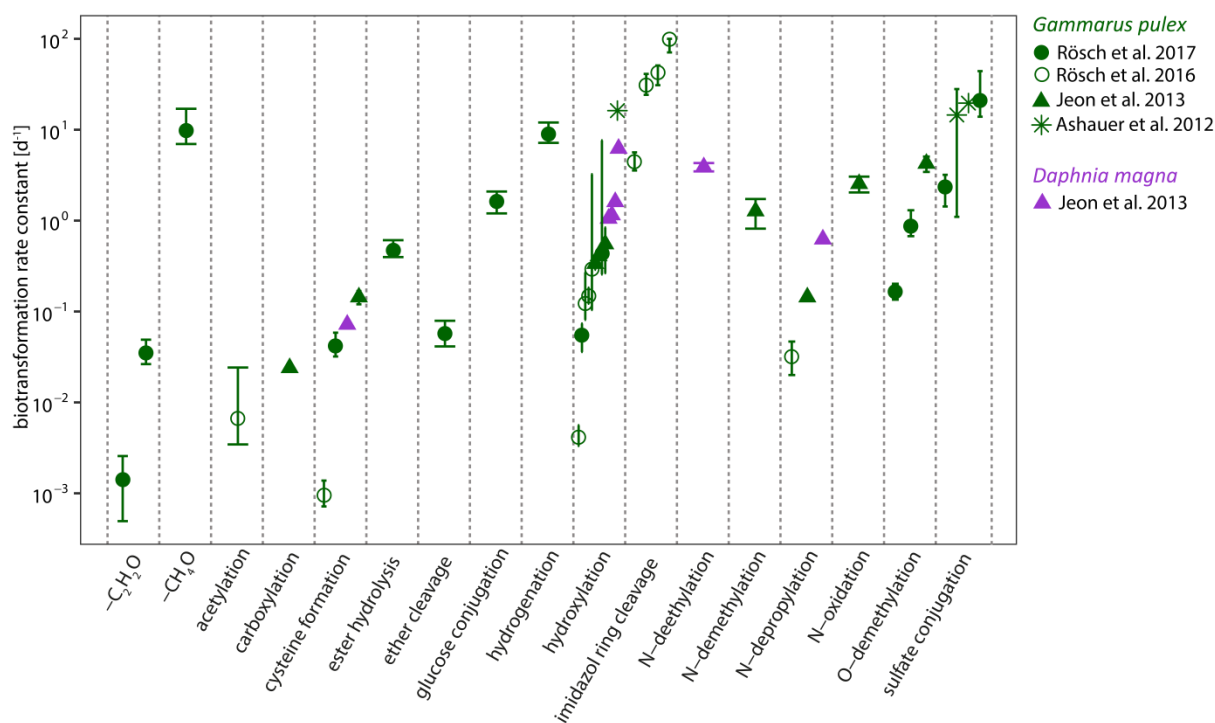


Figure 5-1: Comparison of modeled biotransformation rate constants [d⁻¹] compiled from different studies (Ashauer et al. (2012)²⁵, Jeon et al. (2013)¹³, Rösch et al. (2016)²⁶ and Rösch et al. (2017)²⁷) that identified BTPs of pesticides and pharmaceuticals in aquatic invertebrates and modeled the respective biotransformation rate constants. Error bars represent the corresponding 95% confidence intervals except for the study of Jeon et al. (2013)¹³, in which standard errors were calculated. If the standard error included zero or was below zero it could not be displayed on a log scale.

Our study provides modeled biotransformation rate constants of specific biotransformation reactions based on measured internal BTP concentrations. These biotransformation rate constants, as well as biotransformation rate constants from literature on aquatic invertebrates,^{13, 25} could be used to construct a database that comprises not only information on possible biotransformation reactions in different aquatic invertebrates but also information on their quantitative importance. The compiled data on rate constants available for individual reactions presented in Figure 5-1 show that even for one reaction type, biotransformation rate constants can vary by several orders of magnitude. However, identified BTPs are often characterized by several different reactions, since intermediate BTPs cannot be detected if they rapidly react further. This fact makes it difficult to assess the importance of individual biotransformation reactions since the modeled biotransformation rate constants often comprise several reaction steps. Furthermore, classifying biotransformation reactions can be challenging if the reaction is not distinctly defined, as we have seen, for example, for the imidazole ring cleavage products (PRZ_M382 → PRZ_M353 → PRZ_M325 → PRZ_M282). These reactions occurring at the imidazole ring are N-C cleavages but differ from typical N-dealkylation reactions and show higher biotransformation rate constants.

5.4 Relevance of Synergism in Pesticide Mixtures

Two reviews reported that in approximately 5% of all investigated pesticide mixtures, the observed effect was greater than two compared to the model of concentration addition (CA).²⁸⁻²⁹ The most potent synergists in the pesticide mixtures investigated were cholinesterase inhibitors (organophosphate and carbamate insecticides) and azole fungicides, both of which are known to alter enzyme activity and thereby affect biotransformation.²⁸ However, the concentrations used in these experiments were substantially higher than what is expected in the environment.

Chapter 4 confirms the outcome of the single studies collected in the reviews that azole fungicides are potent synergists. However, out of the six binary fungicide mixtures tested, composed of 40 or 80 $\mu\text{g L}^{-1}$ azoxystrobin and similar molar concentrations of one of the selected azole fungicides (four triazoles: cyproconazole, epoxiconazole, propiconazole, tebuconazole; two imidazoles: ketoconazole, prochloraz), only prochloraz showed CYP inhibition measured in terms of internal concentrations of azoxystrobin and associated BTPs. Furthermore, the observed synergism by prochloraz was not only caused by CYP inhibition, but also by increased azoxystrobin uptake. Determined inhibitory concentrations of prochloraz that cause 10% CYP inhibition ($\text{IC}_{10, \text{PRZ, AZ}}$) of $4 \pm 2 \mu\text{g L}^{-1}$ were around 10 times higher than prochloraz concentrations measured in Swiss surface waters.³⁰⁻³¹ However, surface water concentrations of azoles can be in the low $\mu\text{g L}^{-1}$ range in waters strongly influenced by agriculture and/or wastewater.³²⁻³³ Additionally, there are a few studies that also detected synergism at environmentally realistic concentrations.³⁴⁻³⁵ Nevertheless, in general, threshold concentrations are likely above environmentally realistic concentrations for many synergists, below which potential synergists do not enhance the effect of co-occurring chemicals. The review by Cedergreen (2014)²⁸ shows that for pesticide mixtures it was possible to identify the most potent synergists. Therefore, additional studies are needed that investigate synergistic interaction of those known synergists at chemical concentrations realistic for aquatic environments. In addition, other substance classes such as pharmaceuticals should be further evaluated for possible synergism. Special attention could be paid to those synergists in risk assessment by, for example, adjustment of environmentally quality standards (EQS), if the threshold concentration for synergy is below the determined EQS.

5.5 Toxicokinetic-(Toxicodynamic) Modeling to assess the Importance of Biotransformation and Synergistic Interactions

From a risk assessment point of view, the overall objective would be to link the chemical exposure concentration to the internal concentration at the target site and, consequently, to the effect, also in the presence of co-occurring substances that can cause synergistic effects. Toxicokinetic-toxicodynamic models exist which simulate the processes that lead to toxic effects on organisms.³⁶ In general, such a model should be able to address varying substrate-inhibitor ratios to predict threshold effect concentrations where synergism starts. To establish a link between toxicokinetics and toxicodynamics, time-resolved effect data,

such as mortality, and the (toxico)-kinetics of CYP inhibition would be needed. The model would be substrate-specific, since mortality is driven by the substrates' bioaccumulation, which is influenced by the proportion of CYP-catalyzed biotransformation reactions that lead to detoxification or in some cases, to bioactivation. However, prochloraz did not only inhibit the CYP-catalyzed biotransformation reactions of a co-occurring substrate, but also impacted gammarids' mobility, resulting in different substrate uptake rate constants at different prochloraz exposure concentrations, further complicating toxicokinetic-toxicodynamic modeling.

Differences in species' sensitivity towards the same chemical can be related to both toxicokinetic and toxicodynamic processes. Our study shows that two related species from the same taxonomic order of *Amphipoda* differed in toxicokinetics, *i.e.*, exhibited different rates of chemical uptake, elimination and biotransformation, thereby contributing to the understanding why species sensitivity towards the same chemicals can vary.

The reduced toxicokinetic modeling approach for azoxystrobin, where the time courses of the parent compound, the sum of all primary BTPs and the sum of all secondary BTPs were modeled, showed similar results compared to the detailed modeling of azoxystrobin and of all single BTPs, because similar uptake and total elimination rates were obtained, resulting in similar kinetic BAFs. Both models indicated that the sum of primary biotransformation rate constants $k_{Mx, 1st}$ or the total primary biotransformation rate constant $k_{M, 1st, total}$ contributed to the same percentage to the total elimination of azoxystrobin. Therefore, in the future, it might be sufficient to use the reduced toxicokinetic modeling approach to evaluate the importance of biotransformation, since it reduces parameter uncertainty and only requires the assignment of primary and secondary BTPs, which is much easier compared to the elucidation of a whole biotransformation pathway, where every precursor needs to be correctly assigned.

5.6 Chemical Testing using Aquatic Invertebrates

The principle of the 3R (*i.e.*, replacement, reduction, refinement), first introduced in 1959 by Russell and Burch (1959)³⁷, has been embedded in the EU legislation 2010/63/EU on protection of animals used for scientific purposes³⁸ and describes the need for the replacement of protected animals (mainly vertebrates), for methods to minimize the number of test species in experiments (reduction), and for methods that minimize the pain and suffering of test species (refinement). Invertebrates are not protected within this EU legislation. Since their nervous system is fundamentally different from those of vertebrates they are expected to experience less pain. However, if and to what extent invertebrates are able to experience pain is subject to debate.³⁹ Therefore, *in vitro* cell assays are regarded as a promising alternative chemical testing approach that can reduce and almost replace the number of required vertebrate or invertebrate test species.⁴⁰⁻⁴² However, more investigations are needed to improve the extrapolation from *in vitro* to *in vivo* test systems in relation to toxicokinetics and toxicodynamics, especially concerning the comparability of biotransformation processes.⁴³

References

- [1] Marchant, C. A.; Briggs, K. A.; Long, A., In silico tools for sharing data and knowledge on toxicity and metabolism: Derek for windows, meteor, and vitic. *Toxicology Mechanisms and Methods* **2008**, *18* (2-3), 177-187.
- [2] Kirchmair, J.; Goeller, A. H.; Lang, D.; Kunze, J.; Testa, B.; Wilson, I. D.; Glen, R. C.; Schneider, G., Predicting drug metabolism: experiment and/or computation? *Nature Reviews Drug Discovery* **2015**, *14* (6), 387-404.
- [3] ADMET Predictor (Simulations Plus Inc, 2014).
- [4] Katagi, T., Bioconcentration, Bioaccumulation, and Metabolism of Pesticides in Aquatic Organisms. In *Reviews of Environmental Contamination and Toxicology, Vol 204*, Whitacre, D. M., Ed. 2010; Vol. 204, pp 1-132.
- [5] Guengerich, F. P., Common and uncommon cytochrome P450 reactions related to metabolism and chemical toxicity. *Chem. Res. Toxicol.* **2001**, *14* (6), 611-650.
- [6] Sole, M.; Livingstone, D. R., Components of the cytochrome P450-dependent monooxygenase system and 'NADPH-independent benzo a pyrene hydroxylase' activity in a wide range of marine invertebrate species. *Comparative Biochemistry and Physiology C-Toxicology & Pharmacology* **2005**, *141* (1), 20-31.
- [7] Snyder, M. J., Cytochrome P450 enzymes in aquatic invertebrates: Recent advances and future directions. *Aquat. Toxicol.* **2000**, *48* (4), 529-547.
- [8] James, M. O.; Boyle, S. M., Cytochromes P450 in crustacea. *Comparative Biochemistry and Physiology C-Pharmacology Toxicology & Endocrinology* **1998**, *121* (1-3), 157-172.
- [9] James, M. O., Conjugation of organic pollutants in aquatic species. *Environ. Health Perspect.* **1987**, Vol. 71, 97-103.
- [10] Testa, B.; Kraemer, S. D., The Biochemistry of Drug Metabolism - An Introduction Part 4. Reactions of Conjugation and Their Enzymes. *Chemistry & Biodiversity* **2008**, *5* (11), 2171-2336.
- [11] Gismondi, E.; Thome, J. P., Transcriptome of the freshwater amphipod *Gammarus pulex* hepatopancreas. *Genomics Data* **2016**, *8*, 91-92.
- [12] European Mass Bank Server (NORMAN MassBank) www.massbank.eu.
- [13] Jeon, J.; Kurth, D.; Ashauer, R.; Hollender, J., Comparative toxicokinetics of organic micropollutants in freshwater crustaceans. *Environ. Sci. Technol.* **2013**, *47* (15), 8809-17.
- [14] Brooke, D. N.; Crookes, M. J.; Merckel, D. A., Methods for predicting the rate constant for uptake of organic chemicals from water by fish. *Environ. Toxicol. Chem.* **2012**, *31* (11), 2465-2471.
- [15] Barron, M. G., Bioconcentration. Will water-borne organic chemicals accumulate in aquatic organisms? *Environmental Science & Technology* **1990**, *24* (11), 1612-1618.
- [16] Casey, J. R.; Grinstein, S.; Orłowski, J., Sensors and regulators of intracellular pH. *Nature Reviews Molecular Cell Biology* **2010**, *11* (1), 50-61.
- [17] Bard, S. M., Multixenobiotic resistance as a cellular defense mechanism in aquatic organisms. *Aquat. Toxicol.* **2000**, *48* (4), 357-389.
- [18] Kurelec, B., The multixenobiotic resistance mechanism in aquatic organisms. *Crit. Rev. Toxicol.* **1992**, *22* (1), 23-43.
- [19] Goss, K.-U.; Brown, T. N.; Endo, S., Elimination half-life as a metric for the bioaccumulation potential of chemicals in aquatic and terrestrial food chains. *Environ. Toxicol. Chem.* **2013**, *32* (7), 1663-1671.
- [20] Arnot, J. A.; Mackay, D.; Bonnell, M., Estimating metabolic biotransformation rates in fish from laboratory data. *Environ. Toxicol. Chem.* **2008**, *27* (2), 341-351.
- [21] Arnot, J. A.; Meylan, W.; Tunkel, J.; Howard, P. H.; Mackay, D.; Bonnell, M.; Boethling, R. S., A quantitative structure-activity relationship for predicting metabolic biotransformation rates for organic chemicals in fish. *Environ. Toxicol. Chem.* **2009**, *28* (6), 1168-1177.

- [22] Kuo, D. T.; Di Toro, D. M., Biotransformation model of neutral and weakly polar organic compounds in fish incorporating internal partitioning. *Environ. Toxicol. Chem.* **2013**, *32* (8), 1873-81.
- [23] Van der Linde, A.; Jan Hendriks, A.; Sijm, D. T. H. M., Estimating biotransformation rate constants of organic chemicals from modeled and measured elimination rates. *Chemosphere* **2001**, *44* (3), 423-435.
- [24] Sijm, D. T. H. M.; Rikken, M. G. J.; Rorije, E.; Traas, T. P.; Mclachlan, M. S.; Peijnenburg, W. J. G. M., Transport, Accumulation and Transformation Processes. In *Risk Assessment of Chemicals: An Introduction*, Leeuwen, C. J. v.; Vermeire, T. G., Eds. Springer Netherlands: Dordrecht, 2007; pp 73-158.
- [25] Ashauer, R.; Hintermeister, A.; O'Connor, I.; Elumelu, M.; Hollender, J.; Escher, B. I., Significance of xenobiotic metabolism for bioaccumulation kinetics of organic chemicals in *gammarus pulex*. *Environ. Sci. Technol.* **2012**, *46* (6), 3498-3508.
- [26] Rösch, A.; Anliker, S.; Hollender, J., How Biotransformation Influences Toxicokinetics of Azole Fungicides in the Aquatic Invertebrate *Gammarus pulex*. *Environmental Science & Technology* **2016**, *50* (13), 7175-7188.
- [27] Rösch, A.; Gottardi, M.; Vignet, C.; Cedergreen, N.; Hollender, J., Mechanistic Understanding of the Synergistic Potential of Azole Fungicides in the Aquatic Invertebrate *Gammarus pulex*. *Environmental Science & Technology* **2017**, *51* (21), 12784-12795.
- [28] Cedergreen, N., Quantifying synergy: A systematic review of mixture toxicity studies within environmental toxicology. *PLoS ONE* **2014**, *9* (5), e96580.
- [29] Belden, J. B.; Gilliom, R. J.; Lydy, M. J., How well can we predict the toxicity of pesticide mixtures to aquatic life? *Integrated environmental assessment and management* **2007**, *3* (3), 364-372.
- [30] Moschet, C.; Wittmer, I.; Simovic, J.; Junghans, M.; Piazzoli, A.; Singer, H.; Stamm, C.; Leu, C.; Hollender, J., How a complete pesticide screening changes the assessment of surface water quality. *Environ. Sci. Technol.* **2014**, *48* (10), 5423-5432.
- [31] Doppler, T.; Mangold, S.; Wittmer, I.; Spycher, S.; Comte, R.; Stamm, C.; Singer, H., Hohe PSM-Belastung in schweizer Bächen. *Aqua und Gas* **2017**, *4*, 46-56.
- [32] Battaglin, W.; Sandstrom, M.; Kuivila, K.; Kolpin, D.; Meyer, M., Occurrence of Azoxystrobin, Propiconazole, and Selected Other Fungicides in US Streams, 2005–2006. *Water Air Soil Pollut* **2011**, *218* (1-4), 307-322.
- [33] Riise, G.; Lundekvam, H.; Wu, Q. L.; Haugen, L. E.; Mulder, J., Loss of pesticides from agricultural fields in SE Norway - runoff through surface and drainage water. *Environ. Geochem. Health* **2004**, *26* (2-3), 269-276.
- [34] Laetz, C. A.; Baldwin, D. H.; Collier, T. K.; Hebert, V.; Stark, J. D.; Scholz, N. L., The Synergistic Toxicity of Pesticide Mixtures: Implications for Risk Assessment and the Conservation of Endangered Pacific Salmon. *Environ. Health Perspect.* **2009**, *117* (3), 348-353.
- [35] Bjergager, M.-B. A.; Hanson, M. L.; Lissemore, L.; Henriquez, N.; Solomon, K. R.; Cedergreen, N., Synergy in microcosms with environmentally realistic concentrations of prochloraz and esfenvalerate. *Aquat. Toxicol.* **2011**, *101* (2), 412-422.
- [36] Ashauer, R.; Boxall, A.; Brown, C., Predicting effects on aquatic organisms from fluctuating or pulsed exposure to pesticides. *Environ. Toxicol. Chem.* **2006**, *25* (7), 1899-1912.
- [37] Russell, W. M. S.; Burch, R. L., *The principles of humane experimental technique*. Methuen: London, 1959.
- [38] Directive 2010/63/EU of the European Parliament and of the Council on the protection of animals used for scientific purposes. 2010.
- [39] Sneddon, L. U., Pain in aquatic animals. *J. Exp. Biol.* **2015**, *218* (7), 967-976.
- [40] Stadnicka-Michalak, J.; Tanneberger, K.; Schirmer, K.; Ashauer, R., Measured and Modeled Toxicokinetics in Cultured Fish Cells and Application to In Vitro - In Vivo Toxicity Extrapolation. *Plos One* **2014**, *9* (3).

- [41] Tanneberger, K.; Knoebel, M.; Busser, F. J. M.; Sinnige, T. L.; Hermens, J. L. M.; Schirmer, K., Predicting Fish Acute Toxicity Using a Fish Gill Cell Line-Based Toxicity Assay. *Environmental Science & Technology* **2013**, *47* (2), 1110-1119.
- [42] Lillicrap, A.; Belanger, S.; Burden, N.; Du Pasquier, D.; Embry, M. R.; Halder, M.; Lampi, M. A.; Lee, L.; Norberg-King, T.; Rattner, B. A.; Schirmer, K.; Thomas, P., Alternative Approaches to Vertebrate Ecotoxicity Tests in the 21st Century: A Review of Developments Over the Last 2 Decades and Current Status. *Environ. Toxicol. Chem.* **2016**, *35* (11), 2637-2646.
- [43] Bischof, I.; Koester, J.; Segner, H.; Schlechtriem, C., Hepatocytes as in vitro test system to investigate metabolite patterns of pesticides in farmed rainbow trout and common carp: Comparison between in vivo and in vitro and across species. *Comparative Biochemistry and Physiology C-Toxicology & Pharmacology* **2016**, *187*, 62-73.

Curriculum Vitae

Name: Andrea Rösch
Email: andrea.b.roesch@gmail.com
Nationality: German
Date of birth: March 7, 1986

2013 – 2017: PhD Thesis, Environmental Chemistry, Eawag Dübendorf / ETH Zürich,
Switzerland

2009 – 2012: MSc Marine Environmental Sciences, University of Oldenburg, Germany

2006 – 2009: BSc Environmental Sciences, University of Oldenburg, Germany

2005 – 2006: Voluntary ecological year on Hallig Langeness, Schleswig-Holstein Wadden
Sea, Germany

1997 – 2005: Abitur, Montfortgymnasium Tettnang, Germany

Acknowledgments

My greatest thanks go to Juliane Hollender for her supervision of the thesis and for the opportunity to perform this work. I'm thankful for our weekly meetings, her time whenever I needed support, her quick responses and edits to anything I sent her, and for all her scientific input. I gratefully thank Nina Cedergreen for giving me the opportunity to visit her Environmental Toxicology group at the University of Copenhagen for two months, for the cooperation that developed, for the critical feedback on our manuscript, and for being on my committee. Many thanks go to Roman Ashauer for helpful discussions and advice with toxicokinetic modeling and for being a member of my committee. I also thank Kris McNeill for his contribution as a member of my committee.

Furthermore, I want to thank everyone that directly contributed to this work: Sabine Anliker for the great work on and outcome of her master thesis which resulted in a shared publication; Birgit Beck, Philipp Longrée, Andreas Maccagnan and Bernadette Vogler for their technical support and assistance in the lab; Tjalling Jager for his enormous support concerning toxicokinetic modeling, his time he dedicated to answering my questions, his ideas and his input; Michele Gottardi and the group in Copenhagen for their help with lab work and with data evaluation; Qiuguo Fu for support in the lab, discussion as well as for taking over the *Hyalella* culture; Andreas Scheidegger for support with Bayesian statistics; Emma Schymanski for her assistance in computational MS/MS spectra annotation, uploading my spectra to MassBank and her generously shared knowledge on structure elucidation of biotransformation products; all Uchems dealing with biotransformation in different matrices; Junho Jeon for supervising me when I came to Eawag and started my PhD; and Rebecka Hischer for conducting toxicity tests during her bachelor thesis which is not the type of experiment I enjoy doing.

Thanks to all former and present office girls of E22: Aurea, Christelle, Evelyne, Jen, Paola and Yuije. Special thanks go to Jen. I am very happy that I had the pleasure of sharing the office with her during my entire PhD. I enjoyed turning our chairs, looking into the hallway and chatting when we needed a break (and thereby confusing people), the beautiful calendars she brought every year and our monthly ritual of "choosing everybody's favorite item", and her general support work and non-work related.

Many thanks go to the entire department of Environmental Chemistry. I was lucky to get the chance to work in such a supportive and inspiring working environment. Many Uchems became friends, and I enjoyed lunch breaks, apéros as well as social events outside of Eawag. I want to thank Birgit for many evenings we spent on preparing delicious and complex dinners and for always offering me a bed in *Birgit Becks Bed & Breakfast*, especially during the times when I was doing toxicokinetic experiments; Rebekka and Jen for always being there, at Eawag and in Winterthur/Oerlikon; Martin Loos for picking me up for breaky breaks and talking nonsense – always really great stuff; Nicole and Jonas for sandwich discussion; Rani, the presentation god, for his support and for calming me down before my

defense; Fabian for offering me a beer on the aqa terrace when I was hiding in the library; Michele, Sabine, Matze, Anne, Simon M., Bernadette, Tobi, Christoph, Emma, Simon S., Ash, Philipp, Andreas, Cresten, Fred, Stephie, Urs, Karin, Adi, Sarah, Stefan, Christine, Davide, and many more former and present Uchem members.

Finally, a huge thank you goes to my parents, Iris, Verena and Mathias, for their support and encouragement throughout my entire life.